



UNIVERSITÀ DEGLI STUDI DI PAVIA

Dottorato di Ricerca in Scienze Chimiche e Farmaceutiche (XXXII Ciclo)

Coordinatore: Chiar.mo Prof. Mauro Freccero

**SIGMA 1 RECEPTOR (S1R) MODULATORS AS A THERAPEUTIC STRATEGY FOR
PROMOTING NEUROPLASTICITY. DESIGN AND SYNTHESIS OF NOVEL MONO- AND
BI-VALENT LIGANDS FOR SRS**

Tutor: Chiar.ma Prof. Simona Collina

Tesi di dottorato di

Giacomo Rossino

Curriculum:

Pharmaceutical Sciences

Table of contents

The research	4
List of abbreviations	7
1. Introduction	10
1.1 Sigma receptors: an overview.....	11
1.2 Structure and mechanism of S1R (with a special focus on oligomerization process).....	16
1.3 Sigma 1 Receptor as therapeutic target (with a special focus on neurodegeneration).....	19
1.4 Multi target drugs as a modern approach for neurodegenerative diseases.....	23
2. Targeting the sigma1 receptor system to counteract neurodegeneration	27
2.1 The S1R modulators: state of the art	28
2.2 Design and pharmacokinetic predictions of novel ligands.....	31
2.3 Synthesis.....	35
2.4 Biological investigation.....	38
2.5 Computational studies	44
2.6 Discussion	47
3. Studying the S1R oligomerization process	49
3.1 Design of bivalent ligands.....	50
3.2 Synthesis of enantiopure compound (<i>R</i>)-RC-33A	54
3.3 Synthesis of bivalent ligands.....	60
3.4 Biological evaluation of bivalent ligands	62
3.5 Computational studies	64
3.6 Discussion	67
4. Conclusions	69
5. Experimental section	71
5.1 Laboratory materials and equipment	72
5.2 General experimental details	72
5.3 Synthetic procedures	73
5.3.1 General procedure for the preparation of compounds II – III	73
5.3.2 General procedure for the preparation of compounds Ia-b, IIa-c and IIIa-b.....	73
5.3.3 General procedure for the preparation of compounds 1-31.....	76
5.3.4 synthesis of (<i>R</i>)-RC-33A with route A	87
5.3.5 synthesis of (<i>R</i>)-RC-33A with route B	91
5.3.6 Synthesis of (<i>R</i>)-RC-33A with route C	92
5.3.7 Synthesis of bivalent ligands.....	93
5.4 General protocol for binding assays.....	99

5.4.1 S1R binding assay	99
5.4.2 S2R binding assay	100
5.4.3 GluN2 binding assay	100
5.5 Computational studies	100
5.5.1 Dataset preparation	100
5.5.2 Docking protocol.	105
6. References.....	106
Appendix.....	119
Paper 1	120
Paper 2	142
Paper 3	155
Paper 4	174
Paper 5	192
Paper 6	213

The research

During my three-years-project I focused on the development of novel mono- and bi-valent Sigma1 Receptor (S1R) modulators to address two main objectives: (i) the obtainment of multitarget-directed ligands (MTDLs) endowed with therapeutic potential for the treatment of neurodegenerative diseases; (ii) the preparation of a series of bivalent compounds to be used for the study of S1R oligomerization process. These two major topics are briefly discussed herein.

(i) Neurodegeneration is a key event in many challenging disorders (e.g. Alzheimer's diseases, Parkinson's disease, multiple sclerosis). Such pathologies involve the alteration of several molecular pathways, making the identification of an effective treatment a difficult task. Considering their complex nature, the multi-target paradigm is gaining great consensus in the search for small molecules able to counteract these pathologies. Among the numerous molecular targets that have been correlated with neurodegenerative disorders, S1R has gained great attention from the scientific community, and S1R agonists are considered promising pharmacological tools for their neuroprotective activity. Accordingly, we reasoned that by coupling S1R agonism with modulation of other molecular targets implicated in neurodegenerative processes we might obtain new molecular entities endowed with higher chances to counteract such pathologies. The additional targets of our MTDLs include N-Methyl-D-Aspartate (NMDA) receptor, which plays a relevant role in synaptic plasticity, and acetylcholinesterase (AChE), which regulates acetylcholine levels in central nervous system. A small structurally focused compound library was prepared through a divergent synthesis. The so-obtained compounds were tested for a preliminary biological evaluation, evaluating their affinity and selectivity towards S1R and NMDA receptor, the AChE inhibition and their antioxidant properties, since oxidative stress plays a potential role in the pathogenesis of neurodegenerative disorders. A number of promising compounds, endowed with effective multitarget profile, was identified. These results will pave the way for further biological investigation and structure optimization in order to achieve viable tools for the treatment of neurodegenerative pathologies.

(ii) In the last decade numerous studies have supported the hypothesis that S1R can exist in multiple oligomeric forms. In detail, agonists seem to stabilize S1R monomers and dimers that act as chaperones, whereas antagonists bind to higher oligomer complexes, maintaining them in repository forms. These assumptions were recently confirmed by the elucidation of S1R crystal structure, which highlighted the trimeric form of the receptor. Nevertheless, the mechanism of generation, as well as the precise biological function of S1R oligomers, are still unknown. Accordingly, a series of homo- and hetero-bivalent S1R ligands was designed and synthesized to investigate S1R oligomerization process. Since S1R agonists are known to

exert neuroprotective effects, and S1R can form homo-dimeric structures upon interaction with agonists, we reasoned that promoting dimerization through bivalent agonists might enhance ligand's activity. The designed bivalent compounds consist in two units of (*R*)-RC-33 (a potent and selective S1R agonist developed by our group) tethered by a linker. Different lengths, polarities and spatial constraints were explored for the linker. The key precursor of the synthesis is (*R*)-RC-33A, an aminic derivative of RC-33. For the obtainment of enantiopure (*R*)-RC-33A, three different synthetic approaches have been explored, resulting in the identification of an efficient pathway to access (*R*)-RC-33 derivatives with high yield and chiral purity. Once the designed ligands were obtained in sufficient amount and purity, they were tested in binding assays using radioligands to assess their S1R affinity. Moreover, computational studies were performed on both mono- and bi-valent S1R modulators. In detail, docking into the crystal's binding pocket served as basis for the development of a 3D-QSAR model and for the rationalization of experimental results. Molecular dynamics studies are ongoing, and future functional assays will contribute to shed light on the S1R oligomeric states.

Objectives (i) and (ii) were pursued in parallel during my PhD. Accordingly, the organization of this PhD thesis will not follow the chronological order of the activities performed. Instead, it will be organized according to the topics addressed, as follows:

Section 1: gives an introduction on S1R, its structure and oligomeric states, as well as its therapeutic potential, especially in the treatment of neurodegenerative pathologies. In this section, a brief overview on the multitarget approach for counteracting neurodegeneration will be given.

Section 2: provides a detailed discussion on the first objective of my work, *i.e.* the obtainment of MTDLs targeting the S1R and other related targets to counteract neurodegeneration.

Section 3: describes the pursue of the second objective of my research, *i.e.* the development of bivalent S1R ligands to study the S1R oligomerization.

Section 4: draws the most important conclusions and future perspectives concerning both main objectives of my work.

Section 5: collects all experimental procedures and data.

Section 6: reports all bibliographic references.

Appendix: reports the publications I contributed to, concerning the topics addressed throughout this thesis.

The research is characterized by a high level of interdisciplinarity and involved several researchers with different competences. I mainly worked at the LabMedChem, at the University of Pavia, where I performed the synthesis, purification and characterization of the target products. Moreover, I also had the opportunity to spend part of my PhD in the lab of Julio Caballero (University of Talca, Chile), where I acquired skills in molecular modelling – working on molecular docking and the early development of a 3D-QSAR model – and in the group of Bernhard Wunsch (University of Münster, Germany), where I finalized the synthesis relative to objective (ii) and I was trained to perform displacement binding assays

with radioligands. Finally, I had the opportunity to follow all the different aspects of this interdisciplinary project being involved in the planning of activities and in the discussion of the results with all the research groups involved.

List of abbreviations

AChE	Acetylcholine esterase
ACN	Acetonitrile
AD	Alzheimer's disease
ADME	Absorption, distribution, metabolism, excretion
ALS	Amyotrophic lateral sclerosis
AQP	Aquaporin
ATF6	Activating transcription factor 6
A β	Amyloid beta
BBB	Blood-brain barrier
BDNF	Brain-derived neurotrophic factor
BiP	Binding Immunoglobulin Protein
BuChE	Butyrylcholinesterase
CNS	Central nervous system
COMU	(1-Cyano-2-ethoxy-2-oxoethylidenaminoxy) dimethylamino-morpholino-carbenium hexafluoro-phosphate
DALY	Disability-adjusted life year
DCC	<i>N,N'</i> -Dicyclohexylcarbodiimide
DCFDA	2',7'-Dichlorofluorescein diacetate
DCM	Dichloromethane
DHEA	Dehydroepiandrosterone
DIBAL-H	Diisobutylaluminium hydride
DIPEA	<i>N,N</i> -Diisopropylethylamine
DMF	Dimethylformamide
DMT	<i>N,N</i> -dimethyltryptamine
DRG	Dorsal root ganglia
DTG	Ditolyguanidine
DTNB	5,5'-Dithiobis(2-nitrobenzoic acid)
EDC	1-Ethyl-3-(3-dimethylaminopropyl)carbodiimide
EGF	Epidermal growth factor
EGFR	Epidermal growth factor receptor
ER	Endoplasmic reticulum

FRET	Fluorescence resonance energy transfer
FRS	Free radical scavenging
GDNF	Glial cell-derived neurotrophic factor
H ₃ R	Histamine H ₃ receptor
HD	Huntington's disease
HDAC	Histone deacetylase
HER2	Human epidermal growth factor 2
HPLC	High performance liquid chromatography
I.D.	Internal diameter
IP3	Inositol trisphosphate
IP3R	Inositol trisphosphate receptor
IPA	Isopropyl alcohol
IRE1	Inositol-requiring enzyme 1
IRE1 α	Inositol-requiring enzyme 1 α
MAM	Mitochondria-associated ER membrane
MAO B	Monoamine oxidase B
MS	Multiple sclerosis
MTD	Multitarget drug
MTDL	Multitarget-directed ligand
mw	Microwave
MW	Molecular Weight
NGF	Nerve growth factor
NMDA	<i>N</i> -methyl-D-aspartate
NMDAR	<i>N</i> -methyl-D-aspartate receptor
NMR	Nuclear magnetic resonance
NODMHA	<i>N,O</i> -Dimethylhydroxylamine
NOS	Nitric oxide synthase
NPC1	Niemann-Pick type C protein 1
Nrf2	Nuclear factor erythroid 2-related factor 2
PD	Parkinson's disease
PDB	Protein data bank
PD-LID	Parkinson's Disease Levodopa Induced Dyskinesia
PEA	Phenylethylamine
PEG	Polyethylene glycol
PERK	Protein kinase RNA like ER kinase

PGRMC1	Progesterone Receptor Membrane Component 1
PKC	Protein kinase C
ps	Particle size
PyBroP	Bromo-tris-pyrrolidino-phosphonium hexafluorophosphate
QSAR	Quantitative structure-affinity relationship
ROS	Reactive oxygen species
S1R	Sigma-1 receptor
S2R	Sigma-2 receptor
SAR	Structure-affinity relationship
SCA	Spinocerebellar ataxia
TBTU	2-(1H-Benzotriazole-1-yl)-1,1,3,3-tetramethylammonium tetrafluoroborate
TEAC	Tetraethylammonium chloride
TFA	Trifluoroacetic acid
THF	Tetrahydrofuran
TLC	Thin layer chromatography
TMS	Tetramethylsilane
UPLC-MS	Ultra performance liquid chromatography–mass spectrometry
UPR	Unfolded protein response

1. Introduction

1.1 Sigma receptors: an overview

The term “Sigma Receptor” (SR) was coined in 1976 by Martin *et al.*, in order to identify a new opioid receptor subtype¹, in virtue of its ability to interact with the benzomorphan analogue (\pm)-SKF-10,047 (**Figure 1**). Subsequent pharmacological characterization demonstrated that this classification was an erroneous assumption, since the opioid antagonists naloxone and naltrexone had no activity toward SRs²⁻⁴.

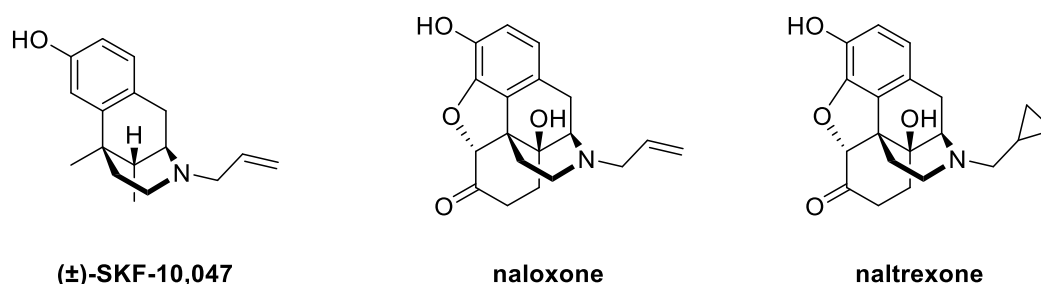


Figure 1. Chemical structure of (\pm)-SKF-10,047, which binds to both Sigma and opioid receptors, and those of naloxone and naltrexone, opioid receptors antagonists.

After years of contradictions and wrong assumptions⁵, the advances in biological and pharmacological fields collimated in defining SRs as an orphan receptor family (**Figure 2**) consisting of two subtypes known as Sigma-1 (S1R) and Sigma-2 (S2R) receptors, which display a different tissue distribution and a distinct physiological and pharmacological profile⁶⁻⁸. Molecular cloning of both receptor subtypes showed that these proteins are genetically unrelated to each other and to the true opioid receptors^{9,10}.

A brief summary of the state-of-art knowledge about S1R and S2R is reported hereafter.

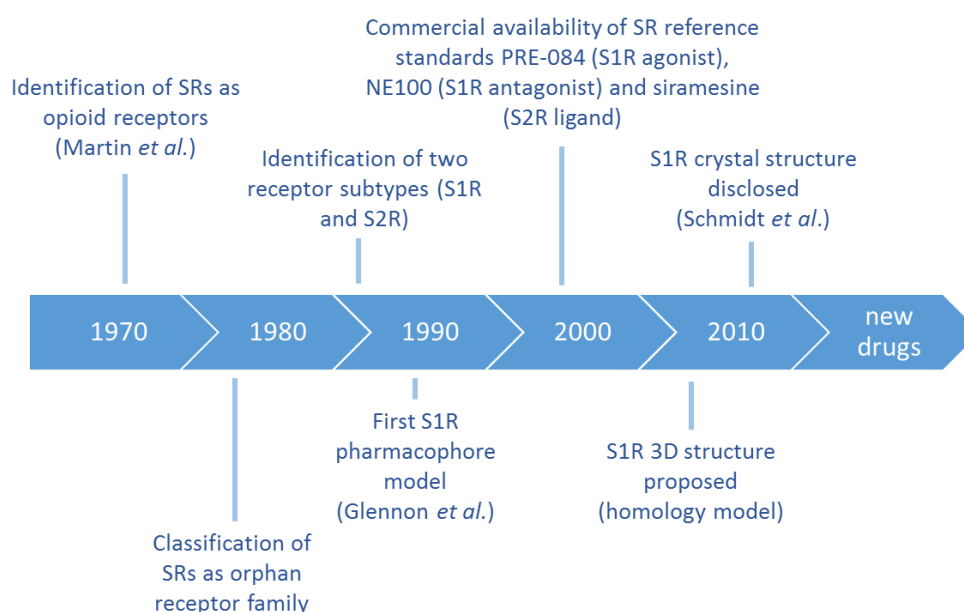


Figure 2. Sigma receptors timeline.

The gene encoding S1R has been cloned from several species, including humans, rats and mice^{9,11}. It expresses an integral membrane protein composed by 223 amino acids, which shows no sequence similarity to any other human protein and has a molecular weight of 25.3 kDa¹². Over the last ten years, several possible structures of S1R have been proposed^{13,14}, until the breakthrough in 2016, when the three-dimensional structure of S1R was finally disclosed (**Figure 3**)¹⁵.

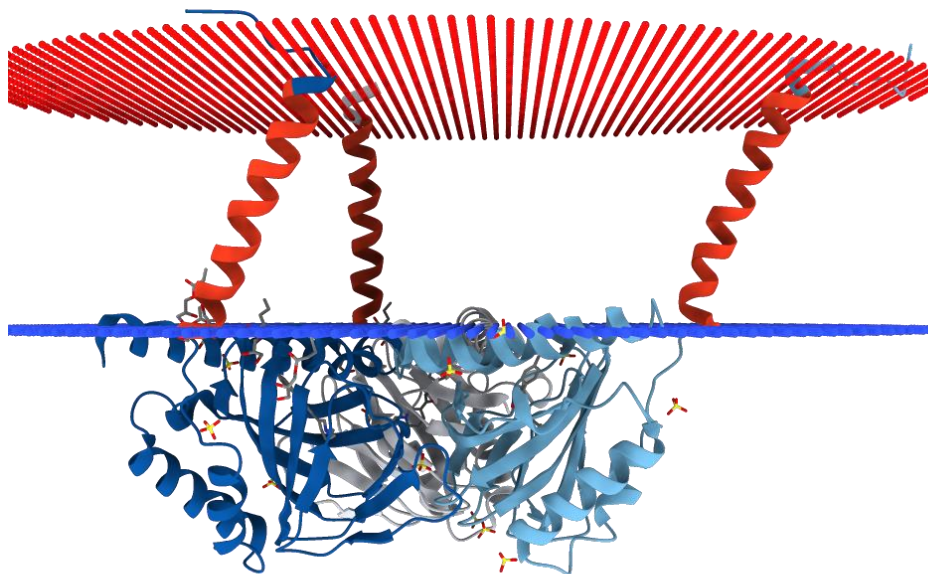


Figure 3. Structure of human sigma-1 receptor bound to antagonist PD144418, elucidated by Schmidt *et al.* (PDB: 5HK1)¹⁵. Transmembrane domains are shown in red, while the cytosolic domains of each monomer are depicted in blue, cyan and grey.

In their outstanding study, Schmidt and collaborators reported two very similar crystal structures, each complexed with a different ligand (*i.e.* PD144418 and 4-IBPP). Both co-crystals are constituted by a trimer, with a single transmembrane helix and a cytosolic domain for each monomer. The ligand binding pocket is placed in the β -barrel region of the cytosolic domain and is constituted mainly by hydrophobic residues. Binding of small molecules is mainly due to an ionic interaction between a positively charged center on the ligand and receptor's Glu172 residue, that is involved in a network of hydrogen bonds with Asp126 and Tyr103. In addition, ligands can form hydrophobic π - π interactions with Tyr103 and other hydrophobic amino acids in the binding site. Regarding the subcellular localization of S1R, we know that the receptor is localized at the endoplasmic reticulum/mitochondria interface, in a region called MAM (Mitochondria-associated ER membrane). Only in 2007, the role played by S1R was clarified. It is now commonly described as a molecular chaperone which, upon activation, can translocate and modulate the activity of different receptors, enzymes and ionic channels¹⁶. In detail, at the MAM level, it ensures the cell survival through different mechanisms:

i) Ca^{2+} homeostasis control, by chaperoning the inositol triphosphate (IP3) receptor; ii) it promotes an increase of antioxidant and antistress proteins, by ensuring the correct transmission of ER stress into the nucleus, through the modulation of Inositol Requiring Enzyme 1 (IRE1); iii) it promotes a decrease of reactive oxygen species (ROS) formation through Nrf2 signaling. Moreover, under stressful conditions or in case of pharmacological manipulations S1R can translocate from the MAM to other cellular compartments, affecting other membranous and soluble proteins. This broad network of interactions determines the involvement of S1R in numerous signal transduction pathways, indeed it can be defined a pluripotent modulator in living systems¹⁷. Macroscopically, S1R is ubiquitously expressed (liver, kidney, heart), but above all it is found in the Central Nervous System (CNS)¹⁸. In fact, it has been regarded as a potential therapeutic target for treating neurodegenerative pathologies (Alzheimer's disease, Parkinson's disease, amyotrophic lateral sclerosis) as well as cocaine addiction, myocardial hypertension and cancer^{8,19-24}. Concerning S1R ligands, it has to be noted that this receptor can bind a wide range of structurally diverse pharmacologically active molecules: benzomorphans, guanidines, phencyclidine-related compounds, morpholine, piperidine and piperazine derivatives are but a few of them²⁵. Interestingly, an endogenous ligand for the S1R receptor has yet to be conclusively identified, although tryptaminergic trace amines, as well as choline and neuroactive steroids such as dehydroepiandrosterone (DHEA) and pregnenolone all activate the receptor^{26,27}. Nevertheless, development of an effective and reliable binding assay protocol, based on displacement of [³H](+)-pentazocine²⁸, allowed the correct evaluation of affinity for a large number of chemically dissimilar small molecules, which in turn led Glennon and co-workers to describe the first S1R binding pharmacophore model in 1994²⁹. This consists in an ionizable amine site flanked by two hydrophobic domains and has been a milestone of crucial importance for the design of new S1R ligands up to the aforementioned publication of the receptor's crystal structure in 2016¹⁵.

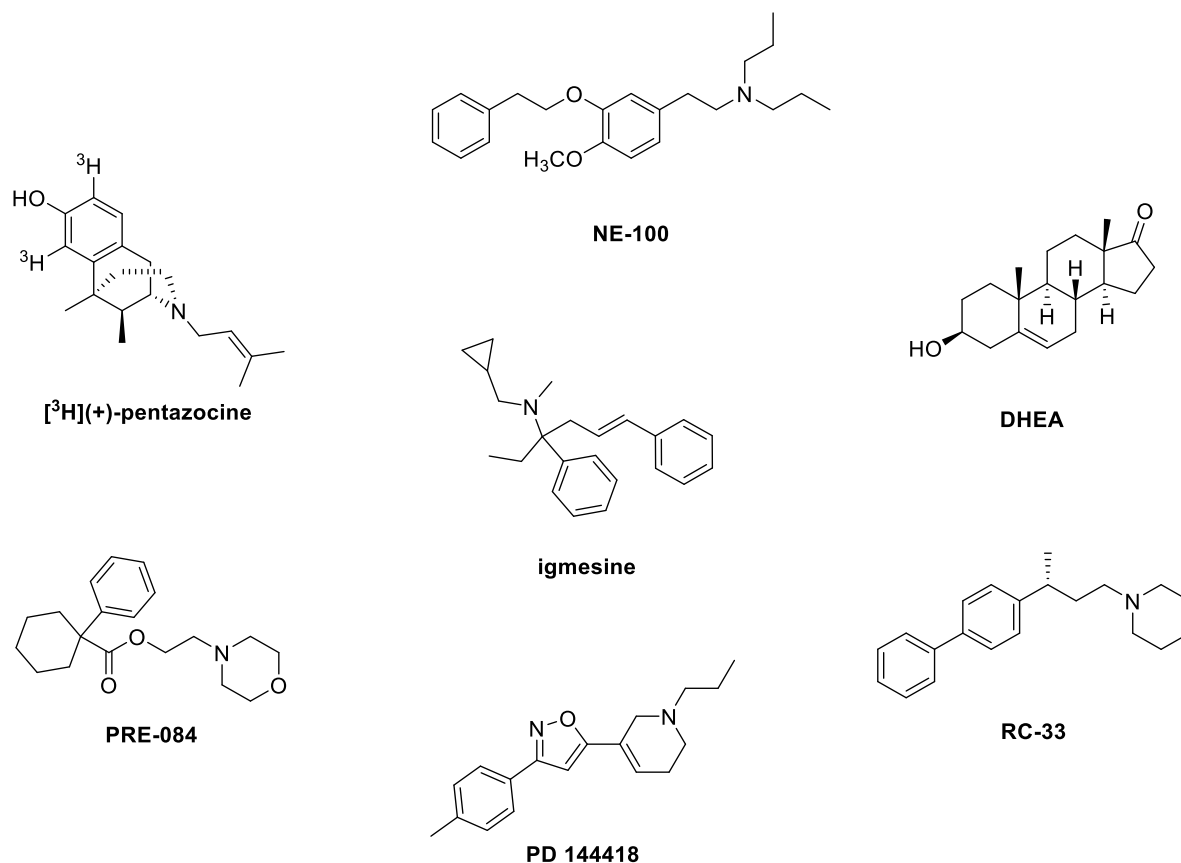


Figure 4. some representative S1R ligands

On the other hand, S2R is a more enigmatic target that eluded molecular identification since its discovery in 1990³⁰, which was based on a photoaffinity labelling study: using 1,3-di(2-tolyl)guanidine (DTG), researchers showed the existence of two protein bands of 25 and 21.5 kDa. The first band was associated to S1R, and this assumption was confirmed after cloning the gene encoding S1R. The second band was assigned to the S2R³⁰. In 2011, Xu *et al.* postulated the possible localization of the S2R binding site on the Progesterone Receptor Membrane Component 1 (PGRMC1)³¹, but later evidences proved this hypothesis to be wrong, since binding of S2R ligands was unaffected by whether PGRMC1 was overexpressed or knocked down^{32–34}. It was not until 2017 that S2R was cloned and finally identified as TMEM97, an endoplasmic reticulum-resident transmembrane protein that regulates the sterol transporter NPC1¹⁰. This paved the way to further development of the already considerable biological investigation on S2R. It is in fact now well-known that this receptor is correlated with different cancer conditions. In detail, evidence of its over-expression in proliferating breast carcinoma cells^{35,36} has led to the development of S2R ligands that are now in clinical trials for the diagnosis of breast cancer³⁷. It is also relevant that high levels of S2R have been detected in pancreatic cancer cell lines (Panc-02, Panc-01, CFPAC-1, AsPC-1)³⁸. Remarkably, the pro-apoptotic effects of S2R ligands suggest the involvement of the Caspase family, protease enzymes playing essential roles in programmed cell death. Moreover, in some other cases S2R ligands are able to promote toxic damages, which trigger autophagy or cell-cycle arrest phenomena³⁹. The high intracellular Ca²⁺ level could be another

implicated mechanism in the cell-death activation. Several organelles and ionic channels are involved in the Ca^{2+} homeostasis control. S2R ligands are able to modulate the activity of these cellular structures, increasing the amount of the ion calcium in the cytosol, thus causing cellular damages and death⁴⁰⁻⁴². It is noteworthy that S2R modulators are able to increase the reactive oxygen species (ROS) formation, a peculiar condition that occurs before apoptosis. Furthermore, S2Rs are widely distributed in the CNS and have been correlated to pivotal cellular processes in neurological disorders. Particularly, experimental evidence suggested that S2R is involved in Alzheimer's disease and some of its modulators are now in clinical trial for the treatment of this challenging pathology⁴³⁻⁴⁵.

As mentioned above, S2R was firstly identified for its ability to bind with high affinity to DTG and haloperidol, but not to benzomorphans³⁰. Since then, a large number of molecules able to interact selectively with this receptor subtype has been reported. These include 6,7-dimethoxytetrahydroisoquinoline analogs, tropane and granatane analogs, cyclohexylpiperazine analogs and indole analogs⁴⁶. In 2017, a manually curated database of the S2R selective ligands was built and is now freely available online^{47,48}.

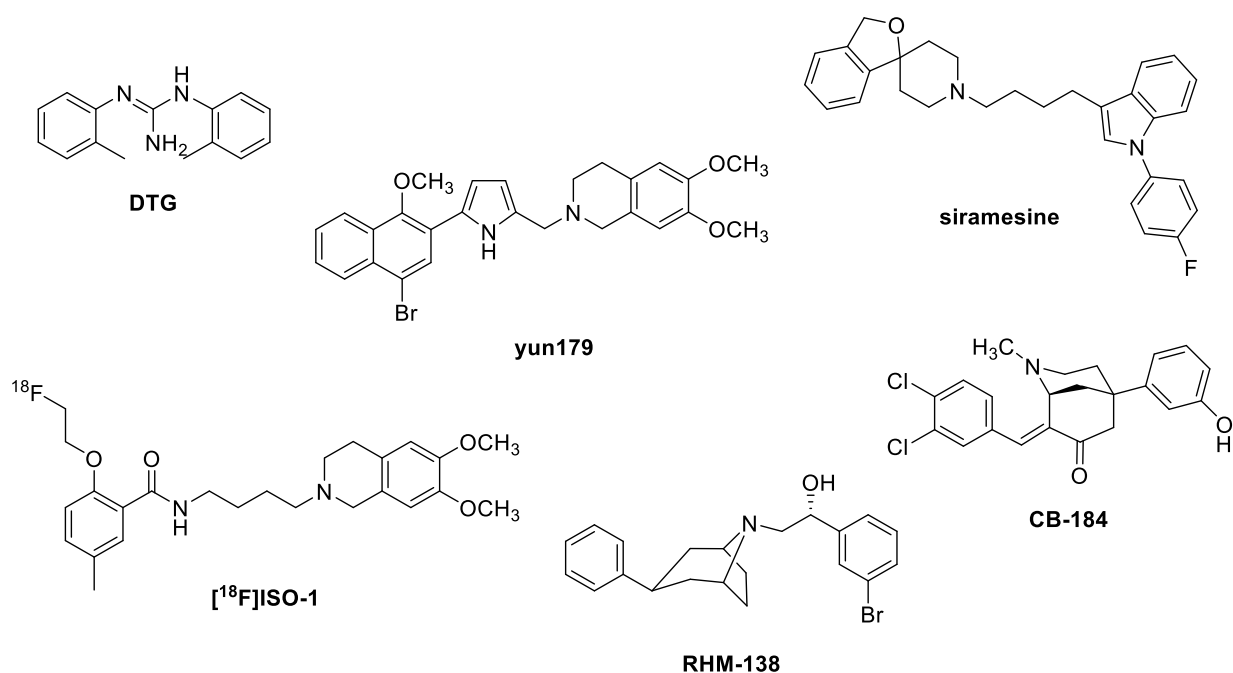


Figure 5. some representative S2R ligands

In conclusion, both Sigma receptor subtypes can be considered promising therapeutic targets in virtue of their involvement in many different pathologies, ranging from CNS-related diseases to cancer. In particular, the recent elucidation of S1R's three-dimensional structure allows a rational approach to the design of new molecules as potential pharmacological tools. A more detailed discussion of S1R's structural features and mode of action, as well as its therapeutic potential will be the focus of the next sections.

1.2 Structure and mechanism of S1R (with a special focus on oligomerization process)

As discussed in the previous section, S1R represents a potential therapeutic target of great interest because of its involvement in several pathological conditions. Nevertheless, despite significant pharmacological interest and investigation, it still remains an enigmatic protein which key features have started to be disclosed only in very recent times, after forty years of studies.

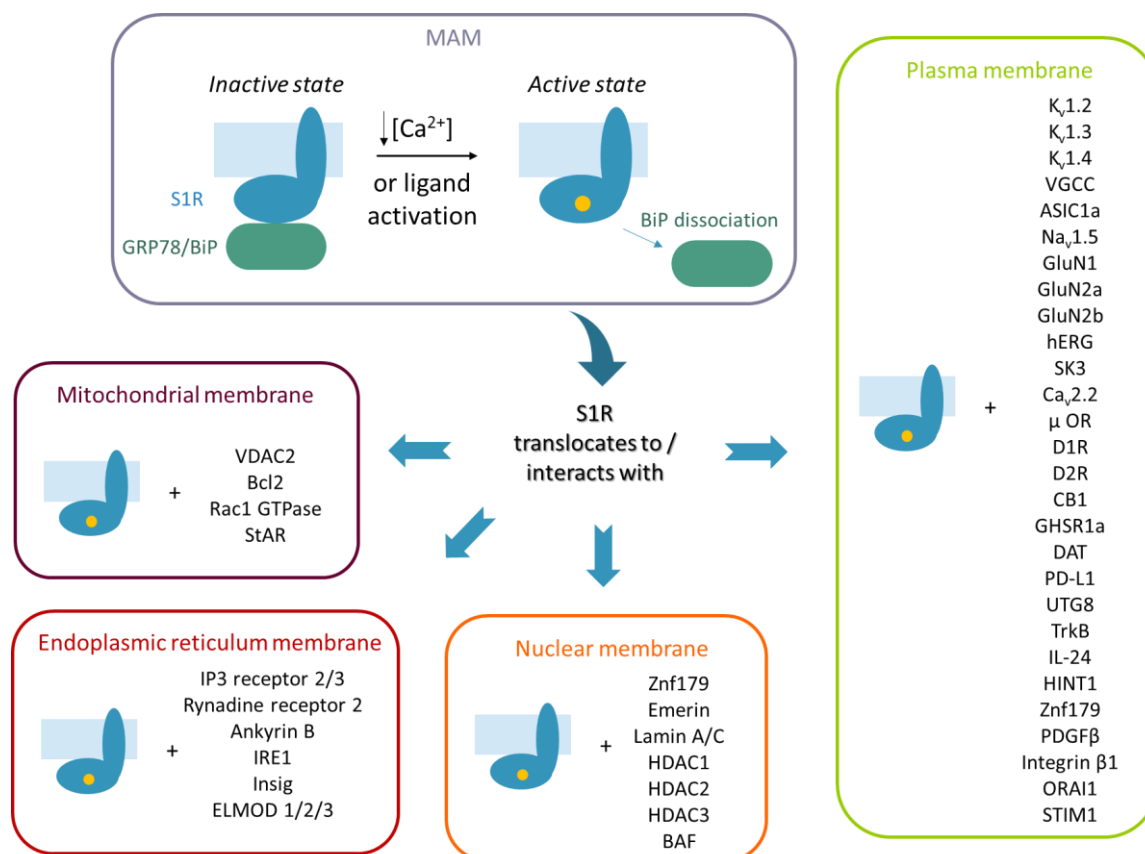


Figure 6. Schematization of the chaperone model for S1R function. Partner proteins are divided based on their subcellular localization (picture adapted from reference⁴⁹).

Nowadays, S1R is unanimously considered a ligand-operated chaperone, able to modulate different signaling pathways through interaction with other proteins¹⁶. Under resting conditions, the receptor is localized at the MAM, in complex with the binding immunoglobulin protein (BiP) – another chaperone, which plays a central role in protein folding and quality control²³. Stressful conditions or interaction with small molecules can modulate S1R's activity. Such small molecules have been divided into agonists and antagonists, on the basis of their ability to recapitulate the effects, respectively, of genetic overexpression and knockout of S1R in animal models⁵⁰. An alternative method to determine agonist/antagonist profile of S1R ligands consist in evaluation of test compounds' effect on neurite outgrowth: several experiments on PC12 cells, an *in vitro* model of neuronal differentiation, demonstrated that S1R agonists are able to potentiate neurite outgrowth

and elongation induced by the nerve growth factor (NGF) or epidermal growth factor (EGF), whereas antagonists block such effects⁵¹⁻⁵³. Activation of S1R by agonists or by a decrease in ER Ca²⁺ concentrations cause the receptor to dissociate from BiP and interact with client proteins in the ER or other organelles. Studies published up to now suggest that S1R is able to interact with more than 40 different proteins, many of which are very different in sequence and structure (**Figure 6**)⁴⁹.

However, one of the most intriguing interaction S1R can take part to, is with itself: there is accumulating evidence suggesting that S1R can exist in a variety of oligomeric forms, which functional consequences still remain poorly understood. The first hints about existence of S1R oligomers came from a couple of work published in 2007. In detail, while studying the binding site of S1R through iodolabelled probes, Pal *et al.* identified high molecular weight protein complexes not completely dissociated during the SDS-PAGE analyses⁵⁴. Considering that S1R contains two GXXXG integral membrane dimerization domains, the authors hypothesized that the receptor could exist as a homo- and/or hetero-oligomers. In the same year, Ramachandran and collaborators showed how the S1R radiolabelled ligand, [³H]-(+)-pentazocine, binds to the molecular target with a molar ratio of 1:2. This event found a possible explanation in the dimerization of the protein⁵⁵. Similarly, a study that involved photo-incorporation of a N-alkylamine derivative resulted in an enhanced electrophoretic mobility of only 50% of the derivatized receptor⁵⁶. Also in this case, a binding model involving a receptor dimer and/or oligomer was proposed. More recently, gel filtration chromatography has been employed to reveal diverse oligomeric forms that are stabilized by ligand binding⁵⁷. Furthermore, FRET spectrometric analyses revealed different S1R oligomerization states, as a consequence of the binding with different ligands⁵⁸. These studies led to the development of a mechanistic model regarding S1R constructs according to which agonists stabilize S1R monomers and dimers that act as chaperones, whereas antagonists bind to higher oligomer complexes, maintaining them in repository forms^{57,58}. This model is the most commonly accepted nowadays, and the recent crystallographic studies confirmed S1R's ability to form homo-oligomer complexes. Nevertheless, the precise mechanism of generation, as well as the biological function of such forms are still not completely understood^{49,59}. These points, along with molecular features of S1R ligands underpinning agonism/antagonism probably represent the major Sigma enigmas to date. It must be noted that Glennon's pharmacophoric model does not differentiate between agonists and antagonists. Even the publication of the first S1R crystal structure in 2016 could not give particular insights into this aspect. In fact, Schmidt and co-workers reported that no clear difference could be observed between interactions of the receptor and the two chemically divergent co-crystallized ligands (*i.e.* the antagonist PD 144418 and compound 4-IBP, with a more ambiguous profile)¹⁵. In a later publication, the authors argued that structural studies of other three well-characterized classical ligands could help to solve the puzzle: crystal structures of S1R bound to the antagonists haloperidol and NE-100, and to the agonist (+)-pentazocine were disclosed in 2018⁵⁹. Crystallographic analysis of ligands in the antagonist-bound S1R confirmed a highly conserved binding mode and receptor conformation even for chemically diverse antagonists. Interestingly, the agonist-bound

receptor crystallized very similarly to antagonist-bound S1R, with the only exception of helix α_4 , which shifts approximately 1.8 Å away from helix α_5 in the (+)-pentazocine-bound structure relative to the PD 144418-bound structure (see **Figure 7**). In addition, the authors performed docking studies which suggested that also other structurally unrelated agonists (such as PRE-084) might adopt a pose very similar to that observed for the crystallographic (+)-pentazocine. These steric constraints force helix α_4 to shift 1.1–1.8 Å away from helix α_5 to accommodate the agonist. Such a modest structural change does not disrupt the oligomerization interface between individual protomers, nor it seems to be easily exploitable for rational design of modulators with a well-defined biological profile. Nevertheless, Schmidt and collaborators pointed out that if α_4 were to move to a greater degree it could disrupt the oligomerization interface, which is consistent with prior data suggesting that S1R agonists bias the receptor toward lower-molecular-weight states, whereas antagonists bias it toward higher-molecular-weight states.

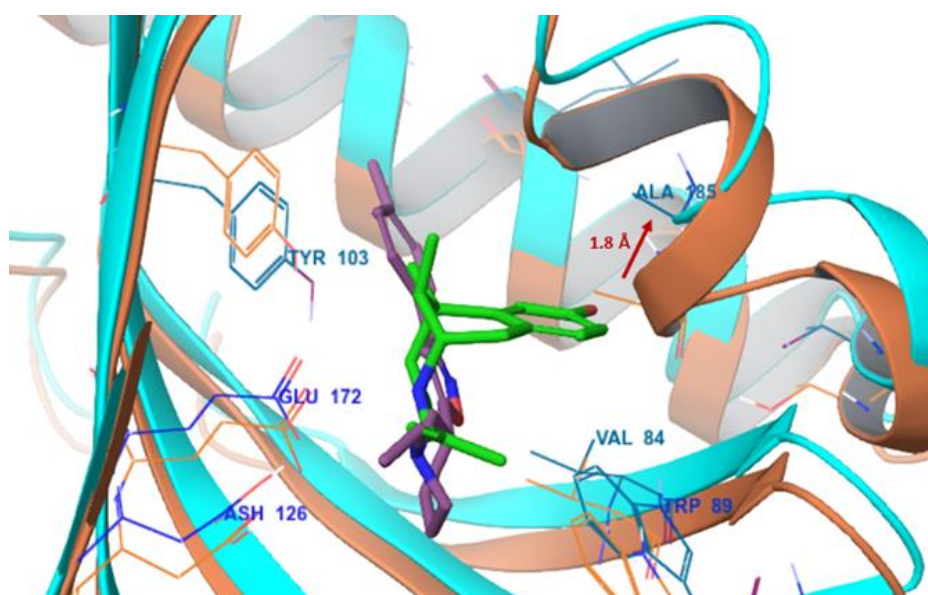


Figure 7. Alignment of the structures of human S1R bound to (+)-pentazocine (PDB 6DK1), shown in blue, and to PD 144418 (PDB 5HK1), shown in orange. The ligands (+)-pentazocine and PD 144418 are shown in green and purple, respectively. The red arrow indicates the shift of helix α_4 .

1.3 Sigma 1 Receptor as therapeutic target (with a special focus on neurodegeneration)

As mentioned above, S1R has been extensively studied from a pharmacological standpoint since its discovery in the 1970s. It has in fact been proposed as drug target for the treatment of various pathologies and conditions. These include neurodegenerative diseases, such as Alzheimer's disease (AD)^{23,50,60}, Parkinson's disease (PD)^{23,50}, Amyotrophic lateral sclerosis (ALS)^{23,50} and multiple sclerosis (MS) (see Paper 1, Appendix, page 119), as well as neuropathic pain^{61,62}, drug and alcohol abuse^{63,64} and cancer⁶⁵⁻⁶⁷. The considerable amount of patented S1R modulators reflects the significant potential of such molecules as pharmacological tools^{8,67}. Interestingly, three of them are currently under clinical trial (**Figure 8**): ANAVEX 2-73, patented by Anavex Life Sciences Corp, is undergoing Phase III clinical trials for the treatment of AD⁶⁰; AVP-786 (deuterated (d6)-dextromethorphan/quinidine), entered Phase III clinical trials to alleviate agitation in patients with AD^{68,69}; S1A or MR309/ E-52862, patented by Esteve, is undergoing Phase II clinical trials for treating neuropathic pain, post-operative pain and opioid analgesia enhancement^{70,71}. Furthermore, pridopidine – originally developed for Huntington disease and thought to be a dopamine D2 receptor antagonist⁷² – has now reached Phase II clinical trial for Parkinson's Disease Levodopa Induced Dyskinesia (PD-LID)⁷³, and has been recently proposed for the treatment of ALS in virtue of its S1R-agonist profile⁷⁴.

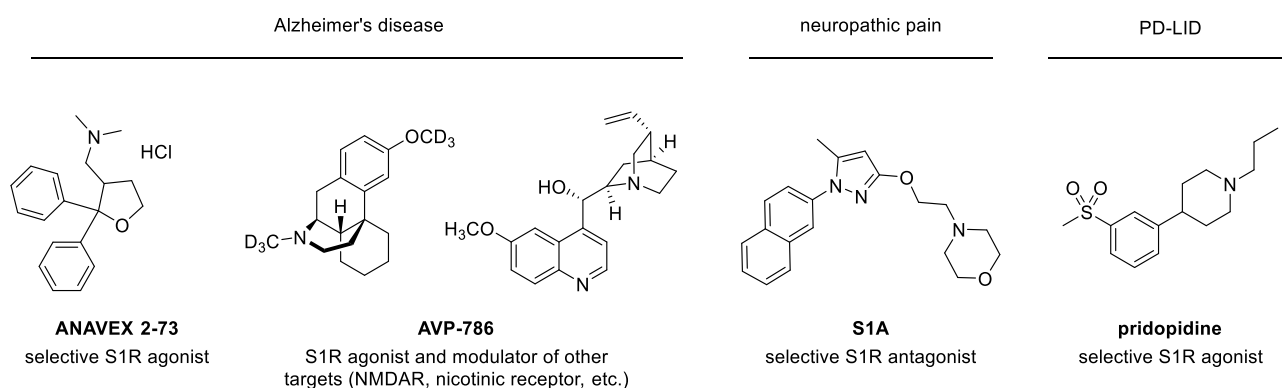


Figure 8. S1R modulators currently under clinical trial

S1R's ability to interact with a wide range of proteins affecting different signaling pathways and biological cascades, as well as its involvement in cell survival and excitability, makes it an attractive target for the treatment of complex multi-factorial pathologies that represent today's major therapeutic challenges. These include CNS-related diseases and cancer. In the following section a brief excursus on neurodegenerative diseases and S1R's correlation with them will be given.

Neurodegeneration is a key feature of many debilitating, incurable diseases that are rapidly rising in prevalence, partly because of elderly population increase in recent years⁷⁵. This heterogeneous group of

disorders, many of which are age-related, includes AD and other dementias, PD, ALS, MS, Huntington's disease (HD), spinocerebellar ataxia (SCA) and post-stroke degeneration⁷⁵⁻⁷⁷. These pathologies are diverse in their pathophysiology – with some causing memory and cognitive impairments and others affecting a person's ability to move, speak and breathe. Recent estimates showed that globally, in 2016, neurological disorders were the leading cause of DALYs (disability-adjusted life years; the sum of years of life lost and years lived with disability) and second leading cause of deaths (affecting about 9.0 million people), representing a tremendous burden to the patients, their families, and society⁷⁸. The current pharmacological scenario is meagre, and disease-modifying therapeutics have yet to emerge: the drugs currently approved only afford symptomatic relief, providing little or no mitigation of the progression of the pathology. Accordingly, there is an urgent need to develop new and more effective therapeutic strategies to combat these devastating diseases. Significant efforts have been made in this field to provide new insights into the complex pathophysiology of such conditions, developing effective models – from cell-based systems, to complex animals – and revealing candidate biomarkers or therapeutic targets⁷⁹. Accumulating evidence suggests that neurodegenerative diseases have a multifactorial origin, being associated with both specific genetic variations and environmental factors (e.g. smoking and stress) that lead to alteration of several molecular cascades^{79,80}. However, progressive loss of structure and/or function of neurons, within the CNS, is the pivotal event leading to neurodegeneration. Hence, besides the distinct genetic etiologies and pathological phenotypes, neurodegenerative disorders appear to share common mechanisms of neuronal cellular dysfunction, which include calcium dysregulation, excitotoxicity, oxidative and ER stress, mitochondrial dysfunction and neuroinflammation. S1R, which is expressed in both neurons and glia cells within the central nervous system, can modulate the aforementioned biological mechanisms associated with neurodegeneration^{23,50,81}.

- Alteration of the intracellular Ca^{2+} levels is often associated with both chronic neurodegenerative diseases and acute CNS damages. S1R is one of the main actors in the sophisticated homeostasis control that avoids pro-apoptotic phenomena⁸². As mentioned in *Section 1.2*, S1R forms a quiescent complex with BiP and this structure is Ca^{2+} -dependent. Ca^{2+} depletion or S1R agonism promote the complex dissociation and thus, the activation of S1R chaperonic activity^{16,23}. Among the S1R client proteins that take part in restoring calcium influx, the most notable are the inositol 1,4,5-triphosphate receptor type 3 (IP3R)⁸³ and protein kinase C (PKC)^{84,85}. On the other hand, high levels of Ca^{2+} are dangerous as well. This state is often a consequence of excitotoxicity, *i.e.* a pathological condition in which high levels of glutamate over-activate *N*-Methyl-D-Aspartate (NMDA) receptors, which in turn cause an excessive calcium influx. This leads to stochastic failure of calcium homeostasis and necrotic cell death^{86,87}. Excitotoxicity occurs in various neurodegenerative pathologies, and it has been correlated with S1R: upon activation it is able to modulate glutamate receptors, albeit the underlying mechanisms are not completely fathomed yet and seem to be numerous⁸⁸⁻⁹¹.

- Reactive oxygen species (ROS) are natural by-products of oxygen metabolism, promoting hormetic responses. In detail, low concentrations of ROS possess beneficial effects in maintaining cellular homeostasis, whereas a disequilibrium between their production and detoxification systems may lead to oxidative damage⁹². Numerous altered conditions contribute in generating ROS, such as mitochondrial dysfunction and sustained neurotransmission (e.g., of glutamate, dopamine, or serotonin), and they may cause severe side effects, damaging lipids, nucleic acids and proteins^{93,94}. The brain is particularly vulnerable to oxidative stress, since it has high oxygen demand, relatively low levels of the antioxidant glutathione and is enriched in polyunsaturated fatty acids that are substrates for lipid peroxidation⁹⁵. Accordingly, oxidative stress has been extensively associated with several CNS-related diseases: strong association between the detection of increased ROS production and the increased oxidative damage observed in CNS disorders has been documented^{76,96}. Activation of S1R may also mitigate ROS accumulation, possibly through modulation of ROS-neutralizing proteins. S1R knockout, knockdown or addition of antagonist haloperidol can increase oxidative damage, whereas addition of (+)-pentazocine counteracts it^{97,98}. Along with ROS, reactive nitrogen species (RNS) can also be generated under pathological conditions in the CNS. Sigma-1 agonists may also ameliorate nitrosative stress. The sigma receptor agonist PPBP (4-phenyl-1-(4-phenylbutyl) piperidine) attenuated nitric oxide (NO) production as well as nitrosative damage to proteins and nucleic acids⁹⁹. The decrease in NO generation may be linked to the ability of sigma-1 receptor activation to decrease nitric oxide synthase (NOS) activity^{100,101}.
- The ER plays an important role in protein synthesis and folding as well as cellular homeostasis. Under stressful conditions (e.g. calcium dysregulation and oxidative stress), unfolded or misfolded proteins can accumulate within the ER lumen and promote the protective unfolded protein response (UPR)^{102,103}. However, in case of prolonged or severe protein accumulation, the ER can eventually trigger cell death, rather than cell maintenance programs. Multiple studies show that S1R agonists interfere with abnormal protein accumulation, modulating the UPR^{24,104,105}. In particular, S1R's localization within the ER and at mitochondrial membranes suggests a role in interorganellar communication and regulation, as well as separate influences in both structures¹⁶. During ER stress or via ligand stimulation, S1R can modulate the activity of other proteins involved in UPR, *i.e.* protein kinase RNA like ER kinase (PERK), inositol requiring enzyme 1 alpha (IRE1 α), and activating transcription factor 6 (ATF6)^{16,104}.
- Mitochondria play multiple critical roles in neuron maintenance. In addition to supplying ATP and providing metabolic and biosynthetic substrates, mitochondria also regulate calcium homeostasis and the initiation of apoptosis. Aberrant mitochondrial function, as well as alterations in mitochondrial structure and dynamics, are associated with multiple neurodegenerative diseases^{76,106}. The close apposition of mitochondria to a particular subset of the ER, the MAM, is

important for multiple aspects of normal mitochondrial and cellular function. Proper interaction between mitochondria and the MAM maintains lipid synthesis and trafficking, calcium homeostasis, and regulation of mitochondrial-dependent apoptosis. As mentioned above, the fact that S1R is localized at the MAM suggests it plays a key role in these biological pathways. Accumulating evidence suggests S1R is an effective protector against mitochondrial damage^{23,50,81}. For example, it has been shown that the S1R agonists BHDP (N-benzyl-N-(2-hydroxy-3,4-dimethoxybenzyl)- piperazine) and SA4503 preserve mitochondrial respiration and ATP synthesis in different *in vitro* models, whereas co-administration of antagonist NE-100 blocks these effects^{107,108}. Additional studies suggested that S1R can also influence the expression of both pro-and anti-apoptotic signals targeting mitochondria. In detail, S1R agonists seems to promote cell survival by increasing the expression of the anti-apoptotic protein Bcl-2 as well as by decreasing the activity of the pro-apoptotic protein Bax^{109,110}.

- One of the most ubiquitous responses to CNS insults including neurodegenerative disorders is reactive gliosis¹¹¹. This is classified as the “activation” of astrocytes within the CNS, which causes astrocytes to proliferate, migrate, and produce several factors to further improve brain damage¹¹². Several recent studies have shown the ability of sigma ligands to ameliorate reactive astroglia¹¹³⁻¹¹⁶. Microglia, on the other hand, are a separate and distinct type of glial cell compared to astrocytes. These are macrophage-derived cells located in the CNS, where they play a key role as mediators of neuroinflammation. They are grouped into two subcategories: M1 microglia, with pro-inflammatory properties involved in CNS damage, and M2 microglia, which are anti-inflammatory and stimulate neuronal regrowth and repair¹¹⁷. Accumulating evidence suggests that S1R can also regulate microglial activity by strengthening the reparative microglia phenotype (M2), while it attenuates the inflammatory response (M1) and hence promotes neuroprotection^{107,109-112}. Recent publications showed that these beneficial effects can be triggered, both *in vitro* and *in vivo*, by S1R agonists such as PRE-084^{110,118-121}.

Altogether, these data corroborate the great potential of S1R as a therapeutic target to counteract CNS-related disorders. In particular, its ability to modulate a wide range of orthogonal biological mechanisms involved in neurodegeneration is generally considered a significant advantage in the fight against such complex multifactorial diseases. Moreover, the possibility to trigger, enhance or suppress many of the aforementioned molecular cascades through small molecules modulators makes viable to adopt a medicinal chemistry approach.

1.4 Multi target drugs as a modern approach for neurodegenerative diseases

As it has been reported in the previous section, neurodegenerative diseases are complex disorders with several pathoetiological pathways leading to cell death. The multifactorial origin of such disorders makes the traditional therapeutic approach, which relies on “one target one drug” paradigm, ineffective. The so-called “magic bullet” – a ligand interacting with a singular drug target at very high potency – has been extensively and successfully used for many diverse pathologies, but fails when applied to diseases involving multiple compensatory mechanisms, namely cancer and CNS-related disorders^{122–125}. Cellular networks involved in such pathologies are robust and prevent major changes in their outputs when a single target is modulated. Hence, current treatment options for neurodegenerative diseases are limited, relying essentially on symptomatic relief rather than disease-modifying therapies^{122,123}. Recently, an alternative strategy has been proposed to alter progression of neurodegenerative diseases: the use of multi-target drugs (MTDs) or multitarget-directed ligands (MTDLs). According to the definition of Melchiorre and colleagues in their pioneer publication these are “... compounds that are effective in treating complex diseases because of their ability to interact with the multiple targets thought to be responsible for the disease pathogenesis...”¹²⁶. It must be noted that many drugs already on the market act *via* interaction with multiple targets, but in those cases the discovery of the mechanism of action was made afterwards and/or serendipitously. On the other hand, with the MTDL approach, a single molecule is designed *a priori* to act by modulating different disease pathways, since it is expected that balanced modulation of diverse selected targets can provide an improved therapeutic effect. One of the main limitations during early years of MTDs rational design was that much of the complexity between linked signaling pathways was still poorly understood. However, continuous efforts in defining those mechanisms are constantly adding new pieces to the jigsaw puzzle of neurodegeneration, eventually paving the way to enhanced treatment options. Accordingly, during recent years, a number of heterogeneous MTDs have been developed that showed promising results *in vitro* and *in vivo*, although issues like side effects and low bioavailability started to emerge during clinical trials. This suggest that, besides the correctness of the basic principle, MTDs represent a big challenge in terms of both discovery and development, prompting the scientific community to pursue further investigations^{127–129}. Nowadays, to build new MTDLs the medicinal chemist decides from the beginning which and how many pharmacophoric groups have to be assembled into a new scaffold, based on the type and number of biological targets to be modulated. This strategy gives significant advantages respect to drug cocktails and multi-component formulations in terms of pharmacodynamic and pharmacokinetic profiles^{130,131}. In order to combine two molecules (or parts of them) in a new, single chemical entity, different approaches can be exploited, as depicted in **Figure 9**. Hybrid compounds can be obtained by linking (either with a cleavable or not cleavable linker) two molecules, or by framework integration, which can be done either by fusing (i.e. connecting

directly) or by merging (i.e. partially superimposing) two scaffolds. In particular, the merging technique enhances the overlap between the two original compounds and diminishes the new molecule's dimensions, which in turn improves ADME profile and drug-like-properties.

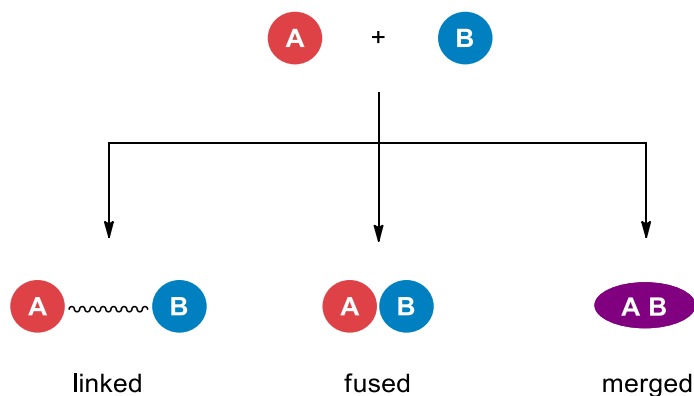


Figure 9. Schematization of various approaches to the design of multi-target directed ligands, starting from two different molecules A and B, endowed with affinity for two different targets.

To date, multi-kinase inhibitors constitute the most successful class of rationally designed MTDLs: for example, lapatinib and neratinib are two notable members of this group that eventually reached the market^{132,133}. These are dual kinase inhibitors active on both epidermal growth factor receptor (EGFR) and human epidermal growth factor receptor 2 (HER2). Lapatinib was discovered by Gilmer and colleagues in the pursuit of a novel compound able to modulate both EGFR and HER2 via the kinase domain, thus obtaining a synergistic effect¹³². It is currently used in the therapy against breast cancer and other solid tumors under the trade names Tykerb and Tyverb¹³⁴. More recently, neratinib was approved by FDA for the treatment of breast cancer¹³⁵. This molecule was designed through computational studies aimed at enhancing affinity profile toward both EGFR and HER2¹³³. Another case worth mentioning in the search for multitarget anti-cancer drugs is CUDC-101, a potent EGFR, HER2, and Histone deacetylase (HDAC) inhibitor¹³⁶. The compound was designed at Curis by linking the quinazoline scaffold of known EGFR/HER2 inhibitors, such as lapatinib, and the hydroxamic acid moiety responsible for the HDAC inhibitory activity. After excellent results in preclinical tests, CUDC-101 entered phase I clinical trials for the treatment of head and neck cancer. Unfortunately, it was later abandoned due to bioavailability issues¹³⁷.

Concerning CNS-related diseases, one of the most studied and promising MTDLs for the treatment of neurodegenerative disorders is ladostigil (**Figure 10**). It acts as a reversible acetylcholinesterase (AChE) and butyrylcholinesterase inhibitor (BuChE), and an irreversible monoamine oxidase B (MAO B) inhibitor. Its scaffold merges the pharmacophoric elements of older drugs like rivastigmine and rasagiline^{138,139}. In addition to its neuroprotective properties, ladostigil enhances the expression of neurotrophic factors like GDNF and BDNF, and may be capable of inducing neurogenesis¹⁴⁰. Ladostigil reached phase II clinical trial for the therapy against cognitive impairments. The results were published very recently and showed that despite a safe

profile and good tolerability, the compound was not able to significantly delay progression to dementia, although it has been associated with reduced brain and hippocampus volume loss¹⁴¹. Other examples of linked, fused or merged MTDLs can be found in recent literature and are reported in **Figure 10**. In 2019 Rajeshwari *et al.* reported the synthesis and evaluation of a series of tacrine and phenylbenzothiazole hybrids potentially useful for the treatment of Alzheimer's disease¹⁴². These compounds are inhibitors of AChE and inhibitors of amyloid- β (A β) self-aggregation endowed with neuroprotective effects. The two scaffolds were joined by a linker. In another recent publication, Lutsenko and collaborators described the preparation of monoamine oxidase B (MAO B) inhibitors and histamine H₃ receptor (H₃R) antagonists as viable tools to counteract neurodegeneration¹⁴³. In this case, the pharmacophoric elements of rasagline and UCL2190 (MAO B and H₃R modulators, respectively) were merged in a single small molecule. Another example of merged dual ligand is PQM130, which is obtained by the combination of the N-benzylpiperidine group present in donepezil (AChE inhibitor) and the feruloyl group present in ferulic acid (a product of degradation of curcumin endowed with neuroprotective, antioxidant and anti-inflammatory properties). This compound resulted effective in ameliorating the cognitive impairments and pathology in a mouse model of Alzheimer's disease¹⁴⁴.

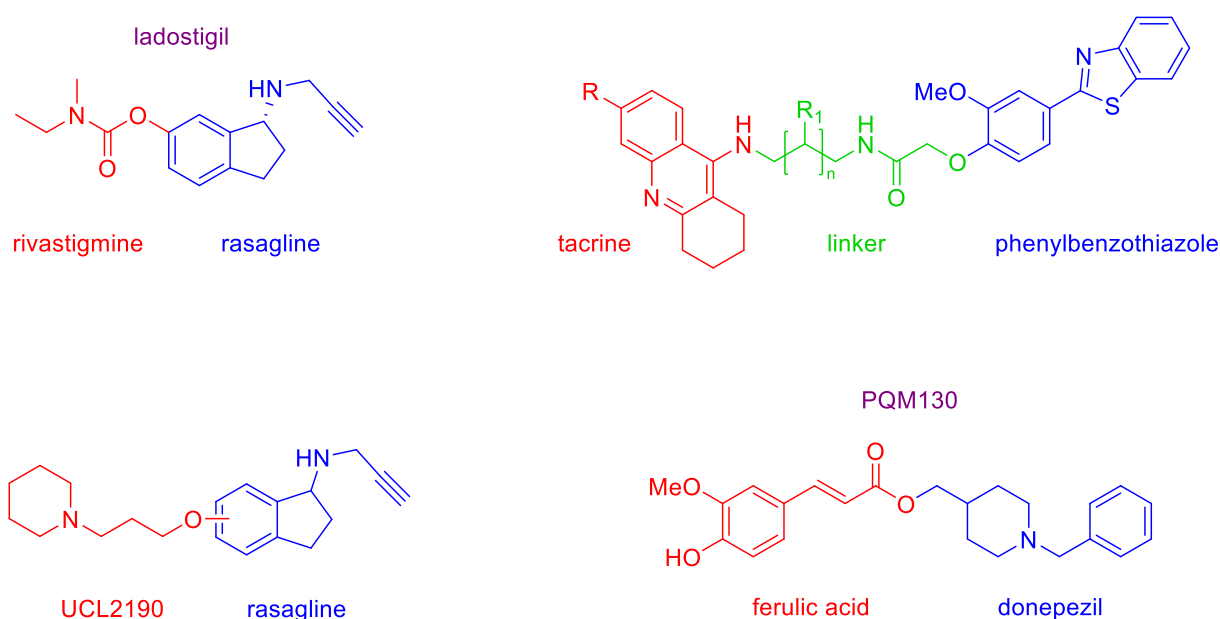


Figure 10. Some examples of MTDLs currently under investigation. Different colors indicate structural elements of older ligands (which names are indicated in the same color) that served as inspiration to build new hybrid compounds (which names are reported in purple, when present).

In conclusion, analysis of recent literature shows that despite promising results in early stages of drug development and the widely recognized therapeutic potential of multi-target drugs, their rational discovery

still represent a great challenge. Nevertheless, some notable rationally designed MTDs have already been approved for therapy (e.g. multi-kinase inhibitors), further supporting the viability of this approach.

2. Targeting the sigma1 receptor system to counteract neurodegeneration.

2.1 The S1R modulators: state of the art

As mentioned above, S1R is able to bind a variety of structurally unrelated compounds. However, to date no endogenous ligand has been definitively identified, although many hypotheses have been advanced. Neurosteroids (such as dehydroepiandrosterone (DHEA), pregnenolone, and progesterone)¹⁴⁵ as well as the hallucinogen *N,N*-dimethyltryptamine (DMT)²⁶, D-erythro-sphingosine¹⁴⁶ and choline²⁷ have all been suggested as putative endogenous S1R ligands (**Figure 11**), but in most cases their low affinity makes these assumptions uncertain.

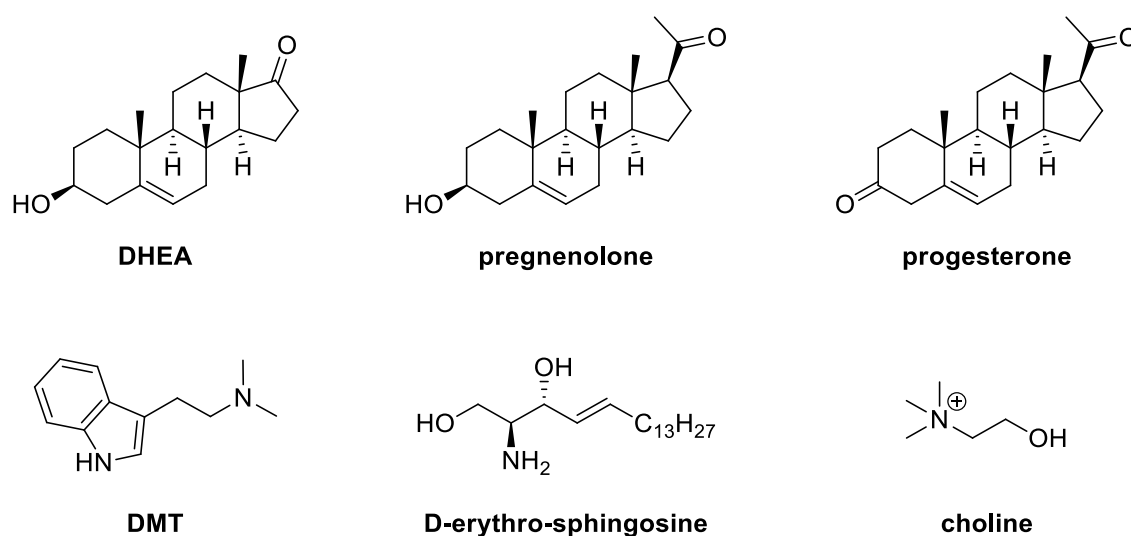


Figure 11. Some putative S1R endogenous ligands

Since the discovery of S1R, there has been an extensive pharmacological investigation, which helped to identify a large number of diverse ligands. Many of these were designed on the basis of the well-known pharmacophoric model published by Glennon and collaborators in 1994, consisting of a basic nitrogen flanked by two hydrophobic moieties²⁹. Besides this rather loose common feature, some recurring structural motives can be identified among the most notable S1R modulators (**Figure 12**). Morpholine is one of these. The first selective S1R agonist identified is in fact the morpholine derivative PRE-084, originally employed to investigate S1R's role in different CNS-related disorders, and still commonly used as a reference standard in *in vitro* and *in vivo* assays of novel ligands^{114,147}. Another important morpholine-based compound with enhanced S1R affinity is Afobazole, endowed with anxiolytic and neuroprotective properties¹⁴⁸. Its ability to interact also with S2R proved beneficial to modulate microglial function¹¹⁸. The already cited S1A (also known as E-52862) contains a morpholine ring too⁷⁰. Esteve is currently investigating this selective S1R antagonist for the treatment of neuropathic pain⁷¹. Another important class of Sigma ligands is constituted by guanidines. In particular, 1,3-di-*o*-tolylguanidine (DTG) deserves to be mentioned for its employment in SRs

binding assays. This compound is in fact a pan-sigma modulator, *i.e.* it can bind both Sigma 1 and Sigma 2 receptors. Its tritiated form is commonly used for determining binding affinity at S2R, in the presence of non-tritiated pentazocine to mask the S1R binding site¹⁴⁹. Piperazine derivatives also account for a large number of S1R ligands. These include SA4503, under investigation for treatment of ischemic stroke^{81,150}, BD1031, which is being studied for the development of a new method to define the S1R agonist/antagonist profile¹⁵¹, and Rimcazole, originally developed as a potential antipsychotic and historically reported as S1R antagonist despite its rather low binding affinity^{152,153}. Finally, many other remarkable S1R modulators share a piperidine scaffold. Among these, 4-IBP deserves to be mentioned: this non-selective SR ligand has been co-crystallized with S1R in the pivotal work by Schmidt *et al*¹⁵. It has been developed as radiopharmaceutical to bind to SRs on the MCF-7 human breast carcinoma cell line, although its functional profile is not unanimously identified, with assays suggestive of either agonist or inverse agonist activity¹⁵⁴. 4-PPBP is another compound belonging to this group (it was discovered by Yang *et al.*, who reported its cytoprotective effect)¹⁵⁵. Moreover, the well-known antipsychotic drug Haloperidol is a S1R antagonist which also contains a piperidine ring¹⁵⁶. Interestingly, this structural motif is sometimes found as part of spirocyclic molecules (see **Figure 11**): this is the case, for example, of L-687,384, a potent S1R agonist and NMDA receptor antagonist developed by Merck Sharp & Dohme¹⁵⁷, which inspired a series of analogues, such as Fluspidine, developed by Wünsch and co-workers^{158,159}. Other nitrogen-containing polycyclic compounds able to bind S1R are benzomorphanes (such as (+)-pentazocine and (+)-SKF-10,047)^{1,28}, cocaine¹⁶⁰ and amantadine¹⁶¹. It is worth noting that from the list of modulators reported in this Section emerges that even compounds sharing a common structural motif can display divergent biological profiles: this is the case of PRE-084 and S1A, SA4503 and Rimcazole, or 4-PPBP and Haloperidol. In fact, as discussed in *Section 1.2*, an elusive aspect of S1R's modulators is which structural elements determine agonist/antagonist behavior^{59,162}. Up to date, classification of small molecules as agonists or antagonists relies therefore on evaluation of their physiological effects in *in vitro* and/or *in vivo* models, such as neurite outgrowth assay^{51,52,81}.

In the pursuit of novel SRs modulators endowed with therapeutic potential, our research group developed, over the last ten years, a large number of molecules bearing the pharmacophoric elements required for interaction with S1R. From these studies emerged compound (*R*)-1-[3-(1,1'-biphen)-4-yl]butylpiperidine (named (*R*)-RC-33, **Figure 12**) as a selective S1R agonist exhibiting excellent affinity ($K_i = 1.8$ nM), high selectivity over other receptors, neuroprotective effects and good *in vitro* metabolic stability^{22,53,163}. The ability of (*R*)-RC-33 to promote the differentiation and the neurite elongation was verified using the rat dorsal root ganglia (DRG) experimental model¹⁶⁴. Moreover, after systemic administration in mice, (*R*)-RC-33 showed an excellent pharmacokinetic profile and CNS distribution⁵³. This hit compound served as the basis for the development of new mono- and bi-valent modulators of S1R that constituted the main focus of my PhD research project.

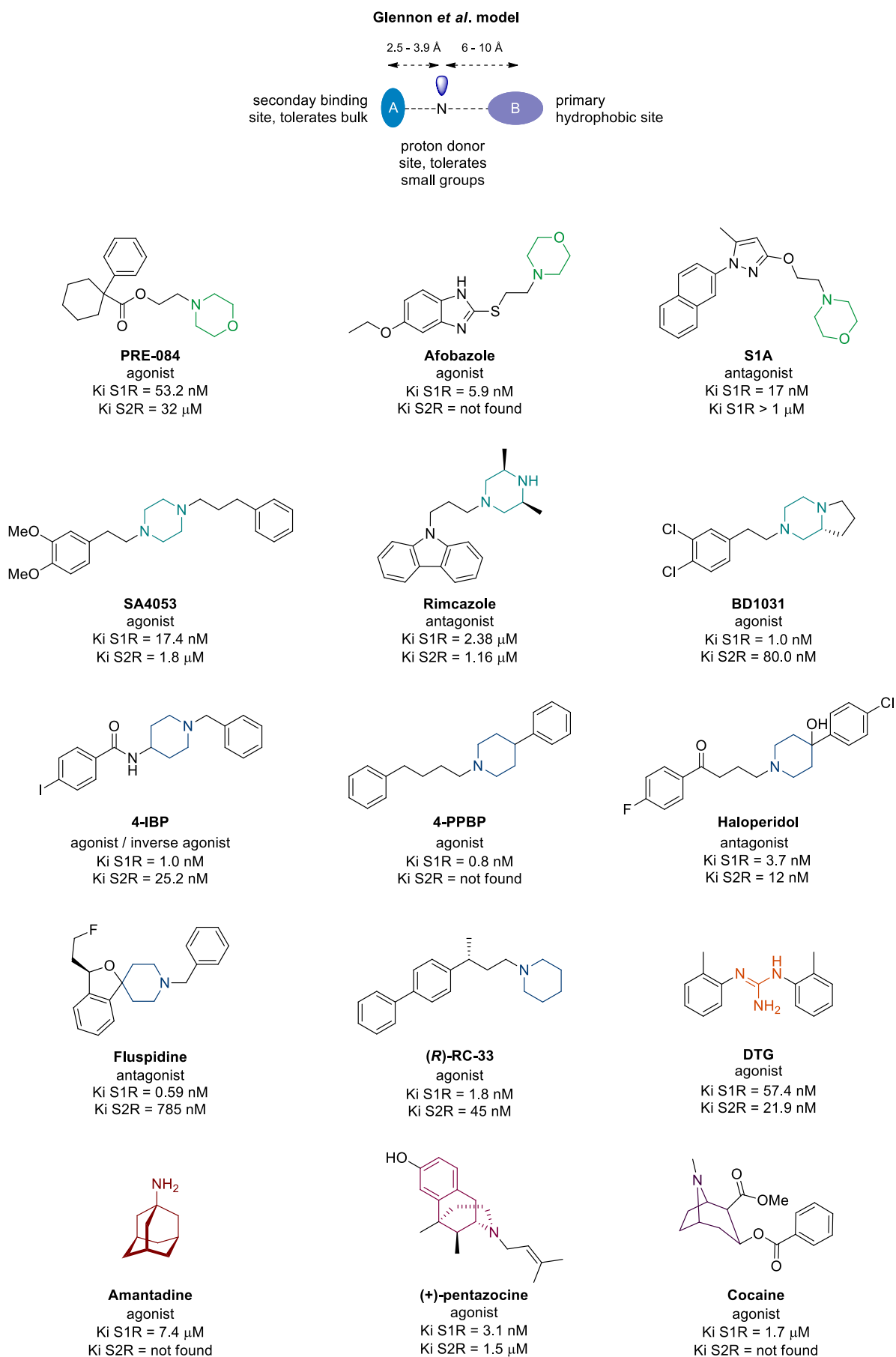


Figure 12. Glennon's pharmacophoric model and some noteworthy S1R modulators. Recurring structural motives are highlighted with different colors.

2.2 Design and pharmacokinetic predictions of novel ligands

As discussed in *Section 1.3*, the involvement of S1R in numerous molecular cascades related to neurodegeneration makes it an attractive target for the development of innovative therapies for CNS-related diseases. Considering the advantages of multitarget-directed ligands presented in *Section 1.4*, we reasoned that coupling S1R agonism with modulation of other molecular targets implicated in neurodegenerative processes, we might obtain new pharmacological tools endowed with higher chances to counteract such pathologies. Among these additional therapeutic targets, we selected acetylcholinesterase (AChE) and *N*-methyl-D-aspartate (NMDA) receptor.

In detail, AChE regulates acetylcholine levels in central nervous system, and since many years is considered one of the major biomarkers for degeneration of the cholinergic neural network. AChE inhibitors are able to restore the physiological amount of acetylcholine and are commonly used in therapy for counteracting the cognitive impairment, a common feature of neurodegenerative diseases^{165,166}. On the other hand, the *N*-methyl-D-aspartate receptor (NMDAR) plays a relevant role in synaptic plasticity and synapse formation underlying memory and learning. This ionotropic glutamate receptor, constituted by two subunits GluN1 and GluN2, is one of the major conduits for calcium entry into neuronal cells¹⁶⁷. An alteration of this neurotransmitter pathway causes accumulation of glutamate in the synaptic terminations that promotes the GluN2 activation and thus, an excessive accumulation of Ca²⁺ inside the cell. This condition, known as excitotoxicity, triggers diverse mechanisms of cell death and is one of the major hallmarks of neurodegeneration^{167,168}. Accumulating evidence suggests that a negative modulation of this molecular target may contribute in slowing the progression of neuropathies¹⁶⁹. In addition to dysregulation of these neurotransmitter pathways (*i.e.* acetylcholine and glutamate systems), an important condition occurring in neurodegenerative disorders is over-production of Reactive Oxygen Species (ROS) due to alterations of mitochondrial respiratory chain activity^{93,170}. While a low ROS level plays a crucial role in cellular pathways, abnormal increase in ROS concentration can overcome the cellular antioxidant machinery and induce macromolecular damages (*i.e.* interaction with the DNA, proteins and lipids), promoting aberrant molecular cascades⁹⁴. Given these premises, we aimed at obtaining molecules able to modulate S1R, to act as AChE and NMDA receptor inhibitors and endowed with antioxidant properties. To reach this goal we designed a library of potential MTDLs bearing the pharmacophoric elements of (*R*)-RC-33, the potent and selective S1R agonist developed by our group (see *Section 2.1*), Donepezil (the well-known AChE inhibitor currently used to counteract cognitive impairment in patients with Alzheimer's disease)¹⁷¹, Ifenprodil (a potent NMDAR inhibitor)^{172,173} and Curcumin, the natural antioxidant produced by *Curcuma longa* plants¹⁷⁴. The new compound series is characterized by a common arylalkylamineketone scaffold reported in **Figure 13**, with three elements of structural diversity: the aromatic ring, the aminic moiety and the length of the linker

between the aromatic and the aminic portions. Exploration of diverse stereo-electronic features, as well as evaluation of commercially available building blocks and synthetic feasibility, prompted us to develop the compound library reported in **Table 1**.

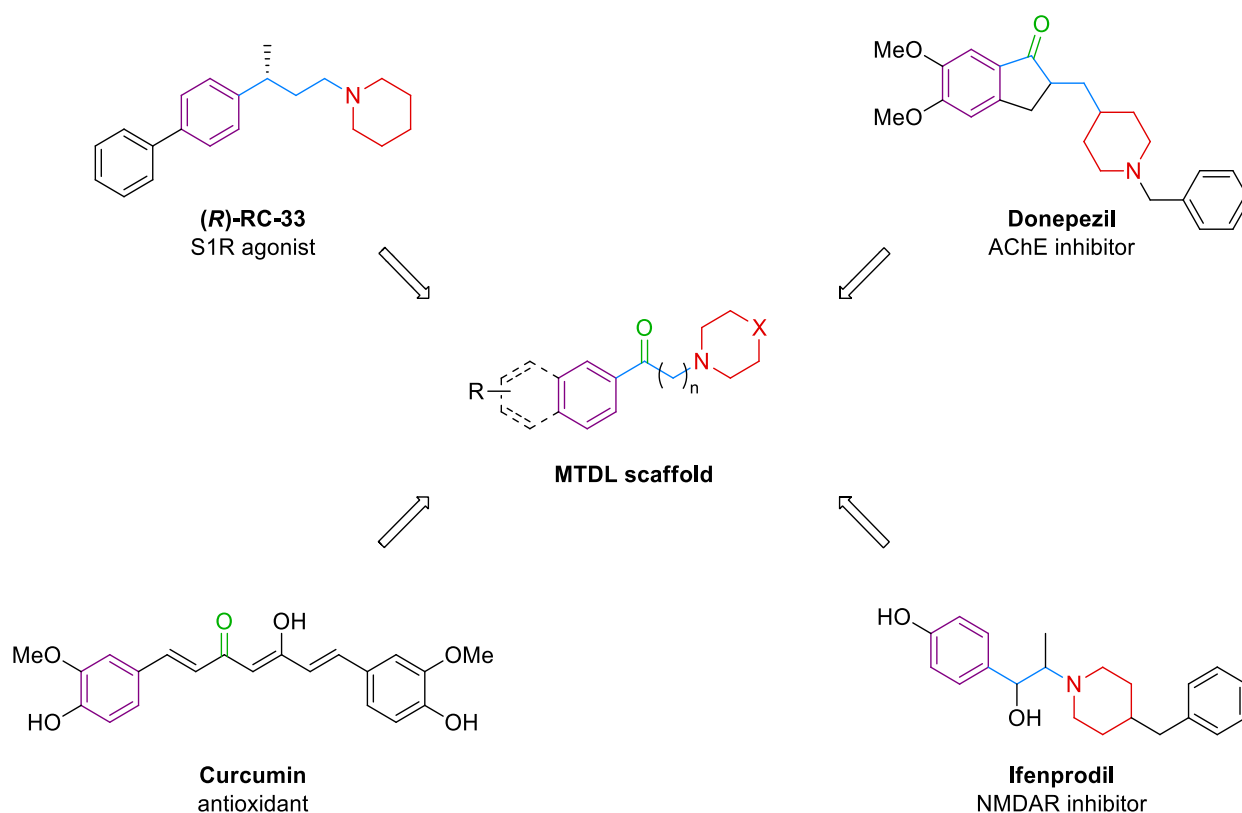
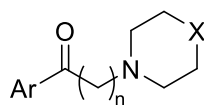


Figure 13. Common arylalkylamineketone scaffold of the new MTDL series and reference compounds that served as inspiration. The pharmacophoric elements that have been implemented in the new library are depicted with different colors. In detail, the keto-group present in Donepezil and Curcumin is retained in the new series, while aromatic ring, amine moiety and alkyl linker are the three elements of structural diversity explored.

Before moving forward to the synthesis of the designed compounds, we evaluated *in silico* their pharmacokinetic profile. In modern drug discovery, *in silico* prediction of absorption, distribution, metabolism and excretion (ADME) parameters is a valuable tool to assess the drug-likeness of a novel compound and its chances to reach the proper body district where the target lies. Such predictions are particularly useful in the development of therapeutic molecules for CNS-related diseases, since the blood-brain barrier (BBB) is able to prevent almost 100% of large molecules and more than 98% of small molecules drugs to reach the brain¹⁷⁵. Notwithstanding that actual and true data regarding the pharmacokinetic properties of a molecule must come from experimental results, in the last few years several computational methods proved to be effective in reducing the attrition rate during the first stages of a drug discovery process, thanks to the early optimization made possible by the information obtained from computational methods. Since the primary targets of the designed library (*i.e.* S1R, AChE and NMDA) are mainly localized in

CNS, the Wager *et al.* model¹⁷⁶ was used to predict our compounds' ability to cross BBB. According to this well-established and broadly employed model, there are six physicochemical parameters that can be computed to assess both the pharmacokinetic properties and the ability of a molecule to reach CNS: (a) partition coefficient (ClogP); (b) distribution coefficient at pH 7.4 (ClogD); (c) molecular weight (MW); (d) topological polar surface area (TPSA); (e) number of hydrogen-bond donors (HBDs); and (f) acid dissociation constant (pK_a)¹⁷⁷. According to the Wager *et al.* model, a score ranging from 0 to 1 is attributed to each property, applying specific functions for ClogP, ClogD, MW, pK_a, HBD and TPSA. The summation of all these values gives a final score (0-6), which can be defined as follows: i) 0-2, compound is unable to cross the BBB; ii) 2-5, compound may reach the CNS; iii) 5-6, compound effectively crosses the BBB¹⁷⁶. Accordingly, this model was exploited to calculate the potential ability of compounds **1-31** in reaching the CNS (**Table 1**). For comparative purposes, we reported also the results obtained for (*R*)-RC-33 and Donepezil, for which is known their good CNS distribution. The tabulated results show that four compounds (**15** and **19-21**) possess a score above 5, whereas the others display values ranging from 2 to 5. Noteworthy, compounds **3, 7, 9, 11, 14, 16-18** and **22** possess good scores (>4). Altogether these values reveal that all molecules **1-31** are able to reach the CNS. Moreover, reference compounds (*R*)-RC-33 and donepezil show scores ranging from moderate to good (2.57 and 4.41, respectively) and this behavior is in line with their *in vivo* CNS distribution, which was extensively confirmed by experimental data and clinical use. With this promising results in our hand, we moved forward to the synthesis of the whole library.

Table 1. Designed compounds and their scores related to the predicted BBB penetration. Colors of the score boxes range from yellow to green as the score increases.

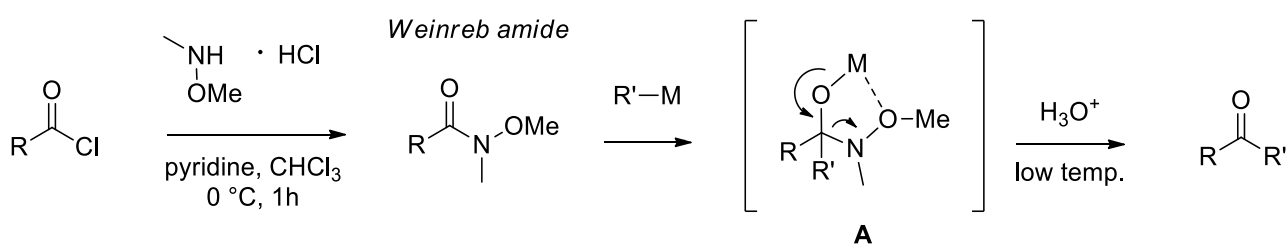


compound	score	Ar	n	X
1	3.47	phenyl	1	CHBn
2	3.57	4-methoxyphenyl		
3	4.04	3-methoxyphenyl		
4	3.02	naphth-2-yl		
5	3.42	6-mehoxynaphth-2-yl		
6	2.97	4-biphenyl		CH ₂
7	4.25	naphth-2-yl		
8	3.65	4-biphenyl		
9	4.15	4-(benzyloxy)phenyl		
10	3.46	phenyl		
11	4.09	4-methoxyphenyl	2	CHBn
12	2.72	naphth-2-yl		
13	2.61	4-biphenyl		
14	4.8	phenyl		
15	5.3	4-methoxyphenyl		
16	4.35	naphth-2-yl		CH ₂
17	4.18	4-biphenyl		
18	4.15	4-(benzyloxy)phenyl		
19	5.48	phenyl		
20	5.94	4-methoxyphenyl		
21	5.28	naphth-2-yl	3	O
22	4.91	4-biphenyl		
23	3.17	phenyl		
24	3.79	4-methoxyphenyl		
25	3.74	3-methoxyphenyl		
26	2.49	naphth-2-yl		CHBn
27	2.73	6-mehoxynaphth-2-yl		
28	2.32	4-biphenyl		
29	3.95	naphth-2-yl		
30	3.35	4-biphenyl		
31	3.85	4-(benzyloxy)phenyl	CH ₂	
(R)-RC-33	2.57			
Donepezil	4.41			

2.3 Synthesis

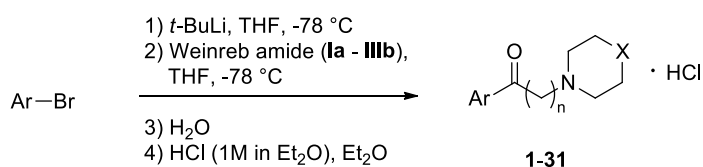
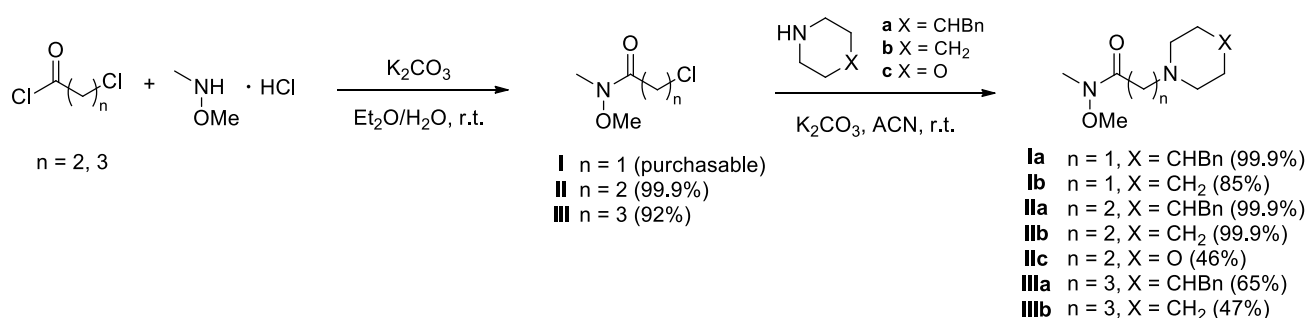
To prepare the designed library we planned to adopt a divergent strategy. This approach is in contrast with target-oriented syntheses, *i.e.* linear and convergent syntheses, which aim to access a precise region of chemical space, often defined by a complex natural product known to have a useful biological function. Divergent synthesis, on the other hand, aims at the preparation of a drug-like or natural product-like compound library by the derivatization of a versatile synthetic intermediate. This strategy is particularly useful to explore wider regions of chemical space in a very efficient way^{178,179}. Consequently, it often led to the discovery of various bioactive compounds, proving its potential to reach a viable drug candidate, and many reviews and research papers on this topic can be found in recent literature^{178–182}.

A retrosynthetic analysis was then performed, in order to identify the most convenient pathway to access the desired compounds. Different well-established approaches for the obtainment of amino-ketones (e.g. Mannich reaction) were taken into consideration (see Paper 2, Appendix, page 141). Finally, we envisaged to exploit the Weinreb ketone synthesis. This classical synthetic protocol developed by Weinreb and Nahm involves two subsequent nucleophilic acyl substitutions: the reaction of an acyl chloride with *N,O*-dimethylhydroxylamine, to form a Weinreb amide, followed by treatment of this species with an organometallic reagent, such as a Grignard reagent or organolithium reagent (**Scheme 1**)¹⁸³. Most importantly, this last step does not produce tertiary alcohols due to over-addition of organometallic reagent. In fact, the reaction proceeds through a metal-chelated intermediate (**A** in **Scheme 1**), which is very stable at low temperature, and therefore requires a low-temperature quench to afford target ketone without over-addition byproducts.



Scheme 1. Generic representation of the Weinreb ketone synthesis.

In our case, we choose lithium arenes as organometallic reagents to be employed in the last step. These can be obtained through bromo-lithium exchange, performed on the corresponding aryl bromide with *t*-butyl lithium in anhydrous THF at -78 °C¹⁸⁴. The detailed route employed to obtain our target compounds **1-31** is reported in **Scheme 2**. This synthetic strategy allowed us to access a wide range of structurally diverse final compounds from a limited number of key intermediates (Weinreb amides **la-IIIb**).



Cmp	Ar	n	X	Yield (%)	Cmp	Ar	n	X	Yield (%)
1	phenyl	1	CHBn	40	17	4-biphenyl	2	CH ₂	35
2	4-methoxyphenyl			37	18	4-(benzyloxy)phenyl			31
3	3-methoxyphenyl			48	19	phenyl			30
4	naphth-2-yl			54	20	4-methoxyphenyl			38
5	6-methoxynaphth-2-yl			49	21	naphth-2-yl			41
6	4-biphenyl			33	22	4-biphenyl			37
7	naphth-2-yl	1	CH ₂	42	23	phenyl	3	CHBn	31
8	4-biphenyl			35	24	4-methoxyphenyl			30
9	4-(benzyloxy)phenyl			29	25	3-methoxyphenyl			33
10	phenyl	2	CHBn	28	26	naphth-2-yl			41
11	4-methoxyphenyl			25	27	6-methoxynaphth-2-yl			25
12	naphth-2-yl			22	28	4-biphenyl			26
13	4-biphenyl			22	29	naphth-2-yl	58		
14	phenyl	2	CH ₂	29	30	4-biphenyl	3	CH ₂	72
15	4-methoxyphenyl			27	31	4-(benzyloxy)phenyl			53
16	naphth-2-yl			23					

Scheme 2. Synthesis of the compound library based on arylalkylaminoketone scaffold. Yields of intermediates are reported in brackets.

Firstly, Weinreb amides **I-III** were either purchased if commercially available (amide **I**) or prepared by reacting the corresponding acyl chloride with *N,O*-dimethylhydroxyamine hydrochloride (compounds **II-III**). The reactions were performed under basic conditions (in presence of K_2CO_3), in a mixture of ether and water 1:1. Afterwards, nucleophilic substitution on Weinreb amides **I-III** was carried out using amines **a-c**, *i.e.* 4-benzylpiperidine, piperidine and morpholine. This led to the key intermediates **Ia-Ib**, **IIa-IIc** and **IIIa-IIIb**, characterized by diverse linker lengths and amine groups. The reaction needed 24 h and the presence of K_2CO_3 as base to yield the crude α , β and γ amino Weinreb amides. In most cases, an acid/base extraction

was sufficient to obtain the key intermediates in modest to excellent yields and suitable purity. Conversely, **IIIa** required a purification through flash chromatography, since the reaction gave some side products. Finally, compounds **1-31** were obtained by coupling intermediates **Ia-IIIb** with different aryl lithium species generated *in situ*. Aromatic moieties thus introduced include phenyl, 4-methoxyphenyl, 3-methoxyphenyl, naphth-2-yl, 6-methoxynaphth-2-yl, 4-biphenyl and 4-(benzyloxy)phenyl (see **Scheme 2**). In detail, this last step involves the smooth bromo-lithium exchange on the aryl bromide to access the lithiated arene that, after addition of Weinreb amides **Ia-IIIb** and quenching with H₂O gave the desired crude ketones **1-31** in good yields. After flash chromatography purification, compounds were converted into their corresponding hydrochlorides by addition of HCl in Et₂O. All the potential MTDLs **1-31** were obtained in a sufficient amount and with the appropriate degree of purity, as confirmed by IR, ¹H NMR, ¹³C NMR and UPLC-MS analysis, for the following biological investigations.

2.4 Biological investigation

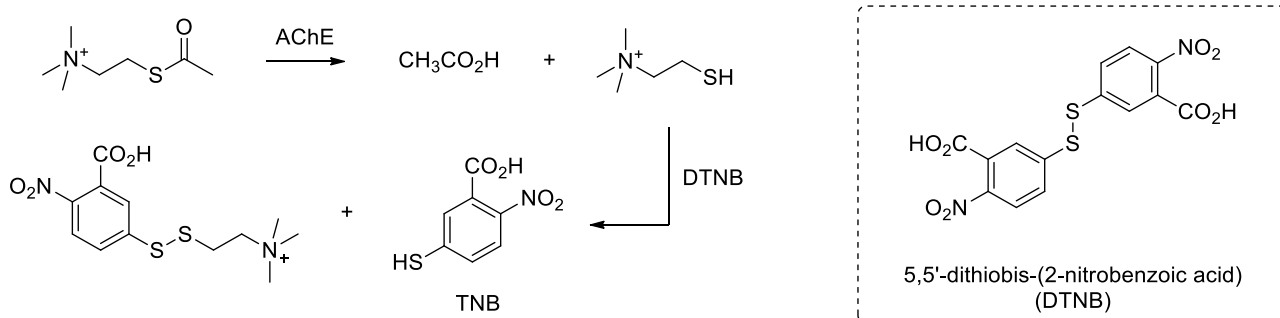
Once all the designed compounds were obtained in suitable amount and purity for preliminary biological investigation, we proceeded in assessing their affinities toward S1R, S2R and NMDA receptor, as well as their anti-AChE activity and antioxidant profile.

Competition experiments with radioligands were employed to determine our compounds' affinities toward both Sigma receptor subtypes. The assay for S1R was performed using homogenized guinea pig cerebral cortex membranes, in the presence of [³H]-(+)-pentazocine, as a potent and selective S1R radioligand. Nonspecific binding values were determined using non-radiolabeled (+)-pentazocine in excess. Conversely, homogenized rat liver membranes were adopted to evaluate the S2R binding values, employing [³H]-DTG. Since this compound is a non-selective S2R ligand, S1R was previously masked with an excess of non-tritiated (+)-pentazocine. Moreover, a high concentration of non-tritiated DTG was used to determine nonspecific binding values. Compounds with high affinity were tested three times, whereas compounds with low SR affinity, only one measure was performed. The SRs affinities of compounds **1-31** and reference compounds (namely, (*R*)-RC-33, Donepezil and Ifenprodil) are presented in **Table 2**. Analogously to (*R*)-RC-33, almost all compounds display a weak affinity toward S2R, and more than half of the series (**2, 4, 9-11, 15-18, 21-26, 29-30**) presents a K_i S1R lower than 50 nM. Some preliminary SAR considerations can be drawn from these results: (i) the 4-methoxyphenyl ring seems to favor the interaction with S1R, as molecules **2, 11, 15** and **24** belonging to the three different n series present good K_i values (27, 11, 8 and 2.9 nM, respectively); (ii) a longer linker adapts well to the S1R binding pocket, as it can be deduced by the 4-benzylpiperidine derivatives (**1-6, 10-13** and **23-28**), which follow 1 < 2 < 3 n-scale in the interaction with S1R; (iii) on the other hand, the length of the linker can limit the selectivity, indeed compounds belonging to the n = 3 series present a S2R/S1R ranging from 1.6 to 11.4 and thus.

Affinity towards GluN2 subunit of NMDA was determined through competitive binding assays on membrane extracts of L cells (tk-), stably transfected with a vector containing the genetic information of GluN1a and GluN2B subunits. [³H]-Ifenprodil was employed as a selective and potent GluN2 inhibitor radioligand. Compounds with high affinity were tested three times. For compounds with low NMDA affinity, only one measure was performed. The results reported in **Table 2** show that the majority of compounds **1-31** possess a rather weak affinity towards NMDA receptor. Noteworthy exceptions are **2-4, 10** and **23-28**, which show a K_i < 150 nM. These results suggest that n = 3 linker and benzylpiperidine moiety are a good combination for NMDAR binding.

Afterwards, compounds **1-31** were tested for defining their potential to inhibit AChE. A spectrophotometric procedure was adopted, based on the well-known Ellman's method¹⁸⁵. The chemical mechanisms at the basis of this assay is reported in **Scheme 3**: acetylthiocholine is hydrolyzed in acetic acid and thiocholine, which

reacts with 5,5'-dithiobis-(2-nitrobenzoic acid) (DTNB, also known as Ellman's reagent) cleaving the disulfide bond to give 2-nitro-5-thiobenzoic acid (TNB), which ionizes to the TNB^{2-} dianion in water at neutral and alkaline pH. This TNB^{2-} ion has a yellow color and can be quantified in a spectrophotometer by measuring the absorbance at 412 nm. Compounds that inhibit AChE activity result in a decrease of the test solution's absorbance at 412 nm.



Scheme 3. Chemical mechanism of Ellman's method for assessment of acetylcholinesterase activity.

An initial screening was performed, employing the target compounds at a concentration of 50 μM . The results of this assay are summarized in **Table 1**. Noteworthy, 12 compounds (**3-4**, **11-12**, **17**, **23-25**, **27-30**) possess a percentage of inhibition $\geq 60\%$. For these most promising molecules, the IC_{50} values were determined. Interestingly, the obtained IC_{50} values resulted lower than 25 μM , with the only exception of **3** ($\text{IC}_{50} = 32.88 \pm 1.77 \text{ mM}$). In particular, **25** and **27** result the most promising AChE inhibitors, with an IC_{50} of 7.64 ± 2.07 and $4.28 \pm 0.23 \mu\text{M}$, respectively (**Table 2**). Interestingly, the most active compounds belong to the $n = 3$ series (**23-25**, **27-28**), and the inhibitory activity progressively decreases for $n = 2$ and $n = 1$ series. Moreover, molecules bearing the 4-benzylpiperidine or piperidine motif are characterized by higher inhibitory activity respect to the morpholine-based compounds. Considering the obtained results, both the amine portion and the linker length seem to be important for the anti-AChE activity, whereas no clear relation between the aromatic portion and AChE inhibition has emerged.

Table 2. Binding affinities of compounds **1-31** towards NMDAR, S1R and S2R and S1R selectivity (K_i S2R/ K_i S1R). AChE inhibition activity and IC_{50} of the most promising compounds. Values of model compounds (*R*)-RC-33, Donepezil and Ifenprodil are reported for comparative purposes.

compound	K_i S1R (nM)	K_i S2R (nM)	S2R/S1R	K_i NMDAR (nM)	% of AChE inhibition (50 μ M)	AChE IC_{50} (μ M)
1	75 \pm 3.6	2300	30.7	215	5.65 \pm 0.10	a
2	27 \pm 1.2	2000	74	16 \pm 1.2	8.21 \pm 0.06	a
3	131 \pm 15	1500	11.5	11 \pm 0.4	75.50 \pm 0.02	32.82 \pm 1.77
4	27 \pm 1.8	802	30	139 \pm 11	87.40 \pm 6.39	9.13 \pm 2.24
5	286	1400	4.9	>1000	48.24 \pm 0.02	a
6	340	>1000	-	>1000	11.41 \pm 0.04	a
7	130 \pm 16	190	1.5	657	b	b
8	132 \pm 55	1200	9.1	3100	b	b
9	48 \pm 12	976	20.3	796	b	b
10	16 \pm 1.8	5800	363	39 \pm 2.1	42.30 \pm 0.21	a
11	11 \pm 2.2	2400	218	198	64.10 \pm 5.58	22.02 \pm 9.12
12	211	6200	29.4	>1000	85.50 \pm 0.02	18.55 \pm 7.72
13	167	3900	23.4	>1000	55.04 \pm 6.69	a
14	171	749	4.4	>1000	b	b
15	7.9 \pm 0.9	2100	256	1700	42.07 \pm 0.04	a
16	2.2 \pm 0.7	178 \pm 12	81	>1000	45.20 \pm 7.07	a
17	15 \pm 1.1	462	30.8	>1000	64.80 \pm 0.35	13.08 \pm 6.31
18	25 \pm 7	972	38.9	954	b	b
19	606	>1000	-	>1000	10.75 \pm 0.01	a
20	301	>1000	-	>1000	59.70 \pm 2.24	a
21	9 \pm 0.7	>1000	-	>1000	24.62 \pm 0.05	a
22	2.9 \pm 0.3	>1000	-	723	12.20 \pm 1.72	a
23	9.0 \pm 0.5	47 \pm 2	5.2	39 \pm 1.1	74.80 \pm 3.56	13.07 \pm 2.10
24	31 \pm 4.2	111 \pm 8	6.8	96 \pm 2.7	80.01 \pm 0.02	12.80 \pm 1.79
25	17 \pm 2.2	43 \pm 1.9	2.5	49 \pm 1.8	71.80 \pm 1.60	7.64 \pm 2.07
26	24 \pm 3.4	58 \pm 2.3	2.4	26 \pm 0.9	b	b
27	68 \pm 1.7	107 \pm 10	1.6	20 \pm 0.7	92.60 \pm 0.03	4.28 \pm 0.23
28	135 \pm 11	704	5.2	96 \pm 2.6	84.10 \pm 0.02	13.94 \pm 2.15
29	4.4 \pm 2.4	50 \pm 19	11.4	462	88 \pm 1,59	3,84 \pm 0,62
30	33 \pm 14	82	2.5	200	72 \pm 0,36	0,68 \pm 0,09
31	87 \pm 28	199	2.3	673	b	b
(<i>R</i>)-RC-33	1.8 \pm 0.1	45 \pm 16	25	>1000	4.82 \pm 2.15	a
Donepezil	14.6 ^c	-	-	-	99.4 \pm 0.01	0.012 \pm 0.01
Ifenprodil	125 \pm 24	98 \pm 34	0.8	10 \pm 0.7	-	-

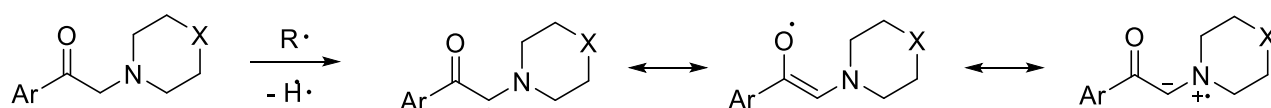
Values are expressed as mean \pm SEM of three experiments. Compounds with high affinity were tested three times. For compounds with low SR and NMDA affinity (K_i > 150 nM) only one measure was performed.

^a Inhibition % < 60% at a concentration of 50 μ M.

^b Compounds were not evaluated for solubility issues.

^c Data taken from reference ¹⁸⁶.

Basing on these preliminary biological investigations, compounds that showed a good multitarget binding profile were selected for evaluation of antioxidant activity. Since counteraction of oxidative stress can be exerted through different biological pathways and molecular mechanisms^{93,94,187}, a number of orthogonal assays was employed. Firstly, free radical scavenging (FRS) activity was determined by 2,2-diphenyl-1-picrylhydrazyl (DPPH) assay, and the results were compared to those of reference molecules (*R*)-RC-33, Donepezil and Curcumin. Stock solutions in EtOH of the test compounds (**2**, **4**, **10-11**, **15-17**, **21-26**) were prepared (5.0 mM). The DPPH absorbance was spectrophotometrically monitored at 515 nm and inhibition percentages calculated. The results demonstrated that compounds **10-11**, **15-17**, **21-26**, as well as (*R*)-RC-33 and Donepezil do not display significant antioxidant activity (values ranging from 2.8% to 32%). Conversely, compounds **2** and **4** exerted a significant FRS activity (65.6 % and 65.7 % respectively), comparable with that of Curcumin (FRS% 71.3 ± 6.74). Since only molecules belonging to the n = 1 series possess intrinsic antioxidant properties, we postulated that this might be due to the methylene spacer adjacent to both carbonyl and amine moieties, which could be crucial to stabilize the radical center (**Scheme 4**)¹⁸⁸.



Scheme 4. Proposed mechanism for the radical scavenging activity of n = 1 series compounds.

To further investigate potential antioxidant activity, we evaluated the ability of some selected compounds in reducing ROS within SH-SY5Y cells after an exposure to oxidative damages mediated by H₂O₂. The assay is performed with the cell-permeable non-fluorescent probe 2',7'-Dichlorofluorescein diacetate (DCFDA). Within the cell, this compound undergoes esterase-mediated de-acetylation and the resulting product is then subjected to oxidation by ROS, giving 2',7'-dichlorofluorescein, a highly fluorescent molecule. As reported in **Figure 14**, Curcumin possesses the ability to reduce ROS up to a 0%, whereas donepezil and (*R*)-RC-33 show no antioxidant properties. Among the tested compounds, **4** and **17** showed the best antioxidant profile, being able to promote ROS reduction up to 43% and 18% respectively.

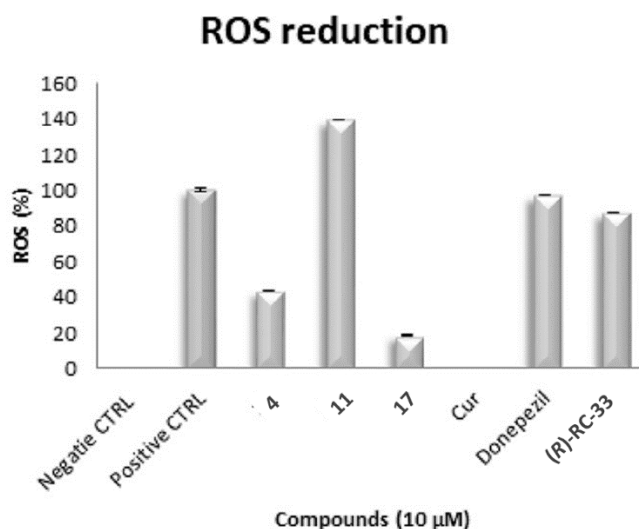


Figure 14. ROS percentage evaluation after administration of test compound in SH-SY5Y cells. Among model compounds, only Curcumin is able to reduce ROS production, whereas Donepezil and RC-33 resulted ineffective. Among novel compounds, **4** and **17** showed promising antioxidant activity (inactive compound **11** is reported for comparison).

Lastly, selected compounds were tested on HeLa cells to evaluate their antioxidant effect mediated by aquaporins (AQPs). Aquaporins are a family of water channel proteins present in mammals in different isoforms and constitute emerging targets in virtue of their role in promoting H₂O₂ diffusion and scavenging reactive oxygen species, thus alleviating oxidative injury^{189,190}. These intriguing membrane proteins are still unexplored from a medicinal chemistry standpoint.

Firstly, osmotic water permeability in oxidative stress conditions was measured by a stopped-flow light scattering method. As reported in **Figure 15**, addition of our test compounds was able to prevent or restore the water permeability decrease in most cases. Then, hydrogen peroxide permeability was evaluated: H₂O₂ levels were measured in heat-stressed HeLa cells using the fluorescent probe CM-H₂DCFDA. Dose-response relationship for two representative compounds (**21** and **22**) are reported in **Figure 15**. The results obtained indicate that our compounds are able to counteract oxidative stress by modulation of Aquaporins activity.

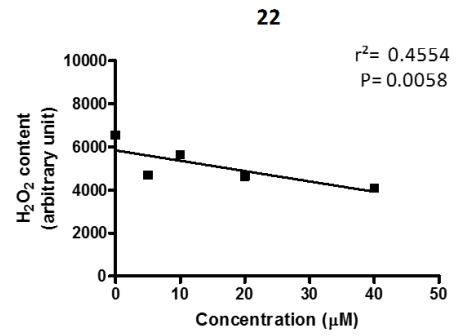
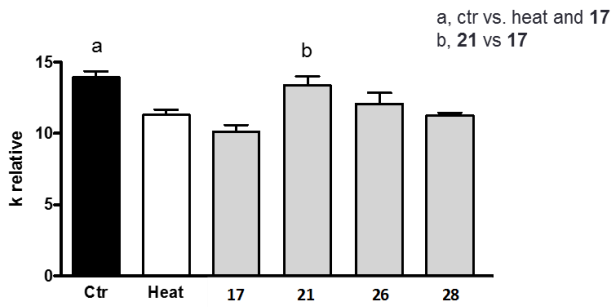
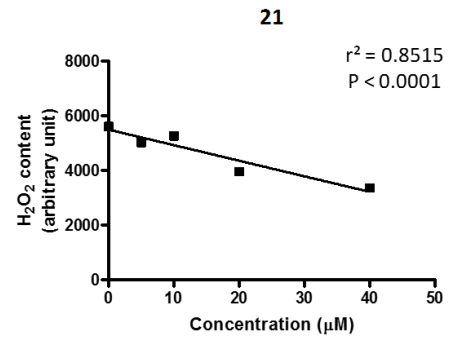
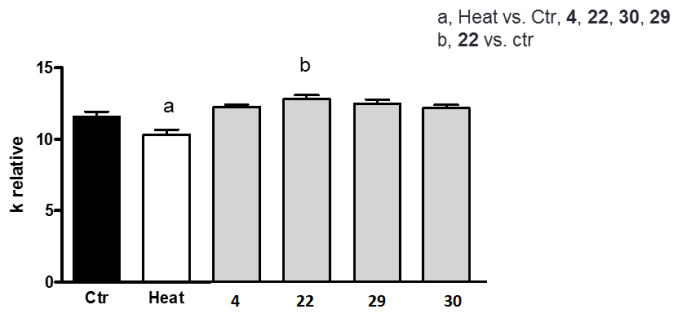


Figure 15. Evaluation of MTDLs' AQPs-mediated antioxidant effect on HeLa cells. Measurement of osmotic water permeability and H₂O₂ levels in oxidative stress conditions.

2.5 Computational studies

In order to rationalize the results obtained from binding assays, computational studies were carried out on the compound library. In detail, the S1R trimeric structure in complex with 4-IBP (PDB: 5HK2) was used to dock our arylalkylaminoketones. Interestingly, all active molecules formed ionic interactions with Glu172 and Asp126 due to their positively charged amine group. By contrast, low-ranked ligands lacked these key residue contacts. The pivotal role of Glu172 is consistent with what was pointed out in the first publication of the S1R crystal structure¹⁵. Other amino acids often involved in protein-ligand interactions include residues Trp89 and Phe107, which can form π -cation interactions with the ligands' protonated amine, and Tyr120 and His154, involved in π - π stacking with ligand aromatic rings. As reported in **Figure 14**, reference compound (*R*)-RC-33 is able to engage most of these stabilizing interactions (i.e. ionic interaction with Glu172 and Asp126, cation- π interaction with Phe107 and hydrophobic contacts between aromatic rings and surrounding amino acids). Upon docking, it was observed that most of compounds **1-31** conserved key interactions with the receptor, although larger molecules with four rings (such as 4-biphenyl derivatives **6**, **13** and **28**) did not fit well into the binding pocket. In detail, either the biphenyl moiety clashed with Tyr206 or the benzyl ring did not have enough space on the opposite side of the pocket. Conversely, molecules **14**, **19** and **20** that have only two rings lacked important hydrophobic contacts resulting in low binding affinity (experimental $K_i > 130$ nM). In conclusion, compounds with three rings, which conserved H-bond and hydrophobic interactions, seem to be the most promising. In **Figure 14**, two representative compounds (**4** and **17**) are reported as examples.

All new derivatives were docked also on AChE using the X-ray crystal structure bound to Donepezil (PDB: 4EY7). The top-ranked ligands adopted poses similar to the co-crystallized Donepezil, forming π - π and π -cation interactions with Trp86, Trp286, Tyr337 and Tyr341 residues of the binding pocket (**Figure 14**). Also, the H-bond with the backbone of Phe295 was mostly conserved. In particular, the presence of the carbonyl enhanced the binding in the $n = 3$ series (compounds **23-31**), which has the optimal linker length to keep both the H-bond to Phe295 and the ionic interaction between amine and Tyr residues. Instead, not all compounds formed hydrogen bond interactions with the hydroxyl group of Tyr amino acids. For instance, the docking pose of compound **17** showed that the charged amine could fit into a deeper binding pocket, where it could form interactions with Glu202. This was possible only for unsubstituted piperidine rings. Furthermore, the naphthalene ring (compounds **10** and **27**) enhanced the π - π stacking with Trp286. In summary, docking poses suggested that the charged amine plays a key role not only for binding to negatively charged amino acids, but also to aromatic residues through cation- π interactions. The binding is strengthened by the presence of aromatic rings, which form hydrophobic and π - π interactions with both S1R and AChE ligand pockets. Several compounds among our new set of derivatives showed protein-ligand interaction

patterns which are similar to reference compounds (*R*)-RC-33 and Donepezil, as shown in **Figure 14**, where the docking poses of **4** and **17** are reported.

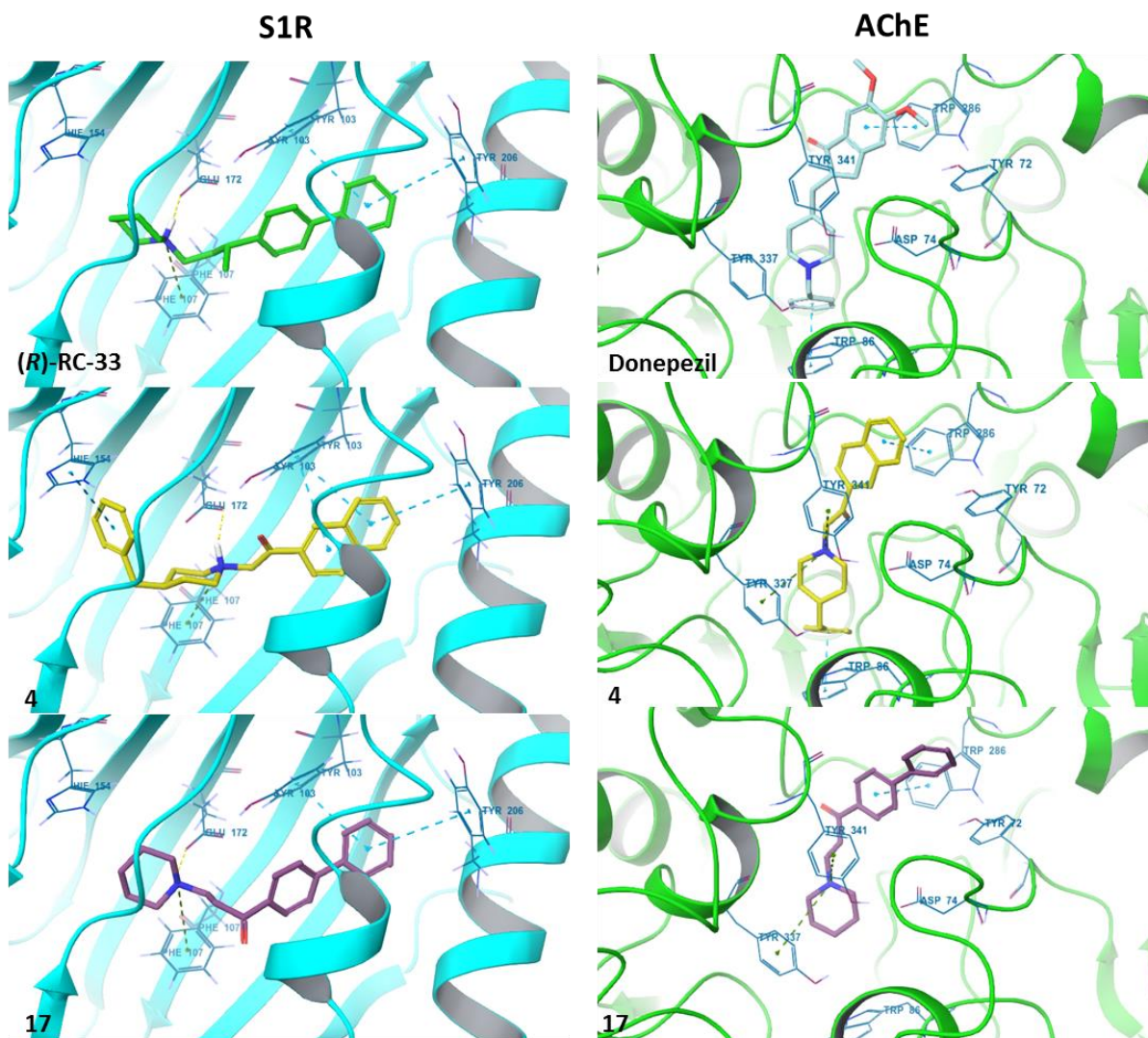


Figure 14. Docking poses of reference compounds (RC-33, green, and Donepezil, turquoise) and of **4** and **17** (yellow and purple, respectively) on S1R and AChE binding pockets. Ligands and key residues are shown as sticks.

Overall, the preparation and evaluation (both *in vitro* and *in silico*) of the reported compound library have been reported in a recent publication (see Paper 3, Appendix, page 154), where additional details can be found about computational and biological investigations (including cell viability and neurotrophic activity). It is worth noting that the ketone moiety of the designed compounds does not interfere with S1R and AChE binding. Hence, it might be exploited for interaction with other molecular targets related to neurodegenerative diseases to develop MTDLs with optimized binding profile. In particular, interaction of our compounds with NMDAR deserves to be further investigated, since only few of them showed a significant inhibitory activity toward this receptor. Although important insights on interaction with GluN2B might come from computational studies, such investigations are particularly demanding due to the broad shape of the receptor's binding pocket. This is in fact constituted from a non-polar cavity and two sub-cavities, separated

by the side chain of Gln110, which are highly accessible to both the solvent and the ligands¹⁹¹. A drawback of this situation is that the large available space makes docking particularly difficult, as well as subsequent free energy calculations, since they highly rely on the correctness of the interactions between the ligands and their environment. These issues will be addressed in next studies in order to draw important SAR considerations. Nevertheless, one should keep in mind that, when dealing with MTDLs, the final goal is an equilibrated and synergistic modulation of selected therapeutic targets, rather than extremely high potency toward all of them. Moreover, since NMDA receptor is one of the client proteins of S1R, even compounds with modest affinity toward NMDAR might result in beneficial modulation of the related biological pathway *via* a Sigma-mediated mechanism.

2.6 Discussion

As extensively reported in *Section 1.3*, S1R is now unanimously considered a promising target for counteracting neuropathies in virtue of its two main features: (i) ability to modulate a wide range of biological pathways involved in cell survival and excitability, (ii) overexpression in central nervous system cells. Its therapeutic potential is confirmed by recent studies that culminated in bringing S1R modulators into clinical trials. This is the case of Anavex 273 and AVP-786 (under evaluation for Alzheimer's disease), S1A (investigated for the treatment of neuropathic pain), and pridopidine, originally developed for Huntington disease and now repositioned for ALS. More S1R agonists are in the pipeline of pharmaceutical industries in pursuit of neuroprotective agents. Furthermore, as outlined in Paper 1 (Appendix, page 119), S1R has been recently proposed as molecular target to counteract multiple sclerosis, thus expanding the spectrum of potential therapeutic application of Sigma1 agonists. This was based on the consideration that S1R plays a pivotal role in regulating synaptogenesis, myelination and cellular homeostasis through different pathways involving microglial activation and protection against mitochondrial damage and oxidative stress.

Given these premises, in my PhD work I considered S1R and other related targets to design novel MTDLs with the final aim to obtain new agents for counteracting neurodegenerative diseases. Among the eligible targets, in the first phase of the work, AChE was selected due to its well-established role in regulation of the cholinergic system, which impairments are considered hallmarks of neurodegeneration. Accordingly, the pharmacophoric elements of RC-33 and Donepezil (S1R agonist and AChE inhibitor, respectively) were assembled in a new scaffold potentially able to bind both targets. Keeping in mind that oxidative stress also plays a role in neuropathies, structural features of the natural antioxidant Curcumin were included as well. The resulting arylalkylaminoketone scaffold served as basis for the design of a compound library of 24 potential MTDLs. Briefly, the designed compounds were efficiently synthesized with a divergent approach and their biological profile was drawn through binding and spectrophotometric assays. The results have been published in Paper 3 (Appendix, page 154). Two compounds resulted of particular interest (*i.e.* compound **4** and **17**), showing high affinity toward both S1R and AChE and exerting antioxidant and neurotrophic properties at non-cytotoxic dose. It is worth noting that (*R*)-RC-33 shows no anti-AChE property, nor antioxidant properties (both in DPPH assay and within SH-SY5Y cells), despite the striking structural similarity with compound **17**. This suggests that even minor structural changes can induce significant amelioration in the compound's biological profile. Prompted by these encouraging results, we decided to extend this approach to a new series of compounds, including investigation on NMDA receptor and Aquaporins (AQPs) (manuscript in preparation). Of note, NMDA is involved in synapse formation and plasticity and is commonly regarded as one of the main S1R client proteins. On the other hand, Aquaporins are a family of integral membrane proteins involved in water and H₂O₂ transport. They represent an emerging target, still poorly

studied from a medicinal chemistry point of view. Interestingly, some AQP subtypes seem to be able to interact with NMDA receptor¹⁹². Triggering this network of mutual modulation and beneficial effects may provide an enhanced therapeutic effect. Accordingly, we designed the new ligands to fill those regions of chemical space unexplored with the first library (**Figure 15**).

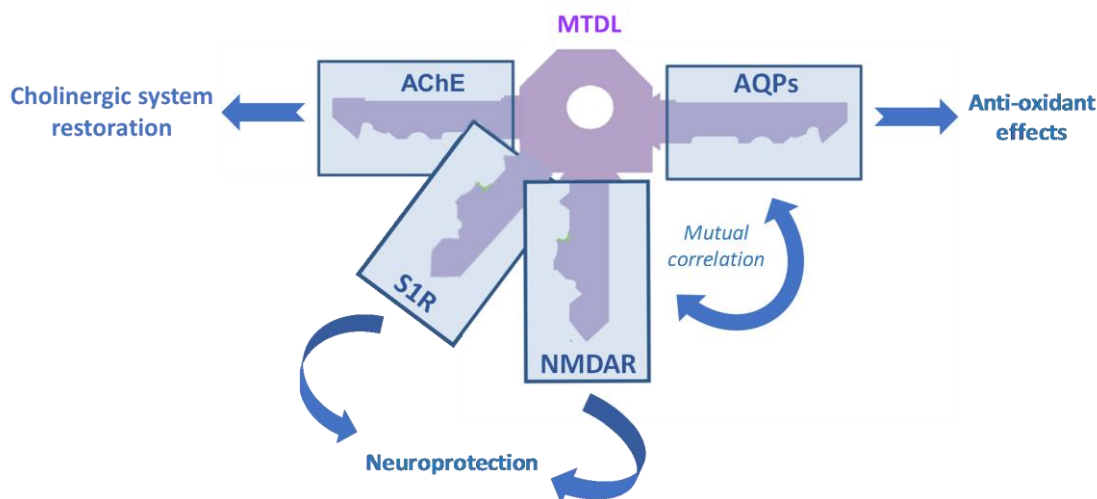


Figure 15. Multitarget approach schematization: interaction of the same molecule with multiple selected targets can promote an enhanced beneficial outcome by activating different molecular cascades, similarly to a key that can open many doors.

Among the newly prepared compounds, four had a $K_i < 50\text{nM}$ toward S1R (**9, 18, 29, 30**) and two of them showed anti-AChE activity (% of inhibition $> 70\%$), although all exhibited a modest binding affinity toward NMDAR ($K_i > 200\text{ nM}$). This last aspect did not discourage us, since NMDAR can be modulated through activation of S1R. Finally, evaluation of some selected molecules – from both the first and second library – on Aquaporins gave interesting results: almost all tested compounds resulted able to counteract oxidative stress conditions by restoring water permeability and lowering H_2O_2 levels in HeLa cells. Notably, some compound (**21, 22** and **26**) that displayed low intrinsic ROS scavenging properties in DPPH assay, here resulted effective, suggesting that their antioxidant activity might be primarily AQP-mediated. The obtained results confirm the potential of these unexplored molecular targets to counteract cell damage caused by oxidative stress, and represent a step forward in understanding their role in cells.

To sum up, a library of MTDLs sharing the pharmacophoric requirements for interaction with S1R, AChE and NMDAR has been prepared. Their binding profile has been determined, as well as their antioxidant properties, revealing a number of compounds endowed with multitarget affinity and able to counteract oxidative stress.

3. Studying the S1R oligomerization process

3.1 Design of bivalent ligands

Over the last 25 years, the use of homo- and hetero-bivalent drugs has been gradually gaining relevant consensus among the scientific community, in virtue of their ability to target a variety of therapeutic targets with improved efficiency and/or selectivity. The progressive recognition of the therapeutic potential of such approach led – from few pioneering studies in the 1990s – to a research outburst in very recent time^{193–199}. Indeed, the ability of a single protein to form dimeric or oligomeric complexes can be crucial to activate a specific molecular cascade and trigger important biological mechanisms^{200–203,160,204}. As reported in *Section 1.2*, S1R can be counted among such proteins, as it is known that agonists bias the receptor toward its monomeric or low-molecular-weight homomers (namely, dimers), whereas antagonists favor the formation of higher order oligomers, although the dominant physiologically form and how oligomerization is connected to agonism are still to be elucidated.

Given these premises, we planned to develop a series of bivalent S1R modulators as useful tools to study molecular mechanisms underlying the receptor's oligomerization, as well as biological effects triggered by this process. In particular, we reasoned that since S1R can form homo-dimeric structures upon interaction with agonists, and S1R agonists are known to exert neuroprotective effects, promoting dimerization through dimeric ligands could enhance ligand's beneficial activity. Accordingly, we designed a series of bivalent ligands consisting in two units of (*R*)-RC-33 (our in-house developed S1R agonist) tethered by a linker (**Figure 16**). Because of the lack of derivatizable functions within (*R*)-RC-33 structure, a structural variation was required. To decide which portion of the original scaffold is best suited for derivatization and attachment of the linker, without disturbing the interaction with the binding pocket, an analysis of the crystal structure published in 2016 was required. Immediately, a main issue arose: the binding site is not exposed to the solvent, and no clear indication on how ligands could access this highly occluded region was available at that time. The authors of the crystallographic study could only hypothesize two main alternatives: one pathway is through a gap between the two membrane-adjacent helices, directly into/out of the plasma membrane, while the other passes through a polar region occluded by residues Gln135, Glu158, and His154, from the cytosolic surface. Notably, the receptor must be endowed with significant conformational plasticity to allow reversible ligand binding.

Computational studies could help to identify the most probable route ligands follow to reach the active site and which conformational changes are involved during this process. Such information would be really useful for the design of bivalent ligands, helping to decide which scaffold derivatization and linker type best adapt to the “open” conformation of the receptor's binding pocket. However, computations of such major conformational changes for proteins as large as S1R (223 aminoacids, 25.3 KDa) are particularly demanding, and their reliability must be confirmed by experimental results. Moreover, S1R has been crystallized only as

trimeric complex, hence, receptor's dimeric structure and the exact distance between two binding sites in this particular form are still unknown.

Given these premises, a preliminary docking study on (*R*)-RC-33 was performed to drive some basic considerations for the development of bivalent ligands. Starting from these first insights, finer computational studies were carried out in parallel with development and experimental evaluation of bivalent ligands.

In detail, the trimeric crystal structure in complex with 4-IBP was used to dock model compound (*R*)-RC-33. The obtained poses were superimposable with the co-crystallized ligand, with the key ionic interaction occurring between the protonated nitrogen of the piperidine ring and Glu172 residue. In addition, hydrophobic contacts are shown between the aromatic rings and surrounding amino acids (Met93, Leu95, Leu105). Considering that the biphenyl portion is more deeply buried into the receptor's structure, whereas piperidine ring points toward one of the putative pathways for accessing the binding site (the one leading to the cytosolic side), we envisaged the introduction of an amminic group at 4-position of the piperidine nucleus (compound (*R*)-RC-33A) for tethering the two sub-units of bivalent derivatives, as reported in **Figure 16**: this allows us to access bivalent compounds through amidation coupling with different di-acidic linkers. To validate the hypothesis that derivatization of the piperidine ring does not affect significantly the affinity toward S1R, we decided to extend investigation to acetamide derivative **32**. The novel bivalent ligands were designed with the aim to explore different linker features as length, hydrophilicity and spatial constrain. Specifically, homo-bivalent ligands can be grouped into three different categories: i) compounds with linear and hydrophobic alkyl-linkers (**33-35**), ii) molecules with hydrophilic linear polyoxyethylene-linkers (**36-38**), iii) one ligand presenting rigid, planar and hydrophobic phenyl-linker (**39**). We also designed the hetero-bivalent compound **40** (**Figure 16**), bearing RC-33 pharmacophore at one end and an inactive moiety, *i.e.* some functional group that is not expected to give specific interaction with a second binding pocket. This will serve as a negative control, to verify the effects of activating two S1R monomers through a bivalent agonist.

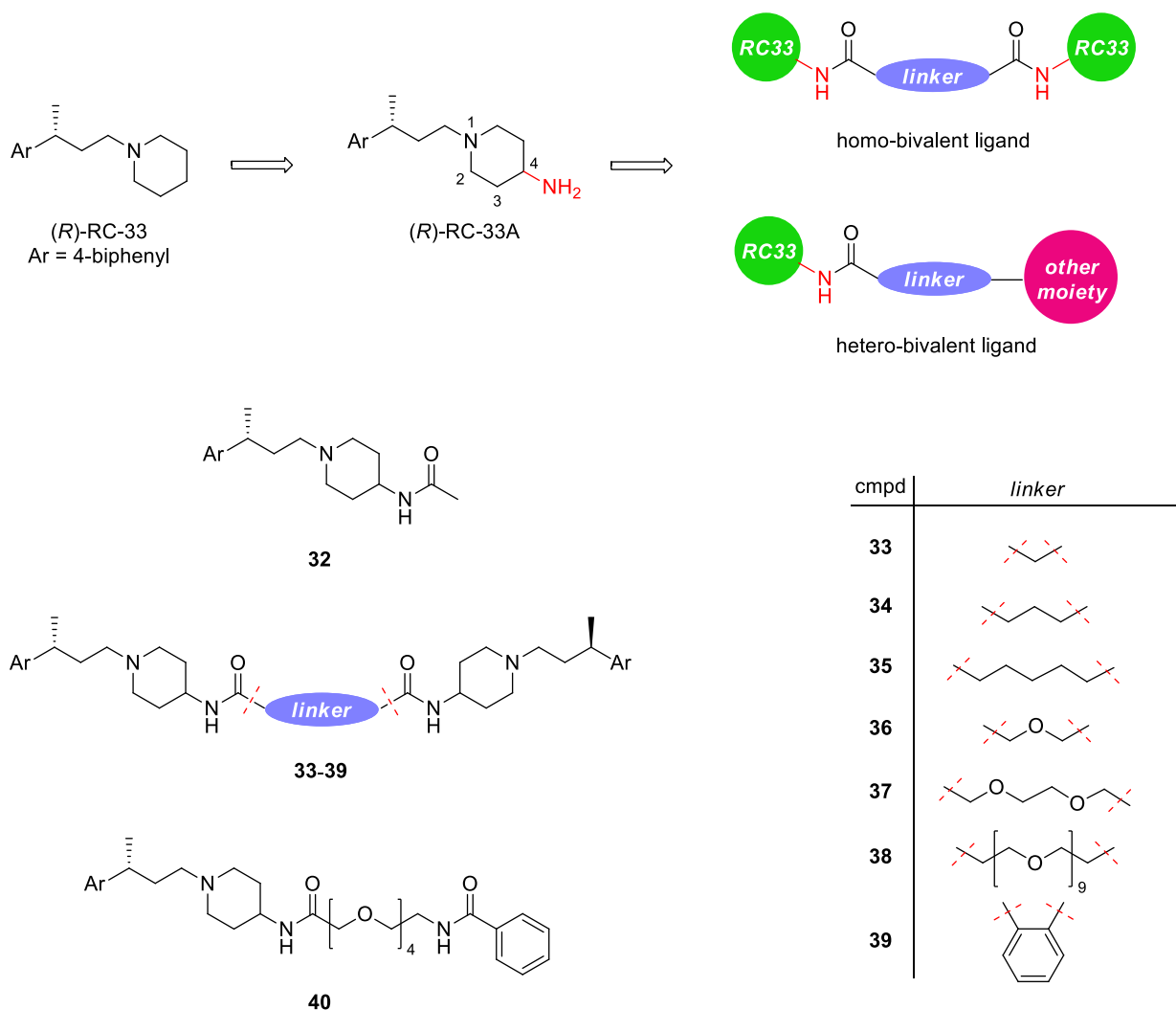


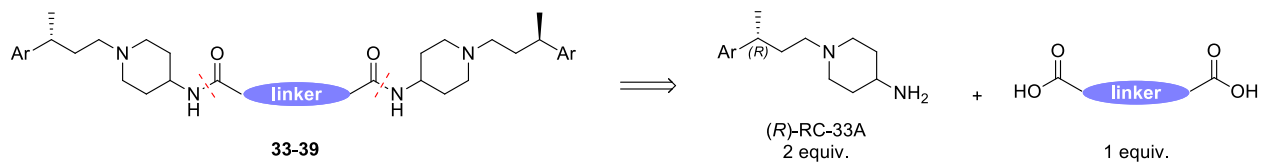
Figure 16. Structures of S1R ligands designed to study the receptor's dimerization.

As mentioned above, for the preparation of homo-bivalent ligands we considered to exploit coupling *via* amidation reaction between two equivalents of key intermediate (R)-RC-33A and one equivalent of commercially available di-acidic symmetric linkers (**Scheme 5**). Obtainment of hetero-bivalent compound **40**, on the other hand, involves the use of asymmetric linker **42**. This can be added to an activated ester of benzoic acid to obtain compound **41**, which in turn is coupled with (R)-RC-33A.

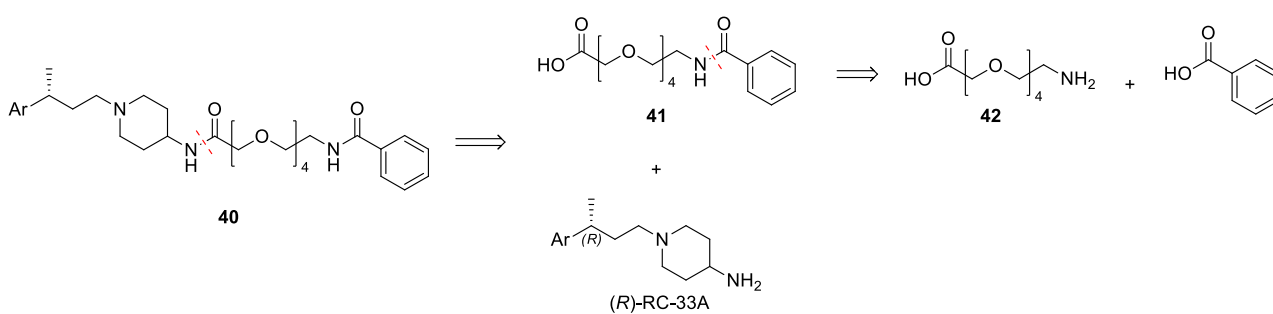
An important issue that must be taken into account when dealing with such bivalent ligands is chirality. If the pharmacophore that has to be coupled twice with the linker bears one chiral center – as in our case – this leads to the possibility to obtain three different products: a couple of enantiomers (with configuration *R,R* and *S,S*) and one meso compound (*R,S*). In early studies performed after the discovery of RC-33, both enantiomers showed superimposable affinities toward S1R and the (*R*) enantiomer was later identified as lead compound in virtue of its higher metabolic stability¹⁶³. Accordingly, we directed our efforts toward the obtainment of enantioenriched (*R,R*) bivalent ligands, in order to i) prevent quicker degradation during

biological investigations and ii) to avoid a final mixture of three different stereoisomers that might give problems during physico-chemical characterization.

homo-bivalent ligands retrosynthesis



hetero-bivalent ligands retrosynthesis



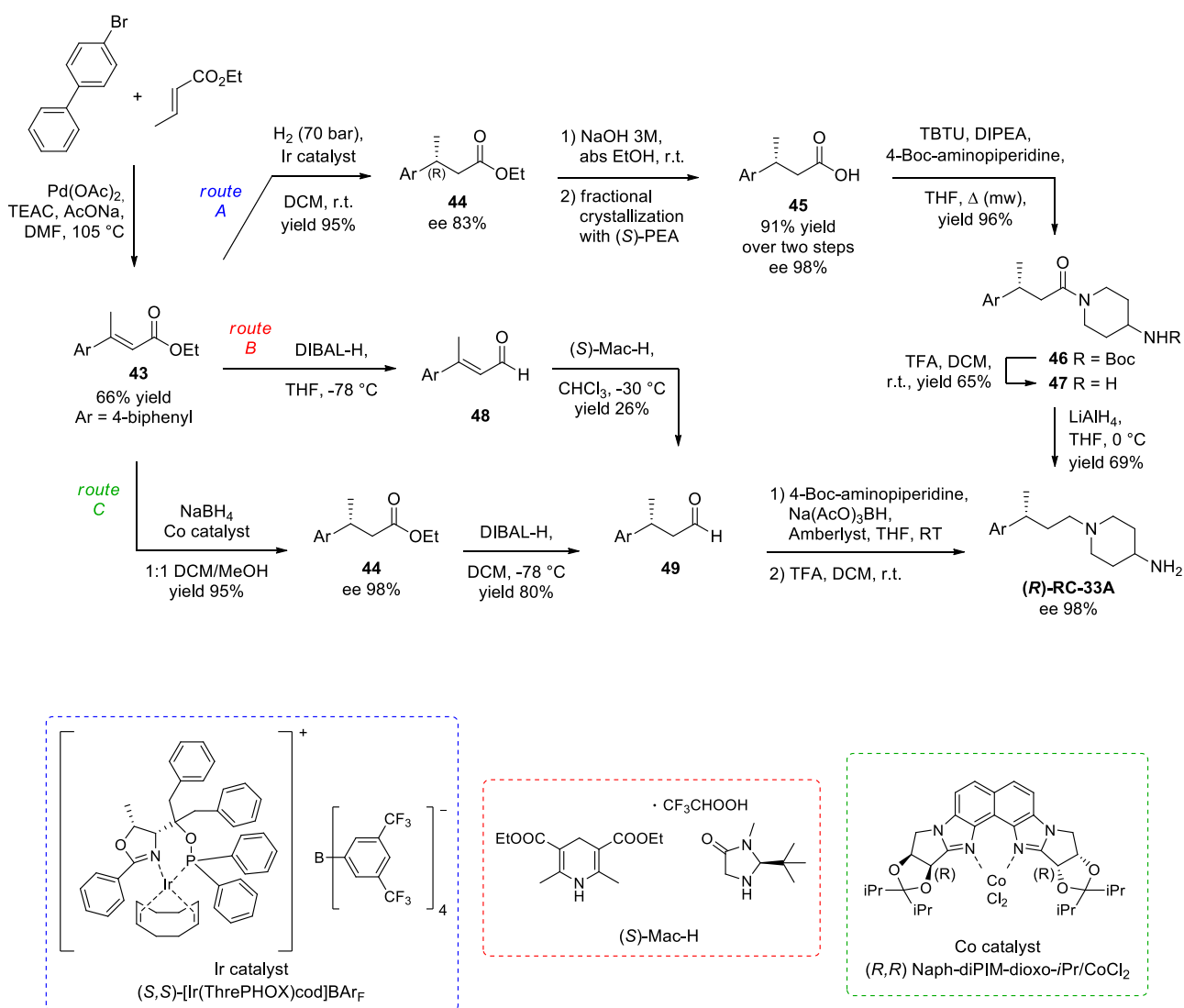
Scheme 5. Retrosynthetic analysis. Compound (R)-RC-33A is the key intermediate for the obtainment of both homo- and hetero-bivalent ligands.

3.2 Synthesis of enantiopure compound (*R*)-RC-33A

The obtainment of enantiomerically pure products is a fundamental requirement in modern drug discovery and development, due to the different behavior each enantiomer can exhibit in chiral environments, such as human body. Depending on the stage of drug discovery process, different techniques and combinations thereof can be employed to obtain enantiopure compounds. Two main approaches can be identified: i) separation of racemates (through chromatography or crystallization) and ii) enantioselective synthesis (exploiting chiral auxiliaries, chiral pool, chiral catalysts, or biocatalysis). In some cases, an integrated approach based on combination of different techniques gives the best results. A detailed review on the methods for obtaining enantiopure compounds during the drug discovery process can be found in Paper 4 (Appendix, page 173).

Three different synthetic pathways (route A, B and C in **Scheme 16**) have been explored for the obtainment of key intermediate (*R*)-RC-33A in suitable amount and chiral purity for the characterization and evaluation of the designed bivalent ligands. As reported in **Scheme 16**, the investigated synthetic strategies have the first step in common, consisting in a Heck reaction between 4-bromobiphenyl and ethyl crotonate. This reaction was performed under Jeffery conditions, *i.e.* with a tetraalkylammonium salt in absence of phosphine ligands²⁰⁵. Tetraethylammonium chloride is used here as a phase-transfer catalyst to improve the yield and accelerate the rate of the reaction. Moreover, Pd(OAc)₂ microencapsulated in polyurea matrix (Pd EnCat®) was used as catalyst, in order to facilitate work-up procedure and limit Pd contamination in products. Consistently with the typical Heck reaction stereoselectivity, the trans α,β -unsaturated ester **43** is obtained as the major product. Identification of the cis/trans products was based on previous works on analogous compounds²⁰⁶. At this point, the first pathway explored is route A (**Scheme 16**), which is based on the protocol already developed for the gram-scale synthesis of (*R*)-RC-33²², properly adapted to access the new target compound. The subsequent enantioselective reduction of the double bond is the key step for the introduction of the chiral center with the desired configuration. The reaction is carried out in a Parr multireactor using the chiral Ir catalyst (*S,S*) Ir(ThrePHOX) under 70 bar of hydrogen pressure at room temperature. Under optimized condition, the saturated ester **44** is obtained with 83% enantiomeric excess (ee). With the aim to enhance chiral purity to a degree suitable for biological investigations, ester **44** is hydrolyzed to the corresponding acid, which undergoes fractional crystallization with (*S*)-phenylethylamine ((*S*)-PEA) in MeOH/H₂O 1:1. This protocol resulted more efficient than the one previously reported for the synthesis of (*R*)-RC-33, in which cinchonidine was used as resolving agent and the crystallization solvent was acetone/H₂O 1:1. In detail, the diastereomeric salt (*S,S*)-**45**·PEA crystallizes as white needles, whereas (*R,S*)-**45**·PEA remains in the mother liquors. For this reason, multiple subsequent crystallizations were needed to

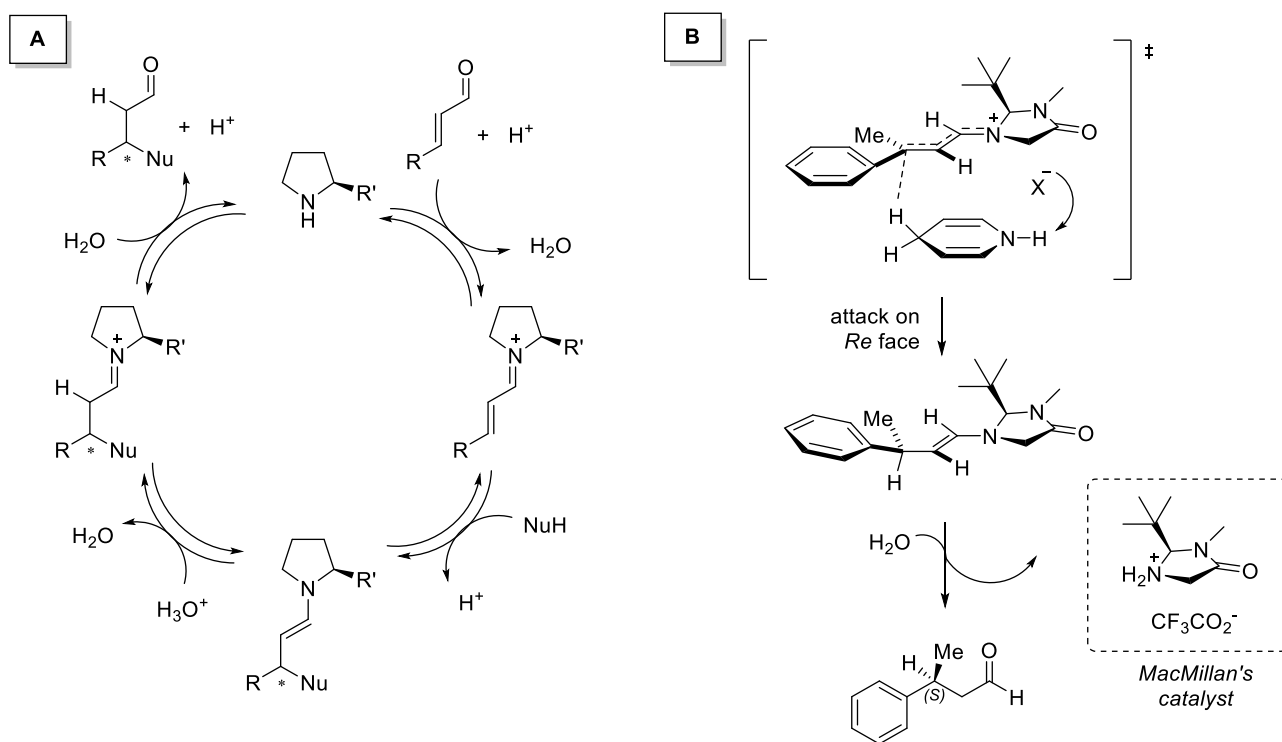
reach the desired chiral purity. The process was monitored by chiral HPLC: after 5 crystallizations, 1.2g of (*R,S*)-**45**·PEA with 94.5% ee and 1.8g of (*R,S*)-**45**·PEA with 98.4% ee were obtained starting from 5g of diastereomeric salt. Free acid **45** (94.5% ee) was then subjected to amidation with 4-Boc-aminopiperidine in the presence of condensing agent 2-(1H-Benzotriazole-1-yl)-1,1,3,3-tetramethylammonium tetrafluoroborate (TBTU). The reaction was performed under microwave (mw) irradiation to easily and quickly access the desired product with high yield. Upon deprotection with trifluoroacetic acid (TFA), amide **46** is subjected to reduction with LiAlH₄. Key intermediate (*R*)-RC-33A is thus obtained with retainment of enantiomeric excess, as confirmed by chiral HPLC.



Scheme 16. Synthesis of key intermediate (*R*)-RC-33A.

With the aim of optimizing the synthesis of RC-33A, an alternative strategy was explored (route B). The key step of this new pathway is the organocatalytic enantioselective reduction of α,β -unsaturated aldehyde **48** to the corresponding saturated product **49**. From the pioneering study published by Hajos and Parrish in 1973, organocatalysis has now become one of the most promising approaches for the obtainment of chiral

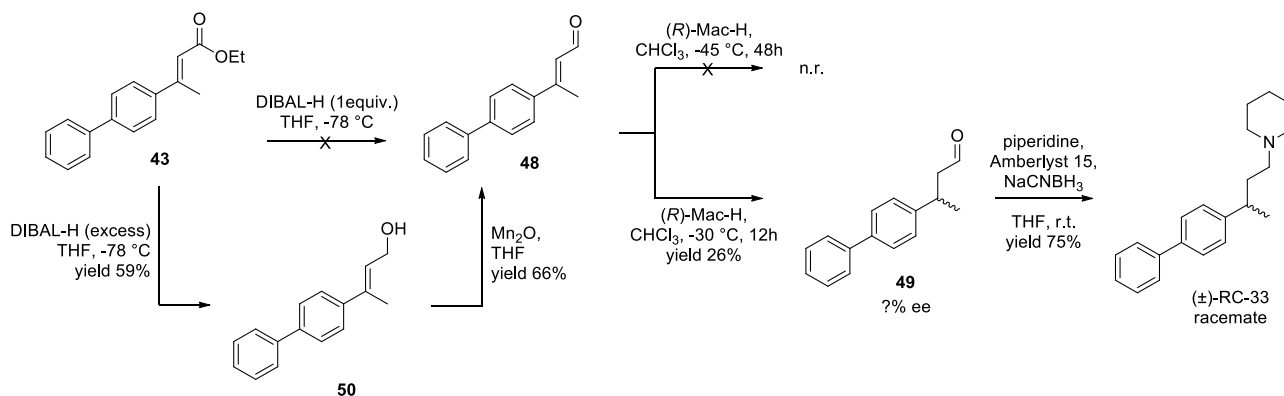
molecules. This approach employs small organic compounds as catalysts, which contain specific functional groups to activate the substrate and special stereo-structures responsible for the stereinduction. Organocatalysis offers several advantages, such as affording asymmetric induction without the use of metal catalysts. Moreover, the scope and generality of suitable reactions is really large, and more than one stereocenters can be generated efficiently in a single pot operation (domino or cascade organocatalysis), although the reactivity of organocatalyst may be lower compared with metal-catalysis, requiring 10-40 mol% of catalyst loading. The use of chiral pyrrolidine derivatives for the stereocontrolled β functionalization of α,β -unsaturated carbonyl compounds (**Scheme 17, A**) constitute an important part of organocatalysis that has been extensively studied and exploited in organic synthesis²⁰⁷. From a mechanistic point of view, the electronic redistribution induced by the iminium intermediates produces a LUMO-lowering effect that facilitates nucleophilic additions, including conjugate additions and pericyclic reactions and enabling the asymmetric introduction of several nucleophiles to the β position.



Scheme 17. A) General representation of the aminocatalytic cycle for the β functionalization of α,β -unsaturated carbonyl compounds *via* iminium activation. B) Transition state involved in asymmetric induction with MacMillan's catalyst.

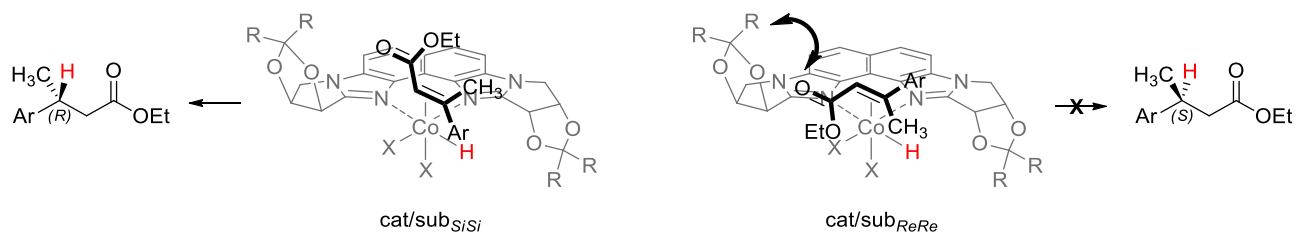
In our case, the reaction to be performed is an enantioselective reduction of the C-C double bond through hydrogen transfer from a dihydropyridine derivative (Hantzsch ester). Such reaction was reported by MacMillan, who demonstrated its high performance in terms of yield and stereocontrol (ee >90%)²⁰⁸. The reaction is performed with the chiral imidazolidinone shown in **Scheme 17** (MacMillan's catalyst), which is purchasable in mixture with the Hantzsch ester under the trade name (*S*)-Mac-H. Another interesting aspect

of this reaction, which prompted us into exploration of its feasibility, is its remarkable enantioconvergence: the authors reported that the product configuration is determined only by the catalyst configuration, independently from the *E/Z* isomerism of the starting material. This represents a significant advantage for our synthesis, since it means that the *Z* isomer of ester **43**, which is inevitably obtained as minor product during Heck arylation, can be recovered. Considering this feature, along with the easier and safer protocol respect to route A (avoidance of transition metals and high-pressure H₂ gas) and the excellent enantiomeric excesses reported in literature, we decided to apply this strategy to our substrate. Notably, route B involves only four synthetic steps starting from ester **43**, whereas route A requires five synthetic steps and a fractional crystallization. The first reaction of the new pathway is therefore the reduction of *E* ester **43** to the corresponding aldehyde with diisobutylaluminium hydride (DIBAL-H). The reaction was performed using one equivalent of reducing agent, at -78 °C, to avoid over-reduction. Unfortunately, allylic alcohol **50** was obtained as sole product, in very low yield. Considering that the outcome of such reactions is often aleatory, especially in the case of conjugated esters, we decided to add DIBAL-H in excess to push the reaction toward complete reduction to allylic alcohol **50** and then to oxidize it to aldehyde with Mn₂O (Scheme 18). In this phase we were not concerned about optimizing this step as our main goal was to obtain aldehyde **48** for testing the feasibility of the organocatalytic reaction. Accordingly, once the α,β -unsaturated aldehyde was obtained, scouting reactions with MacMillan's catalyst were performed. Since (*R*)-Mac-H was already available among our supplies, we employed this catalyst at first, although it was expected to give the saturated aldehyde with the *S* configuration. We started performing the reaction at -45 °C in chloroform with 20 mol% of imidazolidinone and 1.2 equivalent of Hantzsch ester. Under these conditions, no consumption of the starting material could be appreciated, even after 48 hours. A second experiment was then performed, raising the temperature to -30 °C. After 12 hours, TLC analysis showed the appearance of a new product, although the starting material was not completely consumed. The reaction was stopped anyway to evaluate identity and chiral purity of the product. After purification, ¹H-NMR analysis confirmed the obtainment of aldehyde **49**. Since a validated chiral HPLC method was not available for this compound, we opted for a smooth conversion of the aldehyde to RC-33 *via* reductive amination with piperidine, in order to access a product already well-characterized. The experimental conditions can be summarized as follows: Chiralcel OJ-H (4.6 mm I.D. x 250 mm L, ps = 5 μ m); eluent: MeOH/Et₂NH, 100:0,1, (v/v); flux: 0,5 mL/min (λ =250nm). Unfortunately, the chromatogram showed that the obtained product was a racemic mixture. Additional experiments were performed on *Z* aldehyde and on a mixture of *E/Z* aldehydes, obtaining superimposable results. Therefore, we concluded that organocatalytic reduction with MacMillan's catalyst takes place without stereocontrol on our substrate.



Scheme 18. Exploration of synthetic route B.

Lastly, route C was explored. Similarly to route A, this pathway involves enantioselective reduction of conjugated ester **43** to the saturated derivative **44**. In this case, the asymmetric 1,4-reduction is catalyzed by a diamidine cobalt complex developed by Kitamura's group (Naph-diPIM-dioxo-R, **Scheme 19**)²⁰⁹. The advantages of the new protocol are: i) the easier and safer protocol (the reaction exploits NaBH₄ as reducing agent, instead of H₂ gas at high pressure) and ii) the higher enantioselectivity compared to the Ir-catalyzed reduction. In particular, this last feature would bring an additional advantage to route C: obtainment of ester **44** with suitable ee would allow to adopt a strategy similar to route B (*i.e.* reduction to aldehyde followed by reductive amination), avoiding conversion to acid and fractional crystallization. Investigation of this new synthetic pathway was made possible by availability of Co chiral catalyst, kindly provided by prof. Kitamura, at the Institute of Pharmaceutical and Medicinal Chemistry of Münster, where I spent part of my PhD. The synthesis of this family of catalysts, which are not commercially available, has been reported in recent publications²¹⁰, as well as its versatility and efficiency: for example, it has been used for the optimization of the synthesis of Fluspidine, a potent and selective 51R antagonist developed by Wünsch²¹¹. For the synthesis of (*R*)-RC-33A, the (*R,R*)-Naph-diPIM-dioxo-*i*Pr/CoCl₂ complex was used to access the desired (*R*)-**44** enantiomer with high yield and excellent chiral purity (ee 98%), as confirmed by HPLC analysis. The experimental setup is simple, the reaction quick and clean; moreover, the use of ligand with the opposite configuration gave the (*S*) isomer of **44** with comparable yield and enantioselectivity. From a mechanistic standpoint, it has been proposed that the Naph-diPIM-dioxo-*i*Pr-CoH_{*n*} (with *n*=1 or 2) species is generated from the Co^{II}Cl₂ precursor by the action of NaBH₄, and that the hydride is delivered to C3 of the conjugated ester in a 1,4-addition manner by a two-electron-transfer mechanism. Steric hindrance of the dioxolane ring on the (*R,R*) ligand favors the formation of cat/sub_{*SiSi*} complex rather than cat/sub_{*ReRe*}, yielding (*R*)-**44** as major product.



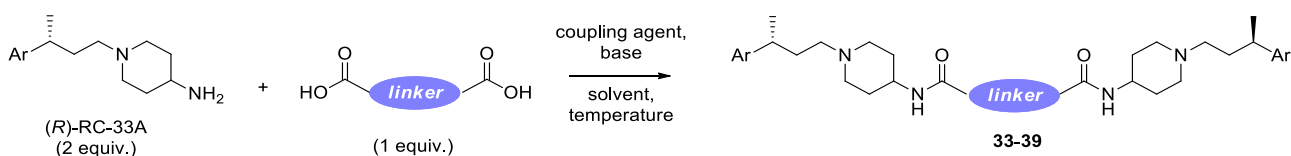
Scheme 19. Proposed rationalization of the observed enantioselectivity: the catalyst/substrate complex $\text{cat}/\text{sub}_{\text{SiSi}}$ is sterically favored. R = *i*Pr, Me or H; Ar = biphen-4-yl.

The subsequent reduction of ester **44** with DIBAL-H gave aldehyde **49** in satisfying yield, in contrast to what it was observed for the attempted reduction of α,β -unsaturated ester **43** to the corresponding aldehyde **48** (**Scheme 18**). The final steps to obtain (*R*)-RC-33A with route C are currently under investigation: these consist in a reductive amination with 4-Boc-aminopiperidine and subsequent deprotection. If the experiments will prove successful, route C will result the most convenient synthetic pathway for the obtainment of (*R*)-RC-33A.

3.3 Synthesis of bivalent ligands

With key intermediate (*R*)-RC-33A in hand, we moved forward to the preparation of the designed ligands. Acetamide derivative **32** was easily obtained by treating (*R*)-RC-33A with acetic anhydride, whereas for compounds **33-39** different coupling reagents (e.g. DCC, EDC, PyBroP, TBTU, COMU) and reaction conditions were explored in scouting reactions. The general procedure involves activation of acidic moieties with a condensing agent, followed by addition of two equivalents of (*R*)-RC-33A. Optimal conditions for the obtainment of each final compound are reported in **Table 3**.

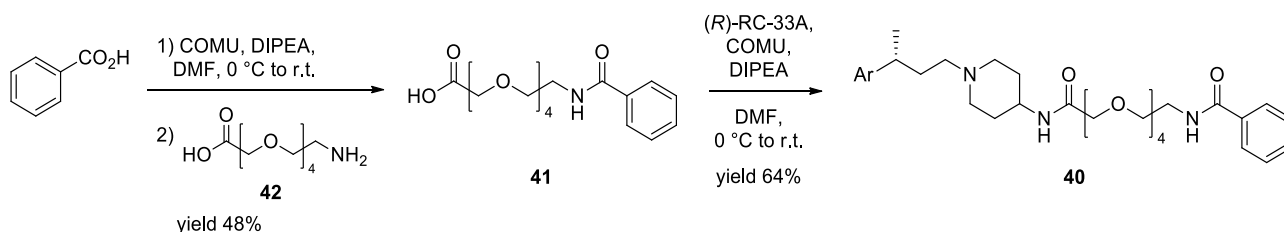
Table 3. Reagents and conditions for the final step in the synthesis of homo-bivalent ligands **33-39**. Ar = Biphen-4-yl; mw = microwave irradiation; (a) the reagent employed is the corresponding acyl chloride; (b) the reagent employed is the corresponding anhydride.



Cmpd	linker	coupling agent	base	solvent	temperature	Yield
33	CH ₂	TBTU	DIPEA	CH ₃ CN	r.t.	63%
34	(CH ₂) ₃	TBTU	DIPEA	CH ₃ CN	mw: 90 °C, 50 W, 5x10 min	32%
35	(CH ₂) ₅	TBTU	DIPEA	CH ₃ CN	mw: 90 °C, 50 W, 5x10 min	59%
36	CH ₂ OCH ₂ ^a	-	Et ₃ N	CH ₂ Cl ₂	r.t.	94%
37	(CH ₂ OCH ₂) ₂	COMU	DIPEA	DMF	0 °C to r.t.	40%
38	CH ₂ (CH ₂ OCH ₂) ₉ CH ₂	COMU	DIPEA	DMF	0 °C to r.t.	59%
39	1,2 phen ^b	TBTU	DIPEA	THF	mw: 120 °C, 50 W, 5x10 min	28%

Uronium salts resulted the best performing condensing agents: compounds **33-35** and **39** were obtained using TBTU, whereas for compounds **37** and **38** COMU was employed. Compound **36** was obtained without the need of such coupling reagents because the commercially available acyl chloride derivative of the linker was employed.

Hetero-bivalent compound **40**, on the other hand was obtained through the convergent synthesis reported in **Scheme 20**.



Scheme 20. Synthesis of hetero-bivalent compound **40**.

To avoid protection/deprotection steps, benzoic acid is first activated with COMU (1), then amino-PEG4-acid linker **42** is added (2) to yield compound **41**. This is then reacted with (*R*)-RC-33A to give target product **40**. Identity of all final products was confirmed by ¹H and ¹³C NMR analysis and their purity was determined *via* HPLC. Assessment of their ee is currently ongoing, through the development of a proper chiral HPLC method. Nevertheless, it is reasonable to assume that chiral purity obtained for (*R*)-RC-33A is retained during the last synthetic step, considering that (i) final compounds retained the levorotatory optical activity observed for intermediates **44-47** and (*R*)-RC-33A, and (ii) coupling with the linker involves the primary amine, which is distant from the chiral center, and the reaction conditions are not too harsh to cause a racemization. To further verify the retainment of the configuration, X-ray crystallography on some representative bivalent compound, such as **33**, was taken into consideration. In the attempt to obtain single crystals suitable for this technique, vapor diffusion was selected as the most promising crystallization technique, and different binary solvent systems (e.g. CHCl₃/Et₂O, CHCl₃/acetone, CHCl₃/petroleum ether) were investigated. Further improvements are needed in order to grow crystals that are fit for purpose.

3.4 Biological evaluation of bivalent ligands

Once compounds **32-40** were obtained in suitable amount and purity, competition experiments with radioligands were performed to determine binding site affinities toward S1R. The test was performed using homogenized guinea pig cerebral cortex membranes, in the presence of [³H]-(+)-pentazocine, as a potent and selective S1R radioligand. Nonspecific binding values were determined using non-radiolabeled (+)-pentazocine and haloperidol in excess (as described in *Experimental Section*). Compounds with high affinity were tested three times. For compounds with low S1R affinity, only one measure was performed. Moreover, compounds considered most promising ($K_i < 200\text{nM}$) were also tested on S2R to evaluate their receptor subtype selectivity. For S2R, homogenized rat liver membranes were adopted to evaluate the binding values, employing [³H]-DTG and non-tritiated (+)-pentazocine to mask the S1R. Moreover, a high concentration of non-tritiated DTG was used to determine nonspecific binding values. The results are reported in **Table 4**, along with the K_i values of parent compound (*R*)-RC-33.

Table 4. Binding affinities of compounds **32-40** toward S1R. K_i values are reported with standard error of the mean (SEM) for compounds tested three times; (a) data retrieved from literature¹⁶³; (b) compound tested as hydrochloride salt to improve its solubility.

cmpd	type	spacer	K_i S1R (nM)	K_i S2R (nM)
(<i>R</i>)-RC-33 ^a	reference cmpd	-	1.8 ± 0.1	45 ± 16
32	acetamide	-	11 ± 4	206
33	homo-bivalent	CH ₂	200 ± 16	Inhibition 0%
34^b		(CH ₂) ₃	622	-
35^b		(CH ₂) ₅	1300	-
36		CH ₂ OCH ₂	Inhibition 0%	-
37		(CH ₂ OCH ₂) ₂	2.6 ± 0.6	46
38		CH ₂ (CH ₂ OCH ₂) ₉ CH ₂	799	-
39		1,2 phenyl	134	6600
40		hetero-bivalent	(CH ₂ OCH ₂) ₄	1600

The K_i values of the smallest ligand of the series, acetamide **32**, show only a modest increase respect to RC-33. This result confirmed our hypothesis that the 4-position of the piperidine ring can be derivatized without significant loss in affinity. However, when derivatization leads to an important change in ligand's dimension – as in the case of bivalent ligands – the resulting binding profile can be more difficult to predict. Both length

and nature of the linker seem to be strongly important in determining affinity toward the receptor. For example, compound **35** bears a linker quite similar in length to that of compound **37**, but the difference in their K_i values is almost three orders of magnitude. In particular, compound **37** is endowed with excellent affinity, comparable to that of our lead compound (*R*)-RC-33 (2.6 nM and 1.8 nM, respectively), which is remarkable for a ligand of that size. Our hypothesis is that compound **37** is able to stabilize the “open” conformation of the binding pocket, *i.e.* those conformational changes that allow ligands to enter and exit the active site. Other bivalent compounds show affinities ranging from modest to low. Interestingly, hetero-bivalent ligand **40** shows a micromolar K_i value. The absence of a second pharmacophore able to interact with the receptor might be the main reason behind this drastic drop in affinity.

Further biological investigations are needed to get a clearer picture of the behavior of our compounds. In particular, functional assays such as NGF-induced neurite outgrowth assay could be the key to evaluate agonism profile of our ligands and the potential enhancement in neuroprotective effect.

To rationalize the results obtained so far, modelling studies were performed on both mono- and bi-valent ligands.

3.5 Computational studies

The recent publication of the first S1R crystal structure was essential for the development of computational studies aimed at better understanding ligand-receptor interactions. Nevertheless, even this milestone left some unanswered questions. First of all, the authors reported that no significant difference could be identified in the 3D-structure of the receptor co-crystallized with two chemically divergent ligands (i.e. antagonist PD 144418 and agonist/inverse agonist 4-IBP). Hence, it was not possible to determine what structural elements and which interactions in the binding pocket are responsible for the agonism and antagonism of small molecules. Secondly, the binding site is not exposed to the solvent. Although this fact accounted for the slow kinetics of ligands binding to S1R, it was unclear how small molecules could access this highly occluded region. During our research, we started from investigation of the interactions of model compound RC-33 and its monovalent analogs with the S1R binding site. Overall, 80 compounds reported in recent publications by our group were selected for this first task (see *Experimental Section*, **Table 5**)^{212–215}. These molecules were originally designed on the basis of the pharmacophoric model proposed by Glennon²⁹, and therefore they share some common structural features (**Figure 17**). Compounds were docked into the active site of S1R crystal structure bound to PD144418 (PDB code: 5HK1) by using the software Glide from the Schrödinger suite. Several poses were obtained for each compound, and both scoring energies (i.e. glide score) and information of PD144418 and 4-IBP crystallographic structures helped to select the best solutions. The results showed how Glennon's pharmacophore is oriented within the S1R binding site and confirmed the key importance of electrostatic interaction between the charged amino group of the ligands and the side chain carboxylate group of the residue Glu172, since the best docking solution for most compounds gave this interaction. The best docking poses of RC-33 and its derivatives resulted superimposable with orientations of the co-crystallized ligands. In particular, docked ligands placed their larger hydrophobic groups near the so-called primary hydrophobic site (delimited by residues Val84, Met93, Leu95, Leu105, Tyr206, Ile178, Leu182, and Tyr103), while their smaller hydrophobic groups locate near the secondary hydrophobic site (residues Phe107, Trp164, His154, and Ile124). Best poses obtained from docking experiments, along with experimental K_i value of each compound, served as the basis for the development of 3D-QSAR models to explain the SAR of the RC-33 analogs. These studies originated as side-project during the development of this thesis, hence they will be discussed only briefly herein. The bioactive conformations predicted by docking were used as the alignment rule for deriving the models. The structural features that affect ligands' activities on S1R were identified by describing steric and electrostatic fields. Fields variables were calculated and processed to construct different 3D-QSAR models. The most accurate model resulted the one combining both steric field, as major contribution (88%), and electrostatic field. This is reasonable considering that the S1R binding site is mostly hydrophobic. In particular, bulky groups are desired in the bigger hydrophobic region –

near residues Tyr103, Tyr206, Thr202 – and in the region delimited by Val84, Trp89, Phe107, Ala185, where RC-33 places its methyl group. Another bulky moiety can be placed in the space near residues Tyr120, Ser117, Trp164, (where the piperidine of RC-33 is placed in the docked structure) although regions where steric hindrance disfavor affinity are also present in the neighboring space, reflecting the complexity of the steric field inside the binding pocket. The electrostatic field, on the other hand, contributes to a lesser extent to the model: smaller regions where an increase in positive charge enhance or diminishes ligands' activity are present in the bigger hydrophobic region. For a more detailed description of these studies, which did not include bivalent ligands, please refer to Paper 5 (Appendix, page 191).

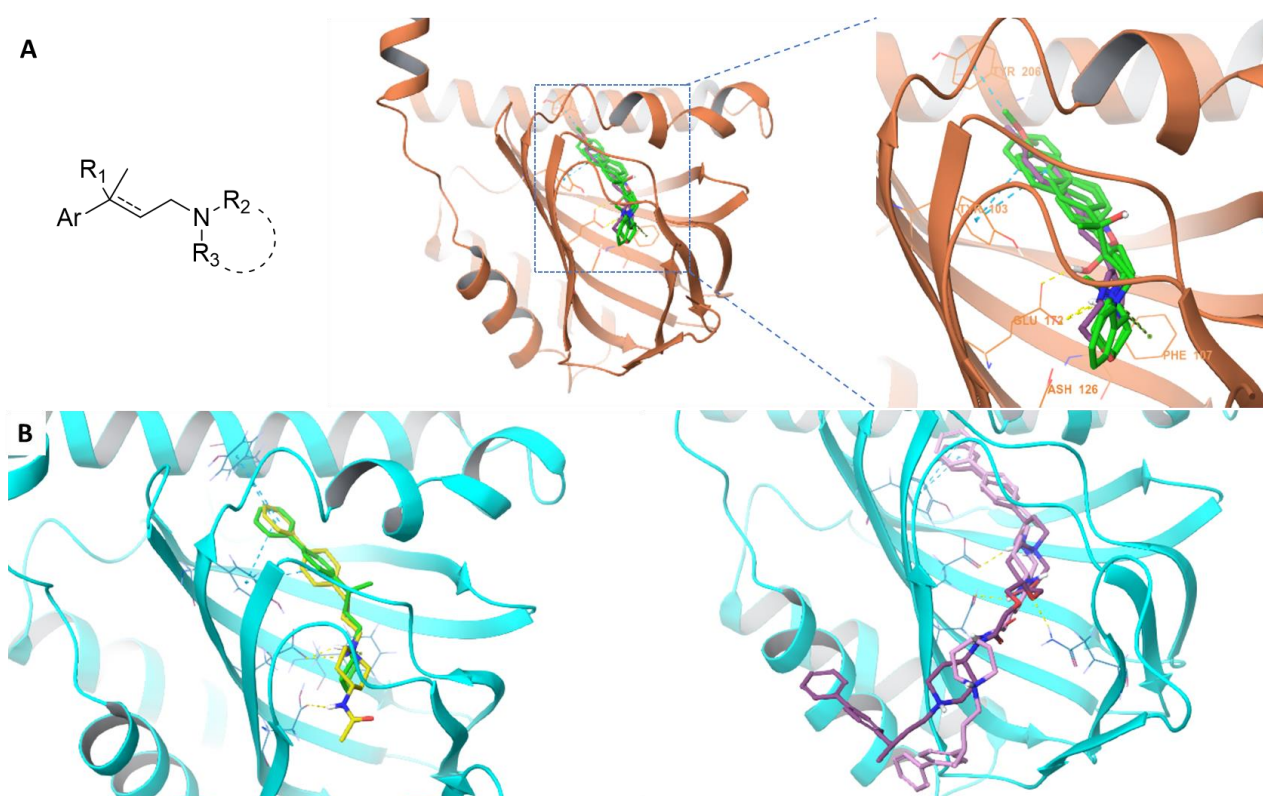


Figure 17. **A** Docking poses of some representative S1R ligand. In green are reported those which general structure is indicated in the Figure and that were used to perform 3D-QSAR studies. In purple is depicted co-crystallized PD144418. All docked compounds show poses similar to PD144418. **B** On the left are reported the docking poses of (*R*)-RC-33 (green) and its acetamide derivative **32** (yellow), on the right are shown the docking poses of **34** (pink) and **37** (purple).

Overall, the most active ligands (*i.e.* those with low experimental K_i values) share a high degree of similarity in the predicted binding poses, which are also similar to the binding mode of the co-crystallized ligands (Figure 17). In particular, it is worth noting that the docking pose of (*R*)-RC-33 and the 3D-QSAR model suggest that derivatization at 4-position of the piperidine nucleus is a good strategy for the obtainment of bivalent ligands. In fact, this portion, which is located in the small hydrophobic region, tolerates bulky groups and points toward one of the postulated pathways for the access to the binding pocket (the one leading to the cytosolic side and occluded by residues Gln135, Glu158, and His154). This intuition was further confirmed by the good binding profile of acetamide derivative **32** (K_i S1R = 11 ± 4 nM), indicating that insertion of an

additional moiety in that position does not compromise receptor's affinity. The pathway between the small hydrophobic region and the cytosol could therefore accommodate a linear chain serving as linker to tether two RC-33 units, as originally envisaged. Accordingly, bivalent ligands were oriented with one end superimposed to the docked (*R*)-RC-33 and the linker occupying the aforementioned region, then macromodel minimization was performed to allow structural rearrangements of the receptor. The output was used to generate a grid box to dock the bivalent ligands. The obtained poses showed that while one extremity of the bivalent ligand fits well into the binding pocket, the other end can barely reach the solvent, meaning that the linkers are too short to reach two different binding sites. The only exception is compound **38**, which is characterized by a very long PEG9 linker. However, it must be noted that every S1R crystal published up to date consists in a trimer, meaning that the precise architecture of dimer and the distance between two binding pockets in this form are still unknown. Moreover, the bivalent ligands developed during this project can be exploited to study how molecules enter the binding site. Particularly, compound **37** exhibited an excellent binding affinity, suggesting that it might stabilize the open conformation of the receptor. To shed light on these intriguing aspects, further investigations involving molecular dynamics simulations are ongoing. These computations are particularly demanding due to the receptor's dimension and the entity of the conformational changes, but we are confident that they will result in important contribution to this research field. Our first paper on the use of bivalent S1R ligands to study receptor's dimerization is currently under review (see Paper 6, Appendix, page 212).

3.6 Discussion

S1R is known to be able to form complexes with many different proteins. However, homo-oligomerization still represent a poorly understood phenomenon. Accumulating evidence suggest that agonists binding promotes formation of low molecular weight species (i.e. monomers and dimers), whereas antagonists shift S1R structure toward higher order oligomers. Nevertheless, the exact molecular mechanism that relates agonism/antagonism to the oligomerization state is still unknown. Considering that S1R agonists exert neuroprotective effects and bias S1R toward dimeric form, we hypothesized that promoting dimerization through bivalent agonists might enhance ligand's activity and biological function of S1R dimers. The designed ligands are based on two (*R*)-RC-33 scaffolds tethered by a linker. The synthesis of such compounds required the obtainment of key intermediate (*R*)-RC-33A in enantiopure form for two reasons: (i) although RC-33 interaction with S1R is not stereoselective, the (*R*) enantiomer was identified as the most stable in biological matrices; (ii) since coupling two RC-33-like scaffolds with a linker implies doubling the chiral centers, using one enantiomer instead of the racemic mixture avoids having a mixture of different entities and the related complication in their isolation and characterization. Accordingly, different approaches (enantioselective metal catalysis, organocatalysis, fractional crystallization) have been explored to identify the most efficient route to access enantiopure (*R*)-RC-33A. The synthetic pathway involving the Co-catalyzed asymmetric 1,4-reduction of ester **43** resulted the best strategy. Thereafter, scouting reactions for the final coupling of the di-acidic linkers with (*R*)-RC-33A have been performed to find the optimal conditions for each target compound. Once the synthetic feasibility of our approach was confirmed, we took advantage of the recent publication of the S1R crystal structure to perform computational studies on our bivalent ligands. At first, docking experiments on RC-33 and its monovalent analogues were performed. These served both to observe how such molecules are oriented within the binding pocket and to elaborate a 3D-QSAR model, which is reported in Paper 5 (Appendix, page 191). We found that the piperidine ring of RC-33 points toward one of the putative pathways to access the occluded binding site, suggesting that the general design of our bivalent ligands, with the linker tethering two RC-33 from the piperidine side, have good chances to be effective in promoting dimerization. Docking of the bivalent ligands revealed that, although one extremity can fit well into the active site, the linkers initially designed are probably too short to reach two binding pockets. A precise estimate of the optimal linker length is difficult, because every S1R crystal structure available so far consists in a trimer with occluded binding pockets. Therefore, the architecture of S1R dimeric form and the conformational changes involved in the binding site opening are unknown. Taking into account these considerations we decided to expand our library introducing a small monovalent analog of RC-33 (compound **32**), a ligand with longer PEG linker (compound **38**, see **Figure 18**) and one hetero-bivalent ligand (compound **40**). Moreover, we set molecular dynamics experiments to get clearer information on possible receptor's

conformational rearrangements during ligands binding. In particular, we reasoned that even shorter bivalent ligands could be exploited in these studies to understand how molecules reach the occluded binding pocket. However, to get reliable information, comparison with experimental binding affinity is necessary. Accordingly, the whole library was tested through binding assays using radiolabeled (+)-pentazocine. Bivalent ligand **37** exhibited the highest affinity ($K_i = 2.6$ nM), comparable to that of model compound (*R*)-RC-33. We hypothesize that **37** is able to bind the receptor's pocket in its open conformation, since the linker seemed too short to join two binding sites. Compound **32** also showed a good binding affinity, confirming that derivatization on the piperidine portion of (*R*)-RC-33 allows to retain key interaction with the binding site of S1R. In contrast, hetero-bivalent ligand **40** exhibited a very low affinity, suggesting that the presence of two RC-33 scaffolds is crucial for interaction with the receptor. The computational and experimental evaluation of the simplest bivalent ligand (compound **33**), as well as comparison with (*R*)-RC-33 and PD144418, is reported in a paper currently under revision (Paper 6, Appendix, page 212). Further *in silico* studies, on the whole compound series, are ongoing, as well as functional assays to define the agonist profile. We are confident that the results obtained from these investigations will be a significant contribution into better understanding S1R molecular mechanisms underpinning agonism and oligomerization.

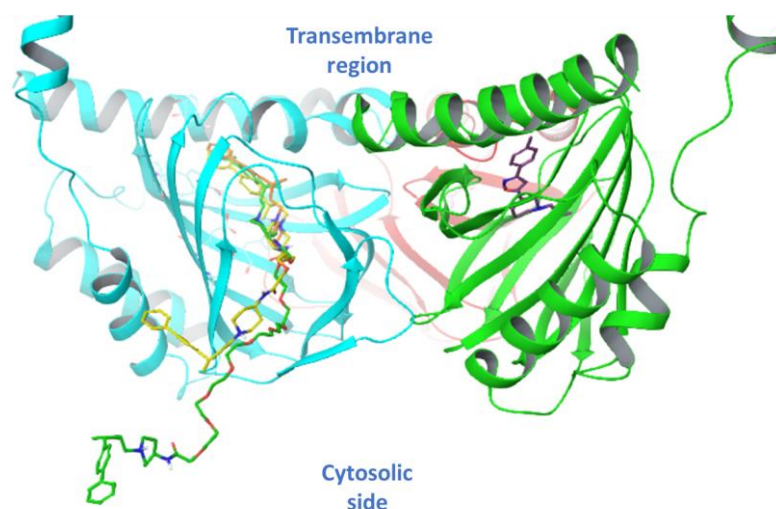


Figure 18. Docking of model compound (*R*)-RC-33 (orange) and bivalent ligands **37** and **38** (yellow and green, respectively) inside one of the monomers that build up the trimeric crystal structure (each monomer is represented in different colors, and co-crystallized ligands are shown in purple).

4. Conclusions

The first main objective of my research project concerned the preparation of novel multitarget directed ligands potentially useful to counteract neurodegenerative diseases through modulation of selected targets – namely S1R, AChE and NMDA – and endowed with antioxidant properties. To achieve this goal, a compound library of 31 arylalkylaminoketones was prepared in a quick and efficient way, exploiting a divergent approach based on Weinreb ketone synthesis. The common scaffold brings the pharmacophoric elements of RC-33 (S1R agonist), Donepezil (AChE inhibitor), Ifenprodil (NMDAR inhibitor) and Curcumin (natural antioxidant). The ability of the designed compound to cross the BBB was assessed *in silico* through a well-established method (Wager *et al.* model). The preliminary biological investigation consisted in assessment of their binding profile through displacement binding assays. Specifically, affinity toward S1R, S2R and NMDAR was evaluated using radioligands. Conversely, inhibition of AChE was evaluated spectrophotometrically. It emerged that more than half of the compound library displayed a good S1R affinity ($K_i < 50$ nM) and selectivity over S2R. Fewer compounds showed a promising activity on NMDA receptor and AChE. Those showing a good multi-target profile were selected for further investigations, which concerned the evaluation of antioxidant activity: DPPH assay allowed to determine intrinsic free radical scavenging properties, whereas tests on HeLa cells indicated Aquaporins-mediated effects on water and H₂O₂ permeability. Interestingly, some of the tested compounds resulted effective in counteracting oxidative stress conditions. Docking studies on S1R and AChE showed that compounds with higher affinity are predicted to assume poses similar to that of parent compounds (*i.e.* RC-33 and Donepezil). Notably, the carbonyl group does not interfere with S1R binding in the active site. Hence, this moiety could be exploited in the design of novel MTDLs with improved binding profile toward NMDA receptor. To address this task, an in-depth computational study will be needed, to determine key interactions inside the broad NMDAR binding site. To sum up, the prepared compound library allowed to identify a number of compounds (e.g. **2**, **4**, **17**, **23-25**) endowed with a promising combination of affinity towards S1R, NMDAR, anti-AChE and antioxidant activity. The results obtained so far were reported in a recent publication (see Paper 3, Appendix). Further biological investigation will hopefully pave the way for achievement of viable therapeutic candidates for the treatment neurodegenerative disorders.

The second objective of this thesis was the development of bivalent S1R ligands, as viable tools for studying the receptor's dimerization process and its physiological role. The homo-bivalent ligands were designed as two units of (*R*)-RC-33 joined by a linker, which can vary in length, hydrophilicity and spatial constraint. To obtain such compounds, an amide coupling between a di-acidic linker and two equivalents of (*R*)-RC-33A was envisaged. Three different synthetic approaches have been explored to access this key intermediate (an

amine derivative of RC-33) in enantiomerically pure form. As a result, a quick, stereoselective and efficient synthetic protocol was set up. After exploration of different coupling agents and reaction conditions, optimal procedures for the obtainment of the designed homo-bivalent compounds were identified. One hetero-bivalent ligand and the acetamide derivative of RC-33 were also prepared to gather additional information. From the subsequent binding assays, two compounds (**32** and **37**) emerged for their high affinity toward S1R ($K_i < 15$ nM). Furthermore, docking studies were carried out on both mono- and bi-valent S1R ligands to rationalize experimental results. From this work, a 3D-QSAR model was developed as reported in our recent publication (see Paper 5, Appendix). Further computational studies, involving molecular dynamics, are currently ongoing, as well as functional assays (*i.e.* evaluation of NGF induced neurite outgrowth). The results are expected to help understand molecular mechanisms at the basis of receptor's oligomerization and ligands' agonism/antagonism activities.

5. Experimental section

5.1 Laboratory materials and equipment

Reagents and solvents for synthesis, TLC and NMR were purchased from Sigma Aldrich. Silica gel for flash chromatography (60 Å, 230-400 Mesh) was purchased from Sigma Aldrich. Solvents were evaporated at reduced pressure with the Heidolph Laborota 4000 Efficient equipment. Analytical thin layer chromatography (TLC) analyses were carried out on silica gel pre-coated glass-backed plates (TLC Silica Gel 60 F254, Merk) impregnated with a fluorescent indicator, and visualised with the instrument MinUVIS, DESAGA® Sastedt-GRUPPE by ultraviolet (UV) radiation from UV lamp ($\lambda = 254$ and 366 nm) or by stain reagents such as Ninidrine and Cerium Molybdate. NMR were measured at room temperature ($15^\circ - 25^\circ\text{C}$) on a Bruker Advance 400 MHz spectrometer, using tetramethylsilane (TMS) as internal standard and a BBI 5 mm probe. All raw FID files were processed with Top Spin program from Bruker and the spectra analysed using the MestRenova 6.0.2 program from Mestrelab Research S.L. Chemical shifts are expressed in parts per million (ppm, δ scale). ^1H -NMR spectroscopic data are reported as follow: chemical shift in ppm (multiplicity, coupling constants J (Hz), integration intensity). The multiplicities are abbreviated with s (singlet), d (doublet), t (triplet), q (quartet), m (multiplet) and brs (broad signal). The chemical shift of all symmetric signals is reported as the centre of the resonance range. ^{13}C -NMR spectroscopic data are reported as follows: chemical shift in ppm.

5.2 General experimental details

Reactions performed under inert atmosphere were carried out with dry glassware, previously dried in oven or flamed with Bunsen burner, fitted with rubber septum, under an atmosphere of nitrogen or argon and with magnetic stirring. Liquid reagents, air-/moisture- sensitive and dry solvents were added using plastic syringes with metal needle, previously conditioned with nitrogen. Solid reagents were transferred opening the rubber septum under nitrogen or argon flow or solubilizing them in appropriate dry solvents. Low temperatures were reached either with a cryostat or with cooling agents, such as ice (0°C), mixture of ice, methanol and sodium chloride (-18°C), or mixture of solid carbon dioxide and acetone (-78°C) placed in a Dewar suitable for the reaction flask. Reactions at high temperature were performed in oil baths heated with heating plates and temperature control probes. Reactions conducted under microwave irradiation were performed in a microwave mono-mode oven, specific for organic synthesis (Discover® Lab-Mate instrument, CEM Corporate). Reactions' progress and ending were monitored by TLC; in addition, the final products were analysed with ^1H and ^{13}C Nuclear Magnetic Resonance (NMR).

5.3 Synthetic procedures

5.3.1 General procedure for the preparation of compounds II – III

To an aqueous solution of potassium carbonate (K_2CO_3 , 2.0 equiv.) was added diethyl ether (Et_2O) and N,O-dimethylhydroxyamine (NODMHA) hydrochloride (1.5 equiv.). The resulting mixture was cooled at 0 °C and then the corresponding acyl chloride (1.0 equiv.) was added dropwise. The reaction was let to reach room temperature and then it was stirred overnight. The reaction mixture was extracted with Et_2O ($2 \times 10mL$) and washed with water (10mL) and brine (20mL). The organic phase was dried (anhydrous sodium sulphate Na_2SO_4), filtered and, after removal of the solvent under reduced pressure, the pure compounds II – III were obtained.

3-Chloro-N-methoxy-N-methylpropanamide (II)

By following the General Procedure, starting from 3-chloropropanoyl chloride (127 mg, 1.00 mmol, 1.0 equiv.), K_2CO_3 (276 mg, 2.0 mmol, 2.0 equiv.), N,O-dimethylhydroxyamine hydrochloride (146 mg, 1.5 mmol, 1.5 equiv.), H_2O (3 mL) and Et_2O (3 mL), the desired product was obtained in 92% (139 mg) as a pale yellow oil. **1H -NMR** (500MHz, $CDCl_3$): δ (ppm) = 3.80 (t, J = 6.9 Hz, 2H, CH_2CH_2Cl), 3.70 (s, 3H, $NOCH_3$), 3.19 (s, 3H, NCH_3), 2.91 (t, J = 6.7 Hz, 2H, CH_2CH_2CO). **^{13}C -NMR** (125 MHz, $CDCl_3$): δ 170.8, 61.4, 39.2, 35.0, 32.0.

4-Chloro-N-methoxy-N-methylbutanamide (III)

By following the General Procedure, starting from 4-chlorobutanoyl chloride (141 mg, 1.00 mmol, 1.0 equiv.), K_2CO_3 (276 mg, 2.0 mmol, 2.0 equiv.), N,O-dimethylhydroxyamine hydrochloride (146 mg, 1.5 mmol, 1.5 equiv.), H_2O (3 mL) and Et_2O (3 mL), the desired product was obtained in a quantitative amount (yield >99.9%) (166 mg) as a bright yellow oil. **1H -NMR** (500MHz, $CDCl_3$): δ 3.70 (s, 3H, $NOCH_3$), 3.63 (t, J = 6.4 Hz, 2H, CH_2CH_2Cl), 3.18 (s, 3H, NCH_3), 2.62 (t, J = 6.7 Hz, 2H, CH_2CH_2CO), 2.11 (m, J = 6.9 Hz, 2H, $CH_2CH_2CH_2$). **^{13}C -NMR** (125 MHz, $CDCl_3$): δ 170.8, 61.4, 39.2, 35.0, 32.0.

5.3.2 General procedure for the preparation of compounds Ia-b, IIa-c and IIIa-b

To a solution of Weinreb amide (1.0 equiv.) in ACN, the corresponding amine (1.0 equiv.) and K_2CO_3 (1.5 equiv.) were added. The mixture was stirred overnight, at room temperature. In case of compound **Ib** the

mixture was stirred for 36h at room temperature; for compound **Ib** four days at room temperature were needed; lastly for compound **IIIb** the temperature was raised to 50 °C for 8h, then it was let to reach room temperature and stirred for five days. After removal of the solvent under reduced pressure, the crude was extracted with DCM (3 x 5 mL) and washed with water (5 mL) and brine (10 mL). In the case of compounds **Ia** and **Ib**, this work-up was sufficient to obtain the pure products. Conversely, an acid (pH = 3-4) / base (pH = 8-9) work-up was required for **Ila-c** and **IIIa-b**, the combined organic phases were dried (anhydrous Na₂SO₄), filtered and, evaporated under vacuum to get the desired compounds. The crude compound **IIIa** was further purified through flash chromatography (silica gel) to afford pure compound **IIIa**.

2-(4-benzylpiperidin-1-yl)-N-methoxy-N-methylacetamide (Ia) By following the General Procedure, starting from 2-chloro-*N*-methoxy-*N*-methylacetamide (138 mg, 1.00 mmol, 1.0 equiv), K₂CO₃ (207 mg, 1.5 mmol, 1.5 equiv), 4-benzylpiperidine (175 mg, 176 mL 1.0 mmol, 1.0 equiv) and ACN (7 mL), the desired product was obtained in quantitative amount (276 mg) as a bright yellow oil. ¹H-NMR (500 MHz, CDCl₃) δ: 7.27 (m, 2H, Ar), 7.18 (t, 1H, *J* = 7.5 Hz, Ar), 7.14 (d, 2H, *J* = 7.3 Hz, Ar), 3.69 (s, 3H, NOCH₃), 3.29 (s, 2H, CH₂N), 3.16 (s, 3H, NCH₃), 2.96 (d, 2H, Pip-2, Pip-6), 2.53 (d, 2H, CH₂Pip-4), 2.07 (t, 2H, Pip-2, Pip-6), 1.62 (d, 2H, Pip-3, Pip-5), 1.51 (m, 1H, Pip-4), 1.40 (q, 2H, Pip-3, Pip-5). ¹³C-NMR (125 MHz, CDCl₃) δ: 171.4, 140.5, 129.1, 128.1, 125.7, 61.3, 58.5, 54.1, 43.1, 37.5, 32.1, 32.0.

N-methoxy-N-methyl-2-(piperidine-1-yl)-acetamide (Ib) By following the General Procedure, starting from 2-chloro-*N*-methoxy-*N*-methylacetamide (**I**, commercially available) (138 mg, 1.00 mmol, 1.0 equiv.), K₂CO₃ (207 mg, 1.5 mmol, 1.5 equiv.), piperidine (175 mg, 176mL 1.0 mmol, 1.0 equiv.) and ACN (10 mL), the desired product was obtained in 85% (235 mg) as a dark oil. ¹H-NMR (500 MHz, CDCl₃) δ: 3.71 (s, 3H, NOCH₃), 3.29 (s, 2H, CH₂N), 3.19 (s, 3H, NCH₃), 2.50 (m, 4H, CH₂ piperidine), 1.71 (m, 4H, CH₂ piperidine), 1.47 (m, 2H, CH₂ piperidine).

3-(4-benzylpiperidin-1-yl)-N-methoxy-N-methylpropanamide (IIa) By following the General Procedure, starting from 3-chloro-*N*-methoxy-*N*-methylpropanamide (152 mg, 1.00 mmol, 1.0 equiv), K₂CO₃ (207 mg, 1.5 mmol, 1.5 equiv), 4-benzylpiperidine (175 mg, 176 mL, 1.0 mmol, 1.0 equiv) and ACN (7 mL), the desired product was obtained in quantitative amount (290 mg) as a bright yellow oil. ¹H-NMR (500 MHz, CDCl₃) δ: 7.27 (m, 2H, Ar), 7.18 (t, 1H, *J* = 7.4 Hz, Ar), 7.13 (d, 2H, *J* = 7.4 Hz, Ar), 3.68 (s, 3H, NOCH₃), 3.16 (s, 3H, NCH₃), 2.95 (d, 2H, Pip-2, Pip-6), 2.72-2.70 (m, 4H, CH₂N, CH₂CH₂N), 2.53 (d, 2H, CH₂Pip-4), 2.00 (t, 2H, Pip-2, Pip-6), 1.65 (d, 2H, Pip-3, Pip-5), 1.54 (m, 1H, Pip-4), 1.36 (q, 2H, Pip-3, Pip-5). ¹³C-NMR (125 MHz, CDCl₃) δ: 173.1, 140.5, 129.1, 128.1, 125.8, 61.3, 53.8, 53.6, 43.0, 37.6, 37.1, 32.1, 29.5.

N-methoxy-*N*-methyl-3-(piperidin-1-yl)propanamide (**IIb**) By following the General Procedure, starting from 3-chloro-*N*-methoxy-*N*-methylpropanamide (152 mg, 1.00 mmol, 1.0 equiv), K₂CO₃ (207 mg, 1.5 mmol, 1.5 equiv), piperidine (85 mg, 99 mL, 1.0 mmol, 1.0 equiv) and ACN (7 mL), the desired product was obtained in quantitative amount (200 mg) as a bright yellow oil. ¹H-NMR (400 MHz, CDCl₃) δ: 3.76 (s, 3H, NOCH₃), 3.24 (s, 3H, NCH₃), 2.76 (s, 4H, CH₂N, CH₂CH₂N), 2.52 (t, 4H, Pip-2, Pip-6), 1.70-1.56 (m, 6H, Pip-3, Pip-4, Pip-5). ¹³C-NMR (100 MHz, CDCl₃) δ: 175.2, 61.3, 54.5, 54.2, 29.7, 25.9, 24.2.

N-methoxy-*N*-methyl-3-morpholinopropanamide (**IIc**) By following the General Procedure, starting from 3-chloro-*N*-methoxy-*N*-methylpropanamide (152 mg, 1.00 mmol, 1.0 equiv), K₂CO₃ (207 mg, 1.5 mmol, 1.5 equiv), morpholine (87 mg, 87 mL, 1.0 mmol, 1.0 equiv) and ACN (7 mL), the desired product was obtained in 46 % (93 mg) as a bright yellow oil. ¹H-NMR (400 MHz, CDCl₃) δ: 3.78-3.73 (m, 4H, NCH₂CH₂O), 3.73 (s, 3H, NOCH₃), 3.22 (s, 3H, NCH₃), 2.81-2.63 (m, 4H, CH₂CH₂N, CH₂CH₂N), 2.56-2.51 (t, 4H, NCH₂CH₂O). ¹³C-NMR (100 MHz, CDCl₃) δ: 175.3, 66.9, 61.3, 53.9, 53.6, 32.2, 29.4.

4-(4-benzylpiperidin-1-yl)-*N*-methoxy-*N*-methylbutanamide (**IIIa**) By following the General Procedure, starting from 4-chloro-*N*-methoxy-*N*-methylbutanamide (166 mg, 1.00 mmol, 1.0 equiv), K₂CO₃ (207 mg, 1.5 mmol, 1.5 equiv), 4-benzylpiperidine (175 mg, 176 mL 1.0 mmol, 1.0 equiv) and ACN (7 mL), the desired product was obtained in 65 % (198 mg) as a bright yellow oil after chromatography on silica gel (60:40 ethylacetate:*n*-hexane). ¹H-NMR (400 MHz, CDCl₃) δ: 7.33-7.12 (m, 5H, Ar), 3.69 (s, 3H, NOCH₃), 3.48 (s, 2H, CH₂N), 3.18 (s, 3H, NCH₃), 2.74-2.66 (m, 2H, Pip-2, Pip-6), 2.60-2.50 (m, 4H, CH₂Pip-4, Pip-2, Pip-6), 2.31-2.21 (m, COCH₂CH₂), 2.09-1.94 (m, 2H, COCH₂CH₂CH₂), 1.82-1.65 (m, 5H, Pip-3, Pip-4, Pip-5). ¹³C-NMR (125 MHz, CDCl₃) δ: 173.6, 139.9, 129.1, 128.3, 126.1, 61.1, 57.1, 53.1, 42.5, 37.2, 30.3, 29.5, 20.3.

N-methoxy-*N*-methyl-4-(piperidin-1-yl)-butanamide (**IIIb**) By following the General Procedure, starting from 4-chloro-*N*-methoxy-*N*-methylbutanamide (166 mg, 1.00 mmol, 1.0 equiv.), K₂CO₃ (207 mg, 1.5 mmol, 1.5 equiv.), piperidine (85 mg, 99 mL, 1.0 mmol, 1.0 equiv.) and ACN (7 mL), the desired product was obtained in 47% (101 mg) as a yellow oil. ¹H-NMR (400 MHz, CDCl₃) δ: 3.70 (s, 3H, NOCH₃), 3.16 (s, 3H, NCH₃), 2.56 (t, *J* = 2.7Hz, 2H, CH₂N), 2.51 (m, 4H, CH₂N piperidine), 2.19 (t, *J* = 7.4Hz, 2H COCH₂), 1.93 (m, 2H, COCH₂CH₂), 1.71 (m, 4H, CH₂ piperidine), 1.46 (m, 2H, CH₂ piperidine).

5.3.3 General procedure for the preparation of compounds 1-31

Under argon atmosphere, *tert*-butyllithium (2.2 equiv., 1.9 M in pentane) was added dropwise to a -78 °C cooled solution of the appropriate arylbromide (1.5 equiv.) in anhydrous THF. After 20 minutes, the solution of the corresponding Weinreb amide in anhydrous THF was added dropwise. The stirring was continued for 5 additional hours and then quenched with water. The reaction was extracted with Et₂O (3 x 5 mL) and washed with water (5 mL) and brine (10 mL). The organic phase was dried (anhydrous Na₂SO₄), filtered and, after removal of the solvent under reduced pressure, the so-obtained crude mixture was subjected to chromatography (silica gel) to afford pure compounds. Lastly, pure compounds were converted into their corresponding hydrochlorides, adding an ethereal solution of HCl (1.0 equiv., 1 M in Et₂O).

4-benzyl-1-(2-oxo-2-phenylethyl)piperidin-1-ium hydrochloride (1) By following the General Procedure, starting from bromobenzene (236 mg, 1.5 mmol, 1.5 equiv.), 2-(4-benzylpiperidin-1-yl)-*N*-methoxy-*N*-methylacetamide (274 mg, 1.00 mmol, 1.0 equiv.), *t*-BuLi (1.9 M, 1.32 mL, 2.5 mmol, 2.5 equiv.) and THF (5 mL), the desired product was obtained in 40% (117 mg) as a bright yellow oil after chromatography on silica gel (60:40 hexane:ethylacetate) and converted into the corresponding hydrochloride. FT-IR (cm⁻¹): 3058, 3023, 2922, 2846, overtones Ar = 2100-1800, 1706, 1598, 1580, 1448. ¹H-NMR (400 MHz, CDCl₃) δ: 12.07 (s, 1H, NH⁺), 7.95 (brs, 2H, Ar), 7.65 (brs, 1H, Ar), 7.50 (brs, 2H, Ar), 7.31 (t, *J* = 7.0 Hz, 2H, Ar), 7.23 (t, *J* = 8.0 Hz, 1H, Ar), 7.16 (d, *J* = 8.0 Hz, 2H, Ar), 4.75 (s, 2H, COCH₂N), 3.55 (brs, 4H, Pip-2, Pip-6), 2.64 (m, 2H, CH₂Pip-4), 2.09-1.85 (m, 5H, Pip-3, Pip-4, Pip-5). ¹³C-NMR (100 MHz, CDCl₃) δ: 190.3, 139.0, 134.9, 133.9, 129.1, 128.9, 128.4, 128.1, 126.3, 59.7, 52.4, 42.0, 35.9, 29.3. UHPLC-ESI-MS: ABS t_R = 1.19, 96% pure (λ = 210 nm), m/z = 294.3 [M + H]⁺.

4-benzyl-1-(2-(4-methoxyphenyl)-2-oxoethyl)piperidin-1-ium hydrochloride (2) By following the General Procedure, starting from 1-bromo-4-methoxybenzene (281 mg, 1.5 mmol, 1.5 equiv.), 2-(4-benzylpiperidin-1-yl)-*N*-methoxy-*N*-methylacetamide (274 mg, 1.00 mmol, 1.0 equiv.), *t*-BuLi (1.9 M, 1.32 mL, 2.5 mmol, 2.5 equiv.) and THF (5 mL), the desired product was obtained in 37% (120 mg) as a bright yellow oil after chromatography on silica gel (60:40 hexane:ethylacetate) and converted into the corresponding hydrochloride. FT-IR (cm⁻¹): 3059, 3013, 2932, overtones Ar = 2100-1750, 1694, 1603, 1578, 1512, 1402. ¹H-NMR (400 MHz, CDCl₃) δ: 11.93 (brs, 1H, NH⁺), 7.90 (d, *J* = 8.0 Hz, 2H, Ar), 7.30 (t, *J* = 8.0 Hz, 2H, Ar), 7.22 (t, *J* = 8.0 Hz, 1H, Ar), 7.15 (d, *J* = 8.0 Hz, 2H, Ar), 6.93 (d, *J* = 8.0 Hz, 2H, Ar), 4.68 (s, 2H, COCH₂N), 3.87 (s, 3H, OCH₃), 3.51 (brd, 4H, Pip-2, Pip-6), 2.63 (d, 2H, CH₂Pip-4), 2.06 (m, 2H, Pip-3, Pip-5), 1.85-1.82 (m, 3H, Pip-3, Pip-4, Pip-5). ¹³C-NMR (100 MHz, CDCl₃) δ: 188.5, 164.8, 148.5, 139.0, 130.5, 128.9, 128.4, 126.9, 126.2,

114.2, 59.1, 55.6, 52.2, 42.0, 35.8, 29.3. UHPLC-ESI-MS: ABP t_R = 1.87, 98% pure (λ = 210 nm), m/z = 324.4 [M + H]⁺.

4-benzyl-1-(2-(3-methoxyphenyl)-2-oxoethyl)piperidin-1-ium hydrochloride (3) By following the General Procedure, starting from 1-bromo-3-methoxybenzene (281 mg, 1.5 mmol, 1.5 equiv.), 2-(4-benzylpiperidin-1-yl)-*N*-methoxy-*N*-methylacetamide (274 mg, 1.00 mmol, 1.0 equiv.), *t*-BuLi (1.9 M, 1.32 mL, 2.5 mmol, 2.5 equiv.) and THF (5 mL), the desired product was obtained in 48% (155 mg) as a bright yellow oil after chromatography on silica gel (60:40 hexane:ethylacetate) and converted into the corresponding hydrochloride. FT-IR (cm⁻¹): 3056, 3026, 3003, 2923, 2841, overtones Ar = 2100-1750, 1696, 1596, 1431. ¹H-NMR (400 MHz, CDCl₃) δ : 11.94 (brs, 1H, NH⁺), 7.49-7.16 (m, 9H, Ar), 4.77 (s, 2H, COCH₂N), 3.84 (s, 3H, OCH₃), 3.56 (m, 4H, Pip-2, Pip-6), 2.63 (brd, 2H, CH₂Pip-4), 2.08 (brs, 2H, Pip-3, Pip-5), 1.86-1.73 (m, 3H, Pip-3, Pip-4, Pip-5). ¹³C-NMR (100 MHz, CDCl₃) δ : 190.1, 160.0, 139.0, 135.2, 130.1, 128.9, 128.4, 126.3, 121.4, 120.6, 112.2, 60.0, 55.6, 52.5, 42.0, 35.8, 29.3. UHPLC-ESI-MS: ABP t_R = 1.85, 99% pure (λ = 220 nm), m/z = 324.4 [M + H]⁺.

4-benzyl-1-(2-(naphthalen-2-yl)-2-oxoethyl)piperidin-1-ium hydrochloride (4) By following the General Procedure, starting from 2-bromonaphthalene (311 mg, 1.5 mmol, 1.5 equiv.), 2-(4-benzylpiperidin-1-yl)-*N*-methoxy-*N*-methylacetamide (274 mg, 1.00 mmol, 1.0 equiv.), *t*-BuLi (1.9 M, 1.32 mL, 2.5 mmol, 2.5 equiv.) and THF (5 mL), the desired product was obtained in 54% (185 mg) as a bright yellow oil after chromatography on silica gel (60:40 hexane:ethylacetate) and converted into the corresponding hydrochloride. FT-IR (cm⁻¹): 3023, 2924, overtones Ar = 2100-1800, 1689, 1599, 1495, 1453. ¹H-NMR (400 MHz, CDCl₃) δ : 11.63 (brs, 1H, NH⁺), 8.51 (s, 1H, Nap), 7.91 (d, 2H, Nap), 7.78 (t, 2H, Nap), 7.59 (t, J = 8.0 Hz, 1H, Nap), 7.51 (t, J = 8.0 Hz, 1H, Nap), 7.28-7.11 (m, 5H, Ar), 4.96 (s, 2H, COCH₂N), 3.60-3.52 (m, 4H, Pip-2, Pip-6), 2.59 (brd, 2H, CH₂Pip-4), 2.04 (m, 2H, Pip-3, Pip-5), 1.82-1.79 (m, 3H, Pip-3, Pip-4, Pip-5). ¹³C-NMR (100 MHz, CDCl₃) δ : 190.2, 139.0, 136.0, 132.0, 131.0, 130.7, 129.8, 129.4, 128.9, 128.4, 127.6, 127.2, 126.2, 122.6, 59.9, 52.7, 41.9, 35.7, 29.3. UHPLC-ESI-MS: ABP t_R = 2.08, 95% pure (λ = 210 nm), m/z = 344.3 [M + H]⁺.

4-benzyl-1-(2-(6-methoxynaphthalen-2-yl)-2-oxoethyl)piperidin-1-ium hydrochloride (5) By following the General Procedure, starting from 2-bromo-6-methoxynaphthalene (256 mg, 1.5 mmol, 1.5 equiv.), 2-(4-benzylpiperidin-1-yl)-*N*-methoxy-*N*-methylacetamide (274 mg, 1.00 mmol, 1.0 equiv.), *t*-BuLi (1.9 M, 1.32 mL, 2.5 mmol, 2.5 equiv.) and THF (5 mL), the desired product was obtained in 49% (183 mg) as a bright yellow oil after chromatography on silica gel (60:40 hexane:ethylacetate) and converted into the corresponding hydrochloride. FT-IR (cm⁻¹): 3023, 2932, overtones Ar = 2100-1800, 1682, 1483. ¹H-NMR (400 MHz, CDCl₃) δ :

11.46 (brs, 1H, NH⁺), 8.38 (s, 1H, Nap), 7.79 (m, 2H, Nap), 7.61 (brd, 1H, Nap), 7.28-7.00 (m, 7H, Ar, Nap), 4.92 (s, 2H, COCH₂N), 3.90 (s, 3H, OCH₃), 3.59-3.53 (m, 4H, Pip-2, Pip-6), 2.58 (brd, 2H, CH₂Pip-4), 2.03 (m, 2H, Pip-3, Pip-5), 1.82-1.79 (m, 3H, Pip-3, Pip-4, Pip-5). ¹³C-NMR (100 MHz, CDCl₃) δ: 189.7, 160.4, 139.0, 137.9, 131.4, 130.5, 129.0, 128.9, 128.3, 127.5, 127.3, 126.2, 123.4, 120.1, 105.7, 59.9, 55.4, 52.7, 42.0, 35.7, 29.3. UHPLC-ESI-MS: ABS t_R = 1.63, 95% pure (λ = 210 nm), m/z = 374.5 [M + H]⁺.

1-(2-([1,1'-biphenyl]-4-yl)-2-oxoethyl)-4-benzylpiperidin-1-ium hydrochloride (6) By following the General Procedure, starting from 4-bromo-1,1'-biphenyl (350 mg, 1.5 mmol, 1.5 equiv.), 2-(4-benzylpiperidin-1-yl)-N-methoxy-N-methylacetamide (274 mg, 1.00 mmol, 1.0 equiv.), *t*-BuLi (1.9 M, 1.32 mL, 2.5 mmol, 2.5 equiv.) and THF (5 mL), the desired product was obtained in 33% (122 mg) as a bright yellow oil after chromatography on silica gel (60:40 hexane:ethylacetate) and converted into the corresponding hydrochloride. FT-IR (cm⁻¹): 3025, 2986, 2935, 2916, 2847, overtones Ar = 2100-1800, 1691, 1603, 1414. ¹H-NMR (400 MHz, CDCl₃) δ: 11.70 (brs, 1H, NH⁺), 8.00 (d, *J* = 6.3 Hz, 2H, Ar), 7.66 (brs, 2H, Ar), 7.55 (ds, *J* = 4.0 Hz, 2H, Ar), 7.44 (m, 3H, Ar), 7.28-7.13 (m, 5H, Ar), 4.88 (s, 2H, COCH₂N), 3.60-3.55 (m, 4H, Pip-2, Pip-6), 2.62-2.52 (brs, 2H, CH₂Pip-4), 2.07 (m, 2H, Pip-3, Pip-5), 1.86-1.83 (m, 3H, Pip-3, Pip-4, Pip-5). ¹³C-NMR (100 MHz, CDCl₃) δ: 189.8, 147.4, 139.0, 138.9, 132.5, 129.0, 128.7, 128.6, 128.4, 127.5, 127.1, 126.2, 60.0, 52.7, 42.0, 35.8, 29.3. UHPLC-ESI-MS: ABP t_R = 2.22, 98% pure (λ = 210 nm), m/z = 370.5 [M + H]⁺.

1-(2-(naphthalen-2-yl)-2-oxoethyl)piperidin-1-ium hydrochloride (7) By following the General Procedure, starting from 2-bromonaphthalene (1.5 equiv.), N-methoxy-N-methyl-2-(piperidin-1-yl)-acetamide (1.0 equiv.), *t*-BuLi (1.7M, 2.5 equiv.) and THF, the desired product was obtained in 42% yield as a yellow solid after chromatography on silica gel (90:10 ethylacetate/methanol) and converted into the corresponding hydrochloride. R_f: 0.27 (80:20 ethylacetate/methanol). mp: 252-253°C. ¹H-NMR (400MHz, MeOD): δ 8.68 (s, 1H, Napht), 8.12 (d, *J*=8.0 Hz, 1H, Napht), 8.07 (s, 2H, Napht), 8.01 (d, *J* = 8.1 Hz, 1H, Napht), 7.73 (t, *J* = 7.5 Hz, 1H, Napht), 7.67 (t, *J* = 7.4 Hz, 1H, Napht), 5.10 (s, 2H, COCH₂N), 3.66 (brs, 2H, pip), 3.17 (brs, 2H, pip), 2.03 (brs, 5H, pip), 1.64 (brs, 1H, pip). ¹³C-NMR (100 MHz, MeOD) δ: 190.51, 136.37, 132.43, 130.94, 130.67, 129.53, 129.28, 128.67, 127.63, 127.09, 122.59, 61.24, 54.27, 22.58, 21.22.

1-(2-([1,1'-biphenyl]-4-yl)-2-oxoethyl)piperidin-1-ium hydrochloride (8) By following the General Procedure, starting from 4-bromo-1,1'-biphenyl (1.5 equiv.), N-methoxy-N-methyl-2-(piperidin-1-yl)-acetamide (1.0 equiv.), *t*-BuLi (1.7M, 2.5 equiv.) and THF, the desired product was obtained in 35% yield as a pale yellow solid after chromatography on silica gel (90:10 ethylacetate/methanol) and converted into the corresponding hydrochloride. R_f: 0.27 (80:20 ethylacetate/methanol). mp: 236-238°C. ¹H-NMR (400MHz, MeOD): δ 8.15 (d,

$J = 8.3$ Hz, 2H, Ph-PhCO), 7.89 (d, $J = 8.3$ Hz, 2H, Ph-PhCO), 7.74 (d, $J = 7.7$ Hz, 2H, Biph), 7.53 (t, $J = 7.5$ Hz, 2H, Biph), 7.46 (t, $J = 7.2$ Hz, 1H, Biph), 4.99 (s, 2H, COCH₂N), 3.65 (brs, 2H, pip), 3.16 (t, $J = 13.1$ Hz, 2H, pip), 2.08 – 1.87 (brs, 5H, pip), 1.69 – 1.55 (brs, 1H, pip). ¹³C-NMR (100 MHz, MeOD) δ : 190.12, 147.42, 139.19, 132.31, 128.81, 128.67, 128.41, 127.17, 126.89, 61.19, 54.23, 22.57, 21.21.

1-(2-(4-(benzyloxy)phenyl)-2-oxoethyl)piperidin-1-ium hydrochloride (9) By following the General Procedure, starting from 1-(benzyloxy)-4-bromobenzene (1.5 equiv.), N-methoxy-N-methyl-2-(piperidin-1-yl)-acetamide (1.0 equiv.), *t*-BuLi (1.7M, 2.5 equiv.) and THF, the desired product was obtained in 29% (90 mg) as a pale yellow solid after chromatography on silica gel (80:20 ethylacetate/methanol) and converted into the corresponding hydrochloride. R_f: 0.19 (80:20 ethylacetate/methanol). mp: 86-88°C. ¹H-NMR (400 MHz, MeOD): δ 8.03 (d, $J = 8.8$ Hz, 2H, OPhCO), 7.47 (d, $J = 7.4$ Hz, 2H, PhCH₂), 7.41 (t, $J = 7.3$ Hz, 2H, PhCH₂), 7.36 (d, $J = 7.2$ Hz, 1H, PhCH₂), 7.19 (d, $J = 8.8$ Hz, 2H, OPhCO), 5.24 (s, 2H, PhCH₂OPh), 4.87 (s, 2H, COCH₂N), 3.61 (d, $J = 12.1$ Hz, 2H, pip), 3.11 (brs, 2H, pip), 1.94 (brs, 5H, pip), 1.60 (m, 1H, pip). ¹³C-NMR (100 MHz, MeOD) δ : 193.52, 130.63, 128.58, 127.74, 115.10, 70.33, 59.24, 52.20, 23.04, 21.50.

3-(4-benzylpiperidin-1-yl)-1-phenylpropan-1-one (10) By following the General Procedure, starting from bromobenzene (236 mg, 1.5 mmol, 1.5 equiv.), 3-(4-benzylpiperidin-1-yl)-*N*-methoxy-*N*-methylpropanamide (290 mg, 1.00 mmol, 1.0 equiv.), *t*-BuLi (1.9 M, 1.32 mL, 2.5 mmol, 2.5 equiv.) and THF (5 mL), the desired product was obtained in 28% yield (86 mg) as a bright yellow oil after chromatography on silica gel (90:10 ethylacetate:methanol) and converted into the corresponding hydrochloride. FT-IR (cm⁻¹): 3059, 3045, 3025, 2996, 2921, overtones Ar = 2100-1700, 1682, 1596, 1447. ¹H-NMR (500 MHz, CDCl₃) δ : 7.88 (d, $J = 8.3$ Hz, 2H, Ar), 7.48 (m, 1H, Ar), 7.38 (t, $J = 7.5$ Hz, 2H, Ar), 7.20 (m, 2H, Ar), 7.11 (t, $J = 7.0$ Hz, 1H, Ar), 7.06 (d, $J = 7.4$ Hz, 2H, Ar), 3.17 (m, 2H, COCH₂CH₂), 2.91 (d, 2H, Pip-2, Pip-6), 2.77 (m, 2H, CH₂CH₂N), 2.47 (d, $J = 7.2$ Hz, 2H, CH₂Pip-4), 1.96 (m, 2H, Pip-2, Pip-6), 1.59 (d, 2H, Pip-3, Pip-5), 1.48 (m, 1H, Pip-4), 1.30 (m, 2H, Pip-3, Pip-5). ¹³C-NMR (125 MHz, CDCl₃) δ : 199.0, 140.4, 136.7, 133.1, 129.0, 128.6, 128.1, 128.0, 125.8, 53.9, 53.3, 43.0, 37.6, 36.1, 31.8. UHPLC-ESI-MS: ABS t_R = 1.25, 95% pure ($\lambda = 254$ nm), m/z = 308.4 [M + H]⁺.

3-(4-benzylpiperidin-1-yl)-1-(4-methoxyphenyl)propan-1-one (11) By following the General Procedure, starting from 1-bromo-4-methoxybenzene (281 mg, 1.5 mmol, 1.5 equiv.), 3-(4-benzylpiperidin-1-yl)-*N*-methoxy-*N*-methylpropanamide (290 mg, 1.00 mmol, 1.0 equiv.), *t*-BuLi (1.9 M, 1.32 mL, 2.5 mmol, 2.5 equiv.) and THF (5 mL), the desired product was obtained in 25% (84 mg) as a bright yellow oil after chromatography on silica gel (90:10 ethylacetate:methanol) and converted into the corresponding hydrochloride. FT-IR (cm⁻¹): 3048, 3030, 3005, 2939, 2918, 2841, overtones Ar = 2100-1700, 1673, 1601, 1457,

1420. **¹H-NMR** (500 MHz, CDCl₃) δ: 7.96 (d, *J* = 8.7 Hz, 2H, Ar), 7.28 (m, 2H, Ar), 7.20 (t, *J* = 6.7 Hz, 1H, Ar), 7.13 (d, *J* = 7.5 Hz, 2H, Ar), 6.93 (d, *J* = 8.7 Hz, 2H, Ar), 3.87 (s, 3H, OCH₃), 3.41 (m, 2H, COCH₂CH₂), 3.17 (m, 2H, Pip-2, Pip-6), 3.07 (m, 2H, CH₂CH₂N), 2.57 (brd, 2H, CH₂Pip-4), 2.28 (m, 2H, Pip-2, Pip-6), 1.73 (brd, 2H, Pip-3, Pip-5), 1.64 (m, 3H, Pip-3, Pip-4, Pip-5). **¹³C-NMR** (125 MHz, CDCl₃) δ: 177.5, 163.8, 139.9, 130.5, 129.2, 129.0, 128.3, 126.1, 113.8, 53.7, 52.8, 42.5, 37.1, 34.6, 30.5. UHPLC-ESI-MS: ABS *t_R* = 1.35, 98% pure (λ = 254 nm), *m/z* = 338.4 [M + H]⁺.

3-(4-benzylpiperidin-1-yl)-1-(naphthalen-2-yl)propan-1-one (12) By following the General Procedure, starting from 2-bromonaphthalene (311 mg, 1.5 mmol, 1.5 equiv.), 3-(4-benzylpiperidin-1-yl)-*N*-methoxy-*N*-methylpropanamide (290 mg, 1.00 mmol, 1.0 equiv.), *t*-BuLi (1.9 M, 1.32 mL, 2.5 mmol, 2.5 equiv.) and THF (5 mL), the desired product was obtained in 22% (79 mg) as a bright yellow oil after chromatography on silica gel (90:10 ethylacetate:methanol) and converted into the corresponding hydrochloride. FT-IR (cm⁻¹): 3059, 3029, 2943, 2921, 2864, overtones Ar = 2000-1700, 1674, 1595, 1495, 1456. **¹H-NMR** (500 MHz, CDCl₃) δ: 8.41 (s, 1H, Nap), 7.95 (d, *J* = 8.7 Hz, 1H, Nap), 7.89 (d, *J* = 8.1 Hz, 1H, Nap), 7.80 (t, *J* = 8.9 Hz, 2H, Nap), 7.54-7.46 (m, 2H, Nap), 7.20 (t, *J* = 7.5 Hz, 2H, Ar), 7.11 (t, *J* = 7.3 Hz, 1H, Ar), 7.06 (d, *J* = 7.5 Hz, 2H, Ar), 3.31 (t, *J* = 7.5 Hz, 2H, COCH₂CH₂), 2.95 (brd, 2H, Pip-2, Pip-6), 2.85 (t, *J* = 7.6 Hz, 2H, CH₂CH₂N), 2.47 (d, *J* = 7.2 Hz, 2H, CH₂Pip-4), 2.00 (m, 2H, Pip-2, Pip-6), 1.61 (brd, 2H, Pip-3, Pip-5), 1.50 (m, 1H, Pip-4), 1.33 (m, 2H, Pip-3, Pip-5). **¹³C-NMR** (125 MHz, CDCl₃) δ: 198.9, 140.4, 135.5, 133.9, 132.4, 129.8, 129.5, 129.0, 128.5, 128.4, 128.2, 127.7, 125.8, 123.7, 53.9, 53.4, 43.0, 37.6, 36.1, 31.7. UHPLC-ESI-MS: ABP *t_R* = 1.62, 98% pure (λ = 254 nm), *m/z* = 358. [M + H]⁺.

1-([1,1'-biphenyl]-4-yl)-3-(4-benzylpiperidin-1-yl)propan-1-one (13) By following the General Procedure, starting from 4-bromo-1,1'-biphenyl (350 mg, 1.5 mmol, 1.5 equiv.), 3-(4-benzylpiperidin-1-yl)-*N*-methoxy-*N*-methylpropanamide (290 mg, 1.00 mmol, 1.0 equiv.), *t*-BuLi (1.9 M, 1.32 mL, 2.5 mmol, 2.5 equiv.) and THF (5 mL), the desired product was obtained in 22% yield (84 mg) as a bright yellow oil after chromatography on silica gel (90:10 ethylacetate:methanol) and converted into the corresponding hydrochloride. FT-IR (cm⁻¹): 3059, 3029, 2916, overtones Ar = 2100-1700, 1677, 1601, 1457, 1402. **¹H-NMR** (400 MHz, CDCl₃) δ: 12.24 (brs, 1H, NH⁺), 8.09 (brd, 2H, Ar), 7.70 (brd, 2H, Ar), 7.63 (brd, 2H, Ar), 7.48 (brt, 2H, Ar), 7.43 (brt, 1H, Ar), 7.29-7.13 (m, 5H, Ar), 3.87 (brs, 2H, COCH₂CH₂), 3.58 (brs, 2H, Pip-2, Pip-6), 3.48 (brs, 2H, CH₂CH₂N), 2.71-2.64 (m, 4H, Pip-2, Pip-6, CH₂Pip-4), 2.08 (brt, 2H, Pip-3, Pip-5), 1.87-1.79 (m, 3H, Pip-3, Pip-4, Pip-5). **¹³C-NMR** (100 MHz, CDCl₃) δ: 195.7, 146.6, 139.4, 138.9, 134.0, 128.9, 128.4, 128.3, 127.3, 127.2, 126.3, 53.6, 52.1, 41.8, 36.4, 33.3, 28.9. UHPLC-ESI-MS: ABP *t_R* = 2.37, 95% pure (λ = 254 nm), *m/z* = 384.4 [M + H]⁺.

1-phenyl-3-(piperidin-1-yl)propan-1-one (14) By following the General Procedure, starting from bromobenzene (236 mg, 1.5 mmol, 1.5 equiv.), *N*-methoxy-*N*-methyl-3-(piperidin-1-yl)propanamide (200 mg, 1.00 mmol, 1.0 equiv.), *t*-BuLi (1.9 M, 1.32 mL, 2.5 mmol, 2.5 equiv.) and THF (5 mL), the desired product was obtained in 29% yield (63 mg) as a bright yellow oil after chromatography on silica gel (60:40 ethylacetate:methanol) and converted into the corresponding hydrochloride. FT-IR (cm⁻¹): 3055, 3021, 2938, 2863, overtones Ar = 2100-1700, 1682, 1597, 1581, 1477, 1456. ¹H-NMR (500 MHz, CDCl₃) δ: 7.95 (dd, *J* = 1.2 and 7.9 Hz, 2H, Ar), 7.55 (m, 1H, Ar), 7.45 (t, *J* = 7.9 Hz, 2H, Ar), 3.24 (t, *J* = 7.4 Hz, 2H, COCH₂CH₂), 2.83 (t, *J* = 7.8 Hz, 2H, CH₂CH₂N), 2.49 (brs, 4H, Pip-2, Pip-6), 1.62 (m, 4H, Pip-3, Pip-5), 1.44 (m, 2H, Pip-4). ¹³C-NMR (125 MHz, CDCl₃) δ: 197.1, 136.7, 133.1, 128.6, 128.0, 54.5, 53.7, 36.0, 25.7, 24.0. UHPLC-ESI-MS: ABP t_R = 1.07, 96% pure (λ = 254 nm), m/z = 218.3 [M + H]⁺.

1-(4-methoxyphenyl)-3-(piperidin-1-yl)propan-1-one (15) By following the General Procedure, starting from 1-bromo-4-methoxybenzene (281 mg, 1.5 mmol, 1.5 equiv.), *N*-methoxy-*N*-methyl-3-(piperidin-1-yl)propanamide (200 mg, 1.00 mmol, 1.0 equiv.), *t*-BuLi (1.9 M, 1.32 mL, 2.5 mmol, 2.5 equiv.) and THF (5 mL), the desired product was obtained in 27% yield (67 mg) as a bright yellow oil after chromatography on silica gel (60:40 ethylacetate:methanol) and converted into the corresponding hydrochloride. FT-IR (cm⁻¹): 2951, 2937, 2875, overtones Ar = 2100-1700, 1672, 1598, 1464, 1442, 1425. ¹H-NMR (500 MHz, CDCl₃) δ: 7.93 (d, *J* = 8.9 Hz, 2H, Ar), 6.91 (d, *J* = 8.7 Hz, 2H, Ar), 3.85 (s, 3H, OCH₃), 3.17 (t, *J* = 7.4 Hz, 2H, COCH₂CH₂), 2.80 (t, *J* = 7.9 Hz, 2H, CH₂CH₂N), 2.47 (brs, 4H, Pip-2, Pip-6), 1.60 (m, 4H, Pip-3, Pip-5), 1.44 (m, 2H, Pip-4). ¹³C-NMR (125 MHz, CDCl₃) δ: 197.8, 163.4, 130.3, 129.9, 113.7, 55.4, 54.5, 53.9, 35.8, 25.8, 24.1. UHPLC-ESI-MS: ABP t_R = 1.24, 98% pure (λ = 254 nm), m/z = 248.3 [M + H]⁺.

1-(naphthalen-2-yl)-3-(piperidin-1-yl)propan-1-one (16) By following the General Procedure, starting from 2-bromonaphthalene (311 mg, 1.5 mmol, 1.5 equiv.), *N*-methoxy-*N*-methyl-3-(piperidin-1-yl)propanamide (200 mg, 1.00 mmol, 1.0 equiv.), *t*-BuLi (1.9 M, 1.32 mL, 2.5 mmol, 2.5 equiv.) and THF (5 mL), the desired product was obtained in 23% yield (61 mg) as a bright yellow oil after chromatography on silica gel (60:40 ethylacetate:methanol) and converted into the corresponding hydrochloride. FT-IR (cm⁻¹): 3037, 2934, 2891, 2855, overtones Ar = 2100-1700, 1676, 1598, 1463. ¹H-NMR (500 MHz, CDCl₃) δ: 8.50 (s, 1H, Nap), 8.02 (d, *J* = 8.5 Hz, 1H, Nap), 7.96 (d, *J* = 8.1 Hz, 1H, Nap), 7.88 (t, *J* = 9.2 Hz, 2H, Nap), 7.62-7.54 (m, 2H, Nap), 3.43 (t, *J* = 7.3 Hz, 2H, COCH₂CH₂), 2.95 (t, *J* = 7.2 Hz, 2H, CH₂CH₂N), 2.59 (brs, 4H, Pip-2, Pip-6), 1.68 (m, 4H, Pip-3, Pip-5), 1.49 (m, 2H, Pip-4). ¹³C-NMR (125 MHz, CDCl₃) δ: 198.9, 135.6, 134.0, 132.5, 129.9, 129.6, 128.5, 127.7, 126.8, 123.7, 54.5, 53.7, 36.0, 25.5, 23.9. UHPLC-ESI-MS: ABS t_R = 1.09, 95% pure (λ = 254 nm), m/z = 268.3 [M + H]⁺.

1-([1,1'-biphenyl]-4-yl)-3-(piperidin-1-yl)propan-1-one (17) By following the General Procedure, starting from 4-bromo-1,1'-biphenyl (350 mg, 1.5 mmol, 1.5 equiv.), *N*-methoxy-*N*-methyl-3-(piperidin-1-yl)propanamide (200 mg, 1.00 mmol, 1.0 equiv.), *t*-BuLi (1.9 M, 1.32 mL, 2.5 mmol, 2.5 equiv.) and THF (5 mL), the desired product was obtained in 35% yield (103 mg) as a bright yellow oil after chromatography on silica gel (60:40 ethylacetate:methanol) and converted into the corresponding hydrochloride. FT-IR (cm⁻¹): 3055, 3027, 2934, overtones Ar = 2100-1700, 1680, 1605, 1560, 1449, 1430. ¹H-NMR (500 MHz, CDCl₃) δ: 8.04 (d, *J* = 8.3 Hz, 2H, Ar), 7.68 (d, *J* = 8.4 Hz, 2H, Ar), 7.62 (d, *J* = 8.0 Hz, 2H, Ar), 7.47 (t, *J* = 7.3 Hz, 2H, Ar), 7.41 (t, *J* = 7.2 Hz, 1H, Ar), 3.27 (t, *J* = 7.4 Hz, 2H, COCH₂CH₂), 2.86 (t, *J* = 7.8 Hz, 2H, CH₂CH₂N), 2.51 (brs, 4H, Pip-2, Pip-6), 1.63 (m, 4H, Pip-3, Pip-5), 1.47 (m, 2H, Pip-4). ¹³C-NMR (125 MHz, CDCl₃) δ: 198.8, 145.7, 139.8, 135.5, 128.9, 128.6, 128.2, 127.2, 54.6, 53.8, 36.2, 25.7, 24.1. UHPLC-ESI-MS: ABP t_R = 1.89, 95% pure (λ = 254 nm), m/z = 294.3 [M + H]⁺.

1-(3-(4-(benzyloxy)phenyl)-3-oxopropyl)piperidin-1-ium hydrochloride (18) By following the General Procedure, starting from 1-(benzyloxy)-4-bromobenzene (1.5 equiv.), *N*-methoxy-*N*-methyl-2-(piperidin-1-yl)-propanamide (1.0 equiv.), *t*-BuLi (1.7M, 2.5 equiv.) and THF (5 mL), the desired product was obtained in 31% yield as a yellow solid after chromatography on silica gel (90:10 DCM/methanol) and converted into the corresponding hydrochloride. ¹H-NMR (400 MHz, MeOD): δ 8.05 (d, *J* = 8.2 Hz, 2H, *O*PhCO), 7.47 (d, *J* = 6.3 Hz, 2H, PhCH₂), 7.40 (t, *J* = 6.5 Hz, 2H, PhCH₂), 7.35 (brs, 1H, PhCH₂), 7.14 (d, *J* = 8.3 Hz, 2H, *O*PhCO), 5.22 (s, 2H, PhCH₂O), 3.62 (brs, 2H, COCH₂CH₂), 3.55 (brs, 4H, pip), 3.04 (t, *J* = 12.5 Hz, 2H, COCH₂CH₂), 1.98 (brs, 2H, pip), 1.82 (brs, 3H, pip), 1.58 (brs, 1H, pip). ¹³C-NMR (125 MHz, MeOD) δ: 194.91, 163.38, 136.55, 131.05, 129.00, 128.08, 127.49, 126.54, 113.90, 69.85, 53.31, 52.22, 32.29, 22.95.

3-morpholino-1-phenylpropan-1-one (19) By following the General Procedure, starting from bromobenzene (236 mg, 1.5 mmol, 1.5 equiv.), *N*-methoxy-*N*-methyl-3-morpholinopropanamide (202 mg, 1.00 mmol, 1.0 equiv.), *t*-BuLi (1.9 M, 1.32 mL, 2.5 mmol, 2.5 equiv.) and THF (5 mL), the desired product was obtained in 30% (66 mg) as a bright yellow oil after chromatography on silica gel (90:10 ethylacetate:methanol) and converted into the corresponding hydrochloride. FT-IR (cm⁻¹): 3086, 2981, 2930, 2872, overtones Ar = 2100-1700, 1685, 1597, 1584, 1445, 1405. ¹H-NMR (500 MHz, CDCl₃) δ: 7.94 (dd, *J* = 1.3 and 7.2 Hz, 2H, Ar), 7.55 (m, 1H, Ar), 7.46 (t, *J* = 7.8 Hz, 2H, Ar), 3.70 (t, *J* = 4.6 Hz, 4H, Mor-3, Mor-5), 3.18 (t, *J* = 7.3 Hz, 2H, COCH₂CH₂), 2.83 (t, *J* = 7.7 Hz, 2H, CH₂CH₂N), 2.50 (brs, 4H, Mor-2, Mor-6). ¹³C-NMR (125 MHz, CDCl₃) δ: 198.9, 136.7, 133.1, 128.6, 128.0, 66.8, 53.6, 53.4, 35.9. UHPLC-ESI-MS: ABP t_R = 0.82, 99% pure (λ = 254 nm), m/z = 220.2 [M + H]⁺.

1-(4-methoxyphenyl)-3-morpholinopropan-1-one (20) By following the General Procedure, starting from 1-bromo-4-methoxybenzene (281 mg, 1.5 mmol, 1.5 equiv.), *N*-methoxy-*N*-methyl-3-morpholinopropanamide (202 mg, 1.00 mmol, 1.0 equiv.), *t*-BuLi (1.9 M, 1.32 mL, 2.5 mmol, 2.5 equiv.) and THF (5 mL), the desired product was obtained in 38% yield (95 mg) as a bright yellow oil after chromatography on silica gel (90:10 ethylacetate:methanol) and converted into the corresponding hydrochloride. FT-IR (cm⁻¹): 2990, 2954, 2932, 2857, overtones Ar = 2100-1700, 1674, 1597, 1427. ¹H-NMR (500 MHz, CDCl₃) δ: 7.94 (d, *J* = 8.9 Hz, 2H, Ar), 6.93 (d, *J* = 8.9 Hz, 2H, Ar), 3.87 (s, 3H, OCH₃), 3.74 (m, 4H, Mor-3, Mor-5), 3.17 (t, *J* = 7.3 Hz, 2H, COCH₂CH₂), 2.86 (t, *J* = 7.2 Hz, 2H, CH₂CH₂N), 2.47 (brs, 4H, Mor-2, Mor-6). ¹³C-NMR (125 MHz, CDCl₃) δ: 197.3, 163.5, 130.3, 129.8, 66.7, 55.5, 53.6, 35.4. UHPLC-ESI-MS: ABP t_R = 0.84, > 99% pure (λ = 254 nm), m/z = 250.2 [M + H]⁺.

3-morpholino-1-(naphthalen-2-yl)propan-1-one (21) By following the General Procedure, starting from 2-bromonaphthalene (311 mg, 1.5 mmol, 1.5 equiv.), *N*-methoxy-*N*-methyl-3-morpholinopropanamide (202 mg, 1.00 mmol, 1.0 equiv.), *t*-BuLi (1.9 M, 1.32 mL, 2.5 mmol, 2.5 equiv.) and THF (5 mL), the desired product was obtained in 41% (110 mg) as a bright yellow oil after chromatography on silica gel (90:10 ethylacetate:methanol) and converted into the corresponding hydrochloride. FT-IR (cm⁻¹): 3018, 2924, 2863, overtones Ar = 2100-1700, 1687, 1594, 1469, 1436. ¹H-NMR (500 MHz, CDCl₃) δ: 8.48 (s, 1H, Nap), 8.02 (dd, *J* = 1.5 and 8.5 Hz, 1H, Nap), 7.95 (d, *J* = 8.5 Hz, 1H, Nap), 7.88 (t, *J* = 9.5 Hz, 2H, Nap), 7.61-7.53 (m, 2H, Nap), 3.76 (t, *J* = 4.5 Hz, 4H, Mor-3, Mor-5), 3.37 (t, *J* = 7.0 Hz, 2H, COCH₂CH₂), 2.94 (t, *J* = 7.5 Hz, 2H, CH₂CH₂N), 2.60 (brs, 4H, Mor-2, Mor-6). ¹³C-NMR (125 MHz, CDCl₃) δ: 198.6, 135.6, 134.0, 132.4, 129.8, 129.5, 128.5, 127.7, 126.8, 123.7, 66.6, 53.6, 53.5, 35.7. UHPLC-ESI-MS: ABP t_R = 1.48, 99% pure (λ = 254 nm), m/z = 270.3 [M + H]⁺.

1-([1,1'-biphenyl]-4-yl)-3-morpholinopropan-1-one (22) By following the General Procedure, starting from 4-bromo-1,1'-biphenyl (350 mg, 1.5 mmol, 1.5 equiv.), *N*-methoxy-*N*-methyl-3-morpholinopropanamide (202 mg, 1.00 mmol, 1.0 equiv.), *t*-BuLi (1.9 M, 1.32 mL, 2.5 mmol, 2.5 equiv.) and THF (5 mL), the desired product was obtained in 37% (109 mg) as a bright yellow oil after chromatography on silica gel (90:10 ethylacetate:methanol) and converted into the corresponding hydrochloride. FT-IR (cm⁻¹): 3023, 2861, overtones Ar = 2100-1700, 1683, 1603, 1451. ¹H-NMR (500 MHz, CDCl₃) δ: 8.03 (d, *J* = 8.4 Hz, 2H, Ar), 7.68 (d, *J* = 8.4 Hz, 2H, Ar), 7.62 (d, *J* = 7.6 Hz, 2H, Ar), 7.47 (t, *J* = 7.4 Hz, 2H, Ar), 7.40 (t, *J* = 7.4 Hz, 1H, Ar), 3.73 (t, *J* = 4.6 Hz, 4H, Mor-3, Mor-5), 3.23 (t, *J* = 7.4 Hz, 2H, COCH₂CH₂), 2.87 (t, *J* = 7.7 Hz, 2H, CH₂CH₂N), 2.54

(brs, 4H, Mor-2, Mor-6). ¹³C-NMR (125 MHz, CDCl₃) δ: 198.4, 145.8, 139.7, 135.4, 128.9, 128.6, 128.2, 127.2, 66.8, 53.6, 53.5, 35.9. UHPLC-ESI-MS: ABP t_R = 1.74, 99% pure (λ = 254 nm), m/z = 296.3 [M + H]⁺.

4-benzyl-1-(4-oxo-4-phenylbutyl)piperidin-1-ium hydrochloride (23) By following the General Procedure, starting from bromobenzene (236 mg, 1.5 mmol, 1.5 equiv.), 4-(4-benzylpiperidin-1-yl)-*N*-methoxy-*N*-methylbutanamide (304 mg, 1.00 mmol, 1.0 equiv.), *t*-BuLi (1.9 M, 1.32 mL, 2.5 mmol, 2.5 equiv.) and THF (5 mL), the desired product was obtained in 31% yield (100 mg) as a bright yellow oil after chromatography on silica gel (80:20 ethylacetate:methanol) and converted into the corresponding hydrochloride. FT-IR (cm⁻¹): 3025, 2930, 2849, overtones Ar = 2100-1700, 1680, 1595, 1580, 1452, 1414. ¹H-NMR (500 MHz, CDCl₃) δ: 12.06 (brs, 1H, NH⁺), 7.94 (d, *J* = 7.2 Hz, 2H, Ar), 7.59 (t, *J* = 7.4 Hz, 1H, Ar), 7.47 (t, *J* = 7.3 Hz, 2H, Ar), 7.29 (t, *J* = 7.1 Hz, 2H, Ar), 7.22 (t, *J* = 7.1 Hz, 2H, Ar), 7.13 (d, *J* = 7.0 Hz, 1H, Ar), 3.60 (brd, 2H, Pip-2, Pip-6), 3.22 (brs, 2H, COCH₂CH₂), 3.04 (brs, 2H, CH₂CH₂N), 2.63 (m, 4H, CH₂Pip-4, Pip-2, Pip-6), 2.34 (brs, 2H, CH₂CH₂CH₂), 2.10 (m, 2H, Pip-3, Pip-5), 1.83 (d, 2H, Pip-3, Pip-5), 1.60 (m, 1H, Pip-4). ¹³C-NMR (125 MHz, CDCl₃) δ: 198.4, 139.1, 136.1, 133.7, 129.0, 128.8, 128.5, 128.0, 126.4, 57.0, 53.1, 41.9, 36.7, 35.6, 28.9, 18.0. UHPLC-ESI-MS: ABP t_R = 2.00, > 99% pure (λ = 254 nm), m/z = 322.5 [M + H]⁺.

4-benzyl-1-(4-(4-methoxyphenyl)-4-oxobutyl)piperidin-1-ium hydrochloride (24) By following the General Procedure, starting from 1-bromo-4-methoxybenzene (281 mg, 1.5 mmol, 1.5 equiv.), 4-(4-benzylpiperidin-1-yl)-*N*-methoxy-*N*-methylbutanamide (304 mg, 1.00 mmol, 1.0 equiv.), *t*-BuLi (1.9 M, 1.32 mL, 2.5 mmol, 2.5 equiv.) and THF (5 mL), the desired product was obtained in 30% yield (106 mg) as a bright yellow oil after chromatography on silica gel (80:20 ethylacetate:methanol) and converted into the corresponding hydrochloride. FT-IR (cm⁻¹): 3024, 3003, 2922, overtones Ar = 2100-1700, 1677, 1603, 1451. ¹H-NMR (500 MHz, CDCl₃) δ: 12.03 (brs, 1H, NH⁺), 7.92 (d, *J* = 8.1 Hz, 2H, Ar), 7.29 (t, *J* = 7.2 Hz, 2H, Ar), 7.21 (t, *J* = 7.2 Hz, 1H, Ar), 7.12 (d, *J* = 7.1 Hz, 2H, Ar), 6.92 (d, *J* = 8.0 Hz, 2H, Ar), 3.87 (s, 3H, OCH₃), 3.59 (brd, 2H, Pip-2, Pip-6), 3.16 (brs, 2H, COCH₂CH₂), 3.03 (brs, 2H, CH₂CH₂N), 2.62 (m, 4H, CH₂Pip-4, Pip-2, Pip-6), 2.32 (brs, 2H, CH₂CH₂CH₂), 2.08 (m, 2H, Pip-3, Pip-5), 1.82 (d, 2H, Pip-3, Pip-5), 1.73 (brs, 1H, Pip-4). ¹³C-NMR (125 MHz, CDCl₃) δ: 196.9, 163.8, 139.1, 130.3, 129.2, 129.0, 128.5, 126.3, 113.9, 57.0, 55.5, 53.0, 41.9, 36.6, 35.1, 28.8, 18.1. UHPLC-ESI-MS: ABS t_R = 1.43, 99% pure (λ = 254 nm), m/z = 352.4 [M + H]⁺.

4-benzyl-1-(4-(3-methoxyphenyl)-4-oxobutyl)piperidin-1-ium hydrochloride (25) By following the General Procedure, starting from 1-bromo-3-methoxybenzene (281 mg, 1.5 mmol, 1.5 equiv.), 4-(4-benzylpiperidin-1-yl)-*N*-methoxy-*N*-methylbutanamide (304 mg, 1.00 mmol, 1.0 equiv.), *t*-BuLi (1.9 M, 1.32 mL, 2.5 mmol, 2.5 equiv.) and THF (5 mL), the desired product was obtained in 33% yield (116 mg) as a bright yellow oil after

chromatography on silica gel (80:20 ethylacetate:methanol) and converted into the corresponding hydrochloride. FT-IR (cm^{-1}): 3022, 2946, 2861, overtones Ar = 2100-1700, 1687, 1595, 1486, 1465. $^1\text{H-NMR}$ (500 MHz, CDCl_3) δ : 12.04 (brs, 1H, NH^+), 7.52 (d, $J = 7.4$ Hz, 1H, Ar), 7.45 (s, 1H, Ar), 7.37 (t, $J = 7.9$ Hz, 1H, Ar), 7.29 (t, $J = 7.2$ Hz, 2H, Ar), 7.21 (t, $J = 7.2$ Hz, 1H, Ar), 7.13 (m, 3H, Ar), 3.85 (s, 3H, OCH_3), 3.59 (brd, 2H, Pip-2, Pip-6), 3.21 (brs, 2H, COCH_2CH_2), 3.03 (brs, 2H, $\text{CH}_2\text{CH}_2\text{N}$), 2.63 (m, 4H, $\text{CH}_2\text{Pip-4}$, Pip-2, Pip-6), 2.33 (brs, 2H, $\text{CH}_2\text{CH}_2\text{CH}_2$), 2.09 (m, 2H, Pip-3, Pip-5), 1.83 (d, 2H, Pip-3, Pip-5), 1.73 (brs, 1H, Pip-4). $^{13}\text{C-NMR}$ (125 MHz, CDCl_3) δ : 198.3, 159.8, 139.1, 137.4, 129.8, 129.0, 128.5, 126.4, 120.6, 120.1, 112.0, 56.9, 55.5, 53.0, 41.9, 36.6, 35.6, 28.8, 18.0. UHPLC-ESI-MS: ABP $t_R = 2.08$, 99% pure ($\lambda = 254$ nm), $m/z = 352.5$ [$\text{M} + \text{H}$] $^+$.

4-benzyl-1-(4-(naphthalen-2-yl)-4-oxobutyl)piperidin-1-ium hydrochloride (26) By following the General Procedure, starting from 2-bromonaphthalene (311 mg, 1.5 mmol, 1.5 equiv.), 4-(4-benzylpiperidin-1-yl)-*N*-methoxy-*N*-methylbutanamide (304 mg, 1.00 mmol, 1.0 equiv.), *t*-BuLi (1.9 M, 1.32 mL, 2.5 mmol, 2.5 equiv.) and THF (5 mL), the desired product was obtained in 41% (152 mg) as a bright yellow oil after chromatography on silica gel (80:20 ethylacetate:methanol) and converted into the corresponding hydrochloride. FT-IR (cm^{-1}): 3055, 3027, 2937, 2907, overtones Ar = 2100-1700, 1681, 1496, 1441. $^1\text{H-NMR}$ (500 MHz, CDCl_3) δ : 12.06 (brs, 1H, NH^+), 8.50 (s, 1H, Nap), 7.98 (d, $J = 8.1$ Hz, 2H, Nap), 7.88 (t, $J = 10.0$ Hz, 2H, Nap), 7.61 (t, $J = 6.8$ Hz, 1H, Nap), 7.57 (t, $J = 6.9$ Hz, 1H, Nap), 7.29 (t, $J = 7.1$ Hz, 2H, Ar), 7.22 (t, $J = 7.1$ Hz, 1H, Ar), 7.14 (d, $J = 7.1$ Hz, 2H, Ar), 3.62 (brd, 2H, Pip-2, Pip-6), 3.37 (brs, 2H, COCH_2CH_2), 3.09 (brs, 2H, $\text{CH}_2\text{CH}_2\text{N}$), 2.64 (m, 4H, $\text{CH}_2\text{Pip-4}$, Pip-2, Pip-6), 2.41 (brs, 2H, $\text{CH}_2\text{CH}_2\text{CH}_2$), 2.11 (m, 2H, Pip-3, Pip-5), 1.84 (d, 2H, Pip-3, Pip-5), 1.71 (m, 1H, Pip-4). $^{13}\text{C-NMR}$ (125 MHz, CDCl_3) δ : 198.4, 139.1, 135.6, 133.4, 132.4, 130.1, 129.7, 129.0, 128.8, 128.7, 128.5, 127.8, 126.4, 123.4, 57.0, 53.1, 41.9, 36.6, 35.7, 28.9, 18.2. UHPLC-ESI-MS: ABS $t_R = 1.67$, > 99% pure ($\lambda = 254$ nm), $m/z = 372.5$ [$\text{M} + \text{H}$] $^+$.

4-benzyl-1-(4-(6-methoxynaphthalen-2-yl)-4-oxobutyl)piperidin-1-ium hydrochloride (27) By following the General Procedure, starting from 2-bromo-6-methoxynaphthalene (256 mg, 1.5 mmol, 1.5 equiv.), 4-(4-benzylpiperidin-1-yl)-*N*-methoxy-*N*-methylbutanamide (304 mg, 1.00 mmol, 1.0 equiv.), *t*-BuLi (1.9 M, 1.32 mL, 2.5 mmol, 2.5 equiv.) and THF (5 mL), the desired product was obtained in 25% (101 mg) as a bright yellow oil after chromatography on silica gel (80:20 ethylacetate:methanol) and converted into the corresponding hydrochloride. FT-IR (cm^{-1}): 3024, 2936, overtones Ar = 2100-1700, 1674, 1482, 1409. $^1\text{H-NMR}$ (500 MHz, CDCl_3) δ : 12.06 (brs, 1H, NH^+), 8.41 (s, 1H, Nap), 7.95 (d, $J = 8.3$ Hz, 1H, Nap), 7.85 (t, $J = 8.7$ Hz, 1H, Nap), 7.76 (d, $J = 8.4$ Hz, 1H, Nap), 7.29 (t, $J = 7.1$ Hz, 2H, Ar), 7.21 (t, 2H, Ar, Nap), 7.13 (d, 3H, Ar, Nap), 3.94 (s, 3H, CH_3), 3.61 (brd, 2H, Pip-2, Pip-6), 3.32 (brs, 2H, COCH_2CH_2), 3.08 (brs, 2H, $\text{CH}_2\text{CH}_2\text{N}$), 2.63 (m, 4H, $\text{CH}_2\text{Pip-4}$, Pip-2, Pip-6), 2.38 (brs, 2H, $\text{CH}_2\text{CH}_2\text{CH}_2$), 2.09 (m, 2H, Pip-3, Pip-5), 1.83 (d, 2H, Pip-3, Pip-5), 1.74 (m, 1H, Pip-4). $^{13}\text{C-NMR}$ (125 MHz, CDCl_3) δ : 198.1, 159.9, 139.1, 137.5, 131.5, 131.3, 129.9, 129.0, 128.5,

127.7, 127.3, 126.4, 124.2, 119.9, 105.6, 57.0, 55.4, 53.0, 41.9, 36.6, 35.4, 28.9, 18.2. UHPLC-ESI-MS: ABS t_R = 1.71, > 99% pure (λ = 254 nm), m/z = 4022.5 [M + H]⁺.

1-(4-([1,1'-biphenyl]-4-yl)-4-oxobutyl)-4-benzylpiperidin-1-ium hydrochloride (28) By following the General Procedure, starting from 4-bromo-1,1'-biphenyl (350 mg, 1.5 mmol, 1.5 equiv.), 4-(4-benzylpiperidin-1-yl)-*N*-methoxy-*N*-methylbutanamide (304 mg, 1.00 mmol, 1.0 equiv.), *t*-BuLi (1.9 M, 1.32 mL, 2.5 mmol, 2.5 equiv.) and THF (5 mL), the desired product was obtained in 26% (103 mg) as a bright yellow oil after chromatography on silica gel (80:20 ethylacetate:methanol) and converted into the corresponding hydrochloride. FT-IR (cm⁻¹): 3083, 3025, 2995, 2850, overtones Ar = 2100-1700, 1684, 1604. ¹H-NMR (500 MHz, CDCl₃) δ : 12.07 (brs, 1H, NH⁺), 8.02 (d, J = 6.3 Hz, 2H, Ar), 7.69 (d, J = 6.3 Hz, 2H, Ar), 7.62 (d, J = 7.2 Hz, 2H, Ar), 7.46 (t, J = 7.1 Hz, 2H, Ar), 7.41 (t, J = 7.2 Hz, 1H, Ar), 7.30 (t, J = 7.1 Hz, 2H, Ar), 7.22 (t, J = 7.2 Hz, 1H, Ar), 7.14 (d, J = 7.0 Hz, 2H, Ar), 3.61 (brd, 2H, Pip-2, Pip-6), 3.26 (brs, 2H, COCH₂CH₂), 3.07 (brs, 2H, CH₂CH₂N), 2.64 (m, 4H, CH₂Pip-4, Pip-2, Pip-6), 2.37 (brs, 2H, CH₂CH₂CH₂), 2.11 (m, 2H, Pip-3, Pip-5), 1.85 (d, 2H, Pip-3, Pip-5), 1.73 (m, 1H, Pip-4). ¹³C-NMR (125 MHz, CDCl₃) δ : 198.0, 146.2, 139.6, 139.1, 134.8, 129.0, 128.7, 128.5, 128.4, 127.4, 127.2, 126.4, 57.0, 53.2, 41.9, 36.7, 35.7, 28.9, 18.1. UHPLC-ESI-MS: ABS t_R = 1.81, 98% pure (λ = 254 nm), m/z = 398.4 [M + H]⁺.

1-(4-(naphthalen-2-yl)-4-oxobutyl)piperidin-1-ium hydrochloride (29) By following the General Procedure, starting from 2-bromonaphthalene (1.5 equiv.), *N*-methoxy-*N*-methyl-4-(piperidin-1-yl)-butanamide (1.0 equiv.), *t*-BuLi (1.7M, 2.5 equiv.) and THF, the desired product was obtained in 58% yield as a pale yellow solid after chromatography on silica gel (60:40 ethylacetate/methanol) and converted into the corresponding hydrochloride. R_f: 0.17 (50:50 ethylacetate/methanol). mp: 213-215°C. ¹H-NMR (400 MHz, MeOD): δ 8.66 (s, 1H, Napht), 8.10 – 8.05 (m, 2H, Napht), 8.01 – 7.94 (m, 2H, Napht), 7.64 (m, 2H, Napht), 3.65 (d, J = 12.3 Hz, 2H, pip), 3.40 (t, J = 6.6 Hz, 2H, CH₂CH₂CH₂), 3.28 – 3.20 (m, 2H, CH₂CH₂CH₂), 3.01 (t, J = 12.4 Hz, 2H, pip), 2.29 – 2.17 (m, 2H, CH₂CH₂CH₂), 2.01 (d, J = 14.9 Hz, 2H, pip), 1.86 (m, 3H, pip), 1.63 – 1.52 (m, 1H, pip). ¹³C-NMR (125 MHz, CDCl₃) δ : 199.1, 130.0, 129.7, 128.7, 128.5, 127.8, 126.1, 122.6, 56.7, 53.1, 35.6, 22.4, 22.1, 18.0.

1-(4-([1,1'-biphenyl]-4-yl)-4-oxobutyl)piperidin-1-ium hydrochloride (30) By following the General Procedure, starting from 4-bromo-1,1'-biphenyl (1.5 equiv.), *N*-methoxy-*N*-methyl-4-(piperidin-1-yl)-butanamide (1.0 equiv.), *t*-BuLi (1.7M, 2.5 equiv.) and THF, the desired product was obtained in 72% yield as a pale yellow solid after chromatography on silica gel (40:60 ethylacetate/methanol) and converted into the corresponding hydrochloride. R_f: 0.23 (40:60 ethylacetate/methanol). mp: 250-251°C. ¹H-NMR (400 MHz, MeOD): δ 8.13 (d, J = 8.3 Hz, 2H, Ph-PhCO), 7.81 (d, J = 8.3 Hz, 2H, PhPhCO), 7.71 (d, J = 7.6 Hz, 2H, PhPhCO), 7.51 (t, J = 7.5 Hz,

2H, *PhPhCO*), 7.43 (t, $J = 7.3$ Hz, 1H, *PhPhCO*), 3.63 (brs, 2H, pip), 3.28 (t, $J = 6.6$ Hz, 2H, $\text{CH}_2\text{CH}_2\text{CH}_2$), 3.25 – 3.18 (m, 2H, $\text{CH}_2\text{CH}_2\text{CH}_2$), 3.00 (brs, 2H, pip), 2.25 – 2.13 (m, 2H, $\text{CH}_2\text{CH}_2\text{CH}_2$), 1.92 (brs, 5H, pip), 1.59 (brs, 1H, pip). $^{13}\text{C-NMR}$ (125 MHz, CDCl_3) δ : 198.8, 145.8, 139.7, 135.7, 130.0, 128.9, 128.6, 128.3, 127.3, 56.7, 53.2, 35.6, 22.5, 22.2, 18.0.

1-(4-(4-(benzyloxy)phenyl)-4-oxobutyl)piperidin-1-ium hydrochloride (31) By following the General Procedure, starting from 1-(benzyloxy)-4-bromobenzene (1.5 equiv.), N-methoxy-N-methyl-4-(piperidin-1-yl)-butanamide (1.0 equiv.), *t*-BuLi (1.7M, 2.5 equiv.) and THF, the desired product was obtained in 53% yield as a pale yellow solid after chromatography on silica gel (60:40 ethylacetate/methanol) and converted into the corresponding hydrochloride. R_f: 0.18 (40:60 ethylacetate/methanol). mp: 188-190°C. $^1\text{H-NMR}$ (400 MHz, MeOD) δ : 8.02 (d, $J = 8.8$ Hz, 2H, *OPhCO*), 7.47 (d, $J = 7.4$ Hz, 2H, *PhCH}_2*), 7.40 (t, $J = 7.3$ Hz, 2H, *PhCH}_2*), 7.35 (d, $J = 7.1$ Hz, 1H, *PhCH}_2*), 7.12 (d, $J = 8.8$ Hz, 2H, *OPhCO*), 5.21 (s, 2H, *PhCH}_2\text{OPh}*), 3.60 (brs, 2H, pip), 3.18 (m, 4H, $\text{CH}_2\text{CH}_2\text{CH}_2$), 2.98 (brs, 2H, pip), 2.21 – 2.08 (m, 2H, $\text{CH}_2\text{CH}_2\text{CH}_2$), 2.04 – 1.72 (brs, 5H, pip), 1.57 (brs, 1H, pip). $^{13}\text{C-NMR}$ (125 MHz, CDCl_3) δ : 198.1, 160.0, 138.1, 137.4, 130.1, 128.1, 127.7, 127.3, 114.4, 69.7, 56.3, 53.1, 31.2, 22.8, 21.5, 18.1.

5.3.4 synthesis of (R)-RC-33A with route A

Synthesis of (E)-ethyl 3-([1,1'-biphenyl]-4-yl)but-2-enoate (43)

In a dry double-necked round bottom flask, under inert atmosphere (N_2), 4-bromo-1,1'-biphenyl (4.00 g, 17.16 mmol, 1 equiv.), TEAC (tetraethylammonium chloride, 9.53 g, 34.3 mmol, 2 equiv.), AcONa (2.81 g, 34.3 mmol, 2 equiv.), $\text{Pd}(\text{Oac})_2$ (0.19 g, 0.86 mmol, 0.05 equiv.) and ethyl crotonate (3.12 ml, 25.74 mmol, 1.5 equiv.) are solubilized in DMF (55 ml). The mixture is kept under magnetic stirring and refluxed overnight. Afterwards, the crude was filtered on Celite and concentrated *in vacuo*. The residue was added to 150 ml of dichloromethane (DCM) and extracted with water (3 × 100 ml). the organic layer is dried on Na_2SO_4 , filtered and concentrated *in vacuo*. The crude product (yellow solid) was purified by flash chromatography on silica gel, eluting with *n*-hexane/ethyl acetate (97/3, v/v). White solid; yield: 66%; m.p.: 82.0- 84.0 °C; R_f = 0.35 (TLC: *n*-hexane/AcOEt, 95/5, v/v); IR (cm^{-1}): 3396, 2935, 1921, 1704, 1623, 1260, 1173, 1041, 839, 768; $^1\text{H-}$

NMR (400 MHz CDCl₃) δ (ppm)= 7.68-7.57 (m, 6H, aromatic), 7.51-7.44 (m, 2H, aromatic), 7.43-7.36 (m, 1H, aromatic), 6.23 (s, 1H, ArCCH), 4.26 (q, $J = 7.1$ Hz, 2H, COOCH₂), 2.64 (s, 3H, ArCCH₃), 1.36 (t, 3H, $J = 7.1$ Hz, CH₂CH₃).

Synthesis of (*R*)-ethyl 3-([1,1'-biphenyl]-4-yl)butanoate (**44**)

Catalyst (*S,S*)-Ir(ThrePHOX) (213 mg, 0.124 mmol, 0.01 equiv.) was weighted in a glass vessel. The vessel was purged with nitrogen, and a 0.362 M DCM solution (34 ml) of **43** (3.301 g, 12.39 mmol, 1 equiv.) was added. The vessel was placed into the autoclave and purged three-times with hydrogen at 70 bar. The reaction was stirred overnight at room temperature under pressure of hydrogen, then hydrogen was released, DCM was evaporated, and the conversion was determined by NMR analysis of the crude. The desired product was obtained after purification by flash chromatography (98:2 and then 97:3 *n*-hexane/ethyl acetate) as a colorless oil. Then the *ee* was determined by enantioselective HPLC. Colorless oil; yield: 95%; $R_f = 0.25$ (TLC: *n*-hexane/AcOEt, 97/3, v/v); IR (cm⁻¹): 3030, 2971, 2926, 1908, 1731, 1487, 1163, 1033, 765, 697; HPLC: $t_R = 11.24$ min, *ee* 83% [Chiralcel OJ-H (4.6 mm I.D. x 150 mm L, ps = 5 μ m); eluent: *n*-heptane/*i*-PrOH = 90/10 (v/v); flux: 0.8 mL/min; ($\lambda = 250$ nm)]; **¹H-NMR** (400 MHz CDCl₃) δ (ppm)= 7.64-7.53 (m, 4H, aromatic), 7.49-7.42 (m, 2H, aromatic), 7.39-7.30 (m, 3H, aromatic), 4.12 (q, $J = 7.1$ Hz, 2H COOCH₂), 3.42-3.30 (m, 1H, ArCH), 2.68 (dd, $J_1 = 15.0$, $J_2 = 7.1$ Hz, 1H, ArCHCH-*H*), 2.60 (dd, $J_1 = 15.0$, $J_2 = 7.1$ Hz, 1H, ArCHCH-*H*), 1.37 (d, $J = 7.0$ Hz, 3H, ArCCH₃), 1.22 (t, $J = 7.1$ Hz, 3H, CH₂CH₃).

Synthesis of (*R*)-3-([1,1'-biphenyl]-4-yl)butanoic acid (**45**)

3M NaOH (65 ml) was added to compound **44** (2.76 g, 10.29 mmol) in 50 ml of abs. EtOH and the reaction mixture was maintained under stirring at room temperature for 2 h. The organic phase was then evaporated, and the residue dissolved in water. The aqueous phase was made acid with 1M HCl (pH 2) and then extracted with ethyl acetate (3 x 100 ml). The combined organic phases were dried over anhydrous Na₂SO₄ and evaporated to dryness, yielding the desired product as a white solid. The *ee* was determined by enantioselective HPLC. [column: ChiralpakTM IC (4.6mm I.D. x 250mm L, ps = 5 μ m); eluent: *n*-heptane/*i*PrOH/TFA, 96/4/0.1 (v/v/v); flow: 0.8 mL/min; ($\lambda = 254$ nm)]. White solid, m.p.= 110.1°C-111.5; yield= 97%; $R_f = 0.33$ (TLC: *n*-hexane:AcOEt:HCOOH, 80:20:1, v/v/v); IR (cm⁻¹) 3033, 2961, 2925, 1705, 1697, 1488, 1409, 1297, 947, 834, 761, 687; HPLC: $t_R = 8.31$ min; e.e. 83% [ChiralpakTM IC (4.6mm I.D. x 250mm L, ps = 5 μ m); eluent: *n*-hexane/*i*-PrOH/TFA, 96/4/0,1 (v/v/v); flux: 0.8 mL/min; ($\lambda = 254$ nm)]; [α]_D²⁰ = -33.6; **¹H-NMR** (400 MHz, CDCl₃) δ (ppm)= 7.57 (dt, $J_1 = 7.06$ Hz, $J_2 = 1.31$ Hz, 2H, aromatic), 7.53 (dt, $J_1 = 8.33$ Hz, $J_2 = 2.51$ Hz, 2H, aromatic), 7.42 (t, $J = 7.32$ Hz, 2H, aromatic), 7.35-7.28 (m, 3H, aromatic), 3.39-3.29 (m, 1H,

CHCH₃), 2.71 (dd, $J_1 = 15.58$ Hz, $J_2 = 6.86$ Hz, 1H, CH₂CH), 2.61 (dd, $J_1 = 15.58$ Hz, $J_2 = 8.17$ Hz, 1H, CH₂CH), 1.35 (d, $J = 6.97$ Hz, 3H, CHCH₃).

Fractional crystallization on acid **45**

A solution of acid **45** (*ee* 83%, 2.483 mmol; 240.3 mg; 1 eq) in MeOH (8 mL) is added to (S)-phenylethylamine (2.483 mmol; 0.312 mL; 1eq; $d = 0.965$ g/mL); the mixture is maintained under magnetic stirring and then concentrated under reduced pressure. The diastereomeric salts of R/S-**45** are crystallized from MeOH/H₂O (1:1 v/v). The white crystals thus obtained are filtered on Buchner and dried, whereas the mother liquor is concentrated *in vacuo* and then extracted with CH₂Cl₂ and a 10% aqueous solution of HCl (3x20 mL). the organic layer is dried on Na₂SO₄ and concentrated under reduced pressure. A white solid is thus obtained, which is analyzed by means of enantioselective HPLC [column: Chiralpak™ IC (4.6mm I.D. × 250mm L, $\psi = 5$ μm); eluent: n-hexane/iPrOH/TFA, 96/4/0.1 (v/v/v); flow: 1 mL/min; ($\lambda = 254$ nm)].

(*R*)-3-([1,1'-biphenyl]-4-yl)butanoic acid [**45**]: white solid. Yield: 94%. Rf: 0.5 (TLC: DCM/MeOH, 9/1 v/v). m.p.= 110-112°C; HPLC: $t_R = 7.49$ min; *ee* 94,5% [Chiralpak™ IC (4.6mm I.D. × 250mm L, $\psi = 5$ μm); eluent: n-hexane/*i*-PrOH/TFA, 96/4/0,1 (v/v/v); flux: 1 mL/min; ($\lambda = 254$ nm)]; [α]_D²⁰ = -21.6 ($c = 0.5\%$ in MeOH). IR (cm⁻¹) 3033, 2961, 2925, 1705, 1697, 1488, 1409, 1297, 947, 834, 761, 687. ¹H-NMR (400 MHz, CDCl₃) δ (ppm)= 7.57 (dt, $J_1 = 1.31$ Hz, $J_2 = 7.06$ Hz, 2H, aromatic), 7.53 (dt, $J_1 = 2.51$ Hz, $J_2 = 8.33$ Hz, 2H, aromatic), 7.43 (t, $J = 7.32$ Hz, 2H, aromatic), 7.35-7.28 (m, 3H, aromatic), 3.39-3.29 (m, 1H; CHCH₃), 2.71 (dd, $J_1 = 6.86$ Hz, $J_2 = 15.58$ Hz, 1H; CH₂CH), 2.61 (dd, $J_1 = 8.17$ Hz, $J_2 = 15.58$ Hz, 1H; CH₂CH), 1.35 (d, $J = 6.97$ Hz, 3H; CHCH₃).

Synthesis of (*R*)-tert-butyl (1-(3-([1,1'-biphenyl]-4-yl)butanoyl)piperidin-4-yl)carbamate (**46**)

Enantioenriched acid **45** (146.8 mg, 0.611 mmol, 1 eq.) is dissolved in acetonitrile (14 mL) with 2-(1H-Benzotriazole-1-yl)-1,1,3,3-tetramethylammonium tetrafluoroborate (TBTU, 235.0 mg, 0.733 mmol, 1.2 eq.) and N,N-diisopropylethylamine (DIPEA, 214.0 μL, 1.222 mmol, 2 eq.). the reaction mixture is heated with a microwave oven to 50 °C for 10 minutes at 200 W. After the formation of acid-TBTU adduct is verified by TLC analysis (DCM/MeOH/NH₃ in MeOH 7 N 90:10:0.1 v/v/v), the proper amount of 4-(N-Boc-amino)piperidine (258.0 mg, 0.611 mmol, 1 eq.) is added to the reaction mixture. This is subjected to 5 heating cycles at the microwave oven at 90 °C and 200 W for 10 minutes. Afterwards, the solvent is evaporated under reduced pressure, the crude product is solubilized in AcOEt (100 mL) and extracted, in order, with an aqueous solution of NaOH 1M (1x100 mL) and with (R/S) tartaric acid 1M (1x100 mL). The organic layer is then dried with Na₂SO₄, filtered and evaporated under reduced pressure. Compound (*R*)-**4** is obtained as a yellow/orange solid and used for the subsequent synthetic step without further purification. Yellow/orange solid. Yield =

95.8%; $R_f = 0.83$ (TLC: DCM/MeOH, 9/1 v/v); m.p. = 130 °C; HPLC: $t_R = 14.2$ min; ee: 93.4% [Chiralpak™ OJ-H (4.6mm I.D. × 150mm L, ps = 5 μm); eluent: MeOH; flux: 0.8 mL/min; ($\lambda = 250$ nm)]; $[\alpha]_D^{20} = -6.4$ (c = 0.5% in MeOH); IR (cm^{-1}) = 606.503, 630.60, 713.533, 751.138, 789.707, 847.561, 1044.26, 1170.58, 1243.86, 1320.04, 1391.39, 1473.35, 1520.6, 1627.63, 1747.19, 1779.01, 2348.87, 2832.92, 2887.88, 2981.41, 3343.96, 3721.94. ¹H-NMR (400MHz, CDCl₃) δ (ppm)= 7.57 (dd, $J = 13.7, 7.6$ Hz, 4H, aromatic), 7.44 (d, $J = 7.3$ Hz, 2H, aromatic), 7.35 (s, 3H, aromatic), 2.86-2.51 (m, 3H, CH₃CHCH₂, CH₂CO, CHNBoc), 2.12 (s, 2H, piperidine), 1.93 (m, 7H, piperidine), 1.45 (d, $J = 10.0$ Hz, 12 H, C-(CH₃)₃), 1.39 (d, $J = 6.3$ Hz, 3H, CHCH₃).

Synthesis of (R)-3-([1,1'-biphenyl]-4-yl)-1-(4-aminopiperidin-1-yl)butan-1-one (**47**)

Compound (R)-**46** (400 mg, 0.947 mmol) is dissolved in DCM (49.76 mL) and then trifluoroacetic acid (12.96 mL) is added dropwise. The reaction is maintained under magnetic stirring for 1 hour at room temperature. After complete conversion of the starting material is confirmed via TLC (DCM/MeOH 9/1 v/v) the solvent is evaporated under reduced pressure. The crude obtained is dissolved in AcOEt (100 mL) and extracted with a saturated aqueous solution of NaHCO₃ (3x100 mL). The organic layer is dried on Na₂SO₄, filtered and evaporated under reduced pressure. The desired product (R)-**5** is obtained as a pale-yellow oil which is used for the subsequent step without further purification. Pale yellow oil. Yield: 65%. $R_f = 0.29$ (TLC: DCM/MeOH 90/10, v/v). HPLC: $t_R = 5.12$ min; ee: 93% [Chiralcel™ OJ-H (4.6mm I.D. × 150mm L, ps = 5μm); eluent: MeOH/DEA, 100/0,1 v/v; flux: 0.8 mL/min; ($\lambda = 250$ nm)]. $[\alpha]_D^{20} = -16.8$ (c = 0.5% in MeOH); IR (cm^{-1})= 696.177, 730.889, 762.709, 838.883, 981.59, 1007.62, 1090.55, 1160.94, 1209.15, 1274.72, 1338.36, 1366.32, 1445.39, 1485.88, 1541.81, 1624.73, 1747.19, 2318.98, 2372.98, 2841.6, 3023.84, 3565.74, 3613.95, 3647.7, 3739.3, 3757.62, 3862.72. ¹H-NMR (400MHz, CDCl₃) δ (ppm)= 7.59 (d, $J = 7.6$ Hz, 2H, aromatic), 7.55 (d, $J = 7.6$ Hz, 2H, aromatic), 7.44 (t, $J = 7.2$ Hz, 2H, aromatic), 7.34 (m, 3H, aromatic), 2.95 (dt, 1H, CH₃CHCH₂), 2.67 (m, 2H, CHHCO, CHNH₂), 2.60-2.51 (m, 1H, CHHCO), 2.04 (bs, 6H, piperidine CH₂, NH₂), 1.91-1.75 (m, 2H, piperidine), 1.38 (d, $J = 6.8$ Hz, 3H, CH₃), 1.35-1.25 (m, 2H, piperidine).

Synthesis of (R)-1-(3-([1,1'-biphenyl]-4-yl)butyl)piperidin-4-amine, (R)-RC-33A

Compound (R)-**47** (180 mg, 0.558 mmol, 1 eq.) is placed in a dry round-bottom flask under inert atmosphere (N₂) and solubilized in anhydrous THF (5.40 mL). The flask is placed in an ice-cold bath and LiAlH₄ (1M in THF, 2.232 mL, 4 eq) is added dropwise. The reaction is left under magnetic stirring at 0° C for 2 hours and monitored via TLC (DCM/MeOH/NH₃ in MeOH 7N, 90:10:0.1, v/v/v). Upon completion, the reaction is quenched by slowly adding few drops of a saturated solution of NH₄Cl, until the effervescence ceases. The reaction mixture is allowed to reach room temperature and then it is extracted with Et₂O (3x20 mL). The reunited organic layers are dried on Na₂SO₄, filtered and evaporated under reduced pressure. The crude

product is further purified through flash chromatography (eluent DCM/MeOH/NH₃ in MeOH, gradient from 90:10:0,1 v/v/v to 90:0:10 v/v/v). The product is obtained as a white solid. White solid; yield: 69%; R_f = 0.16 (TLC: DCM/MeOH/NH₃ in MeOH, 90:10:0.1 v/v/v); HPLC: t_R = 13.6 min; ee 94.5% [Chiralcel™ AD-H (4.6mm I.D. x 150mm L, ps = 5μm); eluent: MeOH/DEA, 100/0,1 v/v; flux: 0.5 mL/min; (λ = 250 nm)]; [α]_D²⁰ = -12.68 (c = 0.5% in MeOH); IR (cm⁻¹) = 1507.1, 1521.56, 1540.85, 1558.2, 1616.06, 1636.3, 1652.7, 1683.55, 1698.02, 1867.72, 2806.88, 2927.41. ¹H NMR (400 MHz, CDCl₃) δ(ppm) = 7.60 (d, J = 7.6 Hz, 1H, aromatic), 7.54 (d, J = 8.1 Hz, 1H, aromatic), 7.45 (t, J = 7.6 Hz, 1H, aromatic), 7.34 (t, J = 7.3 Hz, 1H, aromatic), 7.30-7.25 (m, 1H, aromatic), 2.86 (m, 2H, piperidine CH₂N), 2.78 (m, J = 8.0 Hz, 1H, CH₃CHCH₂), 2.65 (m, 1H, CHNH₂), 2.32 (m, 1H, diastereotopic CHCH₂CHHN), 2.22 (m, 1H, diastereotopic CHCH₂CHHN), 1.97 (m, 2H, piperidine CH₂N), 1.83 (m, 4H, CHCH₂CH₂N and piperidine CH₂), 1.7 (bs, 2H, CHNH₂), 1.39 (m, 2H, piperidine CH₂), 1.31 (d, J = 6.9 Hz, 3H, CH₃).

5.3.5 synthesis of (R)-RC-33A with route B

Synthesis of (E)-3-([1,1'-biphenyl]-4-yl)but-2-en-1-ol (50)

In a round-bottom flask, under N₂ atmosphere, ester **43** (6.19 mmol, 1 equiv.) is solubilized in dry DCM (20 mL), and DIBAL-H (1M solution in toluene, 15.5 mmol, 2.5 equiv.) is added dropwise at -78 °C. The reaction is monitored *via* TLC (n-hexane/AcOEt 75:25) and after 30 minutes is quenched by adding AcOEt (2 mL) and Et₂O (15 mL). The mixture is stirred at room temperature and H₂O (2 mL) and Et₂O (30 mL) are added. After filtration on Celite, the crude is purified through flash chromatography on silica gel (eluent: n-hexane/AcOEt, 75:25) and the pure product is obtained as a yellow solid. Yield = 59%, m.p. = 103.5°C R_f = 0.30 (TLC: n-hexane/AcOEt, 75:25); IR (cm⁻¹): 3659, 3372, 3030, 2911, 1721, 1667, 1600, 1485, 1404, 1267, 831, 760, 694; ¹H-NMR (400 MHz, CDCl₃) δ (ppm): 7.58-7.64 (m, 4H, aromatic), 7.45-7.53 (m, 4H, aromatic), 7.34-7.40 (m, 1H, aromatic), 6.06-6.10 (t, 1H, J = 8.0 Hz, ArCCHCH₂OH), 4.42 (d, 2H, J = 8.0 Hz, ArCCHCH₂), 2.15 (s, 1H, CH₃).

Synthesis of (E)-3-([1,1'-biphenyl]-4-yl)but-2-enal (48)

Allylic alcohol **50** (1.070 mmol, 1 equiv.) is solubilized in THF (8 mL) and MnO₂ (21.4 mmol, 20 equiv.) is added in four equal portions over 6 hours. Then, the reaction mixture is filtered on Celite and the desired product is obtained as a white solid, with sufficient purity for the next step. Yield = 66%, R_f = 0.35 (TLC: n-hexane/AcOEt 85:15); IR (cm⁻¹): 3745, 3714, 2997, 2902, 2846, 2143, 1650, 1486, 1324, 831, 734, 691, 601; ¹H-NMR (400

MHz) (CDCl₃) δ (ppm): 10.23 (d, 1H, COH), 7.61-7.72 (m, 6H, aromatic), 7.47-7.51 (t, 2H, aromatic), 7.40 (m, 1H, aromatic), 6.49 (d, 1H, $J = 8.0$ Hz, ArCCHCOH), 2.6 (s, 1H, ArCCH₃).

Synthesis of (*R*)-3-([1,1'-biphenyl]-4-yl)butanal (**49**)

Compound **48** (0.158mmol, 1 equiv.) is solubilized in CHCl₃ (1 mL), and the flask is placed into an acetone bath kept at -30 °C through a cryostat. Reagent (*S*)-Mac-H is then added to the reaction mixture (0.108 mmol, 0.7 equiv.). The reagent contains a mixture 1:6 of Hantzsch ester and (*S*)-2-(tert-butyl)-3-methyl-4-oxoimidazolidinium trifluoroacetate (MacMillan's imidazolidinone). The reaction is monitored via TLC (n-hexane/DCM/AcOEt 9.5:0.5:0.5). After 12 hours, the reaction is stopped. The mixture is extracted with Et₂O and HCl 10% (3 x 10 mL). The organic layer is dried on Na₂SO₄, filtered and concentrated under vacuum. The crude is purified by flash chromatography on silica gel (eluent: n-hexane/DCM/AcOEt 9.5:0.5:0.5) and the product is obtained as a colorless oil. Yield: 26 % $R_f = 0,39$ (n-hexane/DCM/AcOEt 9.5:0.5:0.5) IR (cm⁻¹): 3667, 3020, 29578, 2930, 1730, 1495, 1407, 865, 770, 734, 697; ¹H-NMR (400 MHz, CDCl₃) δ (ppm): 9.77 (s, 1H, COH), 7.56-7.61 (m, 4H, aromatic), 7.44-7.47 (m, 2H, aromatic), 7.31-7.38 (m, 3H, aromatic), 3.9-3.49 (m, 1H, ArCH), 2.69-2.86 (m, 2H, ArCHCH₂), 1.38 (d, $J = 7.0$ Hz, 3H, ArCHCH₃).

5.3.6 Synthesis of (*R*)-RC-33A with route C

Synthesis of (*R*)-ethyl 3-([1,1'-biphenyl]-4-yl)butanoate (**44**)

To a round-bottom flask previously conditioned with N₂, catalyst (*R,R*) Naph-diPIM-dioxo-*i*Pr/CoCl₂ (1.5 mg, 0.01 equiv.), NaBH₄ (15 mg, 2 equiv.) and ester **43** (49 mg, 1 equiv.) are added in sequence. Then, the flask is placed in an ice-cold bath and the reagents are solubilized in DCM (2 mL). The obtained solution is blue. Afterwards, MeOH (2 mL) is added dropwise under magnetic stirring. After 10 minutes of stirring at 0 °C, the ice bath is removed, and the reaction is left under stirring at r.t. for 1h. After this time the reaction mixture is almost completely clear and TLC analysis (cyclohexane/AcOEt 96:4) confirms complete consumption of the starting material. The reaction is quenched with HCl 1M (4 mL) and extracted with DCM (4 x 4 mL). The organic phase is dried on Na₂SO₄, filtered and concentrated under vacuum. The obtained crude (pale blue solid) is purified through filtration on silica gel (eluent: cyclohexane/AcOEt 96:4). The pure product is a yellowish oil (46 mg). Yield = 94%. HPLC: RT = 17.68 min, ee 98% [Chiralcel OJ-H (4.6 mm I.D. x 150 mm L, ps = 5 μ m); eluent: *n*-heptane/*i*-PrOH = 90/10 (v/v); flux: 0.8 mL/min; ($\lambda = 250$ nm)]; ¹H-NMR (400 MHz CDCl₃) δ

(ppm) = 7.64-7.53 (m, 4H, aromatic), 7.49-7.42 (m, 2H, aromatic), 7.39-7.30 (m, 3H, aromatic), 4.12 (q, $J = 7.1$ Hz, 2H $\text{CO}_2\text{CH}_2\text{CH}_3$), 3.36 (m, 1H, ArCHCH_3), 2.68 (dd, $J_1 = 15.0$, $J_2 = 7.1$ Hz, 1H, diastereotopic ArCHCHH), 2.60 (dd, $J_1 = 15.0$, $J_2 = 7.1$ Hz, 1H, diastereotopic ArCHCHH), 1.37 (d, $J = 7.0$ Hz, 3H, ArCCH_3), 1.22 (t, $J = 7.1$ Hz, 3H, CH_2CH_3).

Synthesis of (R)-3-([1,1'-biphenyl]-4-yl)butanal (49)

In a dry round-bottom flask, under N_2 atmosphere, compound **44** (23 mg, 0.09 mmol, 1 equiv.) is solubilized in anhydrous DCM (4 mL). The flask is placed in a dry ice/acetone bath (-78 °C) and DIBAL-H (1M solution in toluene, 0.09 mL, 1 equiv.) is added dropwise under magnetic stirring. After 15 minutes, TLC analysis (cyclohexane/AcOEt 94:6) confirms complete consumption of the starting material. The reaction is quenched by adding H_2O (3 mL) at -78 °C, then the flask is removed from the bath, diluted with Et_2O (4 mL) and left under magnetic stirring for some minutes. The mixture is then transferred to a separatory funnel and more H_2O (7 mL) and Et_2O (6 mL) are added. After extraction with ether (3 x 6 mL), the organic layers are reunited, dried on Na_2SO_4 , filtered and concentrated under vacuum. The crude is purified through filtration on silica gel (eluent: cyclohexane/AcOEt 92:8). The pure product is obtained as a white solid. Yield = 80%. $^1\text{H-NMR}$ (400 MHz CDCl_3) δ (ppm) = 9.73 (t, $J = 2.0$ Hz, 1H, COH), 7.55 (m, 4H, aromatic), 7.42 (m, 2H, aromatic), 7.30 (m, 3H, aromatic), 3.41 (m, 1H, CH_3CHCH_2), 2.79 (ddd, $J_1 = 16.7$, $J_2 = 6.9$, $J_3 = 1.8$ Hz, 1H, diastereotopic CHCHHCOH), 2.69 (ddd, $J_1 = 16.7$, $J_2 = 7.6$, $J_3 = 2.2$ Hz, 1H, diastereotopic CHCHHCOH), 1.35 (d, $J = 7.0$ Hz, 3H, CH_3).

5.3.7 Synthesis of bivalent ligands

(R)-N-(1-(3-([1,1'-biphenyl]-4-yl)butyl)piperidin-4-yl)acetamide (32)

Acetic anhydride (20 μL , 0.2 mmol, 1.25 eq.) is added to (R)-RC-33A (50 mg, 0.16 mmol, 1.0 eq.) in anhydrous CH_2Cl_2 (2.0 mL) at room temperature under N_2 atmosphere. The reaction mixture is heated to reflux for 1 h, and then cooled on ice. Upon addition of NaOH (10% aqueous solution, 5 mL) the mixture is extracted with DCM (3 x 5 mL). The organic layers are reunited, dried on Na_2SO_4 , filtered and concentrated under vacuum. The crude product is purified by flash chromatography on silica gel (eluent: DCM/MeOH/ NH_3 90:10:0.5). The pure product is obtained as a yellow solid. Yield 95%; $R_f = 0.23$ (DCM/MeOH/ NH_3 90:10:0.5); m.p. = 129.5-132.8; $[\alpha]_D^{20} = -13.64$ (c = 0.5% in CHCl_3); $^1\text{H-NMR}$ (400 MHz, CDCl_3) δ (ppm) = 7.56 (d, $J = 7.1$ Hz, 2H, aromatic), 7.51 (d, $J = 8.2$ Hz, 2H, aromatic), 7.41 (t, $J = 7.6$ Hz, 2H, aromatic), 7.31 (t, $J = 7.3$ Hz, 1H, aromatic), 7.2 (d, J

= 8.3 Hz, 2H, aromatic), 5.51 (d, $J = 7.3$ Hz, 1H, NHCO), 3.80 (m, 1H, piperidine CHNH), 2.93 (brs, 2H, piperidine CH₂N), 2.76 (m, $J = 8.0$ Hz, 1H, CH₃CHCH₂), 2.42 (m, 1H, diastereotopic CH₂CHHN), 2.30 (m, 1H, diastereotopic CH₂CHHN), 2.17 (m, 2H, piperidine CH₂N), 1.94 (s, 3H, COCH₃), 1.86 (m, 4H, piperidine CH₂ and ArCHCH₂CH₂), 1.58 (m, 2H, piperidine CH₂), 1.28 (d, $J = 6.9$ Hz, 3H, CH₃CHCH₂). ¹³C-NMR (400 MHz, CDCl₃) δ(ppm) = 169.43, 145.65, 140.91, 139.06, 128.68, 127.25, 127.17, 127.03, 126.93, 56.73, 52.44, 46.06, 37.87, 34.73, 31.49, 23.45, 22.50.

Synthesis of N¹,N³-bis(1-((R)-3-([1,1'-biphenyl]-4-yl)butyl)piperidin-4-yl)malonamide (33)

A solution of (R)-RC-33A (56 mg, 0.181 mmol, 2 eq.) and diisopropylamine (32 μl, 0.181 mmol, 2 eq.) in CH₃CN (2 mL) is added dropwise to a solution of malonic acid (11.30 mg, 0.109 mmol, 1.2 eq.) and 2-(1H-Benzotriazole-1-yl)-1,1,3,3-tetramethylammonium tetrafluoroborate (TBTU, 58.12 mg, 0.181 mmol, 2 eq.) in 2.4 mL of CH₃CN. The reaction is maintained under magnetic stirring at room temperature for 30 minutes. Upon reaction completion, which is confirmed by TLC analysis (DCM/MeOH/NH₃ in MeOH 90:10:0.1), the solvent is evaporated under reduced pressure. The crude is then dissolved in EtOAc (10 mL) and washed first with a saturated aqueous solution of NaHCO₃ (3x 10mL) and then with Brine (2x10mL). The organic layer is then dried on Na₂SO₄, filtered and concentrated under reduced pressure. The product is further purified through flash chromatography (eluent DCM/MeOH/NH₃ in MeOH, 90:10:0.1 v/v/v) and the desired product is isolated as a pale-yellow oil. Yield: 63%; R_f = 0.72 (DCM/MeOH/NH₃ in MeOH 90:10:0.1); [α]_D²⁰ = -20.30 (c = 0.5% in MeOH); ¹H-NMR (400 MHz, CDCl₃) δ(ppm) = 7.60 (d, $J = 7.6$ Hz, 4H, aromatic), 7.54 (d, $J = 8.0$ Hz, 4H, aromatic), 7.44 (t, $J = 7.6$ Hz, 4H, aromatic), 7.34 (t, $J = 7.2$ Hz, 2H, aromatic), 7.27 (d, $J = 8.4$ Hz, 4H, aromatic), 6.94 (d, $J = 7.2$ Hz, 1H, NH), 3.77 (m, 2H, piperidine), 3.13 (s, 2H, COCH₂CO), 2.79 (m, 6H, CH₃CHCH₂ and piperidine), 2.39-2.19 (m, 4H, CHCH₂CH₂N), 2.16-2.01 (m, 4H, CHCH₂CH₂N), 1.91 (m, 4H, piperidine), 1.83 (dd, $J_1 = 14.8$, $J_2 = 7.6$ Hz, 4H, piperidine), 1.53 (dd, $J_1 = 20.8$, $J_2 = 10.0$ Hz, piperidine), 1.31 (d, $J = 6.8$ Hz, 6H, CH₃CHCH₂). ¹³C-NMR (400 MHz, CDCl₃) δ(ppm) = 171.3, 145.65, 140.91, 139.02, 128.61, 127.28, 127.16, 127.04, 126.98, 56.72, 56.72, 52.04, 52.00, 46.35, 37.80, 35.06, 31.44, 31.38, 22.29.

Synthesis of N¹,N⁵-bis(1-((R)-3-([1,1'-biphenyl]-4-yl)butyl)piperidin-4-yl)glutaramide (34)

Glutaric acid (15.6 mg, 0.118 mmol, 1.2 eq.), TBTU (63.2 mg, 0.197 mmol, 2 eq.) and N,N-diisopropylethylamine (DIPEA, 34.5 μl, 0.197 mmol, 2 eq.) are dissolved in 2 mL of CH₃CN in a vial for microwave oven. The mixture is kept under magnetic stirring at room temperature for 5 minutes to allow reaction between the acid and TBTU. Afterwards, a solution of (R)-RC-33A (60.9 mg, 0.197 mmol, 2 eq.) in 2 mL of CH₃CN is added and the vial undergoes 5 cycles of microwave irradiation (10 minutes each) at 90°C and 50W. The reaction mixture is then evaporated under reduced pressure, giving a brown residue that is

dissolved in CH₂Cl₂ (15 ml) and extracted first with water (3x15 ml) and then with a saturated solution of NaHCO₃ (15 ml). The organic layer is dried on Na₂SO₄, filtered and concentrated under reduced pressure. The brown oil thus obtained is purified through flash chromatography (eluent DCM/MeOH/NH₃ in MeOH, 90:10:0.1 v/v/v) and the pure product is obtained as a yellow solid. Yield: 31.5 %. R_f = 0,83 (TLC: DCM/MeOH/NH₃ in MeOH; 80:20:0.1 v/v/v). m.p.= 207-210°C. [α]_D²⁰= -12.9 (c = 0.5% in DCM); IR (cm⁻¹)= 1473.35, 1488.78, 1507.1, 1540.85, 1557.24, 1645.95, 1670.05, 1683.55, 1698.02, 1716.34, 1748.16, 1867.72, 2343.09, 2359.48. **¹H-NMR** (400 MHz, CDCl₃) δ(ppm)= 7.60 (dd, J₁ = 1.2, J₂ = 8.5, 4H, aromatic), 7.55 (d, J = 8.2 Hz, 4H, aromatic), 7.45 (t, J = 7.6 Hz, 4H, aromatic), 7.35 (t, J = 7.3 Hz, 2H aromatic), 7.26 (d, J = 8.4 Hz, 4H, aromatic), 5.88 (s, 2H, NH), 3.81 (m, 2H, piperidine), 2.95 (d, J = 10.5 Hz, 4H, piperidine), 2.80 (m, 2H, CH₃CHCH₂), 2.48-2.38 (m, 4H, CHCH₂CH₂N), 2.24 (t, J = 7.1 Hz, 4H, NHCOCH₂), 2,18 (m, 4H, piperidine), 1.92 (m, 10H, piperidine, CHCH₂CH₂N, NHCOCH₂CH₂), 1.60 (d, J = 11.3 Hz, 4H, piperidine), 1.32 (d, J = 6.9 Hz, 6H, CH₃CHCH₂). **¹³C-NMR** (400 MHz, CDCl₃) δ(ppm)= 171.9, 146.12, 140.75, 139.02, 128.61, 127.29, 126.17, 127.04, 126.9, 56.7, 52.2, 46.37, 37.8, 35.3, 32.05, 22.3, 21.9.

Synthesis of N¹,N⁷-bis(1-((R)-3-([1,1'-biphenyl]-4-yl)butyl)piperidin-4-yl)heptanediamide (35)

Pimelic acid (17.6 mg, 0.1098 mmol, 1.2 eq.), TBTU (8.7 mg, 0.183 mmol, 2 eq.) and N,N-diisopropylethylamine (DIPEA, 32.0 μl, 0.183 mmol, 2 eq.) are dissolved in 2 ml of CH₃CN in a vial for microwave oven. The mixture is kept under magnetic stirring at room temperature for 5 minutes to allow reaction between the acid and TBTU. Afterwards, a solution of (R)-RC-33A (56.6 mg, 0.183 mmol, 2 eq.) in 2 ml of CH₃CN is added and the vial undergoes 5 cycles of microwave irradiation (10 minutes each) at 90°C and 50W. The reaction mixture is then evaporated under reduced pressure, giving a brown residue that is dissolved in CH₂Cl₂ (15 ml) and extracted first with water (3x15 ml) and then with a saturated solution of NaHCO₃ (15 ml). The organic layer is dried on Na₂SO₄, filtered and concentrated under reduced pressure. The brown oil thus obtained is purified through flash chromatography (eluent DCM/MeOH/NH₃ in MeOH, 80:20:0,1 v/v/v) and the pure product is obtained as white solid. Yield: 58.9%; R_f= 0.64 (TLC: DCM/MeOH/NH₃ in MeOH; 80:20:0.1 v/v/v). m.p.= 192-194°C [α]_D²⁰= -12.1 (c = 0.5% in DCM); IR (cm⁻¹)= 1418.39, 1456.96, 1473.35, 1488.78, 1507.1, 1522.52, 1540.85, 1557.24, 1644.98, 1698.02, 1716.34, 1733.69, 1792.51, 1829.15, 1844.58, 1868.68, 2342.12, 2360.44. **¹H-NMR** (400 MHz, CDCl₃) δ(ppm)= 7.60 (dd J₁= 1.3, J₂ = 8.5 Hz, 4H, aromatic), 7.54 (d, J = 8.2 Hz, 4H, aromatic), 7.45 (t, J = 7.6 Hz, 4H, aromatic), 7.35 (t, J = 7.3 Hz, 2H, aromatic), 7.26 (m, 4H, aromatic), 5.65 (s, 2H, NH), 3.80 (m, 2H, piperidine), 2.99 (d, J = 10.8 Hz, 4H, piperidine), 2.80 (m, 2H, CH₃CHCH₂), 2.47-2.34 (m, 4H, CHCH₂CH₂N), 2.20 (m, 4H, piperidine), 2.17 (t, J = 7.4 Hz, 4H, NHCOCH₂), 1.93 (m, 8H, piperidine, CHCH₂CH₂N), 1.65 (m, 8H, piperidine, NHCOCH₂CH₂), 1.36 (d, J = 6.9, 2H, NHCOCH₂CH₂CH₂), 1.32 (d, J = 6.9 Hz, 6H, CH₃CHCH₂). **¹³C-NMR** (400 MHz, CDCl₃) δ(ppm)= 172.2,

145.90, 140.91, 139.02, 128.61, 127.28, 127.11, 127.04, 126.98 126.95, 56.7, 52.3, 46.19, 37.8, 36.31, 35.17, 31.96, 25.03, 22.47.

Synthesis of 2,2'-oxybis(N-(1-((R)-3-([1,1'-biphenyl]-4-yl)butyl)piperidin-4-yl)acetamide) (36)

Compound (R)-RC-33A (52.9 mg, 0.171 mmol, 2 equiv.) is dissolved in 3 mL of anhydrous CH₂Cl₂ with triethylamine (35.8 μL, 0.256 mmol, 3 equiv.) in a round bottom flask under Nitrogen atmosphere. Then, a solution of diglycolyl chloride (15.2 μL, 0.128 mmol, 1.5 equiv.) in 3.5 mL of CH₂Cl₂ is added dropwise. HCl is released as white gas. After 30 minutes TLC analysis (DCM/MeOH/NH₃ in MeOH 90:10:0.1 v/v/v) confirms reaction completion, with the formation of a spot with R_f = 0.53. The reaction is then quenched by pouring water (6 mL) and the mixture is extracted with a saturated solution of NaHCO₃ (3 x 10 mL). The organic phase is dried on Na₂SO₄, filtered and concentrated under reduced pressure. A brown oil is obtained, which is then purified through flash chromatography (eluent DCM/MeOH/NH₃ in MeOH 90:10:0.1 v/v/v), giving the desired product as a yellowish oil (57.4 mg). Yield = 94%; R_f = 0.53 (TLC: DCM/MeOH/NH₃ in MeOH; 90:10:0.1 v/v/v). [α]_D²⁰ = -13.3 (c = 0.5% in DCM); IR (cm⁻¹) = 1245.79, 1399.1, 1487.81, 1508.06, 1540.85, 1645.95, 1772.26, 2342.12, 2360.44. ¹H NMR (400 MHz, CDCl₃) δ(ppm) = 7.6 (dd, J₁ = 1.3, J₂ = 8.4 Hz, 4H, aromatic), 7.55 (d, J = 8.2 Hz, 4H, aromatic), 7.45 (t, J = 7.4 Hz, 4H, aromatic), 7.35 (t, J = 7.3 Hz, 2H, aromatic), 7.27 (d, 4H, aromatic), 6.69 (s, 2H, NH), 4.03 (s, 4H, NHCOCH₂O), 3.98 (m, 2H, piperidine), 3.05 (d, J = 10.1 Hz, 4H, piperidine), 2.80 (m, 1H, CHNHCO), 2.51-2.38 (m, 4H, CHCH₂CH₂N), 2.27 (d, J = 11.9 Hz, 4H, piperidine), 1.90 (m, 8H, piperidine, CHCH₂CH₂N), 1.77 (d, J = 10.9 Hz, 4H, piperidine), 1.33 (d, J = 6.9 Hz, 6H, CH₃CHCH₂). ¹³C-NMR (400 MHz, CDCl₃) δ(ppm) = 167.78, 145.9, 139.04, 128.68, 127.26, 127.16, 127.02, 126.8, 71.03, 56.58, 52.20, 45.75, 34.74, 31.39, 22.53.

Synthesis of 2,2'-(ethane-1,2-diylobis(oxy))bis(N-(1-((R)-3-([1,1'-biphenyl]-4-yl)butyl)piperidin-4-yl) acetamide) (37)

In a round-bottom flask, under N₂ atmosphere, 3,6-Dioxaoctanedioic acid (6.1 mg, 0.034 mmol, 1 equiv.) is placed with COMU (36.4 mg, 0.085 mmol, 2.5 equiv.) and compound (R)-RC-33A (21 mg, 0.068 mmol, 2 equiv.). The mixture is solubilized in dry DMF (4 mL) under magnetic stirring at 0 °C, then DIPEA (25 μL, 0.14 mmol, 4 equiv.) is added and the reaction mixture turns a bright yellow. After 1h the ice bath is removed, and the reaction is allowed to reach spontaneously room temperature. The reaction progression is monitored via TLC (DCM/MeOH/NH₃ in MeOH 94:6:1.5 v/v/v) and upon completion, after 2h 45min, the mixture is diluted with 20 mL of EtOAc and washed with water (20 mL) and Brine (2 x 25 mL). The reunited aqueous phase is extracted with fresh EtOAc (15 mL). Then, the organic phases are reunited, dried on Na₂SO₄, filtered and concentrated under vacuum. The obtained crude product is purified through flash chromatography on

SiO₂ (eluent DCM/MeOH/NH₃ in MeOH 94:6:1.5 v/v/v) and the desired product is obtained as a whitish solid. Yield = 43%; R_f = 0,29 (TLC: DCM/MeOH/NH₃ in MeOH; 94:6:1.5 v/v/v). [α]_D²⁰ = -10.3 (c = 0.5% in DCM). ¹H NMR (400 MHz, CDCl₃) δ(ppm) = 7.58 (dt, J₁ = 6.8, J₂ = 1.6 Hz, 4H, aromatic), 7.51 (dt, J₁ = 8.4, J₂ = 2 Hz, 4H, aromatic), 7.42 (td, J₁ = 7.2, J₂ = 1.6 Hz, 4H, aromatic), 7.32 (td, J₁ = 6.8, J₂ = 1.6 Hz, 2H, aromatic), 7.24 (dt, J₁ = 8.4, J₂ = 2 Hz, 4H, aromatic), 6.60 (d, J = 8 Hz, 2H, NH), 3.98 (s, 4H, COCH₂O), 3.81 (m, 2H, CHNHCO), 3.68 (s, 4H, OCH₂CH₂O), 2.83 (brs, 4H, piperidine), 2.77 (m, 2H, CH₃CHCH₂), 2.32 (m, 2H, diastereotopic CHCH₂CHHN), 2.22 (m, 2H, diastereotopic CHCH₂CHHN), 2.06 (m, 4H, CHCH₂CH₂), 1.91 (m, 4H, piperidine), 1.80 (m, 4H, piperidine), 1.49 (m, 4H, piperidine), 1.28 (d, J = 6.8, 6H, ArCH₃CH₂). ¹³C-NMR (400 MHz, CDCl₃) δ(ppm) = 168.72, 159.38, 140.91, 139.04, 128.68, 127.26, 127.16, 127.02, 126.93, 70.68, 70.50, 56.68, 53.38, 52.34, 52.10, 37.83, 26.88, 22.51.

Synthesis of N¹,N³¹-bis(1-((R)-3-([1,1'-biphenyl]-4-yl)butyl)piperidin-4-yl)-4,7,10,13,16,19,22,25,28-nonaohaxentriacontane-1,31-diamide (38)

In a round-bottom flask, under N₂ atmosphere, 4,7,10,13,16,19,22,25,28-nonaohaxentriacontane-1,31-dioic acid (bis-PEG9-acid, 21 mg, 0.04 mmol, 1 equiv.) is placed with COMU (34 mg, 0.08 mmol, 2 equiv.) and compound (R)-RC-33A (25 mg, 0.08 mmol, 2 equiv.). The mixture is solubilized in dry DMF (4 mL) under magnetic stirring at 0 °C, then DIPEA (30 μL, 0.16 mmol, 4 equiv.) is added and the reaction mixture turns a bright yellow. After 1h the ice bath is removed, and the reaction is allowed to reach spontaneously room temperature. The reaction progression is monitored via TLC (DCM/MeOH/NH₃ in MeOH 90:10:0.5 v/v/v) and upon completion, after 4h of stirring at room temperature, the mixture is diluted with 25 mL of EtOAc and washed in sequence with 0.5 M HCl (2 x 5 mL), saturated NaHCO₃ (2 x 5 mL) and Brine (2 x 5 mL). The acidic aqueous phase is then extracted with fresh DCM (3 x 10 mL). Then, the organic phases are reunited, dried on Na₂SO₄, filtered and concentrated under vacuum. The crude product is a brown oil which is purified through flash chromatography on SiO₂ (eluent DCM/NH₃ in MeOH 92:8) and the desired product is obtained as a pale-yellow oil. Yield = 59%; R_f = 0.34 (TLC: DCM/NH₃ in MeOH 92:8). [α]_D²⁰ = -9.5 (c = 0.5% in DCM). ¹H NMR (400 MHz, CDCl₃) δ(ppm) = 7.58 (d, J = 7.2 Hz, 4H, aromatic), 7.52 (d, J = 8.4 Hz, 4H, aromatic), 7.42 (t, J = 7.2 Hz, 4H, aromatic), 7.33 (t, J = 7.2 Hz, 2H, aromatic), 7.25 (d, J = 8.4 Hz, 4H, aromatic), 6.33 (d, J = 7.6 Hz, 2H, NHCO), 3.77 (m, 2H, CHNHCO), 3.7 (t, J = 5.8 Hz, 4H, COCH₂CH₂O), 3.62 (m, 32H, OCH₂CH₂O PEG chain), 2.85 (brs, 4H, piperidine CH₂N), 2.77 (m, 2H, CH₃CHCH₂), 2.43 (t, J = 5.8 Hz, 4H, COCH₂CH₂O), 2.33 (m, 2H, diastereotopic CHCH₂CHHN), 2.27 (m, 2H, diastereotopic CHCH₂CHHN), 2.11 (m, 4H, piperidine CH₂), 1.91 (m, 4H, piperidine CH₂), 1.83 (dd, J₁ = 15.2, J₂ = 7.6 Hz, 4H, piperidine CH₂), 1.50 (m, 4H, CH₂ piperidine), 1.29 (d, J = 7.0 Hz, 6H, CH₃). ¹³C-NMR (400 MHz, CDCl₃) δ(ppm) = 173.56, 148.72, 143.64, 141.60, 131.35, 129.96, 129.77, 129.67, 129.60, 73.21, 73.17, 73.04, 72.95, 70.04, 59.51, 55.08, 54.93, 48.79, 40.55, 39.74, 37.88, 34.53, 25.16.

Synthesis of 1-oxo-1-phenyl-5,8,11,14-tetraoxa-2-azahexadecan-16-oic acid (41)

Benzoic acid (17 mg, 0.14 mmol, 1.3 equiv) and COMU (53 mg, 0.12 mmol, 1.1 equiv) are placed in a round-bottom flask under N₂ atmosphere and solubilized in dry DMF (3 mL). The flask is placed in an ice-cold bath and DIPEA (40 μ L) is added under magnetic stirring. The reaction is monitored via TLC (DCM/MeOH 9:1 + 0,1% HCOOH) and after 1h complete consumption of the starting material is observed. Then, the amino-PEG₄-acid **42** (28.6 mg, 0.11 mmol, 1 equiv) is solubilized in 1 mL of dry DMF and is added to the reaction mixture at 0 °C. About 2 mL of dry DMF are used to wash the flask and recover all the amino-PEG₄-acid. The reaction is then allowed to reach spontaneously room temperature and monitored via TLC (DCM/MeOH 9:1 + 0,1% HCOOH). About 1h 30' after addition of the amino acid, the reaction is completed. The mixture is diluted with EtOAc (20 mL) and extracted with a saturated NaHCO₃ solution (20 mL). Then, the aqueous phase is neutralized with conc. HCl and extracted with DCM (2 x 20 mL). The reunited organic layers are dried on Na₂SO₄, filtered and concentrated under vacuum. The crude obtained is a yellowish oil which is then purified through flash chromatography (eluent: DCM/MeOH 9:1 + 0,1% HCOOH). The pure product is a white solid. Yield = 48%, R_f = 0,15 (TLC: DCM/MeOH 9:1 + 0,1% HCOOH). ¹H NMR (400 MHz, CDCl₃) δ (ppm)= 7.83 (d, J = 7.0Hz, 2H, aromatic), 7.47 (t, J = 7.3Hz, 1H, aromatic), 7.41 (t, J = 7.3Hz, 2H, aromatic), 7.14 (brs, 1H, NHCO), 4.10 (s, 2H, OCH₂CO₂H), 3.71-3.62 (m, 16H, CH₂ PEG chain)

Synthesis of (R)-N-(1-(3-([1,1'-biphenyl]-4-yl)butyl)piperidin-4-yl)-14-benzamido-3,6,9,12-tetraoxatetradecan-1-amide (40)

Compound (R)-RC-33A (16.3 mg, 0.05 mmol, 1 equiv.), compound **41** (17.3 mg, 0.05 mmol, 1 equiv.) and COMU (21.4 mg, 0.05 mmol, 1 equiv.) are placed in a round bottom flask, under N₂ atmosphere. The mixture is solubilized in dry DMF (3 mL) under magnetic stirring at 0 °C, then DIPEA (17 μ L, 0.1 mmol, 2 equiv.) is added and the reaction mixture turns a bright yellow. After 1h the ice bath is removed, and the reaction is allowed to reach spontaneously room temperature. The reaction progression is monitored via TLC (DCM/MeOH/NH₃ in MeOH 90:10:0.1 v/v/v) and upon completion, after 4h 30' of stirring at room temperature, the mixture is diluted with 15 mL of EtOAc and washed with Brine (3 x 15 mL). The aqueous phases are reunited and extracted with EtOAc (2 x 15 mL). Then, the organic phases are reunited, dried on Na₂SO₄, filtered and concentrated under vacuum. The crude product is a orange oil which is purified through flash chromatography on SiO₂ (eluent DCM/MeOH/NH₃ in MeOH 90:10:0.1) and the desired product is obtained as a dense yellow oil. Yield = 64%, R_f = 0,5 (DCM/MeOH/NH₃ in MeOH 90:10:0.1 v/v/v), $[\alpha]_D^{20} = -7.0$ (c = 0.5% in DCM). ¹H NMR (400 MHz, CDCl₃) δ (ppm)= 7.81 (d, J = 7.2Hz, 2H, aromatic), 7.55 (d, J = 7.1Hz, 2H, aromatic), 7.51 (d, J = 8.2Hz, 2H, aromatic), 7.47-7.37 (m, 5H, aromatic), 7.31 (t, J = 7.4Hz, 1H, aromatic), 7.21 (d, J = 8.3Hz, 2H, aromatic), 7.14 (brs, 2H, NHCO), 3.92 (s, 2H, COCH₂O), 3.86 (brs, 1H, CHNHCO), 3.66-3.60

(m, 16H, CH₂ PEG chain), 3.16 (brs, 2H, CH₂N), 2.75 (m, 1H, CH₃CHCH₂), 2.49-2.34 (m, 4H, CHCH₂CH₂ and CH₂ piperidine), 1.98 (m, 4H, CH₂ piperidine), 1.85 (brs, 2H, CH₂ piperidine), 1.28 (d, *J* = 6.9Hz, 3H, CH₃)

5.4 General protocol for binding assays

The test compound solutions were prepared by dissolving ≈10 μmol (usually 2-4 mg) of test compound in DMSO (unless otherwise specified), so that a 10 mM stock solution was obtained. To obtain the required test solutions for the assay, the DMSO stock solution was diluted with the respective assay buffer. Due to solubility issues, test compounds **34** and **35** were converted in their hydrochloride salts and dissolved in EtOH to prepare 10 mM stock solutions. The filtermats were presoaked in 0.5% aqueous polyethylenamine solution for 2 h at r.t. before use. All binding experiments were carried out in duplicate in 96-well multiplates. The concentrations given are the final concentrations in the assay. Generally, the assays were performed by addition of 50 μL of the respective assay buffer, 50 μL test compound solution at various concentrations (*i.e.* 10⁻⁵, 10⁻⁶, 10⁻⁷, 10⁻⁸, 10⁻⁹ and 10⁻¹⁰ M), 50 μL of corresponding radioligand solution, and 50 μL of the respective receptor preparation into each well of the multiplate (total volume 200 μL). The receptor preparation was always added last. During the incubation, the multiplates were shaken at a speed of 500-600 rpm at the specified temperature. Unless otherwise noted, the assays were terminated after 120 min by rapid filtration using the harvester. During the filtration each well was washed five times with 300 μL of water. Subsequently, the filtermats were dried at 95 °C. The solid scintillator was melted on the dried filtermats at 95 °C for 5 min. After solidifying of the scintillator at r.t., the trapped radioactivity in the filtermats was measured with the scintillation analyzer. Each position on the filtermat corresponding to one well of the multiplate was measured for 5 min with the [³H]-counting protocol. The overall counting efficiency was 20%. The IC₅₀ values were calculated with GraphPad Prism 3.0 (GraphPad Software, San Diego, CA, USA) by nonlinear regression analysis. The IC₅₀ values were subsequently transformed into K_i values using the equation of Cheng and Prusoff. The K_i values are given as mean value ± SEM from three independent experiments.

5.4.1 S1R binding assay

The assay was performed with the radioligand [³H](+)-pentazocine (22.0 Ci mmol⁻¹; Perkin-Elmer). The thawed membrane preparation of guinea pig brain cortex (≈100 μg protein) was incubated with various concentrations of test compounds, 2 nM [³H](+)-pentazocine, and Tris buffer (50 mM, pH 7.4) at 37 °C. The

nonspecific binding was determined with 10 mM unlabeled (+)-pentazocine. The K_d value of (+)-pentazocine is 2.9 nM.

5.4.2 S2R binding assay

The assay was performed using 150 μg of rat liver homogenate, which was incubated with various concentrations of test compound for 120 min at room temperature, along with 3 nM [^3H]-DTG (Perkin-Elmer, specific activity 58.1 Ci mmol^{-1}) in 50 mM Tris-HCl, pH 8.0, 0.5 mL final volume. (+)-pentazocine (100 nM) and haloperidol (10 μM) were used to mask S1R and to define nonspecific binding, respectively.

5.4.3 GluN2 binding assay

The competitive binding assay was performed with the radioligand [^3H]-ifenprodil (60 Ci mmol^{-1} ; BIOTREND, Cologne, Germany). The thawed cell membrane preparation from the transfected L(tk-) cells (about 20 μg protein) was incubated with various concentrations of test compounds, 5 nM [^3H]-ifenprodil, and TRIS/EDTA buffer (5mM TRIS/1 mM EDTA, pH 7.5) at 37 °C. The non-specific binding was determined with 10mM unlabeled ifenprodil. The K_d value of ifenprodil is 7.6 nM.

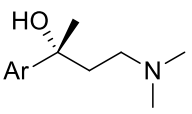
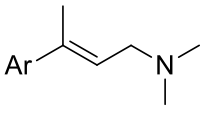
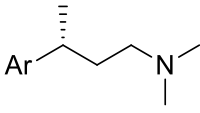
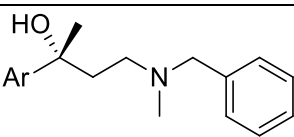
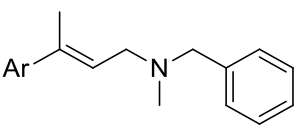
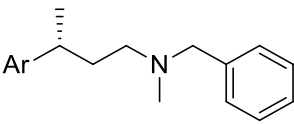
5.5 Computational studies

5.5.1 Dataset preparation

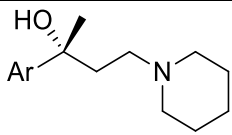
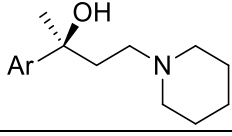
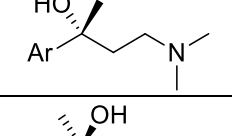
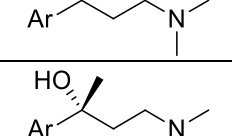
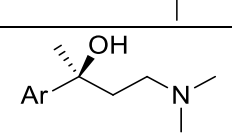
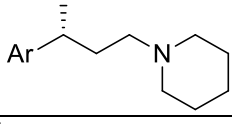
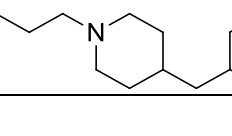
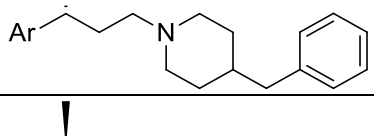
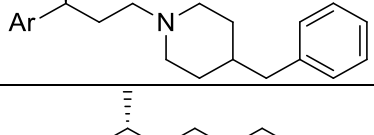
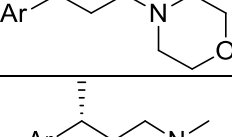
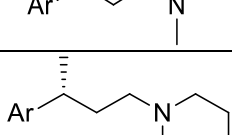
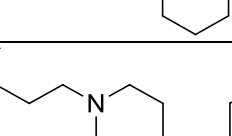
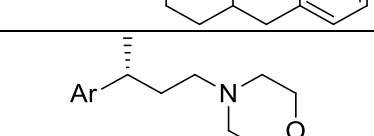
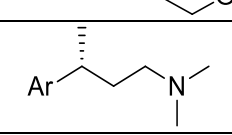

The molecular structures of test compounds were sketched using Maestro's molecular editor (Maestro 10.2.011, Schrödinger LLC). Afterwards, the 3D structures were obtained using the LigPrep module (LigPrep, Maestro 10.2.011, Schrödinger LLC); ionization states were generated at $\text{pH } 7.0 \pm 2.0$ using Epik.

For the development of 3D-QSAR model, 80 monovalent RC-33 analogs were selected from previously reported works by Collina and co-workers (see **Table 5**). The experimental K_i values (ranging from 0.69 nM to 1 μM) were converted into logarithmic $\text{p}K_i$ values. The compound chemical structures and their $\text{p}K_i$ values are depicted in **Table 5**.

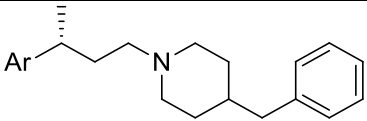
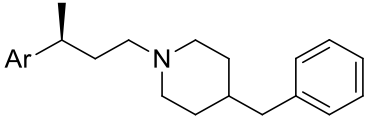
Table 5. Structures, pK_i values and reference of S1R ligands selected for 3D-QSAR study.

Entry	Structure	Ar	pK _i	Ref	
1		Naphth-2-yl	7.6	216	
2		6-Methoxy-naphth-2-yl	7.41	217	
3		Naphth-1-yl	6.99	216	
4		Naphth-2-yl	7.70	216	
5		6-Methoxy-naphth-2-yl	7.67	216	
6		Biphen-4-yl	8.85	218	
7		Phenyl	6.00	218	
8		4-Methoxyphenyl	6.09	218	
9		3-Methoxyphenyl	6.00	218	
10			Naphth-1-yl	7.33	216
11			Naphth-2-yl	8.71	216
12	6-Hydroxy-naphth-2-yl		7.72	216	
13	6-Methoxy-naphth-2-yl		8.64	216	
14	Biphen-4-yl		8.99	216	
15		6-Methoxy-naphth-2-yl	8.22	217	
16		Biphen-4-yl	8.62	217	
17		Naphth-2-yl	8.10	216	
18		Biphen-4-yl	8.20	216	
19		6-Methoxy-naphth-2-yl	7.86	217	
20		Phenyl	7.04	216	
21		4-Methoxyphenyl	8.28	216	
22		Naphth-2-yl	8.27	216	
23		Biphen-4-yl	8.24	216	
24		6-Methoxy-naphth-2-yl	8.64	217	

25		6-Methoxy-naphth-2-yl	7.98	217
26		Naphth-2-yl	9.01	218
27		Biphen-4-yl	9.07	218
28		Phenyl	6.34	218
29		4-Methoxyphenyl	7.85	218
30		3-Methoxyphenyl	7.04	218
31		6-Methoxy-naphth-2-yl	8.36	217
32		Biphen-4-yl	9.16	218
33		6-Methoxy-naphth-2-yl	8.89	217
34		Naphth-2-yl	7.64	218
35		Biphen-4-yl	8.15	218
36		Phenyl	8.97	218
37		4-Methoxyphenyl	8.38	218
38		3-Methoxyphenyl	8.11	218
39		Naphth-2-yl	8.02	218
40		Biphen-4-yl	7.94	218
41		4-Methoxyphenyl	6.00	218
42		3-Methoxyphenyl	6.00	218
43		Naphth-2-yl	6.00	219
44		4-Methoxyphenyl	6.00	219
45		6-Methoxy-naphth-2-yl	6.00	219
46		Biphen-4-yl	6.00	219
47		4-Methoxyphenyl	6.00	219
48		Naphth-2-yl	6.00	219
49		4-Methoxyphenyl	6.00	219

50		biphenyl-4-yl	7.41	215
51			8.33	215
52		naphth-2-yl	6.69	215
53			7.20	215
54		6-methoxy-naphth-2-yl	7.29	215
55			7.60	215
56		naphth-2-yl	8.82	213
57		naphth-2-yl	8.22	213
58			8.16	213
59		naphth-2-yl	8.27	213
60		4-Methoxyphenyl	6.94	213
61			7.70	213
62			8.46	213
63			7.12	213
64			6.62	213

65		3-Methoxyphenyl	7.44	213
66			8.54	213
67			6.86	213
68		Phenyl	6.37	213
69			7.34	213
70			8.54	213
71			8.52	213
72			7.07	213
73			2-Naphtyl	8.00
74		7.96		214
75		Phenyl	7.57	214
76			7.4	214
77		6-Hydroxy naphtyl	7.15	214
78			7.21	214

79			7.46	214
80			7.89	214

5.5.2 Docking protocol.

The ligand-receptor molecular docking experiments of RC-33 and its mono- and bi-valent analogs into the active site of S1R were performed by using the software Glide from the Schrödinger suite. Protein coordinates were extracted from the crystal structure of S1R bound to the selective antagonist PD144418 (PDB code: 5HK1). A grid box of 20 X 20 X 20 Å was centered on the center of mass of the ligand in this crystal structure covering the binding site of S1R. Glide standard (SP) and extra-precision (XP) modes were employed with the same protocol and parameters that were reported by Caballero in previous works^{220,221}. Glide SP was used to evaluate the capability of the Glide method to obtain poses that fit the known pharmacophore of S1R ligands, and the more precise Glide XP was used for finding the final docking poses. After several poses were found for each compound, the ones that showed the best scoring energies (*i.e.* glide score) were considered. The information of PD144418 and 4-IBP in the crystallographic structures was considered for the selection of the best solutions, *i.e.* those with a good Gscore and which docking pose was close to that of co-crystallized ligands.

For bivalent ligands, superimposition tool was used to fit one end of the ligand into the binding pocket, in a position similar to that of docked (*R*)-RC-33. After merging the reoriented bivalent ligand and the protein, minimization was performed using MacroModel application (Force Field: OPLS3). The result was used to generate a new grid and dock the bivalent ligand following the general protocol reported at the beginning of the paragraph.

6. References

- (1) Martin, W. R.; Eades, C. G.; Thompson, J. A.; Huppler, R. E.; Gilbert, P. E. The Effects of Morphine- and Nalorphine- like Drugs in the Nondependent and Morphine-Dependent Chronic Spinal Dog. *J. Pharmacol. Exp. Ther.* **1976**, *197* (3), 517–532.
- (2) Su, T. P. Evidence for Sigma Opioid Receptor: Binding of [3H]SKF-10047 to Etorphine-Inaccessible Sites in Guinea-Pig Brain. *J. Pharmacol. Exp. Ther.* **1982**, *223* (2), 284–290.
- (3) Vaupel, D. B. Naltrexone Fails to Antagonize the Sigma Effects of PCP and SKF 10,047 in the Dog. *Eur. J. Pharmacol.* **1983**, *92* (3–4), 269–274. [https://doi.org/10.1016/0014-2999\(83\)90297-2](https://doi.org/10.1016/0014-2999(83)90297-2).
- (4) Maurice, T.; Lockhart, B. P. Neuroprotective and Anti-Amnesic Potentials of Sigma (Sigma) Receptor Ligands. *Prog. Neuropsychopharmacol. Biol. Psychiatry* **1997**, *21* (1), 69–102.
- (5) Skuza, G. Potential Antidepressant Activity of Sigma Ligands. *Pol. J. Pharmacol.* **2003**, *55* (6), 923–934.
- (6) Quirion, R.; Bowen, W. D.; Itzhak, Y.; Junien, J. L.; Musacchio, J. M.; Rothman, R. B.; Su, T. P.; Tam, S. W.; Taylor, D. P. A Proposal for the Classification of Sigma Binding Sites. *Trends Pharmacol. Sci.* **1992**, *13* (3), 85–86.
- (7) Hellewell, S. B.; Bruce, A.; Feinstein, G.; Orringer, J.; Williams, W.; Bowen, W. D. Rat Liver and Kidney Contain High Densities of $\Sigma 1$ and $\Sigma 2$ Receptors: Characterization by Ligand Binding and Photoaffinity Labeling. *Eur. J. Pharmacol. Mol. Pharmacol.* **1994**, *268* (1), 9–18. [https://doi.org/10.1016/0922-4106\(94\)90115-5](https://doi.org/10.1016/0922-4106(94)90115-5).
- (8) Collina, S.; Gaggeri, R.; Marra, A.; Bassi, A.; Negrinotti, S.; Negri, F.; Rossi, D. Sigma Receptor Modulators: A Patent Review. *Expert Opin. Ther. Pat.* **2013**, *23* (5), 597–613. <https://doi.org/10.1517/13543776.2013.769522>.
- (9) Hanner, M.; Moebius, F. F.; Flandorfer, A.; Knaus, H. G.; Striessnig, J.; Kempner, E.; Glossmann, H. Purification, Molecular Cloning, and Expression of the Mammalian Sigma1-Binding Site. *Proc. Natl. Acad. Sci.* **1996**, *93* (15), 8072–8077. <https://doi.org/10.1073/pnas.93.15.8072>.
- (10) Alon, A.; Schmidt, H. R.; Wood, M. D.; Sahn, J. J.; Martin, S. F.; Kruse, A. C. Identification of the Gene That Codes for the σ_2 Receptor. *Proc. Natl. Acad. Sci.* **2017**, *114* (27), 7160–7165. <https://doi.org/10.1073/pnas.1705154114>.
- (11) Seth, P.; Fei, Y.-J.; Li, H. W.; Huang, W.; Leibach, F. H.; Ganapathy, V. Cloning and Functional Characterization of a σ Receptor from Rat Brain. *J. Neurochem.* **2002**, *70* (3), 922–931. <https://doi.org/10.1046/j.1471-4159.1998.70030922.x>.
- (12) Prasad, P. D.; Li, H. W.; Fei, Y.-J.; Ganapathy, M. E.; Fujita, T.; Plumley, L. H.; Yang-Feng, T. L.; Leibach, F. H.; Ganapathy, V. Exon-Intron Structure, Analysis of Promoter Region, and Chromosomal Localization of the Human Type 1 σ Receptor Gene. *J. Neurochem.* **2002**, *70* (2), 443–451. <https://doi.org/10.1046/j.1471-4159.1998.70020443.x>.
- (13) Laurini, E.; Col, V. D.; Mamolo, M. G.; Zampieri, D.; Posocco, P.; Fermeglia, M.; Vio, L.; Pricl, S. Homology Model and Docking-Based Virtual Screening for Ligands of the σ_1 Receptor. *ACS Med. Chem. Lett.* **2011**, *2* (11), 834–839. <https://doi.org/10.1021/ml2001505>.
- (14) Ortega-Roldan, J. L.; Ossa, F.; Amin, N. T.; Schnell, J. R. Solution NMR Studies Reveal the Location of the Second Transmembrane Domain of the Human Sigma-1 Receptor. *FEBS Lett.* **2015**, *589* (5), 659–665. <https://doi.org/10.1016/j.febslet.2015.01.033>.
- (15) Schmidt, H. R.; Zheng, S.; Gurpinar, E.; Koehl, A.; Manglik, A.; Kruse, A. C. Crystal Structure of the Human $\Sigma 1$ Receptor. *Nature* **2016**, *532* (7600), 527–530. <https://doi.org/10.1038/nature17391>.
- (16) Hayashi, T.; Su, T.-P. Sigma-1 Receptor Chaperones at the ER- Mitochondrion Interface Regulate Ca²⁺ Signaling and Cell Survival. *Cell* **2007**, *131* (3), 596–610. <https://doi.org/10.1016/j.cell.2007.08.036>.
- (17) Su, T.-P.; Su, T.-C.; Nakamura, Y.; Tsai, S.-Y. The Sigma-1 Receptor as a Pluripotent Modulator in Living Systems. *Trends Pharmacol. Sci.* **2016**, *37* (4), 262–278. <https://doi.org/10.1016/j.tips.2016.01.003>.
- (18) Maurice, T.; Su, T.-P. The Pharmacology of Sigma-1 Receptors. *Pharmacol. Ther.* **2009**, *124* (2), 195–206. <https://doi.org/10.1016/j.pharmthera.2009.07.001>.

- (19) Hashimoto, K.; Ishiwata, K. Sigma Receptor Ligands: Possible Application as Therapeutic Drugs and as Radiopharmaceuticals. *Curr. Pharm. Des.* **2006**, *12* (30), 3857–3876. <https://doi.org/10.2174/138161206778559614>.
- (20) Kourrich, S.; Su, T.-P.; Fujimoto, M.; Bonci, A. The Sigma-1 Receptor: Roles in Neuronal Plasticity and Disease. *Trends Neurosci.* **2012**, *35* (12), 762–771. <https://doi.org/10.1016/j.tins.2012.09.007>.
- (21) Peviani, M.; Salvaneschi, E.; Bontempi, L.; Petese, A.; Manzo, A.; Rossi, D.; Salmona, M.; Collina, S.; Bigini, P.; Curti, D. Neuroprotective Effects of the Sigma-1 Receptor (S1R) Agonist PRE-084, in a Mouse Model of Motor Neuron Disease Not Linked to SOD1 Mutation. *Neurobiol. Dis.* **2014**, *62*, 218–232. <https://doi.org/10.1016/j.nbd.2013.10.010>.
- (22) Marra, A.; Rossi, D.; Pignataro, L.; Bigogno, C.; Canta, A.; Oggioni, N.; Malacrida, A.; Corbo, M.; Cavaletti, G.; Peviani, M.; et al. Toward the Identification of Neuroprotective Agents: G-Scale Synthesis, Pharmacokinetic Evaluation and CNS Distribution of (R)-RC-33, a Promising Sigma1 Receptor Agonist. *Future Med. Chem.* **2016**, *8* (3), 287–295. <https://doi.org/10.4155/fmc.15.191>.
- (23) Weng, T.-Y.; Tsai, S.-Y. A.; Su, T.-P. Roles of Sigma-1 Receptors on Mitochondrial Functions Relevant to Neurodegenerative Diseases. *J. Biomed. Sci.* **2017**, *24* (1), 74. <https://doi.org/10.1186/s12929-017-0380-6>.
- (24) Tesei, A.; Cortesi, M.; Zamagni, A.; Arienti, C.; Pignatta, S.; Zannoni, M.; Paolillo, M.; Curti, D.; Rui, M.; Rossi, D.; et al. Sigma Receptors as Endoplasmic Reticulum Stress “Gatekeepers” and Their Modulators as Emerging New Weapons in the Fight Against Cancer. *Front. Pharmacol.* **2018**, *9*, 711. <https://doi.org/10.3389/fphar.2018.00711>.
- (25) Walker, J. M.; Bowen, W. D.; Walker, F. O.; Matsumoto, R. R.; Costa, B. D.; Rice, K. C. Sigma Receptors: Biology and Function. *Pharmacol. Rev.* **1990**, *42* (4), 355–402.
- (26) Fontanilla, D.; Johannessen, M.; Hajipour, A. R.; Cozzi, N. V.; Jackson, M. B.; Ruoho, A. E. The Hallucinogen N,N-Dimethyltryptamine (DMT) Is an Endogenous Sigma-1 Receptor Regulator. *Science* **2009**, *323* (5916), 934–937. <https://doi.org/10.1126/science.1166127>.
- (27) Brailoiu, E.; Chakraborty, S.; Brailoiu, G. C.; Zhao, P.; Barr, J. L.; Ilies, M. A.; Unterwald, E. M.; Abood, M. E.; Taylor, C. W. Choline Is an Intracellular Messenger Linking Extracellular Stimuli to IP 3 -Evoked Ca 2+ Signals through Sigma-1 Receptors. *Cell Rep.* **2019**, *26* (2), 330–337.e4. <https://doi.org/10.1016/j.celrep.2018.12.051>.
- (28) Bowen, W. D.; De Costa, B. R.; Hellewell, S. B.; Walker, J. M.; Rice, K. C. [3 H]-(+)-Pentazocine: A Potent and Highly Selective Benzomorphan-Based Probe for Sigma-1 Receptors. *Mol. Neuropharmacol.* **1993**, *3* (2), 117–126.
- (29) Glennon, R. A.; Ablordeppey, S. Y.; Ismaiel, A. M.; El-Ashmawy, M. B.; Fischer, J. B.; Howie, K. B. Structural Features Important for .Sigma.1 Receptor Binding. *J. Med. Chem.* **1994**, *37* (8), 1214–1219. <https://doi.org/10.1021/jm00034a020>.
- (30) Hellewell, S. B.; Bowen, W. D. A Sigma-like Binding Site in Rat Pheochromocytoma (PC12) Cells: Decreased Affinity for (+)-Benzomorphans and Lower Molecular Weight Suggest a Different Sigma Receptor Form from That of Guinea Pig Brain. *Brain Res.* **1990**, *527* (2), 244–253. [https://doi.org/10.1016/0006-8993\(90\)91143-5](https://doi.org/10.1016/0006-8993(90)91143-5).
- (31) Xu, J.; Zeng, C.; Chu, W.; Pan, F.; Rothfuss, J. M.; Zhang, F.; Tu, Z.; Zhou, D.; Zeng, D.; Vangveravong, S.; et al. Identification of the PGRMC1 Protein Complex as the Putative Sigma-2 Receptor Binding Site. *Nat. Commun.* **2011**, *2*, 380. <https://doi.org/10.1038/ncomms1386>.
- (32) Chu, U. B.; Mavlyutov, T. A.; Chu, M.-L.; Yang, H.; Schulman, A.; Mesangeau, C.; McCurdy, C. R.; Guo, L.-W.; Ruoho, A. E. The Sigma-2 Receptor and Progesterone Receptor Membrane Component 1 Are Different Binding Sites Derived From Independent Genes. *EBioMedicine* **2015**, *2* (11), 1806–1813. <https://doi.org/10.1016/j.ebiom.2015.10.017>.
- (33) Abate, C.; Niso, M.; Infantino, V.; Menga, A.; Berardi, F. Elements in Support of the ‘Non-Identity’ of the PGRMC1 Protein with the $\Sigma 2$ Receptor. *Eur. J. Pharmacol.* **2015**, *758*, 16–23. <https://doi.org/10.1016/j.ejphar.2015.03.067>.
- (34) Pati, M. L.; Groza, D.; Riganti, C.; Kopecka, J.; Niso, M.; Berardi, F.; Hager, S.; Heffeter, P.; Hirai, M.; Tsugawa, H.; et al. Sigma-2 Receptor and Progesterone Receptor Membrane Component 1 (PGRMC1) Are Two Different Proteins: Proofs by Fluorescent Labeling and Binding of Sigma-2 Receptor Ligands to PGRMC1. *Pharmacol. Res.* **2017**, *117*, 67–74. <https://doi.org/10.1016/j.phrs.2016.12.023>.

- (35) Mach, R. H.; Smith, C. R.; al-Nabulsi, I.; Whirrett, B. R.; Childers, S. R.; Wheeler, K. T. Sigma 2 Receptors as Potential Biomarkers of Proliferation in Breast Cancer. *Cancer Res.* **1997**, *57* (1), 156–161.
- (36) Colabufo, N. A.; Berardi, F.; Contino, M.; Ferorelli, S.; Niso, M.; Perrone, R.; Pagliarulo, A.; Saponaro, P.; Pagliarulo, V. Correlation between Sigma2 Receptor Protein Expression and Histopathologic Grade in Human Bladder Cancer. *Cancer Lett.* **2006**, *237* (1), 83–88. <https://doi.org/10.1016/j.canlet.2005.05.027>.
- (37) Imaging of in Vivo Sigma-2 Receptor Expression With 18F-ISO-1 Positron Emission Tomography in Metastatic Breast Cancer - Full Text View - ClinicalTrials.gov <https://clinicaltrials.gov/ct2/show/NCT03057743> (accessed Aug 19, 2019).
- (38) Kashiwagi, H.; McDunn, J. E.; Simon, P. O.; Goedegebuure, P. S.; Xu, J.; Jones, L.; Chang, K.; Johnston, F.; Trinkaus, K.; Hotchkiss, R. S.; et al. Selective Sigma-2 Ligands Preferentially Bind to Pancreatic Adenocarcinomas: Applications in Diagnostic Imaging and Therapy. *Mol. Cancer* **2007**, *6*, 48. <https://doi.org/10.1186/1476-4598-6-48>.
- (39) Zeng, C.; Rothfuss, J.; Zhang, J.; Chu, W.; Vangveravong, S.; Tu, Z.; Pan, F.; Chang, K. C.; Hotchkiss, R.; Mach, R. H. Sigma-2 Ligands Induce Tumour Cell Death by Multiple Signalling Pathways. *Br. J. Cancer* **2012**, *106* (4), 693–701. <https://doi.org/10.1038/bjc.2011.602>.
- (40) Vilner, B. J.; Bowen, W. D. Modulation of Cellular Calcium by Sigma-2 Receptors: Release from Intracellular Stores in Human SK-N-SH Neuroblastoma Cells. *J. Pharmacol. Exp. Ther.* **2000**, *292* (3), 900–911.
- (41) Cassano, G.; Gasparre, G.; Contino, M.; Niso, M.; Berardi, F.; Perrone, R.; Colabufo, N. A. The Sigma-2 Receptor Agonist PB28 Inhibits Calcium Release from the Endoplasmic Reticulum of SK-N-SH Neuroblastoma Cells. *Cell Calcium* **2006**, *40* (1), 23–28. <https://doi.org/10.1016/j.ceca.2006.03.004>.
- (42) Cassano, G.; Gasparre, G.; Niso, M.; Contino, M.; Scalera, V.; Colabufo, N. A. F281, Synthetic Agonist of the Sigma-2 Receptor, Induces Ca²⁺ Efflux from the Endoplasmic Reticulum and Mitochondria in SK-N-SH Cells. *Cell Calcium* **2009**, *45* (4), 340–345. <https://doi.org/10.1016/j.ceca.2008.12.005>.
- (43) Yi, B.; Sahn, J. J.; Ardestani, P. M.; Evans, A. K.; Scott, L.; Chan, J. Z.; Iyer, S.; Crisp, A.; Zuniga, G.; Pierce-Shimomura, J.; et al. Small Molecule Modulator of Sigma 2 Receptor Is Neuroprotective and Reduces Cognitive Deficits and Neuro-Inflammation in Experimental Models of Alzheimer's Disease. *J. Neurochem.* **2017**, *140* (4), 561–575. <https://doi.org/10.1111/jnc.13917>.
- (44) Grundman, M.; Morgan, R.; Lickliter, J. D.; Schneider, L. S.; DeKosky, S.; Izzo, N. J.; Guttendorf, R.; Higgin, M.; Pribyl, J.; Mozzoni, K.; et al. A Phase 1 Clinical Trial of the Sigma-2 Receptor Complex Allosteric Antagonist CT1812, a Novel Therapeutic Candidate for Alzheimer's Disease. *Alzheimers Dement. Transl. Res. Clin. Interv.* **2019**, *5*, 20–26. <https://doi.org/10.1016/j.trci.2018.11.001>.
- (45) Clinical Trial of CT1812 in Mild to Moderate Alzheimer's Disease - Full Text View - ClinicalTrials.gov <https://clinicaltrials.gov/ct2/show/NCT02907567> (accessed Aug 20, 2019).
- (46) Huang, Y.-S.; Lu, H.-L.; Zhang, L.-J.; Wu, Z. Sigma-2 Receptor Ligands and Their Perspectives in Cancer Diagnosis and Therapy. *Med. Res. Rev.* **2014**, *34* (3), 532–566. <https://doi.org/10.1002/med.21297>.
- (47) Nastasi, G.; Miceli, C.; Pittalà, V.; Modica, M. N.; Prezzavento, O.; Romeo, G.; Rescifina, A.; Marrazzo, A.; Amata, E. S2RSLDB: A Comprehensive Manually Curated, Internet-Accessible Database of the Sigma-2 Receptor Selective Ligands. *J. Cheminformatics* **2017**, *9* (1), 3. <https://doi.org/10.1186/s13321-017-0191-5>.
- (48) Home - S2RSLDB <http://www.researchdsf.unict.it/S2RSLDB/> (accessed Aug 20, 2019).
- (49) Schmidt, H. R.; Kruse, A. C. The Molecular Function of σ Receptors: Past, Present, and Future. *Trends Pharmacol. Sci.* **2019**, S0165614719301439. <https://doi.org/10.1016/j.tips.2019.07.006>.
- (50) Nguyen, L.; Lucke-Wold, B. P.; Mookerjee, S. A.; Cavendish, J. Z.; Robson, M. J.; Scandinaro, A. L.; Matsumoto, R. R. Role of Sigma-1 Receptors in Neurodegenerative Diseases. *J. Pharmacol. Sci.* **2015**, *127* (1), 17–29. <https://doi.org/10.1016/j.jphs.2014.12.005>.
- (51) Takebayashi, M.; Hayashi, T.; Su, T.-P. Nerve Growth Factor-Induced Neurite Sprouting in PC12 Cells Involves ζ -1 Receptors: Implications for Antidepressants. *J. Pharmacol. Exp. Ther.* **2002**, *303* (3), 1227–1237. <https://doi.org/10.1124/jpet.102.041970>.
- (52) Ishima, T.; Nishimura, T.; Iyo, M.; Hashimoto, K. Potentiation of Nerve Growth Factor-Induced Neurite Outgrowth in PC12 Cells by Donepezil: Role of Sigma-1 Receptors and IP3 Receptors. *Prog.*

- Neuropsychopharmacol. Biol. Psychiatry* **2008**, *32* (7), 1656–1659.
<https://doi.org/10.1016/j.pnpbp.2008.06.011>.
- (53) Rossi, D.; Marra, A.; Picconi, P.; Serra, M.; Catenacci, L.; Sorrenti, M.; Laurini, E.; Fermeglia, M.; Pricl, S.; Brambilla, S.; et al. Identification of RC-33 as a Potent and Selective $\Sigma 1$ Receptor Agonist Potentiating NGF-Induced Neurite Outgrowth in PC12 Cells. Part 2: G-Scale Synthesis, Physicochemical Characterization and in Vitro Metabolic Stability. *Bioorg. Med. Chem.* **2013**, *21* (9), 2577–2586.
<https://doi.org/10.1016/j.bmc.2013.02.029>.
- (54) Pal, A.; Hajipour, A. R.; Fontanilla, D.; Ramachandran, S.; Chu, U. B.; Mavlyutov, T.; Ruoho, A. E. Identification of Regions of the σ -1 Receptor Ligand Binding Site Using a Novel Photoprobe. *Mol. Pharmacol.* **2007**, *72* (4), 921–933. <https://doi.org/10.1124/mol.107.038307>.
- (55) Ramachandran, S.; Lu, H.; Prabhu, U.; Ruoho, A. E. Purification and Characterization of the Guinea Pig Sigma-1 Receptor Functionally Expressed in Escherichia Coli. *Protein Expr. Purif.* **2007**, *51* (2), 283–292. <https://doi.org/10.1016/j.pep.2006.07.019>.
- (56) Chu, U. B.; Ramachandran, S.; Hajipour, A. R.; Ruoho, A. E. Photoaffinity Labeling of the Sigma-1 Receptor with *N*-[3-(4-Nitrophenyl)Propyl]-*N*-Dodecylamine: Evidence of Receptor Dimers. *Biochemistry* **2013**, *52* (5), 859–868. <https://doi.org/10.1021/bi301517u>.
- (57) Gromek, K. A.; Suchy, F. P.; Meddaugh, H. R.; Wrobel, R. L.; LaPointe, L. M.; Chu, U. B.; Primm, J. G.; Ruoho, A. E.; Senes, A.; Fox, B. G. The Oligomeric States of the Purified Sigma-1 Receptor Are Stabilized by Ligands. *J. Biol. Chem.* **2014**, *289* (29), 20333–20344.
<https://doi.org/10.1074/jbc.M113.537993>.
- (58) Mishra, A. K.; Mavlyutov, T.; Singh, D. R.; Biener, G.; Yang, J.; Oliver, J. A.; Ruoho, A.; Raicu, V. The Sigma-1 Receptors Are Present in Monomeric and Oligomeric Forms in Living Cells in the Presence and Absence of Ligands. *Biochem. J.* **2015**, *466* (2), 263–271. <https://doi.org/10.1042/BJ20141321>.
- (59) Schmidt, H. R.; Betz, R. M.; Dror, R. O.; Kruse, A. C. Structural Basis for $\Sigma 1$ Receptor Ligand Recognition. *Nat. Struct. Mol. Biol.* **2018**, *25* (10), 981–987. <https://doi.org/10.1038/s41594-018-0137-2>.
- (60) An Extension Study of ANAVEX2-73 in Patients With Mild to Moderate Alzheimer’s Disease - Full Text View - ClinicalTrials.gov <https://clinicaltrials.gov/ct2/show/NCT02756858> (accessed Aug 21, 2019).
- (61) Romero, L.; Merlos, M.; Vela, J. M. Chapter Seven - Antinociception by Sigma-1 Receptor Antagonists: Central and Peripheral Effects. In *Advances in Pharmacology*; Barrett, J. E., Ed.; Pharmacological Mechanisms and the Modulation of Pain; Academic Press, 2016; Vol. 75, pp 179–215.
<https://doi.org/10.1016/bs.apha.2015.11.003>.
- (62) Bruna, J.; Videla, S.; Argyriou, A. A.; Velasco, R.; Villoria, J.; Santos, C.; Nadal, C.; Cavaletti, G.; Alberti, P.; Briani, C.; et al. Efficacy of a Novel Sigma-1 Receptor Antagonist for Oxaliplatin-Induced Neuropathy: A Randomized, Double-Blind, Placebo-Controlled Phase IIa Clinical Trial. *Neurotherapeutics* **2018**, *15* (1), 178–189. <https://doi.org/10.1007/s13311-017-0572-5>.
- (63) Katz, J.; Hong, W.; Hiranita, T.; Su, T.-P. A Role for Sigma Receptors in Stimulant Self-Administration and Addiction. *Behav. Pharmacol.* **2016**, *27* (2 and 3-Special Issue), 100–115.
<https://doi.org/10.1097/FBP.0000000000000209>.
- (64) Skuza, G. Ethanol Withdrawal-Induced Depressive Symptoms in Animals and Therapeutic Potential of Sigma1 Receptor Ligands. *Pharmacol. Rep.* **2013**, *65* (6), 1681–1687. [https://doi.org/10.1016/S1734-1140\(13\)71530-5](https://doi.org/10.1016/S1734-1140(13)71530-5).
- (65) Kim, F. J.; Maher, C. M. Sigma1 Pharmacology in the Context of Cancer. In *Sigma Proteins: Evolution of the Concept of Sigma Receptors*; Kim, F. J., Pasternak, G. W., Eds.; Handbook of Experimental Pharmacology; Springer International Publishing: Cham, 2017; pp 237–308.
https://doi.org/10.1007/164_2017_38.
- (66) Georgiadis, M.-O.; Karoutzou, O.; Foscolos, A.-S.; Papanastasiou, I. Sigma Receptor (ΣR) Ligands with Antiproliferative and Anticancer Activity. *Mol. Basel Switz.* **2017**, *22* (9).
<https://doi.org/10.3390/molecules22091408>.
- (67) Collina, S.; Bignardi, E.; Rui, M.; Rossi, D.; Gaggeri, R.; Zamagni, A.; Cortesi, M.; Tesei, A. Are Sigma Modulators an Effective Opportunity for Cancer Treatment? A Patent Overview (1996-2016). *Expert Opin. Ther. Pat.* **2017**, *27* (5), 565–578. <https://doi.org/10.1080/13543776.2017.1276569>.

- (68) Garay, R. P.; Grossberg, G. T. AVP-786 for the Treatment of Agitation in Dementia of the Alzheimer's Type. *Expert Opin. Investig. Drugs* **2017**, *26* (1), 121–132. <https://doi.org/10.1080/13543784.2017.1267726>.
- (69) Efficacy, Safety and Tolerability of AVP-786 for the Treatment of Agitation in Patients With Dementia of the Alzheimer's Type - Full Text View - ClinicalTrials.gov <https://clinicaltrials.gov/ct2/show/NCT02442765> (accessed Aug 21, 2019).
- (70) Díaz, J. L.; Cuberes, R.; Berrocal, J.; Contijoch, M.; Christmann, U.; Fernández, A.; Port, A.; Holenz, J.; Buschmann, H.; Laggner, C.; et al. Synthesis and Biological Evaluation of the 1-Arylpyrazole Class of $\Sigma 1$ Receptor Antagonists: Identification of 4-{2-[5-Methyl-1-(Naphthalen-2-Yl)-1H-Pyrazol-3-Yloxy]Ethyl}morpholine (S1RA, E-52862). *J. Med. Chem.* **2012**, *55* (19), 8211–8224. <https://doi.org/10.1021/jm3007323>.
- (71) Esteve | News | MUNDIPHARMA AND PURDUE REACH A NEW DEAL TO IN-LICENCE FROM ESTEVE FULL GLOBAL RIGHTS AND DEVELOPMENT RESPONSIBILITIES FOR NOVEL FIRST-IN-CLASS SIGMA-1 ANTAGONIST (S1A OR MR309/E-52862) <https://www.esteve.com/global/news/mundipharma-and-purdue-reach-a-new-deal-to-in-licence-from-esteve-full-global-rights-and-development-responsibilities-for-novel-first-in-class-sigma-1-antagonist-s1a-or-mr309e-52862> (accessed Aug 21, 2019).
- (72) Sahlholm, K.; Sijbesma, J. W. A.; Maas, B.; Kwizera, C.; Marcellino, D.; Ramakrishnan, N. K.; Dierckx, R. A. J. O.; Elsinga, P. H.; van Waarde, A. Pridopidine Selectively Occupies Sigma-1 Rather than Dopamine D2 Receptors at Behaviorally Active Doses. *Psychopharmacology (Berl.)* **2015**, *232* (18), 3443–3453. <https://doi.org/10.1007/s00213-015-3997-8>.
- (73) A Study to Assess the Safety and Effectiveness of Pridopidine Compared to Placebo in the Treatment of Levodopa-Induced Dyskinesia in Patients With Parkinson's Disease - Full Text View - ClinicalTrials.gov <https://clinicaltrials.gov/ct2/show/NCT03922711> (accessed Oct 6, 2019).
- (74) Ionescu, A.; Gradus, T.; Altman, T.; Maimon, R.; Avraham, N. S.; Geva, M.; Hayden, M.; Perlson, E. Targeting the Sigma-1 Receptor via Pridopidine Ameliorates Central Features of ALS Pathology in a SOD1 G93A Model. *Cell Death Dis.* **2019**, *10* (3), 1–19. <https://doi.org/10.1038/s41419-019-1451-2>.
- (75) Heemels, M.-T. Neurodegenerative Diseases. *Nature* **2016**, *539* (7628), 179–179. <https://doi.org/10.1038/539179a>.
- (76) Golpich, M.; Amini, E.; Mohamed, Z.; Azman Ali, R.; Mohamed Ibrahim, N.; Ahmadiani, A. Mitochondrial Dysfunction and Biogenesis in Neurodegenerative Diseases: Pathogenesis and Treatment. *CNS Neurosci. Ther.* **2017**, *23* (1), 5–22. <https://doi.org/10.1111/cns.12655>.
- (77) Gao, H.-M.; Hong, J.-S. Why Neurodegenerative Diseases Are Progressive: Uncontrolled Inflammation Drives Disease Progression. *Trends Immunol.* **2008**, *29* (8), 357–365. <https://doi.org/10.1016/j.it.2008.05.002>.
- (78) Feigin, V. L.; Vos, T. Global Burden of Neurological Disorders: From Global Burden of Disease Estimates to Actions. *Neuroepidemiology* **2019**, *52* (1–2), 1–2. <https://doi.org/10.1159/000495197>.
- (79) Gitler, A. D.; Dhillon, P.; Shorter, J. Neurodegenerative Disease: Models, Mechanisms, and a New Hope. *Dis. Model. Mech.* **2017**, *10* (5), 499–502. <https://doi.org/10.1242/dmm.030205>.
- (80) De Felice, A.; Ricceri, L.; Venerosi, A.; Chiarotti, F.; Calamandrei, G. Multifactorial Origin of Neurodevelopmental Disorders: Approaches to Understanding Complex Etiologies. *Toxics* **2015**, *3* (1), 89–129. <https://doi.org/10.3390/toxics3010089>.
- (81) Nguyen, L.; Lucke-Wold, B. P.; Mookerjee, S.; Kaushal, N.; Matsumoto, R. R. Sigma-1 Receptors and Neurodegenerative Diseases: Towards a Hypothesis of Sigma-1 Receptors as Amplifiers of Neurodegeneration and Neuroprotection. In *Sigma Receptors: Their Role in Disease and as Therapeutic Targets*; Smith, S. B., Su, T.-P., Eds.; Springer International Publishing: Cham, 2017; Vol. 964, pp 133–152. https://doi.org/10.1007/978-3-319-50174-1_10.
- (82) Nguyen, L.; Kaushal, N.; Robson, M. J.; Matsumoto, R. R. Sigma Receptors as Potential Therapeutic Targets for Neuroprotection. *Eur. J. Pharmacol.* **2014**, *743*, 42–47. <https://doi.org/10.1016/j.ejphar.2014.09.022>.
- (83) Hayashi, T.; Rizzuto, R.; Hajnoczky, G.; Su, T.-P. MAM: More than Just a Housekeeper. *Trends Cell Biol.* **2009**, *19* (2), 81–88. <https://doi.org/10.1016/j.tcb.2008.12.002>.

- (84) Monnet, F. P.; Morin-Surun, M. P.; Leger, J.; Combettes, L. Protein Kinase C-Dependent Potentiation of Intracellular Calcium Influx by Sigma1 Receptor Agonists in Rat Hippocampal Neurons. *J. Pharmacol. Exp. Ther.* **2003**, *307* (2), 705–712. <https://doi.org/10.1124/jpet.103.053447>.
- (85) Tchedre, K. T.; Huang, R.-Q.; Dibas, A.; Krishnamoorthy, R. R.; Dillon, G. H.; Yorio, T. Sigma-1 Receptor Regulation of Voltage-Gated Calcium Channels Involves a Direct Interaction. *Invest. Ophthalmol. Vis. Sci.* **2008**, *49* (11), 4993–5002. <https://doi.org/10.1167/iovs.08-1867>.
- (86) Lau, A.; Tymianski, M. Glutamate Receptors, Neurotoxicity and Neurodegeneration. *Pflug. Arch. - Eur. J. Physiol.* **2010**, *460* (2), 525–542. <https://doi.org/10.1007/s00424-010-0809-1>.
- (87) Sheldon, A. L.; Robinson, M. B. The Role of Glutamate Transporters in Neurodegenerative Diseases and Potential Opportunities for Intervention. *Neurochem. Int.* **2007**, *51* (6–7), 333–355. <https://doi.org/10.1016/j.neuint.2007.03.012>.
- (88) Fu, Y.; Yu, S.; Guo, X.; Li, X.; Li, T.; Li, H.; Dong, Y. Fluvoxamine Increased Glutamate Release by Activating Both 5-HT(3) and Sigma-1 Receptors in Prelimbic Cortex of Chronic Restraint Stress C57BL/6 Mice. *Biochim. Biophys. Acta* **2012**, *1823* (4), 826–837. <https://doi.org/10.1016/j.bbamcr.2012.01.008>.
- (89) Lu, C.-W.; Lin, T.-Y.; Wang, C.-C.; Wang, S.-J. σ -1 Receptor Agonist SKF10047 Inhibits Glutamate Release in Rat Cerebral Cortex Nerve Endings. *J. Pharmacol. Exp. Ther.* **2012**, *341* (2), 532–542. <https://doi.org/10.1124/jpet.111.191189>.
- (90) Pabba, M.; Sibille, E. Sigma-1 and N-Methyl-D-Aspartate Receptors: A Partnership with Beneficial Outcomes. *Mol. Neuropsychiatry* **2015**, *1* (1), 47–51. <https://doi.org/10.1159/000376549>.
- (91) Rodríguez-Muñoz, M.; Cortés-Montero, E.; Pozo-Rodríguez, A.; Sánchez-Blázquez, P.; Garzón-Niño, J. The ON:OFF Switch, Σ 1R-HINT1 Protein, Controls GPCR-NMDA Receptor Cross-Regulation: Implications in Neurological Disorders. *Oncotarget* **2015**, *6* (34), 35458–35477. <https://doi.org/10.18632/oncotarget.6064>.
- (92) Ray, P. D.; Huang, B.-W.; Tsuji, Y. Reactive Oxygen Species (ROS) Homeostasis and Redox Regulation in Cellular Signaling. *Cell. Signal.* **2012**, *24* (5), 981–990. <https://doi.org/10.1016/j.cellsig.2012.01.008>.
- (93) Gandhi, S.; Abramov, A. Y. Mechanism of Oxidative Stress in Neurodegeneration <https://www.hindawi.com/journals/omcl/2012/428010/> (accessed Aug 23, 2019). <https://doi.org/10.1155/2012/428010>.
- (94) Kim, G. H.; Kim, J. E.; Rhie, S. J.; Yoon, S. The Role of Oxidative Stress in Neurodegenerative Diseases. *Exp. Neurobiol.* **2015**, *24* (4), 325–340. <https://doi.org/10.5607/en.2015.24.4.325>.
- (95) Dringen, R.; Hirrlinger, J. Glutathione Pathways in the Brain. *Biol. Chem.* **2003**, *384* (4), 505–516. <https://doi.org/10.1515/BC.2003.059>.
- (96) Reynolds, A.; Laurie, C.; Lee Mosley, R.; Gendelman, H. E. Oxidative Stress and the Pathogenesis of Neurodegenerative Disorders. In *International Review of Neurobiology*; Neuroinflammation in Neuronal Death and Repair; Academic Press, 2007; Vol. 82, pp 297–325. [https://doi.org/10.1016/S0074-7742\(07\)82016-2](https://doi.org/10.1016/S0074-7742(07)82016-2).
- (97) Mori, T.; Hayashi, T.; Su, T.-P. Compromising σ -1 Receptors at the Endoplasmic Reticulum Render Cytotoxicity to Physiologically Relevant Concentrations of Dopamine in a Nuclear Factor-KB/Bcl-2-Dependent Mechanism: Potential Relevance to Parkinson's Disease. *J. Pharmacol. Exp. Ther.* **2012**, *341* (3), 663–671. <https://doi.org/10.1124/jpet.111.190868>.
- (98) Pal, A.; Fontanilla, D.; Gopalakrishnan, A.; Chae, Y.-K.; Markley, J. L.; Ruoho, A. E. The Sigma-1 Receptor Protects against Cellular Oxidative Stress and Activates Antioxidant Response Elements. *Eur. J. Pharmacol.* **2012**, *682* (1), 12–20. <https://doi.org/10.1016/j.ejphar.2012.01.030>.
- (99) Yang, Z.-J.; Carter, E. L.; Torbey, M. T.; Martin, L. J.; Koehler, R. C. Sigma Receptor Ligand 4-Phenyl-1-(4-Phenylbutyl)-Piperidine Modulates Neuronal Nitric Oxide Synthase/Postsynaptic Density-95 Coupling Mechanisms and Protects against Neonatal Ischemic Degeneration of Striatal Neurons. *Exp. Neurol.* **2010**, *221* (1), 166–174. <https://doi.org/10.1016/j.expneurol.2009.10.019>.
- (100) Vagnerova, K.; Hurn, P.; Bhardwaj, A.; Kirsch, J. Sigma 1 Receptor Agonists Act as Neuroprotective Drugs Through Inhibition of Inducible Nitric Oxide Synthase. *Anesth. Analg.* **2006**, *103* (2), 430–434. <https://doi.org/10.1213/01.ane.0000226133.85114.91>.

- (101) Goyagi, T.; Goto, S.; Bhardwaj, A.; Dawson, V. L.; Hurn, P. D.; Kirsch, J. R. Neuroprotective Effect of Σ 1-Receptor Ligand 4-Phenyl-1-(4-Phenylbutyl) Piperidine (PPBP) Is Linked to Reduced Neuronal Nitric Oxide Production. *Stroke* **2001**, *32* (7), 1613–1620. <https://doi.org/10.1161/01.STR.32.7.1613>.
- (102) Yoshida, H. ER Stress and Diseases. *FEBS J.* **2007**, *274* (3), 630–658. <https://doi.org/10.1111/j.1742-4658.2007.05639.x>.
- (103) Kimata, Y.; Kohno, K. Endoplasmic Reticulum Stress-Sensing Mechanisms in Yeast and Mammalian Cells. *Curr. Opin. Cell Biol.* **2011**, *23* (2), 135–142. <https://doi.org/10.1016/j.ceb.2010.10.008>.
- (104) Mori, T.; Hayashi, T.; Hayashi, E.; Su, T.-P. Sigma-1 Receptor Chaperone at the ER-Mitochondrion Interface Mediates the Mitochondrion-ER-Nucleus Signaling for Cellular Survival. *PLoS One* **2013**, *8* (10), e76941. <https://doi.org/10.1371/journal.pone.0076941>.
- (105) Hayashi, T. Conversion of Psychological Stress into Cellular Stress Response: Roles of the Sigma-1 Receptor in the Process. *Psychiatry Clin. Neurosci.* **2015**, *69* (4), 179–191. <https://doi.org/10.1111/pcn.12262>.
- (106) Twig, G.; Hyde, B.; Shirihai, O. S. Mitochondrial Fusion, Fission and Autophagy as a Quality Control Axis: The Bioenergetic View. *Biochim. Biophys. Acta BBA - Bioenerg.* **2008**, *1777* (9), 1092–1097. <https://doi.org/10.1016/j.bbabi.2008.05.001>.
- (107) Klouz, A.; Saïd, D. B.; Ferchichi, H.; Kourda, N.; Ouanes, L.; Lakhal, M.; Tillement, J.-P.; Morin, D. Protection of Cellular and Mitochondrial Functions against Liver Ischemia by N-Benzyl-N'-(2-Hydroxy-3,4-Dimethoxybenzyl)-Piperazine (BHDP), a Sigma1 Ligand. *Eur. J. Pharmacol.* **2008**, *578* (2), 292–299. <https://doi.org/10.1016/j.ejphar.2007.09.038>.
- (108) Tagashira, H.; Zhang, C.; Lu, Y.; Hasegawa, H.; Kanai, H.; Han, F.; Fukunaga, K. Stimulation of Σ 1-Receptor Restores Abnormal Mitochondrial Ca²⁺ Mobilization and ATP Production Following Cardiac Hypertrophy. *Biochim. Biophys. Acta BBA - Gen. Subj.* **2013**, *1830* (4), 3082–3094. <https://doi.org/10.1016/j.bbagen.2012.12.029>.
- (109) Meunier, J.; Hayashi, T. Sigma-1 Receptors Regulate Bcl-2 Expression by Reactive Oxygen Species-Dependent Transcriptional Regulation of Nuclear Factor KappaB. *J. Pharmacol. Exp. Ther.* **2010**, *332* (2), 388–397. <https://doi.org/10.1124/jpet.109.160960>.
- (110) Behensky, A. A.; Yasny, I. E.; Shuster, A. M.; Seredenin, S. B.; Petrov, A. V.; Cuevas, J. Stimulation of Sigma Receptors with Afobazole Blocks Activation of Microglia and Reduces Toxicity Caused by Amyloid-B25-35. *J. Pharmacol. Exp. Ther.* **2013**, *347* (2), 458–467. <https://doi.org/10.1124/jpet.113.208348>.
- (111) Rodríguez, J. J.; Verkhatsky, A. Neurogenesis in Alzheimer's Disease. *J. Anat.* **2011**, *219* (1), 78–89. <https://doi.org/10.1111/j.1469-7580.2011.01343.x>.
- (112) Koyama, Y. Signaling Molecules Regulating Phenotypic Conversions of Astrocytes and Glial Scar Formation in Damaged Nerve Tissues. *Neurochem. Int.* **2014**, *78*, 35–42. <https://doi.org/10.1016/j.neuint.2014.08.005>.
- (113) Ajmo Jr., C. T.; Vernon, D. O. L.; Collier, L.; Pennypacker, K. R.; Cuevas, J. Sigma Receptor Activation Reduces Infarct Size at 24 Hours after Permanent Middle Cerebral Artery Occlusion in Rats. *Curr. Neurovasc. Res.* **2006**, *3* (2), 89–98. <https://doi.org/10.2174/156720206776875849>.
- (114) Peviani, M.; Salvaneschi, E.; Bontempi, L.; Petese, A.; Manzo, A.; Rossi, D.; Salmona, M.; Collina, S.; Bigini, P.; Curti, D. Neuroprotective Effects of the Sigma-1 Receptor (S1R) Agonist PRE-084, in a Mouse Model of Motor Neuron Disease Not Linked to SOD1 Mutation. *Neurobiol. Dis.* **2014**, *62*, 218–232. <https://doi.org/10.1016/j.nbd.2013.10.010>.
- (115) Prezzavento, O.; Campisi, A.; Parenti, C.; Ronsisvalle, S.; Aricò, G.; Arena, E.; Pistolozzi, M.; Scoto, G. M.; Bertucci, C.; Vanella, A.; et al. Synthesis and Resolution of Cis-(±)-Methyl (1R,2S/1S,2R)-2-[(4-Hydroxy-4-Phenylpiperidin-1-yl)Methyl]-1-(4-Methylphenyl)Cyclopropanecarboxylate [(±)-PPCC]: New σ Receptor Ligands with Neuroprotective Effect. *J. Med. Chem.* **2010**, *53* (15), 5881–5885. <https://doi.org/10.1021/jm100116p>.
- (116) Ruscher, K.; Shamloo, M.; Rickhag, M.; Ladunga, I.; Soriano, L.; Gisselsson, L.; Toresson, H.; Ruslim-Litrus, L.; Oksenberg, D.; Urfer, R.; et al. The Sigma-1 Receptor Enhances Brain Plasticity and Functional Recovery after Experimental Stroke. *Brain* **2011**, *134* (3), 732–746. <https://doi.org/10.1093/brain/awq367>.

- (117) Perry, V. H.; Nicoll, J. A. R.; Holmes, C. Microglia in Neurodegenerative Disease. *Nat. Rev. Neurol.* **2010**, *6* (4), 193–201. <https://doi.org/10.1038/nrneuro.2010.17>.
- (118) Cuevas, J.; Rodriguez, A.; Behensky, A.; Katnik, C. Afobazole Modulates Microglial Function via Activation of Both Sigma-1 and Sigma-2 Receptors. *J. Pharmacol. Exp. Ther.* **2011**, *339* (1), 161–172. <https://doi.org/10.1124/jpet.111.182816>.
- (119) Robson, M. J.; Turner, R. C.; Naser, Z. J.; McCurdy, C. R.; Huber, J. D.; Matsumoto, R. R. SN79, a Sigma Receptor Ligand, Blocks Methamphetamine-Induced Microglial Activation and Cytokine Upregulation. *Exp. Neurol.* **2013**, *247*, 134–142. <https://doi.org/10.1016/j.expneurol.2013.04.009>.
- (120) Wu, Z.; Li, L.; Zheng, L.-T.; Xu, Z.; Guo, L.; Zhen, X. Allosteric Modulation of Sigma-1 Receptors by SKF83959 Inhibits Microglia-Mediated Inflammation. *J. Neurochem.* **2015**, *134* (5), 904–914. <https://doi.org/10.1111/jnc.13182>.
- (121) Mancuso, R.; Oliván, S.; Rando, A.; Casas, C.; Osta, R.; Navarro, X. Sigma-1R Agonist Improves Motor Function and Motoneuron Survival in ALS Mice. *Neurother. J. Am. Soc. Exp. Neurother.* **2012**, *9* (4), 814–826. <https://doi.org/10.1007/s13311-012-0140-y>.
- (122) Morphy, R.; Kay, C.; Rankovic, Z. From Magic Bullets to Designed Multiple Ligands. *Drug Discov. Today* **2004**, *9* (15), 641–651. [https://doi.org/10.1016/S1359-6446\(04\)03163-0](https://doi.org/10.1016/S1359-6446(04)03163-0).
- (123) J. Geldenhuys, W.; J. Van der Schyf, C. Rationally Designed Multi-Targeted Agents Against Neurodegenerative Diseases. *Curr. Med. Chem.* **2013**, *20* (13), 1662–1672. <https://doi.org/10.2174/09298673113209990112>.
- (124) Korcsmáros, T.; Szalay, M. S.; Böde, C.; Kovács, I. A.; Csermely, P. How to Design Multi-Target Drugs: Target Search Options in Cellular Networks. *Expert Opin. Drug Discov.* **2007**, *2* (6), 799–808. <https://doi.org/10.1517/17460441.2.6.799>.
- (125) Talevi, A. Multi-Target Pharmacology: Possibilities and Limitations of the “Skeleton Key Approach” from a Medicinal Chemist Perspective. *Front. Pharmacol.* **2015**, *6*. <https://doi.org/10.3389/fphar.2015.00205>.
- (126) Cavalli, A.; Bolognesi, M. L.; Minarini, A.; Rosini, M.; Tumiatti, V.; Recanatini, M.; Melchiorre, C. Multi-Target-Directed Ligands To Combat Neurodegenerative Diseases. *J. Med. Chem.* **2008**, *51* (3), 347–372. <https://doi.org/10.1021/jm7009364>.
- (127) Medina-Franco, J. L.; Giulianotti, M. A.; Welmaker, G. S.; Houghten, R. A. Shifting from the Single- to the Multitarget Paradigm in Drug Discovery. *Drug Discov. Today* **2013**, *18* (0), 495–501. <https://doi.org/10.1016/j.drudis.2013.01.008>.
- (128) Wang, N.; Qiu, P.; Cui, W.; Zhang, B.; Yan, X.; He, S. Recent Advances in Multi-Target Anti-Alzheimer Disease Compounds (2013 up to Present). *Curr. Med. Chem.* **2018**, *26*. <https://doi.org/10.2174/0929867326666181203124102>.
- (129) Prati, F.; Bottegoni, G.; Bolognesi, M. L.; Cavalli, A. BACE-1 Inhibitors: From Recent Single-Target Molecules to Multitarget Compounds for Alzheimer’s Disease: Miniperspective. *J. Med. Chem.* **2018**, *61* (3), 619–637. <https://doi.org/10.1021/acs.jmedchem.7b00393>.
- (130) Rosini, M. Polypharmacology: The Rise of Multitarget Drugs over Combination Therapies. *Future Med. Chem.* **2014**, *6* (5), 485–487. <https://doi.org/10.4155/fmc.14.25>.
- (131) Van der Schyf, C. J. The Use of Multi-Target Drugs in the Treatment of Neurodegenerative Diseases. *Expert Rev. Clin. Pharmacol.* **2011**, *4* (3), 293–298. <https://doi.org/10.1586/ecp.11.13>.
- (132) Rusnak, D.; Gilmer, T. M. The Discovery of Lapatinib (GW572016). *2*.
- (133) Deeks, E. D. Neratinib: First Global Approval. *Drugs* **2017**, *77* (15), 1695–1704. <https://doi.org/10.1007/s40265-017-0811-4>.
- (134) Burris, H. A. Dual Kinase Inhibition in the Treatment of Breast Cancer: Initial Experience with the EGFR/ErbB-2 Inhibitor Lapatinib. *The Oncologist* **2004**, *9 Suppl 3*, 10–15. https://doi.org/10.1634/theoncologist.9-suppl_3-10.
- (135) FDA approves neratinib for extended adjuvant treatment of early stage HER2-positive breast cancer | FDA <https://www.fda.gov/drugs/resources-information-approved-drugs/fda-approves-neratinib-extended-adjuvant-treatment-early-stage-her2-positive-breast-cancer> (accessed Jan 20, 2020).
- (136) Lai, C.-J.; Tao, X.; Wang, J.; Atoyan, R.; Qu, H.; Wang, D.-G.; Yin, L.; Samson, M.; Forrester, J.; Zifcak, B.; et al. CUDC-101, a Multitargeted Inhibitor of Histone Deacetylase, Epidermal Growth Factor

- Receptor, and Human Epidermal Growth Factor Receptor 2, Exerts Potent Anticancer Activity. *Cancer Res.* 11.
- (137) Phase I Study of CUDC-101 With Cisplatin and Radiation in Subjects With Head & Neck Cancer - Full Text View - ClinicalTrials.gov <https://clinicaltrials.gov/ct2/show/NCT01384799> (accessed Jan 20, 2020).
- (138) Weinreb, O.; Mandel, S.; Bar-Am, O.; Yogev-Falach, M.; Avramovich-Tirosh, Y.; Amit, T.; Youdim, M. B. H. Multifunctional Neuroprotective Derivatives of Rasagiline as Anti-Alzheimer's Disease Drugs. *Neurotherapeutics* **2009**, *6* (1), 163–174. <https://doi.org/10.1016/j.nurt.2008.10.030>.
- (139) Weinstock, M.; Luques, L.; Bejar, C.; Shoham, S. Ladostigil, a Novel Multifunctional Drug for the Treatment of Dementia Co-Morbid with Depression. *J. Neural Transm. Suppl.* **2006**, No. 70, 443–446.
- (140) Weinreb, O.; Amit, T.; Bar-Am, O.; Youdim, M. B. H. Induction of Neurotrophic Factors GDNF and BDNF Associated with the Mechanism of Neurorescue Action of Rasagiline and Ladostigil. *Ann. N. Y. Acad. Sci.* **2007**, *1122* (1), 155–168. <https://doi.org/10.1196/annals.1403.011>.
- (141) Schneider, L. S.; Geffen, Y.; Rabinowitz, J.; Thomas, R. G.; Schmidt, R.; Ropele, S.; Weinstock, M.; Ladostigil Study Group. Low-Dose Ladostigil for Mild Cognitive Impairment: A Phase 2 Placebo-Controlled Clinical Trial. *Neurology* **2019**, *93* (15), e1474–e1484. <https://doi.org/10.1212/WNL.00000000000008239>.
- (142) Rajeshwari, R.; Chand, K.; Candeias, E.; Cardoso, S.; Chaves, S.; Santos, M. New Multitarget Hybrids Bearing Tacrine and Phenylbenzothiazole Motifs as Potential Drug Candidates for Alzheimer's Disease. *Molecules* **2019**, *24* (3), 587. <https://doi.org/10.3390/molecules24030587>.
- (143) Lutsenko, K.; Hagenow, S.; Affini, A.; Reiner, D.; Stark, H. Rasagiline Derivatives Combined with Histamine H3 Receptor Properties. *Bioorg. Med. Chem. Lett.* **2019**, 126612. <https://doi.org/10.1016/j.bmcl.2019.08.016>.
- (144) Morroni, F.; Sita, G.; Graziosi, A.; Ravegnini, G.; Molteni, R.; Paladini, M. S.; Dias, K. S. T.; Dos Santos, A. F.; Viegas, C.; Camps, I.; et al. PQM130, a Novel Feruloyl-Donepezil Hybrid Compound, Effectively Ameliorates the Cognitive Impairments and Pathology in a Mouse Model of Alzheimer's Disease. *Front. Pharmacol.* **2019**, *10*, 658. <https://doi.org/10.3389/fphar.2019.00658>.
- (145) Schwarz, S.; Pohl, P.; Zhou, G.-Z.; Su, T.-P.; London, E. D.; Jaffe, J. H. Steroid Binding at σ -"opioid" Receptors. *Science* **1989**, *246* (4937), 1635–1638. <https://doi.org/10.1126/science.2556797>.
- (146) Ramachandran, S.; Chu, U. B.; Mavlyutov, T. A.; Pal, A.; Pyne, S.; Ruoho, A. E. The Sigma1 Receptor Interacts with N-Alkyl Amines and Endogenous Sphingolipids. *Eur. J. Pharmacol.* **2009**, *609* (1), 19–26. <https://doi.org/10.1016/j.ejphar.2009.03.003>.
- (147) Su, T. P.; Wu, X. Z.; Cone, E. J.; Shukla, K.; Gund, T. M.; Dodge, A. L.; Parish, D. W. Sigma Compounds Derived from Phencyclidine: Identification of PRE-084, a New, Selective Sigma Ligand. *J. Pharmacol. Exp. Ther.* **1991**, *259* (2), 543–550.
- (148) Seredenin, S. B.; Antipova, T. A.; Voronin, M. V.; Kurchashova, S. Y.; Kuimov, A. N. Interaction of Afobazole with Sigma1-Receptors. *Bull. Exp. Biol. Med.* **2009**, *148* (1), 42–44. <https://doi.org/10.1007/s10517-009-0624-x>.
- (149) Keana, J. F. W.; Weber, E. Substituted Guanidines Having High Binding to the Sigma Receptor and the Use Thereof. WO1991018868A1, December 12, 1991.
- (150) Lever, J. R.; Gustafson, J. L.; Xu, R.; Allmon, R. L.; Lever, S. Z. Sigma1 and Sigma2 Receptor Binding Affinity and Selectivity of SA4503 and Fluoroethyl SA4503. *Synap. N. Y. N* **2006**, *59* (6), 350–358. <https://doi.org/10.1002/syn.20253>.
- (151) Matsumoto, R. R.; Bowen, W. D.; de Costa, B. R.; Houk, J. C. Relationship between Modulation of the Cerebellorubrospinal System in the in Vitro Turtle Brain and Changes in Motor Behavior in Rats: Effects of Novel Sigma Ligands. *Brain Res. Bull.* **1999**, *48* (5), 497–508. [https://doi.org/10.1016/s0361-9230\(99\)00029-5](https://doi.org/10.1016/s0361-9230(99)00029-5).
- (152) Eaton, M. J.; Lookingland, K. J.; Moore, K. E. The σ Ligand Rimcazole Activates Noradrenergic Neurons Projecting to the Paraventricular Nucleus and Increases Corticosterone Secretion in Rats. *Brain Res.* **1996**, *733* (2), 162–166. [https://doi.org/10.1016/0006-8993\(96\)00290-9](https://doi.org/10.1016/0006-8993(96)00290-9).
- (153) Arena, E.; Dichiaro, M.; Floresta, G.; Parenti, C.; Marrazzo, A.; Pittalà, V.; Amata, E.; Prezzavento, O. Novel Sigma-1 Receptor Antagonists: From Opioids to Small Molecules: What Is New? *Future Med. Chem.* **2018**, *10* (2), 231–256. <https://doi.org/10.4155/fmc-2017-0164>.

- (154) John, C. S.; Vilner, B. J.; Bowen, W. D. Synthesis and Characterization of [125I]-N-(N-Benzylpiperidin-4-yl)-4-Iodobenzamide, a New σ_1 Receptor Radiopharmaceutical: High-Affinity Binding to MCF-7 Breast Tumor Cells. *J. Med. Chem.* **1994**, *37* (12), 1737–1739. <https://doi.org/10.1021/jm00038a002>.
- (155) Yang, S.; Bhardwaj, A.; Cheng, J.; Alkayed, N. J.; Hurn, P. D.; Kirsch, J. R. Sigma Receptor Agonists Provide Neuroprotection in Vitro by Preserving Bcl-2. *Anesth. Analg.* **2007**, *104* (5), 1179–1184, tables of contents. <https://doi.org/10.1213/01.ane.0000260267.71185.73>.
- (156) Tam, S. W.; Cook, L. Sigma Opiates and Certain Antipsychotic Drugs Mutually Inhibit (+)-[3H] SKF 10,047 and [3H]Haloperidol Binding in Guinea Pig Brain Membranes. *Proc. Natl. Acad. Sci. U. S. A.* **1984**, *81* (17), 5618–5621. <https://doi.org/10.1073/pnas.81.17.5618>.
- (157) McLarnon, J.; Sawyer, D.; Church, J. The Actions of L-687,384, a σ Receptor Ligand, on NMDA-Induced Currents in Cultured Rat Hippocampal Pyramidal Neurons. *Neurosci. Lett.* **1994**, *174* (2), 181–184. [https://doi.org/10.1016/0304-3940\(94\)90016-7](https://doi.org/10.1016/0304-3940(94)90016-7).
- (158) Maier, C. A.; Wünsch, B. Novel Spiropiperidines as Highly Potent and Subtype Selective σ -Receptor Ligands. Part 1. *J. Med. Chem.* **2002**, *45* (2), 438–448. <https://doi.org/10.1021/jm010992z>.
- (159) Maestrup, E. G.; Wiese, C.; Schepmann, D.; Brust, P.; Wünsch, B. Synthesis, Pharmacological Activity and Structure Affinity Relationships of Spirocyclic $\Sigma 1$ Receptor Ligands with a (2-Fluoroethyl) Residue in 3-Position. *Bioorg. Med. Chem.* **2011**, *19* (1), 393–405. <https://doi.org/10.1016/j.bmc.2010.11.013>.
- (160) Jimenez-Panizo, A.; Perez, P.; Rojas, A.; Fuentes-Prior, P.; Estebanez-Perpiña, E. Non-Canonical Dimerization of the Androgen Receptor and Other Nuclear Receptors: Implications for Human Disease. *Endocr. Relat. Cancer* **2019**. <https://doi.org/10.1530/ERC-19-0132>.
- (161) Peeters, M.; Romieu, P.; Maurice, T.; Su, T.-P.; Maloteaux, J.-M.; Hermans, E. Involvement of the Sigma 1 Receptor in the Modulation of Dopaminergic Transmission by Amantadine. *Eur. J. Neurosci.* **2004**, *19* (8), 2212–2220. <https://doi.org/10.1111/j.0953-816X.2004.03297.x>.
- (162) Yano, H.; Bonifazi, A.; Xu, M.; Guthrie, D. A.; Schneck, S. N.; Abramyan, A. M.; Fant, A. D.; Hong, W. C.; Newman, A. H.; Shi, L. Pharmacological Profiling of Sigma 1 Receptor Ligands by Novel Receptor Homomer Assays. *Neuropharmacology* **2018**, *133*, 264–275. <https://doi.org/10.1016/j.neuropharm.2018.01.042>.
- (163) Rossi, D.; Pedrali, A.; Gaggeri, R.; Marra, A.; Pignataro, L.; Laurini, E.; Dal Col, V.; Fermeiglia, M.; Pricl, S.; Schepmann, D.; et al. Chemical, Pharmacological, and in Vitro Metabolic Stability Studies on Enantiomerically Pure RC-33 Compounds: Promising Neuroprotective Agents Acting as σ_1 Receptor Agonists. *ChemMedChem* **2013**, *8* (9), 1514–1527. <https://doi.org/10.1002/cmdc.201300218>.
- (164) Collina, S.; Rui, M.; Stotani, S.; Bignardi, E.; Rossi, D.; Curti, D.; Giordanetto, F.; Malacrida, A.; Scuteri, A.; Cavaletti, G. Are Sigma Receptor Modulators a Weapon against Multiple Sclerosis Disease? *Future Med. Chem.* **2017**, *9* (17), 2029–2051. <https://doi.org/10.4155/fmc-2017-0122>.
- (165) Kása, P.; Rakonczay, Z.; Gulya, K. The Cholinergic System in Alzheimer's Disease. *Prog. Neurobiol.* **1997**, *52* (6), 511–535.
- (166) Colovic, M. B.; Krstic, D. Z.; Lazarevic-Pasti, T. D.; Bondzic, A. M.; Vasic, V. M. Acetylcholinesterase Inhibitors: Pharmacology and Toxicology. *Curr. Neuropharmacol.* **2013**, *11* (3), 315–335. <https://doi.org/10.2174/1570159X11311030006>.
- (167) Zhou, Q.; Sheng, M. NMDA Receptors in Nervous System Diseases. *Neuropharmacology* **2013**, *74*, 69–75. <https://doi.org/10.1016/j.neuropharm.2013.03.030>.
- (168) Kemp, J. A.; McKernan, R. M. NMDA Receptor Pathways as Drug Targets. *Nat. Neurosci.* **2002**, *5* Suppl, 1039–1042. <https://doi.org/10.1038/nn936>.
- (169) Temme, L.; Frehland, B.; Schepmann, D.; Robaa, D.; Sippl, W.; Wünsch, B. Hydroxymethyl Bioisosteres of Phenolic GluN2B-Selective NMDA Receptor Antagonists: Design, Synthesis and Pharmacological Evaluation. *Eur. J. Med. Chem.* **2018**, *144*, 672–681. <https://doi.org/10.1016/j.ejmech.2017.12.054>.
- (170) Lin, M. T.; Beal, M. F. Mitochondrial Dysfunction and Oxidative Stress in Neurodegenerative Diseases. *Nature* **2006**, *443* (7113), 787–795. <https://doi.org/10.1038/nature05292>.
- (171) Birks, J. S.; Harvey, R. J. Donepezil for Dementia Due to Alzheimer's Disease. *Cochrane Database Syst. Rev.* **2018**, *2018* (6). <https://doi.org/10.1002/14651858.CD001190.pub3>.

- (172) pubmeddev; RJ, R. I. and M. Ifenprodil is a novel type of N-methyl-D-aspartate receptor antagonist: interaction with polyamines. - PubMed - NCBI <https://www.ncbi.nlm.nih.gov/pubmed/2555674> (accessed Sep 7, 2019).
- (173) pubmeddev; G, B. I. and D. NR2B selective NMDA antagonists: the evolution of the ifenprodil-type pharmacophore. - PubMed - NCBI <https://www.ncbi.nlm.nih.gov/pubmed/16719809> (accessed Sep 7, 2019).
- (174) Barzegar, A.; Moosavi-Movahedi, A. A. Intracellular ROS Protection Efficiency and Free Radical-Scavenging Activity of Curcumin. *PLOS ONE* **2011**, *6* (10), e26012. <https://doi.org/10.1371/journal.pone.0026012>.
- (175) Daneman, R.; Prat, A. The Blood-Brain Barrier. *Cold Spring Harb. Perspect. Biol.* **2015**, *7* (1), a020412. <https://doi.org/10.1101/cshperspect.a020412>.
- (176) Wager, T. T.; Hou, X.; Verhoest, P. R.; Villalobos, A. Central Nervous System Multiparameter Optimization Desirability: Application in Drug Discovery. *ACS Chem. Neurosci.* **2016**, *7* (6), 767–775. <https://doi.org/10.1021/acschemneuro.6b00029>.
- (177) Muehlbacher, M.; Spitzer, G. M.; Liedl, K. R.; Kornhuber, J. Qualitative Prediction of Blood–Brain Barrier Permeability on a Large and Refined Dataset. *J. Comput. Aided Mol. Des.* **2011**, *25* (12), 1095–1106. <https://doi.org/10.1007/s10822-011-9478-1>.
- (178) Burke, M. D.; Schreiber, S. L. A Planning Strategy for Diversity-Oriented Synthesis. *Angew. Chem. Int. Ed.* **2004**, *43* (1), 46–58. <https://doi.org/10.1002/anie.200300626>.
- (179) Shimokawa, J. Divergent Strategy in Natural Product Total Synthesis. *Tetrahedron Lett.* **2014**, *55* (45), 6156–6162. <https://doi.org/10.1016/j.tetlet.2014.09.078>.
- (180) Lee, Y.-C.; Kumar, K.; Waldmann, H. Ligand-Directed Divergent Synthesis of Carbo- and Heterocyclic Ring Systems. *Angew. Chem. Int. Ed.* **2018**, *57* (19), 5212–5226. <https://doi.org/10.1002/anie.201710247>.
- (181) C. Boruah, R.; S. Nongthombam, G. Divergent Synthesis of Steroid Analogs from Steroidal β -Formylenamides, Conjugated Enones and β -Formylvinyl Halides. *HETEROCYCLES* **2019**, *98* (1), 19. <https://doi.org/10.3987/REV-18-898>.
- (182) Reidl, T. W.; Anderson, L. L. Divergent Functionalizations of Azetidines and Unsaturated Azetidines. *Asian J. Org. Chem.* **2019**, *8* (7), 931–945. <https://doi.org/10.1002/ajoc.201900229>.
- (183) Nahm, S.; Weinreb, S. M. N-Methoxy-n-Methylamides as Effective Acylating Agents. *Tetrahedron Lett.* **1981**, *22* (39), 3815–3818. [https://doi.org/10.1016/S0040-4039\(01\)91316-4](https://doi.org/10.1016/S0040-4039(01)91316-4).
- (184) Leroux, F.; Schlosser, M.; Zohar, E.; Marek, I. The Preparation of Organolithium Reagents and Intermediates. In *PATAI'S Chemistry of Functional Groups*; American Cancer Society, 2009. <https://doi.org/10.1002/9780470682531.pat0305>.
- (185) Ellman, G. L.; Courtney, K. D.; Andres, V.; Featherstone, R. M. A New and Rapid Colorimetric Determination of Acetylcholinesterase Activity. *Biochem. Pharmacol.* **1961**, *7* (2), 88–95. [https://doi.org/10.1016/0006-2952\(61\)90145-9](https://doi.org/10.1016/0006-2952(61)90145-9).
- (186) Meunier, J.; Ieni, J.; Maurice, T. The Anti-Amnesic and Neuroprotective Effects of Donepezil against Amyloid B 25-35 Peptide-Induced Toxicity in Mice Involve an Interaction with the σ 1 Receptor. *Br. J. Pharmacol.* **2006**, *149* (8), 998–1012. <https://doi.org/10.1038/sj.bjp.0706927>.
- (187) Kurutas, E. B. The Importance of Antioxidants Which Play the Role in Cellular Response against Oxidative/Nitrosative Stress: Current State. *Nutr. J.* **2016**, *15*. <https://doi.org/10.1186/s12937-016-0186-5>.
- (188) Poutsma, M. L. The Radical Stabilization Energy of a Substituted Carbon-Centered Free Radical Depends on Both the Functionality of the Substituent and the Ordinality of the Radical. *J. Org. Chem.* **2011**, *76* (1), 270–276. <https://doi.org/10.1021/jo102097n>.
- (189) Bienert, G. P.; Schjoerring, J. K.; Jahn, T. P. Membrane Transport of Hydrogen Peroxide. *Biochim. Biophys. Acta* **2006**, *1758* (8), 994–1003. <https://doi.org/10.1016/j.bbamem.2006.02.015>.
- (190) Pellavio, G.; Rui, M.; Caliozna, L.; Martino, E.; Gastaldi, G.; Collina, S.; Laforenza, U. Regulation of Aquaporin Functional Properties Mediated by the Antioxidant Effects of Natural Compounds. *Int. J. Mol. Sci.* **2017**, *18* (12), 2665. <https://doi.org/10.3390/ijms18122665>.

- (191) Lee, C.-H.; Lü, W.; Michel, J. C.; Goehring, A.; Du, J.; Song, X.; Gouaux, E. NMDA Receptor Structures Reveal Subunit Arrangement and Pore Architecture. *Nature* **2014**, *511* (7508), 191–197. <https://doi.org/10.1038/nature13548>.
- (192) Chen, L.-H.; Zhang, H.-T.; Xu, R.-X.; Li, W.-D.; Zhao, H.; Yang, Y.; Sun, K. Interaction of Aquaporin 4 and N-Methyl-D-Aspartate NMDA Receptor 1 in Traumatic Brain Injury of Rats. *Iran. J. Basic Med. Sci.* **2018**, *21* (11), 1148–1154. <https://doi.org/10.22038/IJBMS.2018.29135.7037>.
- (193) Dvorácskó, S.; Keresztes, A.; Mollica, A.; Stefanucci, A.; Macedonio, G.; Pieretti, S.; Zádor, F.; Walter, F. R.; Deli, M. A.; Kékesi, G.; et al. Preparation of Bivalent Agonists for Targeting the Mu Opioid and Cannabinoid Receptors. *Eur. J. Med. Chem.* **2019**, *178*, 571–588. <https://doi.org/10.1016/j.ejmech.2019.05.037>.
- (194) Sheub, S. S.; Erb, S. J.; Lunzer, M. M.; Speltz, R.; Harding-Rose, C.; Akgün, E.; Simone, D. A.; Portoghese, P. S. Targeting MOR-MGluR5 Heteromers Reduces Bone Cancer Pain by Activating MOR and Inhibiting MGluR5. *Neuropharmacology* **2019**, 107690. <https://doi.org/10.1016/j.neuropharm.2019.107690>.
- (195) Meena, V. K.; Chaturvedi, S.; Sharma, R. K.; Mishra, A. K.; Hazari, P. P. Potent Acetylcholinesterase Selective and Reversible Homodimeric Agent Based on Tacrine for Theranostics. *Mol. Pharm.* **2019**, *16* (6), 2296–2308. <https://doi.org/10.1021/acs.molpharmaceut.8b01058>.
- (196) Raub, A. G.; Hwang, S.; Horikoshi, N.; Cunningham, A. D.; Rahighi, S.; Wakatsuki, S.; Mochly-Rosen, D. Small-Molecule Activators of Glucose-6-phosphate Dehydrogenase (G6PD) Bridging the Dimer Interface. *ChemMedChem* **2019**, *14* (14), 1321–1324. <https://doi.org/10.1002/cmdc.201900341>.
- (197) Halazy, S.; Perez, M.; Fourrier, C.; Pallard, I.; Pauwels, P. J.; Palmier, C.; John, G. W.; Valentin, J.-P.; Bonnafous, R.; Martinez, J. Serotonin Dimers: Application of the Bivalent Ligand Approach to the Design of New Potent and Selective 5-HT_{1B/1D} Agonists. *J. Med. Chem.* **1996**, *39* (25), 4920–4927. <https://doi.org/10.1021/jm960552l>.
- (198) Posner, R. G.; Wofsy, C.; Goldstein, B. The Kinetics of Bivalent Ligand-Bivalent Receptor Aggregation: Ring Formation and the Breakdown of the Equivalent Site Approximation. *Math. Biosci.* **1995**, *126* (2), 171–190. [https://doi.org/10.1016/0025-5564\(94\)00045-2](https://doi.org/10.1016/0025-5564(94)00045-2).
- (199) Posner, R. G.; Subramanian, K.; Goldstein, B.; Thomas, J.; Feder, T.; Holowka, D.; Baird, B. Simultaneous Cross-Linking by Two Nontriggering Bivalent Ligands Causes Synergistic Signaling of IgE Fc Epsilon RI Complexes. *J. Immunol.* **1995**, *155* (7), 3601–3609.
- (200) Bosch, J. PPI Inhibitor and Stabilizer Development in Human Diseases. *Drug Discov. Today Technol.* **2017**, *24*, 3–9. <https://doi.org/10.1016/j.ddtec.2017.10.004>.
- (201) Griffin, M. D. W.; Gerrard, J. A. The Relationship between Oligomeric State and Protein Function. In *Protein Dimerization and Oligomerization in Biology*; Matthews, J. M., Ed.; Springer New York: New York, NY, 2012; Vol. 747, pp 74–90. https://doi.org/10.1007/978-1-4614-3229-6_5.
- (202) Matthews, J. M.; Sunde, M. Dimers, Oligomers, Everywhere. In *Protein Dimerization and Oligomerization in Biology*; Matthews, J. M., Ed.; Advances in Experimental Medicine and Biology; Springer New York: New York, NY, 2012; pp 1–18. https://doi.org/10.1007/978-1-4614-3229-6_1.
- (203) Louw, A. GR Dimerization and the Impact of GR Dimerization on GR Protein Stability and Half-Life. *Front. Immunol.* **2019**, *10*, 1693. <https://doi.org/10.3389/fimmu.2019.01693>.
- (204) Pawar, A. B.; Sengupta, D. Resolving the Conformational Dynamics of ErbB Growth Factor Receptor Dimers. *J. Struct. Biol.* **2019**, *207* (2), 225–233. <https://doi.org/10.1016/j.jsb.2019.05.013>.
- (205) Jagtap, S. Heck Reaction—State of the Art. *Catalysts* **2017**, *7* (9), 267. <https://doi.org/10.3390/catal7090267>.
- (206) Rossi, D.; Baraglia, A. C.; Serra, M.; Azzolina, O.; Collina, S. An Efficient Procedure Based on a MW-Assisted Horner–Wadsworth–Emmons Reaction for the Synthesis of (Z)-3,3-Trisubstituted- α,β -Unsaturated Esters. *Molecules* **2010**, *15* (9), 5928–5942. <https://doi.org/10.3390/molecules15095928>.
- (207) *Green Techniques for Organic Synthesis and Medicinal Chemistry*, Second edition.; Zhang, W., Cue, B. W., Eds.; John Wiley & Sons: Hoboken, NJ, 2018.
- (208) Ouellet, S. G.; Tuttle, J. B.; MacMillan, D. W. C. Enantioselective Organocatalytic Hydride Reduction. *J. Am. Chem. Soc.* **2005**, *127* (1), 32–33. <https://doi.org/10.1021/ja043834g>.

- (209) Shuto, Y.; Yamamura, T.; Tanaka, S.; Yoshimura, M.; Kitamura, M. Asymmetric NaBH₄ 1,4-Reduction of C3-Disubstituted 2-Propenoates Catalyzed by a Diamidine Cobalt Complex. *ChemCatChem* **2015**, *7* (10), 1547–1550. <https://doi.org/10.1002/cctc.201500260>.
- (210) Miyata, K.; Kutsuna, H.; Kawakami, S.; Kitamura, M. A Chiral Bidentate Sp²-N Ligand, Naph-DiPIM: Application to CpRu-Catalyzed Asymmetric Dehydrative C-, N-, and O-Allylation. *Angew. Chem. Int. Ed.* **2011**, *50* (20), 4649–4653. <https://doi.org/10.1002/anie.201100772>.
- (211) Nakane, S.; Yoshinaka, S.; Iwase, S.; Shuto, Y.; Bunse, P.; Wünsch, B.; Tanaka, S.; Kitamura, M. Synthesis of Fluspidine via Asymmetric NaBH₄ Reduction of Silicon Enolates of β -Keto Esters. *Tetrahedron* **2018**, *74* (38), 5069–5084. <https://doi.org/10.1016/j.tet.2018.04.005>.
- (212) Quesada-Romero, L.; Mena-Ulecia, K.; Zuñiga, M.; De-la-Torre, P.; Rossi, D.; Tiznado, W.; Collina, S.; Caballero, J. Optimal Graph-Based and Simplified Molecular Input Line Entry System-Based Descriptors for Quantitative Structure–Activity Relationship Analysis of Arylalkylaminoalcohols, Arylalkenylamines, and Arylalkylamines as Σ_1 Receptor Ligands. *J. Chemom.* **2015**, *29* (1), 13–20. <https://doi.org/10.1002/cem.2650>.
- (213) Rossi, D.; Rui, M.; Di Giacomo, M.; Schepmann, D.; Wünsch, B.; Monteleone, S.; Liedl, K. R.; Collina, S. Gaining in Pan-Affinity towards Sigma 1 and Sigma 2 Receptors. SAR Studies on Arylalkylamines. *Bioorg. Med. Chem.* **2017**, *25* (1), 11–19. <https://doi.org/10.1016/j.bmc.2016.10.005>.
- (214) Rui, M.; Rossi, D.; Marra, A.; Paolillo, M.; Schinelli, S.; Curti, D.; Tesei, A.; Cortesi, M.; Zamagni, A.; Laurini, E.; et al. Synthesis and Biological Evaluation of New Aryl-Alkyl(Alkenyl)-4-Benzylpiperidines, Novel Sigma Receptor (SR) Modulators, as Potential Anticancer-Agents. *Eur. J. Med. Chem.* **2016**, *124*, 649–665. <https://doi.org/10.1016/j.ejmech.2016.08.067>.
- (215) Rossi, D.; Marra, A.; Rui, M.; Laurini, E.; Fermeglia, M.; Pricl, S.; Schepmann, D.; Wuensch, B.; Peviani, M.; Curti, D.; et al. A Step Forward in the Sigma Enigma: A Role for Chirality in the Sigma1 Receptor–Ligand Interaction? *MedChemComm* **2015**, *6* (1), 138–146. <https://doi.org/10.1039/C4MD00349G>.
- (216) Collina, S.; Loddo, G.; Urbano, M.; Linati, L.; Callegari, A.; Ortuso, F.; Alcaro, S.; Laggner, C.; Langer, T.; Prezzavento, O.; et al. Design, Synthesis, and SAR Analysis of Novel Selective Sigma1 Ligands. *Bioorg. Med. Chem.* **2007**, *15* (2), 771–783. <https://doi.org/10.1016/j.bmc.2006.10.048>.
- (217) Rossi, D.; Urbano, M.; Pedrali, A.; Serra, M.; Zampieri, D.; Mamolo, M. G.; Laggner, C.; Zanette, C.; Florio, C.; Schepmann, D.; et al. Design, Synthesis and SAR Analysis of Novel Selective Sigma1 Ligands (Part 2). *Bioorg. Med. Chem.* **2010**, *18* (3), 1204–1212. <https://doi.org/10.1016/j.bmc.2009.12.039>.
- (218) Rossi, D.; Pedrali, A.; Urbano, M.; Gaggeri, R.; Serra, M.; Fernández, L.; Fernández, M.; Caballero, J.; Ronsisvalle, S.; Prezzavento, O.; et al. Identification of a Potent and Selective Σ_1 Receptor Agonist Potentiating NGF-Induced Neurite Outgrowth in PC12 Cells. *Bioorg. Med. Chem.* **2011**, *19* (21), 6210–6224. <https://doi.org/10.1016/j.bmc.2011.09.016>.
- (219) Urbano, M.; Collina, S.; Rossi, D.; Baraglia, A. C.; Alcaro, S.; Artese, A.; Azzolina, O. Design and Synthesis of a (N-Alkylaminoalkyl-Substituted)Arylalkenylamide Drug Discovery Library <https://www.ingentaconnect.com/content/ben/lddd/2007/00000004/00000008/art00011> (accessed Sep 30, 2019). <https://doi.org/info:doi/10.2174/157018007782794581>.
- (220) Quesada-Romero, L.; Caballero, J. Docking and Quantitative Structure–Activity Relationship of Oxadiazole Derivates as Inhibitors of GSK3 β . *Mol. Divers.* **2014**, *18* (1), 149–159. <https://doi.org/10.1007/s11030-013-9483-5>.
- (221) Mena-Ulecia, K.; Tiznado, W.; Caballero, J. Study of the Differential Activity of Thrombin Inhibitors Using Docking, QSAR, Molecular Dynamics, and MM-GBSA. *PLOS ONE* **2015**, *10* (11), e0142774. <https://doi.org/10.1371/journal.pone.0142774>.

Appendix

Paper 1

Sigma Receptors as New Target for Multiple Sclerosis

MARTA RUI, GIACOMO ROSSINO, DANIELA ROSSI AND SIMONA COLLINA*

University of Pavia, Department of Drug Sciences, Via Taramelli 12, Pavia, 27100, Italy

*E-mail: simona.collina@unipv.it

12.1 Introduction

During recent years, new advances in genomics and proteomics have led to the identification of new pharmacological targets, offering new opportunities to discover drugs that could cure several multifactorial pathologies, such as multiple sclerosis (MS), a widespread disease associated with genetic, environmental and sociocultural factors.^{1,2} Indeed, not only may specific genetic variations increase the risk to manifest the pathology (see Chapter 2),³ but also the exposure to infectious agents (*e.g.* human herpes viruses) and to smoking and stress (Figure 12.1).^{4,5}

Accumulating evidence suggests that neurodegeneration, together with immune system abnormalities, represent leading events in the exacerbation of the disease.^{6,7} Oxidative stress, mitochondrial alterations and oligodendrocyte degeneration constitute triggering factors to promote dysfunctions within the central nervous system (CNS).⁷ The main pathophysiological features of MS are represented by the axon demyelination process, inflammation, occurring after the T cells attack the myelin sheaths, and breaching of the blood–brain barrier (BBB) that becomes permeable to T cells (Figure

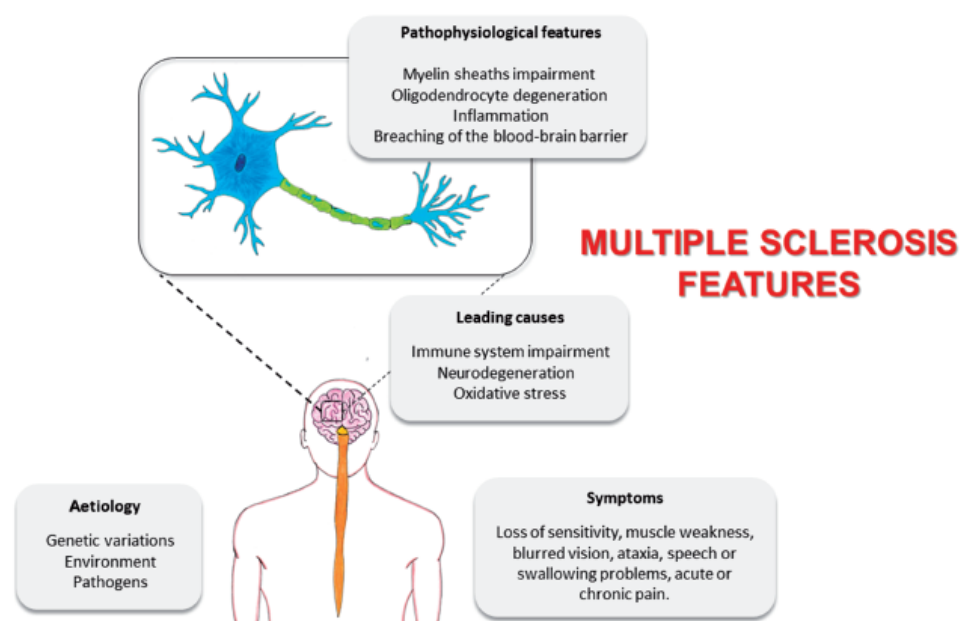


Figure 12.1 Multiple sclerosis features.

12.1).^{8,9} The pathological signs of MS depend on the locations of the lesions within the CNS. Loss of sensitivity, muscle weakness, blurred vision, ataxia, speech or swallowing problems, visual disturbances, fatigue, acute or chronic pain, and bladder and bowel difficulties are some of the main and debilitating MS clinical manifestations (Figure 12.1).³

To date, only few drugs that are able to delay the devastating outcome are available and an effective cure for MS is still missing. Accordingly, there is an urgent need to identify novel and potent remedies suitable to eradicate this debilitating disorder.¹⁰⁻¹⁴ Many efforts have been spent studying the molecular basis underlying this complex disease. The discovery of novel molecular targets and their signalling cascades may open the door to innovative therapeutic strategies. Among the eligible targets, sigma 1 receptor (S1R) has recently attracted the interest of scientists engaged in MS study, in virtue of its involvement in several neurodegenerative phenomena.⁷

12.2 Sigma 1 Receptor

In the late 1970s, sigma receptors (SRs) were identified as an opioid receptor subtype for their capability to interact with the benzomorphan analogue (\pm)-SKF-10,047.¹⁵ Nevertheless, this classification was an erroneous assumption, since the opioid antagonists – naloxone and naltrexone – had no activity towards SRs.¹⁶⁻¹⁸ Subsequently, SRs were proposed as the binding site of phencyclidine, located on the ionic channel associated with the *N*-methyl-D-aspartate (NMDA) receptor. Also in this case the hypothesis was rejected.¹⁹

Despite the SRs discovery pathway presenting several contradictions and wrong assumptions, the advances in biological and pharmacological fields eventually culminated in defining SRs as an orphan receptor family, divided into two receptor subtypes, S1R and S2R.^{20,21} They display a different tissue distribution and a distinct physiological and pharmacological profile.²² Throughout this chapter, the state-of-the-art knowledge about S1R and its modulators will be disclosed, to offer an overview of S1R involvement in neurodegeneration, and how its ligands may be beneficial in counteracting MS.

The gene encoding S1R has been cloned from several species, including humans, rats and mice, and it expresses an integral membrane protein composed of 223 amino acids (homologous only to yeast sterol isomerases), with a molecular weight of 25.3 kDa.^{23–26} The isolated S1R gene is 7 kbp long, localized on 13p band of human chromosome 9, which is a region related to psychiatric disorders.^{23–25,27,28} In recent decades, several possible structures of S1R have been postulated. In detail, at the beginning the analysis of the amino acid sequence of S1R suggested a single trans-membrane segment.^{23,24,27} Subsequently, three hydrophobic domains have been proposed: two trans-membrane-spanning domains connected by a loop, and a third one protruding from the inner face of the membrane.^{29,30} Despite numerous attempts to elucidate the binding site structure, advanced proposals on this crucial element did not match up. Regarding this aspect, the breakthrough took place in 2016, when the three-dimensional structure of S1R was published (co-crystallized with PD144418 and 4-IBP, PDB ID: 5HK1 and 5HK2, respectively). The crystal presents a trimeric architecture, with a single trans-membrane helix and a cytosolic domain for each protomer. The ligand binding pocket, placed in the β -barrel region of the cytosolic domain, consists mainly of hydrophobic residues. The so-obtained crystal structure possesses a high degree of similarity with the previous receptor models, with the exception of the single trans-membrane domain, which is a structural motif in disagreement with the constructs reported in antecedent studies.³¹

At the subcellular level, S1R is localized at the endoplasmic reticulum/mitochondria interface, in a region called the mitochondria-associated endoplasmic reticulum (ER) membrane (MAM) and in 2007, its chaperone behaviour was clarified by Hayashi *et al.*³² In detail, under resting conditions, S1R is in a dormant state, forming a complex with another chaperone, the glucose-regulated protein (BiP) whereas, under stressful conditions or in the case of pharmacological manipulations, S1R can translocate from the MAM to other cellular compartments, regulating the activity of other receptors, enzymes and ionic channels.³³ Moreover, it plays a pivotal role in ensuring the cell's survival, regulating different signal cascades: (1) Ca^{2+} homeostasis control, by chaperoning the inositol triphosphate receptor (IP3-R); (2) increase of antioxidant and anti-stress protein production, by ensuring the correct transmission of ER stress into the nucleus, through the modulation of inositol requiring enzyme 1 (IRE1); (3) decrease of reactive oxygen species (ROS) formation, by promoting the nuclear factor (erythroid-derived 2)-like-2 factor (Nrf2) signalling.³⁴

An interesting theory developed in the last decade concerns the ability of S1R to generate both homodimers and higher order oligomers. The first study, aimed at analysing this structural aspect, was published by Ramachandran *et al.*, who showed how the S1R radiolabelled ligand, [³H]-(+)-pentazocine, binds to the molecular target with a molar ratio of 1:2.³⁵ An explanation of this phenomenon, according to which a molecule interacts with a single receptor subunit, can be found in the putative asymmetric dimerization between two S1R species, endowed with different molecular weights (26 kDa and 23 kDa).³⁶ More recently, fluorescence resonance energy transfer (FRET) spectrometric analyses of S1R constructs, containing monomeric green fluorescent protein 2 (GFP2) and yellow fluorescent protein (YFP) C-terminal fusions, have revealed the presence of higher monomers, dimers and oligomers.³⁷ Lastly, the already mentioned trimeric form of the crystal obtained in 2016 confirmed the ability of S1R to form oligomers, although the mechanism of formation and the biological function of such forms are still unclear. Mechanistic models suggest that these structural changes seem strictly related to the ligands interacting with S1R. In particular, agonists stabilize S1R monomers and dimers that act as chaperones, whereas antagonists bind to higher oligomer complexes, maintaining them in repository forms.^{33,37-39}

Macroscopically, S1R is ubiquitously expressed (liver, kidney, heart), but above all it is found in the CNS tissues (spinal cord, pons, cerebellum, hippocampus, hypothalamus, midbrain, cerebral cortex and pineal gland) and therefore is considered a potential therapeutic target for treating neurodegenerative pathologies.⁴⁰⁻⁴³

12.2.1 Sigma 1 Receptor and MS

From the evidence reported so far, it emerges that S1R could be a viable and innovative target to treat MS, in virtue of its involvement in neurodegeneration, a condition occurring at the onset of MS in some patients.⁷ This molecular target plays a pivotal role in regulating synaptogenesis and myelination, as well as in controlling cellular homeostasis *via* different mechanisms, such as microglial activation, maintenance of mitochondrial integrity and regulation of oxidative stress.⁴⁴⁻⁴⁸

In this section, we will examine the numerous functions that this protein mediates in neuronal cells, along with the neuroprotective effects that can be obtained by regulating S1R and its therapeutic potential in the treatment of MS (Figure 12.2).

12.2.1.1 Calcium Regulation

A microscopic condition, often associated with both chronic neurodegenerative diseases and acute CNS damages, involves an alteration of the intracellular Ca²⁺ levels. Several molecular cascades take part in restoring the cellular physiological condition, and S1R is one of the main actors in this

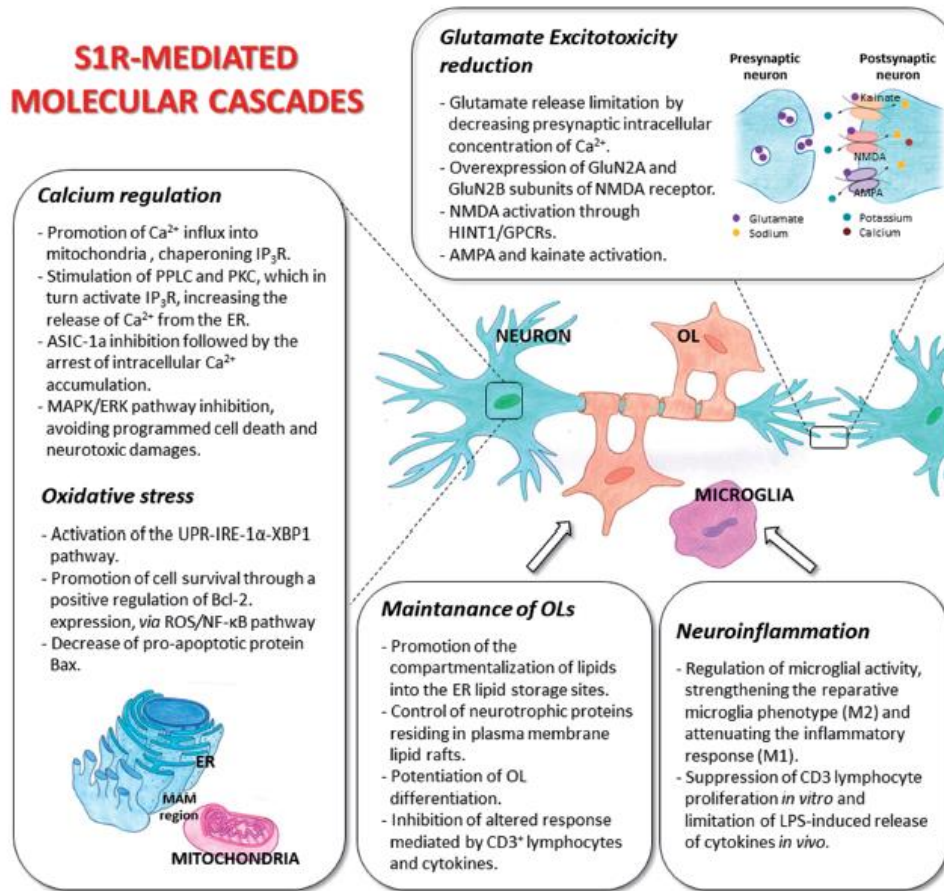


Figure 12.2 S1R-mediated molecular cascades.

sophisticated homeostasis control, avoiding pro-apoptotic phenomena.⁴⁹ As previously mentioned, S1R forms a quiescent complex with BiP and this structure is Ca^{2+} -dependent. Ca^{2+} depletion or decrease in glucose levels, as well as S1R agonism promote the complex dissociation and thus, the activation of S1R chaperonic activity.³² The inositol 1,4,5-triphosphate receptor type 3 (IP_3R) is a client protein of S1R chaperone and it regulates the Ca^{2+} influx into mitochondria for stimulating adenosine triphosphate (ATP) production through Krebs' cycle activation.^{50,51} Another mechanism overcoming the low level of Ca^{2+} takes advantages from the modulation of phospholipase C and protein kinase C. In detail, their S1R-mediated stimulation activates the IP_3R channels, increasing the level of IP_3 in the cytoplasm and the release of Ca^{2+} from the ER.⁵²⁻⁵⁴

A cytoprotective effect guaranteed by S1R provides the acid-sensing ion channel-1a inhibition, arresting intracellular Ca^{2+} accumulation. Specifically, this neuronal Na^+ channel, activated by fluctuation of extracellular H^+ levels, is highly distributed in the central and peripheral nervous system of mammals and is selectively permeable to Ca^{2+} . High levels of intracellular

Ca²⁺ cause membrane depolarization and increase Ca²⁺ influx, activating the mitochondrial permeability transition pore (MPTP). Altogether this cascade provides a sequence of toxic events that culminate in ischaemic neuronal cell death.^{55,56}

The ability of S1R to inhibit the MAPK/ERK pathway is another effective route to regulate the Ca²⁺-associated downstream signalling cascades, which may trigger programmed cell death and neurotoxic damages.⁵⁷

12.2.1.2 Glutamate Excitotoxicity Reduction

Excitotoxicity is a pathological condition in which high levels of glutamate over-activate NMDA receptors, causing high levels of Ca²⁺ to enter the cell, which in turn stimulate various enzymes involved in different mechanisms of programmed cell death. Excitotoxicity occurs in various neurodegenerative pathologies, and it has been correlated with S1R in virtue of its ability to modulate glutamate receptors.⁵⁸ However, the underlying mechanisms are still unclear and seem to be numerous. For example, in a study exploiting a chronic restraint stress model of depression, it has been evidenced that S1R stimulation promotes glutamate release by increasing presynaptic intracellular concentration of Ca²⁺.⁵⁹ This mechanism could be reverted by S1R agonists, which decrease Ca²⁺ entry through presynaptic voltage-dependent Ca²⁺ channels and suppress PKC molecular pathways, causing a limited glutamate release from nerve terminals in the rat cerebral cortex.⁶⁰ This effect can be achieved by preventing small conductance Ca²⁺-activated K⁺ (SK) channel opening, which are strictly related to NMDA activation.⁶¹

NMDA receptors can be regulated by S1R both directly, by binding to specific subunits of the NMDA receptor, and indirectly, modulating the interaction of other proteins with NMDA receptors.⁶²⁻⁶⁴ In fact, S1R antagonists can inhibit the interaction between S1R and the cytosolic C-terminal region of the NMDA receptor GluN1 subunit in recombinant cells, while activation of S1R can stimulate the binding to GluN2 subunit. When this occurs, NMDA receptors are translocated to the cell surface, thus increasing their availability at the plasma membrane.⁶⁵ S1R agonists also increase the overexpression of GluN2A and GluN2B subunits of the NMDA receptor, influencing synaptic plasticity.^{66,67} In another study, conducted on an ischaemia/reperfusion vascular dementia model, S1R agonists were found to be able to increase brain-derived neurotrophic factor (BDNF) levels, by modulating the GluN2A subunit.⁶⁸

Concerning the modulation of NMDA receptors, *via* interaction with other proteins, it has recently been found that S1R agonists promote interaction between histidine triad nucleotide binding protein 1 (HINT1) and G-protein coupled receptors (GPCRs), which eventually improve GPCR-NMDA interaction.⁶⁹ Lastly, recent studies demonstrated that S1R agonism can modulate other glutamate receptors, besides NMDA receptors, such as kainate and alpha-amino-3-hydroxy-5-methyl-5 isoxazole propionic (AMPA) receptors to exert neuroprotection.^{70,71}

Overall, these results suggest that S1R can exert neuroprotection by modulation of glutamatergic neurotransmission, through numerous mechanisms which can be very complex and are not always completely understood.

12.2.1.3 Oxidative and ER Stresses and Mitochondrial Dysfunction

ROS are natural by-products of oxygen metabolism, promoting hormetic responses. In detail, low concentrations of ROS possess beneficial effects in maintaining cellular homeostasis, whereas a disequilibrium between their production and detoxification systems may lead to oxidative damage.⁷² Numerous altered conditions contribute in generating ROS, such as mitochondrial dysfunction and sustained neurotransmission, and they may cause severe side effects, damaging lipids, nucleic acids and proteins.^{73,74} The brain is particularly vulnerable to oxidative stress, since it has high oxygen demand, relatively low levels of the antioxidant glutathione and is enriched in polyunsaturated fatty acids that are substrates for lipid peroxidation.⁷⁵ Accordingly, oxidative stress has been extensively associated with several CNS-related diseases. Moreover, under ER stress, unfolded or misfolded proteins can accumulate within the ER lumen and promote the protective unfolded protein response (UPR), which involves three molecular cascades: (1) activating transcription factor 6 (ATF6); (2) protein kinase RNA like ER kinase (PERK); and (3) inositol requiring enzyme 1 alpha (IRE1 α).^{76,77} Multiple studies show that S1R agonists interfere with ROS production and abnormal protein accumulation, modulating the UPR. More specifically, S1R attenuates the activation of PERK and ATF6, increasing cell survival, whereas it stabilizes IRE-1 α .^{78,79} This last enzyme oligomerizes to activate its cytoplasmic kinase and endoribonuclease domains, which initiate the splicing of the ER stress linked transcriptional factor x-box binding protein 1 (XBP1) mRNA, which encodes for transcription factors necessary for the expression of specific genes to weaken ER stress.^{80,81} The IRE-1 α -XBP1 pathway is involved in several neurodegenerative disorders, and high levels of spliced XBP1 mRNA were also identified in MS demyelinated lesions.⁸²⁻⁸⁵

Mitochondrial abnormalities (*i.e.* mitochondrial DNA mutations, bioenergetic and dynamic impairments) are often associated with neurodegeneration, and accumulating evidence suggests S1R as an effective protector against mitochondrial damage.⁸⁶⁻⁸⁸ S1R is able to influence the expression of both pro- and anti-apoptotic signals targeting mitochondria. In detail, S1R agonists promote cell survival by increasing the expression of the anti-apoptotic protein Bcl-2 – *via* the ROS/NF- κ B pathway – as well as by decreasing the activity of the pro-apoptotic protein Bax.⁸⁹⁻⁹¹

12.2.1.4 Oligodendrocyte Degeneration

Oligodendrocytes (OLs) are non-neuronal cells involved in myelin formation and regulation of myelin protein shunting. Glycosphingolipids are the main fatty substances surrounding axons and they are responsible for nerve

conduction control, as well as for the terminal OL differentiation. Accordingly, an alteration of this refined framework may lead to irreversible CNS damage, causing neurodegeneration.⁹² The role played by S1R in controlling the intracellular lipid flow and the membrane reconstitution in lipid rafts is still clouded, although the ability of S1R to influence the compartmentalization of lipids into the ER lipid storage sites may provide a concrete explanation.⁴⁴⁻⁵¹ Moreover, the up-regulation of S1R affects the function of proteins residing in plasma membrane lipid rafts, such as trophic factor receptors. In this context, it has been highlighted that S1R promotes neurite sprouting by amplifying the activity of the neurotrophin NGF and this synergic effect is a consequence of lipid constituent changes at the plasma membrane lipid rafts. In addition, overexpression of S1R potentiates OL differentiation, while S1R knockdown avoids OL maturation.⁹³ Recently, it has been evidenced that the destruction of OLs and the axonal demyelination may be limited, exploiting the inhibitory aptitude of S1R toward the altered response of CD3⁺ lymphocytes and cytokines (*i.e.* IL-1, IL-6, TNF- α). Indeed, a single injection of S1R ligand in experimental autoimmune encephalomyelitis susceptible mice (animal model for MS) impedes mononuclear cell accumulation and demyelination in brain and spinal cord, reducing the clinical progression of the disease.⁹⁴

12.2.1.5 Neuroinflammation

Microglia are macrophage-derived cells located in the CNS, where they play a key role as mediators of neuroinflammation. They are grouped into two subcategories: M1 microglia, with pro-inflammatory properties involved in CNS damage, and M2 microglia, which are anti-inflammatory and stimulate neuronal regrowth and repair.^{95,96} Accumulating evidence suggests that S1R can regulate microglial activity by strengthening the reparative microglia phenotype (M2), while it attenuates the inflammatory response (M1) and hence promotes neuroprotection. In particular, during a recent study neurotoxic dosing with methamphetamine was observed to activate M1 microglia responses in the mouse striatum, while pre-treatment with S1R ligand prevented it. This process involves variations of the levels of pan-macrophage markers, cluster of differentiation 68 (CD68) and ionized calcium binding adapter molecule 1 (IBA-1).⁹⁷ In another study, conducted on lipopolysaccharide (LPS)-stimulated murine microglial BV2 cells, the authors observed that the S1R agonists suppress M1 microglial activation, also reducing the levels of pro-inflammatory cytokines, such as interleukin (IL)-1 β , tumour necrosis factor- α (TNF- α), and inducible NOS.⁹⁸ Similarly, other S1R agonists have shown the ability to prevent microglial activation and inflammatory cytokines release in response to a number of microglial activators such as LPS, ATP, uridine triphosphate and monocyte chemoattractant protein-1.⁹⁹ PRE-084 was deeply investigated in different studies that confirmed its ability to counteract neuroinflammation: in an *in vivo* model of traumatic brain injury, PRE-084 decreases IBA-1 expression following controlled cortical impact, reduces lesion volume and improves behaviour in mice;¹⁰⁰ in a

mouse model of amyotrophic lateral sclerosis (ALS) it also reduces counts of IBA-1 positive microglial cells;¹⁰¹ and in another study on animals with motor neuron disease, PRE-084 increases the levels of pan-macrophage marker CD68 and CD206, which is associated with M2 microglial responses.⁴¹

Another important pathological scenario in which S1R intervenes is leukocyte extravasation into the brain occurring upon disruption of the BBB by injury, a condition that exacerbates neuroinflammation. Being expressed in lymphocytes, S1R can suppress CD3 lymphocyte proliferation *in vitro* and LPS-induced release of cytokines *in vivo*.^{102,103} This was confirmed by Oxombre *et al.* using an S1R ligand in a mouse autoimmune encephalitis model with peripheral leukocyte infiltration into the brain, demyelination and axonal loss. The ligand considerably reduced the clinical signs of encephalitis by preventing mononuclear cell accumulation and demyelination in the CNS, while also increasing the proportion of B-cell subsets and regulatory T-cells.⁹⁴

Overall, these findings demonstrate the involvement of S1R in neuroinflammation and its potential to counteract this pathological condition.

12.2.2 Sigma 1 Receptor and Its Modulators

Over time, the interest in S1R has increased. It represents an innovative target with a wide spectrum of therapeutic uses, and thus design and synthesis of S1R modulators have gained enormous importance.²²

One critical aspect is represented by the lack of endogenous ligand. Neurosteroids (*i.e.* dehydroepiandrosterone (DHEA), pregnenolone, and progesterone) have been suggested as putative endogenous S1R ligands, despite their low binding affinities (0.3–10 μM).^{104,105} Their compound structures are shown in Figure 12.3.

The long road to discovering a novel S1R modulator begins with the comprehension of the agonist/antagonist behaviour. Defining an S1R profile contributes to depicting the possible pharmacological role of an S1R modulator. A biological test has been set up that provides the evaluation of nerve growth factor (NGF)-induced neurite outgrowth in PC-12 cells (pheochromocytoma of the rat adrenal medulla), a widely accepted neuronal differentiation model. S1R agonists promote neurite elongation, demonstrating their neuroplastic effects. By contrast, S1R antagonists have no effect on this cell line, and several data show their involvement in the treatment of neuropathic pain and cancer conditions.¹⁰⁶ Recently, three drugs in clinical development support this outstanding evidence: (1) ANAVEX 2-73 (Figure 12.3), patented by Anavex Life Sciences Corp, is undergoing Phase III clinical trials for the treatment of Alzheimer's disease (AD);¹⁰⁷ (2) AVP-923 (Dextromethorphan-Quinidine) (Figure 12.3), patented by Concert Pharmaceuticals Inc., is undergoing Phase II clinical trials to alleviate agitation in patients with AD;¹⁰⁸ (3) S1A or MR309/E-52862 (Figure 12.3), patented by Esteve, is undergoing Phase II clinical trials for treating neuropathic pain, post-operative pain and opioid analgesia enhancement.¹⁰⁹

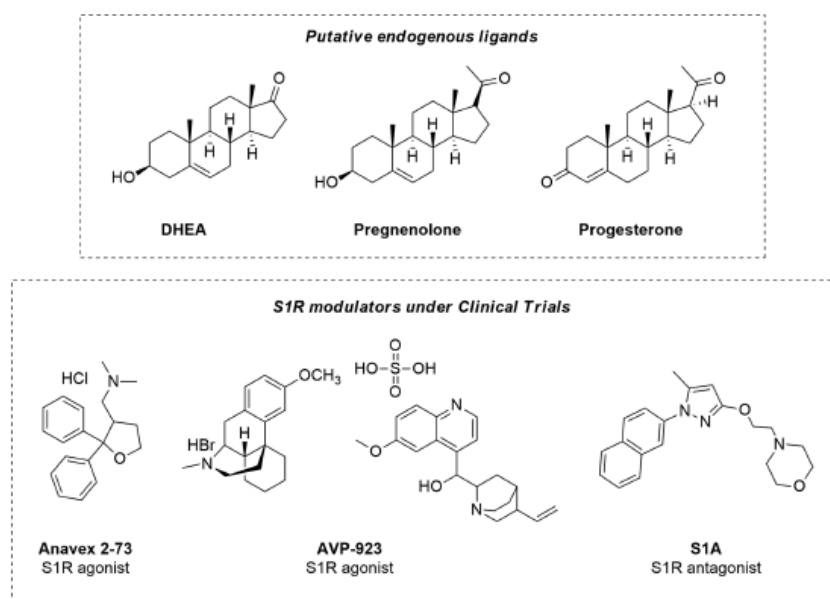


Figure 12.3 Structures of S1R endogenous ligands and S1R modulators under clinical trials.

In this chapter we will focus on the S1R agonists, as potential neuroprotective agents able to counteract MS.⁷

The growing interest in the S1R/neurodegenerative diseases correlation required the identification of molecules able to selectively bind this molecular target. For years this aspect has been a challenge, since several research groups have faced the lack of two fundamental milestones: knowledge of endogenous S1R ligands and the three-dimensional receptor structure. As a result, ligand-based drug design approaches were adopted to identify new molecules targeting S1R. The pioneer was Glennon, who described the first pharmacophore model, in which an ionizable amine site and two hydrophobic domains are essential structural elements.¹¹⁰ Later on, Gund *et al.* introduced an electronegative atom – an oxygen or a sulfur – as an additional pharmacophore element to the previous model.¹¹¹ Nevertheless, in 2005, Laggner *et al.* demonstrated how this electronegative atom is a negligible element and is not required to increase the affinity of a ligand with S1R.¹¹²

Over the years, numerous S1R modulators have been designed, taking into account these structural common features and, the resulted compounds can be grouped into six chemical classes: (1) morpholine derivatives; (2) 1,3-disubstituted guanidines; (3) piperazine-based molecules; (4) spirocycles; (5) cyclopropanes; and (6) piperidine-based compounds. The most representative molecules, belonging to the six different groups, are briefly described in this section.

12.2.2.1 Morpholine Derivatives

The main morpholine-based compound is known as PRE-084 (Figure 12.4). It was the first selective S1R ligand identified as an S1R agonist and has been employed to define the pathophysiological role played by S1R in different CNS-related disorders. Nowadays is still commonly used as an S1R agonist reference standard in *in vitro* and *in vivo* assessments of new compound.^{113,114} In 2009, Seredinin *et al.* reported the high affinity of Afobazole (Figure 12.4) – a morpholine derivative with anxiolytic and neuroprotective properties – towards S1R.¹¹⁵ This molecule is also able to interact with S2R, and in a recent study the pan-SRs affinity of Afobazole was useful to provide

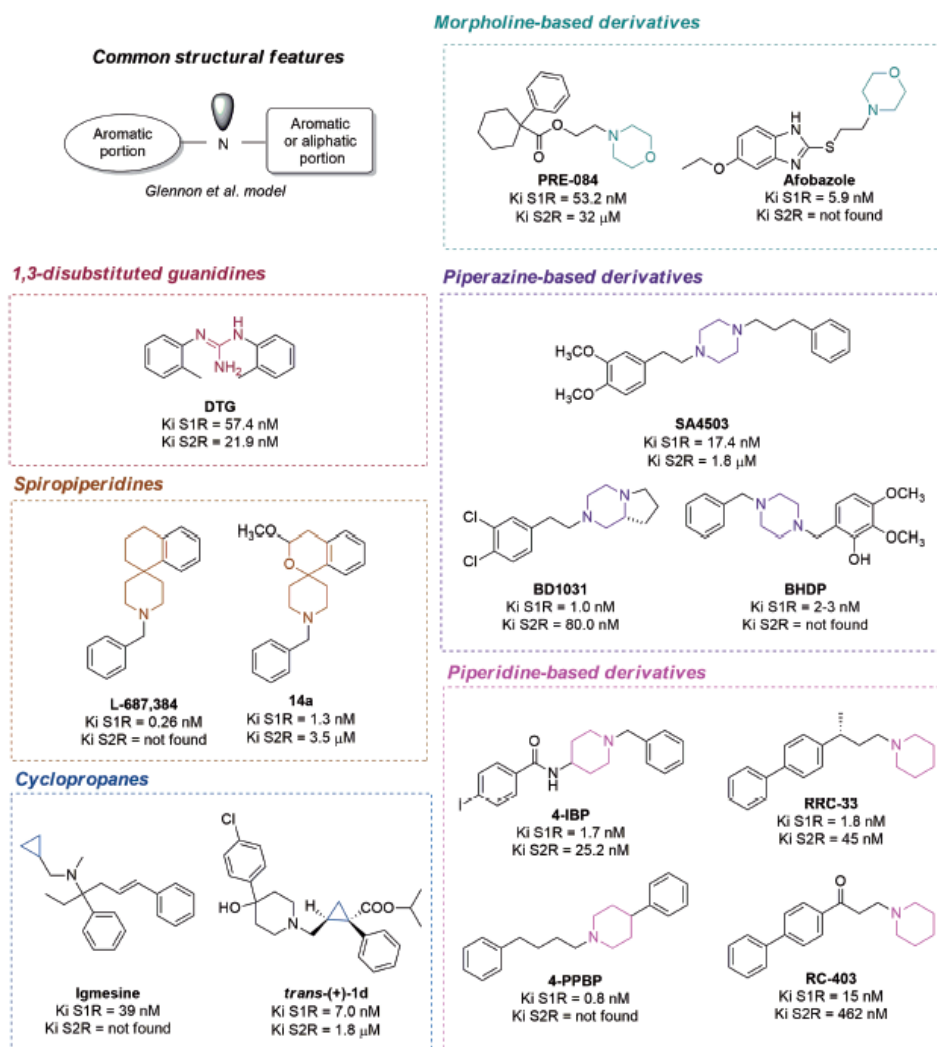


Figure 12.4 S1R agonists.

superior long-term outcomes compared with other S1R ligands in the rat middle cerebral artery occlusion (MCAO) stroke model, by enhancing glial cell survival, blocking ischaemia-induced glial cell activation, and decreasing nitrosative stress.¹¹⁶

12.2.2.2 1,3-Disubstituted Guanidines

1,3-di-*o*-tolylguanidine (DTG) (Figure 12.4) belongs to the second category of S1R agonists. It was patented by researchers at the University of Oregon. In their investigation, the authors claim that the tritiated form, [³H]-DTG, is an effective radioligand for SR binding assays.¹¹⁷ This molecule shows an equal affinity for both SRs, and thus it cannot be considered a selective S1R ligand. Nevertheless, it is a widely accepted reference molecule to perform *in vitro* evaluations, outclassing the previous non-selective radiolabelled SR ligand, (±)-[³H]-SKF 10,047. Indeed, it is still used for determining binding affinity at S2R, in the presence of non-tritiated pentazocine to mask the S1R binding site.¹¹⁸

12.2.2.3 Piperazine-based Molecules

This class of derivatives counts numerous molecules with affinity for S1R. Among them, SA4503, or Cutamesine (Figure 12.4), deserves to be mentioned. It was introduced in the pharmaceutical panorama by Matsuno *et al.*, who described in 1996 this novel S1R agonist.^{119,120} SA4503 reached a phase II clinical trial for evaluating its safety, tolerability, dose range and functional effects in patients with ischaemic stroke. Although this study failed, since no significant effects on functional end points were seen in the treated population compared to the placebo control, post-hoc analysis of subjects with severe or modest ischaemic stroke showed significant improvements. Accordingly, once patient characteristics are optimized to identify a potential responder population, further clinical evaluations will be performed.⁴⁹ The same authors reported on another arylalkylpiperazine derivative in a constrained structure: BD1031 (Figure 12.4). Their work aimed at proposing a novel method to define the S1R agonist/antagonist profile, evaluating the burst duration of red nucleus neurons in the *in vitro* turtle brain. The study revealed that S1R agonists, including BD1031, increase burst duration and produce dystonic postures after microinjection into the red nucleus, whereas antagonists promote the opposite effect.^{121,122} Another member belonging to the piperazine class, structurally related to SA4503, is BHDP (Figure 12.4), defined as an S1R agonist. In a comparative study with other S1R ligands, Klouz *et al.* showed that BHDP possesses a high affinity for S1R in liver mitochondria and rat brain membranes.¹²³ Moreover, the ability of BHDP to prevent hypoxia-induced ATP depletion in cultured astrocytes suggests that this molecule is a potential cytoprotective agent.¹²⁴

12.2.2.4 Spirocycles

The potent S1R agonist L-687,384 (Figure 12.4), developed by Merck Sharp & Dohme, is characterized by a spirocycle structure.¹²⁵ In 1994, it was also evidenced that this molecule promotes a negative effect on *N*-methyl-D-aspartate (NMDA)-induced currents in cultured rat hippocampal pyramidal neurons and thus, it acts as an antagonist at the NMDA receptor-channel complex.¹²⁶ L-687,384-inspired molecules, presenting a heteroatom in the aliphatic part of the tetraline substructure, were designed and synthesized by Wuensch's group. Compound 14a (Figure 12.4), so-numbered in their work, belongs to a broad series of derivatives and shows high S1R affinity and good S1R/S2R-selectivity.¹²⁷

12.2.2.5 Cyclopropanes

Among compounds characterized by a cyclopropane moiety, igmesine is worth noting (Figure 12.4). It is a potent and selective S1R ligand, endowed with neuroprotective and antidepressant-like effects, comparable to those of fluoxetine.^{128,129} It completed Phase II clinical trials for the treatment of depression; however, it failed Phase III clinical trials.¹³⁰ Cyclopropanes, also containing a piperidine motif, are endowed with S1R-mediated neuroprotective effects, as demonstrated by Marrazzo's group. Of particular interest is *trans*-(+)-1d (so-numbered in the work) (Figure 12.4), in virtue of its excellent S1R affinity and selectivity over S2R, and the authors proposed it as a promising tool for the study of S1R.¹³¹

12.2.2.6 Piperidine-based Molecules

Piperidine-based molecules include 4-IBP (Figure 12.4), a non-selective SR modulator, which was co-crystallized with S1R.^{31,132} It has been developed as radiopharmaceutical to bind to SRs on the MCF-7 human breast carcinoma cell line. Moreover, it shows antiproliferative properties, by decreasing the migration of human cancer cells (*e.g.* glioblastoma cells) and sensitizing them to cytotoxic insults of pro-apoptotic and pro-autophagic drugs.¹³³ 4-PPBP (Figure 12.4) is another compound belonging to this group. It was discovered by Yang *et al.*, who reported the cytoprotective effect of this molecule, in virtue of its ability to control a mechanism involving the anti-apoptotic protein bcl-2.¹³⁴ Additionally, this molecule made it possible to individuate a correlation between S1R and the mitogen-activated protein kinase (MAPK) cascade in neuroprotection. Specifically, 4-PPBP promotes the activation of extracellular signal-regulated kinase (ERK1/2) – a subfamily of MAPKs – in glucose-deprived cells (ischaemic models), *via* an S1R-mediated phosphorylation mechanism.¹³⁵

Lastly, a wide series of arylalkylpiperidines with neuroprotective effects have been prepared by Collina's research team.^{136–138} Of particular interest is enantiomeric (R)-1-[3-(1,1'-biphen)-4-yl]butylpiperidine hydrochloride (named RRC33, Figure 12.4), a selective S1R agonist with an excellent S1R affinity ($K_i = 1.8$ nM) along with high selectivity over other receptors

and good *in vitro* metabolic stability. The ability of RRC-33 to promote the differentiation and the neurite elongation was verified using the rat dorsal root ganglia (DRG) experimental model. DRG neurite elongation is a well-accepted simple method to screen the neurotoxic or neuroprotective effect of a drug. The results obtained *in vitro* highlighted the positive neurotrophic role of RRC-33 on neurite outgrowth, and thus support and strengthen the hypothesis to test the effect of this compound in more complex *in vitro* models representing MS. Moreover, after systemic administration in mice, RRC-33 showed an excellent pharmacokinetic profile and CNS distribution. Taken together, these characteristics might potentially be the basis for finding effective treatments against MS. Accordingly, RRC-33 can be considered as a candidate for proof of concept *in vivo* studies in an animal model of MS.^{42,139,140} Another interesting compound is RC-403 (Figure 12.4), a dual S1R agonist/anti-acetylcholinesterase ligand with antioxidant properties, currently under investigation in *in vitro* and *in vivo* neurodegenerative models.¹⁴¹

Before concluding, well-established drugs, in clinical use for the treatment of other pathological conditions such as antitussives, antidepressants, antipsychotics, anti-AD drugs, anti-Parkinson's disease (anti-PD) drugs and some drugs of abuse, are reported to act as S1R agonists.¹⁴²⁻¹⁴⁴ The most effective molecules belonging to the diverse groups have been reported in Figure 12.5.

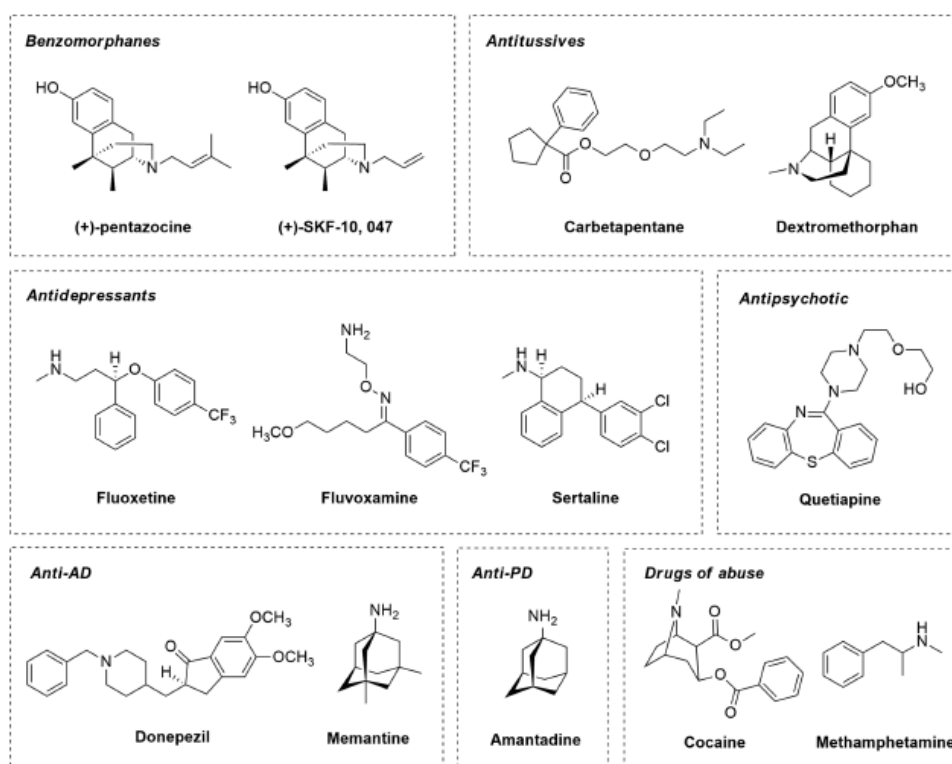


Figure 12.5 Well-established drugs for the treatment of other pathological conditions, able to interact with S1R.

Moreover, the experimental drug ANAVEX2-73 (Figure 12.3), acting as a muscarinic and S1R agonist in clinical trials for AD, is of high interest.¹⁰⁷ All these drugs may have a great relevance for understanding the potential of S1R agonists in MS. Based on the leading principle of translational medicine, which seeks to coordinate the use of new knowledge in clinical practice, clinical observations deriving from the use of such drugs in patients affected by MS may provide feedback about the applications of patient treatment with S1R agonists, confirming the scientific hypotheses of their potential efficacy.

12.3 Conclusions

Over the years S1R agonists have become part of the pharmaceutical panorama; in particular, some of them have become full members of the drug candidates group for the treatment of neurodegenerative diseases. Throughout this work, we pointed out the inestimable value of S1R and its role in modulating different molecular cascades to prevent neurodegeneration, a clinical manifestation accompanying the immune system abnormalities in MS. Although the involvement of S1R in MS deserves to be further investigated, previous data clearly suggests the great potential of S1R as an eligible target to hit for offering an alternative to conventional therapies against MS. Moreover, S1R agonists may be exploited in combinatorial therapeutic strategies to reinforce the beneficial effects of the well-known anti-MS drugs. This synergism may decrease the side effects associated with the disease-modifying drugs in clinical use and improve the probability of success in the fight against MS. Lastly, S1R agonists could be effective molecules to provide a multi-target therapy, in virtue of their ability to activate S1R, which in turn modulates the function of several client proteins.

Acknowledgement

The authors gratefully acknowledge the University of Pavia for the research grant to M.R. and MIUR for the doctoral fellowships to G.R.

References

1. R. L. Zuvich, J. L. McCauley, M. A. Pericak-Vance and J. L. Haines, *Semin. Immunol.*, 2009, **21**, 328.
2. C. C. Bernard and N. Kerlero de Rosbo, *Curr. Opin. Immunol.*, 1992, **4**, 760.
3. A. Compston and A. Coles, *Lancet*, 2008, **372**, 1502.
4. J. O. Virtanen and S. Jacobson, *CNS Neurol. Disord.: Drug Targets*, 2012, **11**, 528.
5. V. Pantazou, M. Schluemp and R. Du Pasquier, *Presse Méd.*, 2015, **44**, e113.
6. W. W. Chen, X. Zhang and W. J. Huang, *Mol. Med. Rep.*, 2016, **13**, 3391.

7. S. Collina, M. Rui, S. Stotani, E. Bignardi, D. Rossi, D. Curti, F. Giordanetto, A. Malacrida, A. Scuteri and G. Cavaletti, *Future Med. Chem.*, 2017, **9**, 2029.
8. B. F. G. Popescu, I. Pirko and C. F. Lucchinetti, *Continuum*, 2013, **19**, 901.
9. M. M. Goldenberg, *Pharm. Ther.*, 2012, **37**, 175.
10. R. Berkovich, *Neurotherapeutics*, 2013, **10**, 97.
11. B. C. Kieseier and P. A. Calabresi, *CNS Drugs*, 2012, **26**, 205.
12. W. Schrempf and T. Ziemssen, *Autoimmun. Rev.*, 2007, **6**, 469.
13. P. S. Rommer, A. Dudsek, O. Stüve and U. K. Zettl, *Clin. Exp. Immunol.*, 2014, **175**, 373.
14. S. R. Mehr and M. P. Zimmerman, *Am. Health Drug Benefits*, 2015, **8**(426), 9.
15. W. R. Martin, C. G. Eades, J. A. Thompson, R. E. Huppler and P. E. Gilbert, *J. Pharmacol. Exp. Ther.*, 1976, **197**, 517.
16. T. P. Su, *J. Pharmacol. Exp. Ther.*, 1982, **223**, 284.
17. T. Maurice and B. P. Lockhart, *Prog. Neuro-Psychopharmacol.*, 1997, **21**, 69.
18. D. B. Vaupel, *Eur. J. Pharmacol.*, 1983, **92**, 269.
19. G. Skuza, *Pol. J. Pharmacol.*, 2003, **55**, 923.
20. R. Quirion, W. D. Bowen, Y. Itzhak, J. L. Junien, J. M. Musacchio, R. B. Rothman, T. P. Su, S. W. Tam and D. P. Taylor, *Trends Pharmacol. Sci.*, 1992, **13**, 85.
21. S. B. Hellewell, A. Bruce, G. Feinstein, J. Orringer, W. Williams and W. D. Bowen, *Eur. J. Pharmacol.*, 1994, **268**, 9.
22. S. Collina, R. Gaggeri, A. Marra, A. Bassi, S. Negrinotti, F. Negri and D. Rossi, *Expert Opin. Ther. Pat.*, 2013, **23**, 597.
23. M. Hanner, F. F. Moebius, A. Flandorfer, H. G. Knaus, J. Striessnig, E. Kempner and H. Glossmann, *Proc. Natl. Acad. Sci. U. S. A.*, 1996, **93**, 8072.
24. P. Seth, Y. J. Fei, H. W. Li, W. Huang, F. H. Leibach and V. Ganapathy, *J. Neurochem.*, 1998, **70**, 922.
25. P. D. Prasad, Y. J. Fei, H. W. Li, W. Huang, F. H. Leibach and V. Ganapathy, *J. Neurochem.*, 1998, **70**, 443.
26. J. M. Walker, W. D. Bowen, F. O. Walker, R. R. Matsumoto, B. De Costa and K. C. Rice, *Pharmacol. Rev.*, 1990, **42**, 355.
27. R. Kekuda, P. D. Prasad, Y. J. Fei, F. H. Leibach and V. Ganapathy, *Biochem. Biophys. Res. Commun.*, 1996, **229**, 553.
28. J. Mei and G. W. Pasternak, *Biochem. Pharmacol.*, 2001, **62**, 349.
29. E. Laurini, V. D. Col, M. G. Mamolo, D. Zampieri, P. Posocco, M. Fermeglia, L. Vio and S. Pricl, *Acs Med. Chem. Lett.*, 2011, **2**, 834.
30. J. L. Ortega-Roldan, F. Ossa, N. T. Amin and J. R. Schnell, *FEBS Lett.*, 2016, **589**, 659.
31. H. R. Schmidt, S. Zheng, E. Gurpinar, A. Koehl, A. Manglik and A. C. Kruse, *Nature*, 2016, **532**, 527.
32. T. Hayashi and T. P. Su, *Cell*, 2007, **131**, 596.
33. U. Chu and A. E. Ruoho, *Mol. Pharmacol.*, 2016, **89**, 142.
34. T. P. Su, T. C. Su, Y. Nakamura and S. Y. Tsai, *Trends Pharmacol. Sci.*, 2016, **37**, 262.

35. S. Ramachandran, H. Lu, U. Prabhu and A. E. Ruoho, *Protein Expression Purif.*, 2007, **51**, 283.
36. U. B. Chu, S. Ramachandran, A. R. Hajipour and A. E. Ruoho, *Biochem. J.*, 2013, **52**, 859.
37. A. K. Mishra, T. Mavlyutov, D. R. Singh, G. Biener, J. Yang, J. A. Oliver, A. E. Ruoho and V. Raicu, *Biochem. J.*, 2015, **466**, 263.
38. K. A. Gromek, F. P. Suchy, H. R. Meddaugh, R. L. Wrobel, L. M. LaPointe, U. B. Chu, J. G. Primm, A. E. Ruoho, A. Senes and B. G. Fox, *J. Biol. Chem.*, 2014, **289**, 20333.
39. A. Tesei, M. Cortesi, A. Zamagni, C. Arienti, S. Pignatta, M. Zanoni, M. Paolillo, D. Curti, M. Rui, D. Rossi and S. Collina, *Front. Pharmacol.*, 2018, 711.
40. T. Maurice and T. P. Su, *Pharmacol. Ther.*, 2009, **124**, 195.
41. M. Peviani, E. Salvaneschi, L. Bontempi, A. Petese, A. Manzo, D. Rossi, M. Salmona, S. Collina, P. Bigini and D. Curti, *Neurobiol. Dis.*, 2014, **62**, 218.
42. A. Marra, D. Rossi, L. Pignataro, C. Bigogno, A. Canta, N. Oggioni, A. Malacrida, M. Corbo, G. Cavaletti, M. Peviani, D. Curti, G. Dondio and S. Collina, *Future Med. Chem.*, 2016, **8**, 287.
43. S. Kourrich, T. P. Su, M. Fujimoto and A. Bonci, *Trends Neurosci.*, 2012, **35**, 762.
44. T. Hayashi and T. P. Su, *Proc. Natl. Acad. Sci. U. S. A.*, 2004, **101**, 14949.
45. A. A. Hall, Y. Herrera, C. T. Ajmo, J. Cuevas and K. R. Pennypacker, *Glia*, 2009, **57**, 744.
46. L. Nguyen, N. Kaushal, M. J. Robson and R. R. Matsumoto, *Eur. J. Pharmacol.*, 2014, **743**, 42.
47. A. Pal, D. Fontanilla, A. Gopalakrishnan, Y. K. Chae, J. L. Markley and A. E. Ruoho, *Eur. J. Pharmacol.*, 2012, **682**, 12.
48. J. Wang, A. Shanmugam, S. Markand, E. Zorrilla, V. Ganapathy and S. B. Smith, *Free Radicals Biol. Med.*, 2015, **86**, 25.
49. L. Nguyen, B. P. Lucke-Wolds, S. Mookerjee, N. Kaushal and R. R. Matsumoto, *Adv. Exp. Med. Biol.*, 2017, **964**, 133.
50. T. Hayashi, R. Rizzuto, G. Hajnoczky and T. P. Su, *Trends Cell Biol.*, 2009, **19**, 81.
51. T. Hayashi and T. P. Su, *J. Pharmacol. Exp. Ther.*, 2003, **306**, 726.
52. H. Ivanova, T. Vervliet, L. Missiaen, J. B. Parys, H. De Smedt and G. Bultynck, *Biochim. Biophys. Acta*, 2014, **1843**, 2164.
53. F. P. Monnet, M. P. Morin-Surun, J. Leger and L. Combettes, *J. Pharmacol. Exp. Ther.*, 2003, **307**, 705.
54. K. T. Tchedre, R. Q. Huang, A. Dibas, R. R. Krishnamoorthy, G. H. Dillon and T. Yorio, *Invest. Ophthalmol. Visual Sci.*, 2008, **49**, 4993.
55. T. W. Sherwood, E. N. Frey and C. C. Askwith, *Am. J. Physiol.: Cell Physiol.*, 2012, **303**, C699.
56. Y. Herrera, C. Katnik, J. D. Rodriguez, A. A. Hall, A. Willing, K. R. Pennypacker and J. Cuevas, *J. Pharmacol. Exp. Ther.*, 2008, **327**, 491.
57. T. Tuerxun, T. Numakawa, N. Adachi, E. Kumamaru, H. Kitazawa, M. Kudo and H. Kunugi, *Neurosci. Lett.*, 2010, **469**, 303.

58. A. L. Sheldon and M. B. Robinson, *Neurochem. Int.*, 2007, **51**, 333.
59. Y. Fu, S. Yu, X. Guo, X. Li, T. Li, H. Li and Y. Dong, *Biochim. Biophys. Acta*, 2012, **1823**, 826.
60. C. W. Lu, T. Y. Lin and S. J. Wang, *Neurochem. Int.*, 2010, **57**, 168.
61. C. W. Lu, T. Y. Lin, C. C. Wang and S. J. Wang, *J. Pharmacol. Exp. Ther.*, 2012, **341**, 532.
62. D. Balasuriya, A. P. Stewart and J. M. Edwardson, *J. Neurosci.*, 2013, **33**, 18219.
63. M. Pabba and E. Sibille, *Molecular Neuropsychiatry*, 2015, **1**, 47.
64. M. Martina, M. E. Turcotte, S. Halman and R. Bergeron, *J. Physiol.*, 2007, **578**, 143.
65. M. Pabba, A. Y. Wong, N. Ahlskog, E. Hristova, D. Biscaro, W. Nassrallah, J. K. Ngsee, M. Snyder, J. C. Beique and R. Bergeron, *J. Neurosci.*, 2014, **34**, 11325.
66. Y. Lin, V. A. Skeberdis, A. Francesconi, M. V. Bennett and R. S. Zukin, *J. Neurosci.*, 2004, **24**, 10138.
67. O. A. Shipton and O. Paulsen, *Philos. Trans. R. Soc., B*, 2014, **369**, 20130163.
68. Q. Xu, X. F. Ji, T. Y. Chi, P. Liu, G. Jin, S. L. Gu and L. B. Zou, *Psychopharmacology*, 2015, **232**, 1779.
69. M. Rodriguez-Munoz, E. Cortés-Montero, A. Pozo-Rodrigálvarez, P. Sánchez-Blázquez and J. Garzón-Niño, *Oncotarget*, 2015, **6**, 35458.
70. H. C. Kim, W. K. Jhoo, W. K. Kim, E. J. Shin, M. A. Cheon, C. Y. Shin and K. H. Ko, *Life Sci.*, 2001, **69**, 915.
71. E. J. Shin, S. Y. Nah, W. K. Kim, K. H. Ko, W. K. Jhoo, Y. K. Lim, J. Y. Cha, C. F. Chen and H. C. Kim, *Br. J. Pharmacol.*, 2005, **144**, 908.
72. P. D. Ray, B. W. Huang and Y. Tsuji, *Cell Signaling*, 2012, **24**, 981.
73. S. Gandhi and A. Y. Abramov, *Oxid. Med. Cell. Longevity*, 2012, 428010.
74. G. H. Kim, J. E. Kim, S. J. Rhie and S. Yoon, *Exp. Neurobiol.*, 2015, **24**, 325.
75. R. Dringen and J. Hirrlinger, *Biol. Chem.*, 2003, **384**, 505.
76. H. Yoshida, *FEBS J.*, 2007, **274**, 630.
77. Y. Kimata and K. Kohno, *Curr. Opin. Cell Biol.*, 2011, **23**, 135.
78. T. Mori, T. Hayashi, E. Hayashi and T. P. Su, *PLoS One*, 2013, **8**, e76941.
79. T. Hayashi, *Psychiatry Clin. Neurosci.*, 2015, **69**, 179.
80. J. Dunys, E. Duplan and F. Checler, *Mol. Neurodegener.*, 2014, **9**, 35.
81. D. Jiang, M. Niwa and A. C. Koong, *Semin. Cancer Biol.*, 2015, **33**, 48.
82. C. Hetz, P. Thielen, S. Matus, M. Nassif, F. Court, R. Kiffin, G. Martinez, A. M. Cuervo, R. H. Brown and L. H. Glimcher, *Genes Dev.*, 2009, **23**, 2294.
83. R. L. Vidal, A. Figueroa, F. A. Court, P. Thielen, C. Molina, C. Wirth, B. Caballero, R. Kiffin, J. Segura-Aguilar, A. M. Cuervo, L. H. Glimcher and C. Hetz, *Hum. Mol. Genet.*, 2012, **21**, 2245.
84. S. Casas-Tinto, Y. Zhang, J. Sanchez-Garcia, M. Gomez-Velazquez, D. E. Rincon-Limas and P. Fernandez-Funez, *Hum. Mol. Genet.*, 2011, **20**, 2144.
85. J. H. Lee, S. M. Won, J. Suh, S. J. Son, G. J. Moon, U. J. Park and B. J. Gwag, *Exp. Mol. Med.*, 2010, **42**, 386.

86. A. Federico, E. Cardaioli, P. Da Pozzo, P. Formichi, G. N. Gallus and E. Radi, *J. Neurol. Sci.*, 2012, **322**, 254.
87. A. Johri and M. F. Beal, *J. Pharmacol. Exp. Ther.*, 2012, **342**, 619.
88. R. K. Chaturvedi and M. Flint Beal, *Free Radicals Biol. Med.*, 2013, **63**, 1.
89. J. Meunier and T. Hayashi, *J. Pharmacol. Exp. Ther.*, 2010, **332**, 388.
90. Y. Ha, Y. Dun, M. Thangaraju, J. Duplantier, Z. Dong, K. Liu, V. Ganapathy and S. B. Smith, *Invest. Ophthalmol. Visual Sci.*, 2011, **52**, 527.
91. A. A. Behensky, I. E. Yasny, A. M. Shuster, S. B. Seredenin, A. V. Petrov and J. Cuevas, *J. Pharmacol. Exp. Ther.*, 2013, **347**, 468.
92. F. Mei, S. Y. Christin Chong and J. R. Chan, *Neurosci. Bull.*, 2013, **29**, 177.
93. T. Hayashi and T. P. Su, *Life Sci.*, 2005, **77**, 1612.
94. B. Oxombre, C. Lee-Chang, A. Duhamel, M. Toussaint, M. Giroux, M. Donnier-Maréchal, P. Carato, D. Lefranc, H. Zéphir, L. Prin, P. Melnyk and P. Vermersch, *Br. J. Pharmacol.*, 2015, **172**, 1769.
95. V. H. Perry, J. A. Nicoll and C. Holmes, *Nat. Rev. Neurol.*, 2010, **6**, 193.
96. N. N. Burke, D. M. Kerr, O. Moriarty, D. P. Finn and M. Roche, *Brain, Behav., Immun.*, 2014, **42**, 147.
97. M. J. Robson, R. C. Turner, Z. J. Naser, C. R. McCurdy, J. D. Huber and R. R. Matsumoto, *Exp. Neurol.*, 2013, **247**, 134.
98. Z. Wu, L. Li, L. T. Zheng, Z. Xu, L. Guo and X. Zhen, *J. Neurochem.*, 2015, **134**, 904.
99. J. Cuevas, A. Rodriguez, A. Behensky and C. Katnik, *J. Pharmacol. Exp. Ther.*, 2011, **339**, 161.
100. H. Dong, Y. Ma, Z. Ren, B. Xu, Y. Zhang, J. Chen and B. Yang, *Cell. Mol. Neurobiol.*, 2015, **36**, 639.
101. R. Mancuso, S. Oliván, A. Rando, C. Casas, R. Osta and X. Navarro, *Neurotherapeutics*, 2012, **9**, 814.
102. J. M. Derocq, B. Bourrié, M. Ségui, G. Le Fur and P. Casellas, *J. Pharmacol. Exp. Ther.*, 1995, **272**, 224.
103. P. Casellas, B. Bourrié, X. Canat, P. Carayon, I. Buisson, R. Paul, J. C. Brelière and G. Le Fur, *J. Neuroimmunol.*, 1994, **52**, 193.
104. A. Urani, F. J. Roman, V. L. Phan, T. P. Su and T. Maurice, *J. Pharmacol. Exp. Ther.*, 2001, **298**, 1269.
105. T. P. Su, E. D. London and J. H. Jaffe, *Science*, 1988, **240**, 219.
106. M. Takebayashi, T. Hayashi and T. P. Su, *J. Pharmacol. Exp. Ther.*, 2002, **303**, 1227.
107. S. Macfarlane, M. Cecchi, D. Moore, P. Maruff, K. M. Capiak, A. Zografidis and C. U. Missling, New Alzheimer's Drug ANAVEX 2-73: A Phase 2a Study, Clinical Safety, Tolerability and Maximum tolerated dose finding in mild-to-moderate Alzheimer's patients, <https://www.anavex.com>, last accessed July 2018.
108. Avanir Pharmaceuticals Announces Positive Phase II Trial Results for AVP-923 in Treatment of Agitation in Patients with Alzheimer's Disease, <https://www.avanir.com>, last accessed July 2018.



109. Mundipharma and Purdue reach a new deal to in-licence from Esteve full global rights and development responsibilities for novel first-in-class Sigma-1 antagonist (S1A or MR309/E-52862).
110. R. A. Glennon, S. Y. Ablordeppey, A. M. Ismaiel, M. B. El-Ashmawy, J. B. Fischer and K. Burke Howie, *J. Med. Chem.*, 1994, **37**, 1214.
111. T. M. Gund, J. Floyd and D. Jung, *J. Mol. Graphics Modell.*, 2004, **22**, 221.
112. C. Laggner, C. Schieferer, B. Fiechtner, G. Poles, R. D. Hoffmann, H. Glossmann, T. Langer and F. F. Moebius, *J. Med. Chem.*, 2005, **48**, 4754.
113. T. P. Su, X. Z. Wu, E. J. Cone, K. Shukla, T. M. Gund, A. L. Dodge and D. W. Parish, *J. Pharmacol. Exp. Ther.*, 1991, **259**, 543.
114. E. Griesmaier, A. Posod, M. Gross, V. Neubauer, K. Wegleiter, M. Hermann, M. Urbanek, M. Keller and U. Kiechl-Kohlendorfer, *Exp. Neurol.*, 2012, **237**, 388.
115. S. B. Seredenin, T. A. Antipova, M. V. Voronin, S. Y. Kurchashova and A. N. Kuimov, *Bull. Exp. Biol. Med.*, 2009, **148**, 42.
116. C. Katnik, A. Garcia, A. A. Behensky, I. E. Yasny, A. M. Shuster, S. B. Seredenin, A. V. Petrov and J. Cuevas, *J. Neurochem.*, 2016, **139**, 497.
117. University of Oregon, Sigma Brain Receptor Ligands and Their Use, *US Pat.*, 4709094, 1986.
118. University of Oregon, Substituted guanidines having high binding to the sigma receptor and the use thereof, *WO Pat.*, 9118868, 1991.
119. K. Matsuno, M. Nakazawa, K. Okamoto, Y. Kawashima and S. Mita, *Eur. J. Pharmacol.*, 1996, **306**, 271.
120. J. R. Lever, J. L. Gustafson, R. Xu, R. L. Allmon and S. Z. Lever, *Synapse*, 2006, **59**, 350.
121. R. R. Matsumoto, W. D. Bowen, B. R. De Costa and J. C. Houk, *Brain Res. Bull.*, 1999, **48**, 497.
122. R. R. Matsumoto, K. A. McCracken, M. J. Friedman, B. Pouw, B. R. De Costa and W. D. Bowen, *Eur. J. Pharmacol.*, 2001, **419**, 163.
123. A. Klouz, J. P. Tillement, M. F. Boussard, M. Wierzbicki, V. Berezowski, R. Cecchelli, S. Labidalle, B. Onténiente and D. Morin, *FEBS Lett.*, 2003, **553**, 157.
124. A. Klouz, D. B. Saïd, H. Ferchichi, N. Kourda, L. Ouanes, M. Lakhal, J. P. Tillement and D. Morin, *Eur. J. Pharmacol.*, 2008, **578**, 292.
125. D. N. Middlemiss, D. Billington, M. Chambers, P. H. Hutson, A. Knight, M. Russell, L. Thorn, M. D. Tricklebank and E. H. F. Wong, *Br. J. Pharmacol.*, 1991, **102**, 153P.
126. J. McLarnon, D. Sawyer and J. Church, *Neurosci. Lett.*, 1994, **174**, 181.
127. C. A. Maier and B. Wünsch, *J. Med. Chem.*, 2002, **45**, 438.
128. F. J. Roman, X. Pascaud, B. Martin, D. Vauché and J. L. Junien, *J. Pharm. Pharmacol.*, 1990, **42**, 439.
129. J. A. Fishback, M. J. Robson, Y. T. Xu and R. R. Matsumoto, *Pharmacol. Ther.*, 2010, **127**, 271.
130. T. Hayashi, S. Y. Tsai, T. Mori, M. Fujimoto and T. P. Su, *Expert Opin. Ther. Targets*, 2011, **15**, 557.

131. E. Amata, A. Rescifina, O. Prezzavento, E. Arena, M. Dichiarà, V. Pittalà, Á. Montilla-García, F. Punzo, P. Merino, E. J. Cobos and A. Marrazzo, *J. Med. Chem.*, 2018, **61**, 372.
132. V. Mégalizzi, V. Mathieu, T. Mijatovic, P. Gailly, O. Debeir, N. De Neve, M. Van Damme, G. Bontempi, B. Haibe-Kains, C. Decaestecker, Y. Kondo, R. Kiss and F. Lefranc, *Neoplasia*, 2007, **9**, 358.
133. C. S. John, B. J. Vilner and W. D. Bowen, *J. Med. Chem.*, 1994, **37**, 1737.
134. S. Yang, A. Bhardwaj, J. Cheng, N. J. Alkayed, P. D. Hurn and J. R. Kirsch, *Anesth. Analg.*, 2007, **104**, 1179.
135. F. Tan, P. L. Guio-Aguilar, C. Downes, M. Zhang, L. O'Donovan, J. K. Callaway and P. J. Crack, *Neuropharmacology*, 2010, **59**, 416.
136. D. Rossi, A. Pedrali, M. Urbano, R. Gaggeri, M. Serra, L. Fernández, M. Fernández, J. Caballero, S. Ronsisvalle, O. Prezzavento, D. Schepmann, B. Wuensch, M. Peviani, D. Curti, O. Azzolina and S. Collina, *Bioorg. Med. Chem.*, 2011, **19**, 6210.
137. D. Rossi, M. Urbano, A. Pedrali, M. Serra, D. Zampieri, M. G. Mamolo, C. Laggner, C. Zanette, C. Florio, D. Schepmann, B. Wuensch, O. Azzolina and S. Collina, *Bioorg. Med. Chem.*, 2010, **18**, 1204.
138. D. Rossi, A. Marra, P. Picconi, M. Serra, L. Catenacci, M. Sorrenti, E. Laurini, M. Fermeglia, S. Pricl, S. Brambilla, N. Almirante, M. Peviani, D. Curti and S. Collina, *Bioorg. Med. Chem.*, 2013, **21**, 2577.
139. D. Rossi, A. Pedrali, A. Marra, L. Pignataro, D. Schepmann, B. Wünsch, L. Ye, K. Leuner, M. Peviani, D. Curti, O. Azzolina and S. Collina, *Chirality*, 2013, **25**, 814.
140. A. Marra, D. Rossi, L. Maggi, F. Corana, B. Mannucci, M. Peviani, D. Curti and S. Collina, *Biomed. Chromatogr.*, 2016, **30**, 645.
141. M. Rui, G. Rossino, S. Coniglio, S. Monteleone, A. Scuteri, A. Malacrida, D. Rossi, L. Catenacci, M. Sorrenti, M. Paolillo, D. Curti, L. Venturini, D. Schepmann, B. Wünsch, K. R. Liedl, G. Cavaletti, V. Pace, E. Urban and S. Collina, *Eur. J. Med. Chem.*, 2018, **158**, 353.
142. N. Narita, K. Hashimoto, M. Iyo, Y. Minabe and K. Yamazaki, *Eur. J. Pharmacol.*, 1995, **293**, 277.
143. N. Narita, K. Hashimoto, S. Tomitaka and Y. Minabe, *Eur. J. Pharmacol.*, 1996, **307**, 117.
144. E. R. Whittmore, V. I. Ilyin and R. M. Woodward, *J. Pharmacol. Exp. Ther.*, 1997, **282**, 326.

Paper 2

Article

PEG 400/Cerium Ammonium Nitrate Combined with Microwave-Assisted Synthesis for Rapid Access to Beta-Amino Ketones. An Easy-to-Use Protocol for Discovering New Hit Compounds

Giacomo Rossino ^{1,†}, Maria Valeria Raimondi ^{2,†}, Marta Rui ¹, Marcello Di Giacomo ¹ , Daniela Rossi ¹ and Simona Collina ^{1,*} 

¹ Drug Sciences Department, Medicinal Chemistry and Pharmaceutical Technology Section, University of Pavia, 27100 Pavia, Italy; giacomo.rossino01@universitadipavia.it (G.R.); marta.rui01@universitadipavia.it (M.R.); marcello.digiacomio@unipv.it (M.D.G.); daniela.rossi@unipv.it (D.R.)

² Department of Biological, Chemical and Pharmaceutical Sciences and Technologies, Medicinal Chemistry and Pharmaceutical Technologies Section, University of Palermo, 90100 Palermo, Italy; mariavaleria.raimondi@unipa.it

* Correspondence: simona.collina@unipv.it; Tel.: +39-0382-987379

† These Authors contributed equally to this work.

Received: 2 March 2018; Accepted: 26 March 2018; Published: 28 March 2018



Abstract: Compound libraries are important requirement in target-based drug discovery. In the present work, a small focused compound library based on β -aminoketone scaffold has been prepared combining microwave-assisted organic synthesis (MAOS) with polymer-assisted solution phase synthesis (PASPS) and replacing reaction workup standard purification procedures with solid phase extraction (SPE). Specifically, the effects of solvent, such as dioxane, dimethylformamide (DMF), polyethylene glycol 400 (PEG 400), temperature, irradiation time, stoichiometric ratio of reagents, and catalysts (HCl, acetic acid, cerium ammonium nitrate (CAN)) were investigated to maximize both conversion and yield. The optimized protocol generally afforded the desired products in satisfying yields and purities. The designed library is a part of our current research on sigma 1 receptor modulators, a valuable tool for the identification of novel potential hit compounds.

Keywords: Mannich reaction; β -aminoketones; microwave-assisted organic synthesis; polymer-assisted solution phase synthesis; solid phase extraction; drug discovery

1. Introduction

Identifying hit compounds is the first step in the complex drug-discovery process, and the degree of structural diversity is an important element, enhancing the rate of success in finding a potential lead candidate. In this context, β -amino carbonyl compounds represent a class of important pharmacophores and useful building blocks for the synthesis of diverse classes of biologically active molecules [1,2].

Numerous β -amino ketones and their analogues exhibit potent activity of great interest in medicinal chemistry, such as anti-inflammatory [3,4], antibacterial [5,6], antiviral [7], antifungal [6,8], analgesic [9], and anticancer activity [10–13], to cite just a few examples (Figure 1). Moreover, β -amino acids are found in some important bioactive natural compounds and are widely employed in the preparation of peptide-based drugs [14–17] (Figure 1). No less important, β -amino ketones can be key intermediates for the synthesis of pharmaceutically relevant compounds [18,19].

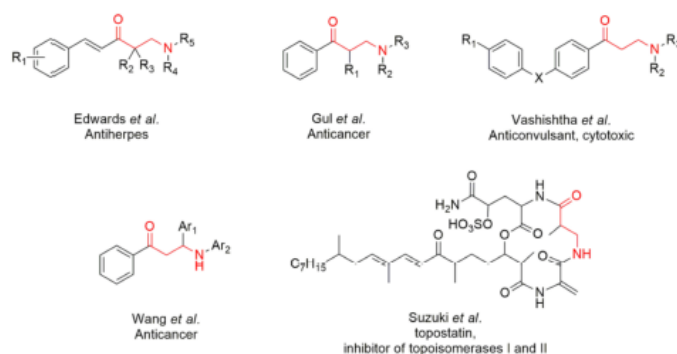


Figure 1. Some important β -amino ketones, both synthetic and natural, and their biological properties.

While many synthetic strategies to achieve β -amino carbonyl compounds can be found in the recent literature (Figure 2), such as aza-Michael reaction [20], enamine-aldehyde cross-coupling via *N*-heterocyclic carbenes [21], copper-catalyzed electrophilic amination of cyclopropanols [22], Pd-catalyzed aminocarbonylation of alkenes [23], and hydrogenolysis of isoxazolines [24], the Mannich multicomponent reaction (Figure 2) remains the most used procedure [2,25], and many improvements to and implementations of the original protocol have been studied [19,26].

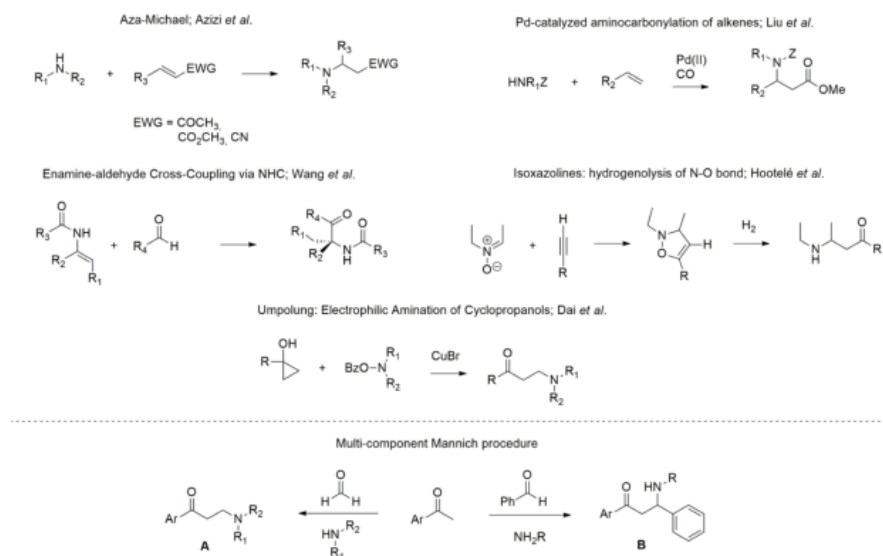


Figure 2. Alternative synthetic routes for accessing β -amino carbonyl compounds.

In particular, the three-component one-pot Mannich reaction allows the formation of β -amino ketones, presenting general structure A or B (Figure 2) with great structural variability, depending on the amine and aldehyde employed [27,28].

In light of these considerations and as part of our ongoing research, we herein focus on the development of an efficient protocol based on the three-component one-pot Mannich reaction for the preparation of a β -amino ketone small library endowed with general formula A (Figure 2), consisting of a tertiary amine bridged to an aromatic ring by a propylenic chain. The final aim is to discover

new potential sigma receptor (SR) modulators [29–32]. We set up an efficient, clean, quick, and scalable protocol based on microwave-assisted organic synthesis (MAOS), using cerium ammonium nitrate (CAN) as a catalyst and polyethylene glycol 400 (PEG 400) as a solvent, combined with polymer-assisted solid phase synthesis (PASPS). Purification of final compounds occurred by solid phase extraction (SPE). Overall, our strategy led us to obtain the desired β -amino ketones efficiently and quickly.

2. Results and Discussion

Through this procedure, a small focused library of 36 β -amino ketones derived from the coupling of aryl-ketones 1–6 with amines a–f (Figure 3) was prepared. Relying on our long experience in the SR field, both building blocks were selected by taking into account the state-of-the-art structure activity relationship (SAR) of SR ligands [33,34]. We exploited aromatic or heterocyclic methyl-ketones (1–6) and cyclic (a, d, f) or benzyl acyclic (b, c, e) secondary amines (Figure 3).

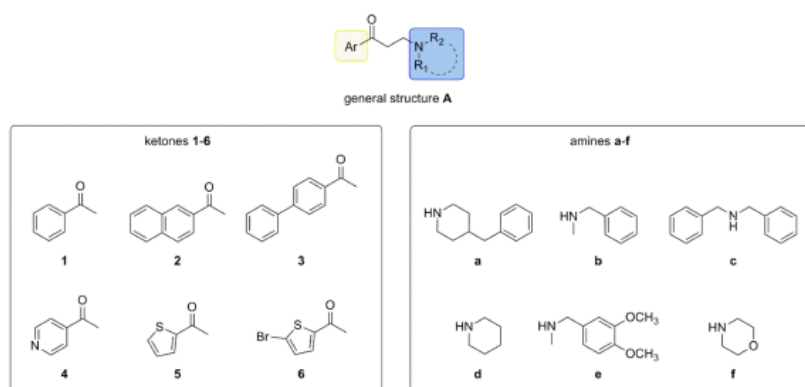


Figure 3. Designed library.

2.1. Setup and Optimization of Synthetic Protocol

According to data in the literature concerning the different reactivities of secondary amines related to their structures and experimental conditions in the Mannich reaction [25,35], we set up a novel protocol using the cyclic and acyclic amines a and b as “building block” models. First, compounds 1a and 1b were synthesized with conventional heating, applying an existing protocol (Figure 4, condition A), and were properly purified [36]. Molar extinction coefficients of acetophenones 1, 1a, and 1b were determined (1.265×10^4 , 6.327×10^3 , and 6.703×10^3 L·mol⁻¹·cm⁻¹, respectively) and high performance liquid chromatography-ultraviolet-photodiode array detector (HPLC-UV-PAD) methods were developed to determine the percentage of conversion and purity of new compounds. Afterwards, based on our own experience, we set up a microwave-assisted synthetic protocol (Figure 4) to obtain our β -amino ketones 1–6, a–f. Of note, MAOS has already been successfully employed in Mannich reactions [37,38]. Microwave oven parameters (i.e., temperature, irradiation power, and time) were explored and different solvents, such as dioxane, dimethylformamide (DMF), tetrahydrofuran (THF), methanol (MeOH), ethanol (EtOH) tested. Temperature and irradiation power varied from 35 °C to 200 °C and from 60 W to 200 W, respectively, as did irradiation time. Lastly, both type and amount of protic acidic additive were evaluated (HCl, HBF₄, HClO₄, acetic acid). Unfortunately, no satisfying results were obtained. Therefore, we considered the use of ceric ammonium nitrate (CAN) as a catalyst in PEG 400, as it had already been used in a three-component Mannich reaction to access β -amino ketones of general structure B (Figure 2) under conventional heating [39]. Accordingly, we employed this catalyst/solvent combination in our microwave-assisted protocol to access the designed compounds of general structure A (Figure 2).

Compounds **1a** and **1b** were obtained under microwave irradiation (60 W, 90 °C for 10 min) using 5% mol of CAN in PEG 400. The HPLC analysis (see Appendix A) showed that the reaction was clean and quick, affording the desired products with 80% conversion. Interestingly, using hydrochloride amines as reagents led to the best results. A schematic comparison between the old and new protocols (path A and path B, respectively) is shown in Figure 4.

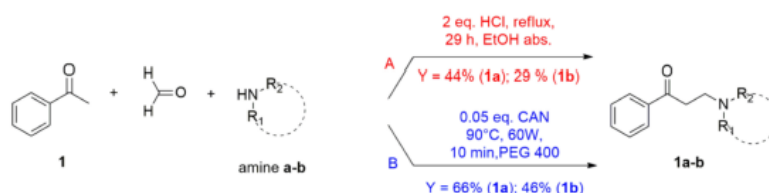


Figure 4. Comparison between (A) traditional and (B) new protocol.

With these promising results, we moved forward to determine the effect of stoichiometric ratio of reagents on both conversion percentage and crude purity. Results are reported in Tables 1 and 2. Reactions conducted with excess amine (entries 2–4 and 10–13) led to high conversion percentages, even if the products had lower purities. An opposite trend was observed using an excess of ketone (entries 5–8 and 14–17). Accordingly, conditions of entries 6 and 15 (i.e., 2 equivalents (eq.) of ketone and 1 eq. of amine) were considered the best compromise and were extended to the other substrate for preparation of the whole library.

Table 1. Investigation of stoichiometric ratio of the reagents on conversion and purity of compound **1a**.

Entry	1 (eq.)	a (eq.)	% Conversion	% Purity
1	1	1	80.0	82.5
2	1	1.5	76.7	77.8
3	1	2	79.9	67.5
4	1	2.5	78.5	60.7
5	1.5	1	67.1	68.9
6	2	1	72.4	97.7
7	2.5	1	77.2	96.1
8	3	1	67.7	95.8

Reagents and reaction conditions: cerium ammonium nitrate (CAN) (0.05 eq.), paraformaldehyde (1.0 eq.), PEG 400, (MW: 90 °C, 60 W, 10 min).

Table 2. Investigation of stoichiometric ratio of the reagents on conversion and purity of compound **1b**.

Entry	1 (eq.)	b (eq.)	% Conversion	% Purity
9	1	1	80.0	60.1
10	1	2	77.2	35.1
11	1	2.5	86.9	34.2
12	1	3	93.4	23.5
13	1	3.5	64.9	23.5
14	1.5	1	81.5	69.4
15	2	1	74.5	81.1
16	3	1	61.6	89.6
17	3.5	1	49.2	92.2

Reagents and reaction conditions: CAN (0.05 eq.), paraformaldehyde (1.0 eq.), PEG 400, (MW: 90 °C, 60 W, 10 min).

2.2. MW-Assisted Library Synthesis

The optimized protocol was then employed to synthesize the small focused library. The following table reports the yields and purities of each compound.

The developed protocol allowed production of the desired compounds (Table 3) with the exception of dibenzylaminic (1–6c) and 4 acetyl-pyridinic (4a–f) compounds (Figure 3). Of note, cyclic amines (a, d, f) were well tolerated in this protocol; in particular, piperidines were the most versatile reagents, since they were able to react with the ketone counterpart, offering products in satisfying yields (Table 3). Relying on the molecules endowed with an acyclic amine, different reactivity was seen: *N*-benzylmethylamine > 3,4-dimethoxy-*N*-methylbenzylamine > dibenzylamine. The failure in the reaction involving dibenzylamine may be attributed to its low basicity, which may slow down the formation of the intermediate imine resulting from the reaction with formaldehyde. This result is not surprising. Indeed, it has been shown that the reactivity in the Mannich reaction is strictly related to the amine structure, and within a homologous series the reactivity may be different. An emblematic example is diethylamine, which is unable to be transformed into β -amino ketone, whereas the superior and inferior amine analogues react efficiently to give access to the desired products [35]. Regarding the ketone building block, the procedure was successfully applied to aromatic ketones, presenting benzene and thienyl nucleus, whereas no product was observed when ketone 4, bearing a pyridine moiety, was used. This behavior can be explained by considering the basic properties of the pyridine ring, which reduced the reactivity of methyl ketone 4. We performed additional model reactions on ketone 4 under traditional conditions at high temperature and for long times to force the reaction. Again, the desired products (compounds 4a and 4b) were not isolated, supporting our hypothesis that the low reactivity of 4 acetyl-pyridine compromised the reaction outcome.

Table 3. Yield and purity of compounds 1a–6f.

Compound	Ar	NR ₁ R ₂	Yield % ^a	Purity % ^a
1a	phenyl	4-benzylpiperidine	72	98
1b		<i>N</i> -benzylmethylamine	70	86
1d		piperidine	58	75
1e		3,4-dimethoxy- <i>N</i> -methylbenzylamine	33	66
1f		morpholine	-	Traces (5)
2a		naphthyl	4-benzylpiperidine	32
2b	<i>N</i> -benzylmethylamine		34	81
2d	piperidine		50	75
2e	3,4-dimethoxy- <i>N</i> -methylbenzylamine		38	54
2f	morpholine		46	71
3a	biphenyl		4-benzylpiperidine	75
3b		<i>N</i> -benzylmethylamine	55	67
3d		piperidine	50	73
3e		3,4-dimethoxy- <i>N</i> -methylbenzylamine	-	Traces (5)
3f		morpholine	50	61
5a		2-thienyl	4-benzylpiperidine	63
5b	<i>N</i> -benzylmethylamine		56	85
5d	piperidine		30	83
5e	3,4-dimethoxy- <i>N</i> -methylbenzylamine		25	66
5f	morpholine		32	77
6a	5-bromo-2-thienyl		4-benzylpiperidine	55
6b		<i>N</i> -benzylmethylamine	40	37
6d		piperidine	29	57
6e		3,4-dimethoxy- <i>N</i> -methylbenzylamine	n.r.	-
6f		morpholine	6	38

Reagents and reaction conditions: ketone (2.0 eq.), amine (1.0 eq.), CAN (0.05 eq.), paraformaldehyde (1.0 eq.), PEG 400, (MW: 90 °C, 60 W, 10 min). ^a determined by LC-MS analysis. - no data. n.r. no reaction.

3. Materials and Methods

Reactions performed under conventional heating were monitored by thin layer chromatography (TLC) with Fluka silica gel 60 F254 (Merck KGaA, Darmstadt, Germany) and purified by automatic flash chromatography with CombiFlash[®]RF (AlfaTech, Teledyne Isco, Inc., Genoa, Italy).

All reactions conducted under microwave irradiation were performed in a microwave mono-mode oven specifically for organic synthesis (Discover[®] LabMate instrument, CEM Corporation, Matthews, NC, USA). The obtained products were purified with Bond Elut SCX[®] cartridge (Varian, Walnut Creek, CA, USA) and silica gel SPE cartridge (Varian, Walnut Creek, CA, USA).

UV spectra were recorded on a LAMBDA[™] 25 UV/VIS spectrometer (Perkin Elmer Inc., Waltham, MA, USA). HPLC analyses were carried out on a Jasco HPLC system (Jasco Europe S.r.l., Cremella, Italy), consisting of a pump model PU 1580, a Reodyne 7125 injector (20 μ L sample loop), and an MD-1510 diode array detector, combined with a Spectra AS3000 autosampler. Experimental data were acquired and interpreted with Borwin PDA and Borwin chromatograph software 1.5. Reversed-phase HPLC analyses were carried out at room temperature on an XTerra RP18 column (3.5 μ m, 4.6 \times 50 mm) (Waters, Milford, MA, USA) and a Hypersil ODS RP18 column (3 μ m, 4.6 \times 100 mm) (VWR, Milano, Italy). The mobile phase was phosphate buffer (pH 7.8) added with acetonitrile as organic modifier; the analysis was carried out using gradient elution (see Tables A1 and A2, Figures A1 and A2 in Appendix A).

Electrospray ionization LC-MS analyses were performed with a single quadrupole AQA ThermoQuest Finnigan (ThermoFinnigan, San Jose, CA, USA) or a Waters Micromass ZQ2000 (Waters, Milford, MA, USA), employing an XBridge C8 column (3.5 μ m, 4.6 \times 50 mm) (Waters, Milford, MA, USA).

¹H-NMR spectra were registered with a Bruker ARX 300 (300 MHz) (Bruker Daltonics, Billerica, MA, USA). Chemical shifts are reported in parts per million (δ) downfield from tetramethylsilane (TMS) as internal standard.

3.1. General Procedure for the Synthesis of β -Aminoketone 1a and 1b under Conventional Heating (Method A)

A solution of acetophenone (1.0 eq.), amine (2.0 eq.), paraformaldehyde (2.0 eq.), and HCl (2.0 eq.) in absolute ethanol (2.25 mL) was refluxed for 24 h in N₂ atmosphere under magnetic stirring. Then, the reaction mixture was evaporated under reduced pressure and the residue purified by automated flash chromatography (CombiFlash[®]RF) using a mixture of 80:20 hexane:diethyl ether, 0.1 NH₃/MeOH as eluent, and silica gel RediSep column (12 g) (particle size: 35–70 μ m).

3.2. General Procedure for the Synthesis of β -Aminoketones 1a–6f under Microwave Heating (Method B)

A mixture of ketone (2.0 eq.), amine hydrochloride (1 eq.), paraformaldehyde (1 eq.), and CAN (0.05 eq.) in PEG 400 (0.8 mL) was irradiated with a microwave power of 60 watts at 90 °C for 10 min. The reaction workup was performed as follows: the mixture was quenched in 2 M NaOH, then the solid was collected by centrifugation, dissolved in methanol or dichloromethane (depending on the solubility of the compound), and purified using SCX cartridge, eluting with a solution of 0.3 M NH₃/MeOH in dichloromethane to remove the excess ketone. Finally, the product was isolated using silica gel SPE cartridge, eluting with dichloromethane to remove the nonreacted amine. Then the organic phase was evaporated to dryness.

3.3. Analytical Data of Prepared Compounds

3-(4-Benzylpiperidin-1-yl)-1-phenylpropan-1-one (1a). Yield: 44% (method A), 72% (method B). Yellow oil; ¹H-NMR (300 MHz, CDCl₃) (ppm): 1.62 (br s, 2H), 1.74 (d, 3H), 2.26 (br s, 2H), 2.58 (d, 2H), 2.95–3.26 (m, 4H), 3.43 (t, 2H), 7.10–7.25 (m, 3H), 7.25–7.33 (m, 2H), 7.43–7.53 (m, 2H), 7.53–7.63 (m, 1H), 7.92–8.03 (m, 2H); LC-MS: Purity 98%; RT 4.53 min. MH⁺ 308.14 [40].

3-[Benzyl(methyl)amino]-1-phenylpropan-1-one (1b). Yield: 70%; Yellow oil; ¹H-NMR (300 MHz, CDCl₃) (ppm): 2.34 (s, 3H), 3.00 (t, 2H), 3.29 (t, 2H), 3.67 (br s, 2H), 7.28–7.32 (m, 1H), 7.32–7.39 (m, 4H), 7.42–7.50 (m, 2H), 7.53–7.61 (m, 1H), 7.92–7.88 (m, 2H); LC-MS: Purity 86%; RT 3.84 min. MH⁺ 254.11 [41].

1-Phenyl-3-(piperidin-1-yl)propan-1-one (1d). Yield: 58%; ¹H-NMR (300 MHz, CDCl₃) (ppm): 1.49–1.57 (m, 2H), 1.62–1.79 (m, 4H), 2.54–2.71 (m, 4H), 2.94 (t, 2H), 3.34 (t, 2H), 7.41–7.52 (m, 2H), 7.53–7.63 (m, 1H), 7.94–8.01 (m, 2H); LC-MS: Purity 75%; RT 3.12 min. MH⁺ 218.16 [42].

3-[(3,4-Dimethoxybenzyl)(methyl)amino]-1-phenylpropan-1-one (1e). Yield: 33%; Yellow oil; ¹H-NMR (300 MHz, CDCl₃) (ppm): 2.34 (s, 3H), 2.94–3.06 (m, 2H), 3.21–3.33 (m, 2H), 3.71 (s, 2H), 3.88 (s, 6H), 6.65–6.77 (m, 2H), 6.77–6.87 (m, 2H), 7.42–7.53 (m, 2H), 7.53–7.62 (m, 1H), 7.91–8.05 (m, 1H); LC-MS: Purity 66%; RT 3.79 min. MH⁺ 314.12.

3-(Morpholin-4-yl)-1-phenylpropan-1-one (1f). LC-MS: Purity 5%; RT 2.73 min. MH⁺ 220.11 [41]

3-(4-Benzylpiperidin-1-yl)-1-(naphthalen-2-yl)propan-1-one (2a). Yield: 32%; Yellow oil; ¹H-NMR (300 MHz, CDCl₃) (ppm): 1.52–1.88 (m, 5H), 2.19–2.48 (m, 2H), 2.60 (d, 2H), 3.04–3.35 (m, 4H), 3.46–3.76 (m, 2H), 7.12–7.24 (m, 3H), 7.28–7.36 (m, 2H), 7.47–7.70 (m, 2H), 7.84–7.94 (m, 2H), 7.95–8.08 (m, 2H), 8.54 (s, 1H); LC-MS: Purity 69%; RT 4.99 min. MH⁺ 358.09 [40].

3-[Benzyl(methyl)amino]-1-(naphthalen-2-yl)propan-1-one (2b). Yield: 34%; ¹H-NMR (300 MHz, CDCl₃) (ppm): 2.38 (s, 3H), 3.06 (t, 2H), 3.43 (t, 2H), 3.71 (s, 2H), 7.30–7.41 (m, 5H), 7.52–7.66 (m, 2H), 7.85–7.93 (m, 2H), 7.97 (d, 1H), 8.02 (dd, 1H), 8.47 (s, 1H); LC-MS: Purity 81%; RT 4.51 min. MH⁺ 304.11 [41].

1-(Naphthalen-2-yl)-3-(piperidin-1-yl)propan-1-one (2d). Yield: 50%; ¹H-NMR (300 MHz, CDCl₃) (ppm): 1.44–1.63 (m, 2H), 1.72–1.91 (m, 4H), 2.60–2.88 (m, 4H), 3.11 (t, 2H), 3.57 (br t, 2H), 7.46–7.68 (m, 2H), 7.83–8.11 (m, 4H), 8.53 (br s, 1H); LC-MS: Purity 75%; RT 4.04 min. MH⁺ 268.14 [42].

3-[(3,4-Dimethoxybenzyl)(methyl)amino]-1-(naphthalen-2-yl)propan-1-one (2e). Yield: 38%; Yellow oil; ¹H-NMR (300 MHz, CDCl₃) (ppm): 2.32 (s, 3H), 2.98 (t, 2H), 3.34 (t, 2H), 3.60 (s, 2H), 3.85 (s, 6H), 6.8 (m, 3H), 7.70 (m, 2H), 7.98–8.15 (m, 4H), 8.50 (s, 1H); LC-MS: Purity 54%; RT 4.41 min. MH⁺ 364.08.

3-(Morpholin-4-yl)-1-(naphthalen-2-yl)propan-1-one (2f). Yield: 46%; ¹H-NMR (300 MHz, CDCl₃) (ppm): 2.76 (br s, 4H), 3.10 (br t, 2H), 3.51 (br t, 2H), 3.86 (br t, 4H), 7.53–7.66 (m, 2H), 7.86–7.94 (m, 2H), 7.96–8.01 (m, 1H), 8.04 (dd, 1H), 8.51 (br s, 1H); LC-MS: Purity 71%; RT 3.78 min. MH⁺ 270.09 [42].

3-(4-Benzylpiperidin-1-yl)-1-(biphenyl-4-yl)propan-1-one (3a). Yield: 75%; ¹H-NMR (300 MHz, CDCl₃) (ppm): 1.67–1.84 (m, 5H), 2.58 (br d, 2H), 3.18–3.37 (m, 4H), 3.53–3.71 (m, 4H), 7.09–7.17 (m, 2H), 7.19–7.24 (m, 1H), 7.28–7.32 (m, 1H), 7.37–7.52 (m, 4H), 7.60–7.66 (m, 2H), 7.67–7.74 (m, 2H), 8.03–8.09 (m, 2H); LC-MS: Purity 75%; RT 5.21 min. MH⁺ 384.12.

3-[Benzyl(methyl)amino]-1-(biphenyl-4-yl)propan-1-one (3b). Yield: 55%; ¹H-NMR (300 MHz, CDCl₃) (ppm): 2.40 (s, 3H), 3.02–3.15 (m, 2H), 3.39 (t, 2H), 3.75 (br s, 2H), 7.28–7.44 (m, 6H), 7.45–7.53 (m, 2H), 7.60–7.66 (m, 2H), 7.66–7.73 (m, 2H), 7.99–8.07 (m, 2H); LC-MS: Purity 67%; RT 4.83 min. MH⁺ 330.11.

1-(Biphenyl-4-yl)-3-(piperidin-1-yl)propan-1-one (3d). Yield: 50%; ¹H-NMR (300 MHz, CDCl₃) (ppm): 1.51–1.66 (m, 2H), 1.72–1.86 (m, 4H), 2.66–2.78 (m, 4H), 3.06 (t, 2H), 3.46 (br t, 2H), 7.38–7.52 (m, 3H), 7.61–7.66 (m, 2H), 7.67–7.73 (m, 2H), 8.03–8.10 (m, 2H); LC-MS: Purity 73%; RT 4.38 min. MH⁺ 294.16.

3-[(3,4-Dimethoxybenzyl)(methyl)amino]-1-(biphenyl-4-yl)propan-1-one (3e). LC-MS: Purity 5%; RT 4.73 min. MH⁺ 390.03.

1-(Biphenyl-4-yl)-3-(morpholin-4-yl)propan-1-one (3f). Yield: 50%; ¹H-NMR (300 MHz, CDCl₃) (ppm): 2.70–2.86 (m, 4H), 3.04–3.16 (m, 2H), 3.38–3.50 (m, 2H), 3.84–3.93 (m, 4H), 7.39–7.53 (m, 3H), 7.61–7.67 (m, 2H), 7.68–7.73 (m, 2H), 8.03–8.09 (m, 2H); LC-MS: Purity 61%; RT 4.18 min. MH⁺ 296.11 [40].

3-(4-Benzylpiperidin-1-yl)-1-(thiophen-2-yl)propan-1-one (5a). Yield: 63%; ¹H-NMR (300 MHz, CDCl₃) (ppm): 1.37–1.77 (m, 5H), 2.12 (t, 2H), 2.57 (d, 2H), 2.92 (t, 2H), 2.98–3.08 (m, 2H), 3.23 (t, 2H), 7.12–7.17 (m, 3H), 7.19–7.28 (m, 2H), 7.28–7.32 (m, 1H), 7.63–7.67 (m, 1H), 7.77 (dd, 1H); LC-MS: Purity 95%; RT 4.40 min. MH⁺ 314.05 [43].

3-[Benzyl(methyl)amino]-1-(thiophen-2-yl)propan-1-one (5b). Yield: 56%; ¹H-NMR (300 MHz, CDCl₃) (ppm): 2.35 (s, 3H), 2.97–3.07 (m, 2H), 3.19–3.29 (m, 2H), 3.68 (s, 2H), 7.13 (dd, 1H), 7.29–7.40 (m, 5H), 7.64 (dd, 1H), 7.73 (dd, 1H); LC-MS: Purity 85%; RT 3.59 min. MH⁺ 260.08 [44].

3-(Piperidin-1-yl)-1-(thiophen-2-yl)propan-1-one (5d). Yield: 30%; ¹H-NMR (300 MHz, CDCl₃) (ppm): 1.33–1.61 (m, 2H), 1.70 (m, 4H), 2.41–2.69 (m, 4H), 2.94 (t, 2H), 3.27 (m, 2H), 7.01–7.19 (m, 1H), 7.63–7.68 (m, 1H), 7.78 (dd, 1H); LC-MS: Purity 83%; RT 2.77 min. MH⁺ 224.13 [42].

3-[(3,4-Dimethoxybenzyl)(methyl)amino]-1-(thiophen-2-yl)propan-1-one (5e). Yield: 25%; ¹H-NMR (300 MHz, CDCl₃) (ppm): 2.38 (s, 3H), 2.97–3.05 (m, 2H), 3.13–3.25 (m, 2H), 3.75 (s, 3H), 3.87–3.91 (m, 5H), 6.61–6.89 (m, 3H), 7.15 (t, 1H), 7.62 (d, 1H), 7.73 (d, 1H); LC-MS: Purity 66%; RT 3.19 min. MH⁺ 320.04.

3-(Morpholin-4-yl)-1-(thiophen-2-yl)propan-1-one (5f). Yield: 32%; ¹H-NMR (300 MHz, CDCl₃) (ppm): 2.63–2.78 (m, 4H), 3.03 (br t, 2H), 3.29 (br t, 2H), 3.78–3.87 (m, 4H), 7.15 (dd, 1H), 7.67 (dd, 1H), 7.79 (dd, 1H); LC-MS: Purity 77%; RT 2.16 min. MH⁺ 226.08 [42].

3-(4-Benzylpiperidin-1-yl)-1-(5-bromothiophen-2-yl)propan-1-one (6a). Yield: 55%. Yellow oil; ¹H-NMR (300 MHz, CDCl₃) (ppm): 1.55–1.81 (m, 5H), 2.22–2.39 (m, 2H), 2.58 (d, 2H), 2.98–3.10 (m, 2H), 3.11–3.22 (m, 2H), 3.33 (t, 1H), 7.07–7.16 (m, 3H), 7.16–7.26 (m, 2H), 7.26–7.34 (m, 2H), 7.57 (d, 1H); LC-MS: Purity 76%; RT 4.83 min. MH⁺ 391.91 [43].

3-[Benzyl(methyl)amino]-1-(5-bromothiophen-2-yl)propan-1-one (6b). Yield: 40%. Yellow oil. ¹H-NMR (300 MHz, CDCl₃) (ppm): 2.40 (s, 3H), 3.08 (d, 2H), 3.26 (br s, 2H), 3.78 (s, 2H), 7.10 (d, 1H), 7.31–7.44 (m, 5H), 7.50 (d, 1H); LC-MS: Purity 37%; RT 4.20 min. MH⁺ 339.93 [45].

1-(5-Bromothiophen-2-yl)-3-(piperidin-1-yl)propan-1-one (6d). Yield: 29%; ¹H-NMR (300 MHz, CDCl₃) (ppm): 0.80–0.94 (m, 1H), 1.49–1.55 (m, 1H), 1.67–1.80 (m, 4H), 2.57–2.68 (m, 4H), 2.96 (t, 2H), 3.24 (br t, 2H), 7.10–7.13 (m, 1H), 7.54 (d, 1H); LC-MS: Purity 57%; RT 3.61 min. MH⁺ 303.97 [45].

1-(5-Bromothiophen-2-yl)-3-(morpholin-4-yl)propan-1-one (6f). Yield: 6%; ¹H-NMR (300 MHz, CDCl₃) (ppm): 2.62–2.89 (m, 4H), 2.99–3.11 (m, 1H), 3.22–3.34 (m, 1H), 3.55–3.67 (m, 3H), 3.86 (br t, 3H), 7.13 (d, 1H), 7.54 (d, 1H); LC-MS: Purity 38%; RT 3.38 min. MH⁺ 305.91.

4. Conclusions

In summary, we have developed a rapid and easy-to-use microwave-assisted protocol based on a combination of PEG 400/CAN, PASPS, and SPE, obtaining the desired products faster than conventional procedures. The reaction optimized with respect to various parameters afforded most of the desired products with good yield and satisfying purity. Our approach could be adapted to a new library of compounds with different aromatic ketones. No less important, the obtained compounds could serve as key intermediates for further functionalization at the ketone group to allow scaffold modifications, suitable for disclosing novel potential hit compounds. We believe that simple reaction procedures and substrate compatibility along with environmentally friendly conditions make our protocol an important supplement to the existing methods.

Lastly, the small focused library we present aims at discovering new potential sigma 1 receptor modulators as part of our ongoing research in this field. From this consideration came our decision to add these products to the library of MuTaLig, an innovative ligand identification platform for the drug-discovery process.

Acknowledgments: MIUR and University of Pavia are gratefully acknowledged for the doctoral and postdoctoral fellowships to G.R. and M.R.

Author Contributions: S.C. conceived the work, contributed to reviewing the manuscript, and was responsible for the correctness of the whole study. M.V.R. and G.R. wrote the manuscript. D.R., M.V.R., and M.D.G. were responsible for the experimental design and for data analysis of the whole study. G.R. and M.R. performed the experiments.

Conflicts of Interest: The authors declare no conflict of interest.

Appendix A

Table A1. HPLC analysis for **1a**. XTerra RP18 column (3.5 μ m, 4.6 \times 50 mm). Flow rate: 1 mL/min.

Time (Minutes)	% Phosphate Buffer	% Acetonitrile
0	90	10
3	90	10
10	60	40
13	60	40
20	5	95
25	90	10
35	90	10

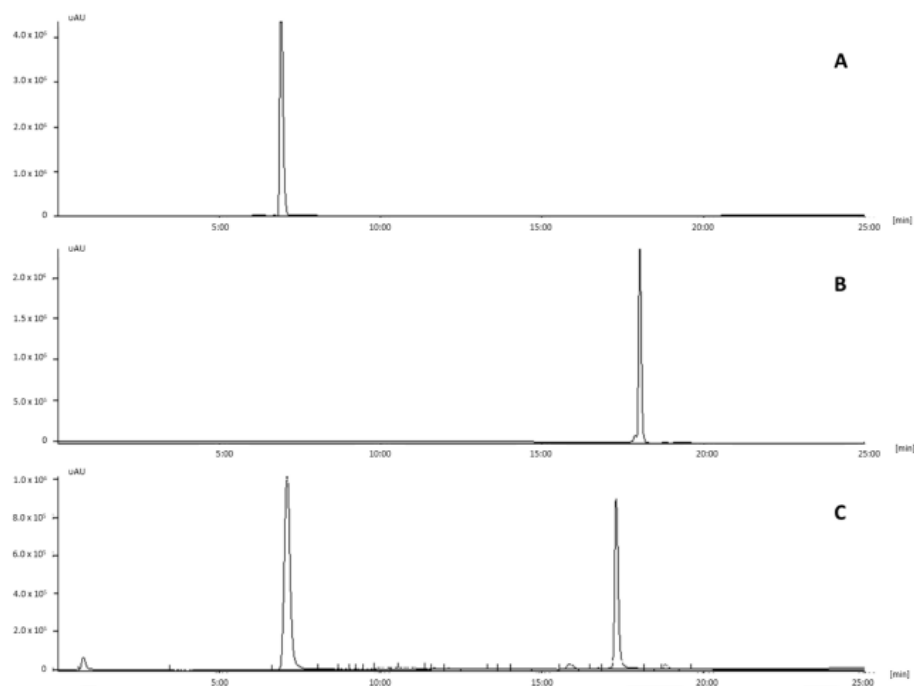
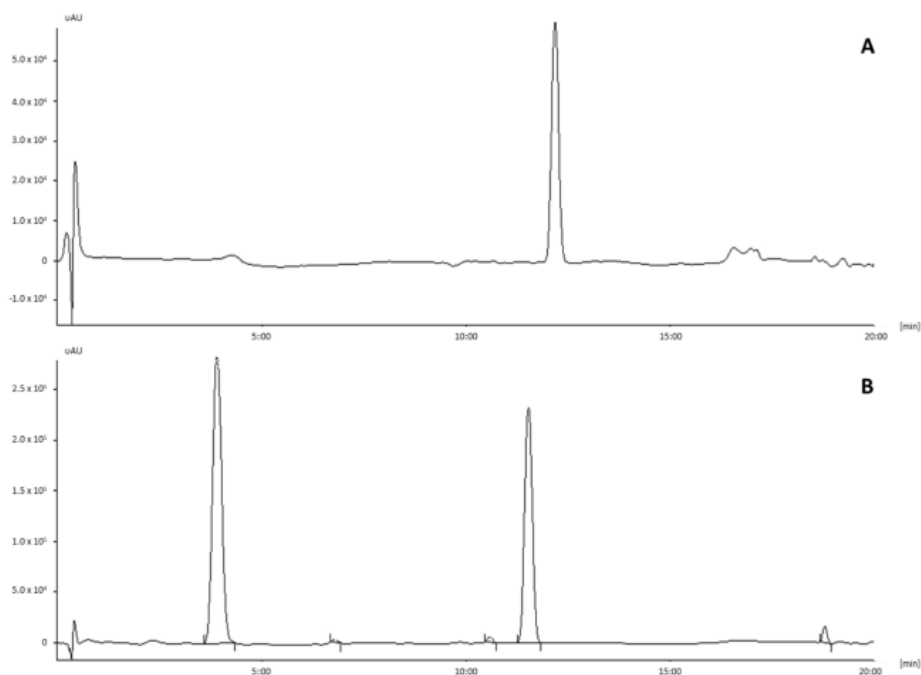


Figure A1. (A) Acetophenone (RT: 6.8 min); (B) compound **1a** (RT: 16 min); (C) reaction mixture (MW) acetophenone (2.0 eq.), 4-benzylpiperidine hydrochloride (1 eq.), paraformaldehyde (1 eq.).

Table A2. HPLC analysis for **1b**. Hypersil ODS RP18 column (3 μ m, 4.6 \times 100 mm). Flow rate: 2 mL/min.

Time (Minutes)	% Phosphate Buffer	% Acetonitrile
0	90	10
3	90	10
10	60	40
13	60	40
20	5	95
30	5	95
35	90	10
40	90	10

**Figure A2.** (A) Compound **1b** (RT: 12 min); (B) reaction mixture (MW) acetophenone (2.0 eq.), *N*-benzylmethylamine hydrochloride (1 eq.), paraformaldehyde (1 eq.).

References

- Bala, S.; Sharma, N.; Kajal, A.; Kamboj, S.; Saini, V. Mannich Bases: An Important Pharmacophore in Present Scenario. *Int. J. Med. Chem.* **2014**, *2014*, 191072. [[CrossRef](#)] [[PubMed](#)]
- Roman, G. Mannich bases in medicinal chemistry and drug design. *Eur. J. Med. Chem.* **2014**, *89*, 743–816. [[CrossRef](#)] [[PubMed](#)]
- Kalluraya, B.; Chimbalkar, R.M.; Hegde, J.C. Anticonvulsant activity of nicotiny/isonicotiny substituted 1,2,4-triazol-5-thione Mannich bases. *Indian J. Heterocycl. Chem.* **2005**, *15*, 15–18.
- Köksal, M.; Gökhan, N.; Küpeli, E.; Yesilada, E.; Erdogan, H. Analgesic and antiinflammatory activities of some new Mannich bases of 5-nitro-2-benzoxazolinones. *Arch. Pharm. Res.* **2007**, *30*, 419–424. [[CrossRef](#)] [[PubMed](#)]
- Ashok, M.; Holla, B.S.; Poojary, B. Convenient one pot synthesis and antimicrobial evaluation of some new Mannich bases carrying 4-methylthiobenzyl moiety. *Eur. J. Med. Chem.* **2007**, *42*, 1095–1101. [[CrossRef](#)] [[PubMed](#)]

6. Pandeya, S.N.; Sriram, D.; Nath, G.; De Clercq, E. Synthesis, antibacterial, antifungal and anti-HIV activities of norfloxacin Mannich bases. *Eur. J. Med. Chem.* **2000**, *35*, 249–255. [[CrossRef](#)]
7. Edwards, M.L.; Ritter, H.W.; Stemerick, D.M.; Stewart, K.T. Mannich bases of 4-phenyl-3-buten-2-one: A new class of antiherpes agent. *J. Med. Chem.* **1983**, *26*, 431–436. [[CrossRef](#)] [[PubMed](#)]
8. Singh, B.N.; Shukla, S.K.; Singh, M. Synthesis and biological activity of sulphadiazine Schiff's bases of isatin and their N-mannich bases. *Asian J. Chem.* **2007**, *19*, 5013–5018.
9. Malinka, W.; Świątek, P.; Filipek, B.; Sapa, J.; Jezierska, A.; Koll, A. Synthesis, analgesic activity and computational study of new isothiazolopyridines of Mannich base type. *Farmaco* **2005**, *60*, 961–968. [[CrossRef](#)] [[PubMed](#)]
10. Gul, H.I.; Vepsäläinen, J.; Gul, M.; Erciyas, E.; Hanninen, O. Cytotoxic activities of mono and bis Mannich bases derived from acetophenone against Renca and Jurkat cells. *Pharm. Acta Helv.* **2000**, *74*, 393–398. [[CrossRef](#)]
11. Vashishtha, S.C.; Zello, G.A.; Nienaber, K.H.; Balzarini, J.; De Clercq, E.; Stables, J.P.; Dimmock, J.R. Cytotoxic and anticonvulsant aryloxyaryl Mannich bases and related compounds. *Eur. J. Med. Chem.* **2004**, *39*, 27–35. [[CrossRef](#)] [[PubMed](#)]
12. Ivanova, Y.; Momekov, G.; Petrov, O.; Karaivanova, M.; Kalcheva, V. Cytotoxic Mannich bases of 6-(3-aryl-2-propenoyl)-2(3H)-benzoxazolones. *Eur. J. Med. Chem.* **2007**, *42*, 1382–1387. [[CrossRef](#)] [[PubMed](#)]
13. Zhang, Z.; Zhu, Y.; Zhou, C.; Liu, Q.; Lu, H.; Ge, Y.; Wang, M. Development of β -amino-carbonyl compounds as androgen receptor antagonists. *Acta Pharmacol. Sin.* **2014**, *35*, 664–673. [[CrossRef](#)] [[PubMed](#)]
14. Lelais, G.; Seebach, D. β^2 -amino acids-syntheses, occurrence in natural products, and components of β -peptides^{1,2}. *Biopolymers* **2004**, *76*, 206–243. [[CrossRef](#)] [[PubMed](#)]
15. Seebach, D.; Beck, A.K.; Bierbaum, D.J. The World of Beta- and Gamma-Peptides Comprised of Homologated Proteinogenic Amino Acids and Other Components. *Chem. Biodivers.* **2004**, *1*, 1111–1239. [[CrossRef](#)] [[PubMed](#)]
16. Seebach, D.; Matthews, J.L.J. β -Peptides: A surprise at every turn. *Chem. Commun.* **1997**, *21*, 2015–2022. [[CrossRef](#)]
17. Suzuki, K.; Nagao, K.; Monnai, Y.; Yagi, A.; Uyeda, M. Topostatin, a Novel Inhibitor of Topoisomerases I and II Produced by *Thermomonospora alba* Strain No. 1520 III. Inhibitory Properties. *J. Antibiot.* **1998**, *51*, 991–998. [[CrossRef](#)] [[PubMed](#)]
18. Ji, J.-X.; Qiu, L.-Q.; Yip, C.W.; Chan, A.S.C. A convenient, one-step synthesis of optically active tertiary aminonaphthol and its applications in the highly enantioselective alkenylations of aldehydes. *J. Org. Chem.* **2003**, *68*, 1589–1590. [[CrossRef](#)] [[PubMed](#)]
19. Huang, P.-J.J.; Youssef, D.; Cameron, T.S.; Jha, A. Microwave-assisted synthesis of novel 2-naphthol bis-Mannich Bases. *Arkivoc* **2008**, *2008*, 165–177. [[CrossRef](#)]
20. Azizi, N.; Baghi, R.; Ghafari, H.; Boloutchian, M.; Hashemi, M. Silicon Tetrachloride Catalyzed Aza-Michael Addition of Amines to Conjugated Alkenes under Solvent-Free Conditions. *Synlett* **2010**, 379–382. [[CrossRef](#)]
21. Wu, J.; Zhao, C.; Wang, J. Enantioselective Intermolecular Enamide–Aldehyde Cross-Coupling Catalyzed by Chiral N-Heterocyclic Carbenes. *J. Am. Chem. Soc.* **2016**, *138*, 4706–4709. [[CrossRef](#)] [[PubMed](#)]
22. Ye, Z.; Dai, M. An Umpolung Strategy for the Synthesis of β -Aminoketones via Copper-Catalyzed Electrophilic Amination of Cyclopropanols. *Org. Lett.* **2015**, *17*, 2190–2193. [[CrossRef](#)] [[PubMed](#)]
23. Cheng, J.; Qi, X.; Li, M.; Chen, P.; Liu, G. Palladium-Catalyzed Intermolecular Aminocarbonylation of Alkenes: Efficient Access of β -Amino Acid Derivatives. *J. Am. Chem. Soc.* **2015**, *137*, 2480–2483. [[CrossRef](#)] [[PubMed](#)]
24. Mancuso, V.; Hootel , C. A new efficient synthesis of β -aminoketones via Δ^4 -isoxazolines. *Tetrahedron Lett.* **1988**, *29*, 5917–5918. [[CrossRef](#)]
25. Tramontini, M. Advances in the chemistry of Mannich bases. *Synthesis* **1973**, *1973*, 703–775. [[CrossRef](#)]
26. Arend, M.; Westermann, B.; Risch, N. Modern Variants of the Mannich Reaction. *Angew. Chem. Int. Ed.* **1998**, *37*, 1044–1070. [[CrossRef](#)]
27. Filho, J.F.A.; Lemos, B.C.; de Souza, A.S.; Pinheiro, S.; Greco, S.J. Multicomponent Mannich reactions: General aspects, methodologies and applications. *Tetrahedron* **2017**, *73*, 6977–7004. [[CrossRef](#)]
28. List, B. The Direct Catalytic Asymmetric Three-Component Mannich Reaction. *J. Am. Chem. Soc.* **2000**, *122*, 9336–9337. [[CrossRef](#)]
29. Rossi, D.; Rui, M.; Di Giacomo, M.; Schepmann, D.; W nsch, B.; Monteleone, S.; Liedl, K.R.; Collina, S. Gaining in pan-affinity towards sigma 1 and sigma 2 receptors. SAR studies on arylalkylamines. *Bioorg. Med. Chem.* **2017**, *25*, 11–19. [[CrossRef](#)] [[PubMed](#)]

30. Marra, A.; Rossi, D.; Pignataro, L.; Bigogno, C.; Canta, A.; Oggioni, N.; Malacrida, A.; Corbo, M.; Cavaletti, G.; Peviani, M.; et al. Toward the identification of neuroprotective agents: G-scale synthesis, pharmacokinetic evaluation and CNS distribution of (R)-RC-33, a promising SIGMA1 receptor agonist. *Future Med. Chem.* **2016**, *8*, 287–295. [CrossRef] [PubMed]
31. Rui, M.; Rossi, D.; Marra, A.; Paolillo, M.; Schinelli, S.; Curti, D.; Tesei, A.; Cortesi, M.; Zamagni, A.; Laurini, E.; et al. Synthesis and biological evaluation of new aryl-alkyl(alkenyl)-4-benzylpiperidines, novel Sigma Receptor (SR) modulators, as potential anticancer-agents. *Eur. J. Med. Chem.* **2016**, *124*, 649–665. [CrossRef] [PubMed]
32. Rossi, D.; Urbano, M.; Pedralia, A.; Serra, M.; Zampieri, D.; Mamolo, M.G.; Laggner, C.; Zanette, C.; Florio, C.; Schepmann, D.; et al. Design, synthesis and SAR analysis of novel selective σ_1 ligands (Part 2). *Bioorg. Med. Chem.* **2010**, *18*, 1204–1212. [CrossRef] [PubMed]
33. Cobos, E.J.; del Pozo, E.; Baeyens, J.M. Irreversible blockade of sigma-1 receptors by haloperidol and its metabolites in guinea pig brain and SH-SY5Y human neuroblastoma cells. *J. Neurochem.* **2007**, *102*, 812–825. [CrossRef] [PubMed]
34. Albayrak, Y.; Hashimoto, K. Sigma-1 Receptor Agonists and Their Clinical Implications in Neuropsychiatric Disorders. *Adv. Exp. Med. Biol.* **2017**, *964*, 153–161. [CrossRef] [PubMed]
35. Blicke, F.F. Mannich Reaction. *Org. React.* **1942**, *1*, 303–341.
36. Azzolina, O.; Collina, S.; Urbano, M.; Fata, E.; Loddo, G.; Linati, L.; Lanza, E.; Barbieri, A. Highly diastereoselective synthesis of enantiopure naphthylaminoalcohols with analgesic properties. *Chirality* **2006**, *18*, 841–848. [CrossRef] [PubMed]
37. Lehmann, E.; Pilotti, Å.; Luthman, K. Efficient large scale microwave assisted Mannich reactions using substituted acetophenones. *Mol. Divers.* **2003**, *7*, 145–152. [CrossRef] [PubMed]
38. Kabalka, G.W.; Zhou, L.L.; Wang, L.; Pagni, R.M. A microwave-enhanced, solventless Mannich condensation of terminal alkynes and secondary amines with para-formaldehyde on cuprous iodide doped alumina. *Tetrahedron* **2006**, *62*, 857–867. [CrossRef]
39. Kidwai, M.; Bhatnagar, D.; Mishra, N.K.; Bansal, V. CAN catalyzed synthesis of β -amino carbonyl compounds via Mannich reaction in PEG. *Catal. Commun.* **2008**, *9*, 2547–2549. [CrossRef]
40. Flynn, G.A.; Lee, S.A.; Faris, M.; Brandt, D.W.; Chakravarty, S. Preparation of Aryl Ketone Derivatives as Intracellular Kinase Inhibitors. U.S. Patent WO 2007136790 A2, 27 November 2007.
41. Jie, X.; Shang, Y.; Zhang, X.; Su, W. Cu-Catalyzed Sequential Dehydrogenation-Conjugate Addition for β -Functionalization of Saturated Ketones: Scope and Mechanism. *J. Am. Chem. Soc.* **2016**, *138*, 5623–5633. [CrossRef] [PubMed]
42. Istanbulu, H.; Erzurumlu, Y.; Kirmizibayrak, P.B.; Erciyas, E. Evaluation of Alkylating and Intercalating Properties of Mannich Bases for Cytotoxic Activity. *Lett. Drug Des. Discov.* **2014**, *11*, 1096–1106. [CrossRef]
43. Debernardis, J.F.; Kerkman, D.J.; Zinkowski, R.P. Preparation of Substituted (1-aryl-3-piperazin-1'-yl)Propanone Antibiotics, Antimycotics and Antineoplastics. U.S. Patent 6,214,994B1, 10 April 2001.
44. Yamada, T.; Sakamoto, K.; Watanabe, K.; Nakano, Y. Process for the Preparation of 1-(2-Thienyl)-3-alkylaminopropanols. U.S. Patent WO 2006104249 A1, 5 October 2006.
45. Mikoshiba, K.; Hamada, K.; Terauchi, A.; Ozaki, S.; Goto, J.I.; Ebisui, E.; Suzuki, A. Transglutaminase-Induced Abnormal Protein Crosslinking Inhibitors Containing Ketone Compounds and Use Thereof. U.S. Patent WO 2011055561 A1, 12 May 2011.

Sample Availability: Samples of the compounds are available from the authors.



© 2018 by the authors. Licensee MDPI, Basel, Switzerland. This article is an open access article distributed under the terms and conditions of the Creative Commons Attribution (CC BY) license (<http://creativecommons.org/licenses/by/4.0/>).

Paper 3



Contents lists available at ScienceDirect

European Journal of Medicinal Chemistry

journal homepage: <http://www.elsevier.com/locate/ejmech>

Research paper

Identification of dual Sigma1 receptor modulators/ acetylcholinesterase inhibitors with antioxidant and neurotrophic properties, as neuroprotective agents



Marta Rui^a, Giacomo Rossino^a, Stefania Coniglio^a, Stefania Monteleone^{b, c},
Arianna Scuteri^d, Alessio Malacrida^d, Daniela Rossi^a, Laura Catenacci^a, Milena Sorrenti^a,
Mayra Paolillo^a, Daniela Curti^e, Letizia Venturini^f, Dirk Schepmann^g,
Bernhard Wünsch^g, Klaus R. Liedl^b, Guido Cavaletti^d, Vittorio Pace^h, Ernst Urban^h,
Simona Collina^{a, *}

^a Department of Drug Sciences, Medicinal Chemistry, Pharmaceutical Technology and Pharmacological Sections, University of Pavia, Viale Taramelli 6 and 12, 27100 Pavia, Italy

^b Institute of General, Inorganic and Theoretical Chemistry, University of Innsbruck, Innrain 80-82, 6020 Innsbruck, Austria

^c Department of Pharmaceutical Chemistry, Philipps-University Marburg, Marbacher Weg 6, 35032 Marburg, Germany

^d School of Medicine and Surgery, University Milano-Bicocca, Via Cadore 48, 20900 Monza, Italy

^e Department of Biology and Biotechnology "L. Spallanzani", Lab. of Cellular and Molecular Neuropharmacology, University of Pavia, Via Ferrata 9, 27100 Pavia, Italy

^f Department of Internal Medicine and Therapeutics, University of Pavia, Via Taramelli 24, 27100 Pavia, Italy

^g Institute of Pharmaceutical and Medicinal Chemistry, University of Muenster, Correnstrasse 48, 48149, Muenster, Germany

^h Department of Pharmaceutical Chemistry, University of Vienna, Althanstrasse 14, 1090 Vienna, Austria

ARTICLE INFO

Article history:

Received 14 June 2018

Received in revised form

3 September 2018

Accepted 4 September 2018

Available online 8 September 2018

Keywords:

Neuroprotective agents

Sigma 1 receptor

Acetylcholinesterase inhibitors

Antioxidant properties

Neurotrophic properties

ABSTRACT

In this manuscript we report on the design, synthesis and evaluation of dual Sigma 1 Receptor (S1R) modulators/Acetylcholinesterase (AChE) inhibitors endowed with antioxidant and neurotrophic properties, potentially able to counteract neurodegeneration. The compounds based on arylalkylaminoketone scaffold integrate the pharmacophoric elements of RRC-33, a S1R modulator developed by us, donepezil, a well-known AChE inhibitor, and curcumin, a natural antioxidant compound with neuroprotective properties. A small library of compounds was synthesized and preliminary *in vitro* screening performed. Some compounds showed good S1R binding affinity, selectivity towards S2R and N-Methyl-D-Aspartate (NMDA) receptor, AChE relevant inhibiting activity and are potentially able to bypass the BBB, as predicted by the *in silico* study. For the hits **10** and **20**, the antioxidant profile was assessed in SH-SY5Y human neuroblastoma cell lines by evaluating their protective effect against H₂O₂ cytotoxicity and reactive oxygen species (ROS) production. Tested compounds resulted effective in decreasing ROS production, thus ameliorating the cellular survival. Moreover, compounds **10** and **20** showed to be effective in promoting the neurite elongation of Dorsal Root Ganglia (DRG), thus demonstrating a promising neurotrophic activity. Of note, the tested compounds did not show any cytotoxic effect at the concentration assayed. Relying on these encouraging results, both compounds will undergo a structure optimization program for the development of therapeutic candidates for neurodegenerative diseases treatment.

© 2018 Elsevier Masson SAS. All rights reserved.

1. Introduction

The progressive loss of structure and/or function of neurons, within the Central Nervous System (CNS), is the prototypical event leading to neurodegeneration, which is an aspect underpinning a

* Corresponding author.

E-mail address: simona.collina@unipv.it (S. Collina).

heterogeneous group of disorders [1,2]. The World Health Organization (WHO) recently reported that neurodegenerative diseases, i.e. Alzheimer's (AD), Parkinson's (PD), Amyotrophic Lateral Sclerosis (ALS) and Multiple Sclerosis (MS), are one of the main causes of death worldwide, causing the death of 6.8 million people annually (Fig. 1) [3–5]. Moreover, the treatment options of neurodegenerative diseases are meagre, since only few molecules able to attenuate the devastating outcome and/or to limit the progression of the diseases are available and thus, there is an urgent need of effective therapies [6]. Neurodegenerative disorders have a multifactorial origin, being associated with both environmental factors, such as smoking, stress and the use of pesticides, and specific genetic variations, leading to alteration of several molecular cascades (Fig. 1) [7,8]. Dysfunction of neurotransmitter pathways (i.e. acetylcholine or dopamine systems) can sometimes occur together with abnormal structure and/or accumulation of proteins – i.e. tau protein hyperphosphorylation, β -amyloid accumulation, further aggravating the pathological condition [9–12]. An important hallmark of neurodegeneration conditions is an over-production of Reactive Oxygen Species (ROS) due to alterations of mitochondrial respiratory chain activity [13,14].

In our continuing efforts towards the design and development of new molecular entities able to counteract neurodegeneration, some years ago we designed and characterized a wide series of Sigma 1 Receptor (S1R) modulators [15]. These compounds may have a great potential as neuroprotective agents, since under pathological conditions S1R operates as a chaperone modulating different proteins, restoring the calcium homeostasis and controlling the generation of ROS, thus preventing cellular damage [16–23]. Accordingly, S1R modulators are able to simultaneously address more than one pathological event and then they represent a good therapeutic opportunity for treating neurodegenerative disorders. At the same time, it is worth noting that the multifactorial origin of such disorders prompted the interest of the scientific community toward the so-called multi-target drugs (MTDs) and along the years, a number of heterogeneous MTDs have been developed combining drugs already used in therapy with several scaffolds endowed with different activities [24–27]. With these premises in mind and in the attempt of obtaining molecules able to modulate S1R, to act as acetylcholinesterase (AChE) inhibitors and endowed with antioxidant properties, herein we report on a new series of dual ligands, designed by focussing on RRC-33, donepezil and curcumin (Cur) (Fig. 2), as reference molecules.

In details, RRC-33 is our most promising compound, showing an excellent affinity and selectivity towards S1R over S2R (Ki S1 = 1.8 ± 0.1 nM; Ki S2 = 45 ± 16 nM) and a high metabolic stability in several biological matrices [28]. Furthermore, it is able to promote neurite differentiation and elongation in rat Dorsal Root Ganglia (DRG) experimental model [29]. Donepezil is an AChE inhibitor able to restore the physiological amount of acetylcholine and it is commonly used in therapy for counteracting the cognitive impairment, a common feature of neurodegenerative diseases [30,31], while Cur (Fig. 2) is an effective ROS scavenging compound [32]. It is the main yellow-colored pigment of *Curcuma longa*, historically employed in Ayurvedic medicine [33]. Although its numerous drawbacks linked to its solubility, instability in physiological fluids, and low bioavailability [34], Cur possesses a wide spectrum of action including antioxidant activities, which may be useful to counteract neurodegenerative diseases [35–37].

Thus, combining the structural features of RRC-33, donepezil and Cur (Fig. 2), we designed a new series of compounds. The newly synthesized compounds were investigated in terms of SRs affinity and inhibitory activity toward AChE enzyme and their mode of interaction with S1R and AChE was *in silico* studied. Furthermore, their *in silico* ADME parameters have been evaluated to assess their ability to cross the blood brain barrier (BBB) and reach the CNS. Lastly, the antioxidant profile and neurotrophic activity of the most interesting derivatives were evaluated.

2. Results and discussion

2.1. Chemistry

We prepared a new compound series, characterized by an arylalkylamineketone scaffold with three elements of structural diversity, i.e. the aromatic ring, the aminic moiety and the length of the linker between the aromatic and the aminic portions (Fig. 2). The conceived arylalkylamineketone scaffold allowed improving synthetic feasibility and chemical tractability by removal of chiral center present in the inspiring S1R modulator RRC-33.

Compounds were synthesized by following the general synthetic route outlined in Scheme 1 and Scheme 2.

A divergent synthesis has been adopted to access the desired products in good yields and in few steps. Target compounds 7–30 were obtained *via* Weinreb ketone synthesis from key intermediates 4a, 5a-c and 6a, which in turn were prepared through:

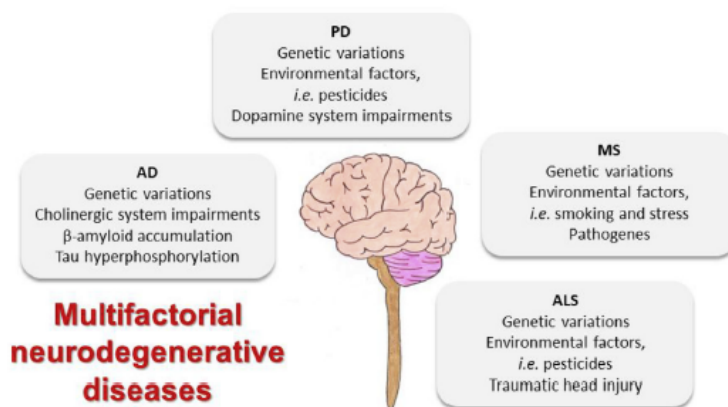


Fig. 1. Some aetiological factors that promote multifactorial neurodegenerative diseases.

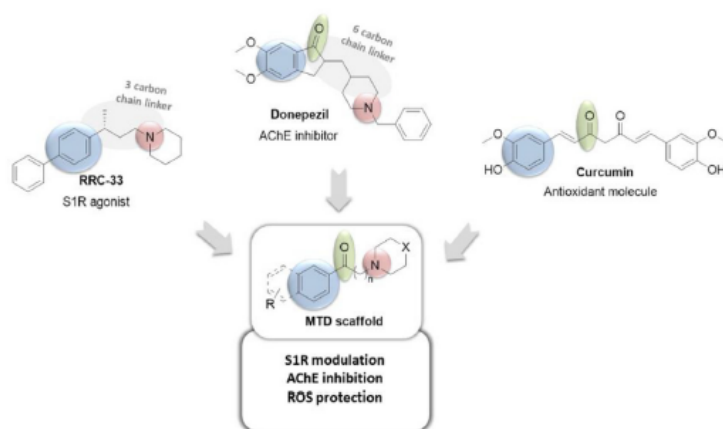
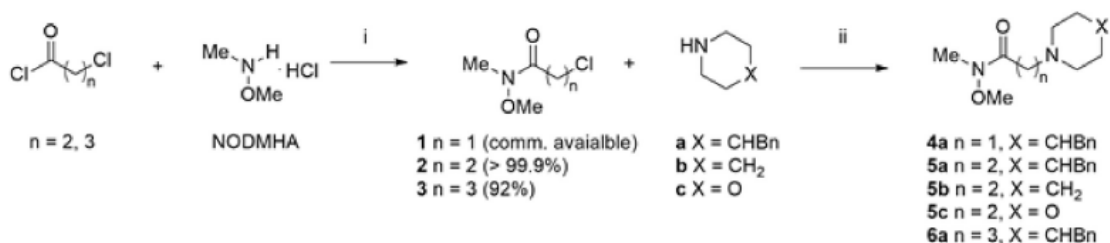
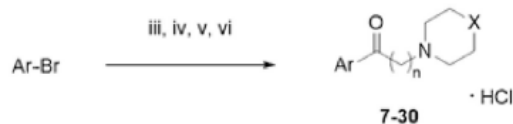


Fig. 2. MTD scaffold merges the key functional groups of S1R agonists, AChE inhibitors and curcumin.



Scheme 1. Weinreb amide formation and nucleophilic substitution. Reagents and reaction conditions: i) K_2CO_3 , $\text{Et}_2\text{O}/\text{H}_2\text{O}$, rt.; ii) K_2CO_3 , ACN, rt.



Cmpd	Ar	n	X	Yield (%)	Cmpd	Ar	n	X	Yield (%)
7	phenyl	1	CHBn	40	19	naphth-2-yl	2	CH ₂	23
8	4-methoxyphenyl			37	20	4-biphenyl			35
9	3-methoxyphenyl			48	21	Phenyl			30
10	naphth-2-yl			54	22	4-methoxyphenyl			38
11	6-methoxynaphth-2-yl			49	23	naphth-2-yl	41		
12	4-biphenyl	33	24	4-biphenyl	37				
13	Phenyl	2	CHBn	28	25	phenyl	3	CHBn	31
14	4-methoxyphenyl			25	26	4-methoxyphenyl			30
15	naphth-2-yl			22	27	3-methoxyphenyl			33
16	4-biphenyl			22	28	naphth-2-yl			41
17	phenyl	2	CH ₂	29	29	6-methoxynaphth-2-yl	30	4-biphenyl	25
18	4-methoxyphenyl			27	30	4-biphenyl			26

Scheme 2. Lithiated arene formation and quenching with the corresponding Weinreb amide. Reagents and reaction conditions: iii) $t\text{-BuLi}$, THF, -78°C ; iv) Weinreb amide (**4a**, **5a-c** or **6a**), -78°C ; v) H_2O ; vi) HCl (1M in Et_2O), Et_2O .

i) the Weinreb amide formation and ii) a nucleophilic substitution (Scheme 1). Specifically, the starting acyl chlorides were easily converted into the desired β and γ chloro Weinreb amides, using the amine *N,O*-dimethylhydroxylamine hydrochloride (NODMHA), in the presence of a basic reagent, K_2CO_3 . The reactions performed in a mixture of ether and water (in equal amount) were stirred for 24 h. A simple extraction provided compounds 2–3 in excellent yields. This reaction was not applied for achieving intermediate 1, since it is commercial available. Accordingly, the Weinreb amides were subjected to a nucleophilic substitution, exploiting the chlorine as good leaving group. The reaction performed with the corresponding secondary amine (a-c), needed 24 h and the presence of K_2CO_3 as base to yield the crude α , β and γ amino Weinreb amides 4a, 5a-c and 6a. An acid/base extraction was essential to obtain the key intermediates, presenting 1 or 2 carbonaceous units, in modest/good yields. Conversely, 6a required a purification through flash chromatography, since the starting material conversion into the desired products furnished some side products. Lastly, the smooth bromo-lithium exchange on the aryl bromide afforded the lithiated arene that, upon quenching with 4a, 5a-c and 6a, gave the desired ketones 7–30 in good yields, after an adequate purification (Scheme 2). Specifically, the corresponding aryl bromide were lithiated, in anhydrous THF at $-78^\circ C$ with *t*-butyl lithium. The subsequent addition of compounds 4a, 5a-c and 6a and quenching with H_2O led to isolate crude compounds, which were purified through flash chromatography. All the potential MTD molecules 7–30 were obtained in a sufficient amount and with the appropriate degree of purity, as confirmed by IR, 1H NMR, ^{13}C NMR and UPLC-MS analysis, as well as thermal analysis, for the following biological investigations. Preliminary solid-state characterization by DSC analysis revealed that all the compounds are crystalline anhydrous phases, with a well-defined melting point followed by sample decomposition, with the only exception of 28 which crystallized as solvatomorph.

2.2. Physicochemical and pharmacokinetic predictions

Molecular descriptors were computed to predict six physicochemical properties of each compound: (a) partition coefficient (ClogP); (b) distribution coefficient at pH 7.4 (ClogD); (c) molecular weight (MW); (d) topological polar surface area (TPSA); (e) number of hydrogen-bond donors (HBDs); and (f) acid dissociation constant (pKa). These parameters are the most representative features to determine the ADME profile, as well as the ability of a compound in reaching the CNS [38]. According to Wager *et al.* model, which is a well-established procedure broadly employed in academic and in industrial settings [39], a score – ranging from 0 to 1 – is attributed to each property, applying a monotonic decreasing function for ClogP, ClogD, MW, pKa, and HBD, whereas a hump function for TPSA (Table S11). The summation of all these values gives access to a final score (0–6), which can be defined as follows: i) 0–2, compound is unable to cross the BBB; ii) 2–5, compound may reach the CNS; iii) 5–6, compound effectively crosses the BBB [39]. Accordingly, we exploited this model to calculate the potential ability of compounds 7–30 in reaching the CNS (Table 1). For comparative purposes, we compared the obtained results with those of RRC-33 and donepezil (Table 1, Table S11), for which is known their good CNS distribution.

The tabulated results show that only four compounds (18 and 21–23) possess a score higher than 5, whereas the other ones possess values ranging from 2 to 5. Noteworthy, compounds 9, 14, 17, 19, 20 and 24 display a good score (>4). Altogether these values reveal that all molecules 7–30 are able to reach the CNS. Moreover, reference compounds RRC-33 and donepezil show good scores (2.57 and 4.41, respectively) and this behaviour is in line with their

in vivo CNS distribution, which was extensively confirmed by experimental data and clinical use.

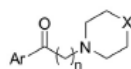
2.3. Binding affinity, enzymatic studies, and structure-activity relationship (SAR) exploration

S1R and S2R binding site affinities of compounds 7–30 were measured through competition experiments, using radioligands. The assay for S1R was performed using homogenized guinea pig cerebral cortex membranes, in the presence of [3H]-(+)-pentazocine, as a potent and selective S1R radioligand. Nonspecific binding values were determined using non-radiolabeled (+)-pentazocine and haloperidol in excess (see experimental section). Conversely, homogenized rat liver membranes were adopted to evaluate the S2R binding values, employing [3H]-DTG – a non-selective S2R radioligand – and, non-tritiated (+)-pentazocine to mask the S1R. Moreover, a high concentration of non-tritiated DTG was used to determine nonspecific binding values. Compounds with high affinity were tested twice. For compounds with low SR affinity, only one measure was performed. The SR affinities of compounds 7–30 towards both S1R and S2R are presented in Table 1.

Similar to reference compound RRC-33, almost all compounds possess a weak affinity for S2R, but only 12 compounds (8, 10, 13–14, 18, 20, 23–28) over 24 present a K_i S1R lower than 50 nM. Altogether these results allow to draw some SAR considerations: i) the 4-methoxyphenyl ring seems to play a key role in the interaction with S1R, in fact molecules 8, 14, 18 and 26 belonging to the three different *n* series present a good K_i values (27, 11, 8 and 2.9 nM, respectively); ii) a longer linker guarantees the S1R binding, as it is evident in the 4-benzylpiperidine derivatives (7–16 and 25–30), which follow $1 = 2 < 3$ *n*-scale in the interaction with S1R; iii) the length of the linker can limit the selectivity, indeed compounds belonging to the *n*=3 series present a S2R/S1R ranging from 1.6 to 6.8 and thus, they may be considered as pan-SR modulators. Lastly, arylalkylamineketones possess a lower S1R affinity than RRC-33 (K_i S1R = 1.8 nM), this difference may be associated to the presence of a novel pharmacophoric element, which can limit the interaction with the molecular target.

At the same time, we extended our study on the *N*-Methyl-D-Aspartate (NMDA) receptor, an ionotropic glutamate receptor, constituted by two subunits GluN1 and GluN2. NMDA receptor plays a relevant role in synaptic plasticity and synapse formation underlying memory and learning. An alteration of this neurotransmitter pathway causes an accumulation of glutamate in the synaptic terminations that promotes the GluN2 activation and thus, the long-term signal enhancement between two neurons. Moreover, the pathological triad, that involves mitochondrial dysfunction, loss of neuronal structures integrity, and disruption of excitation–transcription coupling, may be triggered. Accumulating evidence suggests that a negative modulation of this molecular target may contribute in slowing the progression of neuropathies [40]. Relying on these considerations, we evaluated the affinity of 7–30 towards GluN2 subunit of NMDA. Competitive binding assays on membrane extracts of L cells (tk-), stably transfected with a vector containing the genetic information of GluN1a and GluN2B subunits, were performed, using [3H]-ifenprodil, a selective and potent GluN2 inhibitor radioligand. Compounds with high affinity were tested three times. For compounds with low NMDA affinity, only one measure was performed. The results are reported in Table 1 and they show that 7–30 possess a weak affinity towards NMDA receptor, with the exception of compounds 8–10, 13, 25–29, which show a $K_i < 150$ nM. These results highlight that the affinity towards NMDA receptor depends on the length of the spacer, in fact compounds belonging to the *n*=3 series present good affinity towards GluN2 (20–117 nM). Conversely, molecules

Table 1
Scores related to the potential ability of compounds 7–30 in crossing the BBB. Binding affinities towards NMDA, S1R and S2R and S1R selectivity (Ki S2R/Ki S1R). AChE inhibition activity and IC₅₀ of the most promising compounds.



Cmpd	Score	Ki S1R (nM)	Ki S2R (nM)	S2R/S1R	Ki NMDA (nM)	% of inhibition (50 μM)	IC ₅₀ (μM)
7	3.47	75 ± 3.6	2300	30.7	215	5.65 ± 0.10	^b
8	3.57	27 ± 1.2	2000	74	16 ± 1.2	8.21 ± 0.06	^b
9	4.04	131 ± 15	1500	11.5	11 ± 0.4	75.50 ± 0.02	32.82 ± 1.77
10	3.02	27 ± 1.8	802	30	139 ± 11	87.40 ± 6.39	9.13 ± 2.24
11	3.42	286	1400	4.9	>1000	48.24 ± 0.02	^b
12	2.97	340	>1000	—	>1000	11.41 ± 0.04	^b
13	3.46	16 ± 1.8	5800	363	39 ± 2.1	42.30 ± 0.21	^b
14	4.09	11 ± 2.2	2400	218	198	64.10 ± 5.58	22.02 ± 9.12
15	2.75	211	6200	29.4	>1000	85.50 ± 0.02	18.55 ± 7.72
16	2.61	167	3900	23.4	>1000	55.04 ± 6.69	^b
17	4.80	171	749	4.4	>1000	^a	^a
18	5.30	7.9 ± 0.9	2100	256	1700	42.07 ± 0.04	^b
19	4.35	2.2 ± 0.7	178 ± 12	81	>1000	45.20 ± 7.07	^b
20	4.18	15 ± 1.1	462	30.8	>1000	64.80 ± 0.35	13.08 ± 6.31
21	5.48	606	>1000	—	>1000	10.75 ± 0.01	^b
22	5.94	301	>1000	—	>1000	59.70 ± 2.24	^b
23	5.28	9.0 ± 0.7	>1000	—	>1000	24.62 ± 0.05	^b
24	4.91	2.9 ± 0.3	>1000	—	723	12.20 ± 1.72	^b
25	3.17	9.0 ± 0.5	47 ± 2	5.2	39 ± 1.1	74.80 ± 3.56	13.07 ± 2.10
26	3.79	31 ± 4.2	111 ± 8	6.8	96 ± 2.7	80.01 ± 0.02	12.80 ± 1.79
27	3.74	17 ± 2.2	43 ± 1.9	2.5	49 ± 1.8	71.80 ± 1.60	7.64 ± 2.07
28	2.50	24 ± 3.4	58 ± 2.3	2.4	26 ± 0.9	^a	^a
29	2.73	68 ± 1.7	107 ± 10	1.6	20 ± 0.7	92.60 ± 0.03	4.28 ± 0.23
30	2.32	135 ± 11	704	5.2	96 ± 2.6	84.10 ± 0.02	13.94 ± 2.15
RRC-33	2.57	1.8 ± 0.1	45 ± 16	25	>1000	4.82 ± 2.15	^a
Donepezil	4.41	14.6 ^c	—	—	—	99.4 ± 0.01	0.012 ± 0.01
Ifenprodil	—	125 ± 24	98 ± 34	0.8	10 ± 0.7	—	—

Values are expressed as mean ± SEM of three experiments. Compounds with high affinity were tested three times. For compounds with low SR and NMDA affinity (>150 nM), only one measure was performed.

^a Compounds were not evaluated for solubility issues.

^b Inhibition % < 60% at a concentration of 50 μM.

^c Data taken from Ref. [43].

with 3 carbonaceous units between the aromatic portion and the aminic moiety are endowed with a negligible affinity for the ionotropic glutamate receptor, with the exception of compound 13 (Ki = 39 ± 2.1 nM). Lastly, molecules 7–12 show an intermediate behaviour, presenting a moderate binding affinity. These results did not discourage us, since the affinity towards NMDA receptor is not a necessary condition to define our compounds as MTDs. In fact, as aforementioned S1R can modulate the activity of several client proteins and NMDA receptor is a molecular target of S1R.

Compounds 7–30 were then tested for defining their potential to inhibit AChE. A spectrophotometric procedure was adopted, applying suitable modifications to the original Ellman's method [41,42]. An initial screening was performed, employing the target compounds at a concentration of 50 μM. The results of this assay are summarized in Table 1. Noteworthy, 10 compounds (9–10, 14–15, 20, 25–27, 29–30) over 24 possess a percentage of inhibition ≥ 60%, whereas only five (7–8, 12, 21 and 24) can be considered inactive since they present a percentage of inhibition < 20%.

In the light of these data, for the most promising compounds, showing at a concentration of 50 μM an inhibition percentage more than 60%, the IC₅₀ values were determined. Interestingly, all the tested compounds possess an IC₅₀ lower than 25 μM, with the only exception of 9 (IC₅₀ = 32.88 ± 1.77 μM) (Table 1). In particular, 27 and 29 result the most promising AChE inhibitors, with an IC₅₀ of 7.64 ± 2.07 and 4.28 ± 0.23 μM, respectively.

From a structural point of view, the most interesting compounds are characterized by the presence of 4-benzylpiperidine, as aminic portion, with the exception of compound 20 that is characterized by a piperidine moiety. Moreover, molecules belonging to the n = 3 series (25–27, 29–30) show greater anti-AChE effect; this inhibitory activity progressively decreases for β- and α-amino ketones, respectively (9–10, 14–15 and 20). Basing on the obtained results we can conclude that both the 4-benzylpiperidine portion and the linker length have a crucial role for the anti-AChE activity, whereas no relation between the aromatic portion and the anti-AChE activity has been evidenced. Interestingly, RRC-33, the S1R reference compound, demonstrates no inhibition property against AChE (percentage of inhibition < 5%).

2.4. Molecular dynamic simulations and docking studies

Root mean square deviation (RMSD) values of S1R entire trimeric complex, monomer and binding pocket indicate that the protein structure is stable during MD simulations (RMSD of Cα atoms below 2 Å). The S1R structure in complex with 4-IBP was stable and no conformational changes occurred. The ligand formed H-bonds with the E172 for almost the entire simulation time (above 92%) but only in two binding pockets. In the third one, instead, the interaction was replaced by H-bonds with water molecules. The most representative cluster (occurring 41% of the simulation time) slightly differs from the others (average distance of 1.11 Å).

However, the second cluster has also occurrence of 35% and the RMSD between them is 1.34 Å. They differ from the starting coordinates of 1.53 and 1.56 Å, respectively.

The most representative cluster was used to dock known (training set) and new (test set) S1R ligands. In particular, the best docking results were obtained with rigid docking without any constraints (AUC 0.78). However, not all active compounds were docked to the binding pocket: 4 out of 32 agonists were not successful, probably because they bind to a different conformation of the receptor. Indeed, results did not improve by flexible docking (AUC 0.53), and there is no crystal structure of the receptor in the active state that could be used to specifically investigate agonists.

Nevertheless, all active agonists formed ionic interactions with E172 and D126 due to their positively charged amine group. By contrast, low-ranked ligands lacked of these key residue contacts. Moreover, further amino acids (W89 and F107) were often involved in protein-ligand interactions: for instance, these residues were close to the protonated amine and eventually formed π -cation interactions. Furthermore, Y120 and H154 can form π - π stacking with ligand aromatic rings.

The docking pose of RRC-33 shows that the positively charged nitrogen atom forms ionic interactions with E172 and D126, and cation- π interactions with F107 (Fig. 3). Moreover, hydrophobic contacts (not displayed) occur between the aromatic rings and

surrounding amino acids (M93, L95, L105). The test set of new derivatives (7–30) was docked and all molecules conserved key interactions with the receptor as for the training set. Nevertheless, larger molecules with four rings (such as 4-biphenyl derivatives 12, 16 and 30) did not fit well into the binding pocket in comparison with smaller compounds. Indeed, either the biphenyl moiety clashed with Y206 or the benzyl ring did not have enough space on the opposite side of the pocket. In contrast, molecules 17, 21 and 22 that have only two rings lacked important hydrophobic contacts resulting in low binding affinity. In conclusion, compounds with three rings, which conserved H-bond and hydrophobic interactions, seem to be the most interesting ones. In Fig. 3, compounds 10 and 20 are reported by way of example.

All new derivatives were docked also to AChE. Flexible docking on AChE X-ray structure, both including and excluding water molecules, gave the best results. AUC was 0.71 in both cases, indicating that the model was able to distinguish between active compounds and decoys. The top-ranked ligands formed π - π and π -cation interactions with W86, W286, Y337 and Y341 residues of the binding pocket, as in the donepezil-bound crystal structure (Fig. 3). Also, the H-bond with the backbone of F295 was mostly conserved. In particular, the presence of the carbonyl enhanced the binding when *n* was equal to 3 carbon atoms (compounds 25–30), which is the optimal distance to keep the ionic interaction of the amine and

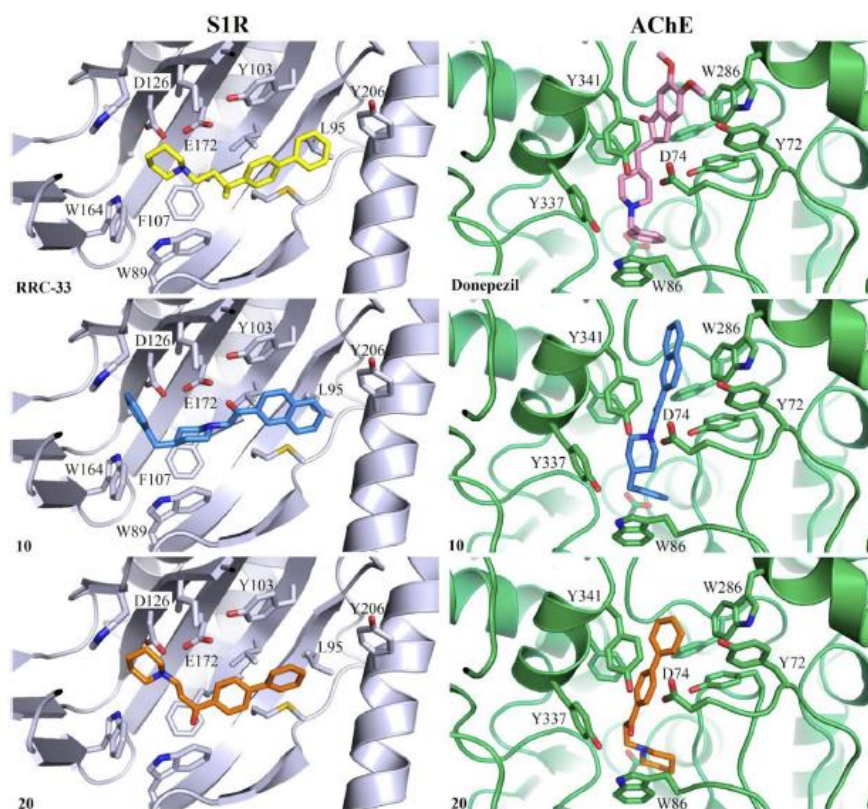


Fig. 3. Docking poses of reference compounds (RRC-33 and donepezil) and of 10 and 20 on S1R (on the left side) and AChE (on the right side) binding pockets. Hydrogen atoms are not displayed. Ligands and key residues are shown as sticks.

the H-bond to F295. Instead, not all compounds formed hydrogen bond interactions with the hydroxyl group of Tyr amino acids (compound **20**). For instance, the docking pose of compound **20** showed that the charged amine could fit into a deeper binding pocket, where it could form interactions with E202 (Fig. 3). This was possible only for unsubstituted piperidine rings. Furthermore, the naphthalene ring (compounds **10** and **29**) enhanced the π - π stacking with W286.

In summary, docking poses suggested that the charged amine plays a key role not only for binding to negatively charged amino acids, but also to aromatic residues through cation- π interactions. The binding is strengthened by the presence of aromatic rings, which form hydrophobic and π - π interactions with both S1R and AChE ligand pockets. Several compounds among our new set of derivatives showed protein-ligand interaction patterns which are similar to reference compounds RRC-33 and donepezil, as shown in Fig. 3, where the docking poses of **10** and **20** are reported.

2.5. Antioxidant profile and neurotrophic activity

Basing on preliminary biological investigations compounds **8**, **10**, **13–14**, **18–20**, **23–28** with either S1R affinity or both good S1R affinity and relevant AChE inhibitory activity were selected for further evaluations.

2.5.1. Free radical scavenging (FRS) activity

FRS activity of **8**, **10**, **13–14**, **18–20**, **23–28** was determined by 2,2-diphenyl-1-picrylhydrazyl (DPPH) assay, and the results were compared to those of reference molecules RRC-33, donepezil and Cur. Stock solutions in EtOH of the tested compounds were prepared (5.0 mM). The DPPH absorbance was spectrophotometrically monitored at 515 nm and at a concentration of 465 μ M; inhibition percentages are reported in Table S12. These preliminary results demonstrated that compounds **13–14**, **18–20**, **23–28**, as well as RRC-33 and donepezil do not display significant antioxidant activity (values ranging from 2.8% up to 32%). Conversely, compounds **8** and **10** could be considered promising antioxidant molecules, since they show an FRS activity (>65%), comparable with the widely recognised Cur antioxidant activity. Accordingly, only molecules belonging to the $n = 1$ series possess intrinsic antioxidant properties, probably due to the methylene spacer adjacent to both carbonyl and amine moieties which stabilize the radical centre (Scheme 3) [44].

In the light of these data, the IC_{50} calculation of **8** and **10** was performed at four different concentrations (ranging from 465 to 45 μ M).

2.5.2. Cell viability and 2',7'-dichlorofluorescein diacetate (DCFDA) assays

Toxicity of **8**, **10**, **13–14**, **18–20**, **23–28** was assessed in SH-SY5Y neuronal cell line, at different concentrations, ranging from 10 to 50 μ M. The cell viability was evaluated through 3-(4,5-dimethylthiazol-2-yl)-5-(3-carboxymethoxyphenyl)-2-(4-sulfophenyl)-2H-tetrazolium (MTS) assay, after exposing cells to these compounds for 24 h and 48 h. The results are reported in Table 2. The tested compounds show a dose-dependent effect on SH-SY5Y cell lines (Homo Sapiens bone marrow neuroblastoma) at different exposure times. Moreover, these values show that almost

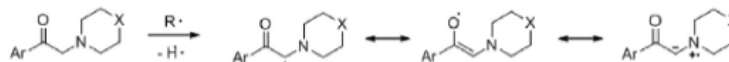
all molecules do not exhibit cytotoxic activities, with the exception of compound **23**, which decreases cell viability even at a 10 μ M concentration (77%). We speculated that this countertrend could be due to the presence of morpholine as aminic moiety. Furthermore, compounds belonging to the $n = 2$ series and presenting a piperidine portion show cytotoxic properties when they are administered for 48 h at a concentration of 25 μ M and 50 μ M. Noteworthy, molecules with a 9-atoms linker between the two aromatic portions do not alter the cell viability even if they are employed at high doses. Lastly, for comparative purpose, RRC-33, donepezil and Cur were subjected to MTS test. Also in this case, the results indicate the lack of toxicity. Considering the results obtained so far (good BBB score, good S1R affinity, high AChE inhibition percentage) compounds **10**, **14** and **20** were selected for a second screening aimed at calculating the IC_{50} value, by testing them at 6 different concentrations (ranging from 1 μ M to 100 μ M) for 24 and 48 h. Compounds **10** and **20** showed an IC_{50} higher than 20 μ M (24 h = 52 and 37, respectively; 48 h = 57 and 22, respectively). The viability trend is reported in Fig. 4.

The major intracellular ROS sources are complex I (NADH dehydrogenase ubiquinone-ubiquinone reductase) and complex III (ubiquinone cytochrome C reductase), both of them take part to the mitochondrial electron transport chain [45]. A low ROS level plays a crucial role in cellular pathways. Nevertheless, when the ROS concentration increases and overcomes the cellular antioxidant machinery, it can induce macromolecular damages (*i.e.* interaction with the DNA, proteins and lipids) and compromise the thiol redox circuits, promoting aberrant molecular cascades [46]. Considering that oxidative stress, induced by the increase of ROS intracellular concentration, is a driving issue in neurodegenerative diseases, we evaluated the ability of **10**, **14** and **20** and reference compounds in reducing ROS within SH-SY5Y cells, after an exposure to oxidative damages mediated by H_2O_2 . The assay provided the employment of DCFDA reagent, which diffuses within the cell and undergoes esterase-mediated de-acetylation. The so-obtained product is then subjected to oxidation by ROS, giving access to 2',7'-dichlorofluorescein, a high fluorescent molecule with adsorption and emission wavelength of 495 and 529 nm, respectively.

The compounds were tested at a concentration of 10 μ M in the presence of H_2O_2 (180 μ M) for 24 h. In parallel experiments, we evaluated the cell viability by MTS assay, to verify the lack of cytotoxicity under the same experimental conditions (Fig. 5). The results reveal that all compounds show a safe profile and thus they can be evaluated through fluorescent assay. As reported in Fig. 5, Cur possesses the ability to reduce ROS up to a 0%, whereas donepezil and RRC-33 show no antioxidant properties. On the basis of our data, **10** and **20** are able to promote ROS reduction up to 43% and 18% respectively and thus can be considered antioxidant molecules, whereas **14** resulted ineffective and it was abandoned.

2.5.3. Neurotrophic activity

Basing on our previous experience, we evaluated the neurotrophic effect of the most interesting compounds **10** and **20**, evaluating the neurite differentiation and elongation by using the straightforward model of Dorsal Root Ganglia (DRG) [29]. Briefly, DRG explants from E15 Sprague – Dawley rat embryos are able to sprout neurites when cultured with pro-differentiation agents, such as Nerve Growth Factor (NGF). The neurite elongation is promoted by neurotrophic drugs and blocked or slowed up by



Scheme 3. Proposed mechanism for the radical scavenging activity of $n = 1$ series compounds.

Table 2
Viability test at 24 h and 48 h.

Cmpd	24 h			48 h		
	10 μ M (%)	25 μ M (%)	50 μ M (%)	10 μ M (%)	25 μ M (%)	50 μ M (%)
8	103 \pm 0.03	98.4 \pm 0.05	87 \pm 0.03	85.5 \pm 0.12	69.3 \pm 0.03	52.5 \pm 0.02
10	107 \pm 0.05	104.2 \pm 0.04	81.3 \pm 0.03	89.5 \pm 0.02	77.6 \pm 0.04	48.4 \pm 0.01
13	93 \pm 0.01	48 \pm 0.01	49 \pm 0.01	106 \pm 0.17	44 \pm 0.04	36 \pm 0.04
14	99.9 \pm 0.01	63.9 \pm 0.04	56.5 \pm 0.05	97.4 \pm 0.02	50.2 \pm 0.05	44.7 \pm 0.01
18	119 \pm 0.02	86 \pm 0.03	63 \pm 0.01	104 \pm 0.08	49.4 \pm 0.06	43.4 \pm 0.01
19	98.6 \pm 0.04	66.4 \pm 0.01	65.4 \pm 0.01	70.3 \pm 0.02	42 \pm 0.01	40 \pm 0.03
20	104 \pm 0.06	95.4 \pm 0.01	64 \pm 0.05	95.9 \pm 0.03	49.3 \pm 0.04	44.7 \pm 0.03
23	77 \pm 0.04	48 \pm 0.01	49 \pm 0.01	79 \pm 0.04	38 \pm 0.06	37 \pm 0.04
24	100 \pm 0.01	73 \pm 0.01	83.3 \pm 0.08	100 \pm 0.06	66 \pm 0.03	62.4 \pm 0.01
25	100 \pm 0.04	100 \pm 0.02	87 \pm 0.01	96 \pm 0.02	95 \pm 0.05	54 \pm 0.02
26	100 \pm 0.01	100 \pm 0.04	84.4 \pm 0.01	97.3 \pm 0.02	87 \pm 0.04	61 \pm 0.01
27	100 \pm 0.03	100 \pm 0.01	98 \pm 0.01	94.8 \pm 0.05	85.6 \pm 0.03	65 \pm 0.01
28	80.2 \pm 0.04	86 \pm 0.01	86 \pm 0.07	77 \pm 0.01	57 \pm 0.01	61 \pm 0.01
RRC-33	100 \pm 0.03	100 \pm 0.03	86 \pm 0.04	84 \pm 0.01	77.1 \pm 0.01	57.3 \pm 0.01
Donepezil	100 \pm 0.01	99.3 \pm 0.02	94.7 \pm 0.01	94.3 \pm 0.01	80.4 \pm 0.01	64.4 \pm 0.02
Curcumin	100 \pm 0.01	76.5 \pm 0.01	71.5 \pm 0.01	100 \pm 0.01	58.7 \pm 0.01	59 \pm 0.02

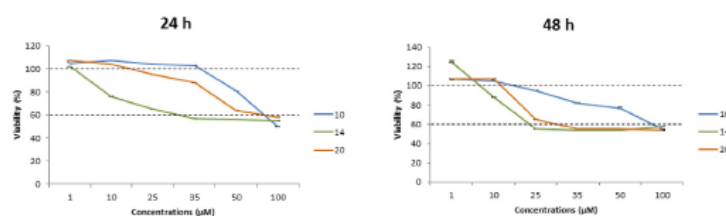


Fig. 4. Viability trends of compounds **10**, **14** and **20**, after 24 and 48 h of exposure.

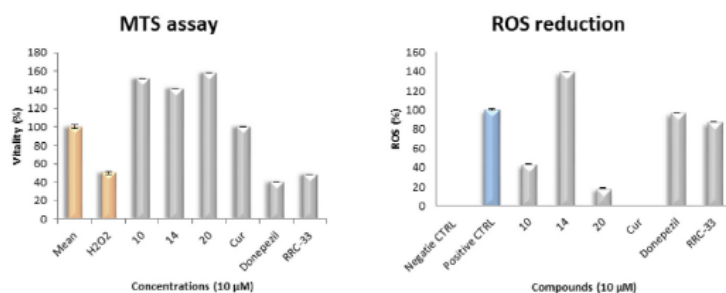


Fig. 5. ROS percentage evaluation after administration of compounds **10**, **14**, **20**, Cur, Donepezil and (R)-RC-33.

neurotoxic agents. Compounds **10** and **20** were tested at different concentration, after 24 and 48 h of exposure (Fig. 6 and Figures S11–S14). Interestingly, both compounds showed neurotrophic effect. In particular, best results were obtained for compound **10** at the concentration of 2.5 μ M, starting from 24 h of exposure and leading to an increase of the neurite length of about 15% with respect to the untreated control DRG. For compound **20**, the concentrations 5 μ M and 2.5 μ M resulted to be the most effective, both after 24 h and after 48 h of exposure, with an increase of neurite length of about 20% with respect to control DRG. For both compounds, none concentrations resulted neurotoxic, except at the concentration 10 μ M, which showed after 24 h of exposure an only transient neurotoxic effect, being disappeared after 48 h. The present results demonstrated the pro-differentiation properties of compounds **10** and **20**, thus confirming their neurotrophic effect.

3. Conclusion

In the present paper we discovered dual S1R modulators/AChE inhibitors endowed with antioxidant and neurotrophic properties. The adopted medicinal chemistry approach led to a novel series of compounds sharing the pharmacophoric requirements for interacting with both S1R and AChE, as confirmed by the molecular modelling study. Within the whole series, three compounds resulted endowed with considerable S1R affinity, good selectivity over S2R and AChE inhibition activity. Their effect on neuroblastoma cell (SH-SY5Y) survival was evaluated and the ROS damage was mimicked by exposing SH-SY5Y cells to H₂O₂. The results highlighted that only compounds **10** and **20** decrease ROS production, thus ameliorating the cellular survival and therefore, they were selected for further experimental investigations. To this

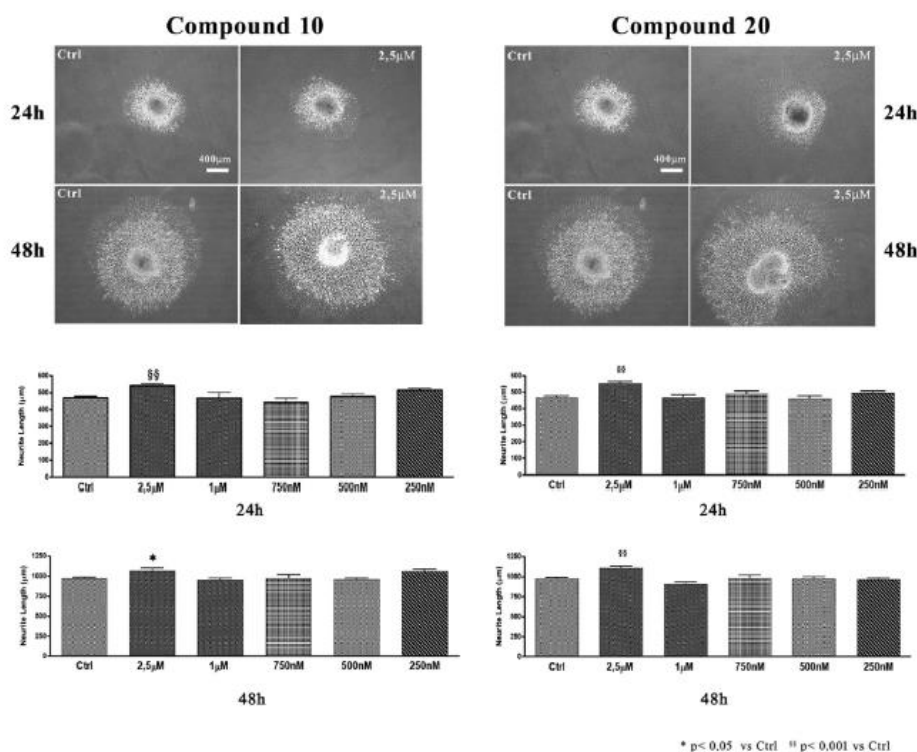


Fig. 6. Evaluation of Neurotrophic activity of compounds **10** and **20**, after 24h and 48h of exposure.

purpose, their effect on neurite outgrowth in DRG *in vitro* model was assessed and their neurotrophic role confirmed. Of note, the tested compounds did not show any cytotoxic effect at the concentration assayed.

Overall, our *hit* compounds **10** and **20** combine in the same molecule the S1R modulation and the AchE inhibition, together with cell damage protection and neurotrophic properties. It is important to underline that RRC-33 has no anti-AChE effect, whereas both RRC-33 and donepezil show no antioxidant properties in our cellular model of ROS damage. Importantly, both compounds maintain the high affinity toward S1R.

Both **10** and **20** compounds will undergo a structure optimization program for the development of therapeutic candidates for neurodegenerative diseases treatment.

4. Materials and methods

4.1. General remarks

Reagents and solvents for synthesis were obtained from Aldrich (Italy). Solvents were purified according to the guidelines in Purification of Laboratory Chemicals. Thermal characterization was performed by using differential scanning calorimetry (DSC) and thermogravimetric analysis (TGA) on a Mettler Star^e System equipped with a DSC 821^e and TGA-DSC1 cell, respectively. Samples were weighed and placed in sealed aluminum (DSC) or alumina (TGA) pans. The samples were heated from 30 °C to 300 °C with a scanning rate of 10 °C/min under nitrogen atmosphere. The instruments were previously calibrated with Indium as standard

reference. For FT-IR analysis a Spectrum One Perkin Elmer spectrophotometer equipped with a MIRacle™ ATR device was used. The IR spectra were scanned over wavenumber range of 4000–650 cm⁻¹ with a resolution of 4 cm⁻¹. Analytical thin-layer chromatography (TLC) was carried out on silica gel precoated glass-backed plates (Fluka Kieselgel 60 F254, Merck); visualized by ultraviolet (UV) radiation, acidic ammonium molybdate (IV), or potassium permanganate. Flash chromatography (FC) was performed with Silica Gel 60 (particle size 230–400 mesh, purchased from Sigma Aldrich). Proton nuclear magnetic resonance (NMR) spectra were recorded on a Bruker Avance 500, 400 and 200 spectrometers operating at 500 MHz, 400 MHz and 200 MHz, respectively. Proton chemical shifts (δ) are reported in ppm with the solvent reference relative to tetramethylsilane (TMS) employed as the internal standard (CDCl₃, δ = 7.26 ppm). The following abbreviations are used to describe spin multiplicity: s = singlet, d = doublet, t = triplet, q = quartet, m = multiplet, br = broad signal, dd = doublet-doublet, td = triplet-doublet. The coupling constant values are reported in Hz. ¹³C NMR spectra were recorded on a 500 MHz, 400 MHz and 200 MHz spectrometers operating at 125 MHz, 100 MHz and 50 MHz, respectively, with complete proton decoupling. Carbon chemical shifts (δ) are reported in ppm relative to TMS with the respective solvent resonance as the internal standard (CDCl₃, δ = 77.23 ppm).

UPLC-UV-ESI/MS analyses were carried out on a Acquity UPLC Waters LCQ FLEET system using an ESI source operating in positive ion mode, controlled by ACQUITY PDA and 4 MICRO (Waters). Analyses were run on a ACQUITY BEH Phenyl (ABP) (50 × 2.1 mm, 1.7 μm) or ACQUITY BEH Shield (ABS) (100 × 2.1 mm, 1.7 μm)

columns, at room temperature, with gradient elution (solvent A: water containing 0.1% of formic acid; solvent B: methanol containing 0.1% of formic acid; gradient: 10% B in A to 100% B in 3 min, followed by isocratic elution 100% B for 1.5 min, return to the initial conditions in 0.2 min) at a flow rate of 0.5 mL min⁻¹. All of the final compounds had 95% or greater purity.

4.2. General procedure for the preparation of compounds 2–3

To an aqueous solution of K₂CO₃ (2.0 equiv.) was added Et₂O and *N,O*-dimethylhydroxyamine hydrochloride (1.5 equiv.). The resulting mixture was cooled at 0 °C and after 2 min the corresponding acyl chloride (1.0 equiv.) was added dropwise. The reaction was stirred overnight until the room temperature was reached. The reaction mixture was extracted with Et₂O (2 × 5 mL) and washed with water (5 mL) and brine (10 mL). The organic phase was dried (anhydrous Na₂SO₄), filtered and, after removal of the solvent under reduced pressure, the pure compounds 2–3 were obtained.

4.2.1. 3-Chloro-*N*-methoxy-*N*-methylpropanamide (2)

By following the General Procedure, starting from 3-chloropropanoyl chloride (127 mg, 1.00 mmol, 1.0 equiv), K₂CO₃ (276 mg, 2.0 mmol, 2.0 equiv), *N,O*-dimethylhydroxyamine hydrochloride (146 mg, 1.5 mmol, 1.5 equiv), H₂O (3 mL) and Et₂O (3 mL), the desired product was obtained in a quantitative amount (>99.9%) (151 mg) as a bright yellow oil. ¹H NMR (500 MHz, CDCl₃) δ: 3.80 (t, *J* = 6.9 Hz, 2H, CH₂CH₂Cl), 3.70 (s, 3H, NOCH₃), 3.19 (s, 3H, NCH₃), 2.91 (t, *J* = 6.7 Hz, 2H, CH₂CH₂CO). ¹³C NMR (125 MHz, CDCl₃) δ: 170.8, 61.4, 39.2, 35.0, 32.0.

4.2.2. 4-Chloro-*N*-methoxy-*N*-methylbutanamide (3)

By following the General Procedure, starting from 4-chlorobutanoyl chloride (141 mg, 1.00 mmol, 1.0 equiv), K₂CO₃ (276 mg, 2.0 mmol, 2.0 equiv), *N,O*-dimethylhydroxyamine hydrochloride (146 mg, 1.5 mmol, 1.5 equiv), H₂O (3 mL) and Et₂O (3 mL), the desired product was obtained in 92% (152 mg) as a bright yellow oil. ¹H NMR (500 MHz, CDCl₃) δ: 3.70 (s, 3H, NOCH₃), 3.63 (t, *J* = 6.4 Hz, 2H, CH₂CH₂Cl), 3.18 (s, 3H, NCH₃), 2.62 (t, *J* = 6.7 Hz, 2H, CH₂CH₂CO), 2.11 (m, *J* = 6.9 Hz, 2H, CH₂CH₂CH₂). ¹³C NMR (125 MHz, CDCl₃) δ: 173.3, 61.3, 44.7, 32.1, 28.6, 27.1.

4.3. General procedure for the preparation of compounds 4a, 5a-c and 6a

To a solution of Weinreb amide (1.0 equiv.) in ACN, the corresponding amine (1.0 equiv.) and K₂CO₃ (1.5 equiv.) were added. The mixture was stirred overnight, at room temperature. After removal of the solvent under reduced pressure, the crude was extracted with DCM (3 × 5 mL) and washed with water (5 mL) and brine (10 mL). In the case of compound 4a, this work-up was sufficient to obtain the pure compound. Conversely, an acid (pH = 3–4)/base (pH = 8–9) work-up was required for 5a-c and 6a, the combined organic phases were dried (anhydrous Na₂SO₄), filtered and, evaporated under vacuum to get the desired compounds. The crude compound 6a was further purified through flash chromatography (silica gel) to afford pure compound 6a.

4.3.1. 2-(4-Benzylpiperidin-1-yl)-*N*-methoxy-*N*-methylacetamide (4a)

By following the General Procedure, starting from 2-chloro-*N*-methoxy-*N*-methylacetamide (138 mg, 1.00 mmol, 1.0 equiv), K₂CO₃ (207 mg, 1.5 mmol, 1.5 equiv), 4-benzylpiperidine (175 mg, 1.0 mmol, 1.0 equiv) and ACN (7 mL), the desired product was obtained in quantitative amount (276 mg) as a bright yellow oil. ¹H NMR (500 MHz, CDCl₃) δ: 7.27 (m, 2H, Ar), 7.18 (t, 1H,

J = 7.5 Hz, Ar), 7.14 (d, 2H, *J* = 7.3 Hz, Ar), 3.69 (s, 3H, NOCH₃), 3.29 (s, 2H, CH₂N), 3.16 (s, 3H, NCH₃), 2.96 (d, 2H, Pip-2, Pip-6), 2.53 (d, 2H, CH₂Pip-4), 2.07 (t, 2H, Pip-2, Pip-6), 1.62 (d, 2H, Pip-3, Pip-5), 1.51 (m, 1H, Pip-4), 1.40 (q, 2H, Pip-3, Pip-5). ¹³C NMR (125 MHz, CDCl₃) δ: 171.4, 140.5, 129.1, 128.1, 125.7, 61.3, 58.5, 54.1, 43.1, 37.5, 32.1, 32.0.

4.3.2. 3-(4-Benzylpiperidin-1-yl)-*N*-methoxy-*N*-methylpropanamide (5a)

By following the General Procedure, starting from 3-chloro-*N*-methoxy-*N*-methylpropanamide (152 mg, 1.00 mmol, 1.0 equiv), K₂CO₃ (207 mg, 1.5 mmol, 1.5 equiv), 4-benzylpiperidine (175 mg, 1.0 mmol, 1.0 equiv) and ACN (7 mL), the desired product was obtained in quantitative amount (290 mg) as a bright yellow oil. ¹H NMR (500 MHz, CDCl₃) δ: 7.27 (m, 2H, Ar), 7.18 (t, 1H, *J* = 7.4 Hz, Ar), 7.13 (d, 2H, *J* = 7.4 Hz, Ar), 3.68 (s, 3H, NOCH₃), 3.16 (s, 3H, NCH₃), 2.95 (d, 2H, Pip-2, Pip-6), 2.72–2.70 (m, 4H, CH₂N, CH₂CH₂N), 2.53 (d, 2H, CH₂Pip-4), 2.00 (t, 2H, Pip-2, Pip-6), 1.65 (d, 2H, Pip-3, Pip-5), 1.54 (m, 1H, Pip-4), 1.36 (q, 2H, Pip-3, Pip-5). ¹³C NMR (125 MHz, CDCl₃) δ: 173.1, 140.5, 129.1, 128.1, 125.8, 61.3, 53.8, 53.6, 43.0, 37.6, 37.1, 32.1, 29.5.

4.3.3. *N*-methoxy-*N*-methyl-3-(piperidin-1-yl)propanamide (5b)

By following the General Procedure, starting from 3-chloro-*N*-methoxy-*N*-methylpropanamide (152 mg, 1.00 mmol, 1.0 equiv), K₂CO₃ (207 mg, 1.5 mmol, 1.5 equiv), piperidine (85 mg, 99 mL, 1.0 mmol, 1.0 equiv) and ACN (7 mL), the desired product was obtained in quantitative amount (200 mg) as a bright yellow oil. ¹H NMR (400 MHz, CDCl₃) δ: 3.76 (s, 3H, NOCH₃), 3.24 (s, 3H, NCH₃), 2.76 (s, 4H, CH₂N, CH₂CH₂N), 2.52 (t, 4H, Pip-2, Pip-6), 1.70–1.56 (m, 6H, Pip-3, Pip-4, Pip-5). ¹³C NMR (100 MHz, CDCl₃) δ: 175.2, 61.3, 54.5, 54.2, 29.7, 25.9, 24.2.

4.3.4. *N*-methoxy-*N*-methyl-3-morpholinopropanamide (5c)

By following the General Procedure, starting from 3-chloro-*N*-methoxy-*N*-methylpropanamide (152 mg, 1.00 mmol, 1.0 equiv), K₂CO₃ (207 mg, 1.5 mmol, 1.5 equiv), morpholine (87 mg, 87 mL, 1.0 mmol, 1.0 equiv) and ACN (7 mL), the desired product was obtained in 46% (93 mg) as a bright yellow oil. ¹H NMR (400 MHz, CDCl₃) δ: 3.78–3.73 (m, 4H, NCH₂CH₂O), 3.73 (s, 3H, NOCH₃), 3.22 (s, 3H, NCH₃), 2.81–2.63 (m, 4H, CH₂CH₂N, CH₂CH₂N), 2.56–2.51 (t, 4H, NCH₂CH₂O). ¹³C NMR (100 MHz, CDCl₃) δ: 175.3, 66.9, 61.3, 53.9, 53.6, 32.2, 29.4.

4.3.5. 4-(4-Benzylpiperidin-1-yl)-*N*-methoxy-*N*-methylbutanamide (6a)

By following the General Procedure, starting from 4-chloro-*N*-methoxy-*N*-methylbutanamide (166 mg, 1.00 mmol, 1.0 equiv), K₂CO₃ (207 mg, 1.5 mmol, 1.5 equiv), 4-benzylpiperidine (175 mg, 1.0 mmol, 1.0 equiv) and ACN (7 mL), the desired product was obtained in 65% (198 mg) as a bright yellow oil after chromatography on silica gel (60:40 ethylacetate:*n*-hexane). ¹H NMR (400 MHz, CDCl₃) δ: 7.33–7.12 (m, 5H, Ar), 3.69 (s, 3H, NOCH₃), 3.48 (s, 2H, CH₂N), 3.18 (s, 3H, NCH₃), 2.74–2.66 (m, 2H, Pip-2, Pip-6), 2.60–2.50 (m, 4H, CH₂Pip-4, Pip-2, Pip-6), 2.31–2.21 (m, COCH₂CH₂), 2.09–1.94 (m, 2H, COCH₂CH₂CH₂), 1.82–1.65 (m, 5H, Pip-3, Pip-4, Pip-5). ¹³C NMR (100 MHz, CDCl₃) δ: 173.6, 139.9, 129.1, 128.3, 126.1, 61.1, 57.1, 53.1, 42.5, 37.2, 30.3, 29.5, 20.3.

4.4. General procedure for the preparation of compounds 7–30

Under argon atmosphere, *tert*-butyllithium (2.2 equiv., 1.9 M in pentane) was added dropwise to a –78 °C cooled solution of the appropriate arylbromide (1.5 equiv.) in anhydrous THF. After 20 min, the solution of the corresponding Weinreb amide in

anhydrous THF was added dropwise. The stirring was continued for 5 additional hours and then quenched with water. The reaction was extracted with Et₂O (2 × 5 mL) and washed with water (5 mL) and brine (10 mL). The organic phase was dried (anhydrous Na₂SO₄), filtered and, after removal of the solvent under reduced pressure, the so-obtained crude mixture was subjected to chromatography (silica gel) to afford pure compounds. Lastly, pure compounds were converted into their corresponding hydrochlorides, adding an ethereal solution of HCl (1.0 equiv., 1 M in Et₂O).

4.4.1. 4-Benzyl-1-(2-oxo-2-phenylethyl)piperidin-1-ium hydrochloride (7)

By following the General Procedure, starting from bromobenzene (236 mg, 1.5 mmol, 1.5 equiv.), 2-(4-benzylpiperidin-1-yl)-N-methoxy-N-methylacetamide (274 mg, 1.00 mmol, 1.0 equiv.), *t*-BuLi (1.9 M, 1.32 mL, 2.5 mmol, 2.5 equiv.) and THF (5 mL), the desired product was obtained in 40% (117 mg) as a bright yellow oil after chromatography on silica gel (60:40 hexane:ethylacetate) and converted into the corresponding hydrochloride. FT-IR (cm⁻¹): 3058, 3023, 2922, 2846, overtones Ar = 2100–1800, 1706, 1598, 1580, 1448. ¹H NMR (400 MHz, CDCl₃) δ: 12.07 (s, 1H, NH⁺), 7.95 (brs, 2H, Ar), 7.65 (brs, 1H, Ar), 7.50 (brs, 2H, Ar), 7.31 (t, *J* = 7.0 Hz, 2H, Ar), 7.23 (t, *J* = 8.0 Hz, 1H, Ar), 7.16 (d, *J* = 8.0 Hz, 2H, Ar), 4.75 (s, 2H, COCH₂N), 3.55 (brs, 4H, Pip-2, Pip-6), 2.64 (m, 2H, CH₂Pip-4), 2.09–1.85 (m, 5H, Pip-3, Pip-4, Pip-5). ¹³C NMR (100 MHz, CDCl₃) δ: 190.3, 139.0, 134.9, 133.9, 129.1, 128.9, 128.4, 128.1, 126.3, 59.7, 52.4, 42.0, 35.9, 29.3. UHPLC-ESI-MS: ABS t_R = 1.19, 96% pure (λ = 210 nm), *m/z* = 294.3 [M + H]⁺.

The thermal profile showed two endothermic effects; the first of little intensity at 136.9 ± 0.5 °C, not associated with a mass loss in TGA curve, was probably attributable to a metastable phase melting, followed by a recrystallization exotherm at around 142 °C and a second endothermic effect due to the melting at 208.4 ± 0.1 °C (ΔH_{fus} = 50 ± 1 J g⁻¹) of a stable phase.

4.4.2. 4-Benzyl-1-(2-(4-methoxyphenyl)-2-oxoethyl)piperidin-1-ium hydrochloride (8)

By following the General Procedure, starting from 1-bromo-4-methoxybenzene (281 mg, 1.5 mmol, 1.5 equiv.), 2-(4-benzylpiperidin-1-yl)-N-methoxy-N-methylacetamide (274 mg, 1.00 mmol, 1.0 equiv.), *t*-BuLi (1.9 M, 1.32 mL, 2.5 mmol, 2.5 equiv.) and THF (5 mL), the desired product was obtained in 37% (120 mg) as a bright yellow oil after chromatography on silica gel (60:40 hexane:ethylacetate) and converted into the corresponding hydrochloride. FT-IR (cm⁻¹): 3059, 3013, 2932, overtones Ar = 2100–1750, 1694, 1603, 1578, 1512, 1402. ¹H NMR (400 MHz, CDCl₃) δ: 11.93 (brs, 1H, NH⁺), 7.90 (d, *J* = 8.0 Hz, 2H, Ar), 7.30 (t, *J* = 8.0 Hz, 2H, Ar), 7.22 (t, *J* = 8.0 Hz, 1H, Ar), 7.15 (d, *J* = 8.0 Hz, 2H, Ar), 6.93 (d, *J* = 8.0 Hz, 2H, Ar), 4.68 (s, 2H, COCH₂N), 3.87 (s, 3H, OCH₃), 3.51 (brd, 4H, Pip-2, Pip-6), 2.63 (d, 2H, CH₂Pip-4), 2.06 (m, 2H, Pip-3, Pip-5), 1.85–1.82 (m, 3H, Pip-3, Pip-4, Pip-5). ¹³C NMR (100 MHz, CDCl₃) δ: 188.5, 164.8, 148.5, 139.0, 130.5, 128.9, 128.4, 126.9, 126.2, 114.2, 59.1, 55.6, 52.2, 42.0, 35.8, 29.3. UHPLC-ESI-MS: ABP t_R = 1.87, 98% pure (λ = 210 nm), *m/z* = 324.4 [M + H]⁺.

The thermal profile was typical of an anhydrous form showing the melting endothermic effect at 233.1 ± 0.7 °C (ΔH_{fus} = 136 ± 4 J g⁻¹).

4.4.3. 4-Benzyl-1-(2-(3-methoxyphenyl)-2-oxoethyl)piperidin-1-ium hydrochloride (9)

By following the General Procedure, starting from 1-bromo-3-methoxybenzene (281 mg, 1.5 mmol, 1.5 equiv.), 2-(4-benzylpiperidin-1-yl)-N-methoxy-N-methylacetamide (274 mg, 1.00 mmol, 1.0 equiv.), *t*-BuLi (1.9 M, 1.32 mL, 2.5 mmol, 2.5 equiv.) and THF (5 mL), the desired product was obtained in 48% (155 mg)

as a bright yellow oil after chromatography on silica gel (60:40 hexane:ethylacetate) and converted into the corresponding hydrochloride. FT-IR (cm⁻¹): 3056, 3026, 3003, 2923, 2841, overtones Ar = 2100–1750, 1696, 1596, 1431. ¹H NMR (400 MHz, CDCl₃) δ: 11.94 (brs, 1H, NH⁺), 7.49–7.16 (m, 9H, Ar), 4.77 (s, 2H, COCH₂N), 3.84 (s, 3H, OCH₃), 3.56 (m, 4H, Pip-2, Pip-6), 2.63 (brd, 2H, CH₂Pip-4), 2.08 (brs, 2H, Pip-3, Pip-5), 1.86–1.73 (m, 3H, Pip-3, Pip-4, Pip-5). ¹³C NMR (100 MHz, CDCl₃) δ: 190.1, 160.0, 139.0, 135.2, 130.1, 128.9, 128.4, 126.3, 121.4, 120.6, 112.2, 60.0, 55.6, 52.5, 42.0, 35.8, 29.3. UHPLC-ESI-MS: ABP t_R = 1.85, 99% pure (λ = 220 nm), *m/z* = 324.4 [M + H]⁺.

The thermal profile showed a first broad endothermic effect at 147.2 ± 0.7 °C followed by melting at 191.4 ± 0.5 °C (ΔH_{fus} = 61 ± 5 J g⁻¹). The first endothermic effect, not associated with a mass loss in TGA curve, was probably attributable to the melting of a metastable phase.

4.4.4. 4-Benzyl-1-(2-(naphthalen-2-yl)-2-oxoethyl)piperidin-1-ium hydrochloride (10)

By following the General Procedure, starting from 2-bromonaphthalene (311 mg, 1.5 mmol, 1.5 equiv.), 2-(4-benzylpiperidin-1-yl)-N-methoxy-N-methylacetamide (274 mg, 1.00 mmol, 1.0 equiv.), *t*-BuLi (1.9 M, 1.32 mL, 2.5 mmol, 2.5 equiv.) and THF (5 mL), the desired product was obtained in 54% (185 mg) as a bright yellow oil after chromatography on silica gel (60:40 hexane:ethylacetate) and converted into the corresponding hydrochloride. FT-IR (cm⁻¹): 3023, 2924, overtones Ar = 2100–1800, 1689, 1599, 1495, 1453. ¹H NMR (400 MHz, CDCl₃) δ: 11.63 (brs, 1H, NH⁺), 8.51 (s, 1H, Nap), 7.91 (d, 2H, Nap), 7.78 (t, 2H, Nap), 7.59 (t, *J* = 8.0 Hz, 1H, Nap), 7.51 (t, *J* = 8.0 Hz, 1H, Nap), 7.28–7.11 (m, 5H, Ar), 4.96 (s, 2H, COCH₂N), 3.60–3.52 (m, 4H, Pip-2, Pip-6), 2.59 (brd, 2H, CH₂Pip-4), 2.04 (m, 2H, Pip-3, Pip-5), 1.82–1.79 (m, 3H, Pip-3, Pip-4, Pip-5). ¹³C NMR (100 MHz, CDCl₃) δ: 190.2, 139.0, 136.0, 132.0, 131.0, 130.7, 129.8, 129.4, 128.9, 128.4, 127.6, 127.2, 126.2, 122.6, 59.9, 52.7, 41.9, 35.7, 29.3. UHPLC-ESI-MS: ABP t_R = 2.08, 95% pure (λ = 210 nm), *m/z* = 344.3 [M + H]⁺.

The thermal profile showed an exothermic effect at 191.9 ± 0.6 °C, probably due to the crystallization of an amorphous portion of sample, induced by heating. The melting of the anhydrous form was recorded at 212.0 ± 0.9 °C (ΔH_{fus} = 69 ± 5 J g⁻¹).

4.4.5. 4-Benzyl-1-(2-(6-methoxynaphthalen-2-yl)-2-oxoethyl)piperidin-1-ium hydrochloride (11)

By following the General Procedure, starting from 2-bromo-6-methoxynaphthalene (256 mg, 1.5 mmol, 1.5 equiv.), 2-(4-benzylpiperidin-1-yl)-N-methoxy-N-methylacetamide (274 mg, 1.00 mmol, 1.0 equiv.), *t*-BuLi (1.9 M, 1.32 mL, 2.5 mmol, 2.5 equiv.) and THF (5 mL), the desired product was obtained in 49% (183 mg) as a bright yellow oil after chromatography on silica gel (60:40 hexane:ethylacetate) and converted into the corresponding hydrochloride. FT-IR (cm⁻¹): 3023, 2932, overtones Ar = 2100–1800, 1682, 1483. ¹H NMR (400 MHz, CDCl₃) δ: 11.46 (brs, 1H, NH⁺), 8.38 (s, 1H, Nap), 7.79 (m, 2H, Nap), 7.61 (brd, 1H, Nap), 7.28–7.00 (m, 7H, Ar, Nap), 4.92 (s, 2H, COCH₂N), 3.90 (s, 3H, OCH₃), 3.59–3.53 (m, 4H, Pip-2, Pip-6), 2.58 (brd, 2H, CH₂Pip-4), 2.03 (m, 2H, Pip-3, Pip-5), 1.82–1.79 (m, 3H, Pip-3, Pip-4, Pip-5). ¹³C NMR (100 MHz, CDCl₃) δ: 189.7, 160.4, 139.0, 137.9, 131.4, 130.5, 129.0, 128.9, 128.3, 127.5, 127.3, 126.2, 123.4, 120.1, 105.7, 59.9, 55.4, 52.7, 42.0, 35.7, 29.3. UHPLC-ESI-MS: ABS t_R = 1.63, 95% pure (λ = 210 nm), *m/z* = 374.5 [M + H]⁺.

The thermal profile showed an exothermic effect at 137.9 ± 0.4 °C, attributable to crystallization, induced by heating, of an amorphous portion of sample. The melting of the anhydrous crystalline form was recorded at 212.9 ± 0.9 °C (ΔH_{fus} = 50 ± 2 J g⁻¹).

4.4.6. 1-(2-([1,1'-biphenyl]-4-yl)-2-oxoethyl)-4-benzylpiperidin-1-ium hydrochloride (**12**)

By following the General Procedure, starting from 4-bromo-1,1'-biphenyl (350 mg, 1.5 mmol, 1.5 equiv.), 2-(4-benzylpiperidin-1-yl)-*N*-methoxy-*N*-methylacetamide (274 mg, 1.00 mmol, 1.0 equiv.), *t*-BuLi (1.9 M, 1.32 mL, 2.5 mmol, 2.5 equiv.) and THF (5 mL), the desired product was obtained in 33% (122 mg) as a bright yellow oil after chromatography on silica gel (60:40 hexane:ethylacetate) and converted into the corresponding hydrochloride. FT-IR (cm^{-1}): 3025, 2986, 2935, 2916, 2847, overtones Ar = 2100–1800, 1691, 1603, 1414. ^1H NMR (400 MHz, CDCl_3) δ : 11.70 (brs, 1H, NH^+), 8.00 (d, $J = 6.3$ Hz, 2H, Ar), 7.66 (brs, 2H, Ar), 7.55 (ds, $J = 4.0$ Hz, 2H, Ar), 7.44 (m, 3H, Ar), 7.28–7.13 (m, 5H, Ar), 4.88 (s, 2H, COCH_2N), 3.60–3.55 (m, 4H, Pip-2, Pip-6), 2.62–2.52 (brs, 2H, $\text{CH}_2\text{Pip-4}$), 2.07 (m, 2H, Pip-3, Pip-5), 1.86–1.83 (m, 3H, Pip-3, Pip-4, Pip-5). ^{13}C NMR (100 MHz, CDCl_3) δ : 189.8, 147.4, 139.0, 138.9, 132.5, 129.0, 128.7, 128.6, 128.4, 127.5, 127.1, 126.2, 60.0, 52.7, 42.0, 35.8, 29.3. UHPLC-ESI-MS: ABP $t_R = 2.22$, 98% pure ($\lambda = 210$ nm), $m/z = 370.5$ [$\text{M} + \text{H}$] $^+$.

The thermal profile was typical of an anhydrous form showing the melting endothermic effect at 208.2 ± 0.4 °C ($\Delta H_{\text{fus}} = 64 \pm 2$ J g $^{-1}$).

4.4.7. 3-(4-Benzylpiperidin-1-yl)-1-phenylpropan-1-one (**13**)

By following the General Procedure, starting from bromobenzene (236 mg, 1.5 mmol, 1.5 equiv.), 3-(4-benzylpiperidin-1-yl)-*N*-methoxy-*N*-methylpropanamide (290 mg, 1.00 mmol, 1.0 equiv.), *t*-BuLi (1.9 M, 1.32 mL, 2.5 mmol, 2.5 equiv.) and THF (5 mL), the desired product was obtained in 28% (86 mg) as a bright yellow oil after chromatography on silica gel (90:10 ethylacetate:methanol) and converted into the corresponding hydrochloride. FT-IR (cm^{-1}): 3059, 3045, 3025, 2996, 2921, overtones Ar = 2100–1700, 1682, 1596, 1447. ^1H NMR (500 MHz, CDCl_3) δ : 7.88 (d, $J = 8.3$ Hz, 2H, Ar), 7.48 (m, 1H, Ar), 7.38 (t, $J = 7.5$ Hz, 2H, Ar), 7.20 (m, 2H, Ar), 7.11 (t, $J = 7.0$ Hz, 1H, Ar), 7.06 (d, $J = 7.4$ Hz, 2H, Ar), 3.17 (m, 2H, COCH_2CH_2), 2.91 (d, 2H, Pip-2, Pip-6), 2.77 (m, 2H, $\text{CH}_2\text{CH}_2\text{N}$), 2.47 (d, $J = 7.2$ Hz, 2H, $\text{CH}_2\text{Pip-4}$), 1.96 (m, 2H, Pip-2, Pip-6), 1.59 (d, 2H, Pip-3, Pip-5), 1.48 (m, 1H, Pip-4), 1.30 (m, 2H, Pip-3, Pip-5). ^{13}C NMR (125 MHz, CDCl_3) δ : 199.0, 140.4, 136.7, 133.1, 129.0, 128.6, 128.1, 128.0, 125.8, 53.9, 53.3, 43.0, 37.6, 36.1, 31.8. UHPLC-ESI-MS: ABS $t_R = 1.25$, 95% pure ($\lambda = 254$ nm), $m/z = 308.4$ [$\text{M} + \text{H}$] $^+$.

The thermal profile was typical of an anhydrous form showing the melting endothermic effect at 193.4 ± 0.7 °C ($\Delta H_{\text{fus}} = 175 \pm 2$ J g $^{-1}$).

4.4.8. 3-(4-Benzylpiperidin-1-yl)-1-(4-methoxyphenyl)propan-1-one (**14**)

By following the General Procedure, starting from 1-bromo-4-methoxybenzene (281 mg, 1.5 mmol, 1.5 equiv.), 3-(4-benzylpiperidin-1-yl)-*N*-methoxy-*N*-methylpropanamide (290 mg, 1.00 mmol, 1.0 equiv.), *t*-BuLi (1.9 M, 1.32 mL, 2.5 mmol, 2.5 equiv.) and THF (5 mL), the desired product was obtained in 25% (84 mg) as a bright yellow oil after chromatography on silica gel (90:10 ethylacetate:methanol) and converted into the corresponding hydrochloride. FT-IR (cm^{-1}): 3048, 3030, 3005, 2939, 2918, 2841, overtones Ar = 2100–1700, 1673, 1601, 1457, 1420. ^1H NMR (500 MHz, CDCl_3) δ : 7.96 (d, $J = 8.7$ Hz, 2H, Ar), 7.28 (m, 2H, Ar), 7.20 (t, $J = 6.7$ Hz, 1H, Ar), 7.13 (d, $J = 7.5$ Hz, 2H, Ar), 6.93 (d, $J = 8.7$ Hz, 2H, Ar), 3.87 (s, 3H, OCH_3), 3.41 (m, 2H, COCH_2CH_2), 3.17 (m, 2H, Pip-2, Pip-6), 3.07 (m, 2H, $\text{CH}_2\text{CH}_2\text{N}$), 2.57 (brd, 2H, $\text{CH}_2\text{Pip-4}$), 2.28 (m, 2H, Pip-2, Pip-6), 1.73 (brd, 2H, Pip-3, Pip-5), 1.64 (m, 3H, Pip-3, Pip-4, Pip-5). ^{13}C NMR (125 MHz, CDCl_3) δ : 177.5, 163.8, 139.9, 130.5, 129.2, 129.0, 128.3, 126.1, 113.8, 53.7, 52.8, 42.5, 37.1, 34.6, 30.5. UHPLC-ESI-MS: ABS $t_R = 1.35$, 98% pure ($\lambda = 254$ nm), $m/z = 338.4$ [$\text{M} + \text{H}$] $^+$.

$z = 338.4$ [$\text{M} + \text{H}$] $^+$.

The DSC curve showed the typical thermal profile of an anhydrous form with a melting endothermic effect recorded at 191.5 ± 0.1 °C ($\Delta H_{\text{fus}} = 129 \pm 7$ J g $^{-1}$).

4.4.9. 3-(4-Benzylpiperidin-1-yl)-1-(naphthalen-2-yl)propan-1-one (**15**)

By following the General Procedure, starting from 2-bromonaphthalene (311 mg, 1.5 mmol, 1.5 equiv.), 3-(4-benzylpiperidin-1-yl)-*N*-methoxy-*N*-methylpropanamide (290 mg, 1.00 mmol, 1.0 equiv.), *t*-BuLi (1.9 M, 1.32 mL, 2.5 mmol, 2.5 equiv.) and THF (5 mL), the desired product was obtained in 22% (79 mg) as a bright yellow oil after chromatography on silica gel (90:10 ethylacetate:methanol) and converted into the corresponding hydrochloride. FT-IR (cm^{-1}): 3059, 3029, 2943, 2921, 2864, overtones Ar = 2000–1700, 1674, 1595, 1495, 1456. ^1H NMR (500 MHz, CDCl_3) δ : 8.41 (s, 1H, Nap), 7.95 (d, $J = 8.7$ Hz, 1H, Nap), 7.89 (d, $J = 8.1$ Hz, 1H, Nap), 7.80 (t, $J = 8.9$ Hz, 2H, Nap), 7.54–7.46 (m, 2H, Nap), 7.20 (t, $J = 7.5$ Hz, 2H, Ar), 7.11 (t, $J = 7.3$ Hz, 1H, Ar), 7.06 (d, $J = 7.5$ Hz, 2H, Ar), 3.31 (t, $J = 7.5$ Hz, 2H, COCH_2CH_2), 2.95 (brd, 2H, Pip-2, Pip-6), 2.85 (t, $J = 7.6$ Hz, 2H, $\text{CH}_2\text{CH}_2\text{N}$), 2.47 (d, $J = 7.2$ Hz, 2H, $\text{CH}_2\text{Pip-4}$), 2.00 (m, 2H, Pip-2, Pip-6), 1.61 (brd, 2H, Pip-3, Pip-5), 1.50 (m, 1H, Pip-4), 1.33 (m, 2H, Pip-3, Pip-5). ^{13}C NMR (125 MHz, CDCl_3) δ : 198.9, 140.4, 135.5, 133.9, 132.4, 129.8, 129.5, 129.0, 128.5, 128.4, 128.2, 127.7, 125.8, 123.7, 53.9, 53.4, 43.0, 37.6, 36.1, 31.7. UHPLC-ESI-MS: ABP $t_R = 1.62$, 98% pure ($\lambda = 254$ nm), $m/z = 358$ [$\text{M} + \text{H}$] $^+$.

The thermal profile was typical of an anhydrous form showing the melting endothermic effect at 199.2 ± 0.2 °C ($\Delta H_{\text{fus}} = 178 \pm 1$ J g $^{-1}$).

4.4.10. 1-([1,1'-biphenyl]-4-yl)-3-(4-benzylpiperidin-1-yl)propan-1-one (**16**)

By following the General Procedure, starting from 4-bromo-1,1'-biphenyl (350 mg, 1.5 mmol, 1.5 equiv.), 3-(4-benzylpiperidin-1-yl)-*N*-methoxy-*N*-methylpropanamide (290 mg, 1.00 mmol, 1.0 equiv.), *t*-BuLi (1.9 M, 1.32 mL, 2.5 mmol, 2.5 equiv.) and THF (5 mL), the desired product was obtained in 22% (84 mg) as a bright yellow oil after chromatography on silica gel (90:10 ethylacetate:methanol) and converted into the corresponding hydrochloride. FT-IR (cm^{-1}): 3059, 3029, 2916, overtones Ar = 2100–1700, 1677, 1601, 1457, 1402. ^1H NMR (400 MHz, CDCl_3) δ : 12.24 (brs, 1H, NH^+), 8.09 (brd, 2H, Ar), 7.70 (brd, 2H, Ar), 7.63 (brd, 2H, Ar), 7.48 (brt, 2H, Ar), 7.43 (brt, 1H, Ar), 7.29–7.13 (m, 5H, Ar), 3.87 (brs, 2H, COCH_2CH_2), 3.58 (brs, 2H, Pip-2, Pip-6), 3.48 (brs, 2H, $\text{CH}_2\text{CH}_2\text{N}$), 2.71–2.64 (m, 4H, Pip-2, Pip-6, $\text{CH}_2\text{Pip-4}$), 2.08 (brt, 2H, Pip-3, Pip-5), 1.87–1.79 (m, 3H, Pip-3, Pip-4, Pip-5). ^{13}C NMR (100 MHz, CDCl_3) δ : 195.7, 146.6, 139.4, 138.9, 134.0, 128.9, 128.4, 128.3, 127.3, 127.2, 126.3, 53.6, 52.1, 41.8, 36.4, 33.3, 28.9. UHPLC-ESI-MS: ABP $t_R = 2.37$, 95% pure ($\lambda = 254$ nm), $m/z = 384.4$ [$\text{M} + \text{H}$] $^+$.

The thermal profile was typical of an anhydrous form showing the melting endothermic effect at 198.9 ± 0.6 °C ($\Delta H_{\text{fus}} = 115 \pm 2$ J g $^{-1}$).

4.4.11. 1-Phenyl-3-(piperidin-1-yl)propan-1-one (**17**)

By following the General Procedure, starting from bromobenzene (236 mg, 1.5 mmol, 1.5 equiv.), *N*-methoxy-*N*-methyl-3-(piperidin-1-yl)propanamide (200 mg, 1.00 mmol, 1.0 equiv.), *t*-BuLi (1.9 M, 1.32 mL, 2.5 mmol, 2.5 equiv.) and THF (5 mL), the desired product was obtained in 29% (63 mg) as a bright yellow oil after chromatography on silica gel (60:40 ethylacetate:methanol) and converted into the corresponding hydrochloride. FT-IR (cm^{-1}): 3055, 3021, 2938, 2863, overtones Ar = 2100–1700, 1682, 1597, 1581, 1477, 1456. ^1H NMR (500 MHz, CDCl_3) δ : 7.95 (dd, $J = 1.2$ and 7.9 Hz, 2H, Ar), 7.55 (m, 1H, Ar), 7.45 (t, $J = 7.9$ Hz, 2H, Ar), 3.24 (t,

$J = 7.4$ Hz, 2H, COCH_2CH_2), 2.83 (t, $J = 7.8$ Hz, 2H, $\text{CH}_2\text{CH}_2\text{N}$), 2.49 (brs, 4H, Pip-2, Pip-6), 1.62 (m, 4H, Pip-3, Pip-5), 1.44 (m, 2H, Pip-4). ^{13}C NMR (125 MHz, CDCl_3) δ : 197.1, 136.7, 133.1, 128.6, 128.0, 54.5, 53.7, 36.0, 25.7, 24.0. UHPLC-ESI-MS: ABP $t_{\text{R}} = 1.07$, 96% pure ($\lambda = 254$ nm), $m/z = 218.3$ [M + H] $^+$.

The thermal profile was typical of an anhydrous form showing the melting endothermic effect at 185.4 ± 0.1 °C ($\Delta H_{\text{fus}} = 147 \pm 1$ J g $^{-1}$).

4.4.12. 1-(4-methoxyphenyl)-3-(piperidin-1-yl)propan-1-one (18)

By following the General Procedure, starting from 1-bromo-4-methoxybenzene (281 mg, 1.5 mmol, 1.5 equiv.), *N*-methoxy-*N*-methyl-3-(piperidin-1-yl)propanamide (200 mg, 1.00 mmol, 1.0 equiv.), *t*-BuLi (1.9 M, 1.32 mL, 2.5 mmol, 2.5 equiv.) and THF (5 mL), the desired product was obtained in 27% (67 mg) as a bright yellow oil after chromatography on silica gel (60:40 ethylacetate:methanol) and converted into the corresponding hydrochloride. FT-IR (cm^{-1}): 2951, 2937, 2875, overtones Ar = 2100–1700, 1672, 1598, 1464, 1442, 1425. ^1H NMR (500 MHz, CDCl_3) δ : 7.93 (d, $J = 8.9$ Hz, 2H, Ar), 6.91 (d, $J = 8.7$ Hz, 2H, Ar), 3.85 (s, 3H, OCH_3), 3.17 (t, $J = 7.4$ Hz, 2H, COCH_2CH_2), 2.80 (t, $J = 7.9$ Hz, 2H, $\text{CH}_2\text{CH}_2\text{N}$), 2.47 (brs, 4H, Pip-2, Pip-6), 1.60 (m, 4H, Pip-3, Pip-5), 1.44 (m, 2H, Pip-4). ^{13}C NMR (125 MHz, CDCl_3) δ : 197.8, 163.4, 130.3, 129.9, 113.7, 55.4, 54.5, 53.9, 35.8, 25.8, 24.1. UHPLC-ESI-MS: ABP $t_{\text{R}} = 1.24$, 98% pure ($\lambda = 254$ nm), $m/z = 248.3$ [M + H] $^+$.

The thermal profile was typical of an anhydrous form showing the melting endothermic effect at 207.3 ± 0.6 °C ($\Delta H_{\text{fus}} = 107 \pm 6$ J g $^{-1}$).

4.4.13. 1-(Naphthalen-2-yl)-3-(piperidin-1-yl)propan-1-one (19)

By following the General Procedure, starting from 2-bromonaphthalene (311 mg, 1.5 mmol, 1.5 equiv.), *N*-methoxy-*N*-methyl-3-(piperidin-1-yl)propanamide (200 mg, 1.00 mmol, 1.0 equiv.), *t*-BuLi (1.9 M, 1.32 mL, 2.5 mmol, 2.5 equiv.) and THF (5 mL), the desired product was obtained in 23% (61 mg) as a bright yellow oil after chromatography on silica gel (60:40 ethylacetate:methanol) and converted into the corresponding hydrochloride. FT-IR (cm^{-1}): 3037, 2934, 2891, 2855, overtones Ar = 2100–1700, 1676, 1598, 1463. ^1H NMR (500 MHz, CDCl_3) δ : 8.50 (s, 1H, Nap), 8.02 (d, $J = 8.5$ Hz, 1H, Nap), 7.96 (d, $J = 8.1$ Hz, 1H, Nap), 7.88 (t, $J = 9.2$ Hz, 2H, Nap), 7.62–7.54 (m, 2H, Nap), 3.43 (t, $J = 7.3$ Hz, 2H, COCH_2CH_2), 2.95 (t, $J = 7.2$ Hz, 2H, $\text{CH}_2\text{CH}_2\text{N}$), 2.59 (brs, 4H, Pip-2, Pip-6), 1.68 (m, 4H, Pip-3, Pip-5), 1.49 (m, 2H, Pip-4). ^{13}C NMR (125 MHz, CDCl_3) δ : 198.9, 135.6, 134.0, 132.5, 129.9, 129.6, 128.5, 127.7, 126.8, 123.7, 54.5, 53.7, 36.0, 25.5, 23.9. UHPLC-ESI-MS: ABP $t_{\text{R}} = 1.09$, 95% pure ($\lambda = 254$ nm), $m/z = 268.3$ [M + H] $^+$.

The thermal profile was typical of an anhydrous form showing the melting endothermic effect at 188.7 ± 0.2 °C ($\Delta H_{\text{fus}} = 130 \pm 3$ J g $^{-1}$).

4.4.14. 1-([1,1'-biphenyl]-4-yl)-3-(piperidin-1-yl)propan-1-one (20)

By following the General Procedure, starting from 4-bromo-1,1'-biphenyl (350 mg, 1.5 mmol, 1.5 equiv.), *N*-methoxy-*N*-methyl-3-(piperidin-1-yl)propanamide (200 mg, 1.00 mmol, 1.0 equiv.), *t*-BuLi (1.9 M, 1.32 mL, 2.5 mmol, 2.5 equiv.) and THF (5 mL), the desired product was obtained in 35% (103 mg) as a bright yellow oil after chromatography on silica gel (60:40 ethylacetate:methanol) and converted into the corresponding hydrochloride. FT-IR (cm^{-1}): 3055, 3027, 2934, overtones Ar = 2100–1700, 1680, 1605, 1560, 1449, 1430. ^1H NMR (500 MHz, CDCl_3) δ : 8.04 (d, $J = 8.3$ Hz, 2H, Ar), 7.68 (d, $J = 8.4$ Hz, 2H, Ar), 7.62 (d, $J = 8.0$ Hz, 2H, Ar), 7.47 (t, $J = 7.3$ Hz, 2H, Ar), 7.41 (t, $J = 7.2$ Hz, 1H, Ar), 3.27 (t, $J = 7.4$ Hz, 2H, COCH_2CH_2), 2.86 (t, $J = 7.8$ Hz, 2H, $\text{CH}_2\text{CH}_2\text{N}$), 2.51 (brs, 4H, Pip-2, Pip-6), 1.63 (m, 4H, Pip-3, Pip-5), 1.47 (m, 2H, Pip-4). ^{13}C NMR

(125 MHz, CDCl_3) δ : 198.8, 145.7, 139.8, 135.5, 128.9, 128.6, 128.2, 127.2, 54.6, 53.8, 36.2, 25.7, 24.1. UHPLC-ESI-MS: ABP $t_{\text{R}} = 1.89$, 95% pure ($\lambda = 254$ nm), $m/z = 294.3$ [M + H] $^+$.

The thermal profile was typical of an anhydrous form showing the melting endothermic effect at 190.6 ± 0.9 °C ($\Delta H_{\text{fus}} = 61 \pm 4$ J g $^{-1}$).

4.4.15. 3-Morpholino-1-phenylpropan-1-one (21)

By following the General Procedure, starting from bromobenzene (236 mg, 1.5 mmol, 1.5 equiv.), *N*-methoxy-*N*-methyl-3-morpholinopropanamide (202 mg, 1.00 mmol, 1.0 equiv.), *t*-BuLi (1.9 M, 1.32 mL, 2.5 mmol, 2.5 equiv.) and THF (5 mL), the desired product was obtained in 30% (66 mg) as a bright yellow oil after chromatography on silica gel (90:10 ethylacetate:methanol) and converted into the corresponding hydrochloride. FT-IR (cm^{-1}): 3086, 2981, 2930, 2872, overtones Ar = 2100–1700, 1685, 1597, 1584, 1445, 1405. ^1H NMR (500 MHz, CDCl_3) δ : 7.94 (dd, $J = 1.3$ and 7.2 Hz, 2H, Ar), 7.55 (m, 1H, Ar), 7.46 (t, $J = 7.8$ Hz, 2H, Ar), 3.70 (t, $J = 4.6$ Hz, 4H, Mor-3, Mor-5), 3.18 (t, $J = 7.3$ Hz, 2H, COCH_2CH_2), 2.83 (t, $J = 7.7$ Hz, 2H, $\text{CH}_2\text{CH}_2\text{N}$), 2.50 (brs, 4H, Mor-2, Mor-6). ^{13}C NMR (125 MHz, CDCl_3) δ : 198.9, 136.7, 133.1, 128.6, 128.0, 66.8, 53.6, 53.4, 35.9. UHPLC-ESI-MS: ABP $t_{\text{R}} = 0.82$, 99% pure ($\lambda = 254$ nm), $m/z = 220.2$ [M + H] $^+$.

The thermal profile was typical of an anhydrous form showing the melting endothermic effect at 178.1 ± 0.8 °C ($\Delta H_{\text{fus}} = 160 \pm 2$ J g $^{-1}$).

4.4.16. 1-(4-methoxyphenyl)-3-morpholinopropan-1-one (22)

By following the General Procedure, starting from 1-bromo-4-methoxybenzene (281 mg, 1.5 mmol, 1.5 equiv.), *N*-methoxy-*N*-methyl-3-morpholinopropanamide (202 mg, 1.00 mmol, 1.0 equiv.), *t*-BuLi (1.9 M, 1.32 mL, 2.5 mmol, 2.5 equiv.) and THF (5 mL), the desired product was obtained in 38% (95 mg) as a bright yellow oil after chromatography on silica gel (90:10 ethylacetate:methanol) and converted into the corresponding hydrochloride. FT-IR (cm^{-1}): 2990, 2954, 2932, 2857, overtones Ar = 2100–1700, 1674, 1597, 1427. ^1H NMR (500 MHz, CDCl_3) δ : 7.94 (d, $J = 8.9$ Hz, 2H, Ar), 6.93 (d, $J = 8.9$ Hz, 2H, Ar), 3.87 (s, 3H, OCH_3), 3.74 (m, 4H, Mor-3, Mor-5), 3.17 (t, $J = 7.3$ Hz, 2H, COCH_2CH_2), 2.86 (t, $J = 7.2$ Hz, 2H, $\text{CH}_2\text{CH}_2\text{N}$), 2.47 (brs, 4H, Mor-2, Mor-6). ^{13}C NMR (125 MHz, CDCl_3) δ : 197.3, 163.5, 130.3, 129.8, 66.7, 55.5, 53.6, 35.4. UHPLC-ESI-MS: ABP $t_{\text{R}} = 0.84$, >99% pure ($\lambda = 254$ nm), $m/z = 250.2$ [M + H] $^+$.

The thermal profile was typical of an anhydrous form showing the melting endothermic effect at 211.0 ± 0.9 °C ($\Delta H_{\text{fus}} = 244 \pm 5$ J g $^{-1}$).

4.4.17. 3-Morpholino-1-(naphthalen-2-yl)propan-1-one (23)

By following the General Procedure, starting from 2-bromonaphthalene (311 mg, 1.5 mmol, 1.5 equiv.), *N*-methoxy-*N*-methyl-3-morpholinopropanamide (202 mg, 1.00 mmol, 1.0 equiv.), *t*-BuLi (1.9 M, 1.32 mL, 2.5 mmol, 2.5 equiv.) and THF (5 mL), the desired product was obtained in 41% (110 mg) as a bright yellow oil after chromatography on silica gel (90:10 ethylacetate:methanol) and converted into the corresponding hydrochloride. FT-IR (cm^{-1}): 3018, 2924, 2863, overtones Ar = 2100–1700, 1687, 1594, 1469, 1436. ^1H NMR (500 MHz, CDCl_3) δ : 8.48 (s, 1H, Nap), 8.02 (dd, $J = 1.5$ and 8.5 Hz, 1H, Nap), 7.95 (d, $J = 8.5$ Hz, 1H, Nap), 7.88 (t, $J = 9.5$ Hz, 2H, Nap), 7.61–7.53 (m, 2H, Nap), 3.76 (t, $J = 4.5$ Hz, 4H, Mor-3, Mor-5), 3.37 (t, $J = 7.0$ Hz, 2H, COCH_2CH_2), 2.94 (t, $J = 7.5$ Hz, 2H, $\text{CH}_2\text{CH}_2\text{N}$), 2.60 (brs, 4H, Mor-2, Mor-6). ^{13}C NMR (125 MHz, CDCl_3) δ : 198.6, 135.6, 134.0, 132.4, 129.8, 129.5, 128.5, 127.7, 126.8, 123.7, 66.6, 53.6, 53.5, 35.7. UHPLC-ESI-MS: ABP $t_{\text{R}} = 1.48$, 99% pure ($\lambda = 254$ nm), $m/z = 270.3$ [M + H] $^+$.

The thermal profile was typical of an anhydrous form showing the melting endothermic effect at 198.9 ± 0.4 °C

($\Delta H_{fus} = 153 \pm 5 \text{ J g}^{-1}$).

4.4.18. 1-([1,1'-biphenyl]-4-yl)-3-morpholinopropan-1-one (24)

By following the General Procedure, starting from 4-bromo-1,1'-biphenyl (350 mg, 1.5 mmol, 1.5 equiv.), *N*-methoxy-*N*-methyl-3-morpholinopropanamide (202 mg, 1.00 mmol, 1.0 equiv.), *t*-BuLi (1.9 M, 1.32 mL, 2.5 mmol, 2.5 equiv.) and THF (5 mL), the desired product was obtained in 37% (109 mg) as a bright yellow oil after chromatography on silica gel (90:10 ethylacetate:methanol) and converted into the corresponding hydrochloride. FT-IR (cm^{-1}): 3023, 2861, overtones Ar = 2100–1700, 1683, 1603, 1451. ^1H NMR (500 MHz, CDCl_3) δ : 8.03 (d, $J = 8.4$ Hz, 2H, Ar), 7.68 (d, $J = 8.4$ Hz, 2H, Ar), 7.62 (d, $J = 7.6$ Hz, 2H, Ar), 7.47 (t, $J = 7.4$ Hz, 2H, Ar), 7.40 (t, $J = 7.4$ Hz, 1H, Ar), 3.73 (t, $J = 4.6$ Hz, 4H, Mor-3, Mor-5), 3.23 (t, $J = 7.4$ Hz, 2H, COCH_2CH_2), 2.87 (t, $J = 7.7$ Hz, 2H, $\text{CH}_2\text{CH}_2\text{N}$), 2.54 (brs, 4H, Mor-2, Mor-6). ^{13}C NMR (125 MHz, CDCl_3) δ : 198.4, 145.8, 139.7, 135.4, 128.9, 128.6, 128.2, 127.2, 66.8, 53.6, 53.5, 35.9. UHPLC-ESI-MS: ABP $t_R = 1.74$, 99% pure ($\lambda = 254$ nm), $m/z = 296.3$ [$\text{M} + \text{H}$] $^+$.

The thermal profile showed a double endothermic effect with a peak at 207.5 ± 0.1 °C and a shoulder at 196.8 ± 0.5 °C, with a total area corresponding to an enthalpy value of $165 \pm 1 \text{ J g}^{-1}$. This behaviour could be attributed to the presence of two solid phases that should be better investigated.

4.4.19. 4-Benzyl-1-(4-oxo-4-phenylbutyl)piperidin-1-ium hydrochloride (25)

By following the General Procedure, starting from bromobenzene (236 mg, 1.5 mmol, 1.5 equiv.), 4-(4-benzylpiperidin-1-yl)-*N*-methoxy-*N*-methylbutanamide (304 mg, 1.00 mmol, 1.0 equiv.), *t*-BuLi (1.9 M, 1.32 mL, 2.5 mmol, 2.5 equiv.) and THF (5 mL), the desired product was obtained in 31% (100 mg) as a bright yellow oil after chromatography on silica gel (80:20 ethylacetate:methanol) and converted into the corresponding hydrochloride. FT-IR (cm^{-1}): 3025, 2930, 2849, overtones Ar = 2100–1700, 1680, 1595, 1580, 1452, 1414. ^1H NMR (500 MHz, CDCl_3) δ : 12.06 (brs, 1H, NH^+), 7.94 (d, $J = 7.2$ Hz, 2H, Ar), 7.59 (t, $J = 7.4$ Hz, 1H, Ar), 7.47 (t, $J = 7.3$ Hz, 2H, Ar), 7.29 (t, $J = 7.1$ Hz, 2H, Ar), 7.22 (t, $J = 7.1$ Hz, 2H, Ar), 7.13 (d, $J = 7.0$ Hz, 1H, Ar), 3.60 (brd, 2H, Pip-2, Pip-6), 3.22 (brs, 2H, COCH_2CH_2), 3.04 (brs, 2H, $\text{CH}_2\text{CH}_2\text{N}$), 2.63 (m, 4H, $\text{CH}_2\text{Pip-4}$, Pip-2, Pip-6), 2.34 (brs, 2H, $\text{CH}_2\text{CH}_2\text{CH}_2$), 2.10 (m, 2H, Pip-3, Pip-5), 1.83 (d, 2H, Pip-3, Pip-5), 1.60 (m, 1H, Pip-4). ^{13}C NMR (125 MHz, CDCl_3) δ : 198.4, 139.1, 136.1, 133.7, 129.0, 128.8, 128.5, 128.0, 126.4, 57.0, 53.1, 41.9, 36.7, 35.6, 28.9, 18.0. UHPLC-ESI-MS: ABP $t_R = 2.00$, >99% pure ($\lambda = 254$ nm), $m/z = 322.5$ [$\text{M} + \text{H}$] $^+$.

The thermal profile showed two well defined endothermic effects; the first at 142.8 ± 0.3 °C attributable to a lower melting phase ($\Delta H_{fus} = 60 \pm 1 \text{ J g}^{-1}$), followed at 148.0 ± 0.3 °C by the exothermic recrystallization into the higher melting phase ($T_{fus} = 157.6 \pm 0.3$ °C, $\Delta H_{fus} = 30 \pm 3 \text{ J g}^{-1}$).

4.4.20. 4-Benzyl-1-(4-(4-methoxyphenyl)-4-oxobutyl)piperidin-1-ium hydrochloride (26)

By following the General Procedure, starting from 1-bromo-4-methoxybenzene (281 mg, 1.5 mmol, 1.5 equiv.), 4-(4-benzylpiperidin-1-yl)-*N*-methoxy-*N*-methylbutanamide (304 mg, 1.00 mmol, 1.0 equiv.), *t*-BuLi (1.9 M, 1.32 mL, 2.5 mmol, 2.5 equiv.) and THF (5 mL), the desired product was obtained in 30% (106 mg) as a bright yellow oil after chromatography on silica gel (80:20 ethylacetate:methanol) and converted into the corresponding hydrochloride. FT-IR (cm^{-1}): 3024, 3003, 2922, overtones Ar = 2100–1700, 1677, 1603, 1451. ^1H NMR (500 MHz, CDCl_3) δ : 12.03 (brs, 1H, NH^+), 7.92 (d, $J = 8.1$ Hz, 2H, Ar), 7.29 (t, $J = 7.2$ Hz, 2H, Ar), 7.21 (t, $J = 7.2$ Hz, 1H, Ar), 7.12 (d, $J = 7.1$ Hz, 2H, Ar), 6.92 (d, $J = 8.0$ Hz, 2H, Ar), 3.87 (s, 3H, OCH_3), 3.59 (brd, 2H, Pip-2, Pip-6),

3.16 (brs, 2H, COCH_2CH_2), 3.03 (brs, 2H, $\text{CH}_2\text{CH}_2\text{N}$), 2.62 (m, 4H, $\text{CH}_2\text{Pip-4}$, Pip-2, Pip-6), 2.32 (brs, 2H, $\text{CH}_2\text{CH}_2\text{CH}_2$), 2.08 (m, 2H, Pip-3, Pip-5), 1.82 (d, 2H, Pip-3, Pip-5), 1.73 (brs, 1H, Pip-4). ^{13}C NMR (125 MHz, CDCl_3) δ : 196.9, 163.8, 139.1, 130.3, 129.2, 129.0, 128.5, 126.3, 113.9, 57.0, 55.5, 53.0, 41.9, 36.6, 35.1, 28.8, 18.1. UHPLC-ESI-MS: ABS $t_R = 1.43$, 99% pure ($\lambda = 254$ nm), $m/z = 352.4$ [$\text{M} + \text{H}$] $^+$.

The thermal profile showed two endothermic effects; the first of little intensity at 119.8 ± 0.9 °C, not associated with a mass loss in TGA curve, was probably due to a metastable phase melting, and the second instead related to a stable phase melting at 157.4 ± 0.5 °C ($\Delta H_{fus} = 61 \pm 1 \text{ J g}^{-1}$).

4.4.21. 4-Benzyl-1-(4-(3-methoxyphenyl)-4-oxobutyl)piperidin-1-ium hydrochloride (27)

By following the General Procedure, starting from 1-bromo-3-methoxybenzene (281 mg, 1.5 mmol, 1.5 equiv.), 4-(4-benzylpiperidin-1-yl)-*N*-methoxy-*N*-methylbutanamide (304 mg, 1.00 mmol, 1.0 equiv.), *t*-BuLi (1.9 M, 1.32 mL, 2.5 mmol, 2.5 equiv.) and THF (5 mL), the desired product was obtained in 33% (116 mg) as a bright yellow oil after chromatography on silica gel (80:20 ethylacetate:methanol) and converted into the corresponding hydrochloride. FT-IR (cm^{-1}): 3022, 2946, 2861, overtones Ar = 2100–1700, 1687, 1595, 1486, 1465. ^1H NMR (500 MHz, CDCl_3) δ : 12.04 (brs, 1H, NH^+), 7.52 (d, $J = 7.4$ Hz, 1H, Ar), 7.45 (s, 1H, Ar), 7.37 (t, $J = 7.9$ Hz, 1H, Ar), 7.29 (t, $J = 7.2$ Hz, 2H, Ar), 7.21 (t, $J = 7.2$ Hz, 1H, Ar), 7.13 (m, 3H, Ar), 3.85 (s, 3H, OCH_3), 3.59 (brd, 2H, Pip-2, Pip-6), 3.21 (brs, 2H, COCH_2CH_2), 3.03 (brs, 2H, $\text{CH}_2\text{CH}_2\text{N}$), 2.63 (m, 4H, $\text{CH}_2\text{Pip-4}$, Pip-2, Pip-6), 2.33 (brs, 2H, $\text{CH}_2\text{CH}_2\text{CH}_2$), 2.09 (m, 2H, Pip-3, Pip-5), 1.83 (d, 2H, Pip-3, Pip-5), 1.73 (brs, 1H, Pip-4). ^{13}C NMR (125 MHz, CDCl_3) δ : 198.3, 159.8, 139.1, 137.4, 129.8, 129.0, 128.5, 126.4, 120.6, 120.1, 112.0, 56.9, 55.5, 53.0, 41.9, 36.6, 35.6, 28.8, 18.0. UHPLC-ESI-MS: ABP $t_R = 2.08$, 99% pure ($\lambda = 254$ nm), $m/z = 352.5$ [$\text{M} + \text{H}$] $^+$.

The thermal profile showed an endothermic effect at 148.9 ± 0.1 °C with a shoulder at 153.9 ± 0.2 ($\Delta H_{fus} = 76 \pm 3 \text{ J g}^{-1}$).

4.4.22. 4-Benzyl-1-(4-(naphthalen-2-yl)-4-oxobutyl)piperidin-1-ium hydrochloride (28)

By following the General Procedure, starting from 2-bromonaphthalene (311 mg, 1.5 mmol, 1.5 equiv.), 4-(4-benzylpiperidin-1-yl)-*N*-methoxy-*N*-methylbutanamide (304 mg, 1.00 mmol, 1.0 equiv.), *t*-BuLi (1.9 M, 1.32 mL, 2.5 mmol, 2.5 equiv.) and THF (5 mL), the desired product was obtained in 41% (152 mg) as a bright yellow oil after chromatography on silica gel (80:20 ethylacetate:methanol) and converted into the corresponding hydrochloride. FT-IR (cm^{-1}): 3055, 3027, 2937, 2907, overtones Ar = 2100–1700, 1681, 1496, 1441. ^1H NMR (500 MHz, CDCl_3) δ : 12.06 (brs, 1H, NH^+), 8.50 (s, 1H, Nap), 7.98 (d, $J = 8.1$ Hz, 2H, Nap), 7.88 (t, $J = 10.0$ Hz, 2H, Nap), 7.61 (t, $J = 6.8$ Hz, 1H, Nap), 7.57 (t, $J = 6.9$ Hz, 1H, Nap), 7.29 (t, $J = 7.1$ Hz, 2H, Ar), 7.22 (t, $J = 7.1$ Hz, 1H, Ar), 7.14 (d, $J = 7.1$ Hz, 2H, Ar), 3.62 (brd, 2H, Pip-2, Pip-6), 3.37 (brs, 2H, COCH_2CH_2), 3.09 (brs, 2H, $\text{CH}_2\text{CH}_2\text{N}$), 2.64 (m, 4H, $\text{CH}_2\text{Pip-4}$, Pip-2, Pip-6), 2.41 (brs, 2H, $\text{CH}_2\text{CH}_2\text{CH}_2$), 2.11 (m, 2H, Pip-3, Pip-5), 1.84 (d, 2H, Pip-3, Pip-5), 1.71 (m, 1H, Pip-4). ^{13}C NMR (125 MHz, CDCl_3) δ : 198.4, 139.1, 135.6, 133.4, 132.4, 130.1, 129.7, 129.0, 128.8, 128.7, 128.5, 127.8, 126.4, 123.4, 57.0, 53.1, 41.9, 36.6, 35.7, 28.9, 18.2. UHPLC-ESI-MS: ABS $t_R = 1.67$, >99% pure ($\lambda = 254$ nm), $m/z = 372.5$ [$\text{M} + \text{H}$] $^+$.

The thermal profile showed a first endothermic effect at 78.1 ± 0.6 °C ($\Delta H = 103 \pm 4 \text{ J g}^{-1}$) attributable to the desolvation of the sample. The TGA mass loss of $10.0 \pm 0.1\%$ recorded in the same DSC temperature range, was in agreement with the theoretical loss of one molecule of ethanol for molecule of compound (10.15%), allowing to presume the crystallization of a solvatomorph. The second endothermic effect at 162.9 ± 0.4 °C ($\Delta H_{fus} = 58 \pm 3 \text{ J g}^{-1}$)

was due to the melting of the anhydrous form.

4.4.23. 4-Benzyl-1-(4-(6-methoxynaphthalen-2-yl)-4-oxobutyl) piperidin-1-ium hydrochloride (29)

By following the General Procedure, starting from 2-bromo-6-methoxynaphthalene (256 mg, 1.5 mmol, 1.5 equiv.), 4-(4-benzylpiperidin-1-yl)-*N*-methoxy-*N*-methylbutanamide (304 mg, 1.00 mmol, 1.0 equiv.), *t*-BuLi (1.9 M, 1.32 mL, 2.5 mmol, 2.5 equiv.) and THF (5 mL), the desired product was obtained in 25% (101 mg) as a bright yellow oil after chromatography on silica gel (80:20 ethylacetate:methanol) and converted into the corresponding hydrochloride. FT-IR (cm^{-1}): 3024, 2936, overtones Ar = 2100–1700, 1674, 1482, 1409. ^1H NMR (500 MHz, CDCl_3) δ : 12.06 (brs, 1H, NH^+), 8.41 (s, 1H, Nap), 7.95 (d, $J = 8.3$ Hz, 1H, Nap), 7.85 (t, $J = 8.7$ Hz, 1H, Nap), 7.76 (d, $J = 8.4$ Hz, 1H, Nap), 7.29 (t, $J = 7.1$ Hz, 2H, Ar), 7.21 (t, 2H, Ar, Nap), 7.13 (d, 3H, Ar, Nap), 3.94 (s, 3H, CH_3), 3.61 (brd, 2H, Pip-2, Pip-6), 3.32 (brs, 2H, COCH_2CH_2), 3.08 (brs, 2H, $\text{CH}_2\text{CH}_2\text{N}$), 2.63 (m, 4H, $\text{CH}_2\text{Pip-4}$, Pip-2, Pip-6), 2.38 (brs, 2H, $\text{CH}_2\text{CH}_2\text{CH}_2$), 2.09 (m, 2H, Pip-3, Pip-5), 1.83 (d, 2H, Pip-3, Pip-5), 1.74 (m, 1H, Pip-4). ^{13}C NMR (125 MHz, CDCl_3) δ : 198.1, 159.9, 139.1, 137.5, 131.5, 131.3, 129.9, 129.0, 128.5, 127.7, 127.3, 126.4, 124.2, 119.9, 105.6, 57.0, 55.4, 53.0, 41.9, 36.6, 35.4, 28.9, 18.2. UHPLC-ESI-MS: ABS $t_{\text{R}} = 1.71$, >99% pure ($\lambda = 254$ nm), $m/z = 4022.5$ [M + H] $^+$.

The thermal profile showed, at 170.5 ± 0.6 °C, an endothermic effect due to a lower melting phase ($\Delta H_{\text{fus}} = 53 \pm 4$ J g^{-1}), followed at 178.1 ± 0.5 °C by the exothermic recrystallization into the higher melting phase ($T_{\text{fus}} = 206.7 \pm 0.2$ °C, $\Delta H_{\text{fus}} = 68 \pm 5$ J g^{-1}).

4.4.24. 1-(4-([1,1'-biphenyl]-4-yl)-4-oxobutyl)-4-benzylpiperidin-1-ium hydrochloride (30)

By following the General Procedure, starting from 4-bromo-1,1'-biphenyl (350 mg, 1.5 mmol, 1.5 equiv.), 4-(4-benzylpiperidin-1-yl)-*N*-methoxy-*N*-methylbutanamide (304 mg, 1.00 mmol, 1.0 equiv.), *t*-BuLi (1.9 M, 1.32 mL, 2.5 mmol, 2.5 equiv.) and THF (5 mL), the desired product was obtained in 26% (103 mg) as a bright yellow oil after chromatography on silica gel (80:20 ethylacetate:methanol) and converted into the corresponding hydrochloride. FT-IR (cm^{-1}): 3083, 3025, 2995, 2850, overtones Ar = 2100–1700, 1684, 1604. ^1H NMR (500 MHz, CDCl_3) δ : 12.07 (brs, 1H, NH^+), 8.02 (d, $J = 6.3$ Hz, 2H, Ar), 7.69 (d, $J = 6.3$ Hz, 2H, Ar), 7.62 (d, $J = 7.2$ Hz, 2H, Ar), 7.46 (t, $J = 7.1$ Hz, 2H, Ar), 7.41 (t, $J = 7.2$ Hz, 1H, Ar), 7.30 (t, $J = 7.1$ Hz, 2H, Ar), 7.22 (t, $J = 7.2$ Hz, 1H, Ar), 7.14 (d, $J = 7.0$ Hz, 2H, Ar), 3.61 (brd, 2H, Pip-2, Pip-6), 3.26 (brs, 2H, COCH_2CH_2), 3.07 (brs, 2H, $\text{CH}_2\text{CH}_2\text{N}$), 2.64 (m, 4H, $\text{CH}_2\text{Pip-4}$, Pip-2, Pip-6), 2.37 (brs, 2H, $\text{CH}_2\text{CH}_2\text{CH}_2$), 2.11 (m, 2H, Pip-3, Pip-5), 1.85 (d, 2H, Pip-3, Pip-5), 1.73 (m, 1H, Pip-4). ^{13}C NMR (125 MHz, CDCl_3) δ : 198.0, 146.2, 139.6, 139.1, 134.8, 129.0, 128.7, 128.5, 128.4, 127.4, 127.2, 126.4, 57.0, 53.2, 41.9, 36.7, 35.7, 28.9, 18.1. UHPLC-ESI-MS: ABS $t_{\text{R}} = 1.81$, 98% pure ($\lambda = 254$ nm), $m/z = 398.4$ [M + H] $^+$.

The thermal profile showed an exothermic effect at 168.7 ± 0.9 °C, probably attributable to a crystallization of an amorphous fraction of sample, induced by heating. The melting of the anhydrous form was then recorded at 216.4 ± 0.4 °C ($\Delta H_{\text{fus}} = 84 \pm 1$ J g^{-1}).

4.5. Physicochemical and pharmacokinetic predictions

The physicochemical properties of compounds 7–30 were calculated by using Chemicalize online property explorer. The *in silico* ability in crossing the BBB was calculated by using the CNS Multiparameter Optimization Desirability (CNS MPO) tool.

4.6. Binding assays

4.6.1. Materials

Guinea pig brains for the S1R binding assays were commercially available (Harlan–Winkelmann, Borchon, Germany). Homogenizer: Elvehjem Potter (B. Braun Biotech International, Melsungen, Germany) and Soniprep 150, MSE, London, UK). Centrifuges: Cooling centrifuge model Rotina 35R (Hettich, Tuttingen, Germany) and High-speed cooling centrifuge model Sorvall RC-5C plus (Thermo Fisher Scientific, Langenselbold, Germany). Multiplates: standard 96-well multiplates (Diagonal, Muenster, Germany). Shaker: self-made device with adjustable temperature and tumbling speed (scientific workshop of the institute). Vortexer: Vortex Genie 2 (Thermo Fisher Scientific, Langenselbold, Germany). Harvester: MicroBeta FilterMate-96 Harvester. Filter: Printed Filtermat Type A and B. Scintillator: Meltilex (Type A or B) solid-state scintillator. Scintillation analyzer: MicroBeta Trilux (all PerkinElmer LAS, Rodgau-Jügesheim, Germany). Chemicals and reagents were purchased from various commercial sources and were of analytical grade.

4.6.2. Preparation of membrane homogenates from Guinea pig brain cortex

Five guinea pig brains were homogenized with the potter (500–800 rpm, 10 up-and-down strokes) in six volumes of cold 0.32 M sucrose. The suspension was centrifuged at $1200 \times g$ for 10 min at 4 °C. The supernatant was separated and centrifuged at $23,500 \times g$ for 20 min at 4 °C. The pellet was resuspended in 5–6 volumes of buffer (50 mM Tris, pH 7.4) and centrifuged again at $23,500 \times g$ (20 min, 4 °C). This procedure was repeated twice. The final pellet was resuspended in 5–6 volumes of buffer and frozen (–80 °C) in 1.5 mL portions containing ~1.5 (mg protein)/mL $^{-1}$.

4.6.3. Preparation of membrane homogenates from rat liver

Two rat livers were cut into small pieces and homogenized with the potter (500–800 rpm, 10 up-and-down strokes) in six volumes of cold 0.32 M sucrose. The suspension was centrifuged at $1200 \times g$ for 10 min at 4 °C. The supernatant was separated and centrifuged at $31,000 \times g$ for 20 min at 4 °C. The pellet was resuspended in 5–6 vol of buffer (50 mM TRIS, pH 8.0) and incubated at rt for 30 min. After the incubation, the suspension was centrifuged again at $31,000 \times g$ for 20 min at 4 °C. The final pellet was resuspended in 5–6 vol of buffer and stored at –80 °C in 1.5 mL portions containing about 2 mg protein/mL.

4.6.4. Cell culture and preparation of membrane homogenates from GluN2B cells

Mouse I(tk-) cells stably transfected with the dexamethasone inducible eukaryotic expression vectors pMSG GluN1a, pMSG GluN2B (1:5 ratio) were grown in Modified Earl's Medium (MEM) containing 10% of standardized FCS (Biochrom AG, Berlin, Germany).

The expression of the NMDA receptor at the cell surface was induced after the cell density of the adherent growing cells had reached approximately 90% of confluency. For the induction, the original growth medium was replaced by growth medium containing 4 μM dexamethasone and 4 μM ketamine (final concentration). After 24 h, the cells were rinsed with phosphate buffered saline solution (PBS, Biochrom AG, Berlin, Germany), harvested by mechanical detachment and pelleted (10 min, $5000 \times g$).

For the binding assay, the cell pellet was resuspended in PBS solution and the number of cells was determined using a Scepter[®] cell counter (MERCK Millipore, Darmstadt, Germany). Subsequently, the cells were lysed by sonication (4 °C, 6×10 s cycles with breaks of 10 s). The resulting cell fragments were centrifuged with a

high performance cool centrifuge ($23,500 \times g$, 4°C). The supernatant was discarded and the pellet was resuspended in a defined volume of PBS yielding cell fragments of approximately 500,000 cells/mL. The suspension of membrane homogenates was sonicated again (4°C , 2×10 s cycles with a break of 10 s) and stored at -80°C .

4.6.5. General protocol for binding assays

The test compound solutions were prepared by dissolving $\sim 10 \mu\text{mol}$ (usually 2–4 mg) of test compound in DMSO so that a 10 mM stock solution was obtained. To obtain the required test solutions for the assay, the DMSO stock solution was diluted with the respective assay buffer. The filtermats were presoaked in 0.5% aqueous polyethylenamine solution for 2 h at rt before use. All binding experiments were carried out in duplicate in 96-well multiplates. The concentrations given are the final concentrations in the assay. Generally, the assays were performed by addition of 50 μL of the respective assay buffer, 50 μL test compound solution at various concentrations (10^{-5} , 10^{-6} , 10^{-7} , 10^{-8} , 10^{-9} and 10^{-10} M), 50 μL of corresponding radioligand solution, and 50 μL of the respective receptor preparation into each well of the multiplate (total volume 200 μL). The receptor preparation was always added last. During the incubation, the multiplates were shaken at a speed of 500–600 rpm at the specified temperature. Unless otherwise noted, the assays were terminated after 120 min by rapid filtration using the harvester. During the filtration each well was washed five times with 300 μL of water. Subsequently, the filtermats were dried at 95°C . The solid scintillator was melted on the dried filtermats at 95°C for 5 min. After solidifying of the scintillator at RT, the trapped radioactivity in the filtermats was measured with the scintillation analyzer. Each position on the filtermat corresponding to one well of the multiplate was measured for 5 min with the [^3H]-counting protocol. The overall counting efficiency was 20%. The IC_{50} values were calculated with GraphPad Prism 3.0 (GraphPad Software, San Diego, CA, USA) by nonlinear regression analysis. The IC_{50} values were subsequently transformed into K_i values using the equation of Cheng and Prusoff. The K_i values are given as mean value \pm SEM from three independent experiments.

4.6.6. S1R binding assay

The assay was performed with the radioligand [^3H](+)-pentazocine ($22.0 \text{ Ci mmol}^{-1}$; PerkinElmer). The thawed membrane preparation of guinea pig brain cortex ($\sim 100 \mu\text{g}$ protein) was incubated with various concentrations of test compounds, 2 nM [^3H](+)-pentazocine, and Tris buffer (50 mM, pH 7.4) at 37°C . The nonspecific binding was determined with 10 mM unlabeled (+)-pentazocine. The K_d value of (+)-pentazocine is 2.9 nM.

4.6.7. S2R binding assay

The assay was performed using 150 μg of rat liver homogenate were incubated for 120 min at room temperature with 3 nM [^3H]-DTG (Perkin–Elmer, specific activity $58.1 \text{ Ci mmol}^{-1}$) in 50 mM Tris–HCl, pH 8.0, 0.5 mL final volume. (+)-pentazocine (100 nM) and haloperidol (10 μM) were used to mask S1R and to define non-specific binding, respectively.

4.6.8. GluN2 binding assay

The competitive binding assay was performed with the radioligand [^3H]-ifenprodil (60 Ci mmol^{-1} ; BIOTREND, Cologne, Germany). The thawed cell membrane preparation from the transfected L(tk-) cells (about 20 μg protein) was incubated with various concentrations of test compounds, 5 nM [^3H]-ifenprodil, and TRIS/EDTA buffer (5 mM TRIS/1 mM EDTA, pH 7.5) at 37°C . The non-specific binding was determined with 10 mM unlabeled ifenprodil. The K_d value of ifenprodil is 7.6 nM.

4.7. Inhibition of AChE

AChE inhibitory activity of compounds 7–30 were determined by the modified Ellman's method. Briefly, stock solutions of tested compounds (5.0 mM) were prepared in DMSO and diluted using 0.1 M $\text{KH}_2\text{PO}_4/\text{K}_2\text{HPO}_4$ buffer (pH 8.0) to afford a final concentration range between 1 and 50 μM . Enzyme solutions were prepared by dissolving lyophilized powder in double-distilled water. The assay solution consisted of 845 μL of 0.1 M phosphate buffer $\text{KH}_2\text{PO}_4/\text{K}_2\text{HPO}_4$, 25 μL of AChE solution (0.22 U/mL, E.C. 3.1.1.7, from electric eel) and 10 μL of various concentrations of test compounds, which was allowed to stand for 5 min at 25°C before 100 μL of 0.01 M DTNB were added. The reaction was started by addition of 20 μL of the 0.075 M substrate solution (acetylthiocholine iodide) and exactly 2 min after substrate addition, the absorption was measured at 25°C at 412 nm. In enzyme-free assay systems the non-enzymatic hydrolysis of acetylthiocholine iodide was measured, and the results were employed as blank. In control experiments, inhibitor-free assay systems were utilized to measure the full activity. A positive control of Donepezil was used to afford a final concentration range between 10 nM–50 μM . The percent inhibition was calculated, using the expression: $(1 - A_i/A_c) \times 100$, where A_i and A_c are the absorbances obtained for AChE in the presence and absence of the inhibitors, respectively, after subtracting the respective background. Each experiment was performed in triplicate, and the mean \pm standard deviation was calculated. Data from concentration-inhibition experiments of the inhibitors were calculated by nonlinear regression analysis, using the Excel program.

4.8. In silico studies

4.8.1. Molecular dynamic simulations

S1R crystal structure in complex with 4-IBP (pdb code 5hk2) [47] was retrieved from the Protein Data Bank [48] and used to investigate the dynamic properties of the receptor. Instead, the X-ray structure of AChE was available in complex with Donepezil (pdb code 4ey7) [49] and we relied on it for molecular docking of our novel compounds.

Molecular dynamic (MD) simulations of S1R were performed in a membrane environment, in the *holo* form (without any ligand) and in complex with the co-crystallized ligand. Structures were prepared with MOE [50] dedicated tools: hydrogen atoms and missing side chains were added. Atomic charges were calculated and the protonation state determined at physiological conditions (pH 7.4). N- and C-termini were capped with acetyl and N-methyl groups, respectively. Salt, detergent and bulk water molecules were removed from the crystal structures, whilst water molecules which were present in the binding site were maintained. The membrane was built around the three alpha helices by using the CHARMM-GUI membrane builder [51]. The protein was embedded in a heterogeneous membrane, composed of POPC (palmitoyl-oleoyl-phosphatidyl-choline) and cholesterol in 3:1 ratio. Potassium ions were added in order to neutralize the system. MD simulations were performed with the AMBER force field and analyzed with Amber tools [52]. The ligand was parametrized by using Antechamber [53] and Parmchk [52]. Dedicated force fields were used for protein (ff99SBonlysc), lipids (lipid14), ions (ionsff99_tip3p) and water (TIP3P) [54]. MD simulations were performed at 300 K, with time step of 2 fs and in anisotropic pressure scaling conditions. Van der Waals and short-range electrostatic interactions were cut off at 10 Å, whilst long-range ones were computed with Particle Mesh Ewald (PME) method. Simulations were carried out for 100 ns for each system.

4.8.2. Molecular docking

The crystal structures and the centroid of the most representative cluster obtained from MD simulations were used to dock ligands into S1R and AChE binding pockets. Ligand docking was carried out with Glide, a grid-based algorithm implemented in Maestro Schrödinger's suite [55]. The grid was generated around the co-crystallized ligands with a radius of 15 Å. Default Van der Waals scaling was used, with scaling factor of 1.0 and partial charge cut-off of 0.25. Partial charges were computed with the OPLS-2005 force field. E172 was selected as possible H-bond constraint for S1R ligand binding. Ligands of the training set were extracted from the ChEMBL database [56] and decoys from the DUDE database [57]. The S1R dataset included 102 agonists and 150 decoys. Whereas, for the AChE dataset we considered 100 inhibitors and 151 decoys. Ligands were processed with Maestro LigPrep, which generated three-dimensional structures and determined the protonation state. Rigid docking was performed for S1R by using a diverse set of 25 conformers for every molecule, which were generated by Maestro ConfGen with default settings. In contrast, flexible docking was applied to AChE ligands. The docking models were then validated with the new dataset of compounds that we present in this paper.

4.9. Antioxidant activity

FRS activity of the examined compounds was determined using the DPPH assay. Briefly, compounds **8**, **10**, **13–14**, **18–20**, **23–28**, **RRC-33**, **donepezil** and **Cur** were dissolved in 1 mL of EtOH, to obtain a stock solution of 5.0 mM. The FRS potential was evaluated at a final concentration of 465 µM. The reaction mixture was prepared by adding 100 µL of each compound solution to 1.875 mL of DPPH solution, freshly prepared by dissolving DPPH in methanol/KH₂PO₄ and NaOH buffer (50/50 v/v) at a concentration of 6×10^{-5} M. After 20 min of incubation at room temperature, the absorbance was measured at 515 nm by the UV–Visible spectrophotometer.

FRS% was expressed as a percent compared with the control, consisting of 1.875 mL of DPPH solution and 100 µL of EtOH. The percent inhibition of the DPPH radical by the test solution was calculated using the following formula:

$$\text{FRS\%} = [(\text{Abs control} - \text{Abs sample}) / \text{Abs control}] \times 100$$

The analyses were carried out in triplicate and results are expressed as mean ± SE.

4.10. MTS assay

CellTiter 96[®] Aqueous One Solution Cell Proliferation Assay (Promega, Milan, Italy) was used on cells seeded onto a 96-well plate at a density of 9×10^3 cells per well. The effect of compounds **8**, **10**, **13–14**, **18–20**, **23–28**, **RRC-33**, **donepezil** and **Cur** was evaluated, at three different concentrations (10, 25 and 50 µM), after 24 h and 48 h of continued exposure. Three independent experiments were performed for each concentration. The optical density (OD) of treated and untreated cells was determined at a wavelength of 490 nm using a plate reader. For compounds **10**, **14** and **20**, a dose response curve was determined by using five different concentrations (1, 10, 25, 35, 50 and 100 µM). IC₅₀ values were calculated by Graph Pad Prism 5 Program.

4.11. Neuroprotection against H₂O₂ induced neurotoxicity

ROS assay was performed in living cells. Human neuroblastoma cell lines (SH-SY5Y) were seeded at 2×10^4 cells per well in 96-well

plates for neuroprotection activity assay. Briefly, intracellular ROS production was measured from SH-SY5Y cells, using ab113851 kit (DCDFA ROS assay kit). Cells were pre-treated with compounds **10**, **14**, **20**, **Cur**, **donepezil** and **RRC-33** for 3 h. The medium was replaced with 100 µL of DCDFA (25 µM) and incubated for 45 min. Afterwards the medium was eliminated and cells were washed with buffer solution. Lastly, cells were treated with 100 µL of each compound (10 µM) and H₂O₂ (180 µM) for 24 h. The total fluorescence was measured using a fluorescence microplate reader (Synergy HTX, Biotek), with excitation and emission wavelengths of 490 nm and 530 nm, respectively.

4.12. Neurotrophic activity

The neurotrophic activity was assessed by measuring the neurite elongation in DRG explants as experimental model. Briefly, compound **10** and **20** were dissolved in DMSO to obtain a stock solution of 10 mM, then diluted in culture medium to obtain the different working concentrations. DRG from E15 Sprague-Dawley rats were aseptically removed and cultured onto a single layer of rat-tail collagen surfaces in 35 mm dishes. DRG were incubated in AN₂ medium (MEM plus 10% Calf Bovine Serum, 50 µg/mL ascorbic acid, 1.4 mM L-glutamine, 0.6% glucose) in the presence of 5 ng/ml NGF and Fudr (10^{-5} M) to remove supporting cells in a 5% CO₂ humidified incubator at 37 °C.

To study the neurotrophic effect of compound **10** and **20** on neurite elongation, DRG explants were treated for 2 h with NGF and then exposed to different compound concentrations (10 µM, 7.5 µM, 5 µM, 2.5 µM, 1 µM, 750 nM, 500 nM, 250 nM) for 24 h and 48 h. DRG treated with AN₂ medium and 5 ng/ml NGF alone represented controls. The neurotrophic effect was evaluated by measuring the length of the longest neurite in each DRG using the ImageJ program (NIH, Bethesda, MD, USA). A statistical analysis was carried out with the one-way Anova test and Tukey post-test with the statistical package GraphPad Prism (GraphPad Software, San Diego, CA, USA). P Value < 0.05 was considered as statistically significant.

Acknowledgement

The Authors gratefully acknowledge University of Pavia for the research grant to M.R. and MIUR for the doctoral fellowship to G.R. Moreover, the authors would like to thank Emanuele Bignardi for his contribution to the biological investigation, and Andrea Sala for his contribution to modeling studies.

Appendix A. Supplementary data

Supplementary data related to this article can be found at <https://doi.org/10.1016/j.ejmech.2018.09.010>.

References

- [1] H.M. Gao, J.S. Hong, Why neurodegenerative diseases are progressive: uncontrolled inflammation drives disease progression, *Trends Immunol.* **29** (2008) 357–365.
- [2] M. Golpich, E. Amini, Z. Mohamed, R. Azman Ali, N. Mohamed Ibrahim, A. Ahmadiani, Mitochondrial dysfunction and biogenesis in neurodegenerative diseases: pathogenesis and treatment, *CNS Neurosci. Ther.* **23** (2017) 5–22.
- [3] report Neurological disorders affect millions globally: WHO report. <http://www.who.int/mediacentre/news/releases/2007/pr04/en/> (Accessed 07 April 2018).
- [4] P. Kovacic, R. Somanathan, Redox processes in neurodegenerative disease involving reactive oxygen species, *Curr. Neuropharmacol.* **10** (2012) 289–302.
- [5] A. Nowacek, L.M. Kosloski, H.E. Gendelman, Neurodegenerative disorders and nanoformulated drug development, *Nanomedicine* **4** (2009) 541–555.
- [6] A.D. Gitler, P. Dhillon, J. Shorter, Neurodegenerative diseases: models, mechanisms, and a new hope, *Dis. Model Mech.* **10** (2017) 499–502.
- [7] A. De Felice, L. Ricceri, A. Venerosi, F. Chiarotti, G. Calamandrei, Multifactorial

- origin of neurodevelopmental disorders: approaches to understanding complex etiologies, *Toxics* 3 (2015) 89–129.
- [8] R. Cacabelos, L. Fernandez-Novoa, V. Lombardi, Y. Kubota, M. Takeda, Molecular genetics of Alzheimer's disease and aging, *Methods Find. Exp. Clin. Pharmacol.* 27 (Suppl A) (2005) 1–573.
 - [9] T. Myhrer, Neurotransmitter systems involved in learning and memory in the rat: a meta-analysis based on studies of four behavioral tasks, *Brain Res. Brain Res. Rev.* 41 (2003) 268–287.
 - [10] S. Perez-Lloret, F.J. Barrantes, Deficits in cholinergic neurotransmission and their clinical correlates in Parkinson's disease, *NPJ Parkinsons Dis* 2 (2016) 16001.
 - [11] M. Jucker, L.C. Walker, Pathogenic protein seeding in Alzheimer's disease and other neurodegenerative disorders, *Ann. Neurol.* 70 (2011) 532–540.
 - [12] P. Sweeney, H. Park, M. Baumann, J. Dunlop, J. Frydman, R. Kopito, A. McCampbell, G. Leblanc, A. Venkateswaran, A. Nurni, R. Hodgson, Protein misfolding in neurodegenerative diseases: implications and strategies, *Transl. Neurodegener.* 6 (2017) 6.
 - [13] X. Chen, C. Guo, J. Kong, Oxidative stress in neurodegenerative diseases, *Neural Regen. Res.* 7 (2012) 376–385.
 - [14] C. Guo, L. Sun, X. Chen, D. Zhang, Oxidative stress, mitochondrial damage and neurodegenerative diseases, *Neural Regen. Res.* 8 (2013) 2003–2014.
 - [15] (a) S. Collina, G. Loddio, M. Urbano, L. Linati, A. Callegari, F. Ortuso, S. Alcaro, C. Lagner, T. Langer, O. Prezzavento, G. Ronisvalle, O. Azzolina, Design, synthesis, and SAR analysis of novel selective σ_1 ligands, *Bioorg. Med. Chem.* 15 (2007) 771–783; (b) D. Rossi, M. Urbano, A. Pedrali, M. Serra, D. Zampieri, M.G. Mamolo, C. Lagner, C. Zanette, C. Florio, D. Schepmann, B. Wuensch, O. Azzolina, S. Collina, Design, synthesis and SAR analysis of novel selective σ_1 ligands (Part 2), *Bioorg. Med. Chem.* 18 (2010) 1204–1212.
 - [16] L. Nguyen, B.P. Lucke-Wold, S. Mookerjee, N. Kaushal, R.R. Matsumoto, Sigma-1 receptors and neurodegenerative diseases: towards a hypothesis of Sigma-1 receptors as amplifiers of neurodegeneration and neuroprotection, *Adv. Exp. Med. Biol.* 964 (2017) 133–152.
 - [17] S. Collina, R. Gaggeri, A. Marra, A. Bassi, S. Negrinotti, F. Negri, D. Rossi, Sigma receptor modulators: a patent review, *Expert Opin. Ther. Pat.* 23 (2013) 597–613.
 - [18] K. Ruscher, T. Wieloch, The involvement of the sigma-1 receptor in neurodegeneration and neurorestoration, *J. Pharmacol. Sci.* 127 (2015) 30–35.
 - [19] L. Nguyen, B.P. Lucke-Wold, S.A. Mookerjee, J.Z. Cavendish, M.J. Robson, A.L. Scandinaro, R.R. Matsumoto, Role of sigma-1 receptors in neurodegenerative diseases, *J. Pharmacol. Sci.* 127 (2015) 17–29.
 - [20] B. Penke, L. Fulop, M. Szucs, E. Frecska, The role of Sigma-1 receptor, an intracellular chaperone in neurodegenerative diseases, *Curr. Neuropharmacol.* 16 (2018) 97–116.
 - [21] T.Y. Weng, S.Y.A. Tsai, T.P. Su, Roles of sigma-1 receptors on mitochondrial functions relevant to neurodegenerative diseases, *J. Biomed. Sci.* 24 (2017) 74.
 - [22] S.Y. Tsai, T. Hayashi, T. Mori, T.P. Su, Sigma-1 receptor chaperones and diseases, *Cent. Nerv. Syst. Agents Med. Chem.* 9 (2009) 184–189.
 - [23] K. Heiss, L. Vanella, P. Murabito, O. Prezzavento, A. Marrazzo, C. Castruccio Castracani, I. Barbagallo, A. Zappala, E. Arena, M. Astuto, A. Giarratano, G. Li Volti, (+)-Pentazocine reduces oxidative stress and apoptosis in microglia following hypoxia/reoxygenation injury, *Neurosci. Lett.* 626 (2016) 142–148.
 - [24] W.J. Geldenhuys, C.J. Van der Schyf, Rationally designed multi-targeted agents against neurodegenerative diseases, *Curr. Med. Chem.* 20 (2013) 1662–1672.
 - [25] E. Arena, I. Cacciatore, L.S. Cerasa, H. Turkez, V. Pittalà, L. Pasquinnuci, A. Marrazzo, C. Parenti, A. Di Stefano, O. Prezzavento, New bifunctional antioxidant/ σ_1 agonist ligands: preliminary chemico-physical and biological evaluation, *Bioorg. Med. Chem.* 24 (2016) 3149–3156.
 - [26] T. Korcsmáros, M.S. Szalay, C. Bóde, I.A. Kovács, P. Cserehely, How to design multi-target drugs: target search options in cellular networks, *Expert Opin. Drug Discov.* 2 (2007) 1–10.
 - [27] A. Talevi, Multi-target pharmacology: possibilities and limitations of the "skeleton key approach" from a medicinal chemist perspective, *Front. Pharmacol.* 6 (2015) 1–7.
 - [28] (a) D. Rossi, A. Pedrali, R. Gaggeri, A. Marra, L. Pignataro, E. Laurini, V. DalCol, M. Fermiglia, S. Pricl, D. Schepmann, B. Wuensch, M. Peviani, D. Curti, S. Collina, Chemical, pharmacological, and in vitro metabolic stability studies on enantiomerically pure RC-33 compounds: promising neuroprotective agents acting as σ_1 receptor agonists, *ChemMedChem* 8 (2013) 1514–1527; (b) D. Rossi, A. Pedrali, A. Marra, L. Pignataro, D. Schepmann, B. Wuensch, L. Ye, K. Leuner, M. Peviani, D. Curti, O. Azzolina, S. Collina, Studies on the enantiomers of RC-33 as neuroprotective agents: isolation, configurational assignment, and preliminary biological profile, *Chirality* 25 (2013) 814–822; (c) A. Marra, D. Rossi, L. Pignataro, C. Bigogno, A. Canta, N. Oggioni, A. Malacrida, M. Corbo, G. Cavalletti, M. Peviani, D. Curti, G. Dondio, S. Collina, Toward the identification of neuroprotective agents: g-scale synthesis, pharmacokinetic evaluation and CNS distribution of (R)-RC-33, a promising Sigma1 receptor agonist, *Future Med. Chem.* 8 (2016) 287–295.
 - [29] S. Collina, M. Rui, S. Stotani, E. Bignardi, D. Rossi, D. Curti, F. Giordanetto, A. Malacrida, A. Scuteri, G. Cavalletti, Are sigma receptor modulators a weapon against multiple sclerosis disease? *Future Med. Chem.* 9 (2017) 2029–2051.
 - [30] M.B. Colović, D.Z. Krstić, T.D. Lazarević-Pašti, A.M. Bondžić, V.M. Vasić, Acetylcholinesterase inhibitors: pharmacology and toxicology, *Curr. Neuropharmacol.* 11 (2013) 315–335.
 - [31] U. Holzgrabe, P. Kapková, V. Alptüzün, J. Scheiber, E. Kugelmann, Targeting acetylcholinesterase to treat neurodegeneration, *Expert Opin. Ther. Targets* 11 (2007) 161–179.
 - [32] A. Barzegar, A.A. Moosavi-Movahedi, Intracellular ROS protection efficiency and free radical-scavenging activity of curcumin, *PLoS One* 6 (2011), e26012.
 - [33] Herbal Medicine: Biomolecular and Clinical Aspects, in: Chapter 13 Turmeric, the Golden Spice, Benzie IFF, Wachtel-galior S, second ed., CRC Press/Taylor & Francis, Boca Raton (FL), 2011.
 - [34] P. Anand, A.B. Kunnumakara, R.A. Newman, B.B. Aggarwal, Bioavailability of curcumin: problems and promises, *Mol. Pharm.* 4 (2007) 807–818.
 - [35] G.M. Cole, B. Teter, S.A. Frautschy, Neuroprotective effects of curcumin, *Adv. Exp. Med. Biol.* 595 (2007) 197–212.
 - [36] A. Monroy, G.J. Lithgow, S. Alavez, Curcumin and neurodegenerative diseases, *Biofactors* 39 (2013) 122–132.
 - [37] A. Amalraj, A. Pius, S. Gopi, S. Gopi, Biological activities of curcuminoids, other biomolecules from turmeric and their derivatives – a review, *J. Tradit. Complement. Med.* 7 (2017) 205–233.
 - [38] M. Muehbacher, G.M. Spitzer, K.R. Liedl, J. Kornhuber, Qualitative prediction of blood-brain barrier permeability on a large and refined dataset, *J. Comput. Aided Mol. Des.* 25 (2011) 1095–1106.
 - [39] T.T. Wager, X. Hou, P.R. Verhoest, A. Villalobos, Central nervous system multiparameter optimization desirability: application in drug discovery, *ACS Chem. Neurosci.* 7 (2016) 767–775.
 - [40] L. Temme, B. Frehland, D. Schepmann, D. Robaa, W. Sippl, B. Wuensch, Hydroxymethyl bioisosteres of phenolic GluN2B-selective NMDA receptor antagonists: design, synthesis and pharmacological evaluation, *Eur. J. Med. Chem.* 144 (2018) 672–681.
 - [41] G.L. Ellman, K.D. Courtney, V. Andres, R.M. Feather-Stone, A new and rapid colorimetric determination of acetylcholinesterase activity, *Biochem. Pharmacol.* 7 (1961) 88–95.
 - [42] C.B. Mishra, A. Manral, S. Kumari, V. Saini, M. Tiwari, Design, synthesis and evaluation of novel indandione derivatives as multifunctional agents with cholinesterase inhibition, anti- β -amyloid aggregation, antioxidant and neuroprotection properties against Alzheimer's disease, *Bioorg. Med. Chem.* 24 (2016) 3829–3841.
 - [43] J. Meunier, J. Ieni, T. Maurice, The anti-amnesic and neuroprotective effects of donepezil against amyloid beta_{25–35} peptide-induced toxicity in mice involve an interaction with the sigma1 receptor, *Br. J. Pharmacol.* 149 (2006) 998–1012.
 - [44] M.L. Poutsma, The radical stabilization energy of a substituted carbon-centered free radical depends on both the functionality of the substituent and the ordinality of the radical, *J. Org. Chem.* 76 (2011) 270–276.
 - [45] A. Phaniendra, D.B. Jestadi, L. Periyasamy, Free radicals: properties, sources, targets, and their implication in various diseases, *Indian J. Clin. Biochem.* 30 (2015) 11–26.
 - [46] E. Fetisova, B. Chernyak, G. Korshunova, M. Muntyan, V. Skulachev, Mitochondria-targeted antioxidants as a prospective therapeutic strategy for multiple sclerosis, *Curr. Med. Chem.* 24 (2017) 2086–2114.
 - [47] H.R. Schmidt, S.D. Zheng, E. Gurpinar, A. Koehl, A. Manglik, A.C. Kruse, Crystal structure of the human sigma 1 receptor, *Nature* 532 (2016) 527–530.
 - [48] H.M. Berman, J. Westbrook, Z. Feng, G. Gilliland, N.N. Bhat, H. Weissig, I.N. Shindyalov, P.E. Bourne, The protein Data Bank, *Nucleic Acids Res.* 28 (2000) 235–242.
 - [49] J. Cheung, M.J. Rudolph, F. Burshsteyn, M.S. Cassidy, E.N. Gary, J. Love, M.C. Franklin, J.J. Height, Structures of human acetylcholinesterase in complex with pharmacologically important ligands, *J. Med. Chem.* 55 (2012) 10282–10286.
 - [50] *Molecular Operating Environment (Moe)* (2016), vol. 2015.1001 ed. (Montreal, QC, Canada: Chemical Computing Group Inc.).
 - [51] S. Jo, T. Kim, W. Im, Automated builder and database of protein/membrane complexes for molecular dynamics simulations, *PLoS One* 2 (2007) e880.
 - [52] D.A. Case, V.B.J.T. Berryman, R.M. Betz, Q. Cai, D.S. Cerutti, T.E. Cheatham, T.A. Darden III, R.E. Duke, H. Gohlke, A.W. Goetz, S. Gusarov, N. Homeyer, P. Janowski, J. Kaus, I. Kolossvary, A. Kovalenko, T.S. Lee, S.L.T. Luchko, R. Luo, B. Madej, K.M. Merz, F. Paesani, D.R. Roe, A. Roitberg, C. Sagui, R. Salomon-Ferrer, G. Seabra, C.L. Simmerling, W. Smith, J. Swails, R.C. Walker, J. Wang, R.M. Wolf, X. Wu, P.A. Kollman, *AMBER 14*, 2014.
 - [53] J.M. Wang, W. Wang, P.A. Kollman, D.A. Case, Automatic atom type and bond type perception in molecular mechanical calculations, *J. Mol. Graph. Model.* 25 (2006) 247–260.
 - [54] C.J. Dickson, B.D. Madej, A.A. Skjevik, R.M. Betz, K. Teigen, I.R. Gould, R.C. Walker, Lipid14: the amber lipid force field, *J. Chem. Theor. Comput.* 10 (2014) 865–879.
 - [55] R.A. Friesner, J.L. Banks, R.B. Murphy, T.A. Halgren, J.J. Klicic, D.T. Mainz, M.P. Repasky, E.H. Knoll, M. Shelley, J.K. Perry, D.E. Shaw, P. Francis, P.S. Shenkin, Glide: a new approach for rapid, accurate docking and scoring. 1. Method and assessment of docking accuracy, *J. Med. Chem.* 47 (2004) 1739–1749.
 - [56] L.J. Bellis, A. Gaulton, A. Hersey, A.P. Bento, J. Chambers, M. Davies, F. Kruger, Y. Light, N. Dedman, S. Mcglinchey, M. Nowotka, G. Papadatos, R. Santos, J.P. Overington, ChEMBL – linking chemistry and biology to enable mapping onto molecular pathways, *Abstr. Pap. Am. Chem. Soc.* 248 (2014).
 - [57] M.M. Mysinger, M. Carchia, J.J. Irwin, B.K. Shoichet, Directory of useful decoys, enhanced (DUD-E): better ligands and decoys for better benchmarking, *J. Med. Chem.* 55 (2012) 6582–6594.

Paper 4

REVIEW



Approaches for multi-gram scale isolation of enantiomers for drug discovery

Daniela Rossi^a, Marilù Tarantino^a, Giacomo Rossino^a, Marta Rui^a, Markus Juza^b and Simona Collina^a

^aDrug Sciences Department, Medicinal Chemistry and Pharmaceutical Technology Section, University of Pavia, Pavia, Italy; ^bCorden Pharma Switzerland LLC, Liestal, Switzerland

ABSTRACT

Introduction: Over the last 30 years, the scientific community has directed its efforts towards the identification of enantioselective approaches to obtain the desired active enantiomer. Accordingly, efficient production of single enantiomers from small to large scale, throughout Drug Discovery (DD) programs, has become of great interest and a fundamental challenge.

Areas covered: This review focuses on two fundamental strategies for preparing enantiomers in high yields and with an excellent enantiomeric excess (ee). Separation of racemates, enantioselective synthesis procedures, and integrated approaches have been extensively reviewed, to offer a guide that enables the selection of the suitable methodology for producing pure enantiomers in scales from small to large.

Expert opinion: Over the past two decades, drug regulatory agencies have set strict rules on the use of racemates and pure enantiomers, leading to the transformation of the drug market. Indeed, the number of drugs approved as a single enantiomer has exponentially increased, outclassing the racemic compounds. As a consequence, the academia and pharmaceutical companies are eager to develop efficient procedures for obtaining enantiopure compounds on the desired scale.

ARTICLE HISTORY

Received 9 July 2017
Accepted 20 September 2017

KEYWORDS

Enantiomers; separation of racemates; enantioselective synthesis; multi grams-scale

1. Introduction


The growing use of enantiopure drugs, pesticides, insecticides, fungicides, and herbicides triggers the increasing market demand for chiral-based products [1–4]. During the last 60 years, scientists learned a lot about the close relationship between enantiopure compounds and human body. It is now well recognized that each enantiomer of a chiral drug may behave differently under physiological conditions (i.e. they can exhibit different pharmacological and/or toxicological profiles), due to the stereochemical discrimination in the interaction with biological molecules that are themselves chiral [5–9].

Despite the complexity associated with chiral chemistry, in 2010 the Transparency Market Research estimated a growth of the global market of chiral technology, which can be divided into enantioselective synthesis, separation of enantiomers, and chiral analysis. From an economic standpoint, in 2010 enantioselective synthesis gained 80% of the total market, generating a revenue of \$3.7 billion, whereas the chiral analysis market was worth \$734 million [10]. Looking at the pharmaceutical industry, most of the commercially available drugs are chiral. Furthermore, the vast majority of new small-molecule drug candidates are enantiomerically pure and thus methods suitable to obtain the target enantiomer in high purity are required [5,11–13].

U.S. Food and Drug Administration (U.S. FDA) and European Medicines Agency are supporting the growth of chiral market. Since 1992, U.S. FDA guidelines and policies require that the absolute stereochemistry of all chiral centers present in a drug must be established. Regulators still allow

the development of racemic mixtures; however, their development has to be justified by an assessment of the risk/benefit ratio [14,15]. To date, pharmaceutical companies involved in Drug Discovery (DD) programs are obliged to prepare single enantiomers, in amount sufficient for testing them separately. At the beginning, only milligrams of enantiomeric compounds should be available, while in the late DD phases the preparation of enantiomeric pure compounds in multi-gram scale is required to evaluate their biological properties. Several procedures can be applied for obtaining enantiomers (Figure 1), depending on the stage of DD (hit identification, lead generation and lead optimization, preclinical evaluation) [16]. Accordingly, robust skills in enantiopure compound preparation and separation techniques are necessary to evaluate all the parameters, having an impact on quality, time, and cost for the identification of new potential drugs [17]. In light of these considerations, the preparation of single enantiomers is a fundamental challenge for both academia and pharmaceutical industry and it plays a key role in DD processes.

In this review, we will focus on the main methodologies commonly used to obtain enantiomeric pure compounds in a suitable amount for performing the biological investigations to move forward in the DD programs. We will particularly discuss the scalable methodologies useful for producing enantiomers from milligrams to multi-grams scale. The main approaches used in the various stages of DD will be discussed: (i) separation of racemates through chromatography or crystallization techniques, (ii) enantioselective synthesis based on

CONTACT Simona Collina  simona.collina@unipv.it

© 2017 Informa UK Limited, trading as Taylor & Francis Group

Article highlights

- The demand for enantiopure drugs has led, during the last decades, to the widespread need of enantiopure compounds, deeply affecting the drug discovery (DD) process in all its phases.
- Different techniques can be exploited to obtain enantiopure compounds, and an accurate evaluation of advantages and limitations of each procedure is essential.
- Two main approaches are usually adopted: either separation of enantiomers (which involves different techniques such as enantioselective chromatography over chiral stationary phases and crystallization) or enantioselective synthesis (which includes chiral pool synthesis, enantioselective catalysis and biocatalysis).
- Depending on DD stage (from hit identification to early development), enantiomeric purity required, synthetic feasibility, environmental impact and economic budget, the best amongst the reported approaches should be identified.
- Sometimes, using only one technique could result in unsatisfactory results in terms of purity, productivity or scalability. In these cases, integrated approaches are crucial: combining two or more of the described techniques could significantly improve the overall efficiency

This box summarizes key points contained in the article.

chiral pool, chiral auxiliaries, chiral catalysts, or biocatalysis, and (iii) integrated approaches based on the combination of different techniques.

2. Separation of racemates

In the initial phase of the DD process, racemic compounds in small quantities are required for a first screening. Once the most active compound has been identified, both enantiomers are needed for the first biological testing at least in the scale of 10 mg [16,17]. For the separation of racemates, enantioselective chromatography using chiral stationary phases (CSPs) is generally considered at first, being a viable route for straightforward and rapid access to both enantiomers with high enantiomeric purity and yields. For the scaling up to multi-grams scale, sometimes the procedure could be revised and crystallization of diastereoisomeric salts may be exploited as a

good alternative. Scalability is the most important factor to be considered for selecting the appropriate resolution method to access enantiomeric compounds for biological/pharmacological testing. If a medicinal chemistry team studied early the issues related to scale-up, it may change the strategy on time, thus avoiding delays in reaching the drug development stage [5,11–13,16–18].

Here, we will focus only on enantioselective chromatography and crystallization of diastereomeric salts (Figure 1) as the major easily scalable resolution approaches used in the last 20 years, as resulted by the numerous reviewed papers.

Some promising and emerging techniques are under investigation, i.e. capillary electrophoresis and membrane-based resolution, but only analytical applications have been reported so far [19,20].

2.1. Enantioselective chromatography

Keeping in mind that enantiomers possess the same physico-chemical properties (i.e. solubility, melting point, pKa), they obviously behave identically in an achiral chromatographic environment. Therefore, enantiodiscrimination can be achieved when enantiomers are converted into covalent (indirect methods) or transient (direct methods) diastereoisomeric derivatives. In the indirect chromatographic methods, an enantiomeric pure chiral agent is employed to transform each enantiomer into a covalent diastereomeric complex that are then separated using an achiral stationary phase, taking advantage of their different chemical or physical properties [21].

As regarding the direct chromatographic methods, the protagonist is a chiral selector – physically or chemically immobilized or coated onto a solid support – which forms with the two enantiomers transient diastereoisomeric derivatives, endowed with different stability and thus the enantiomers are able to migrate through the column with different speed.

The indirect methods are often limited by (i) the additional step of derivatization, (ii) the problems in removing the reagents, and (iii) the necessity to monitor and control

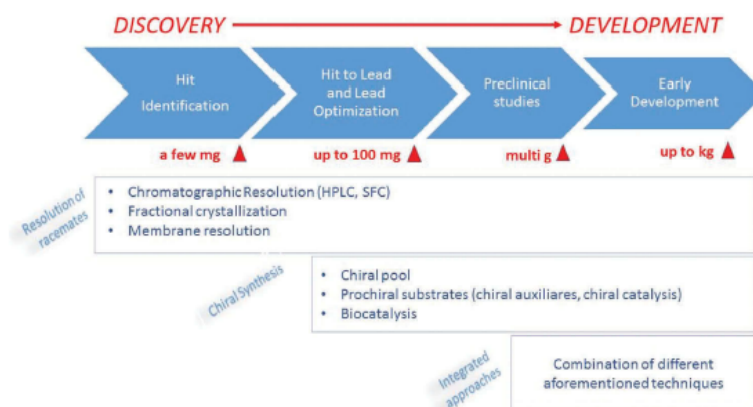


Figure 1. Approaches for isolation of enantiomers in drug discovery and development.

racemization during the resolution process and thus these drawbacks led to antiquating the strategy [22].

Based on literature analysis and our long experience in the preparation of enantiomeric compounds [23–26], high performance liquid chromatography (HPLC) and supercritical fluid chromatography (SFC) using CSPs are powerful and easily scalable tools. In fact, they are perfectly in line with the criteria required at the various stages of DD, such as a quick access to both the enantiomers of a chiral molecule with high enantiomeric excess and amounts ranging from milligrams to multi-gram scale (Figure 1). The chiral selector of the CSP is the core of the enantiodiscrimination process and numerous CSPs became available on the market during the last 30 years for analytical, semi-preparative, and preparative purposes. Among these, the most common CSPs used in DD process are reported in Table 1, together with their chiral selector, the column trade name, and the chromatographic technique (HPLC, SFC, or both) they are suitable for.

The reviewed literature highlights that in the past two decades a limited number of CSPs dominate the chromatographic resolution scenario [13,27]. Particularly, the polysaccharide-based CSPs are the most versatile columns, in virtue of their ability to resolve a wide range of racemates and therefore, they are commonly used in DD. The first generation of these columns is the 'coated polysaccharide-based CSPs', characterized by a good loadability but poor solvent compatibility, i.e. DCM or AcOEt have to be avoided. This drawback was outstandingly overcome by immobilizing the chiral selector onto the solid support, obtaining the new generation of 'immobilized polysaccharide-based CSPs' that allow the use of an extended solvent range, previously incompatible with the coated CSPs [28].

The key point of the chromatographic separation of enantiomers is the selection of CSPs in combination with a suitable mobile phase. Although their structural features diversity could guarantee a complementary recognition, column selection still remains an empirical process, based on the experience of the researchers, on literature suggestion, or more simply, on the classical trial and error process. Accordingly, the setup of a fast, pragmatic, and non-comprehensive column screening in analytical scale could drive the rapid establishment of the optimal experimental conditions for scale-up purposes. A consolidated approach consists in a primary screening with chiral selectors with the broadest application and in including the remaining selectors in a secondary screening. In fact, a significant number of publications deals with this topic [29–31]. Accordingly, the standard screening protocol used in our laboratory for primary screening employs both immobilized and coated cellulose- and amylose-derived CSPs (Table 1). The elution conditions include mixtures of alkane and polar modifiers (i.e. ethanol or 2-propanol), alcohols (methanol, ethanol, and 2-propanol), acetonitrile as well as mixtures of acetonitrile and alcohols [26].

The selection of the optimal combination CSP-mobile phase is guided by enantioselectivity and enantioresolution values. Nevertheless, retention times (they must be as short as possible), high solubility of the racemate and the enantiomers in the eluent/injection solvent, and the use of a mobile phase

consisting of a pure low-cost solvent, thus facilitating workup and re-use of mobile phase, are other important prerequisites for an economic and productive preparative enantiomer separation. Once the analytical resolution method was properly evaluated, optimization of the separation on a given column is a methodical and straightforward process [23].

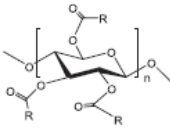
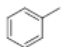
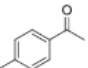
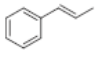
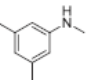
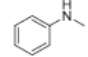
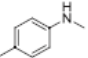
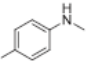
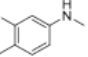
It should be noted that not only polysaccharide-derived CSPs can be used for analytical and preparative enantiomer separations. Other types of chiral selectors include stationary phases based on π - π interactions [32], ligand exchange mechanisms [33], anion exchange CSPs [34] as well as CSPs based on antibiotics [35] or proteins [36], chiral synthetic polymers [37] and many more. All these types of CSPs have merits of their own and are very often alternatives to polysaccharidic CSPs and can provide in some cases unique enantioselectivity complementary to amylose- and cellulose-based CSPs. A number of overviews on CSPs have been published [38].

Among the plethora of works in the field of separation of enantiomers published so far, here we report as an example the resolution of the racemic flavanone Naringenin NRG, (5,7-dihydroxy-2-(4-hydroxyphenyl)chroman-4-one) via enantioselective HPLC on a semi-preparative scale [23]. The application of the mentioned screening protocol for cellulose- and amylose-derived CSPs allowed to quickly identify Chiralpak AD-H (Table 1) and methanol as the best CSP-mobile phase combination, giving rise to relatively short retention times, high enantioselectivity, and good resolution. These experimental conditions were then properly scaled-up, on both a pre-packed Regispack column and a Chiralpak AD column packed and tested in-house with bulk CSP. In both cases, about 2.5 g of racemic NRG were processed in 28 h with an eluent consumption of about 50 L. Therefore, this procedure enabled an exhaustive biological investigation of both NRG enantiomers in very short times.

The major drawback of enantioselective HPLC is related to solvent consumption. To reduce the volumes of solvents, the 'green chromatographic' SFC methodology, which uses carbon dioxide combined with a liquid co-solvent in smaller quantities as eluent, has been developed [39]. The addition of the modifier leads often to subcritical conditions of CO₂; however, the term SFC is used for supercritical and subcritical conditions alike. Over the last few years, SFC has been established as a full analytical technique – not only for separations of enantiomers – that is a very valid and broadly accepted option for efficient method development platforms, as it is testified by the increasing number of works in this field [39–41]. The CO₂ is removed by reducing the pressure, leaving only a smaller amount of modifier to evaporate. This reduction in solvent volumes allows for higher product concentrations and reduces time and cost of purification. Furthermore, the low viscosity and the high diffusivity of CO₂ permit the high flow rates, which reduce analysis and equilibration times and increase the throughput capacity without compromising efficiency.

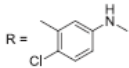
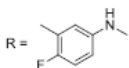
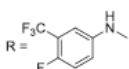
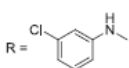
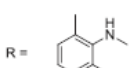
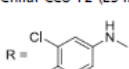
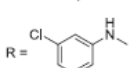
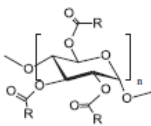
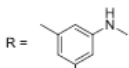
However, some factors still limit the extensive use of SFC. First of all, the higher cost of the instruments in comparison to HPLC units and the larger size of the equipment and reservations about the use of compressed gases hinder the fast implementation of this technology. Nevertheless, the obvious advantages of SFC, i.e. high diffusivity, fast mass transfer, and

Table 1. Commonly used chiral columns for semipreparative scale (I.D. 6–10 mm) or preparative scale (I.D. >21.2 mm) separations.

Chiral selector	Trade name
	
Cellulose	R = -CH ₃
MCTA/CTA-1 (Merck); Chiralcel CA-1, Chiralcel OA (Daicel)	R = 
Chiralcel OB (Daicel); Eurocel 02 (Knauer); Reprosil Chiral-BM (Dr. Maisch HPLC)	R = 
Chiralcel OJ (Daicel); Eurocel 03 (Knauer); CHIRIS-IOJ (CHIRIS); Lux Cellulose-3 (Phenomenex); Reprosil Chiral-JM (Dr. Maisch HPLC); Enantiocel-C3 (Column Tek); Chiral Cellulose T-MB (Silicycle); Chromega Chiral CCI (ES Industries)	R = 
Chiralcel OK (Daicel)	R = 
Chiralcel OD, Chiralcel OD-I, Chiralpak IB (Daicel); Nucleocel Delta (Macherey & Nagel); Eurocel 01 (Knauer); CelluCoate (Akzo Nobel); Lux Cellulose-1 (Phenomenex); RegisCell (Regis); CHIRIS-IOD (CHIRIS); Epitomize CSP-1C (Orochem Technologies); Reflection CL (Sielc Technologies); Chiral-OM (CS-Chromatographie); Cellulose DMP (Sigma-Aldrich (Astec)); Reprosil Chiral-OM (Dr. Maisch HPLC); CHIRAL ART Cellulose-C, CHIRAL ART Cellulose-SB (YMC); Enantiocel-C1 (Column Tek); ACQUITY Trefoil CEL1 (Waters); Chiral Cellulose T-DPC (Silicycle); Chromega Chiral CCO (ES Industries)	R = 
Eurocel 04 (Knauer); CHIRIS-IOB (CHIRIS); Chiralcel OC (Daicel); Reprosil Chiral-CM (Dr. Maisch HPLC)	R = 
Chiralcel OG (Daicel)	R = 
Chiralcel OF (Daicel); Reprosil Chiral-FM (Dr. Maisch HPLC);	R = 
Chiralcel OZ (Daicel); Lux Cellulose-2 (Phenomenex); Epitomize CSP-1Z (Orochem Technologies); Chromega Chiral CC2 (ES Industries); Reprosil Chiral ZM (Dr. Maisch HPLC); Enantiocel-C2 (Column Tek); ACQUITY Trefoil CEL2 (Waters).	

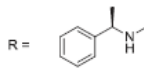
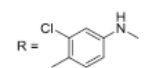
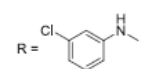
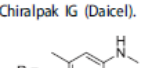
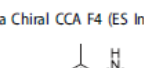

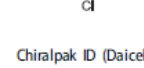
(Continued)

Table 1. (Continued).

Chiral selector	Trade name
	Chiralcel OX (Daicel); Lux Cellulose-4 (Phenomenex); Chromega Chiral CC4 (ES Industries).
	Chromega Chiral CCO F4 (ES Industries).
	Chromega Chiral CCO F4T3 (ES Industries).
	Chiralpak IC (Daicel); CHIRAL ART Cellulose-SC (YMC); Lux i-Cellulose-5 (Phenomenex).
	Chromega Chiral CCO F2 (ES Industries).
	Chromega Chiral CCC (ES Industries).
	Chromega Chiral CCC (ES Industries)
	Amylose
	Chiralpak AD, Chiralpak IA (Daicel); AmyCoate (Akzo Nobel); Nucleocel ALPHA (Macherey & Nagel), Europak 01 (Knauer); RegisPack (Regis)CHIRIS-IAD (CHIRIS); Epitomize CSP-1A (Orochem Technologies)MutoHigh Chiral-AM (CS-Chromatographie); Reprosil Chiral-AM (Dr. Maisch HPLC); CHIRAL ART Amylose-C, CHIRAL ART Amylose-SA (YMC); Enantiopak-A1 (Column Tek); ACQUITY Trefoil AMY1 (Waters); Lux Amylose-1 (Phenomenex); Chiral Amylose T-DPC (Silicycle); Chromega Chiral CCA (ES Industries).

(Continued)

Table 1. (Continued).

Chiral selector	Trade name
	Chiralpak AS-V (Daicel); Reprosil Chiral-AS (Dr. Maisch HPLC); Chromega Chiral CCS (ES Industries).
	Chiralpak AZ, Chiralpak IF (Daicel); Lux Amylose-2 (Phenomenex); Epitomize CSP-1K (Orochem Technologies); Reprosil Chiral-ZA (Dr. Maisch HPLC); Chromega Chiral CC4 (ES Industries).
	Chiralpak IG (Daicel).
	Chromega Chiral CCA F4 (ES Industries).
	Chiralpak AY (Daicel); Chromega Chiral CC3 (ES Industries); RegisPack CLA-1 (Regis); Reprosil Chiral-YM (Dr. Maisch HPLC); Lux Amylose-2 (Phenomenex).
	Chiralpak ID (Daicel).
	Chiralpak IE (Daicel); CHIRAL ART Amylose-SE (YMC).

the resulting short retention times, together with a new generation of reliable SFC systems from major instrument producers will lead inevitably to the adoption of this technology in industry and academia. Especially in the pharmaceutical industry, the higher throughput and productivity of SFC versus HPLC allows for a direct comparison of investment and operating costs and how fast SFC will reach a breakeven point with HPLC.

A number of studies provided by the chiral column producers demonstrated that preparative polysaccharide-based columns gave comparable results both in SFC and HPLC separation conditions.

Recently, we compared HPLC and SFC productivity of enantiomeric 2-(4-phenylphenyl)-4-(1-piperidyl)butan-2-ol RC-34 in multi-gram scale [25]. The sigma-1 receptor (S1R) agonist RC-

34 was subjected to a pilot SFC screening on Chiralpak IA and Chiralpak IC by gradient elution using CO₂ and polar modifiers (MeOH, EtOH, or isopropanol) or a mixture of n-heptane and alcohols (isopropanol or EtOH). Then, isocratic runs were carried out in order to optimize selectivity and resolution. The screening in SFC turned out to be much faster and more straightforward when compared to HPLC. The best separation conditions in terms of enantioselectivity and resolution obtained on Chiralpak IA and on Chiralpak IC (Table 1) were properly scaled-up. As regarding enantioselective HPLC, Chiralcel OJ-H and MeOH resulted the best combination of CSP-mobile phase, and accordingly they were scaled-up. Although HPLC and SFC gave rise to recoveries and yields in the same range as well as compounds with high enantiomeric excess (ee), the specific productivity of SFC method resulted to

be almost four times lower than the specific productivity observed in semi-preparative HPLC.

As discussed above, the well-established and versatile HPLC and SFC techniques are both effective in resolving racemates. Their use depends on the instrumentation availability, as well as the experience of the DD teams involved. SFC and HPLC are often complementary in selectivity and both technologies are useful tools for enantiomer separations. HPLC is mainly widespread in academic labs, while SFC is gaining more and more importance in research and throughput-driven industry. For better insight, important reviews recently published in the field of separations of enantiomers, coming from both academic groups and industry, should be consulted [13,16,17,41–45].

Another up-to-date chromatographic technique to be mentioned is the simulated moving bed (SMB) chromatography. It is employed only in the preparative mode and therefore it is mainly useful for the clinical phases and industrial production, which is a topic not discussed in this review. Broader reviews on SMB are in references [45–47]. Chiral gas chromatography (GC) can also be successfully used for enantiomer separation of volatile compounds of pharmaceutical interest. However, due to low loading and stability issues of many compounds under GC conditions, this remains a niche technology [48].

2.2. Crystallization of diastereomeric salts

Potential drugs with acidic or basic properties can be resolved by crystallization of their diastereomeric salts (sometimes referred to as 'fractional crystallization') [49,50]. The interaction of a racemic mixture with the single enantiomer of a chiral material, called resolving agent, gives rise to two diastereomeric derivatives, with dissimilar physical properties, allowing a separation of enantiomers through crystallization. This approach requires laboratory equipment only and it is suitable for resolutions from the 100-mg scale to industrial processes. On the other hand, sometimes crystallization processes do not provide a product with an enantiomeric purity meeting regulatory requirement due to the phase diagram, and further enantioselective chromatographic purification will be required. Many papers on diastereomeric salt resolution and on the behavior of enantiomeric mixtures can guide researchers in the selection of a proper resolving agent, although this choice depends on the experience of the researchers and still has trial-and-error aspects [49–52].

For identifying crystallization resolution conditions, at least 1–2 g of racemates are needed and a systematic approach has to be applied, taking into account that the use of a resolving agent structurally related to the racemic molecule generally produces a more efficient resolution [12,52]. Different enantiomerically pure acids or bases as resolving agents, depending on the racemate properties, and different solvents (or solvent mixtures) have to be screened. If the crystallization process occurs, the ee of crystals and mother liquors obtained has to be evaluated by analytical HPLC using CSPs.

For the resolution of racemic amines, tartaric acid and its diaryl derivatives (i.e. dibenzoyl-tartaric acid and di-p-toluoyl-L-tartaric acid), mandelic acid, camphor sulphonic acids and some N-acetylated amino acids are widely used, also

considering that they are relatively cheap. Moreover, dehydroabiatic acid (DHAA) is a natural chiral carboxylic acid and can be largely and inexpensively obtained. The application of DHAA and its derivatives for separation of some enantiomers (Figure 2) is well documented [53].

For the resolution of racemic acids, several alkaloids (i.e. brucine, cinchonine, quinine, and quinidine), phenylethylamine, and ephedrine are available (Figure 2). Despite the efficiency of crystallization via diastereomeric salts has been broadly reported, this procedure requires operators with a long experience in this field and an acute ability in choosing the solvents and their quantities [54]. A significant aspect that deserves to be mentioned is the time-consuming precipitation of the desired diastereomeric salt, which may occur slowly. Insights into these considerations, as well as the greater understanding of crystallization processes, are becoming increasingly useful in obtaining new resolving agents.

A variant of the crystallization of diastereomeric salts described above is the so-called 'Dutch resolution' where a mixture of resolving agents with analogous structure (called families) is applied. A mixture of three structurally related and stereochemically homogeneous compounds is generally used as resolving agents instead of a single resolving agent [12,55]. Several families of structurally related resolving agents have been described, including the mandelic acids (M-mix), benzoyl tartaric acids (T-mix), cyclic phosphoric acids (P-mix), chalcones (J-mix), N-benzoylphenylglycines (PGA-mix), amino-phenylethanol (PG-mix), and phenylethylamines (PE-I-mix, PE-II-mix, and PE-III-mix) (Figure 2) [56,57].

This process is extremely useful for resolving racemates up to 100-mg scale, thus filling the gap of the fractional crystallization. This variant generally possesses high success rate and represents a valuable opportunity for reaching enantio-separation in DD process.

A wide number of resolutions by crystallization of diastereomeric salts has been reported in the literature. From the analysis of the papers it clearly emerges that this technique is nowadays preferentially applied in industry for preparative purposes, rather than in academia in the DD process [58,59].

2.3. Preferential crystallization

A very elegant technique to achieve enantiomeric separation is preferential (sometimes called 'direct') crystallization. This approach is applicable only when the racemate is a conglomerate, i.e. a mixture of mirror-image crystallized phases exhibiting symmetrical enantiomeric excess [60]. Unfortunately, conglomerates are not much common: it has been estimated that only 5–10% of the chiral substances belong to this type [61]. However, when it can be performed, preferential crystallization represents a powerful, clean, and scalable technique that does not necessitate chiral auxiliaries. There are two main methods that can be employed: (i) the entrainment process and (ii) simultaneous crystallization [12]. The first one is a kinetic process that exploits the difference in crystallization rates of the enantiomers when homochiral seeds are added to the racemic supersaturated solution. The energy required for the growth of the seeded crystals is lower than the energy required for the spontaneous nucleation of the

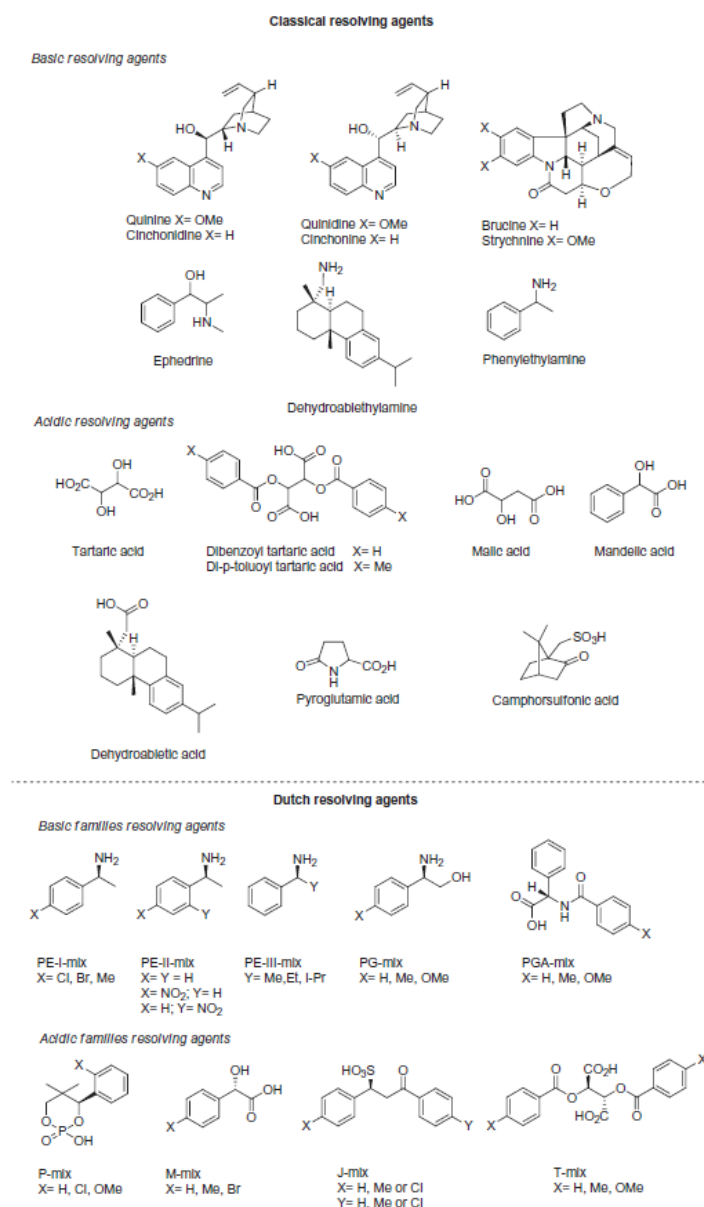


Figure 2. Resolving agents commonly used.

nonseeded enantiomer. However, the process must be stopped before crystallization of the undesired enantiomer becomes likely, so that the system cannot reach equilibrium. This process can be carried out in different modes, the most important of which are known as Seeded Isothermal Preferential Crystallization and Seeded Polythermic Preferential Crystallization [60]. The entrainment process is

mainly employed on smaller scales in a batch mode. Nonetheless, some example of its use on industrial scale is available, such as in the production of broad-spectrum antibiotics (e.g. chloramphenicol, thiamphenicol, and b-lactams) [61]. The second approach, i.e. simultaneous crystallization, is typically used on large scale, both in batch and continuous modes. The two enantiomers are allowed to crystallize

simultaneously, but they are locally separated from a solution that remains close to the racemic composition [12]. Simultaneous crystallization has been used for industrial-scale production of various commercially relevant products and intermediates, such as (-)-menthol, L- α -methyl-dopa, and L-glutamic acid [62]. Many improvements and innovations have been exploited during the years to enhance efficiency, material throughput, batch reproducibility, and crystal quality associated with preferential crystallization. These include, for example, Auto-Seeded Polythermic Programmed Preferential Crystallization, continuous crystallization techniques performed with innovative reactor concepts, and Second-Order Asymmetric Transformation, which exploits racemization of the unwanted enantiomer to increase overall yield and minimize waste. For an in-depth discussion on these topics, we suggest referring to some excellent reviews that can be found in recent literature [12,63].

3. Enantioselective synthesis

In the last stage of DD and in early stage of development, large quantities (100 g upto kg) of a newly identified biologically active compound with a defined stereochemistry are needed. The literature analysis evidenced that in the chemical landscape of modern medicinal chemistry, asymmetric synthesis is currently the preferred approach once the eutomer has been identified [11,12,64–66].

3.1. Chiral pool

Enantiomerically pure compounds can be obtained starting from molecules belonging to the chiral pool, i.e. a set of enantiopure molecules naturally available (carbohydrates, α amino acids, terpenes, hydroxyl acids, and alkaloids). These starting materials are incorporated into the new compounds, providing the chiral center(s) with the desired configuration [67]. Compounds from chiral pool are often relatively cheap and can become the starting materials for efficient synthetic strategy. Nonetheless, they have to present a certain similarity to the desired product; otherwise, the subsequent synthesis can be more challenging, requiring multiple steps with possible racemization. In particular, racemization is a potential issue that should always be kept in mind: all the reactions performed with building blocks from chiral pool must avoid this aspect, otherwise the chiral information of the starting material will be lost [11].

Some recent examples in literature show how chiral pool synthesis is used to successfully access enantiomeric pure products of pharmaceutical interest. For instance, in 2015, an efficient total synthesis of antiepileptic (R)-lacosamide 2 starting from L-serine was developed [68]. The process, consisting in five synthetic steps, has an overall yield of 54% and does not involve kinetic resolution or expensive chiral ligands, making it commercially viable (Figure 3). Another recent study demonstrated the possibility to obtain 1,2-disubstituted 3-benzazepines 4 using natural amino acids as chiral-building blocks [69]. The key step of the synthetic pathway is a calcium-

catalyzed Friedel-Crafts cyclization, which afforded the desired products with high diastereoselectivity (Figure 3).

Several interesting examples of chiral pool synthesis have been properly discussed in a recent literature review [11].

3.2. Chiral auxiliaries

A different synthetic strategy consists in using achiral compounds (prochiral substrates) as starting material, which can be easily converted into enantiopure compounds. Enantiopure chiral auxiliaries can be used for controlling the stereochemical course of specific reactions [12,70]. This approach requires the use of stoichiometric amounts of a chiral auxiliary, which is temporarily coupled with the starting material. The obtained product is involved in a diastereoselective transformation, where the selectivity of the reaction is governed by the configuration of the chiral auxiliary. Despite its use in stoichiometric amount, the chiral auxiliary possesses the advantage to be recovered after a reaction and thus recycled for another process or producing more of the target enantiomer. Racemization is an important drawback related to the enantiopure agent and particular attention is required to avoid this issue to prevent enantiomeric purity lowering.

3.3. Chiral catalysts

Chiral catalysts, such as chiral coordination complexes, in stoichiometric amount can be used to obtain the formation of the desired stereoisomer. The chiral catalyst is not consumed during the process and can be reused, avoiding waste and improving the efficiency of the synthetic procedure. Here below, we highlight a few examples of the two workhorses in DD and development.

Asymmetric hydrogenation (AH) is one of the most relevant enantioselective transformations. During its history of 40 years, thousands of homogeneous catalysts have been developed, allowing the hydrogenation of many substrates with high enantioselectivity [11]. Recently, new ligands suitable for rhodium-catalyzed AH of olefins and ketones have been designed and synthesized. Particularly, a family of supramolecular chiral phosphite ligands, named PhthalaPhos, has been developed using a combinatorial approach. These ligands, which share a common phthalamidic group, are easily prepared from inexpensive starting materials, and showed excellent enantioselectivity in the hydrogenation, on mg scale, of both benchmark olefins and challenging substrates 5–6, 9, 11 of potential interest from a medicinal chemistry standpoint (Figure 3) [71]. To replace the commonly used expensive and highly toxic transition metals (e.g. Ru, Rh, Ir, Pd) with their cheaper and safer first-row counterparts (e.g. Fe, Co, Ni), new BINOL-derived chiral (cyclopentadienone) iron complexes (CK) were prepared. The new compounds catalyze the AH of ketones (i.e. 13) with good enantioselectivities (i.e. 14, up to 77% ee) (Figure 3). These iron catalysts are of interest for DD, in virtue of their stability, low cost, and scalability characteristics and provide compounds with good ee [72].

Another important stereoselective reaction of great relevance in DD is the asymmetric allylic alkylation (AAA). This reaction, originally developed by Trost [73], exploits a chiral palladium

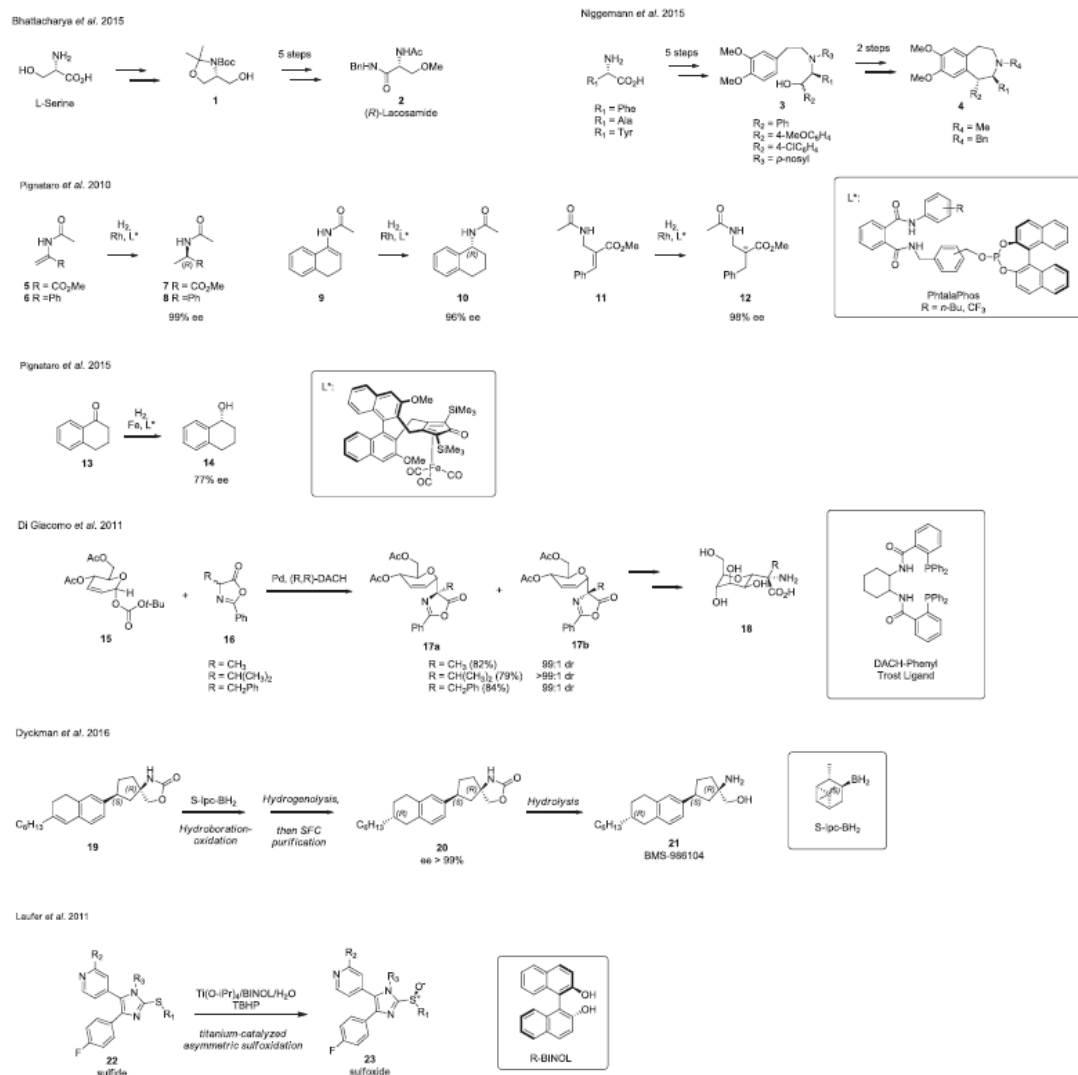


Figure 3. Chiral synthesis examples.

catalyst and has shown good versatility in organic synthesis. Recently, the AAA has been used to access quaternary α -D-C-mannosyl-(S)-amino acids **18** with high yields and excellent diastereoisomeric ratio (dr). The optimal condition provided a Pd source, a chiral diphosphine ligand, and a solvent, affording the desired product in 100-mg scale from commercial 4,6-di-O-acetyl *R*-pseudoglucal carbonate **15** and racemic amino acid-derived azalactones **16**. C-glycosyl α -amino acids have recently emerged as useful building blocks in the synthesis of C-glycosylated peptides, which are important mimics of naturally occurring N- and O-glycoproteins with potential therapeutic applications in a variety of diseases (Figure 3) [74].

Another example regarding AH is the synthesis of BMS-986104 **21**, which is a sphingosine 1-phosphate receptor modulator, which is characterized by the presence of three chiral centers (Figure 3). The originally proposed synthesis was not stereoselective, requiring 11 steps, several resolutions with SFC, and was characterized by low overall yield (<1% yield) [75]. The AH of a trisubstituted alkene was the key step of an alternative synthetic strategy. The use of *S*-isopinocampheylborane (*S*-Ipc-BH₂) allowed high levels of diastereoselectivity, thus providing the desired compound **21** with purity up to 99.8% and an increased overall yield respect to the original synthesis (21% yield, 12 steps) (Figure 3) [76].

Chiral sulfoxides can be found in a number of drugs, containing asymmetric sulfinyl moieties. A metal-catalyzed asymmetric oxidation of prochiral sulfides can be adopted to obtain chiral sulfoxides in high ee (up to 99%). Titanium-catalyzed asymmetric oxidations of tri- and tetrasubstituted 2-thioimidazoles **22** afforded the corresponding sulfoxides **23**. In this way, 11 sulfoxides have been synthesized some of them with high yields and high ee in gram scale. Depending on the configuration of the chiral auxiliaries, *S*-BINOL or *R*-BINOL, both enantiomers are synthetically accessible (Figure 3) [77].

Exploring new reaction conditions is generally time-consuming. Nevertheless, a vast number of asymmetric synthesis currently employed and the systematic literature reviews published so far could be helpful for medicinal chemists [11,64–66,78,79].

3.4. Biocatalysis

Biocatalysis is lately gaining importance for the synthesis of enantiomerically pure drugs [80,81]. The increasing diffusion of this methodology is due to its intrinsic advantages, such as the use of renewable and biodegradable enzymatic catalysts, the reduction of synthetic steps, and the mild reaction conditions. There are hundreds of enzymes that can be used for biocatalysis, belonging to diverse categories, such as lipases, esterases, transaminases, reductases, oxidases, and isomerases [82]. Hereinafter, we focus on some commonly employed enzymes, reporting significant recent examples of their successful application to pharmaceuticals production.

Lipases are among the most commonly employed enzymes in biocatalysis. A recent review reports the most interesting examples found in literature over the last years concerning the use of lipases to obtain enantiopure drugs and/or their intermediates [83]. Most reported biocatalytic processes refer to kinetic resolutions of racemic substrates, which occur under mild conditions with a high degree of regio- or enantioselectivity. Hydrolysis of racemic or prochiral esters along with stereoselective acylation of alcohols are the most popular lipase-catalyzed reactions. A recent example foresees the immobilization of the lipase on synthetic resin in order to

facilitate separation and recycle of the enzyme at the end of the reaction [84].

Among the products of pharmaceutical interest, chiral amines deserve particular mention. They can be easily obtained using biocatalytic approaches. In fact, kinetic resolution of racemic amines through lipases has been extensively used [85,86]. A more efficient strategy, which is currently gaining relevance, consists in the use of transaminases for converting prochiral ketones directly into primary amines in a single operation. Recent studies have been aimed at overcoming the limitations of this method, such as solubility, limited substrate range, and product inhibition. In 2010, an efficient biocatalytic process for the large-scale production of the antidiabetic sitagliptin **25** (Figure 4) was developed. In this procedure, a novel effective transaminase enzyme was used, affording a notable improvement over the previous Rh-catalyzed synthesis [87], with the undesired isomer not being formed in quantities above the limits of detection [88]. Moreover, the enzyme developed showed a broad substrate range and enhanced tolerance toward organic solvents, making it of practical interest for pharmaceutical manufacturing. A further improvement of this process was achieved 2 years later immobilizing the transaminase on hydrophobic resin, making it fully operational in organic solvent and allowing multiple rounds of enzyme reuse [89]. Another enzyme, a ketoreductase, was recently covalently bound to polymer-based resin to obtain enantiopure (*R*)-1-(3,5-bis(trifluoromethyl)phenyl)ethanol **27**, a key intermediate in the synthesis of the antiemetic EMEND **28** (Figure 4). This synthesis showed excellent selectivity, conversion, and versatility, as it was demonstrated to be effective on other ketones. Additionally, it can be applied in both batch mode and continuous plug flow reactor [90].

Although these few examples underline the high potential of biocatalysis for obtaining enantiopure products, this technique is still not widely exploited in industry, mainly owing to the absence of familiarity with the commercially available enzymes. Moreover, enzymes are conceived as biological agents rather than chemical reagents [91].

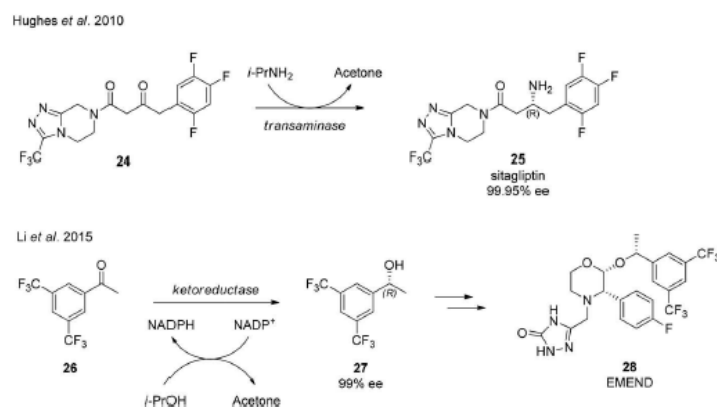


Figure 4. Biocatalysis examples.

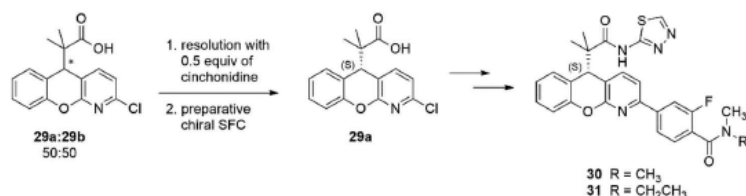
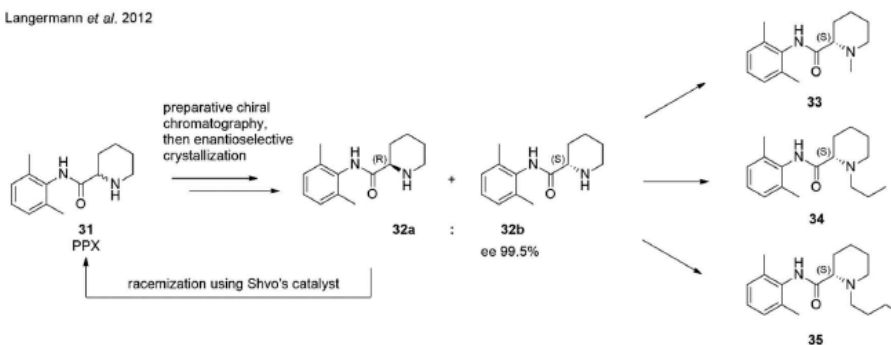
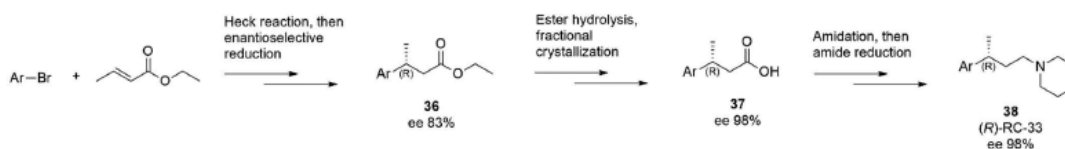
Mas *et al.* 2016Langermann *et al.* 2012Collina *et al.* 2016

Figure 5. Integrated approaches examples.

4. Integrated approaches

As outlined in the previous paragraphs, there are many methods to obtain single enantiomers with high ee and purity in suitable amount for the various phases of DD process. Nevertheless, sometimes each of these methodologies, if performed alone, can be inefficient, leading to low purity, poor yields, or highly time-consuming procedures. In these cases, the use of integrated approaches (i.e. combining different of the aforementioned techniques) can be crucial to obtain the desired results.

Hereinafter, we report some examples in which integrated approach proved to be the winning strategy. The cases described try to cover as diverse as possible technique combinations, among those reported in recent literature.

To synthesize the glucocorticoid receptor modulators 30 and 31 (Figure 5), the key intermediate (S)-29 was initially prepared in kilogram-scale applying SFC. The optimized protocol allowed a processing rate of up to 96 mL/h of a 50:50 solution of 29a and 29b, which provided 31 g/day of enantiomer 29a. This rate failed to satisfy the delivery timeline required for clinical campaign, so other routes were explored

[92]. Since neither enzymatic nor chemical resolutions provided the desired enantiomeric purity (≥ 99.0 HPLC area per cent), the best solution was to use integrated approach. This strategy consisted in a partial resolution of racemate 29a/29b through crystallization of diastereomeric salts, followed by SFC performed on the enantio-enriched mixture, reducing the initial processing time by 54%. In detail, the racemic acid 29 was treated with 0.5 equivalents of the chiral amine cinchonidine, to give the crystalline solid salt of the undesired 29b, while the mother liquor contained an 85:15 mixture of 29a and 29b. This enriched mixture was subsequently purified via preparative SFC to enhance processing rates up to 80 mL/h of the partially resolved mixture, affording a 57 g/day production of 29a with an ee $\geq 99.5\%$. The new protocol satisfied both timeline and enantiomeric purity requests (Figure 5) [92].

Another interesting example is the resolution of 2',6'-Pipicoloxylidide 31 (PPX, Figure 5), a key intermediate in the synthesis of some important anesthetics, such as mepivacaine 33, ropivacaine 34, and bupivacaine 35. Since the (S)-enantiomer of such compounds presents lower system toxicity and allows better surgical results, a large-scale production of enantiopure PPX is of great interest. For many years, a

diastereomeric salt resolution of racemic PPX was the chosen route in industry due to its low cost. Nevertheless, this procedure allows only a maximum of 50% yield and produces a high amount of waste [93]. Accordingly, alternatives have been explored to enhance the process efficiency [94]. Chromatographic separation, crystallization, and asymmetric synthesis were taken into account, but all of these approaches, if considered separately, were not satisfying. Again, an integrated process proved to be successful. First, preparative enantioselective chromatography afforded an enantio-enriched solution, which is then further purified by preferential crystallization. The costs of chromatography can be reduced by lowering purity requirements: the output is an enantio-enriched mixture that can be concentrated by partial solvent evaporation and then charged in the crystallization vessel where it can undergo preferential crystallization by means of proper cooling. It has to be noted that this kind of purification cannot be performed on racemates, since it needs a preliminary enrichment to a composition above the eutectic. The desired enantiomer (S)-PPX 32b is obtained as a crystalline solid with ee \geq 99.5%. The mother liquor derived from this step is recycled to chromatography since it still contains some of the desired enantiomer. This can be easily done because the solvent system is the same for both purifications, requiring simple concentration changes. However, even with this expedient, the combination of chromatography and crystallization does not provide an appealing improvement in the overall process. In this scenario, the introduction of a new step to reduce waste becomes crucial: racemization of the undesired (R)-enantiomer meets this requirement. A homogeneous catalytic racemization was successfully performed using Shvo's catalyst. Thus, combining chromatography, crystallization, and racemization, the authors managed to triumphantly improve the large-scale synthesis of enantiopure (S)-PPX 32b (Figure 5) [94].

Lastly, an integrated approach was applied for the preparation of the 51R agonist (R)-RC-33 38 in g-scale [95]. This compound was originally obtained through preparative HPLC resolution of the racemate in amount suitable for the identification of the eutomer. The original strategy was then revised, to obtain gram-scale amount of the eutomer needed for *in vitro/in vivo* studies. Several strategies have been investigated, such as enantioselective chromatography, fractional crystallization, and enantioselective synthesis alone and in combination to set up the best protocol, in terms of yield, time, and cost. The optimal strategy combined the enantioselective hydrogenation, performed using the (S,S)-Ir(ThrePHOX) complex as catalyst, carried out on (E)-ethyl 3-(biphenyl-4-yl)but-2-enoate, affording (-)-(R)-ethyl 3-(biphenyl-4-yl)butanoate 36 with ee of 83%. The ethyl ester was then converted in the corresponding enantio-enriched acid, which was solved by crystallization of the diastereoisomeric salt with cinchonidine, obtaining the (R) enantiomer 37 with 98% ee. In this case, fractional crystallization presents important advantages compared to enantioselective chromatography, giving excellent results with lower costs and modest environmental impact. The two last steps of the synthesis (amidation with piperidine and reduction of the amide moiety with LiAlH₄) did not affect the excellent ee obtained (Figure 5) [95].

5. Conclusion

The long-standing interest in enantiopure drugs, together with the restriction provided by the leading drug regulatory agencies, has prompted the scientific community to develop straightforward and robust methodologies to obtain enantiomeric compounds in good yields and with excellent ee. This review highlights how different procedures may be combined in promoting the formation of the desired enantiomeric product, underlining the 'pros and cons' of each strategy. We focused our attention, throughout this work, on the main DD phases – from the hit identification up to the preclinical studies – demonstrating that racemic resolution techniques may be effective during all the DD stages. Conversely, enantioselective synthesis represents the current procedure of choice in multi-g scale phase, in virtue of its high versatility and scalability. Lastly, two methods are widely employed for the production of an enantiopure active pharmaceutical ingredient at the development stage: asymmetric synthesis and separation of enantiomers by crystallization. Despite the satisfactory results, these methodologies may be unproductive (low yields and insufficient ee), when they are individually applied. Accordingly, the introduction of integrated approaches may thwart this drawback, since the beneficial effects of each procedure contribute in accessing to the enantiomeric pure compound endowed with the suitable features to perform the *in vitro/in vivo* investigations.

6. Expert opinion

Since 1992, the importance of stereoselective pharmacodynamics and pharmacokinetics has been widely recognized [7]. The evidence that the use of single enantiomer drugs could be beneficial for the human health [96], associated to the impact of the regulatory guidelines, led to an increased development of new single enantiomers and technological improvements [97]. The pharmaceutical market transformations can be appreciated by the trend of new molecular entities approved by U.S. FDA during 2002–2016 (Figure 6) [7,98,99]. The histogram clearly shows that single enantiomer drugs have exponentially increased in the pharmaceutical scenario, outclassing the racemic molecules.

As extensively reported, the desired enantiomeric compounds can be prepared adopting two workable routes: separation of racemates or enantioselective synthesis. In general, a DD process provides an initial rapid screening of the most promising approaches, performing an accurate evaluation of all parameters. Once the optimal method for a mg-scale has been selected, it will be further optimized and scaled-up, saving precious time and money.

When talking about the isolation of enantiopure compounds in large scale, ecological/environmental considerations have also to be taken into account, in order to reduce potential toxicity and hazard of the process. In chromatography using CSPs, large amounts of solvents are used. This aspect is neither desirable nor convenient. Methods able to reduce the amount or to recycle solvents are preferred. In this context, SFC is the ideal method, in virtue of its intrinsic properties and green features. In fact, this procedure requires CO₂ (raw carbon dioxide is recovered as a normal 'by-product' of industrial processes

The chirality of NMEs among 2002-2016

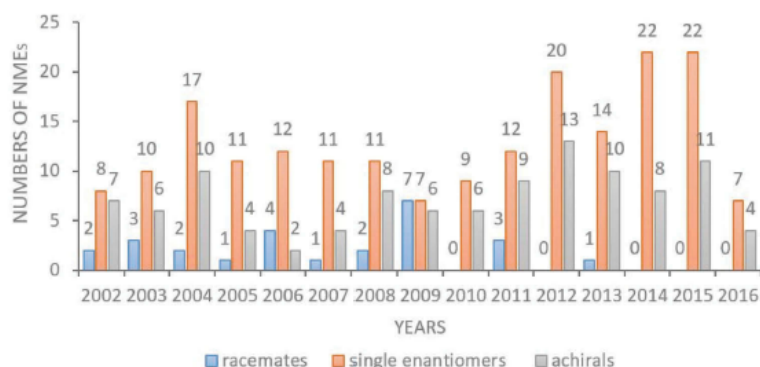


Figure 6. New molecular entities (NMEs) approved by U.S. FDA among 2002-2016 (source: New Drugs at FDA: CDER's New Molecular Entities and New Therapeutic Biological Products. Available at: www.fda.gov/Drugs/DevelopmentApprovalProcess/DrugInnovation/default.htm).

Table 2. Advantages and disadvantages of the main methods for isolating enantiomers.

Pros	Cons
Chiral HPLC	
Wide application	Solvent consumption
Easily scalable method	Low processing rate
High efficiency	
Chiral SFC	
Wide application	High cost of instrumentation
Environmental friendly method	
Easily scalable method	
Efficiency	
Resolution via crystallization of diastereomeric salts	
Low cost	Trial and error approach
Simplicity	Suitable for only acid and basic compounds
Robustness	Low yield
Large/industrial scale	
Enantioselective synthesis (chiral pool and chemocatalysis)	
Wide application	Time-consuming setup
Efficiency	High cost
Suitable for the medium/late stage of DD	Large amount of waste
Biocatalysis	
Efficiency	Cost
Environmental friendly	Enzyme stability
Mild conditions	Solubility issues

and can be used as eluent after purification and liquefaction) and small amounts of alcoholic modifiers, as mobile phase [100]. Furthermore, SFC spans a range from small preparative (a few milligrams to a hundred of grams) up to larger scale. Fractional crystallization is a widely used method, though it allows obtaining only 50% of the final material. For economic and ecological reasons, the racemization of the 'non-desired' enantiomer is advantageous, since it can be reused for further cycles [97]. At the g-scale stage of DD process, enantioselective synthesis may guarantee an indubitable efficacy. In detail, this approach collects a series of appealing procedures – chiral pool, the employment of prochiral substrates, and biocatalysis – able to offer the enantiomeric product endowed with a good ee.

Nevertheless, the efficiency of an enantioselective synthesis process can never be close to 100% and the subsequent purification of the desired enantiomer is generally complex and often unattainable. Moreover, these methodologies may be limited by the costs, since chiral agents (i.e. chiral auxiliaries, chemical, or biocatalysts) are expensive. Several artifices have been developed to counteract these issues, among them the recycling of the chiral agents, as well as the racemization of the enantiomeric counterpart are the main solutions not to burden academic and industrial economy. Lastly, the integrated approaches deserve to be mentioned, since they enable to overcome the major hurdles that can be encountered when a single enantioselective strategy is adopted. We reported few examples that could be sufficient to demonstrate how the synergy among different approaches can provide several benefits in terms of costs and time.

Altogether these data suggest that choosing an appropriate synthetic scheme useful for preparing enantiomers may be tough and requires both scientific and strategic assessments. The decision on which enantioselective approaches to adopt, throughout a DD program, has an immense impact on the project timelines and cost, thus the selection of a gold standard strategy can lead to competitive and fast DD procedures. Conversely, a wrong decision, adopted without rigor, scrutiny, can promote a cascade of events that collimates in a significant waste of time and money.

Table 2 gives a complete picture of the main advantages and disadvantages of the various techniques used for obtaining large-scale enantiomers. This schematic overview may contribute in choosing the right procedure for a g-scale production of enantiopure compounds.

Acknowledgment

The Authors are grateful to Professor Richard Kellogg of Syncom, the Netherlands for his scientific support.

Funding

This manuscript has not been funded.

Declaration of interest

M Juza is an employee of Corden Pharma Switzerland LLC. The authors have no other relevant affiliations or financial involvement with any organization or entity with a financial interest in or financial conflict with the subject matter or materials discussed in the manuscript apart from those disclosed.

References

Papers of special note have been highlighted as either of interest (+) or of considerable interest (++) to readers.

1. Nguyen LA, He H, Chiral drugs P-HC. An overview. *Int J Biomed Sci.* 2006;2:85–100.
2. Williams A. Opportunities for chiral agrochemicals. *Pestic Sci.* 1996;46:3–9.
3. Wu Y, Miao H, Fan S. Separation of chiral pyrethroid pesticides and application in pharmacokinetics research and human exposure assessment. In: *Pesticides in the modern world – effects of pesticides exposure*. Baja California, Mexico InTech, ed. Margarita Stoytcheva; 2011.
4. Regulation (EU) n°528/2012 concerning the making available on the market and use of biocidal products. Evaluation of active substances. Assessment Report. 2013. [cited 23 Jul 2017]. Available from: http://dissemination.echa.europa.eu/Biocides/ActiveSubstances/1409-21/1409-21_Assessment_Report.pdf
5. Sekhon BS. Enantioseparation of chiral drugs – an overview. *Int J PharmTech Res.* 2010;2:1584–1594.
6. McConathy J, Owens MJ. Stereochemistry in drug action. *Prim Care Companion J Clin Psychiatry.* 2003;5:70–73.
7. Agranat I, Caner H, Caldwell J. Putting chirality to work: the strategy of chiral switches. *Nat Rev Drug Discov.* 2002;1:753–768.
8. Andersson T. Single-isomer drugs: true therapeutic advances. *Clin Pharmacokinet.* 2004;43:279–285.
9. Campo VL, Bernardes LS, Carvalho I. Stereoselectivity in drug metabolism: molecular mechanisms and analytical methods. *Curr Drug Metab.* 2009;10:188–205.
10. Chiral technology market - global industry forecast, share, size, growth and industry analysis (2014–2020). Transparency Market Research (TMR). [cited 2 Jul 2017]. Available from: <http://www.transparencymarketresearch.com/chiral-technology-market.html>
11. Rouf A, Taneja SC. Synthesis of single-enantiomer bioactive molecules: a brief overview. *Chirality.* 2014;26:63–78.
 - **This review extensively reports recent examples of synthesis of optically pure drugs and intermediates via different approaches.**
12. Lorenz H, Seidel-Morgenstern A. Processes to separate enantiomers. *Angew Chem Int Ed Engl.* 2014;53:1218–1250.
 - **This review describes the basic concepts of various techniques useful to the enantioseparations.**
13. Leek H, Thunberg L, Jonson AC, et al. Klarqvist M strategy for large-scale isolation of enantiomers in drug discovery. *Drug Discovery Today.* 2017;22:133–139.
14. FDA's policy statement for the development of new stereoisomeric drugs. *Chirality.* 1992;4:338–340.
15. Development of new stereoisomeric drugs US. Food and Drug Administration. 1992. [cited 7 Jul 2017]. Available from: <https://www.fda.gov/drugs/guidancecomplianceregulatoryinformation/guidances/ucm122883.htm>
16. Federsel HJ. Facing chirality in the 21st century: approaching the challenges in the pharmaceutical industry. *Chirality.* 2003;15:5128–5142.
17. Subramanian G. *Chiral separation techniques: a practical approach*. 3rd ed. Weinheim: Wiley-VCH; 2007.
 - **This book is a compendium of techniques that permit the chiral separations.**
18. Lin GQ, You QD, Cheng JF. Overview of chirality and chiral drugs. In: *Chiral drugs: chemistry and biological action*. Weinheim:Wiley-VCH; 2011.
19. Ali I, Suhail M, Al-Othman ZA, et al. Enantiomeric resolution of multiple chiral centres racemates by capillary electrophoresis. *Biomed Chromatogr.* 2016;30:683–694.
 - **A review about application of capillary electrophoresis in chiral separations.**
20. Piacentini E, Mazzei R, Giorno L. Membrane bioreactors for pharmaceutical applications: optically pure enantiomers production. *Curr Pharm Des.* 2017;23:250–262.
 - **Recent review about membrane for the enantioresolution.**
21. Jozwiak K. *Drug stereochemistry: analytical methods and pharmacology*. Boca Raton:3rd ed. CRC Press; 2012.
22. Srinivas NR, Igwemezie LN. Chiral separation by high performance liquid chromatography. I. Review on indirect separation of enantiomers as diastereomeric derivatives using ultraviolet, fluorescence and electrochemical detection. *Biomed Chromatogr.* 1992;6:163–167.
23. Gaggeri R, Rossi D, Collina S, et al. Quick development of an analytical enantioselective high performance liquid chromatography separation and preparative scale-up for the flavonoid naringenin. *J Chromatogr A.* 2011;1218:5414–5422.
24. Collina S, Lodo G, Urbano M, et al. Enantioselective chromatography and absolute configuration of N,N-dimethyl-3-(naphthalen-2-yl)-butan-1-amines: potential sigma1 ligands. *Chirality.* 2006;18:245–253.
25. Rossi D, Marra A, Rui M, et al. "Fit-for-purpose" development of analytical and (semi)preparative enantioselective high performance liquid and supercritical fluid chromatography for the access to a novel $\alpha 1$ receptor agonist. *J Pharm Biomed Anal.* 2016;118:363–369.
26. Rossi D, Nasti R, Marra A, et al. Enantiomeric 4-acylamino-6-alkoxy-2-alkylthiopyrimidines as potential A3 adenosine receptor antagonists: HPLC chiral resolution and absolute configuration assignment by a full set of chiroptical spectroscopy. *Chirality.* 2016;28:434–440.
27. Shen J, Okamoto Y. Efficient separation of enantiomers using stereoregular chiral polymers. *Chem Rev.* 2016;116:1094–1138.
28. Okamoto Y, Ikai T. Chiral HPLC for efficient resolution of enantiomers. *Chem Soc Rev.* 2008;37:2593–2608.
29. Francotte ER. Enantioselective chromatography as a powerful alternative for the preparation of drug enantiomers. *J Chromatogr A.* 2001;906:379–397.
30. Franco P. Common screening approaches for efficient analytical method development in LC and SFC on columns packed with immobilized polysaccharide stationary phases. In *Chiral separations, methods and protocols*. New York: Gerald Gübitz Martin G. Schmid (eds). 2nd ed. Humana Press; 2013.
31. Francotte ER. Chromatography as a separation tool for the preparative resolution of racemic compounds. In: *Chiral separations, applications and technology*. Washington: American Chemical Society; 1997.
32. Pirkle WH, House D, Finn J. Broad spectrum resolution of optical isomers using chiral high-performance liquid chromatographic bonded phases. *J Chromatogr.* 1980;192:143–158.
33. Davankov VA. Chiral selectors with chelating properties in liquid chromatography: fundamental reflections and selective review of recent developments. *J Chromatogr.* 1994;666:55–76.
34. Lämmerhofer M, Lindner W. Quinine and quinidine derivatives as chiral selectors I. Brush type chiral stationary phases for high-performance liquid chromatography based on cinchonan carbamates and their application as chiral anion exchangers. *J Chromatogr A.* 1996;741:33–48.
35. Ward TJ, Farris III AB. Chiral separations using the macrocyclic antibiotics: a review. *J Chromatogr.* 2001;906:73–89.
36. Haginaka J. Protein-based chiral stationary phases for high-performance liquid chromatography enantioseparations. *J Chromatogr A.* 2001;906(1–2):253–273.
37. Allenmark S, Andersson S, Möller P, et al. A new class of network-polymeric chiral stationary phases. *Chirality.* 1995;7:248–256.

38. Allenmark S, Schurig V. Chromatography on chiral stationary phases. *J Mater Chem*. 1997;7:1955–1963.
39. Miller L. Preparative enantioseparations using supercritical fluid chromatography. *J Chromatogr A*. 2012;1250:250–255.
40. Lee J, Lee JT, Watts WL, et al. On the method development of immobilized polysaccharide chiral stationary phases in supercritical fluid chromatography using an extended range of modifiers. *J Chromatogr A*. 2014;1374:238–246.
41. Speybrouck D, Lipka E. Preparative supercritical fluid chromatography: a powerful tool for chiral separations. *J Chromatogr A*. 2016;1467:33–55.
- **An extensive review about Supercritical Fluid Chromatography.**
42. Francotte E. Practical advances in SFC for the purification of pharmaceutical molecules. *LCGC Europe*. 2016;29:194–204.
43. Plotka JM, Biziuk M, Morrison C, et al. Pharmaceutical and forensic drug applications of chiral supercritical fluid chromatography. *Trends Analyt Chem*. 2014;56:74–89.
44. Welch CJ. The use of preparative chiral chromatography for accessing enantiopurity in pharmaceutical discovery and development. In *Comprehensive organic synthesis*. Waltham:2nd ed. Elsevier Ltd; 2014.
45. Imamoglu S. Simulated moving bed chromatography (SMB) for application in bioseparation. *Adv Biochem Eng Biotechnol*. 2002;76:211–231.
46. Juza M, Mazzotti M, Morbidelli M. Simulated moving-bed chromatography and its application to chirotechnology. *Trends Biotechnol*. 2000;18:108–118.
47. Rajendran A, Paredes G, Mazzotti M. Simulated moving bed chromatography for the separation of enantiomers. *J Chromatogr A*. 2009;1216:709–738.
- **Extensive review about Simulated Moving Bed.**
48. Schurig V. Preparative-scale separation of enantiomers on chiral stationary phases by gas chromatography. In: *Enantiomer separation: fundamentals and practical methods*. Fumino Toda (ed). Springer Netherlands; 2004.
49. Kinbara K. Design of resolving agents based on crystal engineering. *Synlett*. 2005;5:732–743.
50. Borghese A, Libert V, Zhang T, et al. Efficient fast screening methodology for optical resolution agents: solvent effects are used to affect the efficiency of the resolution process. *Org Process Res Dev*. 2004;8:532–534.
51. Fogassy E, ACS Maria FF. Pseudosymmetry and chiral discrimination in optical resolution via diastereoisomeric salt formation. The crystal structures of (R)- and (S)-N-methylamphetamine bitartrates (RMERTA and SMERTA). *J Chem Soc Perkin Trans II*. 1986;1881–1886.
52. Kozma D. *CRC handbook of optical resolutions via diastereomeric salt formation*. Boca Raton: CRC Press; 2002.
53. Guangyou Z, Yuqing L, Zhaohui W, et al. Resolution of β -aminoalcohols and 1,2-diamines using fractional crystallization of diastereomeric salts of dehydroabiatic acid. *Tetrahedron: Asymmetry*. 2003;14:3297–3300.
54. Faigl F, Fogassy E, N6gradi M, et al. Strategies in optical resolution: a practical guide. *Tetrahedron: Asymmetry*. 2008;19:519–536.
55. Kellogg RM, Kaptein B, Vries TR. Dutch resolution of racemates and the roles of solid solution formation and nucleation inhibition. *Novel Optical Resolution Technologies*. 2007. Kenichi Sakai, Noriaki Hirayama, Rui Tamura (eds). Springer Berlin Heidelberg.
- **This chapter focuses on the Dutch Resolution.**
56. Vries T, Wynberg H, van Echten E, et al. The family approach to the resolution of racemates. *J Angew Chem Int Ed*. 1998;37:2349–2354.
57. Kellogg RM. Crystallization as a tool in industrial applications of asymmetric synthesis. *Comprehensive Chirality* 2012. Waltham: Elsevier Ltd.
58. Gotrane DM, Deshmukh RD, Ranade PV, et al. A novel method for resolution of amlodipine. *Org Process Res Dev*. 2010;14:640–643.
59. Elati CR, Kolla N, Vankawala PJ, et al. Substrate modification approach to achieve efficient resolution: didesmethylcitalopram: a key intermediate for escitalopram. *Org Process Res Dev*. 2007;11:289–292.
60. Coquerel G. Preferential crystallization. In: Sakai K, Hirayama N, Tamura R, editors. *Novel optical resolution technologies*. Berlin, Heidelberg: Springer-Verlag; 2007. p. 1–51.
61. Collet A. Separation and purification of enantiomers by crystallisation methods. *Enantiomer*. 1999;4:157–172.
62. Jacques J, Collet A, Wilen SH. *Enantiomers, racemates and resolutions*. 1st ed. New York (NY): Wiley; 1991.
63. Rougeot C, Hein JE. Application of continuous preferential crystallization to efficiently access enantiopure chemicals. *Org Process Res Dev*. 2015;19:1809–1819.
64. Farina V, Reeves JT, Senanayake CH, et al. Asymmetric catalysis of active pharmaceutical ingredients. *Chem Rev*. 2006;106:2734–2793.
65. Hong B-C, Raja A, Sheth VM. Asymmetric synthesis of natural products and medicinal drugs through one-pot-reaction strategies. *Synthesis*. 2015;47:3257–3285.
66. Zhan G, Du W, Chen Y-C. Switchable divergent asymmetric synthesis via organocatalysis. *Chem Soc Rev*. 2017;46:1675–1692.
67. Burke D, Henderson DJ. Chirality: a blueprint for the future. *Br J Anaesth*. 2002;88:563–576.
68. Aratikla EK, Bhattacharya AK. Chiral pool approach for the synthesis of functionalized amino acids: synthesis of antiepileptic drug (R)-Lacosamide. *Tetrahedron Lett*. 2015;56:5802–5803.
69. Damsen H, Niggemann M. Calcium-catalyzed synthesis of 1,2-disubstituted 3-benzazepines. *Eur J Org Chem*. 2015;36:7880–7883.
70. Gnas Y, Glorius F. Chiral auxiliaries – principles and recent applications. *Synthesis*. 2006;12:1899–1930.
- **The article is about the most important and common chiral auxiliaries and describes their use in recent works.**
71. Pignataro L, Carboni S, Civera M, et al. PhthalaPhos: chiral supramolecular ligands for enantioselective rhodium-catalyzed hydrogenation reactions. *Angew Chem Int Ed*. 2010;49:6633–6637.
72. Gajewski P, Renom-Carrasco M, Vallati Facchini S, et al. Synthesis of (R)-BINOL-derived (cyclopentadienone)iron complexes and their application in the catalytic asymmetric hydrogenation of ketones. *Eur J Org Chem*. 2015;2015:5526–5536.
73. Trost BM, Van Vranken DL. Asymmetric transition metal-catalyzed allylic alkylations. *Chem Rev*. 1996;96:395–422.
74. Di Giacomo M, Serra M, Brusasca M, et al. Stereoselective Pd-catalyzed synthesis of quaternary α -D-C-Mannosyl-(S)-amino acids. *J Org Chem*. 2011;76:5247–5257.
75. Dhar TG, Xiao HY, Xie J, et al. Identification and preclinical pharmacology of BMS-986104: a differentiated S1P1 receptor modulator in clinical trials. *ACS Med Chem Lett*. 2016;7:283–288.
76. Yang MG, Xiao Z, Murali Dhar TG, et al. Asymmetric hydroboration approach to the scalable synthesis of ((1R,3S)-1-amino-3-((R)-6-hexyl-5,6,7,8-tetrahydronaphthalen-2-yl)cyclopentyl)methanol (BMS-986104) as a potent S1P1 receptor modulator. *J Med Chem*. 2016;59:11138–11147.
77. Böhler S, Goettert M, Schollmeyer D, et al. Chiral sulfoxides as metabolites of 2-thioimidazole-based p38 α mitogen-activated protein kinase inhibitors: enantioselective synthesis and biological evaluation. *J Med Chem*. 2011;54:3283–3297.
78. Gaich T, Mulzer J. Chiral pool synthesis: starting from terpenes. *Comprehensive Chirality* 2012. Waltham: Elsevier Ltd.
79. Chen WW, Xu MH. Recent advances in rhodium-catalyzed asymmetric synthesis of heterocycles. *Org Biomol Chem*. 2017;15:1029–1050.
80. Anthonsen T. Reactions catalyzed by enzymes. In *Applied biocatalysis*. Chur: 2nd ed. Taylor & Francis; 2000.
81. Wells AS, Finch GL, Michels PC, et al. Use of enzymes in the manufacture of active pharmaceutical ingredients – a science and safety-based approach to ensure patient safety and drug quality. *Org Process Res Dev*. 2012;16:1986–1993.
- **This article critically reports recent viable strategies for the use of biocatalysis in pharmaceutical industry.**
82. Liese A, Seelbach K, Wandrey C. *Industrial biotransformations*. 2nd ed. Weinheim: Wiley-VCH; 2006.
- **This book contains an overview of one-step industrially relevant biotransformations and is based on extensive literature and patent research.**

83. Carvalho AC, Fonseca Tde S, de Mattos MC, et al. Recent advances in lipase-mediated preparation of pharmaceuticals and their intermediates. *Int J Mol Sci.* 2015;16:29682–29716.
84. Mohamad NR, Marzuki NHC, Buang NA, et al. An overview of technologies for immobilization of enzymes and surface analysis techniques for immobilized enzymes. *Biotechnol Biotechnol Equip.* 2015;29:205–220.
85. Ismail H, Lau RM, van Rantwijk F, et al. Fully enzymatic resolution of chiral amines: acylation and deacylation in the presence of *Candida antarctica* lipase B. *Adv Synth Catal.* 2008;350:1511–1516.
86. Blacker AJ, Stirling MJ, Page MI. Catalytic racemisation of chiral amines and application in dynamic kinetic resolution. *Org Process Res Dev.* 2007;11:642–648.
87. Hansen KB, Hsiao Y, Xu F, et al. Highly efficient asymmetric synthesis of sitagliptin. *J Am Chem Soc.* 2009;131:8798–8804.
88. Savile CK, Janey JM, Mundorff EC, et al. Biocatalytic asymmetric synthesis of chiral amines from ketones applied to sitagliptin manufacture. *Science.* 2010;329:305–309.
89. Truppo MD, Strotman H, Hughes G. Development of an immobilized transaminase capable of operating in organic solvent. *ChemCatChem.* 2012;4:1071–1074.
90. Li H, Moncecchi J, Truppo MD. Development of an immobilized ketoreductase for enzymatic (R)-1-(3,5-bis(trifluoromethyl)phenyl)ethanol production. *Org Process Res Dev.* 2015;19:695–700.
91. Bryan MC, Dillon B, Hamann LG, et al. Sustainable practices in medicinal chemistry: current state and future directions. *J Med Chem.* 2013;56:6007–6021.
92. De Mas N, Natalie KJ, Quiroz F, et al. A partial classical resolution/preparative chiral supercritical fluid chromatography method for the rapid preparation of the pivotal intermediate in the synthesis of two nonsteroidal glucocorticoid receptor modulators. *Org Process Res Dev.* 2016;20:934–939.
93. Tullar BF. Optical isomers of mepivacaine and bupivacaine. *J Med Chem.* 1971;14:891–892.
94. von Langermann J, Kasperit M, Shakeri M, et al. Design of an integrated process of chromatography, crystallization and racemization for the resolution of 2',6'-pipecoloxylidide (PPX). *Org Process Res Dev.* 2012;16:343–352.
95. Marra A, Rossi D, Pignataro L, et al. Toward the identification of neuroprotective agents: g-scale synthesis, pharmacokinetic evaluation and CNS distribution of (R)-RC-33, a promising SIGMA1 receptor agonist. *Future Med Chem.* 2016;8:287–295.
96. Caldwell J. Through the looking glass in chiral drug development. *Mol Drug Discov.* 1999;2:51–60.
97. Maier NM, Franco P, Lindner W. Separation of enantiomers: needs, challenges, perspective. *J Chromatogr A.* 2001;906:3–33.
98. Shen Z, Lv C, Zeng S. Significance and challenges of stereoselectivity assessing methods in drug metabolism. *J Pharmaceut Anal.* 2016;6:1–10.
99. New drugs at FDA: CDER's new molecular entities and new therapeutic biological products. FDA Public Health Advisory. Washington (DC): FDA/Center for Drug evaluation and Research; 2017. Available from: www.fda.gov/Drugs/DevelopmentApprovalProcess/DrugInnovation/default.htm
100. Taylor LT. Supercritical fluid chromatography for the 21st century. *J Supercritical Fluids.* 2009;47:566–573.

Paper 5

Reprinted with permission from Rossino G, Orellana I, Caballero J, et al. New Insights into the Opening of the Occluded Ligand-Binding Pocket of Sigma1 Receptor: Binding of a Novel Bivalent RC-33 Derivative [published online ahead of print, 2019 Dec 20]. *J Chem Inf Model.* 2019;10.1021/acs.jcim.9b00649. doi:10.1021/acs.jcim.9b00649. Copyright 2020 American Chemical Society



Docking, Interaction Fingerprint, and Three-Dimensional Quantitative Structure–Activity Relationship (3D-QSAR) of Sigma1 Receptor Ligands, Analogs of the Neuroprotective Agent RC-33

José Luis Velázquez-Libera¹, Giacomo Rossino², Carlos Navarro-Retamal¹, Simona Collina² and Julio Caballero^{1*}

¹ Centro de Bioinformática y Simulación Molecular, Facultad de Ingeniería, Universidad de Talca, Talca, Chile,

² Pharmaceutical and Medicinal Chemistry Section, Drug Sciences Department, Università di Pavia, Pavia, Italy

OPEN ACCESS

Edited by:

Teodorico Castro Ramalho,
Universidade Federal de Lavras, Brazil

Reviewed by:

Andrei I. Kheibnikov,
Tomsk Polytechnic University, Russia
Marco Tutone,
University of Palermo, Italy

*Correspondence:

Julio Caballero
jcaballero@utalca.cl

Specialty section:

This article was submitted to
Medicinal and Pharmaceutical
Chemistry,
a section of the journal
Frontiers in Chemistry

Received: 12 April 2019

Accepted: 27 June 2019

Published: 11 July 2019

Citation:

Velázquez-Libera JL, Rossino G,
Navarro-Retamal C, Collina S and
Caballero J (2019) Docking,
Interaction Fingerprint, and
Three-Dimensional Quantitative
Structure–Activity Relationship
(3D-QSAR) of Sigma1 Receptor
Ligands, Analogs of the
Neuroprotective Agent RC-33.
Front. Chem. 7:496.
doi: 10.3389/fchem.2019.00496

The human Sigma1 receptor (S1R), which has been identified as a target with an important role in neuropsychological disorders, was first crystallized 3 years ago. Since S1R structure has no relation with another previous crystallized structures, the presence of the new crystal is an important hallmark for the design of agonists and antagonists against this important target. Some years ago, our group identified RC-33, a potent and selective S1R agonist, endowed with neuroprotective properties. In this work, drawing on new structural information, we studied the interactions of RC-33 and its analogs with the S1R binding site by using computational methods such as docking, interaction fingerprints, and receptor-guided alignment three dimensional quantitative structure–activity relationship (3D-QSAR). We found that RC-33 and its analogs adopted similar orientations within S1R binding site, with high similitude with orientations of the crystallized ligands; such information was used for identifying the residues involved in chemical interactions with ligands. Furthermore, the structure-activity relationship of the studied ligands was adequately described considering classical QSAR tests. All relevant aspects of the interactions between the studied compounds and S1R were covered here, through descriptions of orientations, binding interactions, and features that influence differential affinities. In this sense, the present results could be useful in the future design of novel S1R modulators.

Keywords: sigma1 receptor ligands, RC-33, arylalkylamine derivatives, docking, quantitative structure–activity relationships, interaction fingerprints

INTRODUCTION

The Sigma receptors (SR) have attracted the interest of the scientific community thoroughly in the last decades owing to their potential role in cell survival and function modulation (Walker et al., 1990; Chu and Ruoho, 2016). They were originally misclassified as a subtype of opioid receptors (Martin et al., 1976), but they were later classified as unique class of intracellular proteins,

distinct from other receptors such as GPCRs (G protein-coupled receptors). Sigma receptors (SRs), comprise two subtypes σ_1 and σ_2 receptors (S1R and S2R, respectively) associated with aging- and mitochondria-associated disorders (Tesei et al., 2018). Both subtypes are highly expressed in the central nervous system, but they are derived from completely different genes. S1R was cloned in 1996 (Hanner et al., 1996) and was crystallized for the first time 3 years ago, in 2016 (Schmidt et al., 2016), whereas S2R was cloned only very recently, in 2017, by Alon et al. (2017).

S1R is an intracellular modulator between the endoplasmic reticulum and the mitochondria, the cell nuclei, the membrane, and it also modulates intracellular signaling. It plays a key role in neuropsychological disorders such as depression, enhances the glutamatergic neurotransmission (DeCoster et al., 1995; Meyer et al., 2002), and modulates second messenger systems, such as the phospholipase C/protein kinase C/inositol 1,4,5-trisphosphate system (Morin-Surun et al., 1999). Multiple biological roles of S1R have been identified, which made this protein a relevant target for the future treatment of epilepsy, schizophrenia, sclerosis, Alzheimer, and Parkinson's diseases, cancer, etc. (Mishina et al., 2005; Hashimoto, 2009; Furuse and Hashimoto, 2010; Mavlyutov et al., 2015; Vavers et al., 2017; Tesei et al., 2018). Moreover, S1R agonists enhanced neuroplasticity, and may be effective in amyotrophic lateral sclerosis (Peviani et al., 2014) and multiple sclerosis (Collina et al., 2017b).

Not less important, preclinical studies carried out on different models of memory impairment have revealed that S1R ligands could be promising drugs to treat cognitive dysfunctions (Hayashi and Su, 2004; Monnet and Maurice, 2006; Yagasaki et al., 2006; Collina et al., 2017a). Therefore, the identification of potent and selective S1R modulators is of great interest to develop novel therapeutic strategies focused mainly in the treatment of central nervous system disorders. The list of S1R ligands in the last years includes thioxanthene-derived compounds (Glennon et al., 2004), fenpropimorph-derived analogs (Hajipour et al., 2010), 2(3H)-benzothiazolones (Yous et al., 2005), cyclopropylmethylamines (Prezzavento et al., 2007), benzo[d]oxazol-2(3H)-one derivatives (Zampieri et al., 2009), etc. All these compounds were developed when the three-dimensional (3D) structure of S1R was unknown. Despite this, the pharmacophoric features of S1R were identified and these compounds comply with the general accepted pharmacophoric pattern. It was demonstrated that at least one N positively charged atom is important for binding at sigma receptors and this atom must be flanked by two hydrophobic regions of different sizes (Ablordepey et al., 2000; Glennon, 2005; Caballero et al., 2012).

In the last years, we designed and synthesized compounds that comply with the proposed pharmacophore model and evaluated them as S1R ligands (Collina et al., 2007; Urbano et al., 2007; Rossi et al., 2010, 2011), leading to the finding of compound RC-33 as a potent and selective S1R agonist (Rossi et al., 2013a; Marra et al., 2016). The structure-activity relationship (SAR) of the majority of these compounds was previously described by us by using 2D-QSAR methodologies (Quesada-Romero et al., 2015). With the recent report of the S1R 3D structure (Schmidt et al., 2016), structure-based molecular modeling methods could

be used to investigate S1R ligands with a new glance. With this in mind, we propose in this work the analysis of the SAR of RC-33 and its analogs (in total there were 80 compounds) by combining docking and a 3D-QSAR methodology. This is the first study focused on describing the SAR of S1R ligands by using structure-based molecular modeling methods, after the report of the crystallographic structure of this important biological target.

MATERIALS AND METHODS

Dataset Preparation

The studied compounds were extracted from references (Collina et al., 2007; Urbano et al., 2007; Rossi et al., 2010, 2011, 2015, 2017; Rui et al., 2016). This dataset yielded a total of 80 compounds with reported activities as Ki ranging from 0.00069 to 1 μ M. Ki values were converted into logarithmic pKi values prior 3D-QSAR models' elaboration. The compound chemical structures and their pKi values are depicted in Table 1. The molecular structures were sketched using Maestro's molecular editor (Maestro 10.2.011, Schrödinger LLC). Thereafter, the 3D structures were obtained with the help of the LigPrep module (LigPrep, Maestro 10.2.011, Schrödinger LLC); ionization states were generated at pH 7.0 \pm 2.0 using Epik (Shelley et al., 2007). For compounds containing two possible enantiomers which are reported in racemic form, the R enantiomer was chosen for QSAR experiments because it was determined that both RC-33 enantiomers showed similar affinities for the S1R and they are almost equally effective as S1R agonists (Rossi et al., 2013b). However, both enantiomers were chosen for docking experiments to explore the interactions in the S1R binding site.

Molecular Docking

The ligand-receptor molecular docking experiments of RC-33 analogs into the active site of S1R were performed by using the software Glide from the Schrödinger suite (Friesner et al., 2004). Glide is one of the most effective docking programs at this moment with many successful applications relating to rational design of novel drugs and investigation of protein-ligand interactions. Such applications encompass *in silico* search of novel drugs (Osguthorpe et al., 2012; Amaning et al., 2013), analysis of the SAR of congeneric series of compounds (Almerico et al., 2012; Quesada-Romero and Caballero, 2014; Quesada-Romero et al., 2014; Mena-Ulecia et al., 2015), evaluation of enzymatic reaction pathways (Wu et al., 2011; Batra et al., 2013), etc.

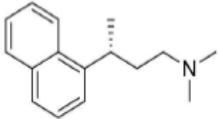
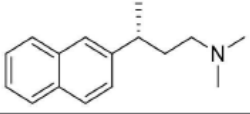
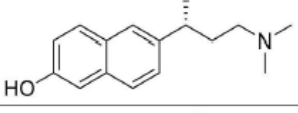
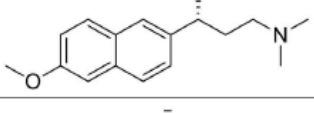
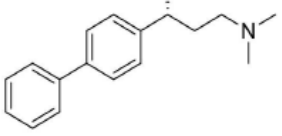
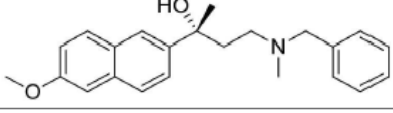
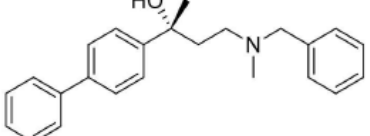
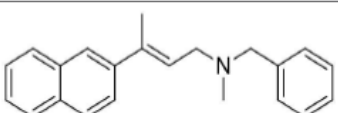
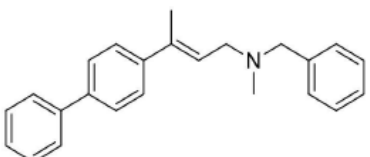
Protein coordinates were extracted from the crystal structure of S1R bound to the selective antagonist PD144418 (code 5HK1 in Protein Data Bank) (Schmidt et al., 2016). A grid box of 20 \times 20 \times 20 Å was centered on the center of mass of the ligand in this crystal structure covering the binding site of S1R. Glide standard (SP) and extra-precision (XP) modes were employed with the same protocol and parameters that were used by us in previous works (Quesada-Romero and Caballero, 2014; Quesada-Romero et al., 2014; Mena-Ulecia et al., 2015). Glide SP was used to evaluate the capability of the Glide method to obtain poses that fit the known pharmacophore of S1R ligands,

TABLE 1 | Structures of RC-33 analogs as S1R ligands.

ID	Structure	Experimental pK _i ^B	Predicted pK _i ^B	References
1 (RC-33)		9.16	9.37	Rossi et al., 2011
2		7.60	7.54	Collina et al., 2007
3		7.41	7.49	Rossi et al., 2010
4		6.99	6.96	Collina et al., 2007
5		7.70	7.62	Collina et al., 2007
6		7.67	7.44	Collina et al., 2007
7		8.85	8.73	Rossi et al., 2011
8 ^a		6.00	6.79	Rossi et al., 2011
9		6.09	6.23	Rossi et al., 2011
10		6.00	6.14	Rossi et al., 2011

(Continued)

TABLE 1 | Continued

ID	Structure	Experimental pK_i^D	Predicted pK_i^D	References
11		7.33	7.11	Collina et al., 2007
12 ^B		8.71	7.99	Collina et al., 2007
13		7.72	7.65	Collina et al., 2007
14		8.64	8.41	Collina et al., 2007
15		8.99	9.05	Collina et al., 2007
16		8.22	8.10	Rossi et al., 2010
17		8.62	8.26	Rossi et al., 2010
18		8.10	8.09	Collina et al., 2007
19		8.20	8.29	Collina et al., 2007

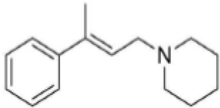
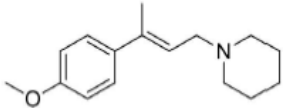
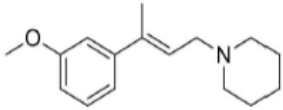
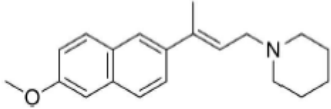
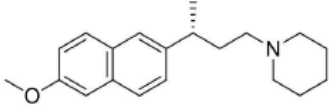
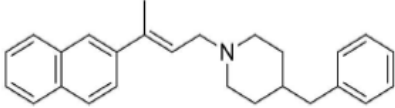
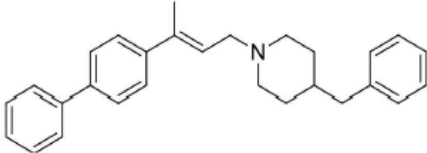
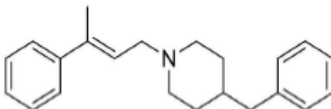
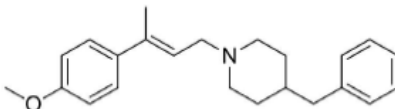
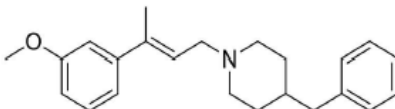
(Continued)

TABLE 1 | Continued

ID	Structure	Experimental pK _i ^b	Predicted pK _i ^b	References
20		7.86	8.22	Fossi et al., 2010
21		7.04	7.06	Collina et al., 2007
22		8.28	8.11	Collina et al., 2007
23 ^a		8.27	8.96	Collina et al., 2007
24		8.24	8.30	Collina et al., 2007
25		8.64	8.52	Fossi et al., 2010
26		7.98	8.01	Fossi et al., 2010
27		9.01	8.79	Fossi et al., 2011
28		9.07	9.22	Fossi et al., 2011

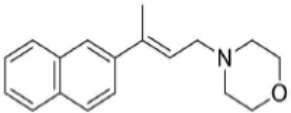
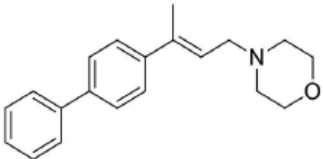
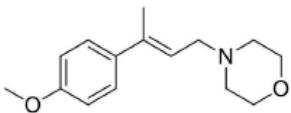
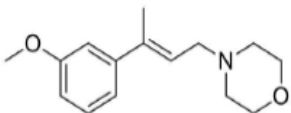
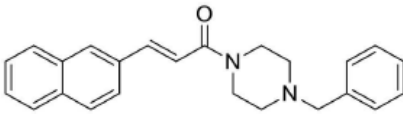
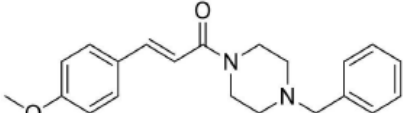
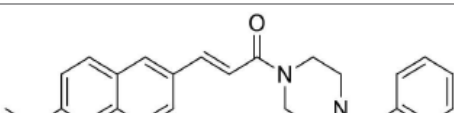
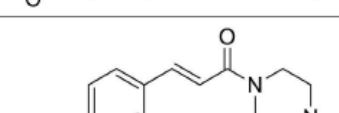
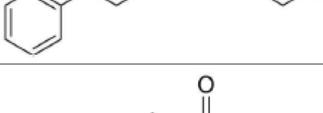
(Continued)

TABLE 1 | Continued

ID	Structure	Experimental pK _i ^b	Predicted pK _i ^b	References
29 ^a		6.34	6.23	Rossi et al., 2011
30		7.85	7.67	Rossi et al., 2011
31		7.04	7.10	Rossi et al., 2011
32		8.36	8.62	Rossi et al., 2010
33		8.89	8.99	Rossi et al., 2010
34 ^a		7.64	7.65	Rossi et al., 2011
35		8.15	8.20	Rossi et al., 2011
36 ^a		8.97	8.56	Rossi et al., 2011
37 ^a		8.38	8.28	Rossi et al., 2011
38 ^a		8.11	7.40	Rossi et al., 2011

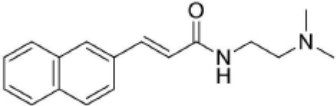
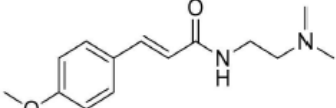
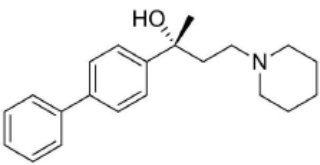
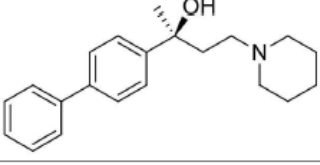
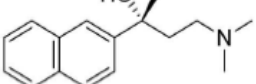
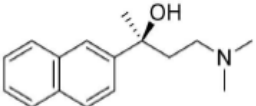
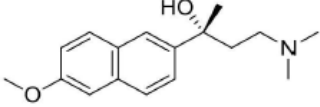
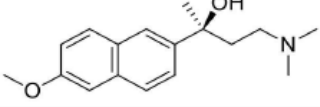
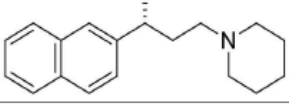
(Continued)

TABLE 1 | Continued

ID	Structure	Experimental pK _i ^b	Predicted pK _i ^b	References
39		8.02	8.04	Fossi et al., 2011
40		7.94	7.83	Fossi et al., 2011
41		6.00	6.38	Fossi et al., 2011
42		6.00	5.98	Fossi et al., 2011
43 ^a		6.00	7.29	Urbano et al., 2007
44		6.00	6.03	Urbano et al., 2007
45		6.00	6.16	Urbano et al., 2007
46		6.00	5.78	Urbano et al., 2007
47 ^a		6.00	6.36	Urbano et al., 2007

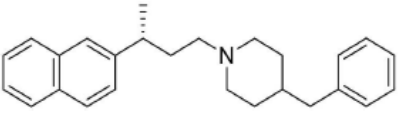
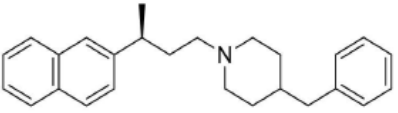
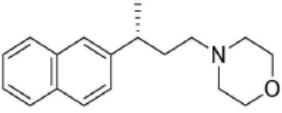
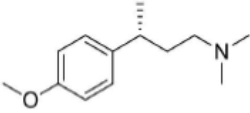
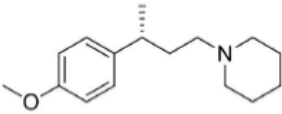
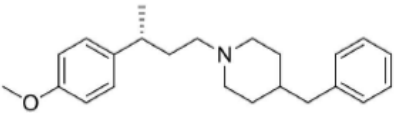
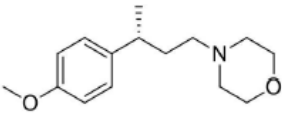
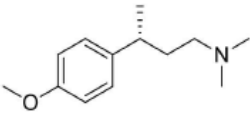
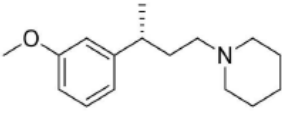
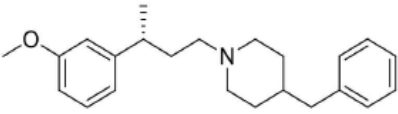
(Continued)

TABLE 1 | Continued

ID	Structure	Experimental pK _i ^D	Predicted pK _i ^D	References
48		6.00	5.89	Urbano et al., 2007
49		6.00	5.75	Urbano et al., 2007
50		7.41	7.52	Rossi et al., 2015
51		8.33	8.37	Rossi et al., 2015
52		6.69	6.81	Rossi et al., 2015
53		7.20	7.40	Rossi et al., 2015
54 ^a		7.29	7.44	Rossi et al., 2015
55		7.60	7.90	Rossi et al., 2015
56		8.82	8.57	Rossi et al., 2017

(Continued)

TABLE 1 | Continued

ID	Structure	Experimental pK _i ^b	Predicted pK _i ^b	References
57		8.22	8.29	Fossi et al., 2017
58		8.16	8.14	Fossi et al., 2017
59		8.27	8.20	Fossi et al., 2017
60		6.94	6.91	Fossi et al., 2017
61		7.70	7.68	Fossi et al., 2017
62		8.46	8.37	Fossi et al., 2017
63		7.12	7.20	Fossi et al., 2017
64		6.62	6.75	Fossi et al., 2017
65 ^a		7.44	6.42	Fossi et al., 2017
66		8.54	8.56	Fossi et al., 2017

(Continued)

TABLE 1 | Continued

ID	Structure	Experimental pK _i ^b	Predicted pK _i ^b	References
67 ^a		6.86	7.25	Rossi et al., 2017
68		6.37	6.35	Rossi et al., 2017
69		7.34	7.37	Rossi et al., 2017
70 ^a		8.54	8.62	Rossi et al., 2017
71		8.52	8.45	Rossi et al., 2017
72 ^a		7.07	6.56	Rossi et al., 2017
73		8.00	8.01	Rui et al., 2016
74		7.96	7.92	Rui et al., 2016
75		7.57	7.73	Rui et al., 2016
76		7.40	7.45	Rui et al., 2016

(Continued)

TABLE 1 | Continued

ID	Structure	Experimental pK _i ^b	Predicted pK _i ^b	References
77		7.15	7.09	Rui et al., 2016
78		7.21	7.18	Rui et al., 2016
79		7.46	7.42	Rui et al., 2016
80 ^a		7.89	7.19	Rui et al., 2016

^aTest set compounds.^bExperimental and predicted pK_i values using Model SE.

and the more precise Glide XP was used for finding the final docking poses.

After several poses were found for each compound, the ones that showed the best scoring energies were considered. The information of PD144418, 4-IBP, haloperidol, NE-100, and (+)-pentazocine in the crystallographic structures recently reported (Schmidt et al., 2016, 2018) was considered for the selection of the best solutions; these compounds show how the previously reported pharmacophoric pattern (Glennon, 2005) is oriented inside the S1R binding site. The essential chemical interactions described for analog ligands (ECIDALs) (Muñoz-Gutierrez et al., 2016; Ramírez and Caballero, 2018) defined for S1R ligands were identified using this information. The most obvious essential chemical interaction is that charged amino group of the ligands must be close to the side chain carboxylate group of the residue Glu172, forming an electrostatic interaction. Therefore, the best docking solution for each compound was the pose that had the best scoring energy and complies with this essential chemical interaction.

The "Interaction Fingerprints Panel" of Maestro (Maestro 10.2.011, Schrödinger LLC) was used for deriving the Interaction fingerprints (IFPs) as described in Singh et al. reports (Deng et al., 2004; Singh et al., 2006). The method accounts for the presence of different types of chemical interactions between ligands and the binding site residues of the target receptor by using bits. For this purpose, distance cutoffs are defined for the binding site, and the interacting set encompasses the residues that contain atoms within the specified cutoff distance from ligand atoms. An interaction matrix is constructed including the bits with relevant information of the defined chemical interactions.

QSAR Modeling

After docking experiments, 3D-QSAR models were performed to explain the SAR of the RC-33 analogs. Their bioactive conformations predicted by using docking were used as the alignment rule for deriving the models. The structural features that affect their activities against the S1R were identified by describing steric and electrostatic fields.

The 80 compounds dataset was randomly partitioned into training (64 compounds) and external (16 compounds) sets. A homogenous distribution of the activities was granted in both training and test sets. 3D-QSAR models were generated using Open3DQSAR (Tosco and Balle, 2011), an open access tool with all the capacities to construct 3D-QSAR models. Steric and electrostatic fields were computed according to classical molecular mechanics equations using the Merck Molecular Force Field (Halgren, 1996).

The field variables were calculated by describing the interaction energies between probe atoms (sp³ carbon atoms with a charge +1) and structures in a 1.0 Å step size grid box surrounding the whole set. Variables were processed as follows: (i) high energies adopted the top value of 30 kcal/mol, (ii) energy values very close to zero (below 0.05 kcal/mol) were set to zero in order to reduce noise, (iii) variables which only assumed a few different values (*n*-level variables) were removed. Thereafter, variables were scaled using the Block Unscaled Weighting procedure (Kastenholz et al., 2000; Boháč et al., 2002) and the predictive power of the models was improved by using the Smart Region Definition algorithm (Pastor et al., 1997).

Partial Least Square (PLS) regression was used to construct 3D-QSAR models, including from one to five Principal Components (PCs) and different combinations of fields. Models

were derived by using one field and by combining them; the best model was selected by considering the higher value of the internal leave-one-out (LOO) cross-validation Q^2 .

RESULTS AND DISCUSSION

Docking Predictions

We have a structural information of the binding poses of S1R ligands such as PD144418, 4-IBP, haloperidol, and NE-100 that similar in shape to RC-33. This information was used for evaluating the quality of the obtained docking results for RC-33 and its analogs. It is known that S1R ligands contain a charged nitrogen central atom flanked by two hydrophobic regions of different size (Glennon, 2005). The above mentioned S1R ligands form electrostatic interactions between the ligand charged nitrogen atoms and the side chain carboxylate of Glu172. In addition, their larger hydrophobic groups locate near the residues Val84, Met93, Leu95, Leu105, Tyr206, Ile178, Leu182, and Tyr103 (primary hydrophobic site), and their smaller hydrophobic groups locate near the residues Phe107, Trp164, His154, and Ile124 (secondary hydrophobic site). It is expected that the studied compounds establish such interactions.

Docking orientations of RC-33 and its analogs are represented in Figure 1. The best docking pose obtained for RC-33 was compared with the orientations of PD144418, 4-IBP, haloperidol, NE-100, and (+)-pentazocine in the reference crystallographic structures 5HK1, 5HK2, 6DJZ, 6DK0, and 6DK1, respectively. (+)-Pentazocine is an agonist as RC-33, but it is shorter than RC-33 and the other crystallized ligands; therefore, it is the least suitable ligand for the structural comparison between the crystallized ligands and the docked RC-33 analogs. Figure 1A shows that the docked structure of RC-33 was similarly oriented as the other crystallized ligands. On the other hand, Figure 1B shows that suitable binding modes of the ligands were found for all the RC-33 analogs. All of them form the conserved salt bridge between the charged N atom of the ligands and the residue Glu172 of the S1R. They also oriented their large hydrophobic groups to the primary hydrophobic site, and oriented their small hydrophobic groups to the secondary hydrophobic site. Representations in Figure 1 show that our docking poses are similar to the S1R-ligand X-ray structures reported to date.

We calculated RMSD values for the studied compounds with respect to the docking result of RC-33 inside the S1R by using an *in-house* script (Velázquez-Libera et al., 2018). These calculations show the similarity in orientations between RC-33 and its analogs in an easy way. Since the RC-33 derivatives are different from the reference compound, RMSD values were calculated by considering only the common graphs between molecules. %RefMatch and %MolMatch values were defined, where %RefMatch refers to the percent of common graphs between the docked compound and RC-33 regarding the total number of atoms of RC-33; meanwhile, %MolMatch refers to the percent of common graphs between the docked compound, and RC-33 regarding the total number of atoms of the docked compound. These values allow identifying the maximal similitude between the docked compound and RC-33; therefore, an RMSD value with high %RefMatch and %MolMatch

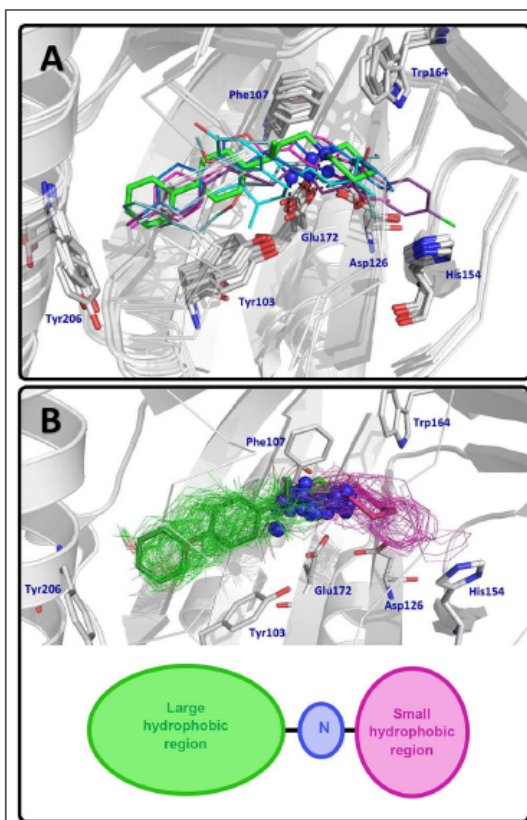


FIGURE 1 | Docking results for RC-33 and its analogs. **(A)** Docking pose obtained for RC-33 (stick representation in green) and comparison with X-ray crystallographic structures of the antagonist PD144418 (thin stick representation in purple, PDB code 5HK1), the ambiguous ligand 4-IBP (thin stick representation in light blue, PDB code 5HK2), the antagonist haloperidol (thin stick representation in ilac, PDB code 6DJZ), the antagonist NE-100 (thin stick representation in teal, PDB code 6DK0), and the agonist (+)-pentazocine (thin stick representation in cyan, PDB code 6DK1). N positively charged atom for each compound is represented by a blue sphere. **(B)** (top) Docking of RC-33 (in sticks representation) and comparison with its analogs (in lines representation); for each compound large hydrophobic group is in green at the left, small hydrophobic group is in purple at the right, and N positively charged atom is a sphere in blue. (bottom) Pharmacophoric model for S1R ligands: N positively charged atom (blue) flanked by large hydrophobic (green) and small hydrophobic (purple) regions.

values reflects that the compound under analysis bears a strong resemblance with RC-33.

The majority of the compounds under study have the 1-(3-phenylbutyl)piperidine or parts of this group in common with RC-33. Their RMSD values are reported in Table 2. In general, RMSD values reflect that the majority of compounds had the 1-(3-phenylbutyl)piperidine (or part of this group) similarly oriented with respect to RC-33 (RMSD < 2 Å). However,

TABLE 2 | RMSD values of the obtained docking pose common fragments for the studied compounds with respect to the docking result of RC-33 inside the S1R.

ID	RMSD (Å) ^a	%RefMatch ^b	%MolMatch ^c	RMSD (Å) ^{a,d}	%RefMatch ^{b,d}	%MolMatch ^{c,d}
1 (RC-33)				0.86	100	100
2	1.70	50	61	2.30	50	61
3	1.40	50	55	1.82	50	55
4	2.61	36	47			
5	2.20	36	47			
6	1.42	36	42			
7	0.46	64	74			
8	2.94	36	62			
9	1.67	36	53			
10	2.50	36	53			
11	2.80	50	65	2.89	50	65
12	2.05	50	65	2.16	50	65
13	2.21	50	61	1.50	50	61
14	1.43	50	58	1.46	50	58
15	0.43	77	89	0.86	77	89
16	1.45	50	42	1.07	50	42
17	0.97	77	65	0.69	77	65
18	1.58	36	35			
19	0.42	64	56			
20	1.29	36	32			
21	2.85	36	42			
22	0.38	36	38			
23	2.09	50	48	1.94	50	48
24	0.94	77	68	0.83	77	68
25	1.22	50	44	0.82	50	44
26	1.23	73	70	1.98	73	70
27	1.38	36	40			
28	0.59	64	64			
29	2.24	36	50			
30	0.85	36	44			
31	1.15	36	44			
32	1.11	36	36			
33	2.15	73	73	1.78	73	73
34	2.14	36	30			
35	0.45	64	48			
36	3.70	36	35			
37	4.17	36	32			
38	2.41	36	32			
39	1.16	36	40			
40	0.63	64	64			
41	0.77	36	44			
42	0.72	36	44			
43	2.10	32	26			
44	1.10	32	28			
45	1.66	32	24			
46	0.67	59	57			
47	1.05	32	37			
48	2.28	32	35			
49	2.23	32	39			
50	0.96	100	96			
51	0.64	100	96			

(Continued)

TABLE 2 | Continued

ID	RMSD (Å) ^a	%RefMatch ^b	%MolMatch ^c	RMSD (Å) ^{a,d}	%RefMatch ^{b,d}	%MolMatch ^{c,d}
52	1.50	50	61			
53	1.87	50	61			
54	1.48	50	55			
55	1.07	50	55			
56	2.19	73	80	1.96	73	80
57	2.63	73	59			
58	2.22	73	59			
59	1.95 ^e	91	100	1.98 ^e	91	100
60	1.80	50	73	2.54	50	73
61	2.63	73	89	1.52	73	89
62	3.02	73	64	6.97	73	64
63	2.38 ^e	82	100	2.51 ^e	82	100
64	2.11	50	73	2.58	50	73
65	2.45	73	89	1.01	73	89
66	2.68	73	64	4.26	73	64
67	2.19 ^e	82	100	1.98 ^e	82	100
68	0.63	50	85	2.96	50	85
69	2.65	73	100	2.73	73	100
70	3.87	73	70			
71	6.66	73	70			
72	2.58 ^e	73	100	1.49 ^e	73	100
73	2.29	73	57			
74	2.20	73	57			
75	4.65	73	67			
76	4.39	73	67			
77	2.72	73	55			
78	2.34	73	55			
79	1.74	73	57			
80	2.08	73	57			

^aRMSD values considering only the common chemical fragments between the docked compound and the reference compound RC-33.

^b%RefMatch refers to the percent of common graphs between the docked and reference compound RC-33 concerning the total number of atoms of the reference compound RC-33.

^c%MolMatch refers to the percent of common graphs between the docked and reference compound RC-33 regarding the total number of atoms of the docked compound.

^dRMSD, %RefMatch, and %MolMatch values for the S enantiomer of the compounds reported as racemic pairs.

^eIn this case, difference in ring heavy atoms were not considered between the docked compound and the reference compound RC-33.

Table 2 reports compounds with RMSD > 2.5 Å (for instance, compounds 11 (R and S), 57, 60 (S), and 77). The 1-(3-phenylbutyl)piperidine group of these compounds is displaced toward the helices $\alpha 4$ and $\alpha 5$; however, their amine groups keep the salt bridge interaction with the residue Glu172. In addition, we found in Table 2 compounds with RMSD > 4 Å (for instance, compounds 37, 62 (S), 66 (S), 75, and 76). The 1-(3-phenylbutyl)piperidine group of these compounds is oriented to the reverse with respect to this group in RC-33; their amine groups also keep the salt bridge interaction with the residue Glu172. These compounds have larger hydrophobic substituents at position 4 of the piperidine, increasing the size of this group. The changed groups fit better inside the bigger hydrophobic cavity close to the helices $\alpha 4$ and $\alpha 5$ when their orientations are opposed to the orientation of the 1-(3-phenylbutyl)piperidine group in RC-33. In this way, these compounds are also adapted to the previous described pharmacophore pattern for S1R ligands

(Ablordeppey et al., 2000; Glennon, 2005; Caballero et al., 2012) (the N positively charged atom flanked by two hydrophobic groups of different sizes), where the charged atom is salt-bridged to Glu172, the bigger hydrophobic group is placed near the helices $\alpha 4$ and $\alpha 5$ at the membrane proximal, and the smaller hydrophobic group is placed near the narrow end of the cupin barrel that is further from the membrane.

The chemical interactions between the RC-33 analogs and the residues at the S1R binding site can be described in detail by using IFPs. This method has been commonly used for identifying the relevant residues involved in protein-ligand affinities (Caballero et al., 2018; Navarro-Retamal and Caballero, 2018; Velázquez-Libera et al., 2018). IFPs capture and label the chemical contacts between a target protein and a set of its ligands as a whole. The chemotypes are identified with the following labels: P (polar groups), H (hydrophobic groups), A (hydrogen bonds where the residue is the acceptor), D (hydrogen bonds

where the residue is the donor), Ar (aromatic groups), and Ch (electrostatic interactions with charged groups). IFPs also differentiate between contacts with backbone and contacts with side-chain functional groups. We calculated IFPs by considering the S1R-ligand complexes formed by our docked structures.

The calculated IFPs are reported in Figure 2. The IFP analysis applied to the complexes between S1R and the RC-33 analogs obtained by docking revealed that 29 S1R residues had contacts with ligands. These residues and their positions in the S1R secondary structure are depicted in Figure 2A. The S1R binding site is mainly hydrophobic; in fact, the vast majority of the observed interactions are hydrophobic or aromatic when

analyzing the occurrence of chemical contacts in the studied structures (Figure 2C).

The residues with polar interactions were identified in the plots of percent of occurrence obtained from IFP calculations (Figure 2). The residue E172 at the sheet β_{10} has polar contributions in 100% of the total structures, forming a salt-bridge and it also acts as HB acceptor in 80% of the studied structures. The residue D126 at the sheet β_5 was identified with polar contributions in more than 50% of the studied structures. The residue T181 at the helix α_4 has polar contributions in more than 80% of the studied structures. Finally, the residues S117 (backbone and side chain), H154 (side chain), and T202

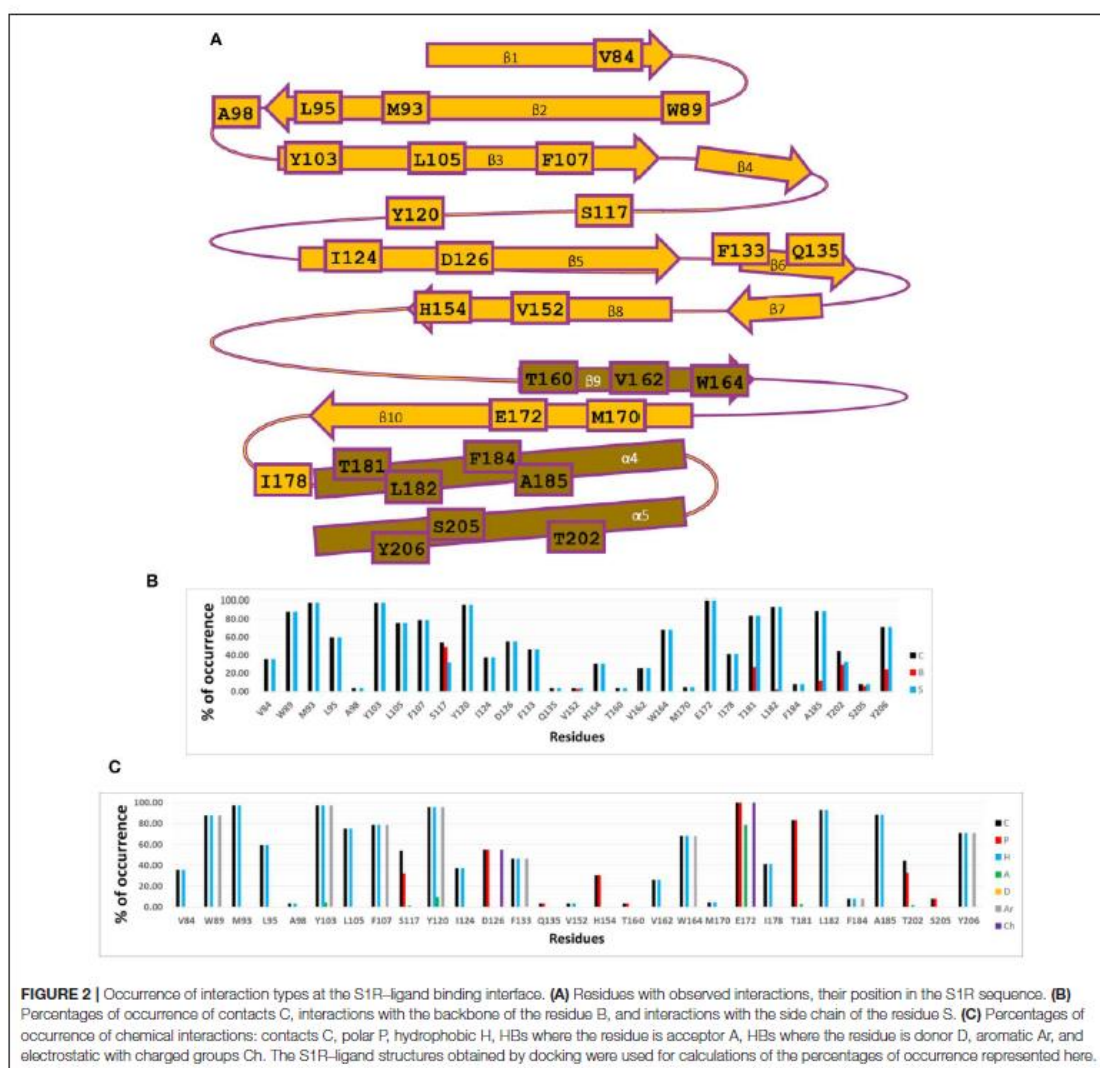
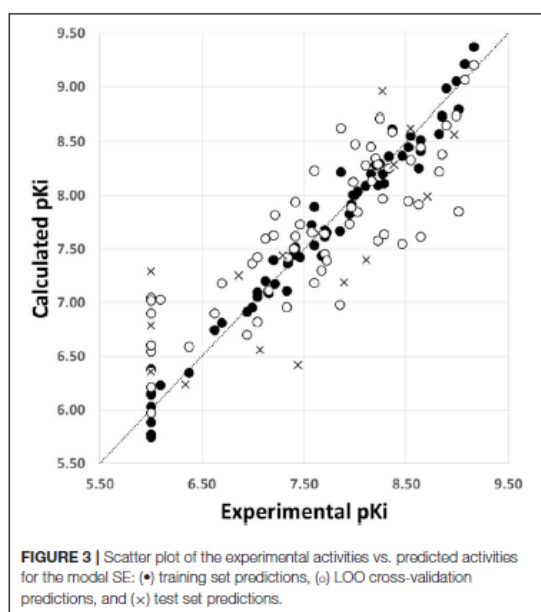


TABLE 3 | Statistical information of the 3D-QSAR models.

Fields	NC	R^2	S	Q^2	S_{LOO}	R^2_{test}	S_{test}	%S	%E
S	8	0.98	0.13	0.64	0.54	0.34	0.81	1	
E	4	0.81	0.39	0.54	0.62	0.59	0.63	–	1
SE	7	0.97	0.15	0.70	0.50	0.61	0.62	0.88	0.12

NC is the number of components; S is the standard deviation of the fitted activity of the training set; R^2 , Q^2 , and R^2_{test} are the coefficients of correlation of the training set, LOO cross validation, and test set, respectively; S_{LOO} is the standard deviation of the LOO cross validation, and S_{test} is the standard deviation of the test predictions. %S and %E are the relative contributions of the steric (S) and the electrostatic (E) fields, respectively.



(backbone and side chain) have polar contributions in around 30% of the studied structures.

Several residues with aromatic interactions were also identified in the plots of percent of occurrence obtained from IFP calculations (Figure 2). The residues with aromatic interactions were important for the shape of the S1R binding site because they restrict the space of the pockets. Four aromatic residues located at the center of the binding site (W89, Y103, F107, and Y120) were identified by the IFP calculations with percent of occurrence values above 80%. These residues cause a bottleneck just in front of the residue E172; therefore they could help to orient the positively charged N of the ligands to form the salt bridge. At the same time, they could stabilize the presence of the positive charge by means of π -cation interactions. The aromatic residues F133 at the sheet β_6 and W164 the sheet β_9 , located close to the narrower end of the cupin β -barrel, have percent of occurrence values of 50 and 70%, respectively. On the other

hand, the residue Y206, located at the helix α_5 , has a percent of occurrence value of 70%.

The remaining residues with hydrophobic interactions were also identified in the plots of percent of occurrence obtained from IFP calculations (Figure 2). The residues identified with percent of occurrence above 75% M93 (at β_2), L105 (at β_3), and L182/A185 (at α_4) are located at the bigger hydrophobic pocket. The residues V84 (at β_1), L95 (at β_2), and I178 (at the loop between β_{10} and α_4) are also located at the bigger hydrophobic pocket and were identified by IFP calculations with lower percent of occurrences, and the residue I124 at β_5 , located at the smaller hydrophobic pocket, had a percent of occurrence below 40%.

In general, the reported IFPs identify the most important S1R residues which establish chemical interactions with RC-33 analogs. Furthermore, it could be useful for the understanding of the interactions between S1R and its ligands.

3D-QSAR Results

We constructed the 3D-QSAR models based on docking alignment; therefore, the docked structures were included in a box for creating the relevant fields, since they are models of the ligand conformations inside the S1R binding site. The docking-based or receptor-guided alignment 3D-QSAR is a well-documented method in literature (Guasch et al., 2012; Navarro-Retamal and Caballero, 2016; Muñoz-Gutiérrez et al., 2017). Three 3D-QSAR models were trained using the steric field (Model S), the electrostatic field (Model E), and the combination of both fields (Model SE). The most reliable models were selected by measuring the LOO cross-validation performance ($Q^2 > 0.5$) and the test set predictions ($R^2_{test} > 0.5$).

Table 3 lists the description and statistical information of the best 3D-QSAR models. This report proved that model S has better (LOO) cross-validation Q^2 than model E. However, when both steric and electrostatic fields are tied together in the more complex model SE, the Q^2 value increases; therefore, this model, which had a $Q^2 = 0.70$ including seven components, containing a major contribution of the steric field (88%), was identified as the model best describing the structure-activity relationship of the studied RC-33 analogs. These results reflect that the steric features are mandatory for modulating the agonistic activities of the studied compounds. This is reasonable considering that the S1R binding site is mostly hydrophobic.

The model SE explains 97% of the variance and has a low standard deviation ($S = 0.15$). The predictions of pKi values for the 64 RC-33 analogs in the training set using the model SE are reported in Table 1 and the correlations between the predicted and experimental pKi values (from training and LOO cross validation) are shown in Figure 3. It is possible to observe that the selected model fitted adequately the whole dataset; it is noteworthy that the more potent compounds had an outstanding performance. When the model SE was used to predict the pKi values of the test set compounds, well results were also found, reflected by the value of $R^2_{test} = 0.61$. The predicted pKi values for the test set are listed in Table 1, and the correlation between the calculated and experimental pKi values are plotted in Figure 3.

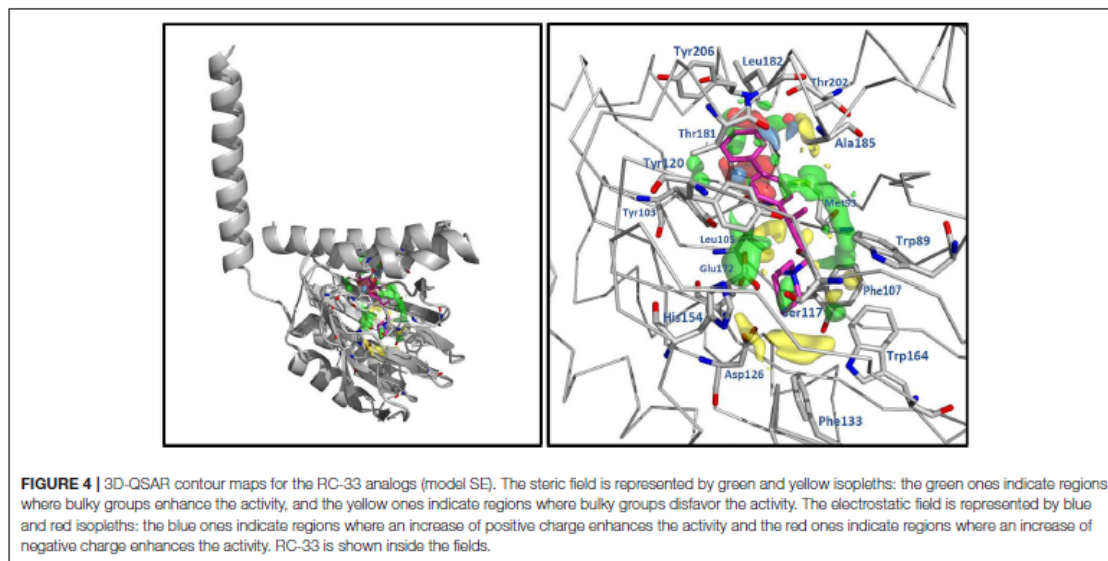


Figure 4 shows contour plots of the steric and electrostatic fields projected onto the docked structure of RC-33 for association between the fields, the compounds of the whole set, and the residues at the S1R binding site. In this figure, green and yellow contours represent regions with positive and negative steric components, respectively. It is noted that positive steric components have a major role. A great green contour in front of the 3-phenylbutylamine, and near the residues V84, W89, F107, and A185, indicates that bulk groups are desired in this region. It is noteworthy that the most active compounds such as RC-33, 7, 15, 27, 28, and 33 has the methyl group of the 3-phenylbutylamine in this region, but the majority of the less active compounds such as 8, 29, 41, 64, and 67 have this group deeper into the bigger hydrophobic pocket. Another three green contours are located near the piperidine of RC-33 and the residues Y120, S117, and W164 indicating that this group or another bulky group in this region is needed. In general, compounds with a dimethylamine in this region (compounds 2–15) are less active than similar compounds that contain piperidine. Another green contour near the residues Y103 and E172 reflects that several active compounds contain the methyl group of the 3-phenylbutylamine in this region. Another green contours are located at the bigger hydrophobic pocket near the residues Y103, Y206, and T202, indicating the preference of a bulky group in this region. For instance, the biphenyl group in compound 7 is preferred instead the phenyl group in compound 8 because the former group fills the entire space of the bigger hydrophobic pocket. Several yellow contours were identified near the residues W164, L105, F107, and T202. All of them are close to the green contours both in the bigger and smaller pockets, and reflect the complexity of the steric field inside the S1R binding site.

In Figure 4, blue and red contours represent regions with positive and negative electrostatic components, respectively; all of them are small and are located inside the bigger hydrophobic pocket. The blue contours are near the residues T181, A185, L182, and the backbone of Y206, and the red contours are near the residues A92, L95, L105, L182, and T202. The blue contours are located in regions where ligands placed hydroxyl groups and their p*K*_i values are between 7 and 7.8 (moderate activities). For instance, compounds 13 and 77 have hydroxyl close to the backbone of Y206, 75, and 76 have hydroxyl close to A185, and 53, 55, and 78 have hydroxyl close to T181. The red contours are located in regions where ligands placed OMe groups and the activity is increased. For instance, compounds 22 and 30 that contain OMe have better activities than compounds 21 and 29 without this group.

The docking-based 3D-QSAR methodology allows establishing a comparison between the chemical features that describe the structure-activity relationship of bioactive ligands and the protein binding site (Alzate-Morales and Caballero, 2010; Caballero et al., 2011; Quesada-Romero et al., 2014; Mena-Ulecia et al., 2015; Muñoz-Gutiérrez et al., 2017). The contour plots in receptor-based 3D-QSAR are not receptor maps, but they solve another key point of the description of the differential activities: different potency in activities is connected with different chemical environments and interactions. The docking and 3D-QSAR methods applied to the study of RC-33 analogs give more information about the structure of S1R-ligand complexes, and identify important chemical features to take into account in the future design of potent S1R ligands. We feel that another similar studies on other series of compounds will be reported during next years.

CONCLUSION

This is the first structure-based molecular modeling investigation a few years after the elucidation of the S1R crystallographic structure; therefore, details of the binding poses and the chemical interactions in the binding site are described. Binding orientations and structure-activity relationship of RC-33 analogs as S1R agonists were studied by using molecular docking and 3D-QSAR methods.

Docking poses obtained for the studied compounds inside the S1R binding site explain the interactions between the well-known theoretical pharmacophore model reported for these compounds (elucidated before the knowledge of the S1R 3D structure) and the residues located at the binding site. They also reproduced structural features reported for complexes between S1R and PD144418, 4-IBP, and other active ligands. The docking analysis, including the IFP calculations, confirmed the preponderant role of E172 forming a salt bridge with the positively charged N of the ligands. Furthermore, docking experiments also identified the importance role of the aromatic residues delimiting the shape of the S1R binding site: specifically, W89, Y103, F107, and Y120 which are at the center of the binding site, F133 and W164 which are close to the narrower end of the cupin β -barrel, and Y206 which is close to the helix α 5.

A receptor-guided alignment 3D-QSAR model with adequate statistical significance and acceptable prediction power was obtained. Steric and electrostatic features had contributions to the differential potency of the agonists, with a major role of the steric ones. The 3D-QSAR model demonstrated that an implicit

correlation is found in the data under analysis between the chemical features of the compounds in their active conformations and their interactions in the pockets of the S1R binding site.

Overall, the information reported here, derived from the recently reported S1R structure, will be useful for the future research in the design of novel S1R ligands.

DATA AVAILABILITY

The raw data supporting the conclusions of this manuscript will be made available by the authors, without undue reservation, to any qualified researcher.

AUTHOR CONTRIBUTIONS

The work was completed by cooperation of all authors. JC was responsible for the study of concept and design of the project. JV-L performed the docking RMSD analysis, IFPs, and 3D-QSAR calculations. GR and CN-R performed the docking calculations. SC and JC drafted and revised the manuscript.

FUNDING

This research was funded by FONDECYT Regular grant number 1170718 (JC) and FONDECYT Postdoc grant number 3170434 (CN-R). The authors gratefully acknowledge MIUR for the doctoral fellowship to GR and thankfully recognize Scuola di Alta Formazione Dottorale of University of Pavia for the mobility research scholarship provided to GR.

REFERENCES

- Ablordepey, S. Y., Fischer, J. B., and Glennon, R. A. (2000). Is a nitrogen atom an important pharmacophoric element in sigma ligand binding? *Bioorg. Med. Chem.* 8, 2105–2111. doi: 10.1016/S0968-0896(00)00148-6
- Almerico, A. M., Tutone, M., and Lauria, A. (2012). Receptor-guided 3D-QSAR approach for the discovery of c-kit tyrosine kinase inhibitors. *J. Mol. Model.* 18, 2885–2895. doi: 10.1007/s00894-011-1304-0
- Alon, A., Schmidt, H. R., Wood, M. D., Sahn, J. J., Martin, S. F., and Kruse, A. C. (2017). Identification of the gene that codes for the σ 2 receptor. *Proc. Natl. Acad. Sci. U.S.A.* 114, 7160–7165. doi: 10.1073/pnas.1705154114
- Alzate-Morales, J., and Caballero, J. (2010). Computational study of the interactions between guanine derivatives and cyclin-dependent kinase 2 (CDK2) by CoMFA and QM/MM. *J. Chem. Inf. Model.* 50, 110–122. doi: 10.1021/ci900302z
- Amaning, K., Lowinski, M., Vallee, F., Steier, V., Marcireau, C., Ugolini, A., et al. (2013). The use of virtual screening and differential scanning fluorimetry for the rapid identification of fragments active against MEK1. *Bioorg. Med. Chem. Lett.* 23, 3620–3626. doi: 10.1016/j.bmcl.2013.04.003
- Batra, J., Szabó, A., Caulfield, T. R., Soares, A. S., Sahin-Tóth, M., and Radisky, E. S. (2013). Long-range electrostatic complementarity governs substrate recognition by human chymotrypsin C, a key regulator of digestive enzyme activation. *J. Biol. Chem.* 288, 9848–9859. doi: 10.1074/jbc.M113.457382
- Bohác, M., Loeprecht, B., Damborský, J., and Schüürmann, G. (2002). Impact of Orthogonal Signal Correction (OSC) on the predictive ability of CoMFA models for the ciliate toxicity of nitrobenzenes. *Q. Struct. Activit. Relationsh.* 21, 3–11. doi: 10.1002/1521-3838(200205)21:1<3::AID-QSAR3>3.0.CO;2-D
- Caballero, J., Morales-Bayuelo, A., and Navarro-Retamal, C. (2018). *Mycobacterium tuberculosis* serine/threonine protein kinases: structural information for the design of their specific ATP-competitive inhibitors. *J. Comput. Aided Mol. Des.* 32, 1315–1336. doi: 10.1007/s10822-018-0173-3
- Caballero, J., Quiliano, M., Alzate-Morales, J. H., Zimic, M., and Deharo, E. (2011). Docking and quantitative structure-activity relationship studies for 3-fluoro-4-(pyrrolo[2,1-f][1,2,4]triazin-4-yloxy)aniline, 3-fluoro-4-(1H-pyrrolo[2,3-b]pyridin-4-yloxy)aniline, and 4-(4-amino-2-fluorophenoxy)-2-pyridinylamine derivatives as c-Met kinase inhibitors. *J. Comput. Aided Mol. Des.* 25, 349–369. doi: 10.1007/s10822-011-9425-1
- Caballero, J., Zilocchi, S., Tiznado, W., Rossi, D., and Collina, S. (2012). Models of the pharmacophoric pattern and affinity trend of methyl 2-(aminomethyl)-1-phenylcyclopropane-1-carboxylate derivatives as σ 1 ligands. *Mol. Simul.* 38, 227–235. doi: 10.1080/08927022.2011.614243
- Chu, U. B., and Ruoho, A. E. (2016). Biochemical pharmacology of the sigma-1 receptor. *Mol. Pharmacol.* 89, 142–153. doi: 10.1124/mol.115.101170
- Collina, S., Bignardi, E., Rui, M., Rossi, D., Gaggeri, R., Zamagni, A., et al. (2017a). Are sigma modulators an effective opportunity for cancer treatment? A patent overview (1996–2016). *Expert Opin. Ther. Pat.* 27, 565–578. doi: 10.1080/13543776.2017.1276569
- Collina, S., Loddò, G., Urbano, M., Linati, L., Callegari, A., Ortuso, F., et al. (2007). Design, synthesis, and SAR analysis of novel selective [sigma]1 ligands. *Bioorg. Med. Chem.* 15, 771–783. doi: 10.1016/j.bmc.2006.10.048
- Collina, S., Rui, M., Stotani, S., Bignardi, E., Rossi, D., Curti, D., et al. (2017b). Are sigma receptor modulators a weapon against multiple sclerosis disease? *Future Med. Chem.* 9, 2029–2051. doi: 10.4155/fmc-2017-0122
- DeCoster, M. A., Klette, K. L., Knight, E. S., and Tortella, F. C. (1995). σ receptor-mediated neuroprotection against glutamate toxicity in primary rat neuronal cultures. *Brain Res.* 671, 45–53. doi: 10.1016/0006-8993(94)01294-R
- Deng, Z., Chuaqui, C., and Singh, J. (2004). Structural interaction fingerprint (SIF): a novel method for analyzing three-dimensional protein-ligand binding interactions. *J. Med. Chem.* 47, 337–344. doi: 10.1021/jm030331x

- Friesner, R. A., Banks, J. L., Murphy, R. B., Halgren, T. A., Klicic, J. J., Mainz, D. T., et al. (2004). Glide: a new approach for rapid, accurate docking and scoring. 1. Method and assessment of docking accuracy. *J. Med. Chem.* 47, 1739–1749. doi: 10.1021/jm0306430
- Furuse, T., and Hashimoto, K. (2010). Sigma-1 receptor agonist fluvoxamine for delirium in patients with Alzheimer's disease. *Ann. Gen. Psychiatry* 9:6. doi: 10.1186/1744-859X-9-6
- Glennon, R. A. (2005). Pharmacophore identification for sigma-1 (sigma1) receptor binding: application of the "deconstruction-reconstruction-elaboration" approach. *Mini Rev. Med. Chem.* 5, 927–940. doi: 10.2174/138955705774329519
- Glennon, R. A., Ismaiel, A. M., Ablordeppey, S., El-Ashmawy, M., and Fisher, J. B. (2004). Thioxanthene-derived analogs as sigma(1) receptor ligands. *Bioorg. Med. Chem. Lett.* 14, 2217–2220. doi: 10.1016/j.bmcl.2004.02.018
- Guasch, L., Sala, E., Valls, C., Mulero, M., Pujadas, G., and Garcia-Vallvé, S. (2012). Development of docking-based 3D-QSAR models for PPARgamma full agonists. *J. Mol. Graph. Model.* 36, 1–9. doi: 10.1016/j.jmgm.2012.03.001
- Hajipour, A. R., Fontanilla, D., Chu, U. B., Arbabian, M., and Ruoho, A. E. (2010). Synthesis and characterization of N,N-dialkyl and N-alkyl-N-alkyl fenpropimorph-derived compounds as high affinity ligands for sigma receptors. *Bioorg. Med. Chem.* 18, 4397–4404. doi: 10.1016/j.bmc.2010.04.078
- Halgren, T. A. (1996). Merck molecular force field. II. MMFF94 van der Waals and electrostatic parameters for intermolecular interactions. *J. Comput. Chem.* 17, 520–552. doi: 10.1002/(SICI)1096-987X(199604)17:5<520::AID-JCC2>3.0.CO;2-W
- Hanner, M., Moebius, F. F., Flandorfer, A., Knaus, H. G., Striessnig, J., Kempner, E., et al. (1996). Purification, molecular cloning, and expression of the mammalian sigma1-binding site. *Proc. Natl. Acad. Sci. U.S.A.* 93, 8072–8077. doi: 10.1073/pnas.93.15.8072
- Hashimoto, K. (2009). Can the sigma-1 receptor agonist fluvoxamine prevent schizophrenia? *CNS Neurol. Disord. Drug Targets* 8, 470–474. doi: 10.2174/187152709789824633
- Hayashi, T., and Su, T.-P. (2004). Sigma-1 receptor ligands: potential in the treatment of neuropsychiatric disorders. *CNS Drugs* 18, 269–284. doi: 10.2165/00023210-200418050-00001
- Kastenholz, M. A., Pastor, M., Cruciani, G., Haaksma, E. E., and Fox, T. (2000). GRID/CPCA: a new computational tool to design selective ligands. *J. Med. Chem.* 43, 3033–3044. doi: 10.1021/jm000934y
- Marra, A., Rossi, D., Pignataro, L., Bigogno, C., Canta, A., Oggioni, N., et al. (2016). Toward the identification of neuroprotective agents: g-scale synthesis, pharmacokinetic evaluation and CNS distribution of (R)-RC-33, a promising SIGMA1 receptor agonist. *Future Med. Chem.* 8, 287–295. doi: 10.4155/fmc.15.191
- Martin, W. R., Eades, C. G., Thompson, J. A., Huppler, R. E., and Gilbert, P. E. (1976). The effects of morphine- and nalorphine- like drugs in the non-dependent and morphine-dependent chronic spinal dog. *J. Pharmacol. Exp. Ther.* 197, 517–532.
- Mavlyutov, T. A., Guo, L.-W., Epstein, M. L., and Ruoho, A. E. (2015). Role of the sigma-1 receptor in Amyotrophic Lateral Sclerosis (ALS). *J. Pharmacol. Sci.* 127, 10–16. doi: 10.1016/j.jphs.2014.12.013
- Mena-Ulecia, K., Tiznado, W., and Caballero, J. (2015). Study of the differential activity of thrombin inhibitors using docking, QSAR, molecular dynamics, and MM-GBSA. *PLoS ONE* 10:e0142774. doi: 10.1371/journal.pone.0142774
- Meyer, D. A., Carta, M., Partridge, L. D., Covey, D. F., and Valenzuela, C. F. (2002). Neurosteroids enhance spontaneous glutamate release in hippocampal neurons possible role of metabotropic σ -like receptors. *J. Biol. Chem.* 277, 28725–28732. doi: 10.1074/jbc.M202592200
- Mishina, M., Ishiwata, K., Ishii, K., Kitamura, S., Kimura, Y., Kawamura, K., et al. (2005). Function of sigma1 receptors in Parkinson's disease. *Acta Neurol. Scand.* 112, 103–107. doi: 10.1111/j.1600-0404.2005.00432.x
- Monnet, F. P., and Maurice, T. (2006). The sigma1 protein as a target for the non-genomic effects of neuro(steroid)s: molecular, physiological, and behavioral aspects. *J. Pharmacol. Sci.* 100, 93–118. doi: 10.1254/jphs.CR0050032
- Morin-Surun, M. P., Collin, T., Denavit-Saubié, M., Baulieu, E. E., and Monnet, F. P. (1999). Intracellular sigma1 receptor modulates phospholipase C and protein kinase C activities in the brainstem. *Proc. Natl. Acad. Sci. U.S.A.* 96, 8196–8199. doi: 10.1073/pnas.96.14.8196
- Muñoz-Gutiérrez, C., Adasme-Carreño, F., Fuentes, E., Palomo, I., and Caballero, J. (2016). Computational study of the binding orientation and affinity of PPAR γ agonists: inclusion of ligand-induced fit by cross-docking. *RSC Adv.* 6, 64756–64768. doi: 10.1039/C6RA12084A
- Muñoz-Gutiérrez, C., Cáceres-Rojas, D., Adasme-Carreño, F., Palomo, I., Fuentes, E., and Caballero, J. (2017). Docking and quantitative structure-activity relationship of bi-cyclic heteroaromatic pyridazinone and pyrazolone derivatives as phosphodiesterase 3A (PDE3A) inhibitors. *PLoS ONE* 12:e0189213. doi: 10.1371/journal.pone.0189213
- Navarro-Retamal, C., and Caballero, J. (2016). Flavonoids as CDK1 inhibitors: insights in their binding orientations and structure-activity relationship. *PLoS ONE* 11:e0161111. doi: 10.1371/journal.pone.0161111
- Navarro-Retamal, C., and Caballero, J. (2018). "Molecular modeling of tau Proline-Directed Protein Kinase (PDPK) inhibitors," in *Computational Modeling of Drugs Against Alzheimer's Disease Neuromethods*, ed K. Roy (New York, NY: Humana Press), 305–345. doi: 10.1007/978-1-4939-7404-7_13
- Osguthorpe, D. J., Sherman, W., and Hagler, A. T. (2012). Generation of receptor structural ensembles for virtual screening using binding site shape analysis and clustering. *Chem. Biol. Drug Des.* 80, 182–193. doi: 10.1111/j.1747-0285.2012.01396.x
- Pastor, M., Cruciani, G., and Clementi, S. (1997). Smart region definition: a new way to improve the predictive ability and interpretability of three-dimensional quantitative structure-activity relationships. *J. Med. Chem.* 40, 1455–1464. doi: 10.1021/jm9608016
- Peviani, M., Salvaneschi, E., Bontempi, L., Petese, A., Manzo, A., Rossi, D., et al. (2014). Neuroprotective effects of the Sigma-1 receptor (S1R) agonist PRE-084, in a mouse model of motor neuron disease not linked to SOD1 mutation. *Neurobiol. Dis.* 62, 218–232. doi: 10.1016/j.nbd.2013.10.010
- Prezzavento, O., Campisi, A., Ronsisvalle, S., Li Volti, G., Marrazzo, A., Bramanti, V., et al. (2007). Novel sigma receptor ligands: synthesis and biological profile. *J. Med. Chem.* 50, 951–961. doi: 10.1021/jm0611197
- Quesada-Romero, L., and Caballero, J. (2014). Docking and quantitative structure-activity relationship of oxadiazole derivatives as inhibitors of GSK3 β . *Mol. Divers.* 18, 149–159. doi: 10.1007/s11030-013-9483-5
- Quesada-Romero, L., Mena-Ulecia, K., Tiznado, W., and Caballero, J. (2014). Insights into the interactions between maleimide derivatives and GSK3 β combining molecular docking and QSAR. *PLoS ONE* 9:e102212. doi: 10.1371/journal.pone.0102212
- Quesada-Romero, L., Mena-Ulecia, K., Zuñiga, M., De-la-Torre, P., Rossi, D., Tiznado, W., et al. (2015). Optimal graph-based and simplified molecular input line entry System-based descriptors for quantitative structure-activity relationship analysis of arylalkylaminoalcohols, arylalkenylamines, and arylalkylamines as σ 1 receptor ligands. *J. Chemom.* 29, 13–20. doi: 10.1002/cem.2650
- Ramírez, D., and Caballero, J. (2018). Is it reliable to take the molecular docking top scoring position as the best solution without considering available structural data? *Molecules* 23:1038. doi: 10.3390/molecules23051038
- Rossi, D., Marra, A., Picconi, P., Serra, M., Catenacci, L., Sorrenti, M., et al. (2013a). Identification of RC-33 as a potent and selective σ 1 receptor agonist potentiating NGF-induced neurite outgrowth in PC12 cells. Part 2: g-scale synthesis, physicochemical characterization and *in vitro* metabolic stability. *Bioorg. Med. Chem.* 21, 2577–2586. doi: 10.1016/j.bmc.2013.02.029
- Rossi, D., Marra, A., Rui, M., Laurini, E., Fermeleglia, M., Pricl, S., et al. (2015). A step forward in the sigma enigma: a role for chirality in the sigma1 receptor–ligand interaction? *Med. Chem. Commun.* 6, 138–146. doi: 10.1039/C4MD00349G
- Rossi, D., Pedrali, A., Gaggeri, R., Marra, A., Pignataro, L., Laurini, E., et al. (2013b). Chemical, pharmacological, and *in vitro* metabolic stability studies on enantiomerically pure RC-33 compounds: promising neuroprotective agents acting as σ 1 receptor agonists. *ChemMedChem* 8, 1514–1527. doi: 10.1002/cmdc.201300218
- Rossi, D., Pedrali, A., Urbano, M., Gaggeri, R., Serra, M., Fernández, L., et al. (2011). Identification of a potent and selective σ 1 receptor agonist potentiating NGF-induced neurite outgrowth in PC12 cells. *Bioorg. Med. Chem.* 19, 6210–6224. doi: 10.1016/j.bmc.2011.09.016
- Rossi, D., Rui, M., Di Giacomo, M., Schepmann, D., Wunsch, B., Monteleone, S., et al. (2017). Gaining in pan-affinity towards sigma 1 and sigma 2 receptors. SAR studies on arylalkylamines. *Bioorg. Med. Chem.* 25, 11–19. doi: 10.1016/j.bmc.2016.10.005

- Rossi, D., Urbano, M., Pedrali, A., Serra, M., Zampieri, D., Mamolo, M. G., et al. (2010). Design, synthesis and SAR analysis of novel selective sigma1 ligands (Part 2). *Bioorg. Med. Chem.* 18, 1204–1212. doi: 10.1016/j.bmc.2009.12.039
- Rui, M., Rossi, D., Marra, A., Paolillo, M., Schinelli, S., Curti, D., et al. (2016). Synthesis and biological evaluation of new aryl-alkyl(alkenyl)-4-benzylpiperidines, novel Sigma Receptor (SR) modulators, as potential anticancer-agents. *Eur. J. Med. Chem.* 124, 649–665. doi: 10.1016/j.ejmech.2016.08.067
- Schmidt, H. R., Betz, R. M., Dror, R. O., and Kruse, A. C. (2018). Structural basis for σ_1 receptor ligand recognition. *Nat. Struct. Mol. Biol.* 25, 981–987. doi: 10.1038/s41594-018-0137-2
- Schmidt, H. R., Zheng, S., Gurpinar, E., Koehl, A., Manglik, A., and Kruse, A. C. (2016). Crystal structure of the human σ_1 receptor. *Nature* 532, 527–530. doi: 10.1038/nature17391
- Shelley, J. C., Cholleti, A., Frye, L. L., Greenwood, J. R., Timlin, M. R., and Uchimaya, M. (2007). Epik: a software program for pK(a) prediction and protonation state generation for drug-like molecules. *J. Comput. Aided Mol. Des.* 21, 681–691. doi: 10.1007/s10822-007-9133-z
- Singh, J., Deng, Z., Narale, G., and Chuaqui, C. (2006). Structural interaction fingerprints: a new approach to organizing, mining, analyzing, and designing protein-small molecule complexes. *Chem. Biol. Drug Des.* 67, 5–12. doi: 10.1111/j.1747-0285.2005.00323.x
- Tesei, A., Cortesi, M., Zamagni, A., Arienti, C., Pignatta, S., Zanoni, M., et al. (2018). Sigma receptors as endoplasmic reticulum stress “Gatekeepers” and their modulators as emerging new weapons in the fight against cancer. *Front. Pharmacol.* 9:711. doi: 10.3389/fphar.2018.00711
- Tosco, P., and Balle, T. (2011). Open3DQSAR: a new open-source software aimed at high-throughput chemometric analysis of molecular interaction fields. *J. Mol. Model.* 17, 201–208. doi: 10.1007/s00894-010-0684-x
- Urbano, M., Collina, S., Rossi, D., Baraglia, A. C., Alcaro, S., Artese, A., et al. (2007). Design and synthesis of a (N-Alkylaminoalkyl-Substituted)arylalkenylamide drug discovery library. *Lett. Drug Des. Discov.* 4, 605–610. doi: 10.2174/157018007782794581
- Vavers, E., Svalbe, B., Lauberte, L., Stonans, I., Misane, I., Dambrova, M., et al. (2017). The activity of selective sigma-1 receptor ligands in seizure models in vivo. *Behav. Brain Res.* 328, 13–18. doi: 10.1016/j.bbr.2017.04.008
- Velázquez-Libera, J. L., Navarro-Retamal, C., and Caballero, J. (2018). Insights into the structural requirements of 2(S)-amino-6-boronohexanoic acid derivatives as arginase I inhibitors: 3D-QSAR, docking, and interaction fingerprint studies. *Int. J. Mol. Sci.* 19:2956. doi: 10.3390/ijms19102956
- Walker, J. M., Bowen, W. D., Walker, F. O., Matsumoto, R. R., De Costa, B., and Rice, K. C. (1990). Sigma receptors: biology and function. *Pharmacol. Rev.* 42, 355–402.
- Wu, D., Wang, Q., Assary, R. S., Broadbelt, L. J., and Krilov, G. (2011). A computational approach to design and evaluate enzymatic reaction pathways: application to 1-butanol production from pyruvate. *J. Chem. Inf. Model.* 51, 1634–1647. doi: 10.1021/ci2000659
- Yagasaki, Y., Numakawa, T., Kumamaru, E., Hayashi, T., Su, T.-P., and Kunugi, H. (2006). Chronic antidepressants potentiate via sigma-1 receptors the brain-derived neurotrophic factor-induced signaling for glutamate release. *J. Biol. Chem.* 281, 12941–12949. doi: 10.1074/jbc.M508157200
- Yous, S., Wallez, V., Belloir, M., Caignard, D. H., McCurdy, C. R., and Poupaert, J. H. (2005). Novel 2(3H)-benzothiazolones as highly potent and selective sigma-1 receptor ligands. *Med. Chem. Res.* 14, 158–168. doi: 10.1007/s00044-005-0131-1
- Zampieri, D., Grazia Mamolo, M., Laurini, E., Zanette, C., Florio, C., Collina, S., et al. (2009). Substituted benzo[d]oxazol-2(3H)-one derivatives with preference for the sigma1 binding site. *Eur. J. Med. Chem.* 44, 124–130. doi: 10.1016/j.ejmech.2008.03.011

Conflict of Interest Statement: The authors declare that the research was conducted in the absence of any commercial or financial relationships that could be construed as a potential conflict of interest.

Copyright © 2019 Velázquez-Libera, Rossino, Navarro-Retamal, Collina and Caballero. This is an open-access article distributed under the terms of the Creative Commons Attribution License (CC BY). The use, distribution or reproduction in other forums is permitted, provided the original author(s) and the copyright owner(s) are credited and that the original publication in this journal is cited, in accordance with accepted academic practice. No use, distribution or reproduction is permitted which does not comply with these terms.

Paper 6

Reprinted with permission from Giacomo Rossino, Ivana Orellana, Julio Caballero, Dirk Schepmann, Bernhard Wünsch, Marta Rui, Daniela Rossi, Mariela González-Avendaño, Simona Collina, and Ariela Vergara-Jaque *Journal of Chemical Information and Modeling* **Article ASAP** DOI: 10.1021/acs.jcim.9b00649. Copyright (2020) American Chemical Society.

New Insights into the Opening of the Occluded Ligand-Binding Pocket of Sigma1 Receptor: Binding of a Novel Bivalent RC-33 Derivative

Giacomo Rossino,[†] Ivana Orellana,[‡] Julio Caballero,^{‡,§} Dirk Schepmann,[§] Bernhard Wunsch,^{§,||} Marta Rui,[†] Daniela Rossi,[†] Mariela González-Avendaño,[‡] Simona Collina,^{*,†,||,⊥} and Ariela Vergara-Jaque^{*,‡,||,⊥}

[†]Department of Drug Sciences, University of Pavia, Viale Taramelli 12, 27100 Pavia, Italy

[‡]Center for Bioinformatics and Molecular Simulation, Universidad de Talca, 1 Poniente, 1141 Talca, Chile

[§]Institute of Pharmaceutical and Medicinal Chemistry, University of Muenster, Correnstrasse 48, 48149 Münster, Germany

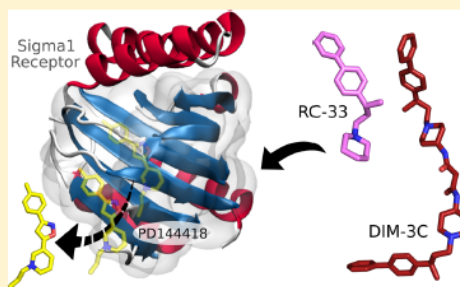
^{||}Multidisciplinary Scientific Nucleus, Universidad de Talca, 1 Poniente, 1141 Talca, Chile

[⊥]Millennium Nucleus of Ion Channels-associated Diseases (MiNICAD), Santiago, Chile

Supporting Information

ABSTRACT: Significant progresses have been made to understand the molecular basis of the Sigma1 receptor (S1R) operating in normal and pathological conditions. S1R is a transmembrane protein that participates in a wide variety of processes at the central nervous system; hence, its function has been associated with mental and neurological disorders. Several ligands have been proposed to regulate the function of S1R revealing a high plasticity of the ligand-binding pocket. Previous drug-design studies have been mainly based on pharmacophore models; however, the recently revealed crystal structure of S1R provides an excellent opportunity for verifying previous predictions and for evaluating the binding of novel compounds. Interestingly, the crystal structure shows that the binding pocket of S1R is highly occluded from solvent; therefore, it is not clear how ligands access this site.

In the present work, we applied steered molecular dynamics (SMD) simulations to open the occluded ligand-binding pocket in the S1R crystal structure and to determine the preferred ligand pathway to enter and exit the binding site. The intracellular surface of the β -barrel ligand-binding region was found the most favorable route to accommodate ligands. This route supports the binding of RC-33 (our in-house-developed S1R modulator) and a new bivalent derivative that constitutes the first divalent structure shown to interact with S1R. Free energy calculations of these compounds associated with S1R agree with experimental K_i values and provide molecular insights of the binding mode of modulators that could access the S1R ligand-binding pocket through the cytoplasmic region.



INTRODUCTION

The Sigma1 receptor (S1R) is a known drug target implicated in a variety of pathologies related to the cardiovascular and nervous systems.¹ Many psychostimulant drugs interact with this receptor in the brain and heart,² making it clear that S1R is a critical target for designing and developing novel pharmaceutical compounds. The gene encoding S1R is located on the human chromosome 9 band p13, a region associated with different psychiatric disorders.³ Behavioral phenotype of knockout S1R in mice revealed gender-related anxiety and depression-like and memory alterations.^{4,5} The central nervous system, therefore, appears to be the primary site of S1R activity and modulation.

The Sigma1 gene has been cloned from various organisms, namely, guinea pig, human, rat and mouse,^{6–8} exhibiting a

greater than 90% species homology.⁹ In humans, the Sigma1 gene is expressed as a small protein of 223 amino acids, acting as chaperone at the endoplasmic reticulum,¹⁰ where it modulates the activity of protein receptors, ion channels, and kinases.^{11,12} Because of the difficulty of expressing, purifying, and crystallizing membrane-bound proteins, the S1R crystal structure has been only recently elucidated, 20 years after its cloning and expression in mammals.⁶ Schmidt et al. reported the first full-length S1R structure in complex with two

Special Issue: Molecular Simulation in Latin America: Coming of Age

Received: August 3, 2019

Published: December 6, 2019

chemically divergent ligands, PD144418 and 4-IBP.¹³ The overall structure shows a trimeric architecture, with each protomer containing a single transmembrane segment and a cytosolic domain termed as the β -barrel ligand-binding region. Interestingly, this large hydrophobic ligand-binding cavity shows remarkable plasticity to bind unrelated ligand structures in a similar orientation and position. The ligand-binding site of each protomer at the crystal structure is occupied by one single molecule, and its interior is completely occluded from solvent. It is necessary, therefore, to understand how ligands enter and exit from this site.

A fascinating feature of SIR is that it binds ligands with very different structures. These include psychostimulant drugs such as cocaine, metamphatamine, haloperidol, dextrometorphan, fluoxetine, donepezil, and others.^{2,14} Based on structure–activity relationship studies, a pharmacophore model of SIR ligands has been proposed, including two hydrophobic constituents attached to a central nitrogen atom.¹⁵ Most SIR agonists, antagonists, and allosteric modulators fit this pharmacophore model.¹⁶ Ligand-based molecular modeling methodologies, integrating the pharmacophore information, have been employed in the design of active ligand series.^{17–22} Additionally, low-quality protein models^{11,23,24} were previously used to identify SIR ligands through studies of structure-based drug design. Nonetheless, taking into account that the quality of homology models is affected by low sequence identity and the use of multiple templates, the recent reported SIR crystal structure provides an excellent frame for corroborating previous predictions and for extending binding studies of novel ligand compounds.

In an effort to better understand the mechanism of interaction between SIR and its modulators, especially the way they reach the ligand-binding pocket, we decided to compare, by both *in silico* and *in vitro* analyses, the binding of the cocrystallized PD144418 ligand with two in-house developed SIR agonists, namely, 1-[3-(1,1'-biphen)-4-yl]butyl-piperidine (RC-33)^{25–27} and a novel RC-33 bivalent derivative N^1, N^3 -bis(1-((R)-3-([1,1'-biphenyl]-4-yl)butyl)piperidin-4-yl)malonamide (DIM-3C), whose structures are reported in Figure 1. In particular, RC-33 was identified as a SIR agonist with an excellent affinity in the nanomolar range and high selectivity as compared with the Sigma2, μ -, and κ -opioid receptors.^{25,26} *In vitro* assays of (*S*) and (*R*) enantiomers of RC-33 revealed that both molecules exhibit a

comparable receptor binding profile, a similar effect in promoting NGF neurite outgrowth, and similar behavior in a calcium influx assay.^{27,28} As a result of further studies, however, we identified the (*R*) enantiomer as a lead compound, due to its metabolic stability and an optimal *in vivo* distribution.²⁹ In the present work, (*R*)-RC-33 was used as a template for designing a bivalent compound (i.e., DIM-3C), which constitutes a bulkier ligand potentially able to induce a conformational change in SIR keeping the ligand-binding pocket open. Taking advantage of the SIR crystal structure, we evaluated its association *in silico* with both RC-33 and DIM-3C. Conformational change studies in the SIR ligand-binding cavity were carried out to identify the ligand access pathway and to evaluate the binding of these two new compounds. The steered molecular dynamics (SMD) method³⁰ was used to induce unbinding of the PD144418 ligand from the crystal structure and to generate the opening of the ligand-binding pocket. Two ligand access pathways were explored, with the cytosolic surface of the β -barrel ligand-binding region showing greater flexibility and providing a transient ligand access pathway from the solvent to the binding site. Molecular docking, molecular dynamics (MD) simulations, and free energy perturbation (FEP) calculations were used to describe the binding mode of RC-33 and DIM-3C into the open SIR structure and to determine their relative binding affinities, which were compared with experimental K_i values corroborating theoretical predictions.

METHODS

Molecular Dynamics Simulations. The crystal structure of the human SIR in complex with the PD144418 chemical compound (PDB code SHK1)¹³ was used to characterize the SIR ligand-binding site and to evaluate the association of new compounds. The structure reveals a trimeric architecture; however, only the protomer with the longest sequence length was selected for our study. The protomer ligand-free form as well as the protomer bound to the PD144418 molecule were embedded in a fully hydrated palmitoyl-oleyl-phosphatidylcholine (POPC) bilayer solvated with explicit water molecules. Sodium and chloride ions (0.15 M NaCl) were added to the aqueous phase to ensure charge neutrality. The protonation states of the residues were analyzed with PropKa.³¹ The Asp126 residue was considered protonated at neutral pH. The parameters for the positively charged PD144418 ligand were obtained from the ParamChem server, using the CGenFF force field.³² The initial configurations of the systems were optimized by means of 30,000 steps of energy minimization, followed by equilibration and relaxation in a 120–435 ns MD simulation at 300 K in the isobaric–isothermal ensemble. Soft harmonic constraints were applied to the protein backbone and ligand during the first 10 ns of simulation, which were decreased gradually from 20 to 0 kcal mol⁻¹ Å⁻² over this period. Constant temperature was enforced using a Langevin thermostat with a damping coefficient of 1 ps⁻¹. The Langevin piston method³³ was used to maintain constant pressure (101.325 kPa). Long-range electrostatic interactions were computed using the particle-mesh Ewald summation method,³⁴ with a smooth real-space cutoff applied between 8 and 9 Å. All covalent bonds involving hydrogen as well as the intramolecular geometries of water molecules were constrained using the SETTLE algorithm.³⁵ The Verlet-I/r-RESPA multiple time-step integrator³⁶ was used with a time step of 2 fs. All MD simulations were performed using the program NAMD

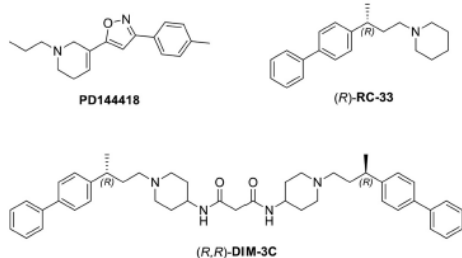


Figure 1. Structures of the compounds evaluated to interact with SIR. Only the (*R*) isomers of RC-33 and DIM-3C are shown; however, both (*S*) enantiomers of RC-33 and DIM-3C and the meso compound (*R,S*)-DIM-3C were also studied, as discussed in the main text.

B

DOI: 10.1021/acs.jcim.9b00649
J. Chem. Inf. Model. XXXX, XXX, XXX–XXX

v2.12-GPU³⁷ with the standard ions, lipids, and water molecules of the CHARMM36³⁸ force field. The root-mean-square deviation (RMSD) for the position of protein and ligand atoms in the simulated systems was utilized to evaluate the stability and thermodynamic equilibrium.

Steered Molecular Dynamics for Studying the Unbinding of PD144418. After equilibration and relaxation of the SIR bound to PD144418, an external force was applied to the ligand in order to open the access to the binding pocket, which could not usually be achieved by standard MD simulations. The steered molecular dynamics (SMD) method³⁰ implemented in NAMD v2.12³⁷ was used. Two ligand access pathways were evaluated: one directed toward the intracellular milieu and another directed toward the plasma membrane (Figure 2). The PD144418 molecule was pulled in

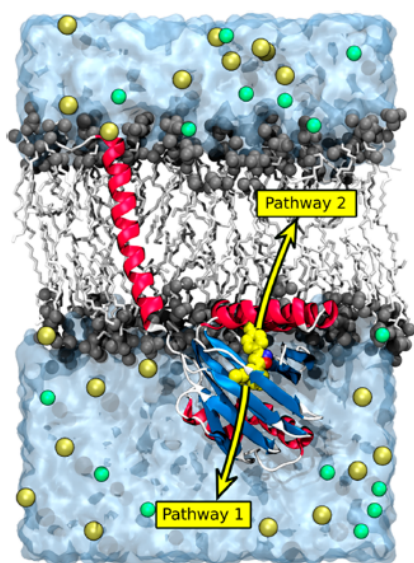


Figure 2. Ligand access pathways to the binding pocket. The presumed ligand-accessible pathways are illustrated using yellow arrows. All-atom simulation system of SIR bound to PD144418 is represented. SIR is shown in a cartoon representation and colored by secondary structure. PD144418 is displayed as spheres colored by atom type: carbon in yellow, oxygen in red, and nitrogen in blue. POPC lipid head groups and tails are shown as gray spheres and white sticks, respectively. TIP3P water molecules are represented by a blue transparent surface. Na⁺ and Cl⁻ ions are shown in light yellow and green spheres, respectively.

both directions using a parallel vector passing through the center of mass of the benzene and pyridine rings. The pulled atoms were harmonically constrained with a force constant of 5 kcal mol⁻¹ Å⁻². Different velocities were tested to avoid any distortion of the ligand or the protein as a consequence of pulling, i.e., 0.002, 0.005, and 0.02 Å ps⁻¹. The SMD simulations time was ≈20 ns, which was enough to observe the ligand completely outside the binding pocket. All calculations were performed using the simulation conditions described in the Molecular Dynamics Simulations section. The force acting on the PD144418 ligand was monitored over time

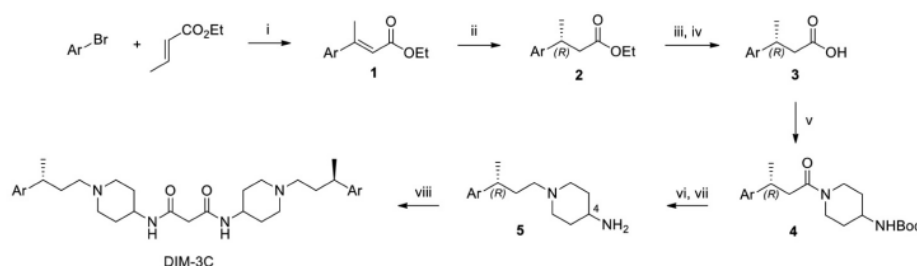
course of simulations to appraise the ligand unbinding event and, therefore, the opening of the occluded binding pocket.

Analysis of Ligand-Binding Cavity Dimensions. The HOLE³⁹ program was used to calculate the dimensions of the cavity connecting the ligand-binding site of SIR with the intracellular region. Analyses were performed for both the SIR crystal structure and the conformation adopted by the protein in the last 10 ns of the SMD trajectory, i.e., for the occluded and open ligand-binding cavities. HOLE algorithm uses the Metropolis Monte Carlo simulated annealing procedure⁴⁰ to find the largest sphere which can be accommodated in each point on the plane normal to the vector passing through the ligand-binding cavity. The center of mass of the benzene and pyridine rings of the PD144418 ligand were used to define the searching vector. The series of spheres of maximum radius were calculated at a distance of 0.25 Å in the vector direction. The values used for van der Waals radii of the protein atoms were taken by default from the AMBER⁴¹ force field. Structural analyses of HOLE outputs were carried out with the VMD v1.9.3 software.⁴²

Molecular Docking of RC-33 and DIM-3C. The association of RC-33⁴³ and the divalent DIM-3C compound was evaluated into three different open conformations of the SIR ligand-binding pocket obtained through SMD simulations. The structural stability of these conformations was evaluated through HOLE³⁹ and root-mean-square fluctuation (RMSF) analyses (Figure S1). An extensive conformational search in different states of the protein was conducted to ensure that all possible poses of the ligands into the binding site were sampled. All stereoisomers of the compounds were considered for this study (i.e., (R)-RC-33, (S)-RC-33, (R,R)-DIM-3C, (S,S)-DIM-3C, and (R,S)-DIM-3C), which were built with the ACD/ChemSketch v15.01 software (Advanced Chemistry Development, Inc., Toronto, On, Canada). LogP octanol/water values were calculated for each compound by using the QikProp program implemented in Maestro (Schrödinger, LLC, New York, USA). The three conformational states of the protein as well as all structural isomers of the ligands were prepared for docking with AutoDockTools v1.5.6,⁴⁴ assigning Gasteiger partial charges. Based on previous reports,^{13,45} the amine group of the ligands and the residue Asp126 of the protein were defined as protonated. Docking simulations were carried out with the AutoDock Vina v1.1.2 software.⁴⁶ Search space for docking was demarcated through a grid box large enough (25 Å × 25 Å × 50 Å) to accommodate free motion of the ligands into the binding site. The grid center was defined as the mass center of PD144418 in the ligand-bound SIR crystal structure.¹⁵ Residues Asp126 and Glu172 were defined to be flexible during the docking simulation. Ten conformations of the ligands were generated for each receptor–ligand complex, which were analyzed with the software PyMOL v1.7.7 (Schrödinger, LLC). The distances of the mass center of the docked conformations against PD144418 in the crystallographic structure were calculated in order to cluster the conformers at RMSD values of 2.5, 5, 7.5, 10, and 15 Å. The lowest scoring conformations in the most populated cluster for both the (S/R) RC-33 and (S,S/R,R/R,S) DIM-3C ligand sets were selected as the most probable binding conformations. It should be noted that AutoDock Vina was used only to obtain a very rough idea of the ligands' affinity. Free energy calculations were subsequently carried out to estimate the relative binding free energy and the precise orientation of the ligands into the SIR binding site.

C

DOI:10.1021/acs.jcim.9b00649
J. Chem. Inf. Model. XXXX, XXX, XXX–XXX

Scheme 1. Synthesis of DIM-3C⁴⁴

^aAr = Biphen-4-yl; reagents and conditions: (i) Pd(OAc)₂ 5 mol %, TBAC, AcONa, DMF, 105°C, yield 66%. (ii) H₂ (70 bar), (S,S)-[Ir(ThrePHOX)cod]BARF, DCM, r.t., yield 95%, ee 83%. (iii) NaOH 3M, abs EtOH, r.t., yield 97%. (iv) fractional crystallization with (S)-phenylethylamine in MeOH/H₂O (1:1 v/v), yield 94%, ee 98%. (v) TBTU, 4-Boc-aminopiperidine, DIPEA, THF, Δ (MW), yield 96%. (vi) TFA, DCM, r.t., yield 65%; (vii) LiAlH₄, THF, r.t., yield 69%; (viii) malonic acid (0.5 equiv), TBTU, DIPEA, CH₃CN, r.t., yield 63%.

Free Energy Perturbation for Studying the RC-33 and DIM-3C Binding. The most probable receptor–ligand complexes yielded by molecular docking, for the RC-33 and DIM-3C compounds, were used as the starting point for determining the relative binding affinity and the specific interactions of the ligands into the open ligand-binding pocket of S1R. Each complex was embedded in a pre-equilibrated palmitoyl-oleyl-phosphatidyl-choline (POPC) bilayer solvated with explicit water molecules. Sodium and chloride ions (0.15 M NaCl) were added to the aqueous phase. The initial configurations of the systems were minimized and equilibrated under MD simulation conditions similar to those described in the *Molecular Dynamics Simulations* section. The equilibration time for each system was ≈70 ns. The parameters for the positively charged RC-33 and DIM-3C ligands were obtained from the ParamChem server, using the CGenFF force field.³² The relative binding free energy of the ligands bound to S1R was estimated employing the free energy perturbation (FEP) method.⁴⁷ Each ligand molecule was gradually annihilated from bulk solution as it gradually appeared on the S1R binding site. The binding energy of the PD144418-bound S1R structure was also estimated as a reference. For each FEP calculation, 80–160 intermediate states ($\lambda = 0.0125$; $\lambda = 0.00625$) were considered in the forward and backward directions,⁴⁸ involving for each state 0.1 ns of equilibration followed by 0.15 ns of data collection. A total simulation time of 320 ns was invested. Weak harmonic distance restraints were used to keep the ligand molecule near the protein binding site, whereas the molecule in bulk solution was kept at a distance far enough from the protein applying positional and orientational restraints. All restraints were applied using the collective variable (COLVAR) module⁴⁹ available in NAMD v2.12.³⁷ The ParseFEP plugin implemented in VMD v1.9.3⁴² was used to determine the BAR⁵⁰ estimators alongside with its statistical error by combining forward and backward transformations. The statistical data obtained from these analyses were used to evaluate the convergence of the FEP calculations (Figures S2 and S3).

Synthesis of DIM-3C. For the synthesis of bivalent compound DIM-3C (Figure 1), we envisaged a coupling via amidation reaction between malonic acid, which serves as linker, and two units of compound 5, a derivative of our in-house developed hit compound RC-33,⁴³ bearing a primary amine at the C-4 position of piperidine. To obtain compound

5, we properly modified the protocol reported in our previous work for the synthesis of (R)-RC-33,^{43,51} with the aim of introducing the primary aminic moiety on the piperidine ring. The synthetic pathway and conditions are reported in Scheme 1. First, a Heck arylation was performed to access α,β -unsaturated ester 1. This was subjected to an enantioselective reduction of the double bond with a chiral Ir catalyst. After subsequent hydrolysis and fractional crystallization, an excellent enantiomeric excess (ee 98%) was obtained. Acid 3 was then subjected to amidation with 4-Boc-aminopiperidine in the presence of condensing agent TBTU. Afterward, reduction of the amide moiety with LiAlH₄ and subsequent Boc cleavage afforded key intermediate 5. Once we verified that the ee had been preserved, we proceeded to the coupling with malonic acid using TBTU. Upon reaction completion, the crude was purified, and target compound DIM-3C was obtained as a yellowish oil.

Binding Assays. K_i values were retrieved from literature for compounds PD144418⁵² and RC-33,²⁸ whereas for the novel compound DIM-3C, a well-established competition binding assay was exploited. This involves the use of homogenized guinea pig cerebral cortex membranes in the presence of [³H]-(+)-pentazocine, a selective S1R ligand (the same assay was used in our previous work to assess RC-33 affinity toward S1R).

RESULTS

Opening of the Occluded Ligand-Binding Pocket.

The crystal structure of the human S1R has been recently elucidated,¹³ providing an unique opportunity for structure-based drug design. In this work, the best resolution S1R structure (i.e., 2.5 Å) containing the PD144418 ligand was chosen to generate the opening of the ligand-binding pocket and, subsequently, evaluate the association of the RC-33 and DIM-3C compounds. Initially, the unbound S1R was relaxed in a 435 ns MD simulation to promote the binding pocket opening; however, during this time, no significant distortions in the dimensions of the ligand-binding cavity were observed. It is possible that the binding pocket opening might happen on longer time scales, which implies a high computational cost. We opted, therefore, for applying an external force to pull the ligand from the occluded β -barrel binding region causing its opening.

D

DOI:10.1021/acs.jcim.9b00649
J. Chem. Inf. Model. XXXX, XXX, XXX–XXX

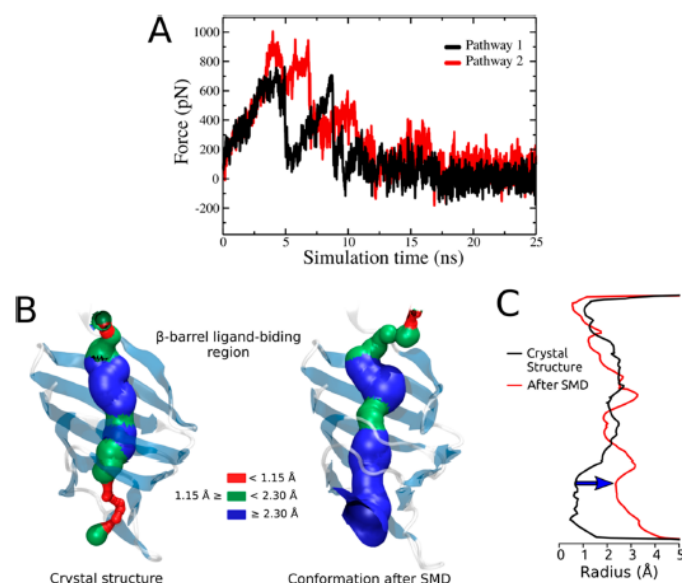


Figure 3. Opening of the occluded ligand-binding pocket. (A) Force-time profile of PD144418 pulled in the two pathways proposed to the ligands enter and exit from the binding site. (B) Surface representation of the ligand-binding cavity, calculated by HOLE,³⁹ in the S1R crystal structure (occluded state) and last frame of the SMD trajectory (open state). Surface is colored according to binding cavity dimensions. (C) HOLE-radius profile of the ligand-binding cavity calculated for the S1R crystal structure and as an average over last 10 ns of the SMD simulation.

Considering the highly occluded ligand-binding cavity in the S1R, the ligand pathway to enter and exit from the binding pocket remains poorly understood. One proposed pathway involves a gap between the two membrane-adjacent helices D and E, where the ligand is exposed directly into/out of the plasma membrane. Another pathway implicates that it accesses the binding pocket through the intracellular medium. Here, we defined a vector crossing both pathways and used the SMD method³⁰ to estimate the force required to pull out the PD144418 ligand from the binding site either toward the membrane or toward the intracellular side (Figure 2). At the beginning of the SMD simulation ($t = 0$ ns), the ligand was in the bound state, interacting with the protein residues as described in the crystal structure.¹³ After 3 ns of SMD simulation applying a pulling velocity of $0.005 \text{ \AA ps}^{-1}$ (Figure 3A), the ligand was moved through Pathway 1 experiencing a dissociative force of ~ 600 pN, while the same molecule going through Pathway 2 required ~ 900 pN to move out of the binding site. The duration of this primary rupture force was longer along Pathway 2, which could be used to determine the difficulty of dissociating the ligand along the two access pathways. A second force peak was observed around 8 ns, where the ligand in Pathway 1 showed a rupture force equivalent to the first peak, whereas the ligand in Pathway 2 exhibited a lower and longer dissociative force of ~ 400 pN. After 13 ns, the pulling force applied to the ligand in both access pathways becomes close to zero, indicating that PD144418 was completely dissociated from the protein. Based on the first rupture force peak observed for the ligand along the two unbinding pathways, we determined Pathway 1 as the most probable ligand access route. The structural

unbinding mechanisms associated with this pathway are explained below.

The unbound S1R structure obtained from the SMD simulation for PD144418 going through access Pathway 1 was analyzed with the program HOLE.³⁹ This algorithm is used to determine the size and shape of cavities in proteins. As shown in Figure 3B, the dimensions of the intracellular β -barrel ligand-binding region in the conformation obtained by SMD simulation were analyzed and compared with the dimensions in the X-ray structure (PDB code 5HK1).¹³ Overall, at the top of the ligand-binding cavity, both structures show roughly the same size and shape; however, the bottom region occluded from solvent in the crystal structure is completely open in the conformation obtained from SMD. This latter structure exhibits a continuous central cavity of at least 5 \AA diameter (Figure 3C), which is open enough to evaluate binding of RC-33 and the novel bivalent DIM-3C compound.

Dissociation of PD144418 and Binding of RC-33 and the Novel Bivalent Derivative DIM-3C. SMD simulations can provide important insights into the binding and unbinding mechanisms in protein–ligand complexes.⁵³ The peaks in the force profiles along the trajectories can be assigned to the forming and breaking of specific interactions. Here, we identified the structural factors determining the unbinding force peaks when the PD144418 ligand was pulled out toward the intracellular region (Figure 3A, Pathway 1). The mechanism of the contacts rupture into the β -barrel ligand-binding region was separated into three distinct stages (Figure 4A). Initially, as described in previous reports,^{13,54} PD144418 interacts with the glutamate residue at position 172 (Glu172) and the protonated aspartic residue at position 126 (Asp126), which have shown to be essential for ligand binding. This

E

DOI:10.1021/acs.jcim.9b00649
J. Chem. Inf. Model. XXXX, XXX, XXX–XXX

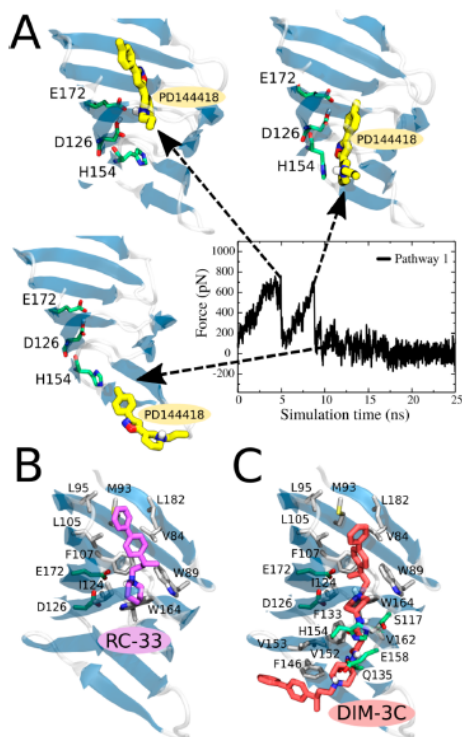


Figure 4. Mechanistic features of PD144418 unbinding process and association of RC-33 and the novel compound DIM-3C. (A) Dependence of dissociation forces experienced by PD144418 on its displacement toward the intracellular region (Pathway 1). The β -barrel ligand-binding region is shown in a blue cartoon representation. PD144418 is displayed as sticks colored by atom type: carbon in yellow, oxygen in red, nitrogen in blue, and hydrogen in white. (B) Preferred binding conformations of (*R*)-RC-33 and (C) (*R,R*)-DIM-3C, derived from docking calculations, into the open ligand-accessible conformation of SIR. The two molecules are shown in sticks with the carbon atoms colored in violet and red, respectively. Key residues making contact with the ligands are exhibited with the carbon atoms colored in green (polar residues) and gray (hydrophobic residues).

interaction is established mainly through the positively charged piperidine nitrogen of PD144418. As the ligand is pulled out of the binding site, a second interaction is formed with residue His154 in its neutral form. Derivatization studies have shown His154 to be in direct contact with SIR ligands.⁵⁵ We hypothesize here the formation of a cation- π interaction,⁵⁶ although no explicit terms for this type of contacts are

contained in the CHARMM force field.³⁸ At the end of the pulling simulation, the breakage of all stabilizing interactions for PD144418 in the binding site was observed, and the ligand is slowly moved toward the bulk solvent.

As was mentioned above, employing SMD simulations the narrow end of the β -barrel ligand-binding region of SIR was opened, allowing thus the evaluation of new ligand compounds to interact with the protein. Starting from the three distinct open conformations of the β -barrel ligand-binding region previously described, protein-ligand docking simulations were carried out for all stereoisomeric structures of RC-33 and the novel bivalent DIM-3C compound. For RC-33, a total of 78 docking poses including (*S*) and (*R*) enantiomers were generated, whereas for DIM-3C, 115 poses were obtained including the (*S,S*), (*R,R*), and (*R,S*) isomers. The best docked conformation of each compound was selected as that with the lowest AutoDock Vina score energy and the lowest distance of the mass center calculated against PD144418 in the crystallographic structure. In agreement with a previous report,⁵⁷ the two RC-33 enantiomers can be accommodated within the SIR ligand-binding site, though (*R*)-RC-33 was identified as the conformation with a more favorable binding energy. For DIM-3C, the (*S,S*) and (*R,R*) isomers showed higher affinity than (*R,S*); however, their affinities were predicted as equivalent.

As shown in Figure 4B, (*R*)-RC-33 is bound to the β -barrel ligand-binding region of SIR through an electrostatic interaction between the protonated piperidine nitrogen and the side chain of residue E172, which is in close contact with the residue D126. Additionally, the large hydrophobic group of the ligand is located near the residues V84, W89, M93, L95, L105, F107, and L182 (primary hydrophobic site), whereas the small hydrophobic group of the ligand is located near the residues I124 and W164 (secondary hydrophobic site). Such contacts are equivalent to those described for the PD144418 ligand in the SIR crystal structure.¹⁵ Thus, (*R*)-RC-33 adopts a similar position, orientation, and interactions as those elucidated for PD144418. On the other hand, DIM-3C (Figure 4C) forms a salt bridge with the negatively charged residue E172 and one of its monomers is placed with the same orientation of (*R*)-RC-33 (i.e., its large and small hydrophobic groups occupying the primary and secondary hydrophobic sites, respectively), while the second monomer is oriented toward the open cavity obtained through SMD calculations. Because of its bivalent structure, DIM-3C forms additional polar contacts with the residues S117, Q135, H154, and E158 located at the opened end of the β -barrel. The hydrophobic contacts network around DIM-3C contemplates the above-mentioned hydrophobic residues, further including the residues F133, F146, V152, V153, and V162 also located at the opened end of the β -barrel.

The association of DIM-3C into the β -barrel ligand-binding region supports the ligand access pathway to the binding site from intracellular region. Based on the docked conformation of

Table 1. Comparison of Experimental and Theoretical Predicted ΔG Binding Energies (kcal/mol) for PD144418, RC-33, and DIM-3C

Binding complex	K_i (nM)	Experimental ΔG (kcal/mol)	FEP ΔG (kcal/mol)	BAR estimator
SIR: PD144418	0.08 ± 0.01^a	-13.76	-13.24	-15.49 ± 0.17
SIR: RC-33	1.8 ± 0.1^b	-11.92	-11.32	-12.81 ± 0.12
SIR: DIM-3C	200 ± 16	-9.10	-9.65	-6.36 ± 0.34

^a K_i taken from Akunne et al. in ref 52. ^b K_i taken from Rossi et al. in ref 28.

F

DOI:10.1021/acs.jcim.9b00649
J. Chem. Inf. Model. XXXX, XXX, XXX-XXX

DIM-3C, one of its monomers needs the opening of the β -barrel ligand-binding region to be oriented in a similar conformation as that found to RC-33. If the pathway directed toward the plasma membrane is considered, an opposite orientation of the DIM-3C monomer with respect to RC-33 would be required in order to locate the second monomer between the membrane-adjacent helices D and E.

To corroborate the predicted ligand binding modes into the open β -barrel ligand-binding region and to estimate the relative binding energies of the SIR:RC-33 and SIR:DIM-3C complexes, free energy perturbation (FEP) calculations were carried out. The SIR:PD144418 complex was also evaluated as a reference. As mentioned above, the three ligands were bound in the same binding pocket establishing polar and hydrophobic contacts with residues lining the β -barrel ligand-binding region. Calculated affinities for each complex are reported in Table 1. The highest affinity (-13.24 kcal/mol) was observed for the crystallographic PD144418 ligand, which is a known SIR antagonist.⁵⁸ In agreement with previous experiments,^{27,28} RC-33 exhibited a binding free energy of -11.32 kcal/mol, whereas the lowest affinity was found for the bivalent compound DIM-3C (-9.65 kcal/mol). It should be noted that although the predicted binding energy for DIM-3C exhibits a moderate affinity as compared with the monomeric ligands these results suggest a possible role of divalent ligands to modulate the SIR function. Overall, the binding free energies (ΔG) obtained by the FEP method agree with experimental K_i values previously reported for PD144418⁵² and RC-33,²⁸ while the energy value calculated for DIM-3C is consistent with our current experimental K_i analysis ($K_i = 200$ nM as reported in Table 1). Binding free energies and statistical errors determined using the BAR estimator,⁴⁸ a combination of the forward and backward transitions to obtain free energy differences, follow the same trend as the experimental K_i values. It should be noted that a non-negligible hysteresis between the forward and backward transformations was observed for DIM-3C (Figure S3), which may be attributed to the size and flexibility of this compound. On other hand, the effect of Colvars restraints on the binding free energy was estimated for each complex as reported by Gumbart et al.,⁵⁹ finding a minimal contribution (≈ 0.3 kcal/mol).

DIM-3C Synthesis and Ligand Binding assays. The synthetic approach described above allowed us to obtain the first reported bivalent SIR ligand. To obtain the DIM-3C compound, we envisaged the symmetric dimerization of RC-33. Specifically, we employed a reactive RC-33 derivative (compound 5), in which the piperidine ring bears a primary amine on the C-4 position, as reported in Scheme 1. This particular position was chosen for derivatization because in the docked pose of RC-33 it is the one pointing toward the proposed entrance of the ligand-binding pocket (Figure 4B). Accordingly, two equivalents of compound 5 were coupled via amide bond to one equivalent of a diacidic linker (i.e., malonic acid) for obtaining the target compound DIM-3C (Scheme 1). Thus, the designed (*R,R*)-DIM-3C molecule consists in two subunits—corresponding to the (*R*)-RC-33 scaffold—joined together by a three-carbon atom chain. The target compound was obtained in suitable amount and purity for further biological evaluation, i.e., competition assay with [³H]-(+)-pentazocine. The symmetry of (*R,R*)-DIM-3C allows it to reach the SIR ligand-binding site indifferently from both ends, which may compensate the expected decrease in binding

affinity due to its larger volume. We also envisaged that this compound represents a viable tool to validate the ligand access pathways to enter and exit the SIR binding pocket.

DIM-3C showed a decreased affinity toward SIR in comparison with the parent compound RC-33 (K_i values are 200 and 1.8 nM, respectively); nevertheless, the new bivalent ligand is able to displace the radiolabeled pentazocine in a dose-dependent manner, indicating its ability to bind the receptor. A lower affinity was expected for this compound due to its bigger dimension as compared to RC-33, which was correctly predicted by *in silico* simulations.

DISCUSSION

As an initial step toward evaluating the association of new ligands at the SIR crystal structure and identifying key residues for binding interactions, the occluded ligand-binding pocket was opened by pulling out the crystallographic PD144418 ligand. The SMD method, employed for this purpose, has been demonstrated as a promising computational tool for inducing unbinding of ligands and evaluating conformational changes in biomolecules.^{53,60–62} It is still uncertain how ligands enter and exit the SIR binding site; therefore, we explored two putative pathways for extracting the PD144418 ligand from the crystal structure. As described in previous reports,^{13,45,63} the proposed pathways include a cytoplasmic entrance passing through the narrow polar region occluded by the residues Q135, H154, and E158, and a gap between the helices D and E adjacent to the plasma membrane. Based on force profiles obtained from SMD calculations, which can be quantitatively correlated with protein–ligand binding affinity, the pathway going through the cytoplasmic region was selected as the most accessible for ligands. Analyses of the internal geometry of the β -barrel ligand-binding region, after its opening applying an external force, show enough space to accommodate ligands entering from the intracellular space.

SMD simulations also provide a detailed atomistic description of the unbinding mechanism of a ligand out of its binding pocket at the protein, which can be used to identify key structural elements in the formation of protein–ligand complexes. Previous studies have revealed that SMD simulations are more suited for identifying electrostatic interactions rather than hydrophobic contacts.⁶¹ Our simulations, indeed, showed that the polar residues D126, H154, and E172 mainly determine the association of the PD144418 ligand to SIR. Seth et al. previously identified the residues D126 and E172 as essentials for ligand binding.⁶⁴ Moreover, a protonated state for D126 has been proposed when ligands are bound to SIR,¹³ which was certainly considered in our study. The open ligand-binding pocket structure of SIR, with special emphasis in these three polar residues, was employed to evaluate the binding of two additional compounds. RC-33 has been recognized as a potent and selective SIR ligand,^{27,43} therefore, its association was evaluated at the atomic level against the open SIR structure. Docking studies support the binding of RC-33 to the open β -barrel ligand-binding region and denote a similar orientation and interactions with surrounding residues as those observed for the PD144418 ligand in the SIR crystal structure.

To validate the proposed ligand access pathway in SIR and to test the binding of a new compound, we designed a bivalent ligand based on the RC-33 structure. DIM-3C constitutes a bulkier ligand with the potential to occupy the binding pocket in its open conformation. For this work, we decided to

G

DOI:10.1021/acs.jcim.9b00649
J. Chem. Inf. Model. XXXX, XXX, XXX–XXX

synthesize only the (*R,R*) DIM-3C dimer for the following reasons: (i) Physicochemical characterization is easier when dealing with a single stereoisomer. (ii) Based on current and previous studies, there is no significant difference between (*R*)- and (*S*)-RC-33 interaction with the S1R ligand-binding pocket.^{27,28} (iii) Since (*R*)-RC-33 was earlier identified as hit compound for its higher metabolic stability,²⁹ the synthetic strategy to obtain this enantiomer was recently optimized by our group, and the same protocol could be used to obtain (*R,R*)-DIM-3C.

The association of DIM-3C with S1R was evaluated by computational studies. This compound forms similar interactions into the β -barrel ligand-binding region as those found for RC-33. A comparable binding association was in fact expected, as DIM-3C is a divalent RC-33 derivative. This ligand corresponds to the first bivalent structure shown to interact with S1R. DIM-3C was of particular interest in our study, allowing us to validate the ligand access pathway from the intracellular space to reach the binding site. Our study, therefore, argues against the ligand entering through the two adjacent helices to the plasma membrane, at least for large ligands. In addition, the interaction of DIM-3C with the residues Q135, H154, and E158—forming the occluded narrow polar region in the S1R crystal structure—allows us to hypothesize that S1R ligands initially interact with these residues and then reach the binding site. This is particularly interesting considering that lipid/water partition coefficients calculated for the three studied compounds denote a preference to be associated into lipid environments.

Computationally demanding MD simulations using the FEP method were carried out to estimate the relative binding free energies of PD144418, RC-33, and DIM-3C interacting with S1R. Our results corroborate the predicted ligand-binding modes obtained by docking and agree with experimental K_i values. The best affinity was found for PD144418, whereas the binding free energy calculated for RC-33 shows the potential of this compound to modulate the S1R activity, which agrees with its reported apparent affinity.²⁸ Experimental affinity assays for DIM-3C were also performed. For this compound, the binding affinity was found to be moderate in comparison with monomeric structures, in accordance with predicted ΔG energy (Table 1). Interestingly, its dose-dependent displacement of [³H]-(+)-pentazocine in the binding assays confirms the ability of DIM-3C to accommodate into the S1R ligand-binding pocket in its open conformation, penetrating through the intracellular side.

In conclusion, while the calculations presented here have a number of limitations—exploration of only two defined pathways for ligands entering and leaving the S1R binding site, the use of approximate force field parameters for ligands, and free energy calculations based on representative stereoisomers—our results suggest that ligands access the S1R binding site through the cytoplasmic region. A conformation opened at the narrow end of the β -barrel seems to be favorable for ligands diffusion from the intracellular space toward the binding site, particularly, for large ligands whose access through the plasma membrane could imply a great structural distortion. Our study also proves an updated characterization of the RC-33 binding into the S1R ligand-binding pocket based on a high-resolution structure of the protein. In addition, the association of S1R with the bivalent RC-33 derivative ligand (i.e., DIM-3C) is demonstrated by our analyses, revealing a molecular structure without precedent to modulate the S1R

activity. DIM-3C is the first divalent compound associated with S1R and represents a good example to argue the ligand access pathway to the binding pocket from the intracellular region. We emphasize that although the ability of DIM-3C to regulate the S1R function is significantly less than that of monomeric ligands, it may be an adequate molecule to describe the opening of the binding pocket for the entrance of ligands. Our study, therefore, is envisioned to prove useful for better understanding the binding mechanism of different compounds into the S1R ligand-binding pocket, providing the molecular basis to design new S1R modulators based on its structure.

■ ASSOCIATED CONTENT

Supporting Information

The Supporting Information is available free of charge at <https://pubs.acs.org/doi/10.1021/acs.jcim.9b00649>.

Information as mentioned in the text. (PDF)

■ AUTHOR INFORMATION

Corresponding Authors

*E-mail: simona.collina@unipv.it (S.C.).

*E-mail: arvergara@utalca.cl (A.V.-J.).

ORCID

Julio Caballero: 0000-0003-0182-1444

Bernhard Wünsch: 0000-0002-9030-8417

Simona Collina: 0000-0002-2954-7558

Ariela Vergara-Jaque: 0000-0002-1236-013X

Author Contributions

A.V.-J., J.C., and S.C. conceived the project. A.V.-J., I.O., and M.G.-A. carried out the computational simulations and analyzed data. G.R. and M.R. performed the synthesis. D.S. performed the binding assays. D.S., B.W., D.R., and S.C. analyzed the data. A.V.-J. and J.C. wrote the manuscript. All authors contributed to the editing of the paper and to scientific discussions.

Notes

The authors declare no competing financial interest.

■ ACKNOWLEDGMENTS

A.V.-J. thanks the academic program “Núcleo Científico Multidisciplinario” and is thankful for the FONDECYT Research Initiation Grant No. 11170223. The Millennium Nucleus of Ion Channels-Associated Diseases (MiNICAD) is a Millennium Nucleus supported by the Iniciativa Científica Milenio of the Ministry of Economy, Development and Tourism (Chile). J.C. is thankful for the FONDECYT Regular Grant No. 1170718 and CONICYT-FONDEQUIP-EQM160063. G.R. and S.C. thankfully recognize Scuola di Alta Formazione Dottorale of the University of Pavia for the mobility research scholarship provided. S.C. gratefully acknowledges the University of Pavia (Italy) for the research grant to M.R. and MIUR for the doctoral fellowship to G.R.

■ ABBREVIATIONS

S1R, Sigma 1 receptor; PD144418, 1,2,3,6-tetrahydro-5-[3-(4-methylphenyl)-5-isoxazolyl]-1-propylpyridine; RC-33, 1-[3-(1,1'-biphenyl)-4-yl]butyl-piperidine; DIM-3C, *N*¹*N*³-bis(1-((*R*)-3-([1,1'-biphenyl]-4-yl)butyl)piperidin-4-yl)malonamide; SMD, steered molecular dynamics; FEP, free energy perturbation

H

DOI:10.1021/acs.jcim.9b00649
J. Chem. Inf. Model. XXXX, XXX, XXX–XXX

REFERENCES

- (1) Su, T.-P.; Hayashi, T.; Maurice, T.; Buch, S.; Ruoho, A. E. The Sigma-1 Receptor Chaperone as an Inter-Organellar Signaling Modulator. *Trends Pharmacol. Sci.* **2010**, *31* (12), 557–566.
- (2) Hayashi, T.; Su, T.-P. An Update on the Development of Drugs for Neuropsychiatric Disorders: Focusing on the Sigma 1 Receptor Ligand. *Expert Opin. Ther. Targets* **2008**, *12* (1), 45–58.
- (3) Prasad, P. D.; Li, H. W.; Fei, Y. J.; Ganapathy, M. E.; Fujita, T.; Plumley, L. H.; Yang-Feng, T. L.; Leibach, F. H.; Ganapathy, V. Exon-Intron Structure, Analysis of Promoter Region, and Chromosomal Localization of the Human Type 1 Sigma Receptor Gene. *J. Neurochem.* **1998**, *70* (2), 443–451.
- (4) Sabino, V.; Cottone, P.; Parylak, S. L.; Steardo, L.; Zorrilla, E. P. Sigma-1 Receptor Knockout Mice Display a Depressive-like Phenotype. *Behav. Brain Res.* **2009**, *198* (2), 472–476.
- (5) Chevallier, N.; Keller, E.; Maurice, T. Behavioural Phenotyping of Knockout Mice for the Sigma-1 (Σ 1) Chaperone Protein Revealed Gender-Related Anxiety, Depressive-like and Memory Alterations. *J. Psychopharmacol. (London, U. K.)* **2011**, *25* (7), 960–975.
- (6) Hanner, M.; Moebius, F. F.; Flandorfer, A.; Knaus, H. G.; Striessnig, J.; Kempner, E.; Glossmann, H. Purification, Molecular Cloning, and Expression of the Mammalian Sigma-1-Binding Site. *Proc. Natl. Acad. Sci. U. S. A.* **1996**, *93* (15), 8072–8077.
- (7) Seth, P.; Leibach, F. H.; Ganapathy, V. Cloning and Structural Analysis of the cDNA and the Gene Encoding the Murine Type 1 Sigma Receptor. *Biochem. Biophys. Res. Commun.* **1997**, *241* (2), 535–540.
- (8) Kekuda, R.; Prasad, P. D.; Fei, Y. J.; Leibach, F. H.; Ganapathy, V. Cloning and Functional Expression of the Human Type 1 Sigma Receptor (HSigmaR1). *Biochem. Biophys. Res. Commun.* **1996**, *229* (2), 553–558.
- (9) Pan, L.; Pasternak, D. A.; Xu, J.; Xu, M.; Lu, Z.; Pasternak, G. W.; Pan, Y.-X. Isolation and Characterization of Alternatively Spliced Variants of the Mouse Sigma 1 Receptor Gene, SigmaR1. *PLoS One* **2017**, *12* (3), No. e0174694.
- (10) Hayashi, T.; Justinova, Z.; Hayashi, E.; Cormaci, G.; Mori, T.; Tsai, S.-Y.; Barnes, C.; Goldberg, S. R.; Su, T.-P. Regulation of Sigma-1 Receptors and Endoplasmic Reticulum Chaperones in the Brain of Methamphetamine Self-Administering Rats. *J. Pharmacol. Exp. Ther.* **2010**, *332* (3), 1054–1063.
- (11) Aydar, E.; Palmer, C. P.; Klyachko, V. A.; Jackson, M. B. The Sigma Receptor as a Ligand-Regulated Auxiliary Potassium Channel Subunit. *Neuron* **2002**, *34* (3), 399–410.
- (12) Morin-Surun, M. P.; Collin, T.; Denavit-Saubié, M.; Baulieu, E.-E.; Monnet, F. P. Intracellular Σ 1 Receptor Modulates Phospholipase C and Protein Kinase C Activities in the Brainstem. *Proc. Natl. Acad. Sci. U. S. A.* **1999**, *96* (14), 8196–8199.
- (13) Schmidt, H. R.; Zheng, S.; Gurpinar, E.; Koehl, A.; Manglik, A.; Kruse, A. C. Crystal Structure of the Human Σ 1 Receptor. *Nature* **2016**, *532* (7600), 527–530.
- (14) Sánchez-Fernández, C.; Entrena, J. M.; Baeyens, J. M.; Cobos, E. J. Sigma-1 Receptor Antagonists: A New Class of Neuro-modulatory Analgesics. *Adv. Exp. Med. Biol.* **2017**, *964*, 109–132.
- (15) Glennon, R. A. Pharmacophore Identification for Sigma-1 (Sigma1) Receptor Binding: Application of the “Deconstruction-Reconstruction-Elaboration” Approach. *Mini-Rev. Med. Chem.* **2005**, *5* (10), 927–940.
- (16) Chu, U. B.; Ruoho, A. E. Biochemical Pharmacology of the Sigma-1 Receptor. *Mol. Pharmacol.* **2016**, *89* (1), 142–153.
- (17) Gund, T. M.; Floyd, J.; Jung, D. Molecular Modeling of [Sigma]1 Receptor Ligands: A Model of Binding Conformational and Electrostatic Considerations. *J. Mol. Graphics Modell.* **2004**, *22* (3), 221–230.
- (18) Laggner, C.; Schieferer, C.; Fiechtner, B.; Poles, G.; Hoffmann, R. D.; Glossmann, H.; Langer, T.; Moebius, F. F. Discovery of High-Affinity Ligands of Σ 1 Receptor, ERG2, and Emopamil Binding Protein by Pharmacophore Modeling and Virtual Screening. *J. Med. Chem.* **2005**, *48* (15), 4754–4764.
- (19) Jung, D.; Floyd, J.; Gund, T. M. A Comparative Molecular Field Analysis (CoMFA) Study Using Semiempirical, Density Functional, Ab Initio Methods and Pharmacophore Derivation Using DISCOtech on Sigma 1 Ligands. *J. Comput. Chem.* **2004**, *25* (11), 1385–1399.
- (20) Quesada-Romero, L.; Mena-Ulecia, K.; Zuniga, M.; De-la-Torre, P.; Rossi, D.; Tiznado, W.; Collina, S.; Caballero, J. Optimal Graph-based and Simplified Molecular Input Line Entry System-based Descriptors for Quantitative Structure-Activity Relationship Analysis of Arylalkylaminoalcohols, Arylalkenylamines, and Arylalkylamines as Σ 1 Receptor Ligands. *J. Chemom.* **2015**, *29* (1), 13–20.
- (21) Caballero, J.; Zilocchi, S.; Tiznado, W.; Rossi, D.; Collina, S. Models of the Pharmacophoric Pattern and Affinity Trend of Methyl 2-(Aminomethyl)-1-Phenylcyclopropane-1-Carboxylate Derivatives as Σ 1 Ligands. *Mol. Simul.* **2012**, *38* (3), 227–235.
- (22) Oberdorf, C.; Schmidt, T. J.; Wunsch, B. SD-QSAR for Spirocyclic Sigma 1 Receptor Ligands by Quasar Receptor Surface Modeling. *Eur. J. Med. Chem.* **2010**, *45* (7), 3116–3124.
- (23) Laurini, E.; Col, V. D.; Mamolo, M. G.; Zampieri, D.; Posocco, P.; Fermeglia, M.; Vio, L.; Pricl, S. Homology Model and Docking-Based Virtual Screening for Ligands of the Σ 1 Receptor. *ACS Med. Chem. Lett.* **2011**, *2* (11), 834–839.
- (24) Ortega-Roldan, J. L.; Ossa, F.; Amin, N. T.; Schnell, J. R. Solution NMR Studies Reveal the Location of the Second Transmembrane Domain of the Human Sigma-1 Receptor. *FEBS Lett.* **2015**, *589* (5), 659–665.
- (25) Rossi, D.; Urbano, M.; Pedrali, A.; Serra, M.; Zampieri, D.; Mamolo, M. G.; Laggner, C.; Zanette, C.; Florio, C.; Schepmann, D.; et al. Design, Synthesis and SAR Analysis of Novel Selective Σ 1 Ligands (Part 2). *Bioorg. Med. Chem.* **2010**, *18* (3), 1204–1212.
- (26) Rossi, D.; Pedrali, A.; Urbano, M.; Gaggeri, R.; Serra, M.; Fernández, L.; Fernández, M.; Caballero, J.; Ronisvalle, S.; Prezzavento, O.; et al. Identification of a Potent and Selective Σ 1 Receptor Agonist Potentiating NGF-Induced Neurite Outgrowth in PC12 Cells. *Bioorg. Med. Chem.* **2011**, *19* (21), 6210–6224.
- (27) Rossi, D.; Pedrali, A.; Marra, A.; Pignataro, L.; Schepmann, D.; Wunsch, B.; Ye, L.; Leuner, K.; Peviani, M.; Curti, D.; et al. Studies on the Enantiomers of RC-33 as Neuroprotective Agents: Isolation, Configurational Assignment, and Preliminary Biological Profile. *Chirality* **2013**, *25* (11), 814–822.
- (28) Rossi, D.; Pedrali, A.; Gaggeri, R.; Marra, A.; Pignataro, L.; Laurini, E.; Dal Col, V.; Fermeglia, M.; Pricl, S.; Schepmann, D.; et al. Chemical, Pharmacological, and in Vitro Metabolic Stability Studies on Enantiomerically Pure RC-33 Compounds: Promising Neuroprotective Agents Acting as Σ 1 Receptor Agonists. *ChemMedChem* **2013**, *8* (9), 1514–1527.
- (29) Marra, A.; Rossi, D.; Pignataro, L.; Bigogno, C.; Canta, A.; Oggioni, N.; Malacrida, A.; Corbo, M.; Cavaletti, G.; Peviani, M.; et al. Toward the Identification of Neuroprotective Agents: G-Scale Synthesis, Pharmacokinetic Evaluation and CNS Distribution of (R)-RC-33, a Promising SIGMA1 Receptor Agonist. *Future Med. Chem.* **2016**, *8* (3), 287–295.
- (30) Lu, H.; Schulten, K. Steered Molecular Dynamics Simulations of Force-Induced Protein Domain Unfolding. *Proteins: Struct., Funct., Genet.* **1999**, *35* (4), 453–463.
- (31) Olsson, M. H. M.; Søndergaard, C. R.; Rostkowski, M.; Jensen, J. H. PROPKA3: Consistent Treatment of Internal and Surface Residues in Empirical PKa Predictions. *J. Chem. Theory Comput.* **2011**, *7* (2), 525–537.
- (32) Vanommeslaeghe, K.; Hatcher, E.; Acharya, C.; Kundu, S.; Zhong, S.; Shim, J.; Darian, E.; Guvench, O.; Lopes, P.; Vorobyov, I.; Mackerell, A. D. CHARMM General Force Field (CGenFF): A Force Field for Drug-like Molecules Compatible with the CHARMM All-Atom Additive Biological Force Fields. *J. Comput. Chem.* **2009**, *31* (4), 671–690.
- (33) Feller, S. E.; Zhang, Y.; Pastor, R. W.; Brooks, B. R. Constant Pressure Molecular Dynamics Simulation: The Langevin Piston Method. *J. Chem. Phys.* **1995**, *103* (11), 4613–4621.

- (34) Essmann, U.; Perera, L.; Berkowitz, M. L.; Darden, T.; Lee, H.; Pedersen, L. G. A Smooth Particle Mesh Ewald Method. *J. Chem. Phys.* **1995**, *103* (19), 8577–8593.
- (35) Miyamoto, S.; Kollman, P. A. Settle: An Analytical Version of the SHAKE and RATTLE Algorithm for Rigid Water Models. *J. Comput. Chem.* **1992**, *13* (8), 952–962.
- (36) Tuckerman, M.; Berne, B. J.; Martyna, G. J. Reversible Multiple Time Scale Molecular Dynamics. *J. Chem. Phys.* **1992**, *97* (3), 1990–2001.
- (37) Phillips, J. C.; Braun, R.; Wang, W.; Gumbart, J.; Tajkhorshid, E.; Villa, E.; Chipot, C.; Skeel, R. D.; Kalé, L.; Schulten, K. Scalable Molecular Dynamics with NAMD. *J. Comput. Chem.* **2005**, *26* (16), 1781–1802.
- (38) MacKerell, A. D.; Bashford, D.; Bellott, M.; Dunbrack, R. L.; Evanseck, J. D.; Field, M. J.; Fischer, S.; Gao, J.; Guo, H.; Ha, S.; et al. All-Atom Empirical Potential for Molecular Modeling and Dynamics Studies of Proteins. *J. Phys. Chem. B* **1998**, *102* (18), 3586–3616.
- (39) Smart, O. S.; Neduvellil, J. G.; Wang, X.; Wallace, B. A.; Sansom, M. S. HOLE: A Program for the Analysis of the Pore Dimensions of Ion Channel Structural Models. *J. Mol. Graphics* **1996**, *14* (6), 354–360.
- (40) Metropolis, N.; Rosenbluth, A. W.; Rosenbluth, M. N.; Teller, A. H.; Teller, E. Equation of State Calculations by Fast Computing Machines. *J. Chem. Phys.* **1953**, *21*, 1087–1092.
- (41) Weiner, S. J.; Kollman, P. A.; Case, D. A.; Singh, U. C.; Ghio, C.; Alagona, G.; Profeta, S.; Weiner, P. A New Force Field for Molecular Mechanical Simulation of Nucleic Acids and Proteins. *J. Am. Chem. Soc.* **1984**, *106* (3), 765–784.
- (42) Humphrey, W.; Dalke, A.; Schulten, K. VMD: Visual Molecular Dynamics. *J. Mol. Graphics* **1996**, *14* (1), 33–38.
- (43) Rossi, D.; Marra, A.; Picconi, P.; Serra, M.; Catenacci, L.; Sorrenti, M.; Laurini, E.; Fermeglia, M.; Pricl, S.; Brambilla, S.; et al. Identification of RC-33 as a Potent and Selective $\Sigma 1$ Receptor Agonist Potentiating NGF-Induced Neurite Outgrowth in PC12 Cells. Part 2: G-Scale Synthesis, Physicochemical Characterization and in Vitro Metabolic Stability. *Bioorg. Med. Chem.* **2013**, *21* (9), 2577–2586.
- (44) Morris, G. M.; Huey, R.; Lindstrom, W.; Sanner, M. F.; Belew, R. K.; Goodsell, D. S.; Olson, A. J. AutoDock4 and AutoDock Tools4: Automated Docking with Selective Receptor Flexibility. *J. Comput. Chem.* **2009**, *30* (16), 2785–2791.
- (45) Ossa, F.; Schnell, J. R.; Ortega-Roldan, J. L. A Review of the Human Sigma-1 Receptor Structure. *Adv. Exp. Med. Biol.* **2017**, *964*, 15–29.
- (46) Trott, O.; Olson, A. J. AutoDock Vina: Improving the Speed and Accuracy of Docking with a New Scoring Function, Efficient Optimization and Multithreading. *J. Comput. Chem.* **2009**, *31* (2), 455–461.
- (47) Zwanzig, R. W. High-Temperature Equation of State by a Perturbation Method. I. Nonpolar Gases. *J. Chem. Phys.* **1954**, *22*, 1420–1426.
- (48) Pohorille, A.; Jarzynski, C.; Chipot, C. Good Practices in Free-Energy Calculations. *J. Phys. Chem. B* **2010**, *114* (32), 10235–10253.
- (49) Fiorin, G.; Klein, M. L.; Hémin, J. Using Collective Variables to Drive Molecular Dynamics Simulations. *Mol. Phys.* **2013**, *111*, 3345–3362.
- (50) Bennett, C. H. Efficient Estimation of Free Energy Differences from Monte Carlo Data. *J. Comput. Phys.* **1976**, *22*, 245–268.
- (51) Marra, A.; Rossi, D.; Maggi, L.; Corana, F.; Mannucci, B.; Peviani, M.; Curti, D.; Collina, S. Development of Easy-to-Use Reverse-Phase Liquid Chromatographic Methods for Determining PRE-084, RC-33 and RC-34 in Biological Matrices. The First Step for in Vivo Analysis of Sigma1 Receptor Agonists. *Biomed. Chromatogr.* **2016**, *30* (4), 645–651.
- (52) Akunne, H. C.; Whetzel, S. Z.; Wiley, J. N.; Corbin, A. E.; Ninteman, F. W.; Teclé, H.; Pei, Y.; Pugsley, T. A.; Heffner, T. G. The Pharmacology of the Novel and Selective Sigma Ligand, PD 144418. *Neuropharmacology* **1997**, *36* (1), 51–62.
- (53) Do, P.-C.; Lee, E. H.; Le, L. Steered Molecular Dynamics Simulation in Rational Drug Design. *J. Chem. Inf. Model.* **2018**, *58* (8), 1473–1482.
- (54) Seth, P.; Ganapathy, M. E.; Conway, S. J.; Bridges, C. D.; Smith, S. B.; Casellas, P.; Ganapathy, V. Expression Pattern of the Type 1 Sigma Receptor in the Brain and Identity of Critical Anionic Amino Acid Residues in the Ligand-Binding Domain of the Receptor. *Biochim. Biophys. Acta, Mol. Cell Res.* **2001**, *1540* (1), 59–67.
- (55) Chu, U. B.; Ramachandran, S.; Hajipour, A. R.; Ruoho, A. E. Photoaffinity Labeling of the Sigma-1 Receptor with N-[3-(4-Nitrophenyl)Propyl]-N-Dodecylamine: Evidence of Receptor Dimers. *Biochemistry* **2013**, *52* (5), 859–868.
- (56) Liao, S.-M.; Du, Q.-S.; Meng, J.-Z.; Pang, Z.-W.; Huang, R.-B. The Multiple Roles of Histidine in Protein Interactions. *Chem. Cent. J.* **2013**, *7* (1), 44.
- (57) Velázquez-Libera, J. L.; Rossino, G.; Navarro-Retamal, C.; Collina, S.; Caballero, J. Docking, Interaction Fingerprint, and Three-Dimensional Quantitative Structure-Activity Relationship (3D-QSAR) of Sigma1 Receptor Ligands, Analogs of the Neuroprotective Agent RC-33. *Front. Chem.* **2019**, *7*, 496.
- (58) Lever, J. R.; Miller, D. K.; Ferguson-Cantrell, E. A.; Green, C. L.; Watkinson, L. D.; Carmack, T. L.; Lever, S. Z. Relationship between Cerebral Sigma-1 Receptor Occupancy and Attenuation of Cocaine's Motor Stimulatory Effects in Mice by PD144418. *J. Pharmacol. Exp. Ther.* **2014**, *351* (1), 153–163.
- (59) Gumbart, J. C.; Roux, B.; Chipot, C. Standard Binding Free Energies from Computer Simulations: What Is the Best Strategy? *J. Chem. Theory Comput.* **2013**, *9* (1), 794–802.
- (60) Moore, D. S.; Brines, C.; Jewhurst, H.; Dalton, J. P.; Tikhonova, I. G. Steered Molecular Dynamics Simulations Reveal Critical Residues for (Un)Binding of Substrates, Inhibitors and a Product to the Malarial M1 Aminopeptidase. *PLoS Comput. Biol.* **2018**, *14* (10), No. e1006525.
- (61) Patel, J. S.; Berteotti, A.; Ronsisvalle, S.; Rocchia, W.; Cavalli, A. Steered Molecular Dynamics Simulations for Studying Protein-Ligand Interaction in Cyclin-Dependent Kinase 5. *J. Chem. Inf. Model.* **2014**, *54* (2), 470–480.
- (62) Caballero, J.; Zamora, C.; Aguayo, D.; Yañez, C.; González-Nilo, F. D. Study of the Interaction between Progesterone and Beta-Cyclodextrin by Electrochemical Techniques and Steered Molecular Dynamics. *J. Phys. Chem. B* **2008**, *112* (33), 10194–10201.
- (63) Alon, A.; Schmidt, H. R.; Wood, M. D.; Sahn, J. J.; Martin, S. F.; Kruse, A. C. Identification of the Gene That Codes for the $\Sigma 2$ Receptor. *Proc. Natl. Acad. Sci. U. S. A.* **2017**, *114* (27), 7160–7165.
- (64) Seth, P.; Ganapathy, M. E.; Conway, S. J.; Bridges, C. D.; Smith, S. B.; Casellas, P.; Ganapathy, V. Expression Pattern of the Type 1 Sigma Receptor in the Brain and Identity of Critical Anionic Amino Acid Residues in the Ligand-Binding Domain of the Receptor. *Biochim. Biophys. Acta, Mol. Cell Res.* **2001**, *1540* (1), 59–67.